Geology, Geochronology and Structural Evolution of La Escondida Copper District, Northern Chile

Felipe Urzúa

Submitted in fulfilment of the requirements
for the degree of Doctor of Philosophy

Hobart, Australia
February, 2009

UNIVERSITY OF TASMANIA

Declaration

This thesis contains no material which has been accepted for the awards of any other degree or diploma in any tertiary institution and, to the best of my knowledge and belief, contains no copy or paraphrase of material previously published or written by another person, except where due reference is made in the text of the Thesis.

Felipe Urzúa
February, 2009

This thesis may be available for loan. Copying of any part of this thesis is in accordance with the *Copyright Act 1969*

Felipe Urzúa 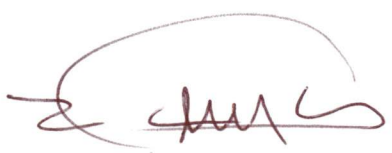
Date: 19/02/2009

To Patricia,
who brought me back from the night

In memory of Alamiro, Roberto and Don Lucho, those
who through different ways embraced the Andes

ABSTRACT

La Escondida district is one of the largest copper concentrations within the late Eocene-early Oligocene porphyry copper metallogenic belt of northern Chile. The district occurs in the north-trending Domeyko Cordillera, an orogenic chain associated with the Domeyko Fault System since the uppermost Late Cretaceous.

The results of a 1:25,000-scale geological mapping of La Escondida district have revealed an intricate juxtaposition of Late Paleozoic to Eocene sedimentary, volcanic and intrusive rock packages. These occur in fault-bounded structural panels and their locations can be predicted underneath the post-Eocene unconsolidated alluvial blanket. Previously defined and new geological units define two major tectonostratigraphic cycles in La Escondida region: a Late Carboniferous-Permian to Triassic-age Pre-Andean (Gondwanian) cycle; and Late Triassic-Present Andean cycle. The former includes La Tabla Formation, which resulted from widespread terrestrial volcanism and cogenetic granitoids. Minor, weakly mineralised porphyry copper-type intrusions and Michigan-style copper occurrences are part of this cycle. The Pre-Andean cycle was characterised by caldera complexes, resurgent intrusions (domes and plutons) and fluvio-lacustrine sedimentation. Major and trace element compositions of volcanic and intrusive rocks are consistent with a destructive continental margin setting. Calc-alkaline, dominantly siliceous explosive volcanism and I-type intrusions were emplaced in a mature magmatic arc governed by an extensional regime.

The Andean cycle in La Escondida district started with deposition of a mixed calcareous-siliciclastic sequence on the eastern margin of a back-arc basin, between the Late Triassic and Neocomian. An almost 2,000 m thick pile of sedimentary rocks was deposited and subsequently folded and thrusted by the 90-80 Ma Peruvian compressional tectonic phase. Three successive magmatic events occurred from 81 Ma to 34 Ma. These events were characterised by volcanic and intrusive episodes that have geochemical signatures typical of arc and transitional/back-arc settings.

During the Late Cretaceous-lowermost early Paleocene, three north- to northeast-elongated plutonic complexes were emplaced (81-79 Ma Sombrero, 77-72 Ma Cerro Bayo and 66-64 Ma Torcaza complexes) that range in composition from monzogabbro, monzodiorite to monzogranite and dacite porphyries. Andesitic volcaniclastic rocks of Las Torres igneous complex were deposited between ca. 70 and 66 Ma, within a small tectonovolcanic basin. Effusive volcanism was preceded and probably accompanied by the intrusion of a north-northeast-oriented dyke swarm of monzogabbro, diorite and andesite, between 82-70 Ma. Structural data suggest that these north- to northeast-elongated intrusions were emplaced and an extensional to transtensional stress regime. The dykes were deformed by the K-T deformational tectonic phase at ca. 64-62 Ma, although those bodies emplaced early were affected by the Peruvian tectonic movements.

The Paleozoic and Mesozoic rocks are unconformably overlain by the late Paleocene-early Eocene Augusta Victoria Formation. This unit consists of extensive ignimbrite flows,

coarse-grained volcano-sedimentary rocks and subordinate basaltic andesite and andesite, and was deposited between 57 and 53 Ma. Minor intrusive activity at 60-61 Ma produced andesite dikes and other subvolcanic bodies as a precursor to widespread volcanism. Subsequent E-W contractional deformation produced large-scale open folds with axes that slightly plunge to the north. Folding and associated reverse faulting were followed by dextral and sinistral strike-slip faulting that only produced minor offsets.

The middle-late Eocene magmatism started with the intrusion of the 43-41 Ma Cerro Rincones plutonic complex, the largest in La Escondida district. It contains nine phases that range from diorite, through monzodiorite and granodiorite, to quartz-monzonite and microgranite. Although early discrete phases were preferentially emplaced along fold axes in the Augusta Victoria Formation, larger phases display ring-shapes in plane-view.

Emplacement of the porphyry Cu-style intrusive complexes at La Escondida and Escondida Norte-Zaldivar deposits occurred between 38 and 34 Ma, and the Domeyko Fault System was a major control on the mineralising intrusions. The kinematic history of its eastern branch, the Escondida master fault, consisted of an early compressional stage (<51-50 Ma), followed by dextral strike-slip transpressional activity (ca. 40-37 Ma) during the emplacement of Escondida Norte-Zaldivar porphyries and later sinistral transpressional movement (> 37 Ma) that controlled the intrusion of La Escondida porphyry (ca. 38-34 Ma). Deformation continued up to ca. 20 Ma, with a minimum average exhumation rate of ca 0.05 km/m.y. Significant extensional and left-lateral transtensional movements occurred on La Escondida master fault at ca. 18-10 Ma (Quechua deformation phase) that produced the triangular pull-apart basin of the Salar de Hamburgo. Dissection of the Hamburgo basin occurred during the early Miocene by NNE-striking faults.

The 39-38 Ma Capella stocks, 38-36 San Carlos strata volcaniclastic rocks and microdiorite bodies were respectively emplaced prior to and during mineralisation at La Escondida and Escondida Norte-Zaldivar. A large family of post-mineralisation porphyritic diorite, andesite-diorite porphyry and andesite pyroxene dykes and minor stocks were also intruded between 38 and 35 Ma. Major and trace elements compositions of the Eocene intrusions suggest increasing pressure and depth of magma source from the pre-to post-mineralisation magmatic products. There was a change from a dry magmatic source regime (pre-mineralisation Cerro Rincones and Capella intrusions), through wet magma (syn-to post-mineralisation porphyritc diorite, andesite-diorite porphyry and San Carlos strata), and back to dry magma (post-mineralisation pyroxene andesite porphyry dyke), based on the available geochemical data. Appreciable Late Paleozoic crustal inheritance has been detected during analyses of zircons from the Andean magmatic rocks, revealing a crustal role in the petrogenesis of these predominantly asthenospheric mantle wedge-derived rocks.

Two sub-belts of Eocene hydrothermal alteration systems in La Escondida district have been identified during this study: (1) an eastern sub-belt that includes La Escondida and Escondida Norte-Zaldivar deposits and several peripheral mineralised intrusions; and (2) a poorly constrained western sub-belt that consists of advanced argillic altered and silicified rocks, the most significant of which is the Chimborazo high sulfidation epithermal Au-Cu-(Fe) deposit. Future exploration should be focused along the La Escondida master faults in the eastern sub-belt beneath the extended Late Cenozoic alluvial cover as these faults appears to have localised the most productive mineralised systems in the district.

ACKNOWLEDGMENTS

The assistance of J. Alfaro, K. Blanco, A. Crawford, P. Cornejo, F. Crignola, M. Croaker, L. Cuitiño, O. Dominguez, G. Gamboa, R. Guerra, C. López, S. Matthews, D. Mena, S. Meffre, P. Morales, M. Mpodozis, H. Niemeyer, B. Quiroz, A. Perı, S. Pizarro, A. Rae, R. Sapiaín, A. Tunks, P. Vargas, W. Véliz and Ch. Wong, significantly facilitated the current study. To all of them, I extend my sincerely thanks. Particular mention is given to J. Camacho, D. Cooke, J. Gilligan, M. Hervé, J. Larson, P. Lazcano, P. Sepúlveda, L. Urzúa, M. Urzúa and V. Urzúa. This study would not have seen the end without their respective contributions.

Table of Content

Page

Volume 1

CHAPTER 6

List of Figures

Page

CHAPTER 1

CHAPTER 2

CHAPTER 3

CHAPTER 4

CHAPTER 5

CHAPTER 6

CHAPTER 7

List of Tables

Page

CHAPTER 3

CHAPTER 4

CHAPTER 5

Table of Content

Page

Volume 2 – Appendices

List of Figures

Page

Appendix 6

List of Tables

Page

Appendix 4

Appendix 5

Appendix 6

Appendix 7

Appendix 8

CHAPTER 1
Introduction

This thesis is part of an integrated, ongoing program carried out by BHP-Billiton to improve the understanding of the alteration and mineralisation processes, the evolution of the magmatic system and the geological setting of La Escondida district in northern Chile. Its limits have been defined arbitrarily, but they encompass the main deposits, prospects and hydrothermal alteration zones adjacent to La Escondida ore body, in conjunction with geological features of major significance in the evolution of the region. The district contains giant porphyry copper-molybdenum deposits at La Escondida and Escondida Norte-Zaldivar and high sulfidation copper veins at Chimborazo. Together, these deposits represent one of the largest concentrations of copper mineralisation (>40Mt of fine Cu) known on Earth (Camus, 2003). This research reports the results of a district-scale geological study which aimed to improve the understanding of the geological setting of this world-class porphyry cluster, and to explore relationships between La Escondida copper mineralisation and the tectonomagmatic history of the northern Chilean Andes (24°S).

1.1 LOCATION

La Escondida porphyry copper district is located in the Domeyko Cordillera or Andean Precordillera, 2nd Region of Antofagasta, northern Chile, approximately 180 km east-southeast of the port city of Antofagasta (Figure 1.1). The central UTM (WGS 84) are 7,319,000m N and 493,000m E and the average altitude is about 3,200 m above sea level. Access is via sealed road from Antofagasta.

The major morphotectonic units of the Antofagasta region include, from west to east: the Coastal Cordillera, Central Depression, Domeyko Cordillera (or Precordillera), Pre-Andean Basin (Atacama and Punta Negra salt pans) and finally, the Western Andean Cordillera, capped by the Miocene to Recent volcanoes (Figure 1.2).

The Domeyko Cordillera is a narrow (<70 km wide) structural element (Figure 1.2) that extends for more than 800 km from Collahuasi southwards as far as Copiapó. In the study

Figure 1.1 Location map of the study area, which encompasses La Escondida porphyry copper district, northern Chile.

area, the Domeyko Cordillera is approximately 60 km wide, and has a maximum altitude of 3,600 m above sea level. It includes, from east to west, three main physiographic elements (Figure 1.3), which are: (a) the roughly northeast and north- northwest trending Sierra de San Carlos and Sierra de Imilac basement-cored uplifts; (b) a triangular-shaped central depression of 3,000 m elevation that hosts the Salar de Hamburgo endorheic basin and other smaller sub-basin as the Laguna Seca; and (c) a series of discontinuous, north-trending ranges of moderate relief, separated by relatively narrow alluvial plains and aprons (bajadas), on the western side of the district (Figure 1.3).

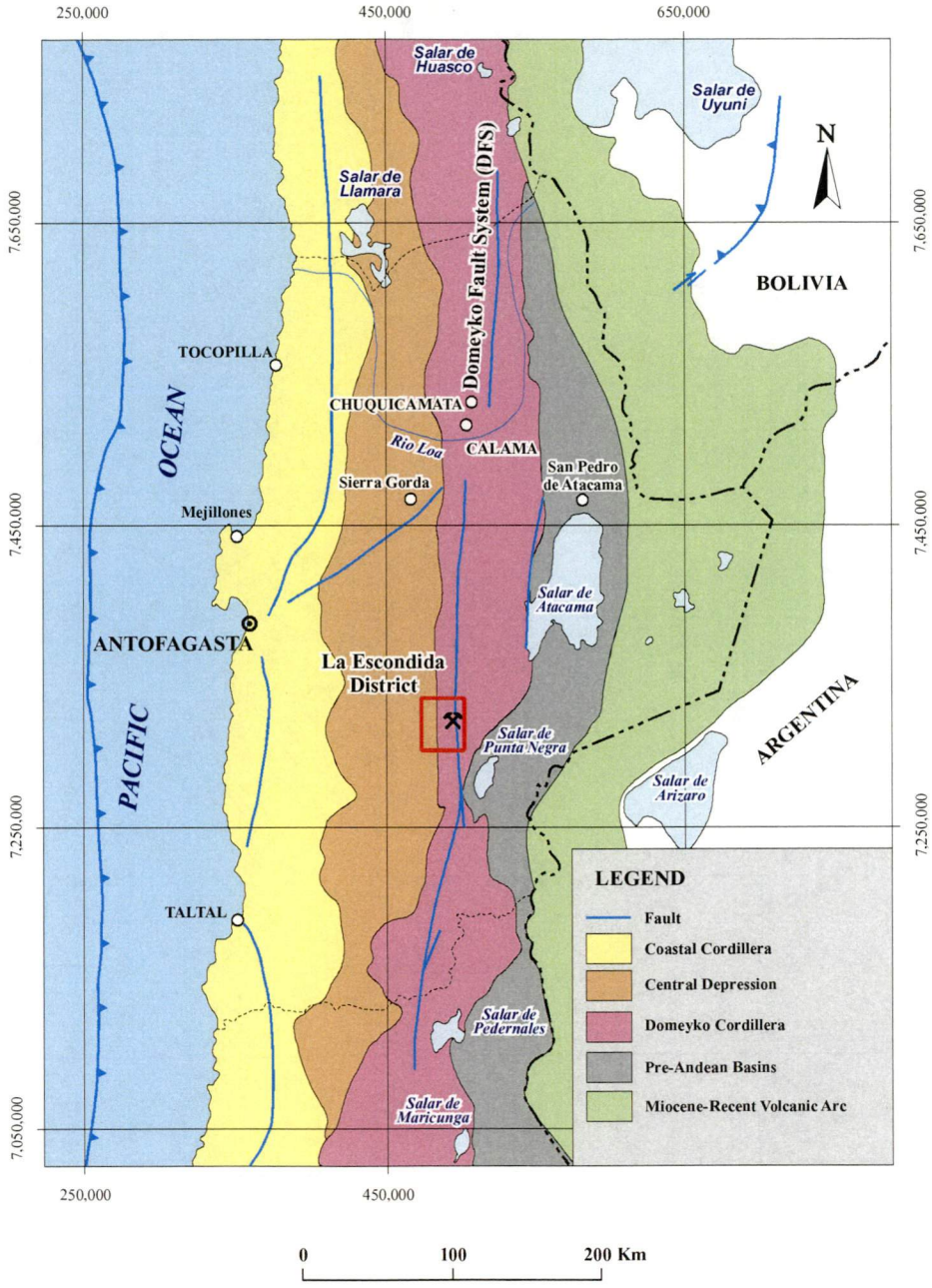

Figure 1.2 Simplified sketch of principal morphotectonics units in northern Chile, showing La Escondida district location (adapted from Arriagada et al., 2003).

1.2 OBJECTIVES

This project has been funded jointly by Minera Escondida and BHP-Billiton as part of a large programme designed to determine the geological evolution of La Escondida district, specifically in order to differentiate alteration zones and exploration targets concealed below Late Cenozoic gravels. The specifics aims of the Ph.D. project are as follows:

- To determine the spatial distribution and ages of sedimentary, volcanic and intrusive rocks through detailed geological mapping.

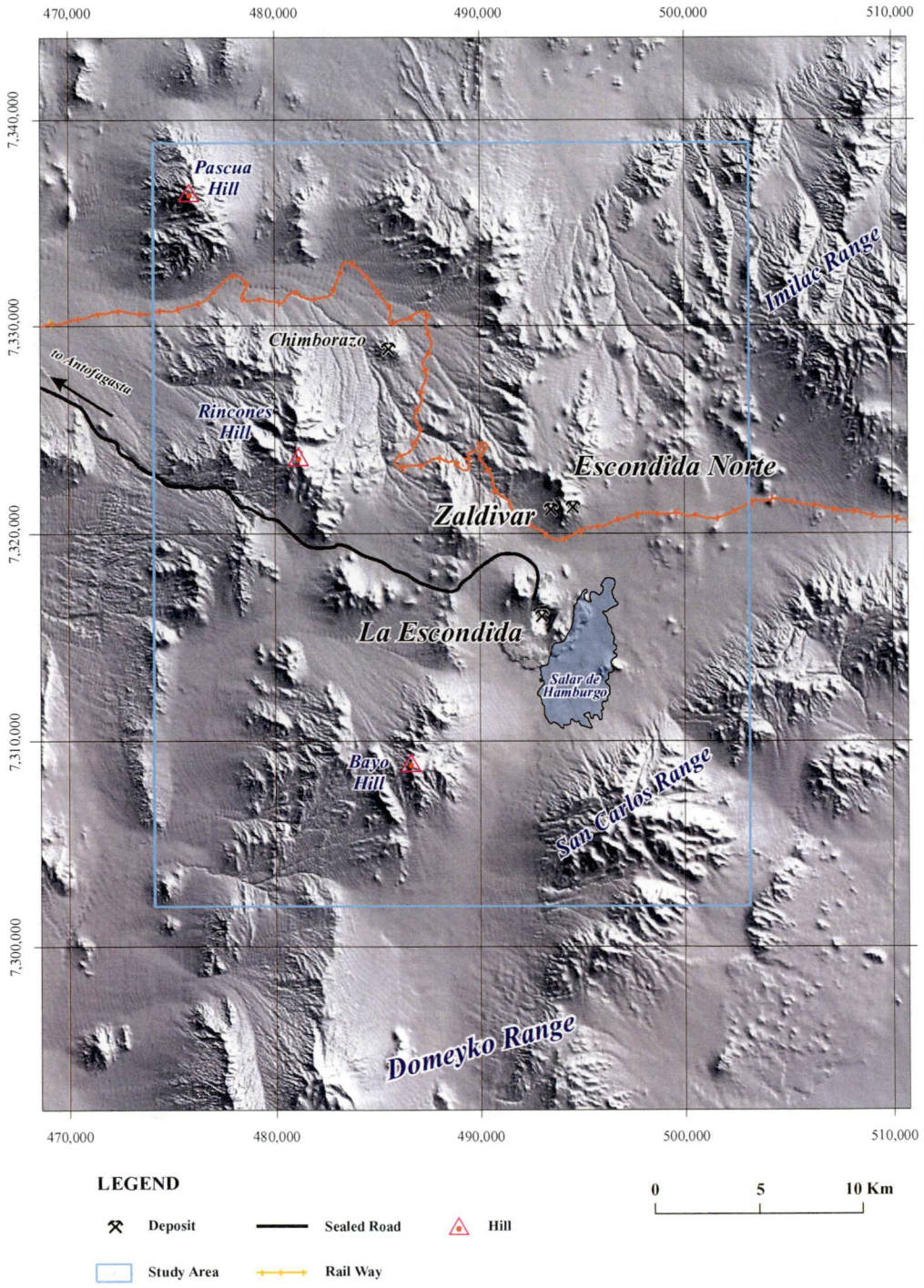

Figure 1.3 Main physiographic units of La Escondida district, northern Chile.

- To investigate the district-scale structural geology based on the outcrop-scale study of key localities.
- To characterise the diverse Meso-Cenozoic intrusive complexes exposed in the region geochemically.
- To highlight alteration zones and other targets hidden by the Late Cenozoic gravel cover.

The objectives have been achieved through detailed geological mapping (scale 1:25,000) of an area of 29 x 35 km in dimension, totalling 1,015 km^2 (Figure 1.3). Geological mapping was supplemented by structural measurements of selected key outcrops and the construction of four east-west cross-sections, incorporating data from exploration drill holes. Representative samples of the major intrusive and volcanic units were collected for K-Ar, ^{40}Ar-^{39}Ar and U-Pb geochronological analyses, and also for major and trace element geochemistry.

1.3 THESIS ORGANISATION

The thesis is organised into two volumes. Volume 1 contains seven chapters and references. Chapter 1 includes an introduction and general thesis outline. Chapter 2 describe the study area within the tectonostratigraphic framework of the Central Andes. Chapter 3 gives an account of the stratigraphy of sedimentary and volcanic sequences, including a classification of the main intrusive units based on the new field data and high-resolution geochrological analyses. Chapter 4 examines the structural geology and discusses the chronology of the major tectonic episodes. Chapter 5 describes the alteration zones and mineral occurrences in La Escondida district, outside of the major porphyries and high sulphidation deposits. Chapter 6 presents the geochemistry of the principal magmatic units. Finally, Chapter 7 summarises the main conclusions, proposes a model for the geological evolution of La Escondida district, and discusses the possible link between regional tectonics and mineralisation episodes. Volume 2 contains eight appendices that include geological maps and cross sections, maps of distribution of hydrothermal alteration zones, tables of sample location and core logs, structural data, geochronological analyticals and geochemical analyses. New geochronological data are presented in Chapters 3 and 5, with analytical procedures and details of the analyses provided in Appendix 6.

1.4 METHODOLOGY

1.4.1 Geological Mapping

The 1:25,000 district geological map (Appendix 1) was constructed using UTM (Universal Transverse Mercator projection) georeferenced aerial photos (scaled 1:25,000), produced by the Servicio Aerofotogramétrico de Chile (SAF) in 1993 and rasterised by Geoingeniería Digital Ltda in 2000. Sample localities and structural measurements were positioned on the georeferenced aerial photographs and geological map using a Trimble

GPS (Geographic Position System) receiver. Rock samples were numbered (FU-XXXX) and stored at the core house of Minera Escondida in Antofagasta, whereas the samples selected for geochemical and geochronological analyses were labelled using an ESC-XX code. Geological maps (Appendix 1), cross-sections (Appendix 2) and alteration map (Appendix 3) are enclosed in pockets from Volume 2 of this thesis.

Fieldwork, which totalled approximately six months, was carried out in four periods (March-May, 2002; August-November, 2002; March-April, 2003; and August-October, 2003). However, numerous outcrops were revised between July, 2005 and March, 2006. A total of 27 structural stations covering geological units from Paleozoic to Eocene were studied by the author. Kinematic measurements from 4 stations were collected with the guidance of H. Niemeyer (Universidad Católica del Norte, Antofagasta) and other 6 localities with the support provided by F. Crignola (Brownfield Exploration Program, Minera Escondida). In order to integrate all available structural information, a comprehensive paleostress study completed by H. Niemeyer in the Chimborazo area has been incorporated into the structural evolution model presented here. Paleomagnetic samples were collected in conjunction with P. Roperch (IPR/Universidad de Chile, Santiago), although a general lack of in-situ outcrops and the complex deformation history made it difficult to interpreted the results. Consequently, these data have been excluded from the present study.

A total of 14,000 meters of cuttings and drill core were logged by the author, at a scale of 1:2,000, with the assistance of J. Alfaro (Brownfield Exploration Program, Minera Escondida) for hole CHD-3265 from Chimborazo. Structural data were processed and analysed employing the computer programs "Stress" (B. Sperner, 1993) and "FaultKin" (Allmendinger, 2001). Sample locations, drill hole logs, geochronological and geochemical analyses, structural measurements and other associated data are presented in appendices 4 to 8 (Volume 2).

1.4.2 Petrography

Approximately one hundred and forty thin sections were described petrographically by the author, initially supervised by L. Cuitiño (Sernageomin, Santiago) and then in partial discussion with A. Rae and T. Crawford at the Centre for Ore Deposit Research, University of Tasmania (CODES), using the BGS Rock Classification Scheme (1999). Additional petrographic descriptions from rock units and alteration zones that crop out at

Chimborazo were provided by the Brownfield Exploration Program (Minera Escondida), including data from the former Minera Orion Chile and Cyprus Minerals (S. Williams, 1988-1994; S. Kim, 2001-2002).

1.4.3 Whole rock geochemistry

Forty samples were collected for analysis of major- and trace-elements and REE, with supervision and guidance provided by P. Cornejo and S. Matthews from Sernageomin for the first 10 samples. These were analysed by inductively coupled plasma mass spectrometry (ICP-MS) at the Sernageomin laboratories in Santiago. Further details of sample selection and location, preparation and analysis are given in Appendix 8 and Chapter 6. Geochemical classification of igneous rocks, elementary plotting and normalised diagram were made employing the "GCDkit" (version 2.2) computer program from V. Jaunousek, C. Farrow and V. Erban (2007).

1.4.4 Geochronology and Thermochronology

Five samples were collected by the author, together with the guidance of P. Cornejo and S. Matthews for ^{40}Ar-^{39}Ar geochronology. Analyses were conducted by C. Pérez de Arce and S. Matthews at the Sernageomin Geochronology Laboratory in Santiago. An additional three K-Ar whole rock analyses were carried out at Sernageomin in order to determinate the age of altered porphyry-type intrusions when the mapping was in progress. Another forty two samples were collected for U/Pb zircon determinations (LA-ICP-MS), initially guided by P. Cornejo and S. Matthews (Sernageomin), and then assisted by C. López, P. Sepúlveda and F. Crignola (Brownfields Exploration Program, Minera Escondida). These analyses were performed by S. Meffre at CODES and are presented in Appendix 6. Finally, eleven apatite and zircon samples were submitted to B. McInnes for U-Th-(He) thermochronological analysis at CSIRO Exploration & Mining in Perth. Unfortunately, analytical procedures and associated relevant data involved in the U-Th-(He) dating were never provided, and cannot be included here.

1.5 PREVIOUS STUDIES

Previous investigations within the Domeyko Cordillera around La Escondida include regional scale maps (1:100,000 and 1:250,000) published by Sernageomin (Maksaev et al., 1991; Marinovic et al., 1995) and publications concerning the large-scale tectonics of the Domeyko Cordillera (Reutter et al., 1991; Mpodozis et al. 1993a and 1993b). Also, a large volume of geological information has been produced during the intensive copper and

precious metals exploration activity carried out during the past two decades in the Antofagasta region, although mining companies have generally not made these data available publically (Petersen et al., 1995, Peri and Palma, 1997).

The first modern geological investigation of La Escondida area was by Garcia (1967), who undertook an extensive regional geological study of northern Chile sponsored by ENAP, the Chilean governmental oil company. He was the first to describe the Augusta Victoria Formation (tentatively assigned to Upper Cretaceous). Later authors recognised that the volcanic rocks outcropping in the vicinity of La Escondida belong to this formation. Ferraris and Di Biase (1978) published the 1:250,000 Antofagasta geological map sheet, covering the area immediately northwest of La Escondida. They recognised the regional extension of the Augusta Victoria Formation from Garcia (1967), and also several plutonic complexes thought to be of Cretaceous age. Boric et al. (1990) provided a detailed synthesis of the geology and mineral deposits of the Antofagasta region. They documented the Late Paleozoic volcanoplutonic basement of the Domeyko Cordillera in the Imilac and San Carlos massifs to the east of La Escondida. They also documented the Triassic-Lower Cretaceous back-arc basin sedimentary pile and associated volcanic rocks of the Augusta Victoria Formation to the west, and various diorite and monzodiorite stocks considered to be of Late Cretaceous-Eocene age. Boric et al. (1990) also included a summary geological description of the La Escondida, Zaldivar and Chimborazo deposits, along with data on other minor mineral occurrences within the district. Maksaev et al. (1991) published the preliminary 1:100,000 Augusta Victoria map sheet, which includes the Escondida area. This map was subsequently incorporated into the 1:250,000 geological map of the Aguas Blancas sheet (Marinovic et al., 1995), which encompasses the area region from the Domeyko Cordillera to the Central Depression and Coastal Cordillera between 24°S and 25°S.

Initial research into the diverse magmatic and metallogenetic aspects of the mineralized porphyry systems was published by Ojeda (1986, 1990). He presented the first geological description of La Escondida, K/Ar ages indicative of an Eocene age for the main mineralisation and alteration events, and data from drill holes and mining-scale surface mapping. Alpers and Brimhall (1988, 1989) reported the results of a detailed investigation into supergene processes and the paleohydrology regime prevailing during the development of the secondary enrichment at La Escondida. Maturana and Saric (1991)

published the first geological model of Zaldivar, where they used information from drill holes and surface outcrops to outline alteration and mineralisation zones in the system.

In more recent times, Richards et al. (1999) reported a geochronology study in La Escondida and Zaldivar deposits, and concluded that the main ore-forming magmatism occurred at around 38 Ma. Monroy (2000) presented an updated geological description of Zaldivar and recognised diverse stages of mineralisation associated with two principal intrusive pulses. Richards et al. (2001) studied La Escondida-Zaldivar porphyry copper cluster, and reported several U/Pb zircon and ^{40}Ar-^{39}Ar ages. These ages were provided in conjunction with petrological data and a 1:50,000 geological map and were used to propose a geological model for the formation of La Escondida. Richards (2001) discussed the geological evolution of La Escondida district and the relative importance of crustal-scale sutures (lineaments) in localising the porphyry systems at La Escondida and elsewhere in northern Chile. Padilla et al. (2001) and Padilla-Garza (2003) combined isotopic, structural and geochronological information to provide an evolutionary model for La Escondida. Campos (2002) and Campos et al. (2003) provided a detailed geochronology and fluid-inclusion study of two mineralising pulses at Zaldivar. Quiroz (2003) detailed several alteration and mineralisation events associated with the emplacement of La Escondida's quartz-monzonite to granodiorite intrusive complex. Véliz and Camacho (2003) updated La Escondida's geology, separating the porphyry complex into two main intrusive phases, on the basis of ongoing resource exploitation and development.

CHAPTER 2
Tectonostratigraphic Setting

La Escondida district is part of the Domeyko Cordillera (Figure 1.2), a major morphotectonic feature located in the fore-arc zone of the active stratovolcanic chain of the Andean Cordillera. The Andean orogen is the product of prolonged convergence between the subducting Nazca (former Farallon) oceanic plate and the overriding continental South American plate (Jordan et al., 1983; Cahill and Isacks, 1992). The region has been the locus of subduction-related magmatism from the Early Mesozoic (ca. 200 Ma) onwards (Coira et al, 1982; Mpodozis and Ramos, 1989). However, the pre-Mesozoic geological history remains poorly understood. This chapter summarises the tectonostratigraphic evolution of northern Chile (24°S), and highlights features relevant to the current studies of La Escondida district.

2.1 TECTONOSTRATIGRAPHY

In broad terms, the Phanerozoic history of northern Chile can be divided into three major tectonic cycles: the Famatinian cycle (Early Paleozoic), the Gondwanian cycle (Late Paleozoic to Middle Triassic); and the Andean cycle (Jurassic to present day; Mpodozis and Ramos, 1989). A schematic east-west tectonostratigraphic and chronologic chart for the Phanerozoic record in northern Chile, at the latitude of La Escondida (24°15'S), is provided in Figure 2.1. Simplified sketches of evolutionary tectonic models for the Early Paleozoic, Late Paleozoic and Meso-Cenozoic periods are shown in Figures 2.2, 2.3 and 2.4, respectively.

2.1.1 Famatinian Cycle (Early Paleozoic)

The Early Paleozoic history of southwestern South America is the subject of continuing debate, due to the complexity of geological processes involved and the lack of outcrop, which hinders accurate reconstructions. The geological record in the pre-Cordilleran region is restricted to submarine bimodal volcanic and deep-water turbidite sedimentary rocks (Middle Arenigian Cordon de Lila igneous-sedimentary complex; Niemeyer, 1989; Pérez et al., 2006 and 2007) exposed in an isolated block of uncertain tectonic

significance, located immediately south of Salar de Atacama. The Cordón de Lila volcanic rocks have a geochemical signature typical of a magmatic arc environment (Niemeyer, 1985; Coira et al., 1999; Pérez et al., 2006). They are overlain by platform-type siliciclastic deposits of the late Arenigian-middle Llanvirnian and Early Silurian periods (González et al., 2006; Navarro et al., 2006).

As a result of several investigations undertaken on the Early Paleozoic metasedimentary and metavolcanic sequences of northwestern Argentina and southwestern Bolivia, a number of conflicting tectonic models have been proposed (Mpodozis and Ramos, 1989; Bahlburg and Hervé, 1997; Isaacson and Díaz-Martinez, 1995; Mon and Salfity, 1995; Ramos and Alemán, 2000; Bahlburg et al., 2000). These models fall into two main groups. Mpodozis and Ramos (1989), Mon and Salfity (1995) and Ramos and Alemán (2000) have argued that the exotic Arequipa and Antofalla terrain collided with the paleo-margin of South America (Figure 2.2). They infer that the final amalgamation to South America occurred during the Ordovician Ocloyic Orogeny at ca. 460 Ma (Coira et al., 1982; Mpodozis and Ramos, 1989; Ramos and Alemán, 2000). An alternative hypothesis has been advocated by Tosdal (1996), Bahlburg and Hervé (1997), Lucassen et al. (1999), Bock et al. (2000) and Bahlburg et al. (2000), who ruled out any collision of exotic terrains during the Ocloyic Orogeny, mainly based on a series of Sm-Nd isotopic data indicating crustal a common origin for the Ordovician to Permian magmatic and sedimentary rocks. Bahlburg and Hervé (1997) prefer a model of subduction-related arc magmatism alternating with passive margin sedimentation in an overall convergent plate setting during the Early Paleozoic (Cambrian-Ordovician). They argue that Early Paleozoic subduction-associated submarine magmatism was followed by passive margin sedimentation in Devonian-Carboniferous times (Section 2.2.2), with subduction renewed during the Late Carboniferous to Permian.

2.1.2 Gondwanian Cycle (Late Paleozoic-Middle Triassic)

2.1.2.1 Devonian-Early Carboniferous

In northern Chile, the early stage of the Gondwanian Cycle is represented by over 3,000 m of siliciclastic sediments that were deposited in tidal-dominated shelf and deltaic environments, with a predominantly eastward provenance from an elevated region in northwestern Argentina (Devonian-Early Carboniferous Zorritas Formation; Davidson et al., 1985; Niemeyer et al., 1985; Urzúa, 1989; Niemeyer et al., 1997). This sequence was deformed by a contractional event that affected this portion of Gondwanian land at the

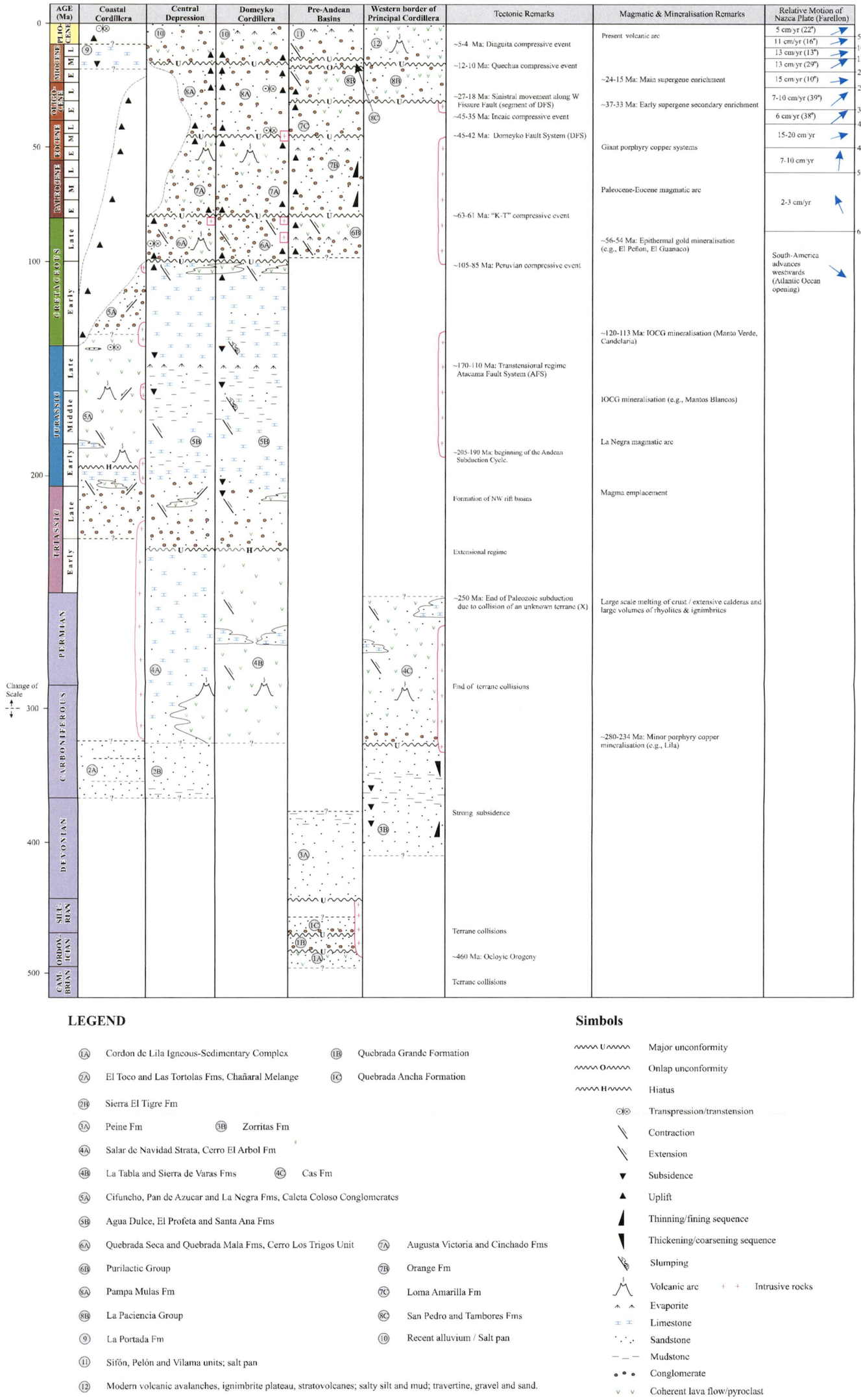

Figure 2.1 Comparative longitudinal tectonostatigraphic chart, including significant magmatic and mineralisation events, for northern Chile (~24ºS). Abbreviations: E = Early; M = Middle; L = Late; Fm = Formation; Fms = 'Formations (adapted from Scheuber et al., 2000; Mpodozis and Thiele, 2002; Mpodozis et al., 2005; May et al., 2005).

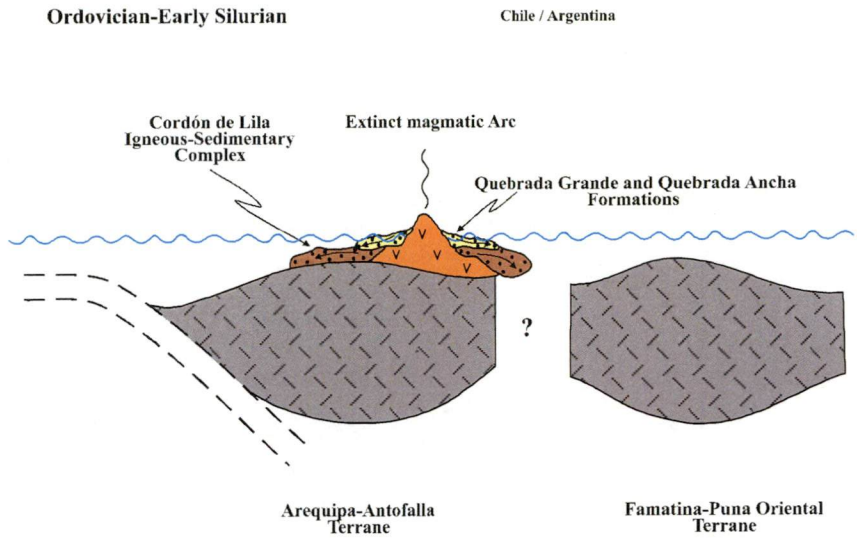

Figure 2.2 Schematic tectonic model for the Ordovician-Early Silurian Cordón de Lila Igneous-Sedimentary Complex (adapted from Bahlburg and Hervé, 1997; Coira et al., 1999; Pérez et al., 2006; González et al., 2006; Navarro et al., 2006).

Early to Late Carboniferous boundary (Urzúa, 1989; Niemeyer et al., 1997).

There are two interpretations for sedimentation in the Devonian-Early Carboniferous period. Lucassen et al. (1999) and Bahlbugh et al. (2002) argued for a passive margin setting dominated by a transpressive-transtensive regime based on the lack of arc-related volcano-plutonic rocks in the region. In contrast, Niemeyer et al. (1985), Urzúa (1989) and Niemeyer et al. (1997) suggested that the Zorritas Formation was deposited in the inland part of a back-arc basin related to an eastward-dipping subduction zone, with the arc rocks located further west in the Central Depression (Figure 2.3a), and now covered by the Mesozoic units. However, it should be mentioned that no significant field evidence supporting the occurrence of a magmatic arc for this period have been identified in the Central Depression and Coastal Cordillera. The gap occupied by the Meso-Cenozoic cover along the Central Depression is on the order of one hundred kilometres. To the west, in the Coastal Cordillera, the Carboniferous Chañaral Melánge is inferred to have been deposited in a forearc setting (Bell, 1987).

2.1.2.2 Late Carboniferous-Middle Triassic

The uppermost Late Paleozoic was characterized by extensive rhyolitic to dacitic volcanic activity dominated by large ignimbrite eruptions, calderas and domes, and subordinate andesitic volcanism and fluvio-lacustrine mixed clastic-calcareous sedimentation. This occurred along the southwestern margin of Gondawana (La Tabla, Sierra de Varas and

Cas Formations, and El Choiyoi silicic volcanic province of Coira et al., 1982), and immediately preceded the intrusion of large volumes of calc-alkaline granitoids at 340-260 Ma (Figure 2.3b). It has been argued that magmatism was triggered by the collision of an unknown exotic terrain at around 245 Ma (Mpodozis and Kay, 1992). The interpreted paleogeographic realm for southwestern Gondwanian during the Late Paleozoic, illustrating the multiple exotic blocks accreted since the Early Paleozoic, is shown in Figure 2.3c. There are a series of uneconomic, small porphyry copper systems that crop out along the Domeyko Cordillera that are associated with El Choiyoi magmatic province (i.e., El Loa, Cerro Redondo, Lila, Los Morros, and Perla). These porphyry systems appear to be related to two phases of intrusive activity within the Late Paleozoic-Triassic magmatic arc and are as young as Late Triassic (Davidson et al., 1985; Mpodozis et al., 1993a; Cornejo et al., 2006; Munizaga et al., 2008; this study).

2.1.3 Andean Cycle (Late Triassic-Recent)

The period encompassing the Permian to Middle Triassic was dominated by extensional tectonics as part of a global plate reorganization, which eventually led to the break up of Pangaea at approximately 235 Ma (Ramos and Alemán, 2000). This generalized extension allowed the formation of a series of *en echelon* and discontinuous, asymmetric, north-northwest-elongate rift basins in northern Chile. These basins were subsequently filled by several thousand meters of marine and continental clastic and volcaniclastic sediments, volcanics and coeval subvolcanic intrusions (Charrier, 1983; Uliana et al., 1985; Mpodozis and Ramos, 1989; Salfity and Marquillas, 1994; Cornejo and Mpodozis, 1996). Well recognized syn-rift and thermal subsidence sequences have been described in Peru, Bolivia and Argentina, but the Chilean equivalents are poorly preserved owing to the Andean deformation and magmatism.

Since the Jurassic, almost 200 m.y. of continuous subduction of the oceanic Nazca plate beneath the South America plate has involved alternation of oblique and orthogonal subduction periods, variable slab-dip angles and convergence rates, and extended tectonic erosion of pre-Miocene fore-arc zone terrains (i.e., Allmendinger et al., 1997). The Andean cycle has been characterised by generally eastward migration of four successive magmatic fronts built on ensialic crust:

- The Jurassic-Lower Cretaceous La Negra arc magmatism localized in the Coastal Range (ca. 180-120 Ma).
- The Late Cretaceous-lowermost early Paleocene arc, which developed principally

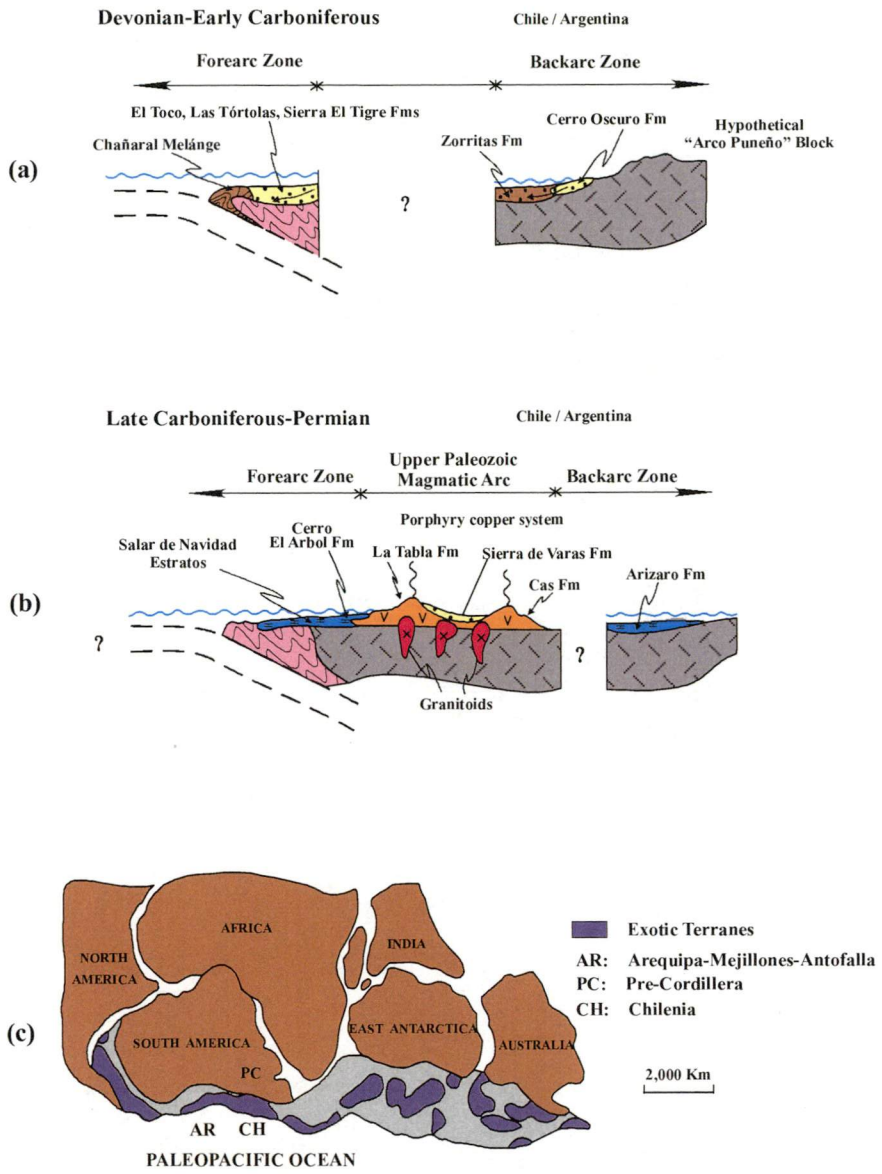

Figure 2.3 Schematic Late Paleozoic tectonic evolution of the Central Andes Cordillera, in northern Chile (adapted from Mpodozis and Ramos, 1989; Coney et al., 1990). Abbreviation: Fm = Formation.

along the Central Depression (ca. 85-63 Ma).

- Late Paleocene-Eocene arc magmatism, which is exposed in the Central Depression and western foothills of the Domeyko Cordillera (ca. 60-35 Ma).
- The late Miocene-Recent arc represented by the Ignimbritic Plateau and the stratovolcanoes emplaced along the western border of the Puna (i.e., Arriagada et al., 2003, and references therein).

A major magmatic quiescence is inferred to have occurred during the Oligocene (ca. 35-25 Ma, Scheuber et al., 1994). The existence of a Late Cretaceous magmatic gap at 90-80 Ma, which was postulated by Scheuber et al. (1994), remains uncertain due to the

poor regional geochronological coverage, and also due to the low-precision geochronological data available from Antofagasta region (Marinovic et al., 1996) that shows significant magmatic activity between 87 and 67 Ma. Moreover, the division of the Late Cretaceous-Paleogene magmatic activity into two north-trending magmatic arcs, as adopted in the present study, is in conflict with previous tectomagmatic reconstructions that have inferred a single Late Cretaceous-Eocene (78-37 Ma) magmatic arc (Scheuber and Reutter, 1992; Haschke et al., 2002a; Haschke et al., 2006). Indeed, cyclic patterns of Andean-style magmatic and tectonic activity since the Jurassic to the present makes occurrence of a single, long-lived continental magmatic arc of almost 40 m.y. unlikely.

2.1.3.1 Late Triassic-Early Cretaceous

The Jurassic-Lower Cretaceous was characterized by a magmatic arc related to an active continental margin (Oliveros et al, 2006, and references therein). Approximately 9,000 m of calc-alkaline- and tholeiitic-affinity andesites and basaltic andesites were erupted (La Negra Formation; Garcia, 1967) coeval with the intrusion of gabbros and granites (ca. 190-115 Ma; Mpodozis and Ramos, 1989; Grocott and Taylor, 2000; Oliveros et al., 2006). The broad Tarapacá back-arc basin (*sensu* Vicente, 2006) accommodated the deposition of clastic, mixed siliciclastic-carbonate and evaporate rocks at this time (Ardill et al., 1998), with variable volcanic supply from the foreland edge of the arc. The regional tectonic regime of the arc was controlled by arc-normal extension and arc-parallel sinistral strike-slip motion along the Atacama Fault System (AFS, i.e., Arabaz, 1971; Scheuber and Andriessen, 1990; Brown et al., 1993), which has been constrained to have occurred between 90 and 80 Ma (Peruvian Phase, i.e., Scheuber and Andriessen, 1990; Grocott and Taylor, 2000; Figure 2.4a). At the same time, the back-arc domains were also undergoing extension during their earlier stages of evolution. Reactivated ancient faults and/or basin-margin growth faults are suspected to have controlled the eastern and western limits of the back-arc Tarapacá Basin (Vicente, 2006), although none have yet been identified (Grocott and Taylor, 2002). The compressive Peruvian deformation started at the end of the Early Cretaceous (Mégard, 1987). It reached maximum intensity by the uppermost Late Cretaceous (ca. 107-83 Ma, Ladino et al., 1999). This resulted in deformation and tectonic inversion of the Tarapacá Basin, including thick- and thin-skinned folding and thrusting in the Late Triassic to Early Cretaceous El Profeta sedimentary sequence exposed along the Central Depression and Domeyko Cordillera (Figure 2.4a; Coira et al., 1982; Mpodozis and Ramos, 1989; Reutter et al., 1991; Scheuber and Reutter, 1992; Mpodozis et al., 1996a, 1996b; Amilibia et al., 2000; Tomlinson et al., 2001a; Muñoz et al.,

2005; Vicente, 2006). At this time, construction of the proto-Domeyko Cordillera started by the reactivation of ancient faults, and/or the onset of the Domeyko Fault System (Amilibia et al., 2000; Mpodozis et al., 2005; Muñoz et al., 2005).

2.1.3.2 Late Cretaceous-Early Paleocene

The Late Cretaceous volcano-plutonic arc has been inferred from discontinuous outcrops of fine- to coarse-gained red beds and volcaniclastic sedimentary rocks, ignimbrite flows, minor andesitic lava flows and subvolcanic intrusions of similar composition, formerly ascribed a lowermost Late Cretaceous-Paleocene age (specifically the Cerro Empexa, Quebrada Mala, Aeropuerto, Quebrada Seca Formations and the Carrizo strata). They now have been constrained to the period of 80 to 63 m.y. (Figure 2.4b; Marinovic et al., 1996; Cornejo and Mpodozis, 1996; Tomlinson et al., 2001a; Cornejo et al., 2003). At this time, the arc was affected by transtensional deformation, producing north-northeast-elongated tectonovolcanic basins (Marinovic et al., 1996; Cornejo and Mpodozis, 1996). Small calc-alkaline granodiorite-monzodiorite plutonic complexes occur as discrete magmatic centers, but have a widespread distribution, extending >1,000 km south from Quebrada Blanca (Cornejo et al., 2003). The tectono-volcanic basins were inverted and deformed by a compressive event at the Cretaceous-early Paleocene boundary, ca. 65-62 Ma ("K-T" deformation phase of Cornejo et al., 2003). This tectonic phase is poorly documented in the Antofagasta region, although it has been recognized widely in adjacent parts of Peru, Bolivia and northwestern Argentina (Peruvian deformation pulse; i.e., Mégard, 1987; Sempere, 1995; Sempere et al., 1997).

The Domeyko proto-Cordillera may have been an active and elevated physiographic unit during this period, separating the Late Cretaceous-early Paleocene intra-arc to back-arc tectonovolcanic basins on the west from the hinterland zones of the Late Cretaceous-Paleocene Purilactic "foreland" basin to the east (Mpodozis et al., 2005). The Purilactic basin was connected to the east with the Cretaceous Salta Group rift basins in northwestern Argentina (Viramonte et al., 1999; Mpodozis et al., 2005).

2.1.3.3 Late Paleocene-Eocene

The Late Paleocene-Middle Eocene magmatic arc is recognized principally along the Central Depression and western flank of the Domeyko Cordillera, including its northernmost ranges (Sierra de Moreno and Sierra de del Medio). Most of the volcanic activity occurred between 60 Ma and 45 Ma (Figure 2.4c), with several discrete and

independent volcanic centres (i.e., Pampa Rubia complex ca. 57-54 Ma, Guanaco-El Peñón ignimbrite complex ca. 60-51 Ma; Pampa Lorca ca. 47-45 Ma; Cornejo et al., 2003). Activation of the Domeyko Fault System was triggered in response to the major Incaic deformation phase (ca. 45-35 Ma; Maksaev, 1990; Boric et al., 1990, Coira et al., 1982; Mpodozis and Ramos, 1989; Scheuber and Reutter, 1992; Tomlinson and Blanco, 1997a and 1997b).

The porphyry copper clusters were emplaced rapidly and syntectonically (Maksaev, 1990; Boric et al., 1990; Scheuber and Reutter, 1992; Cornejo et al., 1997; Tomlinson et al., 2001a; Tomlinson and Blanco, 1997a; Padilla-Garza, 2003; Niemeyer and Munizaga, 2008; this study). They were apparently guided by a marked compartmentalization of deformation along the Domeyko Cordillera, in intimate association with dip-slip and strike-slip movements along of the 1,000 km long Domeyko Fault System (Chapter 4). Syn-orogenic terrestrial sedimentation occurred contemporaneously with the mineralizing intrusives in the Chuquicamata (Blanco et al., 2003) and La Escondida districts.

2.1.3.4 Miocene-Recent

For the last 33 Ma, magmatism has not occurred on the Domeyko Cordillera due to the eastwards migration (ca. 60 km) of the magmatic axis to its present position in the Western Cordillera. Instead, the orogen was affected by folding, uplift and erosion related to increasing subduction rates and increasingly oblique convergence (Maksaev and Zentilli, 1999; Masterman et al., 2005). Rapid denudation rates (100-200 m/My) have been determined along the Central Depression and part of the Principal Cordillera (Maksaev and Zentilli, 1999). The entire Andean arc zone underwent substantial crustal thickening and shortening between 30 Ma and 10 Ma mostly in response to contractional deformation, along with a modest contribution from magmatism (Beck, 1996; Allmendinger, 1997; Jordan et al., 1997; Victor et al., 2005). Although shortening continued from 10 Ma up to 2-1 Ma, the present landscape division of northern Chile is thought to have been initiated in the Early Miocene and completely established with the Quechua tectonic pulse (ca. 12-10 Ma; May et al., 2005). Radiometric ages for ignimbrite flows interbedded in the Andean piedmont and intermontane closed basins (i.e., upper strata of the Calama basin), suggest a diachronous peneplanization between 24 Ma and 9 Ma (May et al., 1997; Blanco et al., 2003; May et al., 2005). On-going magmatism and contractional tectonism may have caused further crustal thickening and uplift between the Middle Eocene and Early Pliocene (ca. 12-4 Ma), but was centered principally in the Puna

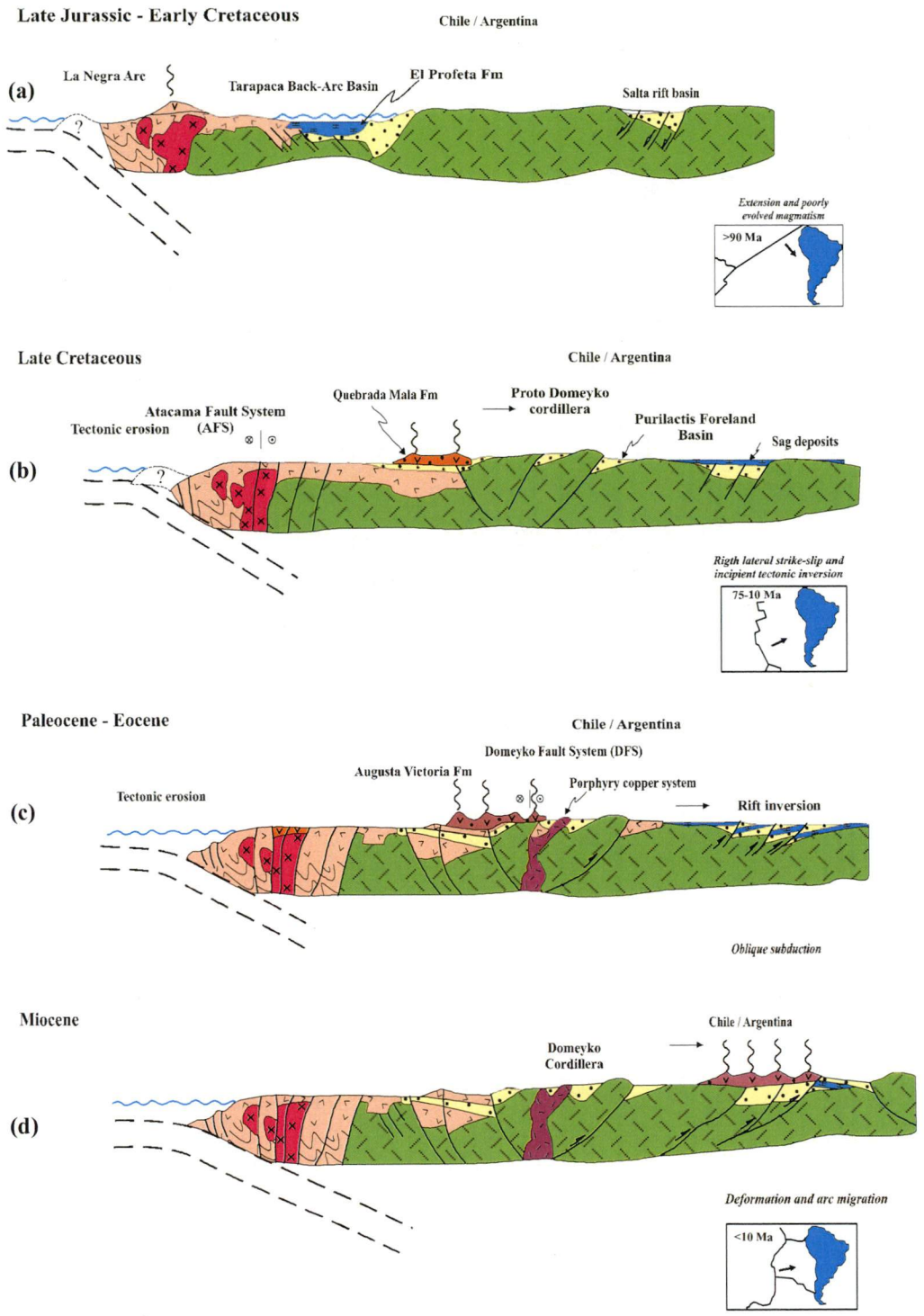

2.4. Schematic Meso-Cenozoic evolution of the Central Andes Cordillera, in northern Chile (adapted from Mpodozis and Ramos, 1989; Ramos and Alemán, 2000).

of Argentina (Allmendinger at al., 1997). The Miocene to Recent arc magmatism is temporally and spatially zoned (Figure 2.4d). Voluminous intra-arc and subordinate back-arc ignimbrite eruptions (ca. 23-5 Ma) have been dominant throughout the Altiplano plateau region whereas active andesitic to dacitic stratovolcanoes centers (ca. 15-11 Ma)

occur along the western border of the Puna (Mpodozis and Ramos, 1989; Allmendinger et al., 1997; Ramos and Alemán, 2000).

The relative tectonic "quiescence" and the onset of fluctuating arid/semi-arid condition punctuated by rainy periods allowed the development of the main secondary enrichment event (ca. 22-15 Ma) observed in the porphyry copper deposits of northern Chile (Gustafson and Hunt, 1975; Alpers and Brimhall, 1988; Sillitoe and McKee, 1996; Marsh et al., 1997; Mote et al., 2001; Hartley and Rice, 2005). However, recent studies indicate that supergene oxidation and enrichment processes have been active since 44 Ma and up to 6 Ma (Rowland and Clark, 2001; Bouzari and Clark, 2002; Hartley and Rice, 2005). The hyper-aridity and fossilization of the landscape since the Middle Miocene (ca. 10 Ma) may have been critical in preserving the enriched copper blankets associated with the Eocene-Oligocene porphyry systems (Sillitoe and McKee, 1996; Camus, 2003). However, this hypothesis has been questioned recently (Hartley and Chong, 2002; Hartley, 2003; Hartley and Rice, 2005; Arancibia et al., 2006), with semi-arid conditions believed to have prevailed until 4-3 Ma, and being interrupted by increased aridity and moderate pluvial precipitation throughout the Oligocene and Miocene (Arancibia et al., 2006). The establishment of true hyperaridity is inferred to have take place in the last few millions years.

2.2 SUMMARY

The Phanerozoic history of the southwestern margin of South America records an intricate interaction of magmatic, tectonic and sedimentary processes linked to three main tectonic cycles. The most relevant aspects are as follow:

- The Early Paleozoic Famatian Cycle was dominated by amalgamation of allochthonous or parautochthonous terrains (i.e., Arequipa and Antofalla) that exerted an important but still poorly understood control over subsequent Meso-Cenozoic processes.
- Since the Jurassic onwards, the key attributes of the Andean cycle have been:

  1. The formation of an unusually thickened continental crustal lithosphere (ca. 72-74 km, Wigger et al., 1994; Beck et al., 1996) beneath the Andes Cordillera (21°-22°S).

  2. Continuous subduction of the oceanic Nazca plate underneath the South America plate marked by oblique and orthogonal convergence periods, variable

subduction rates and variable dip of the subducted slab.

3. Eastwards migration of magmatism and deformation across the South America plate since the Early Mesozoic.

4. Long-lived tectonic erosion of the pre-Miocene fore-arc.

5. Widespread pre-Miocene clockwise tectonic rotation (around vertical axes) of diverse structural blocks from the arc/fore-arc zones.

6. Stress and strain partitioning along the upper plate, which was characterized by arc-parallel translation and arc-normal shortening.

- The Eocene porphyry copper systems were emplaced syn-tectonically with the Incaic deformation phase (ca. 40-35 Ma). This model is supported by detailed kinematic studies of mineralised intrusions at Chuquicamata (Reutter et al., 1996; Lyndsay et al., 1995), Radomiro Tomic (Niemeyer and Leiva, 2000), Escondida (Véliz and Padilla, 1997; Vergara, 2002; this study), Sierra Exploradora (Niemeyer, 1999), Potrerillos and El Salvador (Mpodozis et al., 1994; Cornejo et al., 1993; Niemeyer and Munizaga, 2008). Secondary enrichment required low denudation rates during the Late Oligocene-Middle Miocene times. The semi-aridity punctuated by increased aridity and humidity and tectonic quiescence was established by the Middle Miocene, and allowed the preservation of these world-class supergene-enriched copper deposits.

CHAPTER 3
General Geology

This chapter describes the geological units of La Escondida district based on new mapping and petrographic investigations. Taking into account the diversity of magmatic and sedimentary rocks, unit descriptions have been organised in relation to major time-periods. General maps of outcrops, tables that summarise the key features, and brief comments of rock units, are provided for each geological period of relevance to the district. Detailed field observations are summarized in the geological maps (Appendix 1) and cross-sections (Appendix 2). This information is complemented with maps of alteration and mineralisation zones, tables of sample location and core logging (Appendices 3 to 5). Results of new U-Pb age determinations are used in this chapter to help constrain the sequence of events. Detailed descriptions of the geochronological results are reported in Appendix 6.

3.1 LATE PALEOZOIC-LATE TRIASSIC

In La Escondida district, Late Carboniferous-Permian magmatism produced a series of mafic to silicic volcanic rocks, subvolcanic porphyritic intrusions and contemporaneous granitoids (Figure 3.1; Table 3.1). The Late Carboniferous to Triassic rocks make up elevated structural blocks and correspond to the basement in the region. They also include hypabyssal, porphyry copper-type, intermediate and silicic intrusive rocks, which have been affected by intense hydrothermal alteration (Chapter 5), and which formed at the end of this magmatic event in the Middle to Late Triassic.

3.1.1 La Tabla Formation *(Pzlt)*

La Tabla Formation is a bimodal volcanic sequence of ignimbrites, rhyolites and interlayered andesites and sedimentary rocks that crop out in the eastern portion of La Escondida district (Figure 3.1). The formation has been described from many localities along the Domeyko Cordillera (García, 1967; Mpodozis et al., 1993a; Gardeweg et al., 1994; Marinovic et al., 1995; Marinovic et al., 1996; Cornejo and Mpodozis, 1996; Munizaga et al., 2008). The base of the unit is not exposed in the study area. However, a gently angular unconformity separates La Tabla from the underlying Devonian-Late

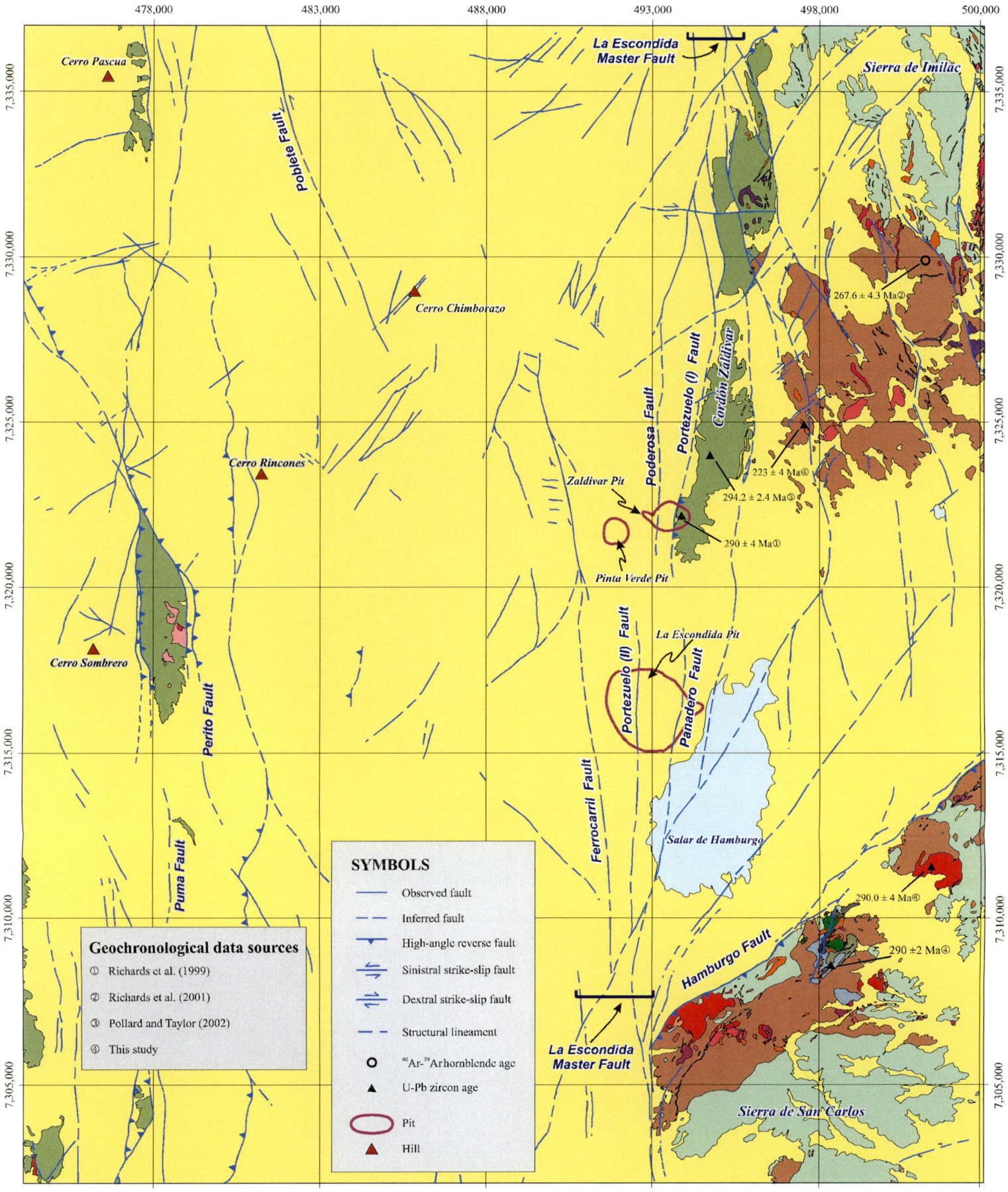

LEGEND

La Tabla Formation (Late Carboniferous-Permian)

Pzlt(c) Eastern volcanic sub-unit: massive, welded and non-welded, rhyolite to dacite crystal-rich tuff and associated subvolcanic rhyolite.

Pzlt(b) Central volcano-sedimentary sub-unit: andesitic to dacitic lava flow, vitric and crystal tuff, volcanic breccia and volcanic sandstone; interbedded redbeds and lacustrine limestones (▲ 287 ± 3 Ma③, ▲ 286 ± 2 Ma①, ▲ 284 ± 4 Ma④; ▲ 282 ± 2 Ma④,○ 267.6 ± 4.3 Ma②).

Pzlt(a) Western volcanic sub-unit: massive, welded and non-welded, coarse-grained, rhyolitic to dacitic crystal-rich tuff; minor massive and auto brecciated lava flow and subvolcanic rhyolite (▲ 294.2 ± 2.4 Ma③, ▲290 ± 4 Ma①).

La Tabla Formation-coeval subvolcanic intrusions

Pzda Greenish-grey, coarse-grained dacite porphyry (▲ 293 ± 4 Ma④)

Pzan Greenish-grey, coarse-grained andesite porphyry

Modern cover and omitted outcrops of non-Late Paleozoic to Triassic sequences

Intrusive rocks of Late Paleozoic-Late Triassic age

Trdp Altered, medium-grained dacite and rhyolite porphyry (▲ 227 ± 3 Ma④; ▲ 223 ± 4 Ma④)

Imilac plutonic complex (Late Carboniferous-Permian)

Pzic8 Reddish brown, medium-grained biotite-quartz-feldspar-phyric rhyolite

Pzic7 Aplitic micromonzonite and microgranite

Pzic6 Grayish red, medium-to coarse-grained granite and granodiorite porphyry

Pzic5 Fine- to medium-grained porphyritic monzonite and quartz monzonite

Pzic4 Coarse-grained granodiorite and monzonite (▲ 290 ± 2 Ma④)

Pzic3 Medium-grained porphyritic quartz diorite

Pzic2 Metamorphosed microdiorite and microtonalite

Pzic1 Metamorphosed medium- to coarse-grained quartz monzodiorite

Figure 3.1 Simplified distributions of Late Paleozoic-Late Triassic volcanic and intrusive units in La Escondida district.

Carboniferous Zorritas Formation in Sierra de Almeida, 60 km east of La Escondida district (Niemeyer et al., 1985; Urzúa, 1988). Weathered exposures of the upper strata are overlain unconformably by conglomerates assigned to the Late Triassic by Fuenzalida (1986) and Marinovic et al. (1995). La Tabla Formation is up to 800 m thick (Marinovic et al., 1995), and massive beds have been folded into open folds with kilometre-scale wavelengths (Chapter 4). Indeterminate low-grade metamorphism of Mesozoic age and low-temperature alteration have affected the volcanic rocks. Gardeweg et al. (1994) proposed three lithological subdivisions for La Tabla Formation, and these have been retained in the present study. However, the stratigraphic position for these three sub-units has been uncertain due to the extensive Cenozoic alluvial cover, and the lack of detailed stratigraphic and geochronological studies. A tentative stratigraphic organization of La Tabla sequence is presented below. Brief summaries of the most relevant features of, and age determinations for, this unit are provided in Table 3.1 and Figure 3.7, respectively.

3.1.1.1 Western Volcanic Sub-Unit *(Pzlt-a)*

This sub-unit crops out to the west of a major structure known as La Escondida master fault (Figure 3.1; Appendix 1). Contacts with the two other sub-units of La Tabla Formation are structurally controlled (Figure 3.2a). The *Pzlt-a* sub-unit is a massive series of reddish grey and coarse-grained, crystal-rich rhyolitic ignimbrites, and rare autobrecciated lava flows (Figures 3.2b 3.3a and b). Several subvolcanic rhyolites (domes?) and andesite plugs form part of the sequence (Marinovic et al., 1995; Richards et al., 2001). The *Pzlt-a* is the wall rock of the Eocene Escondida Norte-Zaldivar porphyry copper deposit (Appendix 2B). Two SHRIMP U-Pb zircon dates constrain an age of 294.2 ± 2.4 Ma and 290 ± 4 Ma for the *Pzlt-a* (Richards et al., 1999; Pollard and Taylor, 2002; Table 3.2). Drill core descriptions from Escondida Norte and Zaldivar mines indicates that the *Pzlt-a* sub-unit has been intruded by syenogranites and granodiorites, with Late Paleozoic U-Pb zircon crystallization ages of 298.9 ± 2.6 Ma and 293 ± 6 Ma, respectively (Pollard and Taylor, 2002; La Escondida brownfields exploration program, 2003-2007; Table 3.4; Appendix 6).

3.1.1.2 Central Volcano-Sedimentary Sub-Unit *(Pzlt-b)*

This sub-unit is poorly exposed on low-relief sectors, but boreholes indicate that it also occurs beneath the alluvial fill of the Salar de Hamburgo basin (Appendix 1B). It forms the wall rock at La Escondida porphyry copper deposit (Appendix 2C). Recent drill holes have identified this unit under other minor basins filled by Neogene gravels (Figure 4.39).

Table 3.1 Summary of Late Paleozoic volcanic and subvolcanic units exposed in La Escondida district.

Unit (Abbreviation)	Age	Regional Description Contact relationships and lithology	La Escondida District Contact relationships and lithology	References
La Tabla Formation ***(Pzlt)***	Late Carboniferous-Permian (~294-282 Ma)	- The unit unconformably overlays Ordovician granitoids, the Argomedo Strata and Zorritas Formation (Devonian-Early Carboniferous), and is covered unconformably by El Profeta Formation (Late Triassic-Late Jurassic) - Terrestrial and bimodal volcanic sequence 800-1000 m thick. Dominantly rhyolitic lava flows, tuffs and volcanic breccias, and subvolcanic intrusives of similar composition. Interbedding of minor epiclastic rocks and andesitic to basaltic lava flows.	- The lower limit of the unit is not exposed and the top is unconformably overlain by the Late Triassic-Late Jurassic El Profeta Formation - Composed of three distinctive sub-units: (1) the Western volcanic sub-unit *(Pzlt-a)* of massive silicic ignimbrite, lava flow and subvolcanic intrusive; (2) the Central volcano-sedimentary sub-unit *(Pzlt-b)* of andesitic to basaltic-andesitic lava flow and subordinate tuff, sandstone, limestone and conglomerate; (3) the Eastern volcanic succession *(Pzlt-c)* comprising dacitic to rhyolitic crystal-rich tuff and rare lapilli-tuff Estimated thickness of <800 m for the entire sequence	García (1967) Davidson et al (1985) Brook et al. (1986) Urzúa (1988) Mpodozis et al (1993a) Gardeweg et al (1994) Marinovic et al (1995)
Andesite porphyry ***(Pzan)***	Late Carboniferous-Early Permian	Small- to medium-sized subvolcanic intrusives of intermediate to silicic composition, which are inferred to be cogenetic with La Tabla sequence Widespread occurrence along the Domeyko Cordillera	- Has intruded the Central volcano-sedimentary sub-unit *(Pzlt-b)* of La Tabla Formation. - Light grey, coarse-grained plagioclase-mafic-phyric andesite - Has intruded the Central volcano-sedimentary sub-unit *(Pzlt-b)* of La Tabla Formation and the andesite porphyry *(Pzan)* - Light grey, coarse grained porphyric dacite, with sparsely well-developed phenocrysts of plagioclase, embayed quartz and chloritised mafic minerals It has intruded Pzan and contains numerous microdioritic enclaves.	Mpodozis et al. (1993a) Marinovic et al. (1995)
Dacite porphyry ***(Pzda)***	Late Carboniferous-Early Permian (293 ± 4 Ma)			

Table 3.2 Radiometric ages for La Tabla Formation and associated subvolcanic intrusions in La Escondida district and adjacent sectors.

Sample	Rock/Sub-unit	Method (material)	Age & Error (Ma, 2σ)	Source of data (*)
La Tabla Formation *(Pzlt)*				
QFP1	Rhyolite porphyry */Pzlt-a*	U-Pb (zircon)	294.2 ± 2.4	3
ZAL3	Antigua porphyry (rhyolite)/*Pzlt-a*	U-Pb (zircon)	290 ± 4	1
ESC-45	Andesitic tuff/*Pzlt-b*	U-Pb (zircon)	287 ± 3	4
ESC-36	Andesitic tuff/*Pzlt-b*	U-Pb (zircon)	286 ± 2	4
ESC-47	Andesitic tuff/*Pzlt-b*	U-Pb (zircon)	284 ± 4	4
ESC-37	Andesitic tuff/*Pzlt-b*	U-Pb (zircon)	282 ± 2	4
IM-86	Amphibole dacite */Pzlt-b*	^{40}Ar-^{39}Ar (hornblende)	267.6 ± 4.3	2
Coarse dacite porphyry *(Pzda)*				
ESC-50	Feldspar-phyric dacite	U-Pb (zircon)	293 ± 4	4

(*) Source of data. (1) Richards et al. (1999); (2) Richards et al. (2001); (3) Pollard and Taylor (2002); (4) this study. Abbreviations: *Pzlt-a* = Western volcanic sub-unit; *Pzlt-b* = Central volcano-sedimentary sub-unit

It is a green to greenish brown, crudely stratified succession of andesites, dacites, basaltic andesites, levels of vitric and crystal tuffs, and interbedded volcanic sandstones, Cu-(Fe)-oxides and native Cu locally along the eastern flank of San Carlos range (La Escondida brownfields exploration program, 2003-2007; Chapter 5). Various *Pzlt-b* samples from surface exposures proved unsuitable for using LA-ICP-MS U-Pb dating on zircon as part of this study. Instead, samples from drill holes located in the Salar de Hamburgo and surrounding La Escondida and Escondida Norte-Zaldivar deposits were used. These samples yielded ages of 287 Ma to 282 Ma (Table 3.2), substantial older than the 267.6 ± 4.3 ^{40}Ar-^{39}Ar hornblende age determination from Richards et al. (2001) and the apparently thermally reset 212-186 Ma K-Ar biotite ages obtained by Marinovic et al. (1995) for andesites and dacites from the sequence (Table 3.2; Appendix 6). Conversely, the clustered 287-282 Ma U-Pb ages are slightly younger than the coeval dacite and andesite porphyry *(Pzap)* intrusions of 293 ± 4 Ma (U-Pb zircon; Table 3.2; Appendix 6), which is described in the following section.

3.1.1.3 Eastern Volcanic Sub-Unit *(Pzlt-c)*

This sequence stratigraphically overlies the *Pzlt-b* sub-unit (Figure 3.5a), and has a similar composition to *Pzlt-a*. The *Pzlt-c* sub-unit comprises massive and reddish brown, flow-banded, welded and non-welded, rhyolitic to dacitic coarse-grained crystal-rich tuffs. Associated flow-banded and massive, porphyritic dacite is surrounded by a brecciated carapace (Figure 3.5b). No reliable radiometric ages have been reported for these rocks in the vicinity of La Escondida district (Davidson et al., 1985; Brook et al., 1986; Gardeweg et al., 1994; Appendix 6). However, they are intruded by a 290 ± 2 Ma granodiorite (U-Pb

zircon age) from the Imilac plutonic complex (Table 3.4; Appendix 6). This establishes a minimum age of ca. 290 Ma for the *Pzlt-c* sub-unit.

3.1.1.4 Age and Depositional Setting

Breitkreuz (1991) proposed a paleogeographic reconstruction for the Late Paleozoic sequences exposed between 23°S and 24°30'S, which consists of large paleo-lake that received calcareous, clastic and volcanic sediments, along with subordinate pillowed lava flows. But it has been questioned on the basis of new U-Pb radiometric ages and fossil fauna, which indicate a Middle to Late Triassic age for part of the sucessions involved in the lacustrine depositional setting (Basso and Marinovic, 2003; Mpodozis, oral comm., 2006). Based on previous age determinations and new SHRIMP and LA-ICP-MS U-Pb zircon dates, a range of ages between 294 Ma and 282 Ma has been established for La Tabla Formation (Figure 3.7; Appendix 6). The unit is interpreted to have been deposited subaerially in caldera and volcanic dome settings (Davidson et al., 1985; Brook et al., 1986; Mpodozis et al., 1993a). Terrestrial explosive volcanism was accompanied by clastic and mixed calcareous-clastic sedimentation, although the resulting facies architecture remains poorly understood. The fine-grained clastic and calcareous rocks that are interbedded in the volcaniclastic succession were deposited subaqueously, below wave-base under low energy conditions of sedimentation, most likely a restricted lacustrine environment (Collinson, 1996; Talbot and Allen, 1996). Interbedded channelised conglomerates, cross-bedded pebbly sandstones, siltstones that have mud cracks, and volcaniclastic deposits suggest complex interaction of distal braided fluvial distributaries, flood plains, lakes, and subaerial and subaqueous volcanic environments (Breitkreuz, 1991; McPhie et al., 1993; Orton, 1996).

Individual volcanic centres have not been identified in the Escondida area, but intra- and extra-caldera facies, post-collapse domes and resurgent plutons have been described about 30 to 50 km to the north, in Sierra Mariposa and Pampa Elvira (Mpodozis et al., 1993a), and also further northwards in the Salar de Atacama region at 23°S (Breitkreuz, 1991).

3.1.2 Dacite and Andesite Porphyries *(Pzda/Pzan)*

Two small nested bodies (< 1.8 km^2) with associated minor plugs of dacitic and andesitic composition have intruded the *Pzlt-b* sub-unit of La Tabla sequence (Figure 3.1; Table 3.1). Both are greenish-grey coarse-grained porphyritic rocks and contain sparse, well-developed phenocrysts of plagioclase, resorbed quartz (including xenocrysts) and

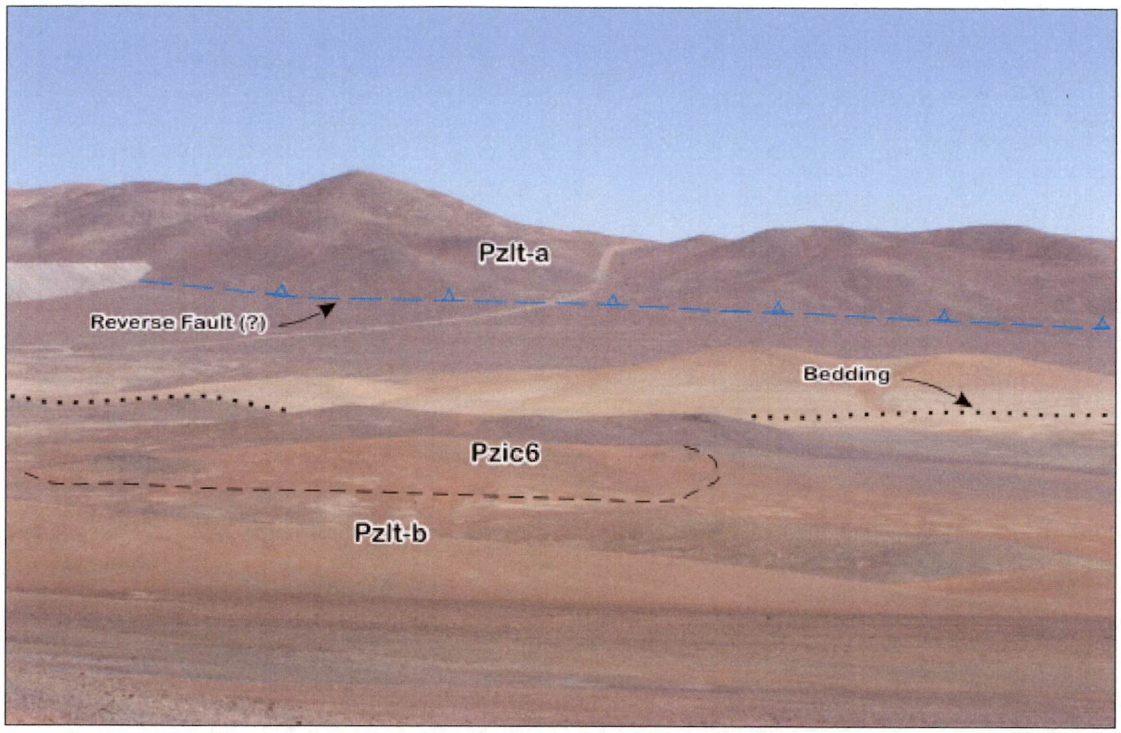

Figure 3.2a General view (looking west) of the massive ignimbrites of the Western volcanic sub-unit *(Pzlt-a)* from the Late Carboniferous-Permian La Tabla Formation. These rocks are separated, by a narrow alluvial plain controlled by La Escondida master fault, from the andesites and white tuffs of the central volcano-sedimentary sub-unit *(Pzlt-b)*. Small granite porphyry *(Pzic6)* has intruded *Pzlt-b*. Cordón Zaldivar (7,324,000m N; 496,000m E).

Figure 3.2b Hand specimen of red-coloured and coarse-grained, poorly-welded rhyolitic crystal-rich ignimbrite of the Central volcanic sub-unit *(Pzlt-b)*. Note the large (**Q**) quartz and feldspars (**F**) immersed in a fine-grained matrix, giving the appearance of coherent lava or subvolcanic intrusive rhyolite with flow-banding. North of the Escondida Norte-Zaldivar deposit (7,328,800m N; 497,200m E).

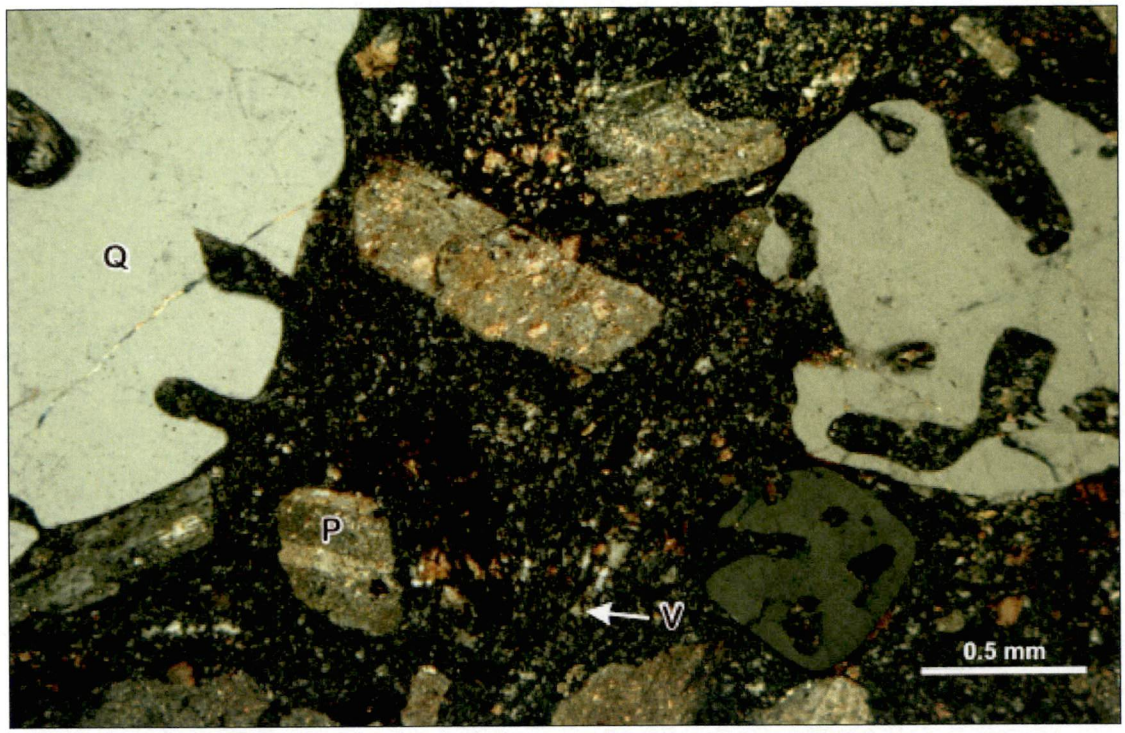

Figure 3.3a Photomicrograph (crossed nicols) of a coarse-grained, welded crystal-rich ignimbrite, with large phenocrysts (including xenocrysts) of resorbed quartz (**Q**) and argillised plagioclase (**P**) set in a devitrified (?), clay-rich quartz+feldspar-bearing matrix. Note the variolitic (**V**) texture in the matrix. La Tabla Formation (Late Carboniferous-Permian). Sample FU-457 (7,336,768m N; 498,552m E).

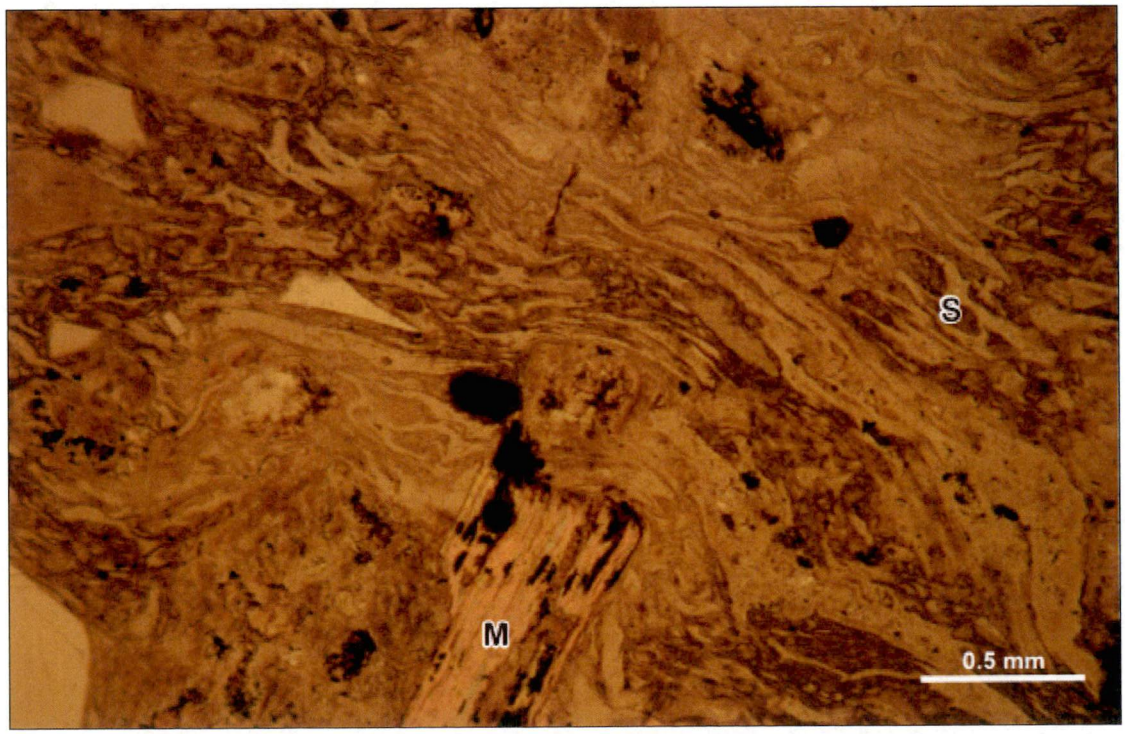

Figure 3.3b Photomicrograph (plane polarised light) of a medium-grained welded ignimbrite, with sparse phenocrysts of broken quartz (**Q**), clay-altered feldspars and rare muscovite (**M**) in a flow-laminated vitric matrix composed of flattened shards (**S**), abundant Fe-oxides and minor microcrystals of quartz, opaques and feldspars. La Tabla Formation. Sample FU-411 (7,333,837m N; 477,195m E).

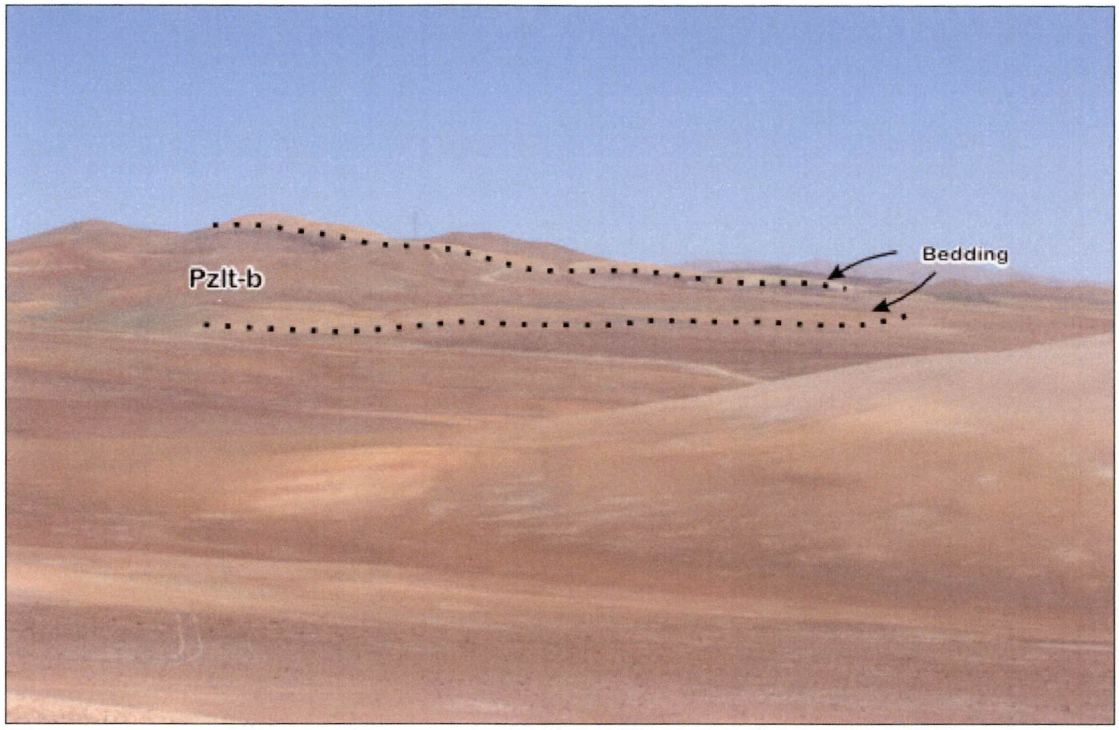

Figure 3.4a General view (looking southeast) of the andesite lava flows and the characteristic interbedding of reddish white-stained vitric tuffaceous rocks in the Central volcano-sedimentary sub-unit *(Pzlt-b)* from La Tabla Formation (Late Carboniferous-Permian). Note the gentle dip of the pyroclastic beds. Northeast of Escondida Norte pit (7,327,300m N; 500,000m E).

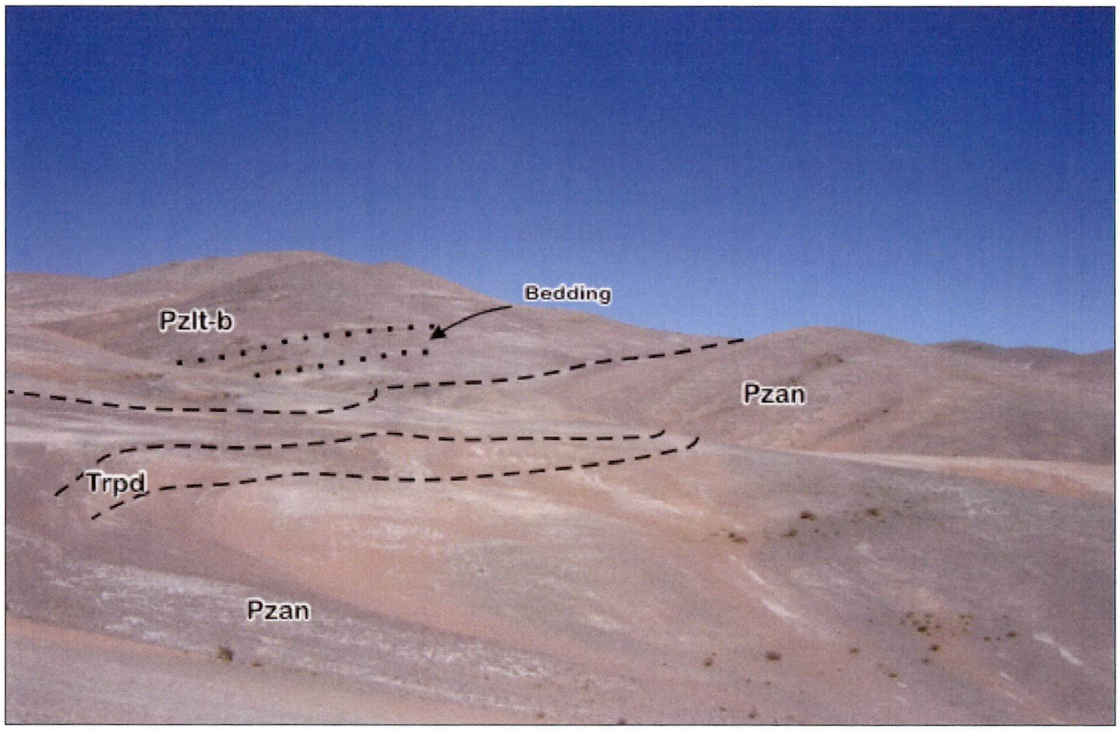

Figure 3.4b General view (looking southeast) of a poorly exposed sequence of volcaniclastic sandstones, andesitic ignimbrites and lava flows of the Central volcano-sedimentary sub-unit *(Pzlt-b)* from La Tabla Formation. Andesitic porphyry *(Pzan)* has intruded the sequence as well as other altered rhyolitic dykes *(Trdp)*. Sierra de San Carlos (7,309,000m N; 498,300m E).

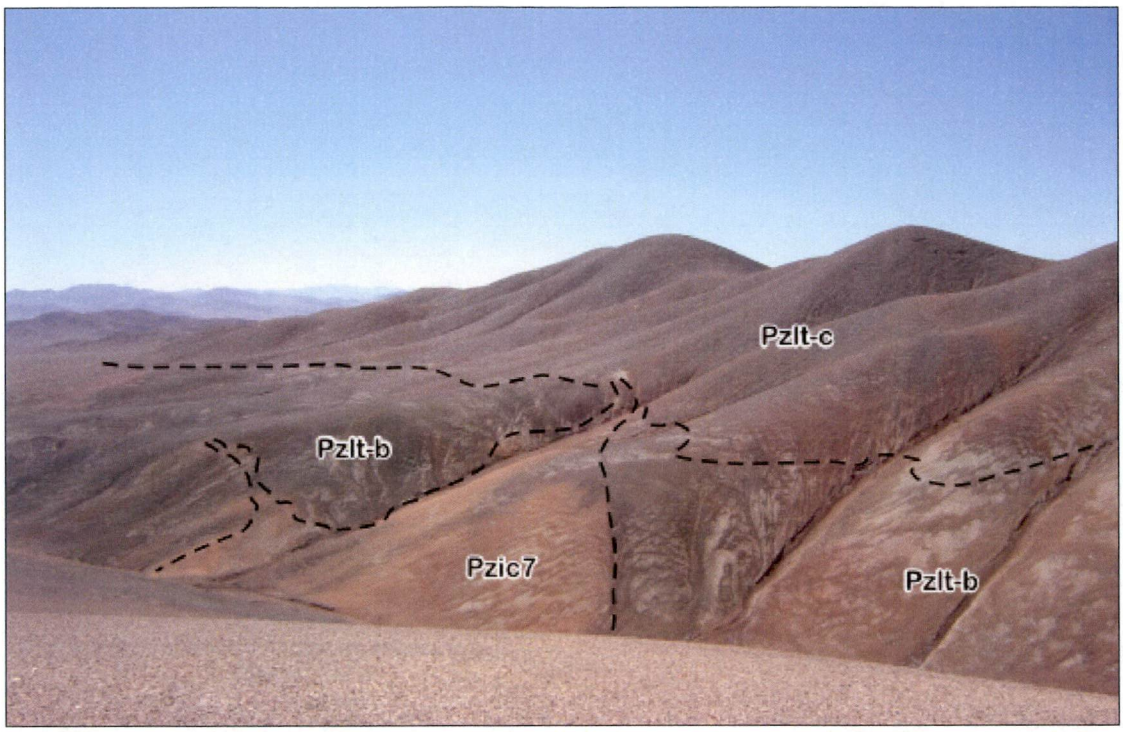

Figure 3.5a General view (looking northwest) of the andesites of the Central volcano-sedimentary sub-unit *(Pzlt-b)* overlain, with an obscured contact, by the massive ignimbrites of the Eastern volcanic sub-unit *(Pzlt-c)* of La Tabla Formation. Note the irregular rhyolite dykes *(Pzic7)* of the Imilac plutonic complex *(Pzic)* cutting the volcanic pile. Quebrada Larga sector (7,334,100m N; 499,900m E).

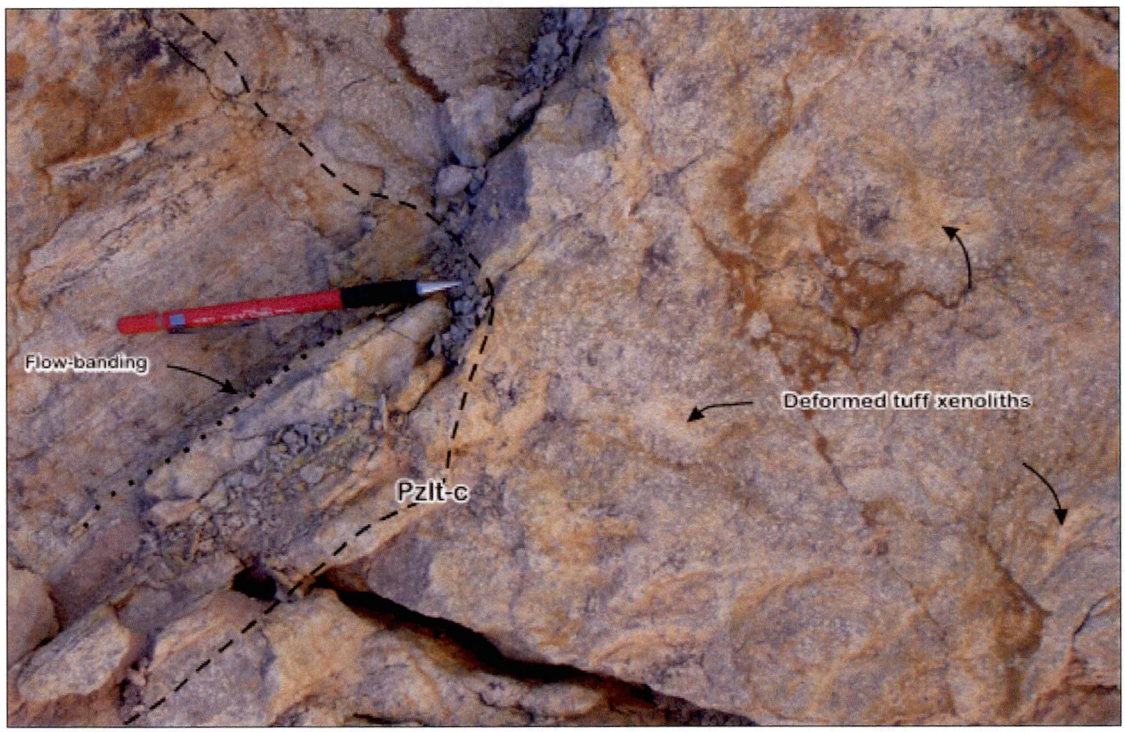

Figure 3.5b Flow-laminated tuffaceous rocks of the Eastern volcanic sub-unit *(Pzlt-c)* from La Tabla Formation intruded by a cogenetic flow-foliated rhyolite, with a narrow brecciated zone along the contact. Note the deformed tuffaceous xenoliths. Sierra de Imilac (7,335,900m N; 502,800m E).

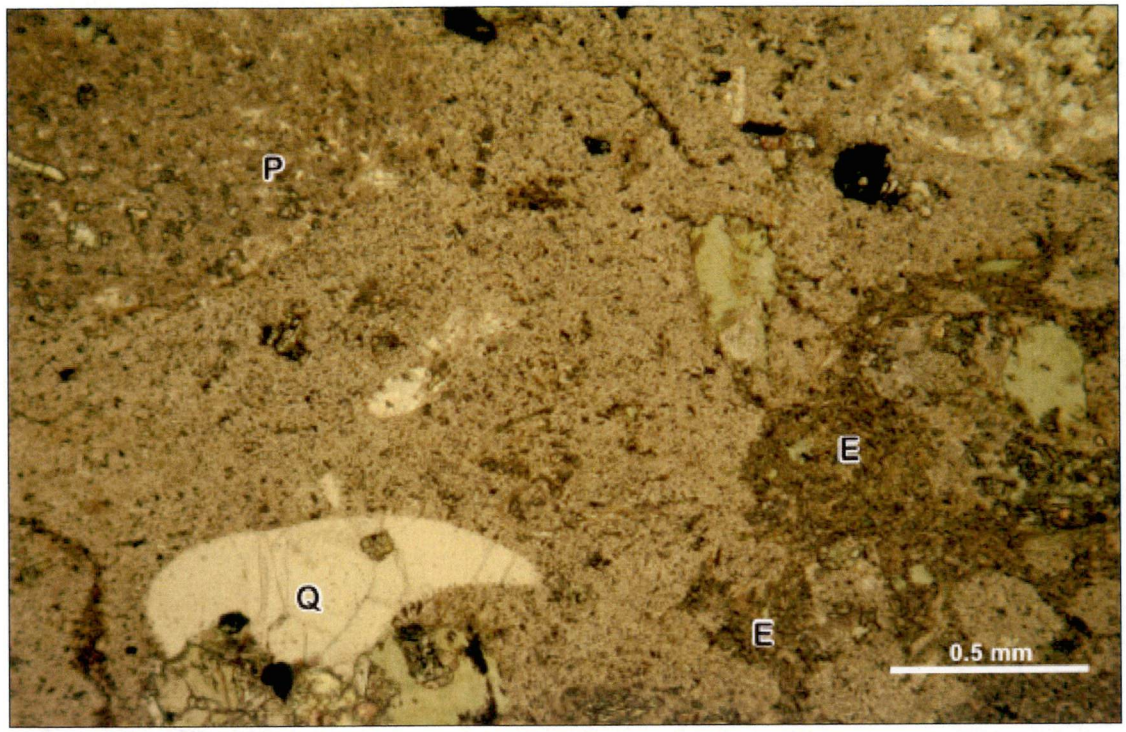

Figure 3.6a Photomicrograph (plane polarised light) of a medium- to coarse-grained dacite porphyry *(Pzdp)* composed of resorbed quartz (**Q**) and strongly argillised and epidotised plagioclase (**P**) phenocrysts in an altered quartz+feldspar-rich groundmass. Note the irregular andesitic enclaves (**E**). Dacite porphyry (293.0 ± 4.0 Ma; LA-ICP-MS U-Pb zircon method). Sample ESC-50 (7,308,600m N; 498,370m E).

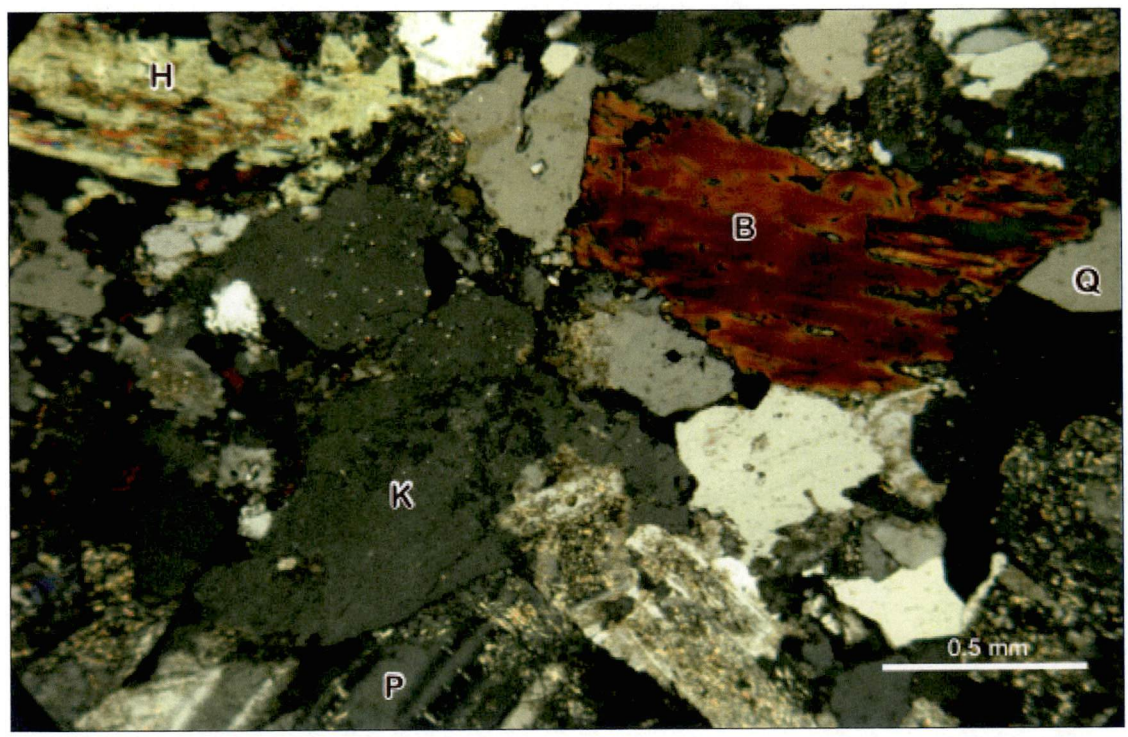

Figure 3.6b Photomicrograph (crossed nicols) of a coarse-grained, moderately porphyritic monzonite *(Pzic4)*. Note the chloritised hornblende (**H**) and biotite (**B**), the weakly sericitised K-feldspars (**K**) and plagioclase (**P**), and interstitial quartz (**Q**). Imilac plutonic complex (290 ± 2 Ma; LA-ICP-MS U-Pb zircon method). Sample ESC-49 (7,311,529m N; 501,363m E).

ferromagnesian minerals that have been replaced by chlorite, biotite and magnetite, all set in a hyalopilitic groundmass. The *Pzda* unit contains numerous microdioritic and andesitic enclaves (Figures 3.6a), as well as chilled-margin xenoliths of the *Pzan* unit. A 293 ± 4 Ma LA-ICP-MS U-Pb zircon age has been determined for the *Pzda* unit during the current study (Table 3.2; Figure 3.7; Appendix 6). Based on textural attributes and field occurrences, a hypabyssal emplacement has been inferred for the intermediate porphyries of the *Pzan* and *Pzda* units.

3.1.3 Imilac Plutonic Complex *(Pzic)*

The Imilac plutonic complex comprises diverse medium-sized stocks, minor apophyses and dykes that range in composition from diorite to porphyritic granite and aplite (Figure 3.1; Table 3.3). The complex is enclosed by a narrow contact metamorphic aureole (< 10-15 m wide, of at least biotite grade, in La Tabla volcanic rocks. Earliest stage intrusive sub-units are discrete quartz monzodiorite *(Pzic1)*, microdiorite and microtonalite *(Pzic2)*, which have all been partially metamorphosed by later silicic intrusions. Several small apophyses and plugs of medium-grained quartz diorite *(Pzic3)* are located at the margins of the main intrusive phase *(Pzic4)*. The *Pzic4* sub-unit is a composite stock (1.5 to 2.5 km^2) dominated by coarse-grained, weakly porphyritic to equigranular biotite-hornblende granodiorite and monzodiorite (Figure 3.6b). Fine- to medium-grained monzonite and quartz monzonite *(Pzic5)*, granite and granodiorite porphyries *(Pzic6)* grade into aplitic micromonzonite and microgranite dykes *(Pzic7)*. A swarm of distinctive reddish brown rhyolite coloured porphyry dykes *(Pzic8)* cross cut all other phases of the Imilac plutonic complex. K-Ar and Rb-Sr ages between 297 Ma and 271 Ma have been reported for the Imilac granitoids (Davidson et al., 1985; Brook et al., 1986; Gardeweg et al., 1994; Figure 3.7; Appendix 6), although the authors did not provide unambiguous locations for their samples. This has caused some doubt regarding the sample coordinates on the geological map of Gardeweg et al. (1994). New LA-ICP-MS U-Pb zircon dating performed for this study establishes an age of 290 ± 2 Ma for a granodiorite from the *Pzic4* intrusive phase of the Imilac plutonic complex (Table 3.4; Figure 3.7; Appendix 6).

3.1.4 Other Late Paleozoic Intrusive Rocks

Intriguing intrusive rocks have been intercepted by drill holes at the Escondida Norte-Zaldivar deposit, for which geochronological studies indicate Late Paleozoic ages (Table 3.4). Petrographically, they are strongly porphyritic to equigranular, medium- to coarse-grained monzogranite, syenogranite, granodiorite and diorite that should cross cut La

Table 3.3 Summary of Late Paleozoic-Late Triassic intrusive units exposed in La Escondida district.

Unit (Abbreviation)	Age	Regional Description Contact relationships and lithology	La Escondida District Contact relationships and lithology	References
Imilac plutonic complex *(Pzic)*	Late Carboniferous-Permian	- Has intruded Precambrian? metamorphic basement, the Lower Paleozoic granitoids and several clastic and volcanic units ranging from Devonian to Permian in ages - Large composite stocks that comprise mesozonal diorite, granodiorites, monzonites and granites (e g Salar Verónica intrusive complex)	- Has intruded the Late Carboniferous-Permian La Tabla volcanic sequence - Mesozonal to epizonal composite intrusive complexes ranging from microdiorite and quartz- diorite, through monzonite and granodiorite, to granitic and rhyolitic porphyries Later felsic dykes and veins are common	Davidson et al (1985) Brook et al (1986) Mpodozis et al (1993a) Gardeweg et al (1994) Marinovic et al (1995) Lucassen et al (1999)
Other intrusive rocks	Late Carboniferous-Early Permian	- There are no clearly comparable intrusive rocks along the Domeyko Cordillera However, medium- to coarse-grained granodiorite and diorite phases of some Late Paleozoic plutons exposed in La Escondida district are strong candidates for correlation	- Blind bodies of monzogranitic and dioritic composition, with unknown size, shape and contact relationship, at the Escondida Norte-Zaldivar deposit They should cross cut La Tabla Formation, but Middle Eocene porphyry-style alteration and mineralization have obscured the contacts - Well-developed K-silicate and quartz-sericite alteration assemblage on medium- to coarse-grained granodiorite and diorite "porphyries" Hydrothermal breccias and porphyry-type mineralization Probably wall-rocks of the Tertiary porphyries systems	Pollard and Taylor (2002) Williams et al (2002) Williams (2003) Escondida brownfields exploration program (2003-2007)
Altered dacite and rhyolite porphyry *(Trdp)*	Middle-Late Triassic	- Has intruded the Late Carboniferous-Permian El Bordo Strata and La Tabla Formation and coeval intrusive complexes - Medium- to small-sized bodies of dacitic-rhyolitic and dioritic composition, with associated epithermal- and porphyry-style alteration and mineralization	- Small apophyses and dikes that cut La Tabla Formation - Pervasively silicified and advanced argillic altered dacite to rhyolite porphyries Large colour anomalies, hydrothermal breccias, and porphyry-type mineralization.	Davidson et al (1985) Brook et al (1986) Mpodozis et al. (1993a) Marinovic et al (1995) Marquardt et al. (1997) Cornejo et al (2006)

Table 3.4 Radiometric ages for Late Paleozoic-Late Triassic intrusive units in La Escondida district and adjacent sectors.

Sample	Rock/Sub-unit	Method (material)	Age & Error (Ma, 2σ)	Source of Data (*)
Imilac plutonic complex *(Pzic)*				
N.D.	(◆) Granitoid/N.D.	K-Ar (sericite)	298 ± 7	1
N.D.	Granitoid/N.D.	K-Ar (biotite)	279 ± 7	1
ESC-49	Monzonite/*Pzic5*	U-Pb (zircon)	290 ± 2	4
Other intrusive rocks				
ZERD356	Quartz porphyry (syenogranite)/N.D	U-Pb (zircon)	298.9 ± 2.6	2
ZERD958	Coarse-grained porphyry (granodiorite)/N.D.	U-Pb (zircon)	293 ± 6	3
Altered dacite and rhyolite porphyry *(Trdp)*				
ESC-51	Feldspar porphyry	U-Pb (zircon)	227 ± 3	4
ESC-52	Feldspar porphyry	U-Pb (zircon)	223 ± 4	4

(*) Source of data: (1) Davidson et al. (1985) and Brook et al. (1986); (2) Pollard and Taylor (2002); (3) La Escondida brownfields exploration program (2003-2007); (4) this study. (◆) Indicates altered rock. Abbreviations: N.D. = Not described.

Tabla Formation. However, the mineralisation and alteration processes associated with the middle Eocene porphyry complex have obscured the contact relationships, sizes and occurrences of these granitoids. They were previously considered intrusive phases of the later porphyry complex, with informal names such as quartz porphyry and coarse-grained porphyry (Williams et al., 2002; Williams, 2003). Two U-Pb zircon ages of 298.9 ± 2.6 Ma and 293 ± 6 Ma by Pollard and Taylor (2002) and La Escondida brownfields exploration program (2003-2007) indicate a Late Carboniferous-Early Permian age for two of those blind intrusions intercepted by drill holes (Sepúlveda, written comm., 2007; Table 3.4; Figure 3.7; Appendix 6).

3.1.5 Altered Dacite and Rhyolite Porphyries *(Trdp)*

Numerous Carboniferous-Permian and Permo-Triassic dacite and rhyolite porphyries occur along the Domeyko Cordillera (Davidson et al., 1985; Mpodozis et al., 1993a; Marinovic et al., 1995; Cornejo et al., 2006). They have been subjected to intense exploration due to their association with large colour anomalies and conspicuous epithermal- and porphyry-type hydrothermal alteration zones (Chapter 5). In La Escondida district, the porphyries occur as dykes and apophyses emplaced in pyroclastic rocks of La Tabla sequence (Figure 3.1; Table 3.3). They have been recognized in outcrops and boreholes, but typically have contact relationships obscured by hydrothermal alteration. Hand specimens are characterised by phenocrysts of embayed quartz and pseudomorphs feldspars and subordinate amphibole altered to sericite, pyrophyllite and alunite; all of them embedded in a groundmass replaced by a similar

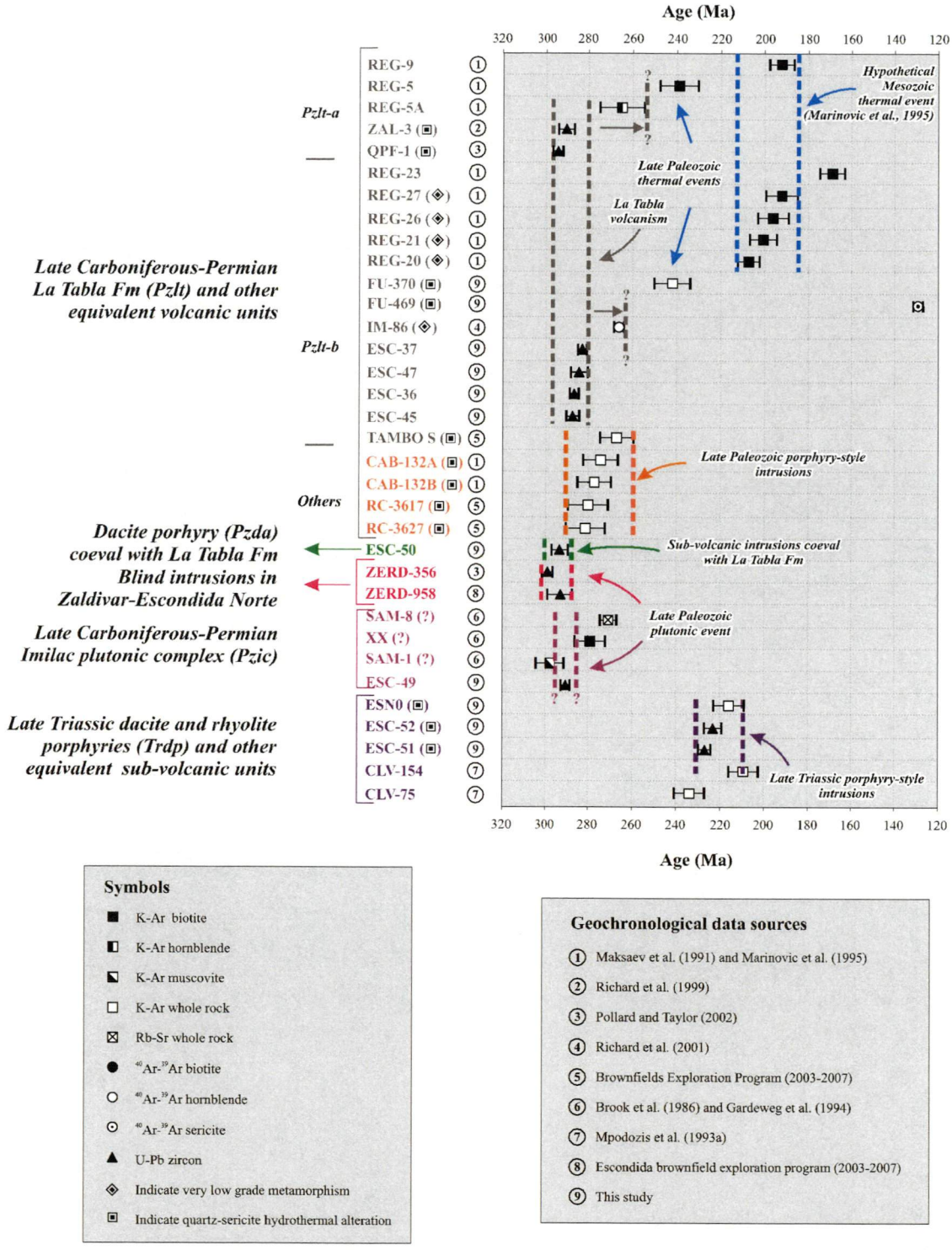

Figure 3.7 Age distribution for selected, altered and unaltered, Late Paleozoic-Triassic igneous rocks in La Escondida district and adjacent sectors. Analytical details provided in Appendix 6.

mineralogical assemblage and abundant quartz.

Two LA-ICP-MS U-Pb zircon analyses of these rocks obtained during the course of the present study have yielded ages of 227 ± 3 Ma and 223 ± 4 Ma (Middle to Late Triassic;

Table 3.4; Figure 3.7). However, other similarly altered intrusives exposed along the Domeyko Cordillera are considerable older (ca. 285-284 Ma; Cornejo et al., 2006; Chapter 5). Based on these data, two different, Late Paleozoic and Middle-Late Triassic, porphyry-style intrusive events have been identified in La Escondida (Figure 3.7; Chapter 5).

3.1.6 Geological Summary for the Late Paleozoic-Triassic

La Tabla Formation and associated plutons, stocks and dykes form part of El Choiyoi granite-rhyolite province, which extended for 2,500 km along the southwestern border of Gondwana (Coira et al., 1982; Mpodozis and Kay, 1992). Magmatism occurred in a series of tectono-volcanic basins, which were characterised by the eruption of large volumes of crystal-rich ignimbrite deposits. In other parts of the Domeyko Cordillera, previous workers inferred a volcanic setting comprising several overlapping caldera complexes, and associated domes and resurgent plutons, emplaced under an extensional tectonic regime (Davidson et al., 1985; Brook et al., 1986; Mpodozis et al., 1993a).

3.2 LATE TRIASSIC-EARLY CRETACEOUS

The Late Triassic-Early Cretaceous saw deposition of a thick sequence of clastic and calcareous rocks in the back-arc Taracapá Basin (Vicente, 2006). These rocks now crop out as relatively narrow, intensely deformed belts flanking the Late Paleozoic basement blocks (Figure 3.8; Chapter 4). The stratigraphic and depositional attributes of the sedimentary units (Table 3.5) imply a complete transgression-regression cycle, with modest explosive volcanic input in the early stage of the evolution of the Tarapacá Basin.

3.2.1 El Profeta Formation *(TJep)*

The Late Triassic-Kimmerigdian El Profeta Formation is a 1,500 m-thick succession of fossiliferous limestones, shale and sandstones, with interbedded conglomerates and pebbly sandstones, tuffs and evaporites (Chong, 1973). The unit is transitional to the red beds of the overlying Late Jurassic-Neocomian Santa Ana Formation (Marinovic et al., 1995). Fuenzalida (1986) and Marinovic et al. (1995) distinguished two main members of El Profeta Formation in La Escondida district (Figure 3.8; Table 3.5). These are described below.

3.2.1.1 Lower Member *(TJep-a)*

This member comprises massive to crudely stratified, monomictic and clast- and matrix-supported, boulder and cobble conglomerates, with boulders up to 1 m diameter

(Figures 3.9a and b). The dominant clasts come from the underlying rhyolites of the Late Paleozoic La Tabla Formation, together with occasional clasts of Cu-bearing quartz diorites and tourmaline breccias (Chapter 5). Intercalations of normal-graded and massive sandstones, flow-banded crystal tuffaceous rock and subordinate volcaniclastic sandstones are common throughout the entire succession. Parting lineations are commonly observed on the bedding planes, along with occasional small-scale cross-beds. Fossiliferous and cherty limestones have been described in the upper sections (Fuenzalida, 1987; Marinovic et al., 1995). Rare invertebrate fossils have been found in Cerro Pascua (Appendix 1A), and they indicate an age range from Late Triassic (Rhaetian) to Early Jurassic (Sinemurian) for this member of El Profeta Formation (Fuenzalida, 1987; Marinovic et al., 1995).

3.2.1.2 Upper Member *(TJep-b)*

This unit is over 700 m thick and is composed of interbedded limestones, sandy limestones and mudstone (Figure 3.10a). The strata are 5-15 cm thick, laterally continuous for tens of meters, with wavy laminations, cross-beds and planar-beds, convolutions, abundant concretions and invertebrate fossils. Small ripple-marks have been draped by muddy laminations that are commonly bioturbated. Thin intercalations of coarse-grained sandstones and granitoid clast-rich conglomerates have recently recognized in the carbonate intervals (Figure 3.10b). A well-known evaporitic stratigraphic marker up to 8-10 m thick of Oxfordian-Kimmeridgian age occurs in the uppermost levels (Ardill et al., 1998). The abundant and widespread faunal content indicates Early Jurassic.

3.2.1.3 Age and Depositional Setting

Late Triassic-Tithonian age for El Profeta Formation, as defined by Marinovic et al. (1995), has been established by a conspicuous fossil content (Ardill et al., 1998; and references therein). In a broad sense, the *TJep-a* is interpreted to be the product of high-energy sedimentation from high-density flows, along with minor debris flows and debris avalanches, in an alluvial fan to coastal setting (fan-delta?) fringing the front of structural bounded regions (Wescott and Ethridge, 1980; Stow, 1985; Collinson, 1996). In contrast, the *TJep-b* represents a carbonate ramp association of offshore to shoreface facies with coral reefs, followed by a gradual transition from carbonate-dominated to a progradational sequence of sandstones deposited in lagoon and tidal flats (Tucker, 1985; Ardill et al., 1998). However, the interbedded coarse-grained rocks are thought to be associated with mass flow (Stow, 1985; Gani, 2004), in concordance with intraformational breccias and slump structures observed 9 km to the north of the study area (Chapter 4) and elsewhere

along the Domeyko Cordillera (Lira, 1991; Orrego, 1992; Niemeyer, oral comm., 2005; Vicente, 2007). The importance of these mass flow deposits in the evolution of the carbonatic Tarapacá basin is poorly understood at present. They are, however, probably indicative of active tectonism during the Late Jurassic, predominantly along the eastern border of the basin.

3.2.2 Santa Ana Formation *(JKsa)*

The Santa Ana Formation, as defined by Marinovic et al. (1995), is a series of redbeds and intercalated lavas, breccias and andesitic tuffs. However, the sections of this formation mapped in the present study do not contain significant amounts of volcanic rocks (Figure 3.7; Table 3.5). The Santa Ana Formation unit concordantly overlies El Profeta Formation (Figure 3.10a) and in turn is covered with marked angular unconformity by the late Paleocene-early Eocene Augusta Victoria Formation. A low angle unconformity, even though it is partly obscured by magmatism and folding, has been observed during the course of the present study between the Santa Ana Formation and the overlying ca. 70-66 Ma Las Torres igneous complex.

The thickness of the Santa Ana Formation is less than 300 m. In general, the unit is largely dominated by interbedded siltstones and sandstones (Figure 3.11b) that are internally micro-laminated and with subordinate beds of cross-bedded medium- to coarse-grained sandstones (Figures 3.12a and b). Scarce paleocurrent readings in trough cross-bedded sandstones yielded a predominant provenance from the east-southeast (Appendix 7). Well-preserved fossil wood rods and rare coquinas of gastropods of little chronological value are exposed in the succession near La Escondida pit (Appendix 1B).

3.2.2.1 Age and Depositional Setting

The rhythmic alternation of cross-rippled sandstone and mudstone that characterizes much of the part of Santa Ana sequence represents successive subaqueous sedimentation of sand and mud in an above-wave base, relatively calm environment. The probable depositional setting is a coastal system, i.e., estuarine or back-barrier lagoons, with marshes (i.e., Tucker, 1985; Reading and Collinson, 1996). In contrast, the medium-scale cross-bedded sandstones intercalated in the uppermost portions of the sequence are associated with minor distal braided fluvial channels in conditions transitional to a terrestrial setting that supported plants and tree found at the top of the sequence (Reading and Collinson, 1996).

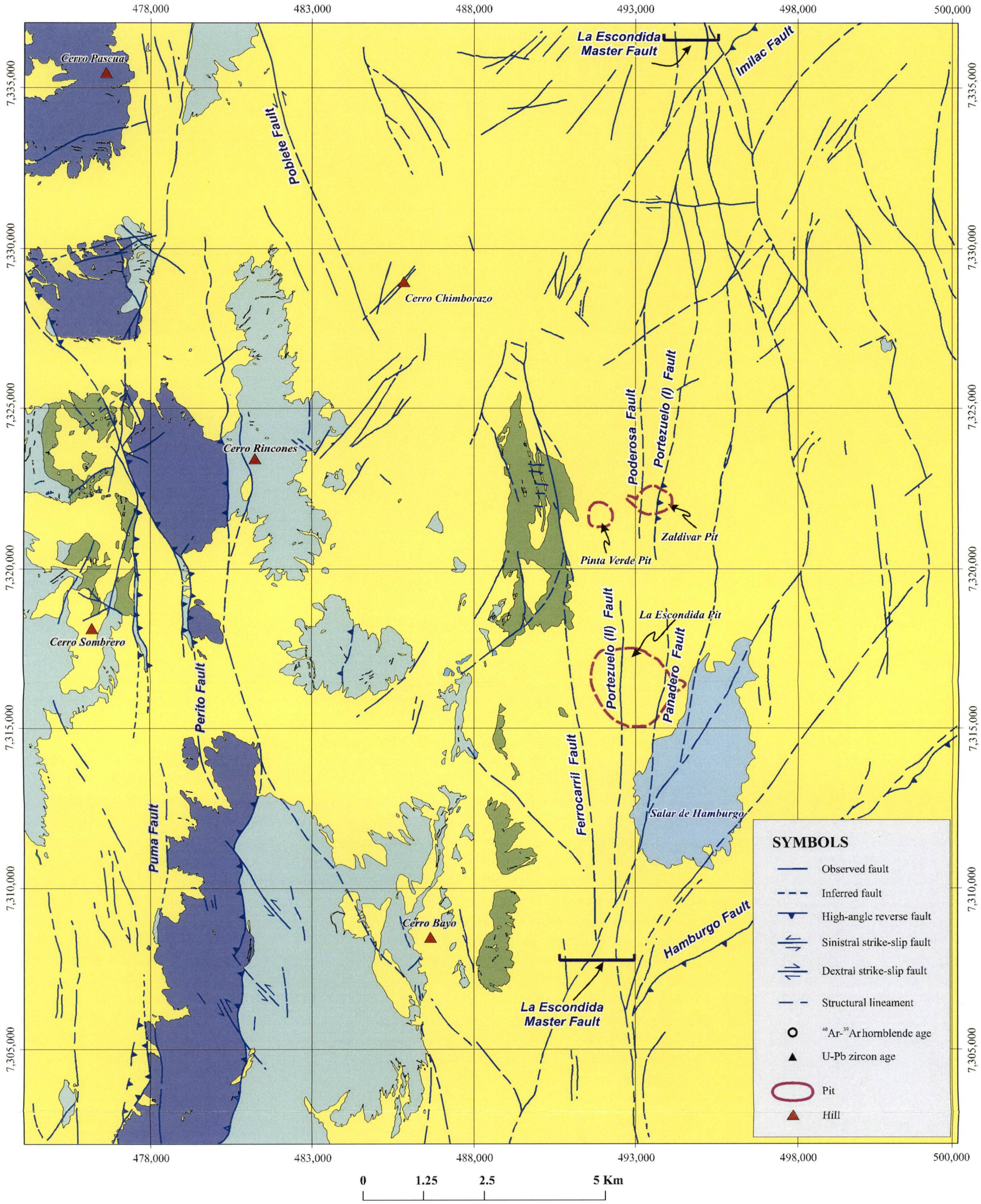

LEGEND

El Profeta Formation (Late Triassic-Kimmeridgian)

TJep(b) Upper Member (Early Jurassic-Kimmeridgian): fossiliferous limestone, calcareous sandstone and mudstone; interbedded evaporite.

TJep(a) Lower Member (Late Triassic-Early Jurassic): conglomerate, conglomeratic sandstone, volcanic breccia and tuff, mudstone; interbedded fossiliferous limestone, calcareous siltstone and chert.

Santa Ana Formation (Late Jurassic-Neocomian)

JKsa Calcareous sandstone, mudstone, minor biogenic limestone, conglomerate and conglomeratic sandstone; common fossil wood.

Modern cover and omitted outcrops of non-Late Triassic to Neocomian sequences

Figure 3.8 General distributions of Late Triassic-Neocomian sedimentary units in La Escondida district.

Table 3.5 Summary of Late Triassic-Neocomian sedimentary units exposed in La Escondida district.

Unit (Abbreviation)	Age	Regional Description Contact relationships and lithology	La Escondida District Contact relationships and lithology	References
El Profeta Formation (TJep)	Late Triassic-Kimmeridgian	- The unit unconformably overlays La Tabla Formation (Late Carboniferous-Permian) and the Late Paleozoic granitoids, and is in turn concordantly covered by the Santa Ana Formation (Late Jurassic-Neocomian) - A fossiliferous succession of 1,500 m thick consisting of limestones, calcareous shales and sandstones, with interbedded coarse-grained conglomerates and conglomeratic sandstones, tuffs and evaporites Biostratigraphically divided into several members and sub-members along the Domeyko Cordillera.	- Transitional contact with the overlaying Santa Ana Formation and also unconformably overlain by the Augusta Victoria Formation (Late Paleocene-Early Eocene). - Composed of two members. (1) Lower Member (*TJep-a*), consisting of boulder-bearing conglomerates and coarse-grained sandstones, along with minor tuffaceous and calcareous beds, and (2) Upper Member (*TJep-b*), composed of fossiliferous limestones, calcareous sandstones, mudstones and evaporites	Chong (1973) Chong and von Hillebrandt (1985) Naranjo and Puig (1984) Fuenzalida (1987) Mpodozis et al (1993a) Marinovic et al (1995) Ardill et al. (1998) Vicente (2006)
Santa Ana Formation *(JKsa)*	Late Jurassic-Neocomian	- The unit is unconformably covered by the Quebrada Seca Formation (Upper Cretaceous) and Augusta Victoria Formation (Late Paleocene-Early Eocene). - A coastal-continental succession of calcareous sandstones, mudstones and minor fine-grained conglomerates, < 400 m thick	- Unconformably covered by the Augusta Victoria Formation (Late Paleocene-Early Eocene) - A rhythmic alternation of cross-rippled sandstones and mudstones, and interbedded sandy limestones and cross-bedded conglomeratic sandstones Rare fossil wood rods Estimated thickness of around 300 m	Naranjo and Puig (1984) Mpodozis et al (1993a) Marinovic et al (1995) Marinovic et al (1996) Cornejo and Mpodozis (1996) Ardill et al. (1998)

Figure 3.9a General view (looking south) of the crudely stratified conglomerates and pebbly sandstones of the Late Triassic-Early Jurassic Lower Member *(TJep-a)* from El Profeta Formation (Late Triassic-Kimmeridgian). Puma sector (7,312,200m N; 488,100m E).

Figure 3.9b Clast-supported monolithic conglomerate from the Lower Member *(TJep-a)* of El Profeta Formation. Note the boulder- and pebble-sized clasts derived from the underlying La Tabla Formation (Late Paleozoic) and the matrix-poor texture. Quebrada Oxidos sector (7,303,600m N; 478,000m E).

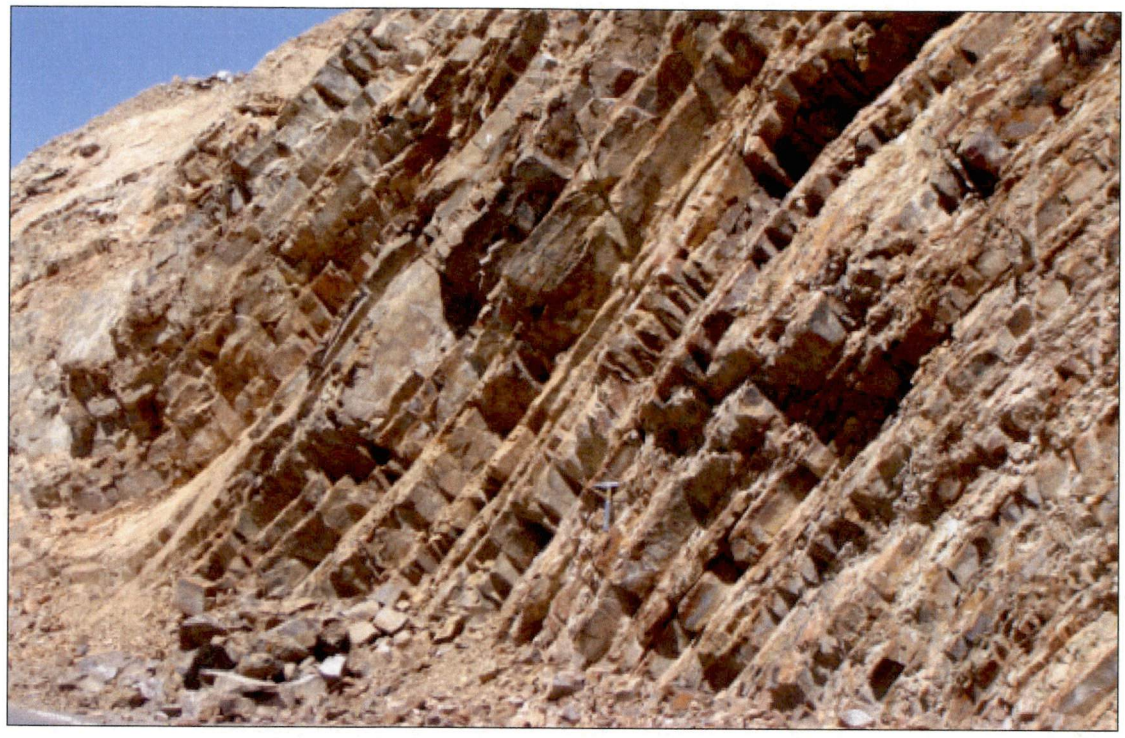

Figure 3.10a General view (looking southeast) of the continuous, well-stratified beds of limestones and subordinates siltstones of the Early Jurassic-Kimmeridgian Upper Member *(TJep-b)* from El Profeta Formation. Paved road to La Escondida operation (7,322,375m N; 479,495m N).

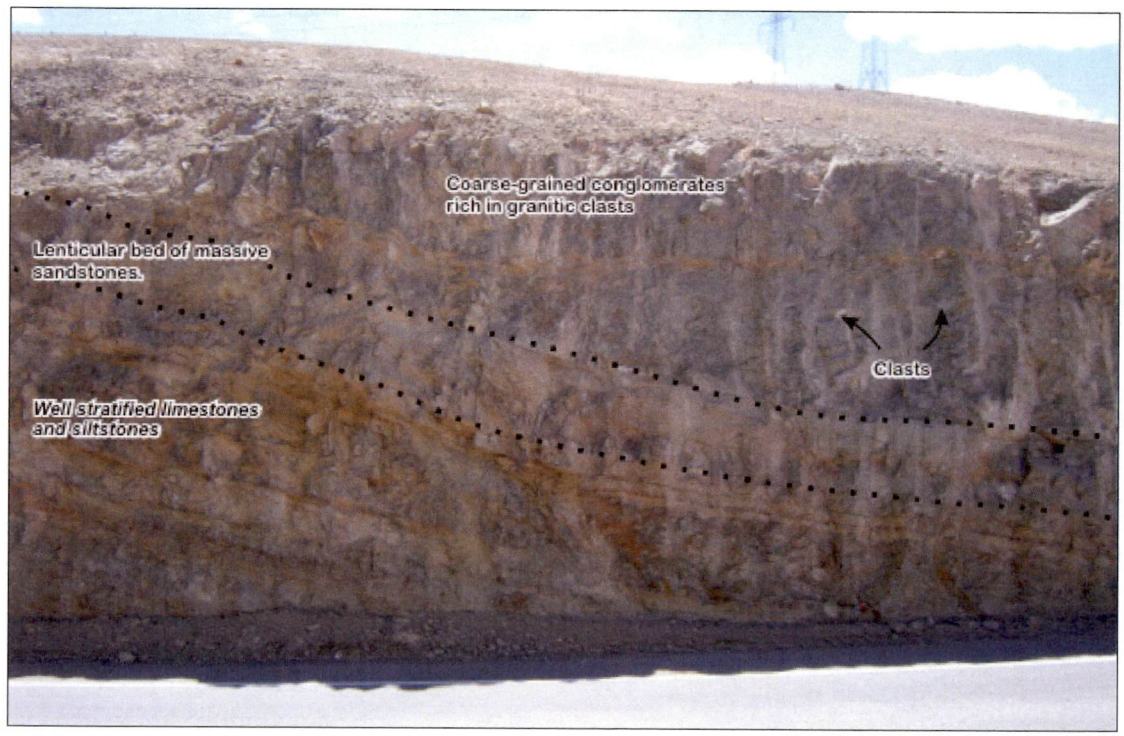

Figure 3.10b General view (looking north) of the well-stratified beds of limestones and siltstones covered by massive sandstones and coarse-grained conglomerates of Early Jurassic-Kimmeridgian Upper Member *(TJep-b)* from El Profeta Formation. Note the planar and non-erosive base of the clastic beds interpreted as high-density turbiditic deposits and debris flows. Paved road to La Escondida operation (7,322,375m N; 479,495m N).

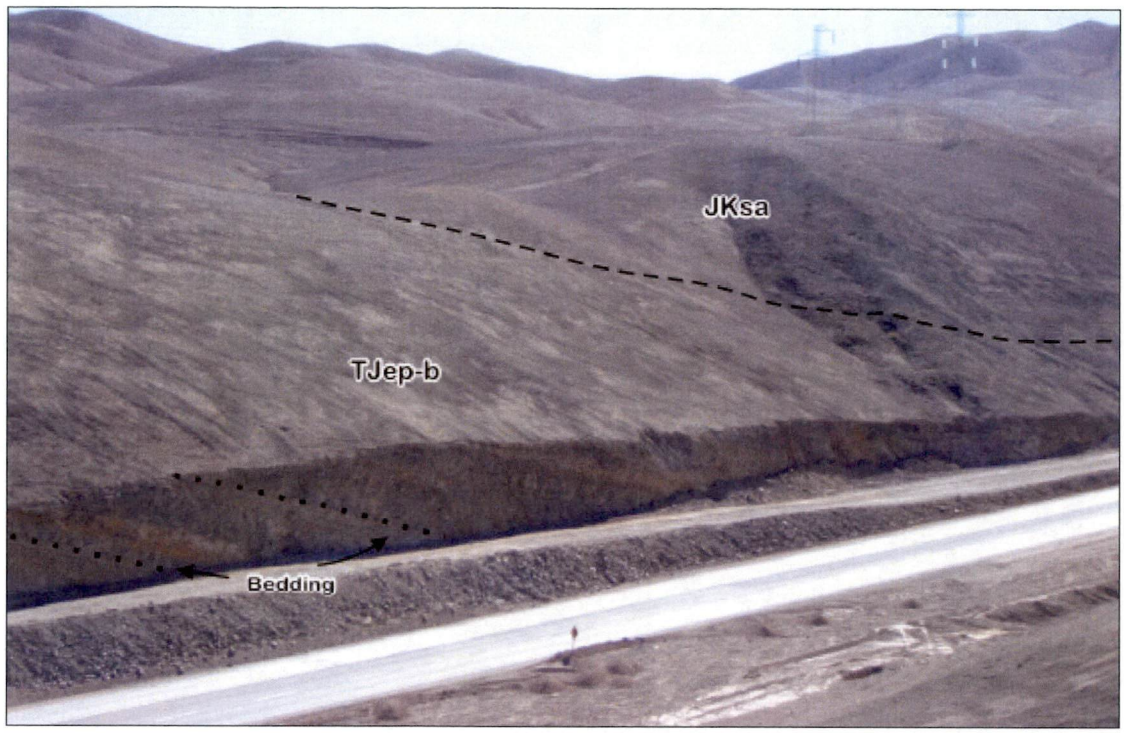

Figure 3.11a General view (looking north) of the transitional passage from the light brown limestones of the Late Jurassic-Kimmeridgian Upper Member *(TJep-b)* of El Profeta Formation to the red sandstones of the Late Jurassic-Neocomian Santa Ana Formation *(JKsa)*. Paved road to Escondida mine (7,322,200m N; 475,500m E).

Figure 3.11b General view (looking southeast) of the typical section of fine- to medium-bedded sandstones, siltstones and mudstones from the Santa Ana Formation (Late Jurassic-Neocomian). Antofagasta-Salta railway (7,323,500m N; 489,500m E).

Figure 3.12a Overturned (?) thinly-bedded fine-grained sandstones and mudstones of the Santa Ana Formation (Late Jurassic-Neocomian). Note the tiny flaser and cross laminations. Antofagasta-Salta railway (7,323,500m N; 489,500m E).

Figure 3.12b Medium-scale trough cross bedding in beds of medium-grained sandstones of the Santa Ana Formation (Late Jurassic-Neocomian), which yielded paleocurrent directions from the east-southeast. Cerro Bayo sector (7,689,900m N; 489,300m E).

Marginal sabkha evaporites deposits have been described in chronologically similar sequences along the eastern margin of the Tarapacá Basin; i.e., Quebrada Monardes Formation in Copiapó (Suarez and Bell, 1992), Cerro Jaspe strata in Sierra del Medio (Ardill et al., 1998), and part of El Profeta Formation in Sierra Exploradora (Cornejo and Mpodozis, 1996). Clear indications of dry climate have not been recognised in the strata studied in La Escondida area. Contemporaneous, Bajocian alkaline basaltic volcanic rocks have not been also documented in the study area, even though they occur in other time-equivalent units on the eastern margin of the Tarapacá Basin nearby Cerro Jaspe region, north of Chuquicamata (Gröschke and Wilke, 1986; Kramer et al., 2005).

3.2.3 Geological Summary of Late Triassic-Early Cretaceous

El Profeta and Santa Ana sedimentary formations record up to 2,600 m of deposition in the Tarapacá back-arc basin (Vicente, 2006). The facies exposed in La Escondida district were deposited along its eastern margin, far from the influence of La Negra volcanic arc (Chapter 2). Whilst the Late Triassic conglomerates of the Lower Member are interpreted as syn-rift deposits, the Jurassic carbonate-clastic rocks of the Upper Member have been inferred to be post-rift sag deposits (i.e., Suarez and Bell, 1992; Ardill et al., 1998 and references therein). A series of *en echelon* depocentres proposed by Prinz et al. (1994) require the formation of several pull-apart sub-basins in the Tarapacá Basin, in response to motions along the fault-bounded eastern margin in the Middle Jurassic (Figure 3.13). This interpretation is consistent with: (1) the absence of Late Triassic-Jurassic sedimentary rocks to the east of La Escondida master fault (Chapter 4); and (2) slump structures and mass flow deposits within the Upper Member of El Profeta Formation, as observed in the study area, and turbiditic fan sequences documented by Orrego (1992) at 20°-21°S. Subsequent contractional movements associated with the lowermost Late Cretaceous Peruvian tectonic phase deformed and inverted the Tarapacá Basin (i.e., Coira et al, 1982; Mpodozis and Ramos, 1989; Marinovic et al., 1995; Cornejo and Mpodozis, 1996; Vicente, 2006; Chapter 4).

3.3 LATE CRETACEOUS-EARLY PALEOCENE

The Late Cretaceous to early Paleocene was a period of widespread, but volumetrically minor, pluton emplacement into the Late Triassic-Necomian carbonate-clastic sequences. The intrusions produced large zones of skarn. Discrete stocks and other minor intrusives, which range in composition from gabbro to aplite and granite porphyry, delineate the occurrence of four magmatic centres: Torcaza pluton, Cerro Bayo plutonic complex,

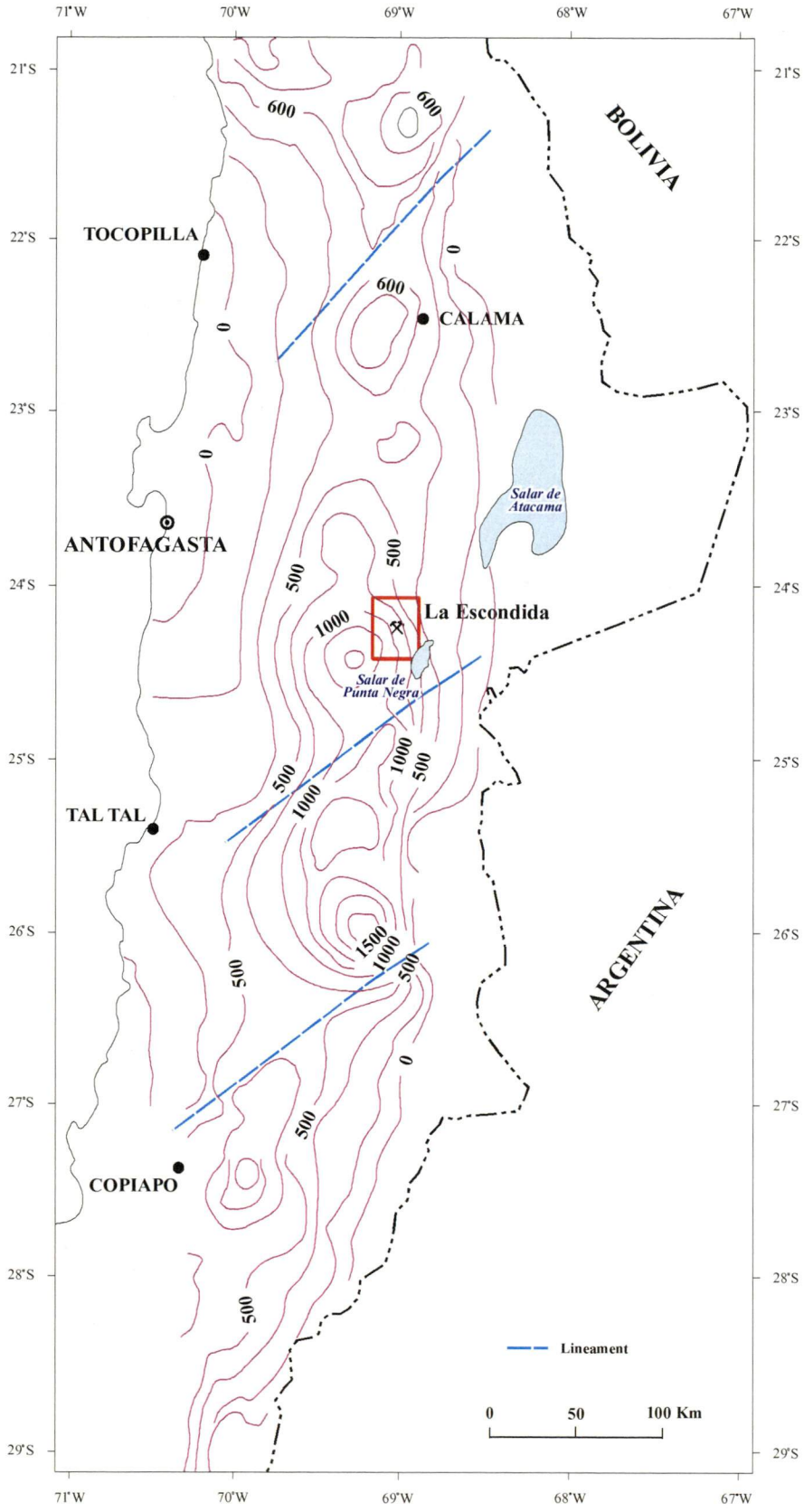

Figure 3.13 Distribution of main depocentres of the Tarapacá Basin, indicating the total sediment thickness for the Upper Triassic-Kimmeridgian times, isopach contours (adapted from Prinz et al., 1994). Note the NNE-elongated sub-basins and the location of La Escondida district.

Sombrero plutonic complex and Las Torres igneous complex (Figure 3.14; Table 3.6). The three former intrusions are a subset of a larger Late Cretaceous magmatic suite that occurs along the Domeyko Cordillera and the eastern side of the Central Depression (Mpodozis et al., 1993a, Cornejo and Mpodozis, 1996), but which remains poorly studied at present. Conversely, the occurrence of a volcanic and volcaniclastic sequence such as Las Torres igneous complex has major relevance because previous descriptions of similar volcanic events do not exist along the Domeyko Cordillera between 22° and 25°S.

Brief summary of the most relevant features and ages distribution of the Late Cretaceous-lowermost early Paleocene rock units are provided in Table 3.6 and Figure 3.22, respectively.

3.3.1 Torcaza Pluton *(LKtp)*

The Torcaza pluton is a small, northeast-elongated composite intrusion that consists of three main phases: monzodiorite, monzonite and diorite (Figure 3.14; Table 3.6). Ca-silicate metamorphic aureoles up to several of tens meters wide occur in the adjacent Mesozoic calcareous country rocks, which host several polymetallic Cu-Pb-Ag veins at the Alicia Mine (Appendix 3; Chapter 5). Secondary chlorite and actinolite occur within the pluton. Two LA-ICP-MS U-Pb zircon age determinations in the Torcaza pluton have given crystallization ages of ca. 81-79 Ma (Table 3.7; Appendix 6).

3.3.1.1 Pyroxene-bearing Amphibole Monzodiorite *(LKtp1)* and Medium-grained Monzonite *(LKtp2)*

The monzodiorite and monzonite form a composite stock about 1 km^2 in plan and elongated on a northerly trend that crops out near the western margin of the pluton (Figures 3.14 and 3.15a). The *LKtp1* sub-unit is an equigranular to glomeroporphyritic monzodiorite, with partially chloritized amphibole and pyroxene phenocrysts. It has gradational contact with a monzonite of *LKtp2* at its northern end. Several leucocratic felsic veins, which are a few centimetres wide, have cross cut *LKtp1* and *LKtp2*. An 81.3 ± 1.0 Ma LA-ICP-MS U-Pb zircon age was obtained for the *LKtp1* sub-unit (Table 3.7; Appendix 6).

3.3.1.2 Bleached Amphibole-rich Diorite *(LKtp3)*

This is a narrow, north-northeast-elongated, heterogeneous stock (<1 km^2; Figures 3.14). The predominant rock type, a fine- to medium-grained amphibole-rich diorite porphyry

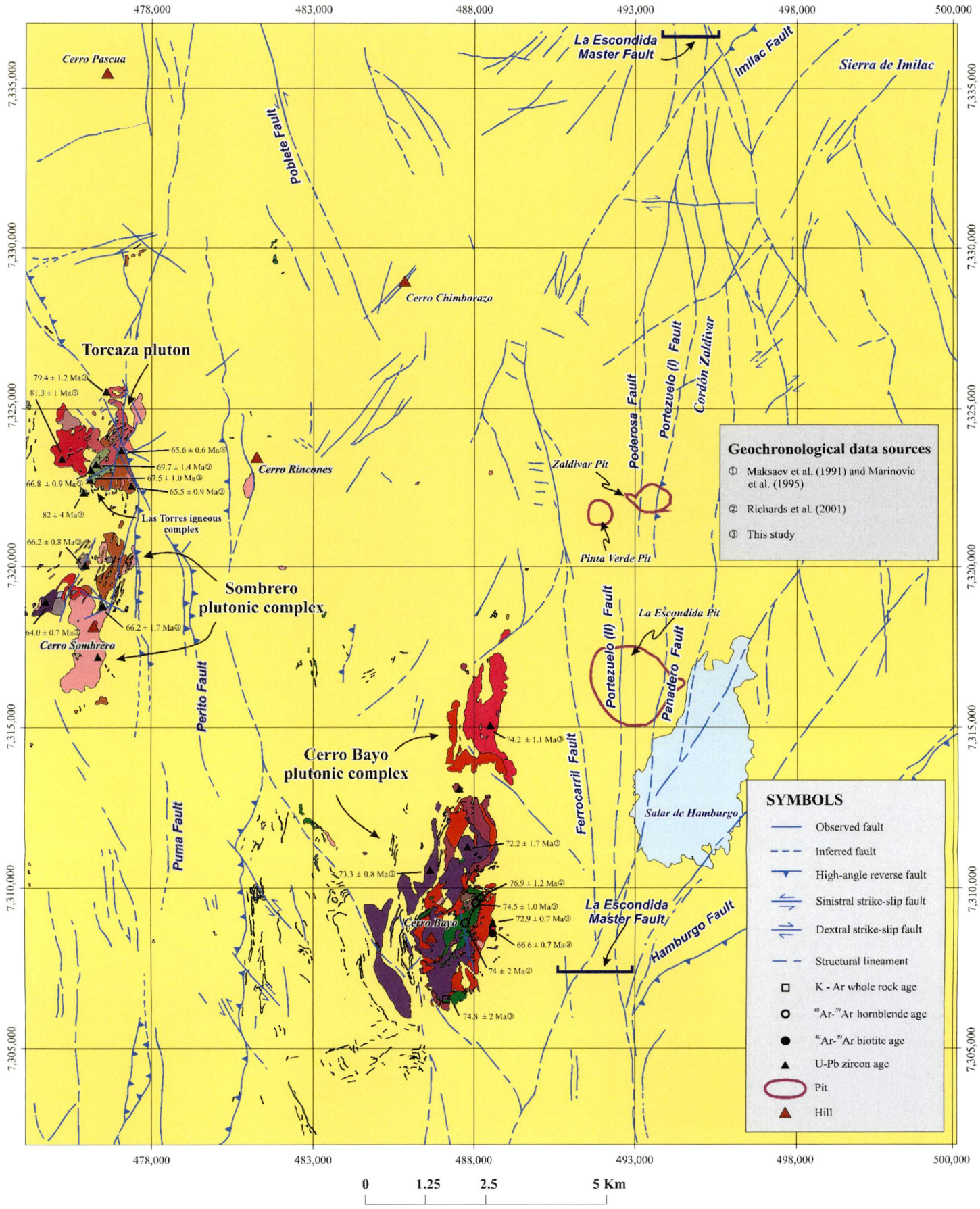

LEGEND

Sombrero plutonic complex (Early Paleocene, ~67-64 Ma)

- TPsb8 Aplitic micromonzonite and microgranite
- TPsb7 Medium- to coarse-grained granodiorite and granite porphyry
- TPsb6 Coarse-grained, biotite-amphibole granodiorite (▲ 64.0 ± 0.7 Ma③)
- TPsb5 Coarse-grained monzonite and quartz monzonite
- TPsb4 Medium-grained, porphyritic monzogranite (▲ 66.2 ± 0.8 Ma③)
- TPsb3 Fine- to medium-grained, porphyritic quartz monzodiorite to monzodiorite (▲ 65.1 ± 0.7 Ma③)
- TPsb2 Early, medium-grained monzonite (▲ 66.2 ± 1.7 Ma③)
- TPsb1 Greenish gray, fine-grained pyroxene diorite (▲ 65.6 ± 0.6 Ma③, ▲ 65.5 ± 0.9 Ma③)

Torcaza pluton (Late Cretaceous, ~81-79 Ma)

- LKtp3 Bleached amphibole-rich diorite (▲ 79.4 ± 1.2 Ma①)
- LKtp2 Medium-grained monzonite
- LKtp1 Pyroxene-bearing amphibole monzodiorite (▲ 81.3 ± 1.0 Ma③)

Modern cover and omitted outcrops

Cerro Bayo plutonic complex (Late Cretaceous, ~ 77-72 Ma)

- LKcb9 Late diorite and andesite dykes and sills
- LKcb8 Leucocratic micromonzonite and microquartz monzonite (▲ 73.3 ± 0.8 Ma③ , ▲ 72.2 ± 1.7 Ma③)
- LKcb7 Medium- to coarse-grained biotite-amphibole monzonite (▲ 72.9 ± 0.7 Ma③, ● 66.5 ± 0.7 Ma③)
- LKcb6 Fine- to medium-grained monzonite and quartz monzonite (▲ 74.3 ± 1.3 Ma③, ▲ 74.2 ± 1.1 Ma③)
- LKcb5 Fine- to medium-grained porphyritic monzodiorite
- LKcb4 Olive gray, medium-grained miarolitic diorite
- LKcb3 Fine-to medium-grained diorite
- LKcb2 Gabbro, monzogabbro and diorite (○ 76.9 ± 1.2 Ma②, □ 74.8 ± 2 Ma①, ○ 74.5 ± 1 Ma③, ○ 74 ± 2 Ma②)
- LKcb1 Coarse-grained quartz diorite and quartz monzodiorite

Las Torres igneous complex (Late Cretaceous, ~70-66 Ma)

- LKlt2 Coarse-grained lapilli-tuff, volcanic breccia, volcanic sandstone and coherent andesite (▲ 69.7 ± 1.4 Ma③, ▲67.5 ± 1.0 Ma③, ▲ 66.8 ± 0.9③)
- LKlt1 Monzogabbro, diorite and andesite dykes and sills (▲ 82 ± 4 Ma③)

Figure 3.14 Simplified distributions of Late Cretaceous-lowermost early Paleocene volcanic and intrusive units in La Escondida district.

Table 3.6 Summary of Late Cretaceous-lowermost early Paleocene intrusive units exposed in La Escondida district.

Unit (Abbreviation)	Age	Regional Description Contact relationships and lithology	La Escondida District Contact relationships and lithology	References
Torcaza pluton *(LKtp)*	Late Cretaceous (~81-79 Ma)	A series of medium-sized composite intrusion aligned on the Domeyko Cordillera, ranging from gabbros to porphyritic rhyolitic (e.g. Guacate, Caracoles, Chinchilla, etc), and with ages between 78 and 74 Ma Las Tinajas gabbro and diorite-andesite are 85-75 Ma, and crop out in El Salvador region.	- Has intruded the calcareous and clastic rocks of the El Profeta and Santa Ana Formations. - Mesozonal intrusive complex composed of three main units. (1) amphibole monzodiorite *(LKtp1)*, (2) medium-grained monzonite *(LKtp2)*, and (3) bleached amphibole-rich diorite *(LKtp3)* Calc-silicate metamorphic aureoles in the calcareous country rocks, which host modest polymetallic Cu-Pb-Ag veins.	Cornejo et al. (1993) Mpodozis et al. (1993a) Marinovic et al (1995) Richards et al (2001)
Cerro Bayo plutonic complex *(LKcb)*	Late Cretaceous (~77-72 Ma)		- Has intruded the calcareous and clastic rocks of the El Profeta and Santa Ana Formations - Mesozonal to epizonal, medium-sized sheeted intrusive complex ranging from banded gabbro and diorite, through monzodiorite and quartz diorite, to micromonzonite Late felsic and mafic dykes and sills are present. A total of nine intrusive units are recognized, with marked north-northeast elongation Calc-silicate metasomatic zones are developed in the country rocks, along with limonitic gossans and veins	Cornejo et al (1993) Mpodozis et al (1993a) Marinovic et al. (1995) Richards et al. (2001)
Las Torres igneous complex *(LKlt)*	Late Cretaceous (~70-66 Ma)	There is no other rock unit comparable with the *LKlt* along the Cordillera de Domeyko. In other regions, these packages correlate with: - La Totola Formation, which occurs in the Salar de Atacama Depression and consists of volcanic rocks and associated basaltic-dacitic dykes and granodiorite-diorite intrusives (ca 70-64 Ma) - Cerro Azabache volcanic and intrusive complex (ca 84 Ma) in the Central Depression province, which includes andesitic porphyries that grade into porphyritic diorites, and subordinate lava flows of similar composition.	- Layered volcaniclastic rocks unconformably overlain the Santa Ana red beds Dykes and other apophyses of the complex have intruded the calcareous and clastic rocks of the El Profeta and Santa Ana Formations. - Small-sized, hypabyssal igneous complex composed of two sub-units (1) poorly constrained andesitic lapilli-tuff and subordinated volcanic breccia, flow-banded andesite (lava-dome?) and volcanic sandstone *(LKlt1)*, and (2) a family of dykes and sills of monzogabbro, diorite, diorite and andesite *(LKlt2)*.	Marinovic et al. (1995) Marinovic et al (1996) Mpodozis et al (2005)
Sombrero plutonic complex *(TPsb)*	lowermost early Paleocene (~67-64 Ma)	Numerous intrusive complexes have been recognized in the Domeyko Cordillera (1) Cerro del Quimal monzonite and granodiorites of ca. 66-64 Ma; (2) Cerro Corral de Alambre granodiorite porphyry (ca. 65-61 Ma), which hosts quartz-stockworks and related skarn, and (3) dioritic to monzodioritic stocks of 66-62 Ma, in El Salvador District.	- Intrude the calcareous and clastic rocks of the El Profeta and Santa Ana Formations and Las Torres Igneous Complex - Small-sized, zoned intrusive complex composed of eight units which varies from diorite, through monzonite, to granodiorite and granite porphyry with advanced argillic alteration.	Cornejo et al (1993) Cornejo and Mpodozis (1995) Mpodozis et al. (2005)

with limonitic patches, is characterised by bleached exposures. The contacts with other intrusive rocks are all ambiguous. This unit has been dated in the current study at 79.4 ± 1.2 Ma by LA-ICP-MS U-Pb analysis of zircons (Table 3.7; Appendix 6).

3.3.2 Cerro Bayo Plutonic Complex *(LKcb)*

The Cerro Bayo plutonic complex (~15 km^2) is a multi-stage and roughly tabular complex exposed in the Cerro Bayo (Figure 3.14; Table 3.6). It appears to have propagated outward as sheeted bodies oriented along north-northeast trends. There are also numerous plugs. Compositionally, the complex ranges from gabbro to micromonzonite, the latter being the dominant facies (Figure 3.15b). Several cogenetic felsic and mafic sills are thickened in the hinge zones of folds in the Jurassic sedimentary rocks (Figures 3.16a and b; Chapter 4). The mafic sheets typically have marginal reaction rims and fine-grained (chilled?) margins against the earlier-formed intrusive phases. Narrow aureoles of skarn and gossanous veins are spatially associated with the largest phases of the Cerro Bayo plutonic complex (Chapter 5). Based on field mapping and geochronological data, the Cerro Bayo complex is divided into at least nine intrusive units (Table 3.6). The older units are more mafic than the younger, felsic intrusions. Ten LA-ICP-MS U-Pb zircon ages for Cerro Bayo plutonic complex have established a crystallisation age between 77 and 72 Ma (Table 3.7; Appendix 6).

3.3.2.1 Coarse-grained Quartz Diorite and Quartz Monzodiorite *(LKcb1)*

These are very small bodies (<0.1 km^2; Figure 3.14) of hypidiomorphic-granular and intergranular-textured hornblende diorite and quartz monzodiorite that have been locally cataclastised and metamorphosed by the *LKcb2* sub-unit (Figure 3.17a). Contact relationships are strongly obscured, with intense recrystallisation observed in thin sections. The intense retexturing suggests that *LKcb1* predates the 77 Ma *LKcb2* sub-unit (Richards et al., 2001). Rock samples of *LKcb1* collected during the current study proved unsuitable for ^{40}Ar-^{39}Ar dating (Appendix 6).

3.3.2.2 Gabbro, Monzogabbro and Diorite *(LKcb2)*

The *LKcb2* sub-unit includes a series of NNE-elongated, tabular-shaped (Figure 3.14) and compositionally banded gabbro, monzogabbro and diorite bodies (Figure 3.17b), which have been intruded by abundant aplite and micromonzonite of the *LKcb8* sub-unit. Mafic enclaves and magmatic layering are commonly observed (Chapter 4). Several radiometric K-Ar and ^{40}Ar-^{39}Ar ages (Marinovic et al., 1995; Richards et al., 2001; this study), indicate

crystallization ages of 77 to 74 Ma for the *LKcb2* sub-unit (Table 3.7; Appendix 6).

3.3.2.3 Fine- to Medium-grained Diorite *(LKcb3)* and Olive Grey Miarolitic Diorite *(LKcb4)*

These dykes and clusters of thin sills are largely concordant with the Jurassic country rocks (Figure 3.14). They can reach 0.5-15 m wide and a few tens of meters in length. Hand specimens consists of randomly oriented plagioclase, biotite and interstitial hornblende. Locally these rocks contain miarolites (< 6-8 mm) partially filled by quartz, calcite and rare epidote. Based on the close occurrence and similar textural attributes, they are interpreted to be coeval with the gabbros of *LKcb2*.

3.3.2.4 Fine- to Medium-grained Monzodiorite *(LKcb5)*

This intrusive phase occurs in two main north-northeast trending belts that are more than 6 km long (Figure 3.14). *LKcb5* is the largest intermediate composition unit of the Cerro Bayo plutonic complex. It broadly surrounds and has intruded the *LKcb2* gabbro bodies. In outcrop, the biotite-bearing amphibole-phyric monzodiorite is characteristically light grey coloured, texturally homogenous and fine-grained. This unit is cut by fine-grained monzonite and quartz-monzonite of the *LKcb6* sub-unit (Figure 3.18a). The age of the *LKcb5* sub-unit is constrained to approximately 74 Ma, based on the intrusive contact with *LKcb2* (ca. 77-74 Ma) and truncation by *LKcb6* (ca. 74 Ma).

3.3.2.5 Fine- to Medium-grained Monzonite and Quartz Monzonite *(LKcb6)*

These rocks are volumetrically the most abundant facies in the Cerro Bayo complex (Figure 3.14), and postdate all of the previously described rock units. The outcrops are characteristically reddish and yellowish brown, showing abundant syn-plutonic aplitic dykes and enclaves of dioritic composition. Hand specimens are porphyritic- and glomeroporphyritic-textured, with few phenocrysts of plagioclase set in an aplitic quartz+feldspar-rich groundmass. Two samples of *LKcb6* have LA-ICP-MS U-Pb zircon ages of 74.3 ± 1.3 Ma and 74.2 ± 1.1 Ma (Table 3.7; Appendix 6).

3.3.2.6 Medium- to Coarse-grained Biotite-amphibole Monzonite *(LKcb7)*

This satellite plug (<0.1 km^2) has been emplaced in the Santa Ana sandstones and the *LKcb5* sub-unit (Figure 3.14). It is the coarsest-grained felsic phase of the complex. Petrographically, it is a medium-grained amphibole-biotite monzonite. A 66.5 ± 0.7 Ma $^{40}Ar/^{39}Ar$ amphibole age and an LA-ICP-MS U-Pb zircon date of 72.9 ± 0.7 Ma have

been obtained from *LKcb 7* during the present study (Table 3.7; Appendix 6).

3.3.2.7 Leucocratic Micromonzonite and Microquartz Monzonite *(LKcb8)*

These occur as a broadly distributed swarm of sill and dykes that usually are less than 5 m thick, but locally can attain thicknesses of up to 20-30 m (Figure 3.14). Texturally, *LKcb8* intrusives are very heterogeneous, ranging from micro-aplitic and vesicular felsite (vesicles <1 cm diameter), to a flow-banded, porphyritic rhyolite. Richards et al. (2001) interpreted these rocks to be domes and pyroclastic deposits of Triassic-Late Jurassic El Profeta Formation. However, their field occurrence and textural attributes, as well as two LA-ICP-MS U-Pb zircon ages of 73.3 ± 0.8 Ma and 72.2 ± 1.7 Ma (Table 3.7; Appendix 6), all point to an intrusive origin, and a genetic link with the Late Cretaceous Cerro Bayo complex.

3.3.2.8 Late Diorite and Andesite Dykes *(LKcb9)*

Minor dykes crop out as thin, dark-greenish grey rocks that are less than 0.5 m thick (Figure 3.14). They have been emplaced chiefly in the *LKcb8*, near the summit of Bayo Hill. Petrographically they are fine-grained amphibole-rich diorite and andesite, along with minor coarse-grained diorite with amphibole phenocrysts up to 1 cm long. Based on the close spatial occurrence of the dykes with intermediate to felsic facies of the Cerro Bayo plutonic complex, *LKcb9* dykes have been assigned to the Late Cretaceous.

3.3.3 Las Torres Igneous Complex *(LKlt)*

Las Torres igneous complex consists of poorly exposed volcanic breccia, lapilli-tuff, lithic-crystal tuff, coherent andesite and calcareous lithic-vitric sandstones numerous coeval to slightly older shallow-level intrusions ranging from monzogabbro, through diorite, to andesite in composition (Figure 3.14; Table 3.6). The unit is poorly exposed between the Alicia mine and the paved road to the Escondida and Zaldivar mines (Appendix 1A), where their steeply dipping (70°-80°) volcaniclastic strata cover unconformably folded calcareous sandstones of the Santa Ana Santa Formation (Late Jurassic-Neocomian). Dykes and small apophyses of Las Torres complex have intruded the El Profeta and Santa Ana Formations. The relative chronology of the diverse volcanic and intrusive facies of Las Torres igneous complex has proven difficult to establish due to poor exposures and contacts obscured by larger Early Tertiary intrusions. The present study divides the unit into two informal sub-units, which are described below.

3.3.3.1 Monzogabbro, Diorite and Andesite Dykes and Sills *(LKlt1)*

The *LKlt1* sub-unit is composed of four main families of intrusions: (1) dark greenish grey coloured and fine-grained, biotite-pyroxene-phyric diorite, which grades to fine-grained, trachytic-textured andesite; (2) light brown coloured, fine-grained and amygdaloidal, pilotaxitic-textured amphibole-rich andesite (Figure 3.18b), (3) coarse-grained, amphibole-phyric andesite (Figures 3.19a); and (4) subordinate amphibole-pyroxene gabbro. They occur in clusters, as sills and dyke swarms, and also as irregular plugs. Correlation of these bodies with other units exposed in the area has been difficult to establish due to the poor exposures and lack of visible contacts. However, chilled and sharp margins have been observed locally on road cuts. North-northeast-oriented dykes occur as tabular bodies 0.3-4 m wide. Field observations indicate that the light brown fine-grained andesite and dark greenish grey diorite bodies have intruded the gabbros. Bleaching and silicic-carbonatic alteration are characteristic of the andesitic intrusive phase. An LA-ICP-MS U-Pb zircon age of 82 ± 4 Ma has been established for a light brown amphibole-rich andesite dyke that intruded the Late Jurassic-Neocomian Santa Ana Formation (Table 3.7; Appendix 6). However, correlation with the main intrusive event of the *LKlt2* sub-unit is only tentative due to two reasons. Firstly, the dykes have not intruded the bedded volcaniclastic beds of the ca. 70-66 Ma *LKlt2* sub-unit and can therefore be somewhat older. Second, the LA-ICP-MS U-Pb zircon age of 82 ± 4 Ma for an early andesite dyke indicate a significantly older age of ca. 10-8 m.y., although the age may be suspect due to the large amount of inherited zircons (Appendix 6). Additional radiometric dating is required in order to determinate the temporal relationships within the spectrum of small intrusions from the *LKlt2* sub-unit.

3.3.3.2 Volcaniclastic Breccia, Lapilli-tuff, Lithic-crystal Tuff, Coherent Andesite and Volcaniclastic Sandstone *(LKlt2)*

The dark green and crudely stratified *LKlt2* sub-unit is exposed in two isolated outcrops that are only a few meters long (Figure 3.14). Thick-bedded volcaniclastic rocks have not been seen to have been intruded in the field by the abundant monzogabbro to diorite-andesite dykes swarms of the *LKlt1* sub-unit (Figure 3.19b). The dominant lithologies of *LKlt2* are lapilli-tuff and volcaniclastic breccia (Figure 3.20a), with abundant lithic clasts, subordinate crystals (mainly plagioclase and quartz) and pumiceous fragments of andesitic to dacitic composition. Phenocrysts of plagioclase, amphibole and clinopyroxene are intensely altered to albite, chlorite, calcite, epidote, opaque minerals and clays. Suboriented plagioclase and ferromagnesian microlites, accompanied by vitric fragments, are

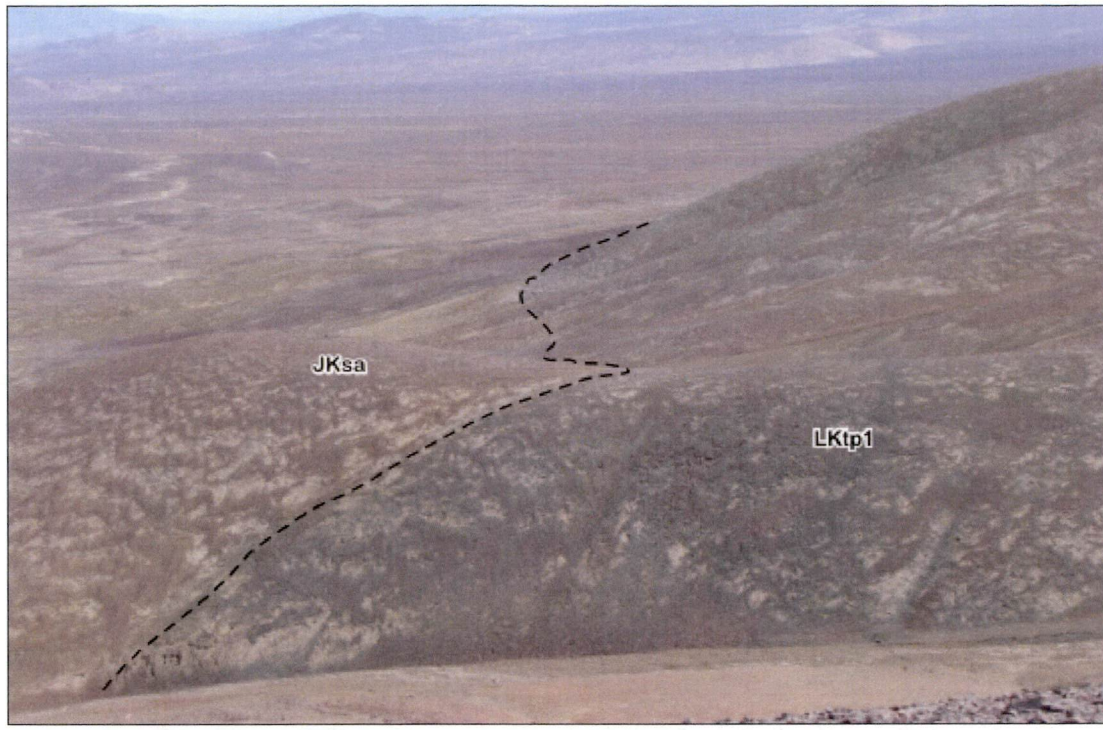

Figure 3.15a General view (looking northwest) of the early monzodioritic sub-unit *(LKtp1)* of the Torcaza pluton (ca. 81-79 Ma) that has intruded red beds of the Santa Ana Formation (Late Jurassic-Neocomian). West of Cerro Rincones sector (7,323,200m N; 575,200n E).

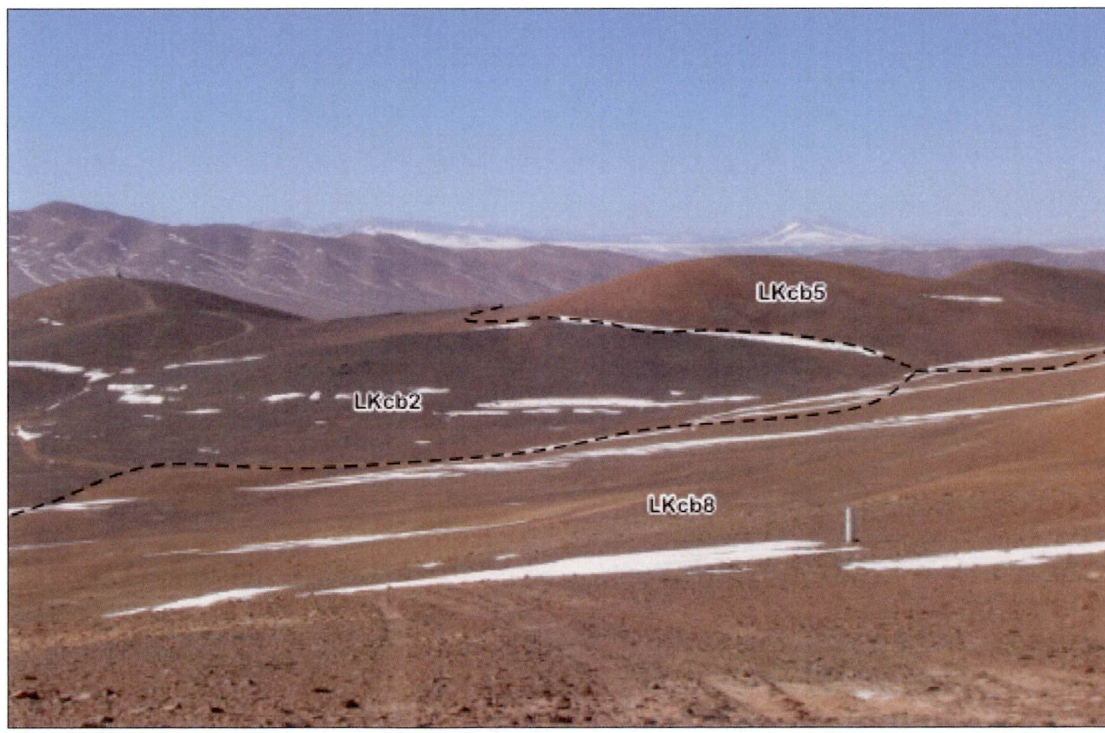

Figure 3.15b General view (looking southeast) of the Cerro Bayo plutonic complex (*LKcb*; ca. 77-72 Ma) including early gabbros and monzogabbros (*LKcb2*; ca. 77-74 Ma), fine-grained monzodiorites (*Kcb5*; ca. 74 Ma) and later microquartz monzonites (*LKcb8*; ca. 73-72 Ma). Cerro Bayo sector (7,309,000m N; 487,000m E).

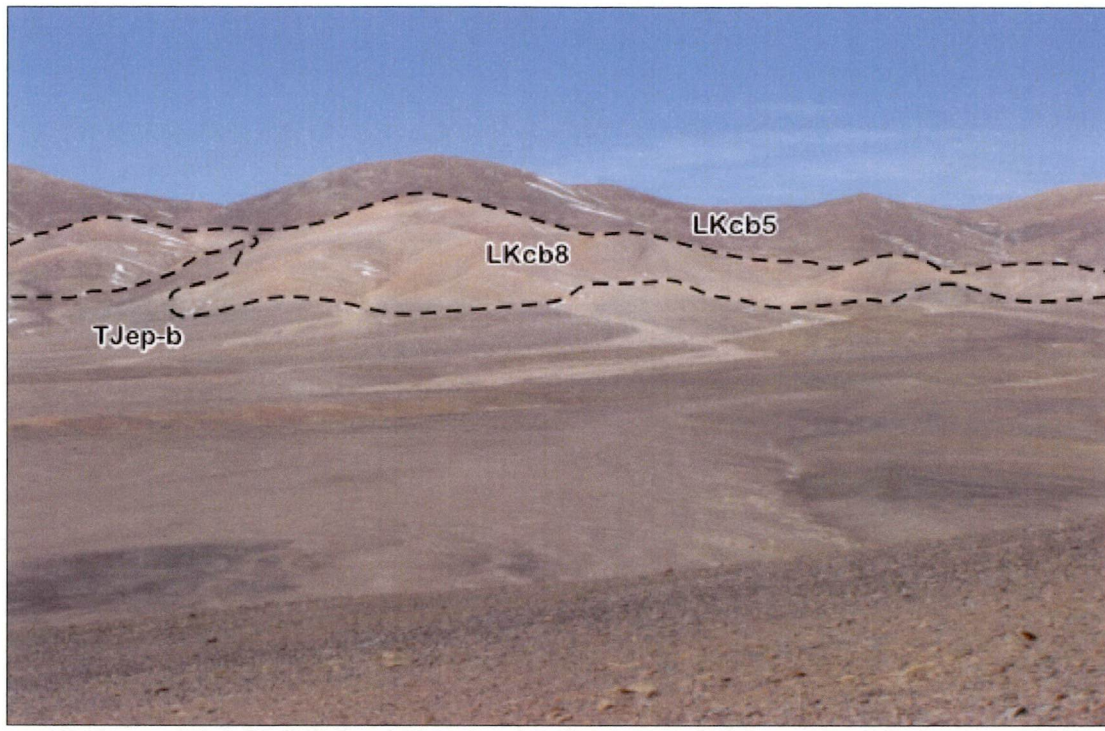

Figure 3.16a General view (looking east) of leucoquartz monzonite sills (*LKcb8*; ca 73-72 Ma) and monzodiorites (*LKcb5*; ca. 74 Ma) of the Cerro Bayo plutonic complex within the folded calcareous beds *(TJep-b)* of El Profeta Formation (Late Triassic-Kimmeridgian). Cerro Bayo sector (7,311,100m N; 486,700n E).

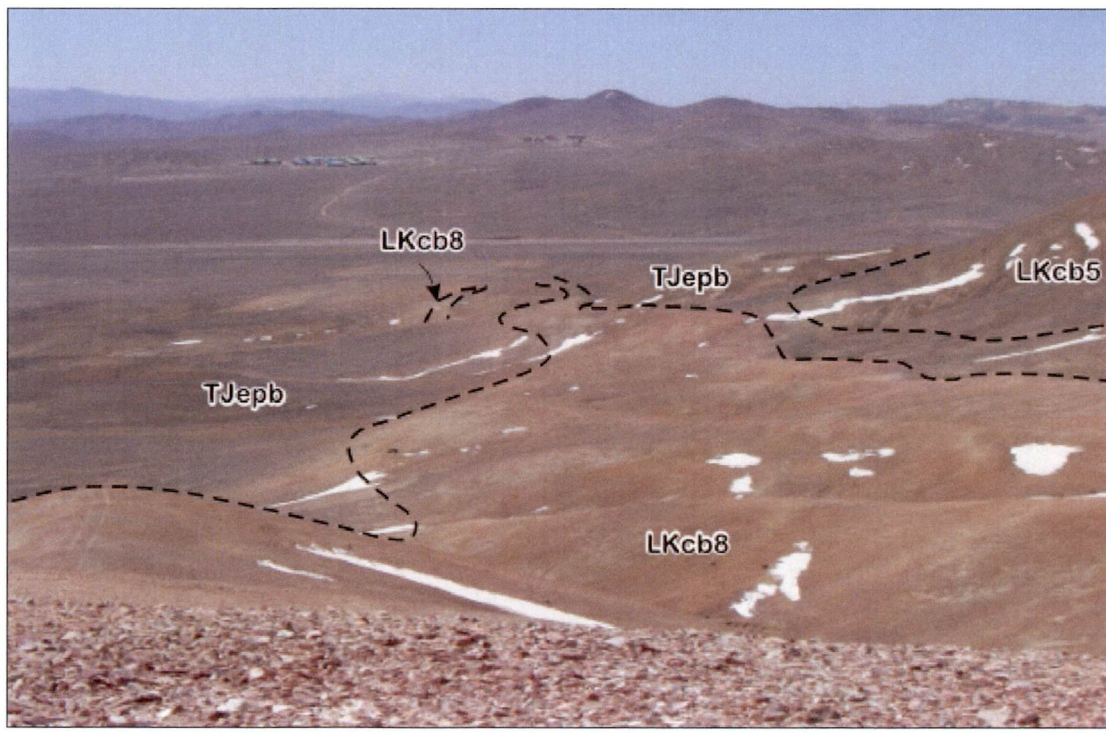

Figure 3.16b General view (looking north) of the leucoquartz monzonite sills (*LKcb8*; ca. 73-72 Ma) concordantly emplaced in the Jurassic calcareous beds *(TJep-b)* of El Profeta Formation. Note the monzodiorites (*LKcb5*; ca. 75 Ma) to the east. Cerro Bayo sector (7,309,700m N; 486,800m E).

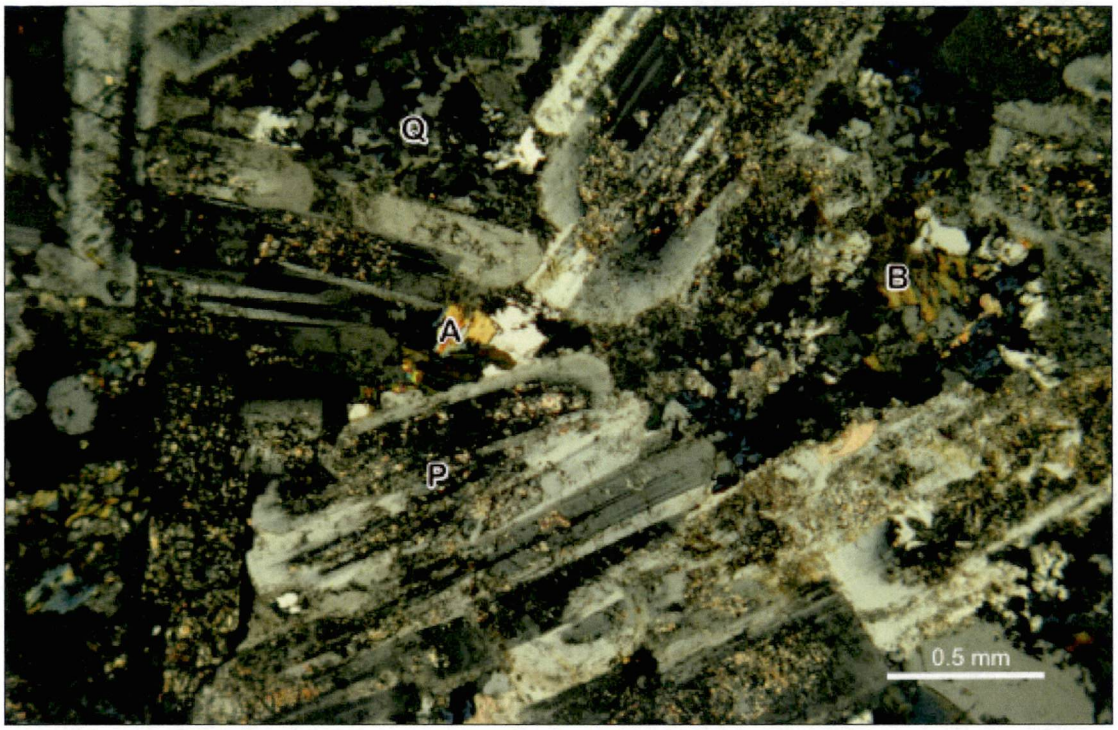

Figure 3.17a Photomicrograph (crossed nicols) of a medium-grained quartz diorite sub-unit *(LKcb1)* from the Cerro Bayo plutonic complex (ca. 77-72 Ma). Note the brittle comminution, grain size reduction and recrystallized hypidiomorphic assemblage of zoned plagioclase (P) replaced by sericite and clays, interstitial amphibole (A) and biotite (B) altered to chlorite, along with abundant polycrystalline quartz (Q). Sample ESC-2 (7,309,707m; 487,863m E).

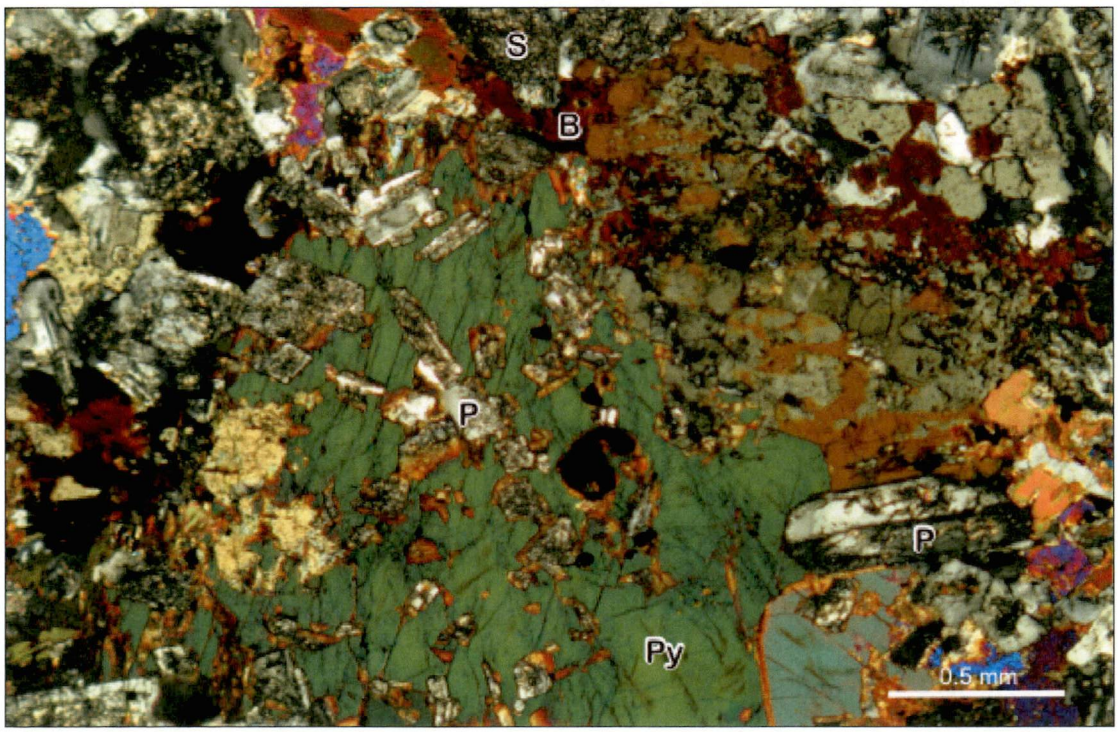

Figure 3.17b Photomicrograph (crossed nicols) of a coarse-grained monzogabbro sub-unit *(LKcb2)* from the Cerro Bayo plutonic complex (ca. 77-72 Ma). Note the hypidiomorphic assemblage of augitic pyroxene (**Py**), locally as large poykilitic crystals, abundant biotite (**B**), plagioclase (**P**) replaced by sericite and clays, and sphene (**S**) as accessory phases. Sample ESC-3 (7,309,584m N; 488,017m E).

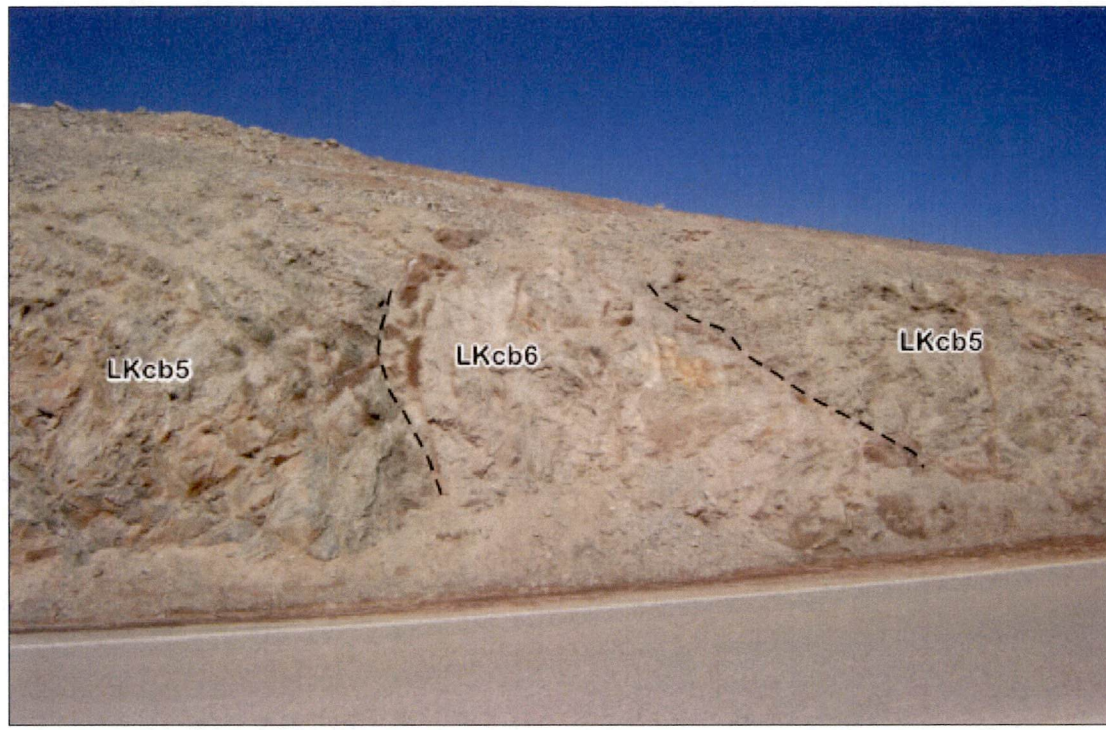

Figure 3.18a Faulted intrusive contact between monzonite (*LKcb6*; ca. 74 Ma) and the slightly older monzodiorite (*LKcb5*; ca. 74 Ma) of the Cerro Bayo plutonic complex. Paved road to the 5000 Camp, La Escondida operation (7,313,500m N; 488,900m E).

Figure 3.18b Late light brown fine-grained andesite dyke *(LKlt1)* of Las Torres igneous complex (70-66 Ma), with somewhat flatted amygdules oriented parallel to walls of the intrusive. Paved road to La Escondida operation (7,322,100m N; 476,400m E).

Figure 3.19a Hand specimen of a dark green coloured and strongly porphyritic andesite dyke *(LKlt1)* of Las Torres igneous complex (70-66 Ma), with characteristic large phenocrysts of amphibole and plagioclase. This family of dykes are clearly intruded by the light brown fine-grained andesite dykes observed in Figure 3.19a. West of Cerro Rincones (7,323,000m N; 276,300m E).

Figure 3.19b Crudely stratified lapilli-tuff and volcaniclastic breccia *(LKlt2)* of Las Torres igneous complex (ca. 70-66 Ma). A U-Pb zircon age of 66.8 ± 0.9 Ma has been obtained from these outcrops. West of Cerro Rincones (7,332,900m N; 476,050m E).

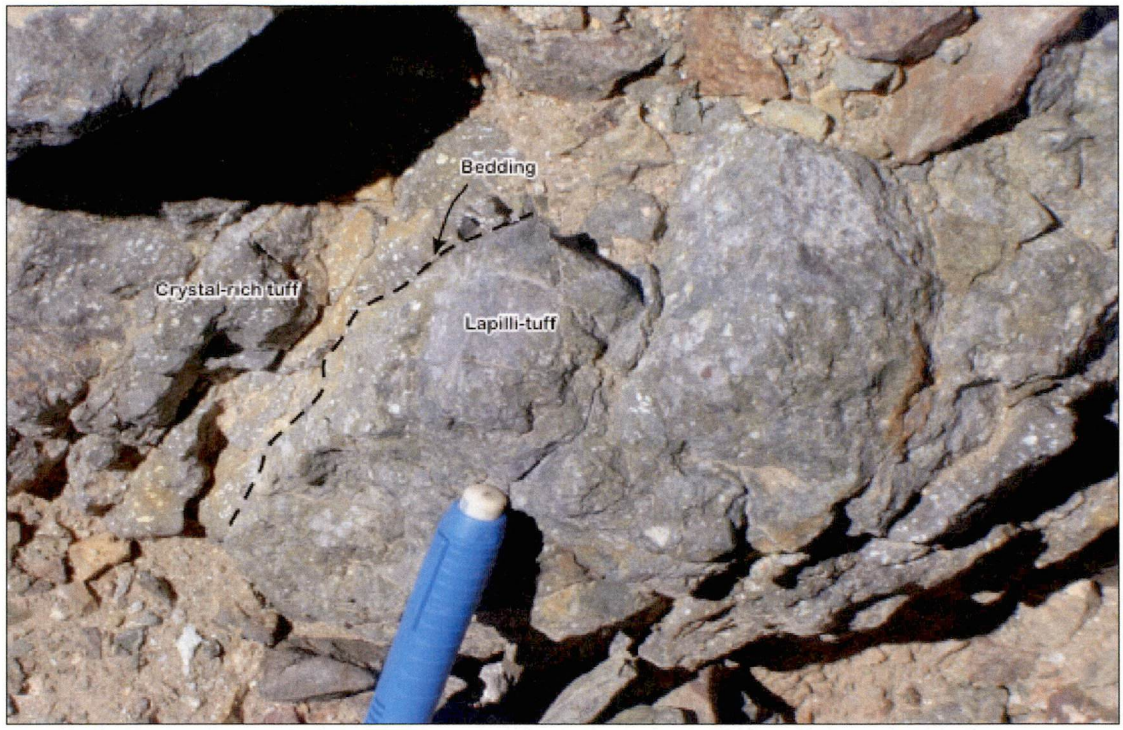

Figure 3.20a Lapilli-tuff with common angular to subrounded lithic clasts. *(LKlt2)* of Las Torres igneous complex (ca. 70-66 Ma) Note the abrupt change from the fragmental rock to a massive crystal-rich tuff. West of Cerro Rincones (7,332,900m N and 476,050m E).

Figure 3.20b Flow-foliated andesite *(LKlt2)* of Las Torres igneous complex (ca. 70-66 Ma), which contain abundant xenoliths of similar composition. A U-Pb zircon age of 67.5 ± 1.4 Ma has been obtained from this outcrop. Note the pebble dyke cutting the volcanic rocks. West of Cerro Rincones (7,332,900m N; 476,050m E).

embedded in a dusty, devitrified and microcrystalline matrix. Flow-banded and coherent, vesicle-rich andesitic lava flows are also observed to have been locally intruded by pebble dykes less than 15 cm thick (Figures 3.20b). Medium-to coarse-grained lithic sandstones are cemented by carbonates. Three rock samples from the *LKlt1* sub-unit have been dated during the present study using the LA-ICP-MS U-Pb U-Pb zircon method. They have determined a narrow age range of ca. 70-66 Ma, uppermost Late Cretaceous (Table 3.7; Appendix 6), for these layered volcaniclastic rocks.

3.3.3.3 Age and Depositional Setting

Las Torres igneous complex is the product of comparatively minor Late Cretaceous volcanic and sub-volcanic andesitic activity in La Escondida district. The LA-ICP-MS U-Pb zircon ages in coherent andesites and pyroclastic rocks from the *LKlt1* sub-unit support an age range of ca. 70-66 Ma (Table 3.7; Figure 3.22). The 82 ± 4 Ma andesite dyke (LA-ICP-MS U- Pb zircon method) tentatively assigned to *LKlt2* determines the occurrence of an early and discrete andesitic intrusive event, which does not correlate with the most probable range of intrusion ages of *LKlt2* sub-unit, around 66-65 Ma. Based on contact relationships, the bulk of *LKlt2* should be contemporaneous and/or slightly younger than *LKlt1*.

The attributes of the volcaniclastic rocks are consistent with a terrestrial, proximal alluvial fan depositional environment (i.e., Suthren, 1985; McPhie et al., 1993; Collinson, 1996). An intramontane, restricted tectono-volcanic depression is considered the most probable sedimentary setting, where subaqueous and subaerial mass flow and pyroclastic flow deposits were deposited together with minor lava flows. Hypabyssal andesite and diorite dyke swarms may have been volcanic feeders. These ideas remain highly speculative at this time, and more detailed facies analysis is required to satisfactorily understanding the paleoenvironment depositional setting of Las Torres complex.

3.3.4 Sombrero Plutonic Complex *(TPsb)*

The Sombrero plutonic complex crops out along a roughly north-northeast trending body, covering an area less than 2.5 km^2 (Figure 3.14; Table 3.6). It has intruded the calcareous sandstones of the Santa Ana Formation, and volcanic rocks of Las Torres igneous complex. It has been intruded by the 43-41 Ma Cerro Rincones plutonic complex at its northern end (Appendix 1A). The plutonic complex is composed of intermediate and felsic rocks, which appear to have an asymmetrical arrangement (Figure 3.14) rather

than the symmetric zoning that might be expected in a compositionally zoned pluton. Contacts between all major intrusive phases are either not exposed, or are partly obscured by felsic dykes (Figures 3.21a and b). Significant domains of skarn-altered calcareous rocks are related to contacts with the granodiorite and monzodiorite intrusive phases (Chapter 5). Five LA-ICP-MS U-Pb ages have been determined for diverse phases of the Sombrero Plutonic Complex, which have established an emplacement age between 67 and 64 Ma (Table 3.7; Appendix 6).

3.3.4.1 Fine-grained Pyroxene Diorite *(TPsb1)*

This narrow body (< 6 km^2) has a marked north-northeast elongation (Figure 3.14). Hand specimen of a typical diorite from *TPsb1* is a dark brown coloured and slightly porphyritic, fine-grained rock. It has been strongly hornfelsed adjacent to the contact with monzodiorite and diorite of the ca. 43-41 Ma Cerro Rincones plutonic complex. A metamorphic association of biotite, pyroxene, orthoclase, polycrystalline quartz and magnetite, along with minor epidote, has been observed in thin sections. New LA-ICP-MS U-Pb zircon ages of 65.6 ± 0.6 and 65.5 ± 0.9 Ma have been obtained for *TPsb1* (Table 3.7; Appendix 6).

3.3.4.2 Medium-grained quartz monzonite *(TPsb2)*

This intrusive phase occurs as metre-wide rims around pyroxene quartz monozodiorite from the *TPsb3* sub-unit (Figure 3.14). In outcrops, a biotite-amphibole-pyroxene quartz monzonite from *TPSb2* is dark brown coloured, characteristically fractured and moderately hornfelsed. The later is manifested by silicification, weak recrystallization, the occurrence of magnetite crystals and laths of neomorphic biotite. This unit has been dated during the present study at 66.2 ± 1.7 Ma by the LA-ICP-MS U-Pb zircon method (Table 3.7; Appendix 6).

3.3.4.3 Fine- to Medium-grained, Pyroxene-phyric Quartz Monzodiorite *(TPsb3)*

This is the principal intrusive phase of the complex, occupying a surface area of nearly 0.8 km^2 (Figure 3.14). Petrographically it is a fine- to medium-grained, porphyritic amphibole-biotite-bearing pyroxene quartz monzodiorite. Close to its margins, the quartz monzodiorite has been weakly hornfelsed by intrusion of a coarse-grained granodiorite from *TPsb6*. The age of the *TPsb3* sub-unit is constrained by a LA-ICP-MS U-Pb zircon age of 65.1 ± 0.7 Ma (Table 3.7; Appendix 6).

3.3.4.4 Pyroxene-amphibole-phyric Monzogranite *(TPsb4)* and Monzonite and Quartz Monzonite (*TPsb5)*

These units are minor intrusive phases of Cerro Sombrero complex and are characterised by marked textural and grain-size changes. Their contacts with other rocks are poorly exposed in the field, but a series of roughly northeast-trending tabular bodies have detected. In some places, they are transitional and/or gradational to adjacent units. Closely-spaced anastomosed fracture cleavage is well-developed locally in some outcrops (Chapter 4). The 66.2 ± 0.8 Ma LA-ICP-MS U-Pb zircon age obtained for a leucomonzogranite from *TPsb4* implies an intrusion age similar to *TPsb3* (Table 3.7; Appendix 6).

3.3.4.5 Coarse-grained Granodiorite *(TPsb6)* and Granite Porphyry *(TPsb7)*

These rocks constitute a texturally and compositionally zoned stock (Figure 3.14), which varies from a marginal pale pink coarse-grained amphibole granodiorite *(TPsb6)* to a light reddish and strongly porphyritic core of granitic to granodioritic composition *(TPsb7)*. The latter facies contain considerable hydrothermal alteration (Appendix 3; Chapter 5). Common microdiorite enclaves of a few centimetres diameter are observed in the granodiorites. The age of a granodiorite of the *TPsb6* sub-unit is given by a LA-ICP-MS U-Pb zircon date of 64.0 ± 0.7 Ma (Table 3.7; Appendix 6), coinciding with its intrusive contacts against *TPsb3*.

3.3.4.6 Aplitic Micromonzonite, Microgranite and Dacite Dykes *(TPsb8)*

This swarm of felsic dykes has a marked north-northeast strike over an area more than 800 km long (Figure 3.21b). No detailed work has been done on this unit, and contact relationships with surrounding units are rarely exposed. They are commonly light brown to reddish white, fine-grained equigranular to weakly inequigranular rocks that are stained by limonites. Locally they contain fine-grained pyrite crystals that have been partially replaced by limonites. The dykes are assigned to the Sombrero plutonic complex based on their close spatial associations with other intrusive phases of the complex. However, it is very difficult in some outcrops to separate these dykes from other family of dacite dykes attributed to the *LKlt2* sub-unit of Las Torres igneous complex.

3.3.5 Geological Summary of Late Cretaceous-Early Paleocene

Several regional studies have proposed that the Domeyko Cordillera has been a positive feature within a contractional tectonic regime since the Late Cretaceous, because the

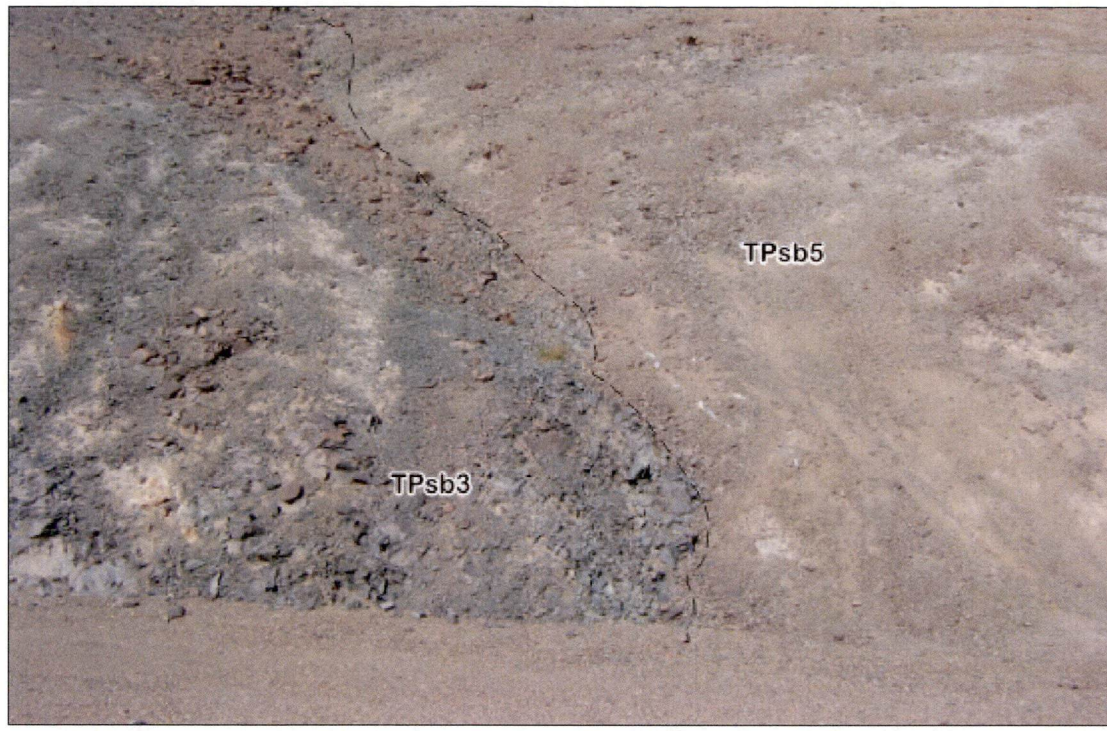

Figure 3.21a Poorly exposed contact between metamorphosed quartz monzodiorite (*TPsb3*; ca. 66-65 Ma) and monzonite (*TPsb5*; ca. 66 Ma) of the Sombrero intrusive complex (*TPsb*; ca. 67-64 Ma). Quebrada Sombrero sector (7,319,600m N; 476,700m E).

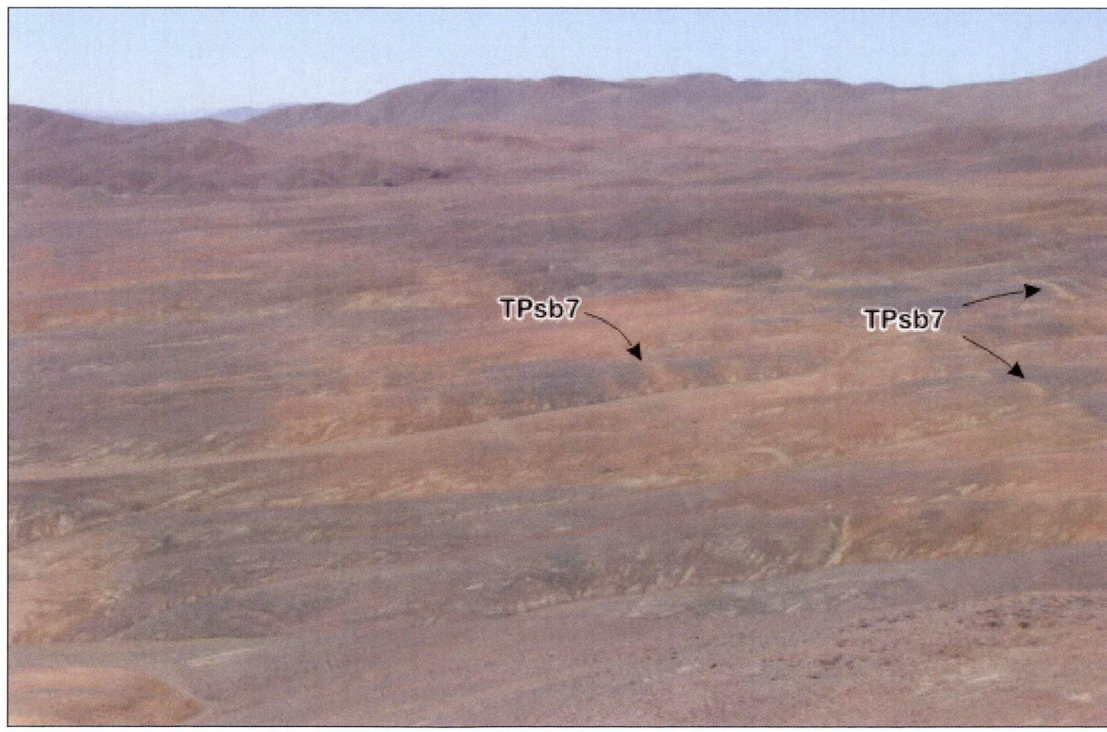

Figure 3.21b General view (looking north) of aplitic dykes *(TPsb7)*, which have cut the older sub-units of the Sombrero intrusive complex (*TPsb*; ca. 67-64 Ma). Sombrero hills (7,318,200m N; 476,200m E).

Table 3.7 Radiometric ages for Late Cretaceous-early Paleocene rock units in La Escondida district and adjacent sectors.

Sample	Rock/Sub-Unit	Method (material)	Age & Error (Ma, 2 σ)	Source of Data (*)
Torcaza pluton (LKtp)				
ESC-42	Monzodiorite/*LKtp1*	U-Pb (zircon)	81.3 ± 1.0	3
ESC-35	Diorite/*LKtp3*	U-Pb (zircon)	79.4 ± 1.2	3
Cerro Bayo plutonic complex *(LKcb)*				
REG-11	Gabbro/*LKcb2*	K-Ar (biotite)	74.8 ± 2	1
IM-158	Gabbro/*LKcb2*	$^{40}Ar/^{39}Ar$ (amphibole)	76.9 ± 1 2	2
IM-159	Gabbro/*LKcb2*	$^{40}Ar/^{39}Ar$ (amphibole)	74.0 ± 2.0	2
ESC-3	Monzogabbro/*LKcb2*	$^{40}Ar/^{39}Ar$ (amphibole)	74.5 ± 1	3
ESC-5	Monzonite/*LKcb6*	U-Pb (zircon)	74 3 ± 1.3	3
ESC-12	Quartz monzonite /*LKcb6*	U-Pb (zircon)	74.2 ± 1.1	3
ESC-24	Monzonite/*LKcb7*	U-Pb (zircon)	72.9 ± 0.7	3
ESC-24	Monzonite/*LKcb7*	$^{40}Ar/^{39}Ar$ (hornblende)	66 5 ± 0.7	3
ESC-4	Microquartz monzonite/*LKcb8*	U-Pb (zircon)	73.3 ± 0.8	3
ESC-11	Microquartz monzonite/*LKcb8*	U-Pb (zircon)	72.2 ±. 1.7	3
Las Torres igneous complex *(LKlt)*				
ESC-19	Andesite/*LKlt2*	U-Pb (zircon)	69.7 ± 1.4	3
ESC-54	Andesite/*LKlt2*	U-Pb (zircon)	67.5 ± 1.0	3
ESC-53	Lapilli tuff/*LKlt2*	U-Pb (zircon)	66.8 ± 0.9	3
ESC-22	Andesite dyke/*LKlt1*	U-Pb (zircon)	82 ± 4	3
Sombrero plutonic complex *(EPsb)*				
ESC-44	Pyroxene-amphibole diorite/*TPsb1*	U-Pb (zircon	65.6 ± 0.6	3
ESC-41	Pyroxene-amphibole diorite/*TPsb1*	U-Pb (zircon)	65.5 ± 0.9	3
ESC-40	Pyroxene-hornblende monzonite/*TPsb2*	U-Pb (zircon)	66.2 ± 1.7	3
ESC-16	Quartz monzodiorite /*TPsb3*	U-Pb (zircon)	65.1 ± 0.7	3
ESC-20	Monzogranite/*TPsb4*	U-Pb (zircon)	66 2 ± 0.8	3
ESC-17	Granodiorite/*TPsb6*	U-Pb (zircon)	64.0 ± 0.7	3

(*) Source of data: (1) Maksaev et al. (1991) and Marinovic et al. (1995); (2) Richards et al. (2001); (3) this study. Abbreviations: *LKtp1* = Pyroxene-bearing amphibole monzodiorite; *LKtp3* = Bleached amphibole-rich diorite; *LKcb2* = Gabbro, monzogabbro and diorite, *LKcb6* = Fine- to medium-grained monzonite and quartz monzonite; *LKcb7* = Medium- to coarse-grained biotite-amphibole monzonite; *LKcb8* = Leucocratic micromonzonite and microquartz monzonite; *LKlt1* = Volcaniclastic breccia, lapilli-tuff, lithic-crystal tuff, coherent andesite and volcaniclastic sandstone; *LKlt2* = Monzogabbro, diorite and andesite dykes and sills; *TPsb1* = Fine-grained pyroxene diorite; *TPsb2* = Medium-grained quartz monzonite; *TPsb3* = Fine- to medium-grained, pyroxene-phyric quartz monzodiorite; *TPsb4* = Pyroxene-amphibole-phyric monzogranite; *TPsb6* = Coarse-grained granodiorite.

lowermost Late Cretaceous Peruvian deformation phase and other Tertiary orogenies have deformed the Paleozoic basement and the Mesozoic sedimentary cover (Coira et al.,1982; Mpodozis and Ramos, 1989; Reutter et al., 1991; Mpodozis et al., 1993a; Mpodozis et al., 2005). A magmatic gap occurred along the axis of the proto-Domeyko Cordillera between 100 and 80 Ma, whereas volumetrically important volcanism and sedimentation occurred during this period within a series of north-northeast-oriented tectono-volcanic basins to the west (i.e., Quebrada Mala and Llanta Formations, Marinovic et al., 1996; Cornejo and Mpodozis, 1996; Mpodozis et al., 2005; Figure 3.23).

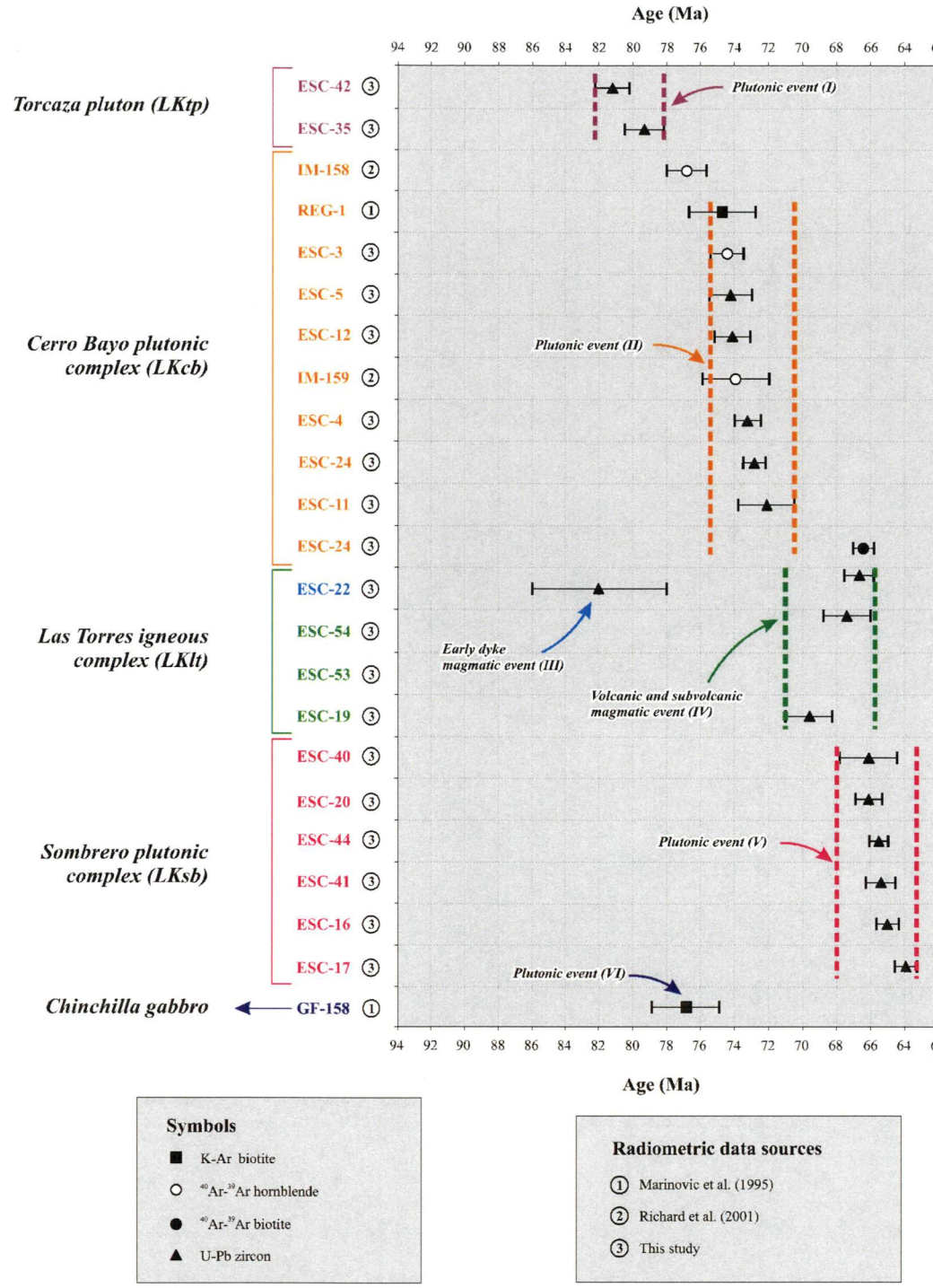

Figure 3.22 Age distribution for Late Cretaceous-lowermost early Paleocene igneous units in La Escondida district and adjacent sectors. Analytical details provided in Appendix 6.

Less significant alkaline volcanism and plutonism started at ca. 80 Ma to the east of the proto-Domeyko Cordillera (i.e., Cerro Quimal gabbros and La Totola Formation; Mpodozis et al., 2005), associated with the Purilactic Basin (Figure 3.24). Synchronous with this magmatism was the emplacement of the Torcaza pluton at 81-79 Ma in La Escondida district, followed by the Cerro Bayo intrusive complex from ca. 77 to 72 Ma.

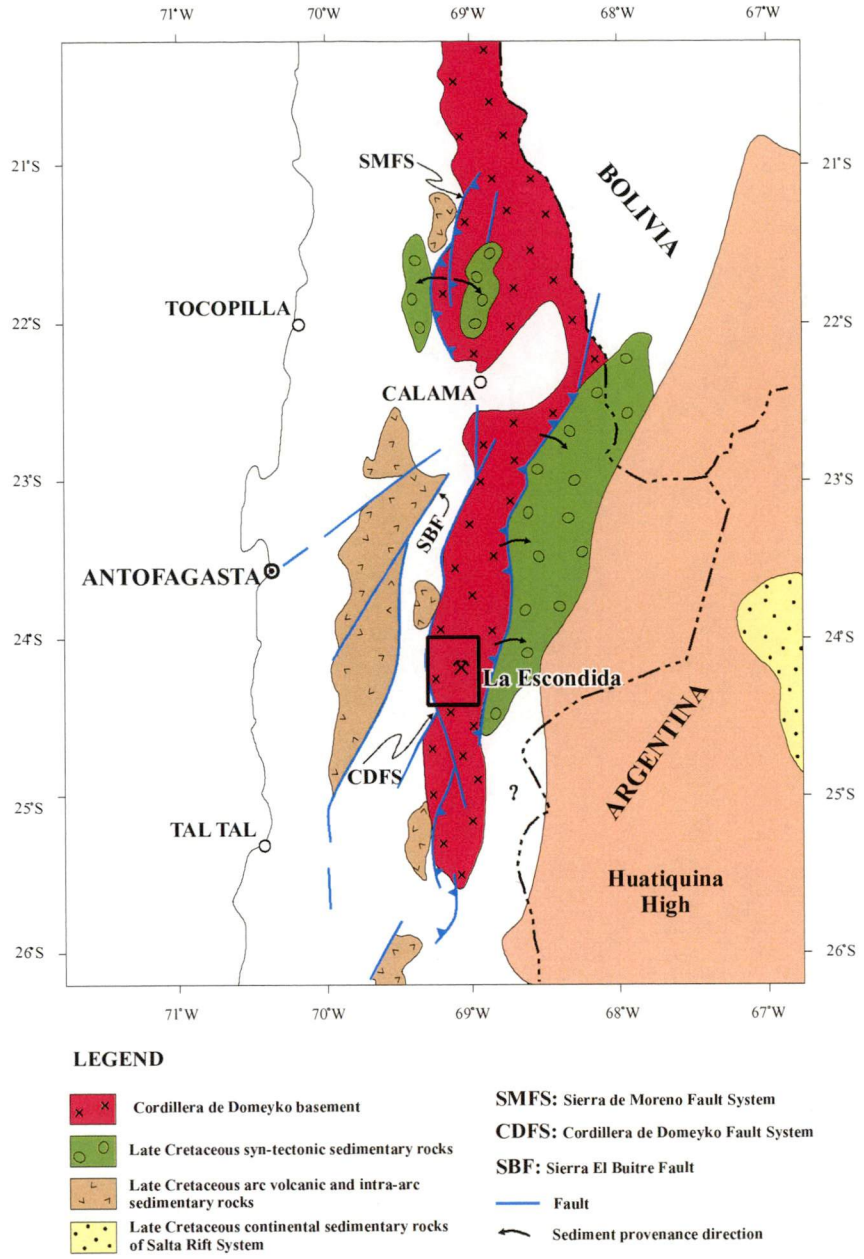

Figure 3.23 Lowermost Late Cretaceous (~100-80 Ma) paleogeographic reconstruction of northern Chile (21°-26°S) showing La Escondida region as an emerged portion of the proto-Domeyko Cordillera block (adapted from Mpodozis et al., 2005).

Magmatism continued from 70 to 66 Ma with the emplacement of Las Torres igneous complex along the western flank of the orogen (Figure 3.24), and concluded with the 67-64 Ma Sombrero intrusive complex.

The existence of a magmatic arc during the Late Cretaceous and early Paleogene was first proposed by Coira et al. (1982) and Mpodozis and Ramos (1989). Recent geological information (Marinovic et al., 1996; Tomlinson et al., 2001a; Cornejo et al., 2003) has helped to define a 1,000 km-long arc-zone of this age that is partially preserved in the

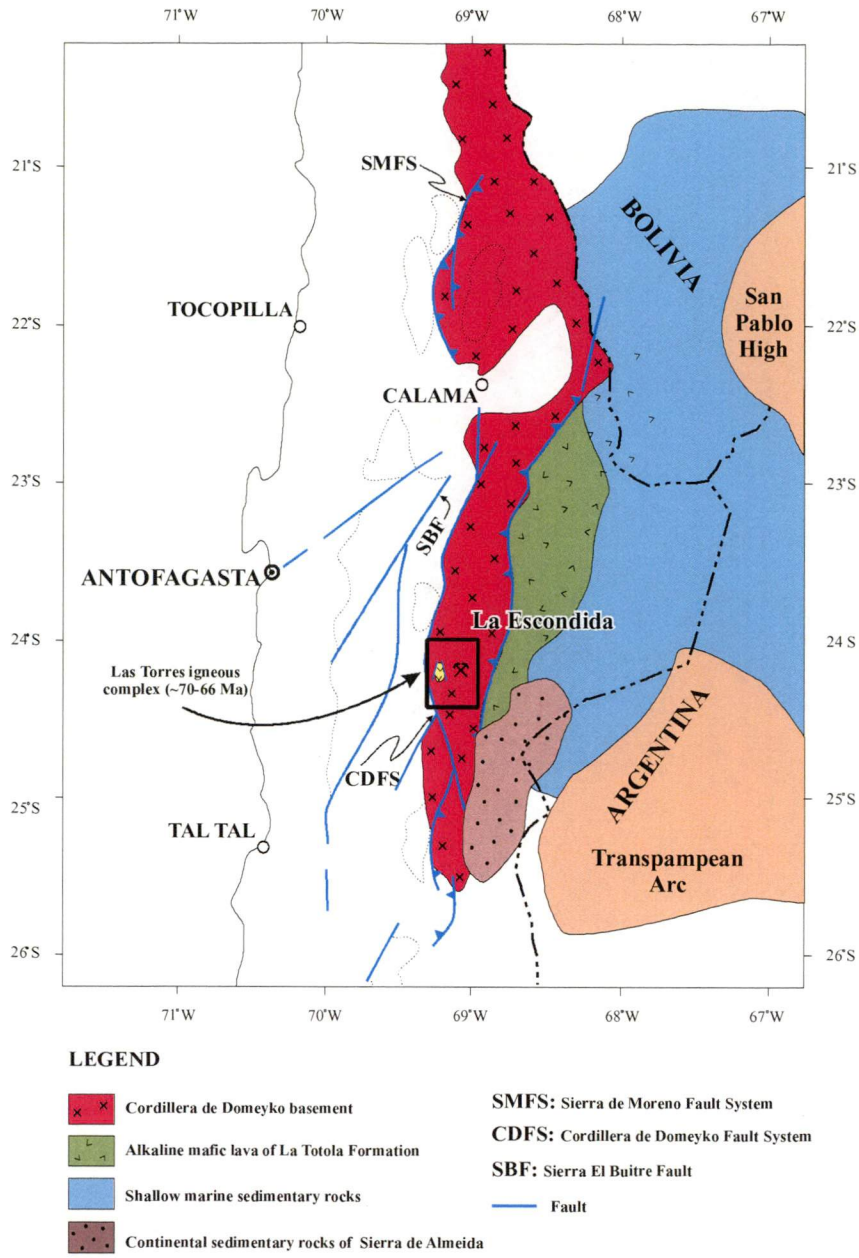

Figure 3.24 Uppermost Late Cretaceous (~70-64 Ma) paleogeographic reconstruction of northern Chile (21°-26°S) showing La Escondida region as an emerged portion of the proto-Domeyko Cordillera block (adapted from Mpodozis et al., 2005). The volcaniclastic and subvolcanic sequence of Las Torres igneous complex (ca. 70-66 Ma) is indicated as the main subaerial volcanic sedimentation event for the Late Cretaceous period in that portion of the orogen.

Central Depression morphotectonic province (Chapter 2). Exact delineation of the arc-back-arc couple remains unclear, although Cornejo et al. (2003) have localise the magmatic arc proper more than 150 km to the west of La Escondida district. There is no well-established tectonic setting for the 81-64 Ma period when basic to silicic magmatism occurred in La Escondida. These intrusions seem to have the chemical affinity of a back-arc environment (Chapter 6). The arc and part of the back-arc regions most likely would

have been affected by the recently identified "K-T" deformation phase (Cornejo et al., 2003) which occurred around 64-62 Ma at La Escondida district (Chapter 4). This deformation phase is clearly recorded by the angular unconformity that separates the Late Jurassic-Neocomian Santa Ana Formation from the overlaying late Peolecene-early Eocene Augusta Victoria Formations.

3.4 LATE PALEOCENE-EARLY EOCENE

After the "K-T" deformation phase in the lowermost early Paleocene (Chapters 2 and 4), the Domeyko Cordillera was the site for renewed volcanism of intermediate to felsic compositions. These rocks are commonly described as the Augusta Victoria Formation, and are associated with small, coeval, diorite and andesite intrusions. The late Paleocene-early Eocene rocks are exposed in large discontinuous belts that occupy the low relief areas of the study area, and are generally bounded by major regional north-trending faults (Figure 3.25; Appendices 1A and B). The Augusta Victoria Formation and comtemporaneous volcanic sequences are the main wall rocks to several of the Eocene Cu-Au porphyry deposits as well as significant high- and low-sulfidation epithermal Au-Ag mineralisation in northern Chile (Chapter 2).

Brief summary of the most relevant features and ages distribution of the late Paleocene-early Eocene rock units are provided in Table 3.8 and Figure 3.30, respectively.

3.4.1 Augusta Victoria Formation *(PEav)*

The late Paleocene-Eocene Augusta Victoria volcanic sequence overlies the Mesozoic El Profeta and Santa Ana Formations unconformably. It is in turn overlain unconformably by sub-horizontal gravels of the late Oligocene-middle Miocene Pampa Mula Formation (Marinovic et al, 1995; Figure 3.25). The Augusta Victoria volcanic pile has undergone very low grade metamorphism and/or hydrothermal alteration to chlorite and other low temperature phases (i.e., calcite, montmorillonite, rutile). To the west of Ferrocarril fault (Figure 3.25), the exposed section includes a crudely stratified lower sequence of pebbly conglomerates and red beds, which are overlain by conglomeratic sandstones and volcaniclastic boulder-rich conglomerates (Figures 3.26a and b). The middle to upper parts of the formation are dominated by interbedded lava flows and tuffs of andesitic to dacitic composition, and characteristic interbedded white rhyolitic vitric tuffs (Figures 3.27a and b). The total thickness is estimated to be less than 700 m. The sequence to the east of Ferrocarril fault is limited to isolated outcrops of fine-grained andesite and

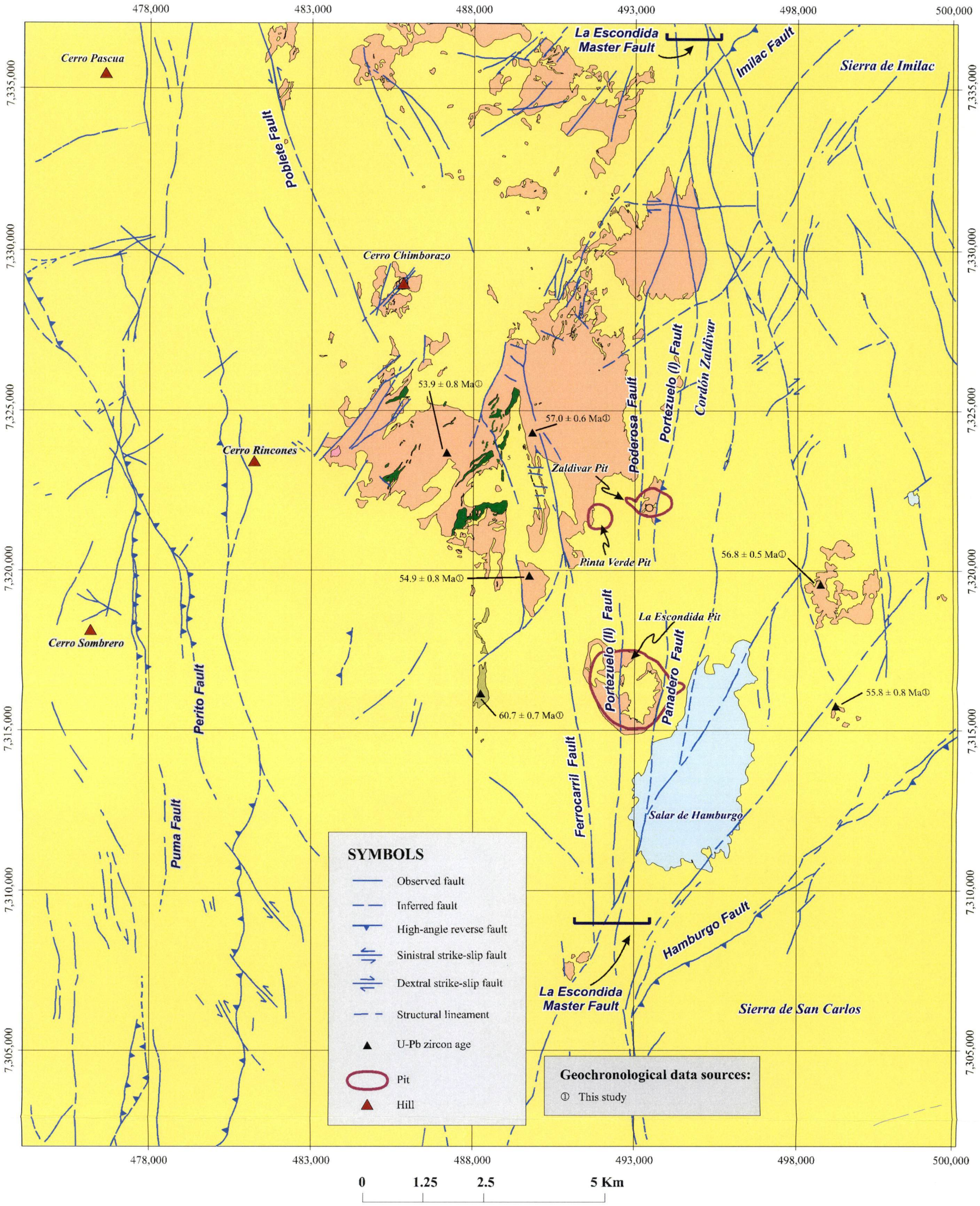

LEGEND

Augusta Victoria Formation (late Paleocene-early Eocene, ~57-53 Ma)

PEav Andesitic to trachyitic lava flow, volcanic breccia and lithic-crystal tuff; interbedded redbeds (▲ 57.0 ± 0.6 Ma① , ▲ 56.8 ± 0.5 Ma , ▲ 55.8 ± 0.8 Ma① , ▲ 54.9 ± 0.8 Ma①, ▲ 53.9 ± 0.8 Ma①)

Augusta Victoria Formation-related intrusions

PEdi Light olive, fine- to medium-grained, pyroxene-amphibole-phyric diorite dike and sill

Pan Medium-grained amphibole-phyric andesite dyke (▲ 60.7 ± 0.6Ma①)

Modern cover and omitted outcrops of non-Late Paleocene to Early Eocene sequences

Figure 3.25 Simplified distributions of late Paleocene-early Eocene volcaniclastic and intrusive units in La Escondida district.

Table 3.8 Summary of late Paleocene-early Eocene igneous units exposed in La Escondida district.

Unit (Abbreviation)	Age	Regional Description Contact relationships and lithology	La Escondida District Contact relationships and lithology	References
Augusta Victoria Formation (PEav)	late Paleocene-early Eocene (~57-53 Ma)	- The sequence unconformably overlies the Late Triassic-Neocomian El Profeta and Santa Ana Formations. - About 1000 m-thick packages of terrestrial and bimodal volcanic rocks divided in several individual volcanic centres between 24°-26° S (e g the shield volcano of Pampa Rubia, El Soldado-Cachinal calderas, El Peñón domes and caldera), with ages between Late Paleocene and Early Eocene To the north (23°-24° S), the time-equivalent units are the Paleocene-Middle Eocene Cinchado Formation, and the Orange Formation (Paleocene-Lower Eocene) in the Salar de Atacama region This unit hosts important high- and low-sulfidation gold and silver mineralisation (e g El Peñón, El Guanaco, Vaquillas, Cachinal de la Sierra)	- The unit is unconformably overlain by the sub-horizontal gravels of the Pampa Mulas Formation (Late Oligocene-Middle Miocene) - Characterized by two distinct sections. a) To the west of La Escondida master fault, a crudely stratified succession of boulder-rich conglomerates and sandstones, with strong volcanic provenance, and minor interbedded lava flows and tuffs of andesitic to dacitic composition Characteristic intercalations of white rhyolitic tuffaceous rocks. Estimated thickness <500 m b) To the east of La Escondida master fault, section of poorly stratified succession of greenish-grey fine-grained andesite, locally autobrecciated, and subordinate fine-grained tuff of similar composition Estimated thickness <350 m	García (1967) Montaño (1976) Mpodozis et al (1993a) Marinovic et al. (1995) Marinovic et al. (1996) Richards et al (2001) Cornejo et al (2003) Mpodozis et al (2005)
Augusta Victoria Formation-related intrusions (PEdi)	late Paleocene-early Eocene		- Intrusives emplaced cogenetically into the Augusta Victoria Formation (57-52 Ma) - Dykes, sills and plugs composed of olive green diorites transitions to porphyritic andesite. Poorly defined contact with wall-rocks. Regional low-grade metamorphism	Marinovic et al. (1995) Richards et al. (2001)
Medium-grained amphibole-phyric andesite (Pan)	late Paleocene (~61-60 Ma)		- Sharp intrusive contacts with monzonites of the Cerro Bayo Plutonic Complex (ca. 77-72 Ma) - Northerly-trending andesite dyke, 4 km long and less than 350 m wide.	Marinovic et al. (1995) Richards et al (2001)

Table 3.9 Radiometric ages for late Paleocene-early Eocene rock units in the study area and adjacent sectors

Sample	Rock	Method (material)	Age &Error (Ma, 2 σ)	Source of Data (*)
Augusta Victoria Formation *(PEav)*				
ESC-30	Vitric tuff	U-Pb (zircon)	57.0 ± 0.6	3
ESC-31	Fine-grained andesite	U-Pb (zircon)	56.8 ± 0.5	3
ESC-32	Pyroxene andesite	U-Pb (zircon)	55.8 ± 0.8	3
ESC-39	Vitric tuff	U-Pb (zircon)	54.9 ± 0.8	3
ESC-7	Vitric tuff	U-Pb (zircon)	53.9 ± 0.8	3
II/68	Ignimbrite	K-Ar (biotite)	59.0 ± 11.6	1
II/402	Rhyolitic breccia	K-Ar (biotite)	56.9 ± 1.6	1
II/147	Ignimbrite	K-Ar (biotite)	55.0 ± 1.4	1
A-247	Andesite	K-Ar (whole rock)	47.7 ± 1.8	1
II-473	Dacite	K-Ar (whole rock)	42.1 ± 1.5	1
DCM-027	Rhyolitic ignimbrite	K-Ar (biotite)	59.2 ± 1.6	2
H8-3	Rhyodacitic dome	K-Ar (biotite)	56.5 ± 1.5	2
DR-4	Dacite dome	K-Ar (biotite)	55.8 ± 1.5	2
DCM-17	Biotite rhyolite	^{40}A-^{39}Ar (biotite)	54 5 ± 0.6	2
DCM-24	Rhyolite dome	U-Pb (zircon)	54.5 ± 0.6	2
Medium-grained amphibole-phyric andesite dyke *(Pan)*				
ESC-21	*Amphibole andesite*	*U-Pb (zircon)*	*60.7 ± 0.6*	*3*

(*) Source of data: (1) Maksaev et al. (1991) and Marinovic et al. (1995), (2) Cornejo et al. (2003); (3) this study.

volcanic breccia, but probably extends for considerable distances beneath the gravels of the Hamburgo salt pan (Figures 3.28a and b; Appendices 2C and D). Boreholes in the Hamburgo basin have revealed the occurrence of coarse-grained volcanogenic rocks that contrast with western sections of the study area. The sequence in the Hamburgo basin is dominantly composed of fine-grained dacitic and andesitic crystal-lithic sandstones and lava flows. It occurs in fault contact with older units and with erosive unconformity underneath the San Carlos strata of 38-36 Ma (Appendix 2D; Chapter 4). The maximum thickness in this sector is estimated to be around 350 m, based on drill core logging.

3.4.1.1 Age and Depositional Setting

The Augusta Victoria Formation has been dated previously by K-Ar and ^{40}Ar-^{39}Ar methods. It has an age distribution of 57 to 42 Ma (Table 3.9; Appendix 6). New radiometric LA-ICP-MS U-Pb zircon dates cluster around 57-53 Ma, suggesting a late Paleocene-early Eocene age (Table 3.9; Appendix 6). A maximum age for the Augusta Victoria sequence has been well constrained at 57 Ma from a sample obtained a few metres above the unconformity that separates the unit from the underlying Santa Ana Formation. In contrast, the minimum age of the formation remains uncertain due to faulting (Chapter 4).

The most remarkable sedimentological feature of the Augusta Victoria Formation in La

Figure 3.26a General view (looking west) of the crudely stratified volcaniclastic conglomerates from the basal sections of the Augusta Victoria Formation (*PEav*; 57-53 Ma) to the west of La Escondida master fault. Antofagasta-Salta railway (7,324,900m N; 487,000m E).

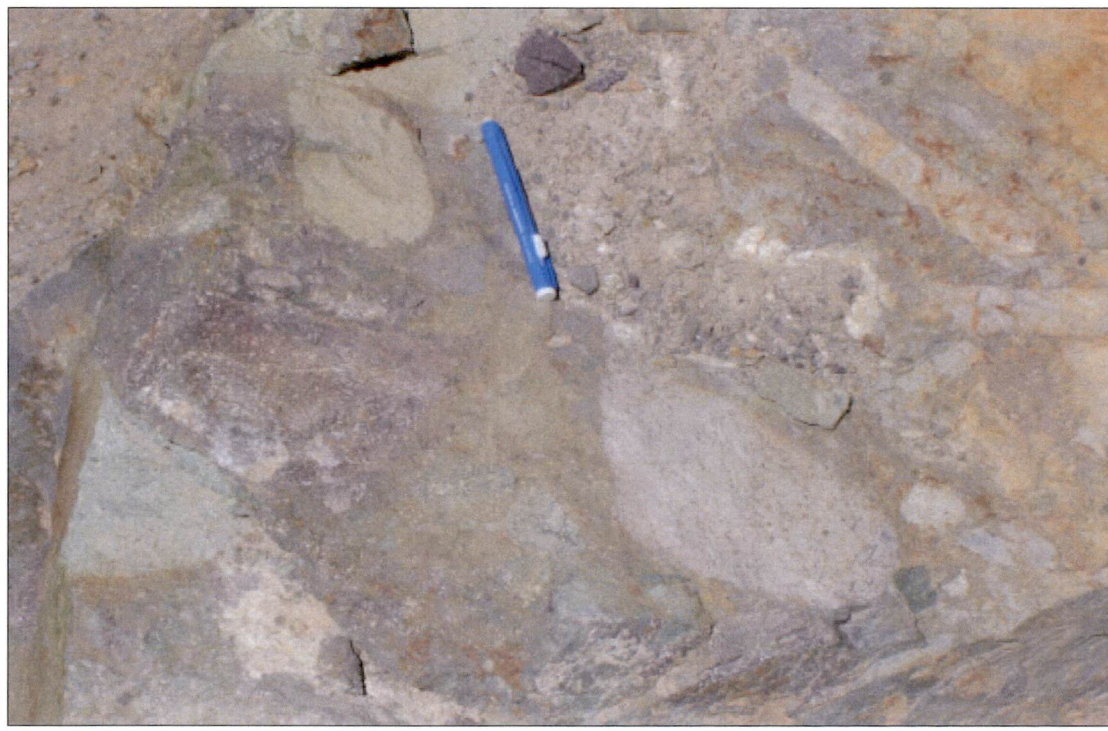

Figure 3.26b Large boulders and pebbles, mostly of andesitic composition in clast-supported volcaniclastic conglomerates from the Augusta Victoria Formation (*PEav*; 57-53 Ma). Antofagasta-Salta railway (7,324,900m N; 487,000m E).

Figure 3.27a General view (looking east) of reddish white rhyolitic to dacitic tuffaceous rocks interbedded within the andesitic volcaniclastic basal sections of the Augusta Victoria Formation (*PEav*; 57-53 Ma). Chimborazo sector (7,325,600m N; 489,200m E).

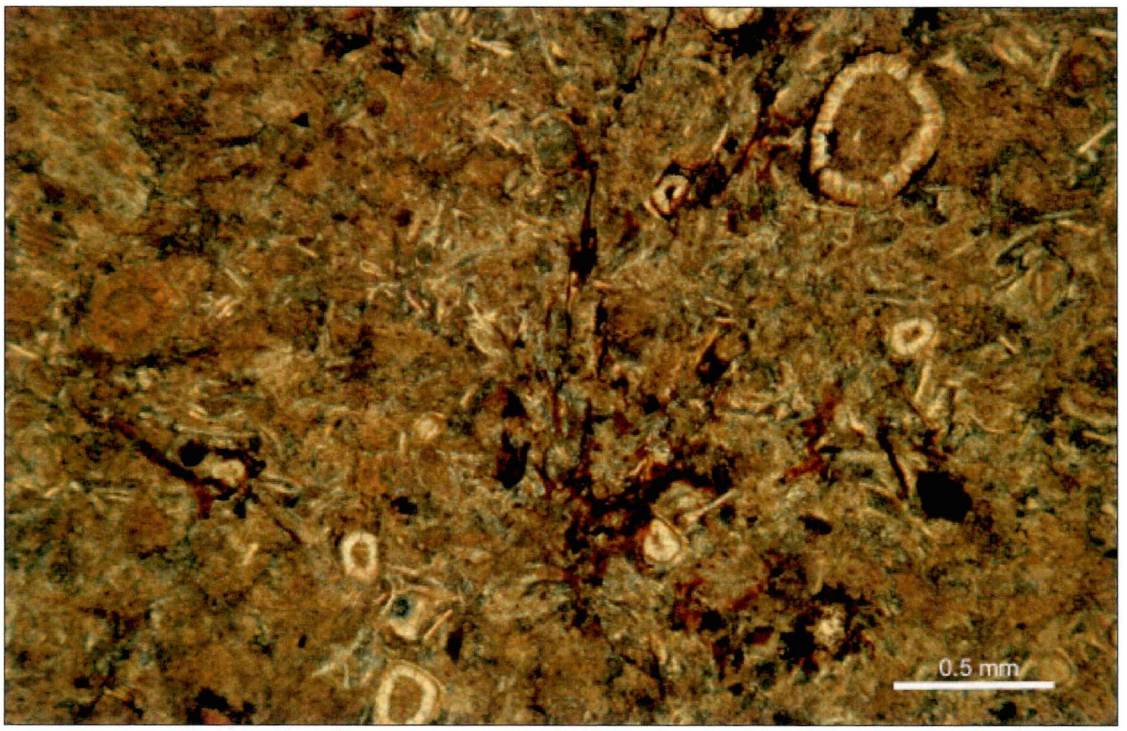

Figure 3.27b Photomicrograph (plane polarised light) of a fine-grained and limonitic vitric tuffaceous rock. This rock is interbedded with conglomerates and sandstones from the Augusta Victoria Formation (*PEav*; 57-53 Ma). Note the abundant spherulites and poorly deformed shards. Sample FU-408 (7,323,626m N; 487,256m E).

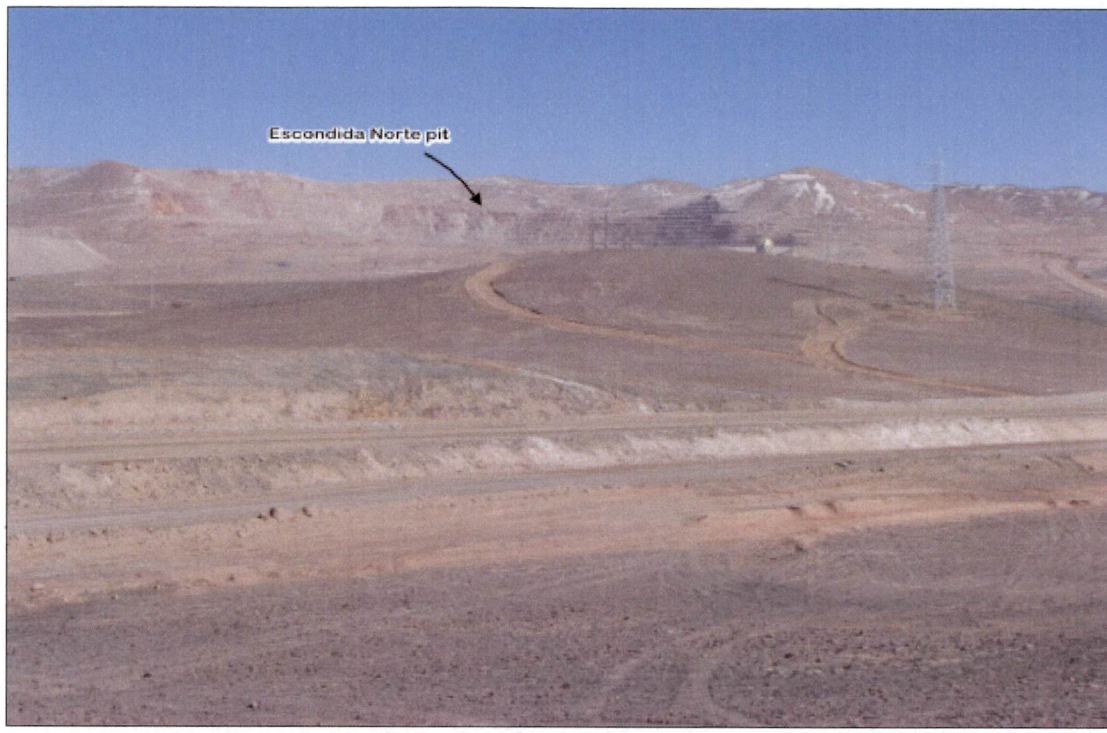

Figure 3.28a General view (looking northwest) of poor outcrops of massive and brown-coloured, fine-grained andesites of the Augusta Victoria Formation (*PEav*; 57-53 Ma), to the east of La Escondida master fault. This photo taken from the northern border of the Hamburgo salt pan (7,319,400m N; 499,200m E).

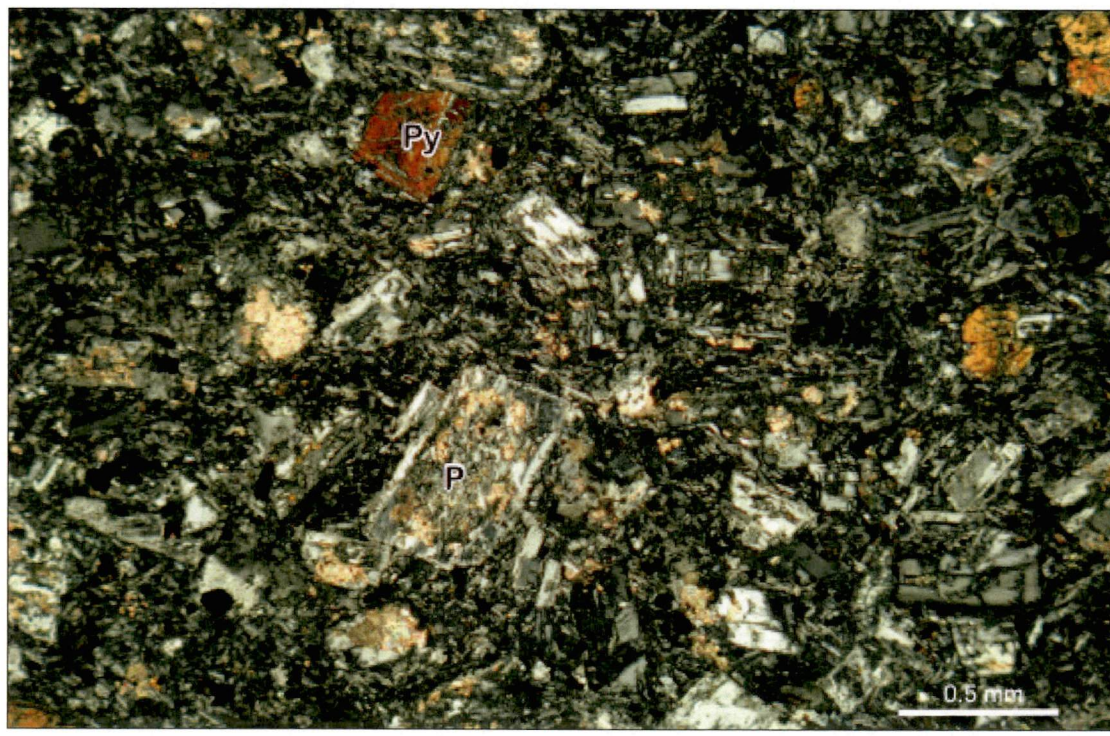

Figure 3.28b Photomicrograph (crossed nicols) of a fine-grained and porphyritic andesite of the Augusta Victoria Formation (*PEav*; 57-53 Ma), exposed to the east of La Escondida master fault. Note that some phenocrysts of plagioclase (**P**) have been altered to calcite and minor sericite. Pyroxene (**Py**) is altered to actinolite. The phenocrysts are hosted by a partially chloritized plagioclase microlite-rich groundmass, which locally developed a pilotaxitic texture. Sample ESC-32 (7,315,757m N ; 499,313m E).

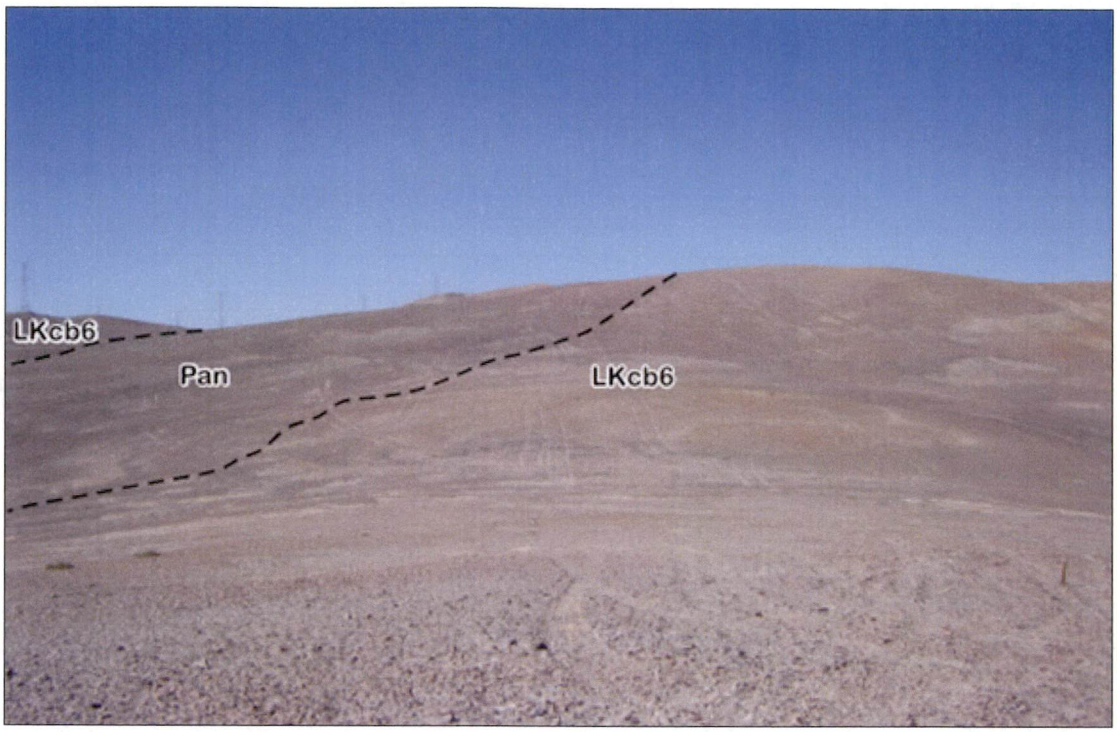

Figure 3.29a Amphibole-phyric andesite dyke (*Pan*; 60.7 ± 0.6 Ma) that has intruded fine-grained monzonite (*LKcb6*; 72 Ma) of the Late Cretaceous Cerro Bayo plutonic complex (77-72 Ma). Note the poor outcrops and the approximate trace of the contacts. San Lorenzo camp sector (7,316,200m N; 488,300m E).

Figure 3.29b Photomicrograph (crossed nicols) of the amphibole-phyric andesite dyke of *Pan*. Note strongly fractured and calcite-altered plagioclase (**P**) phenocrysts and minor amphibole (**A**) pervasively replaced by an association of epidote-chlorite-actinolite-calcite. The groundmass is composed of plagioclase and subordinate amphibole microlites, along with magnetite. Sample ESC-21 (7,316,105m N; 488,330m E).

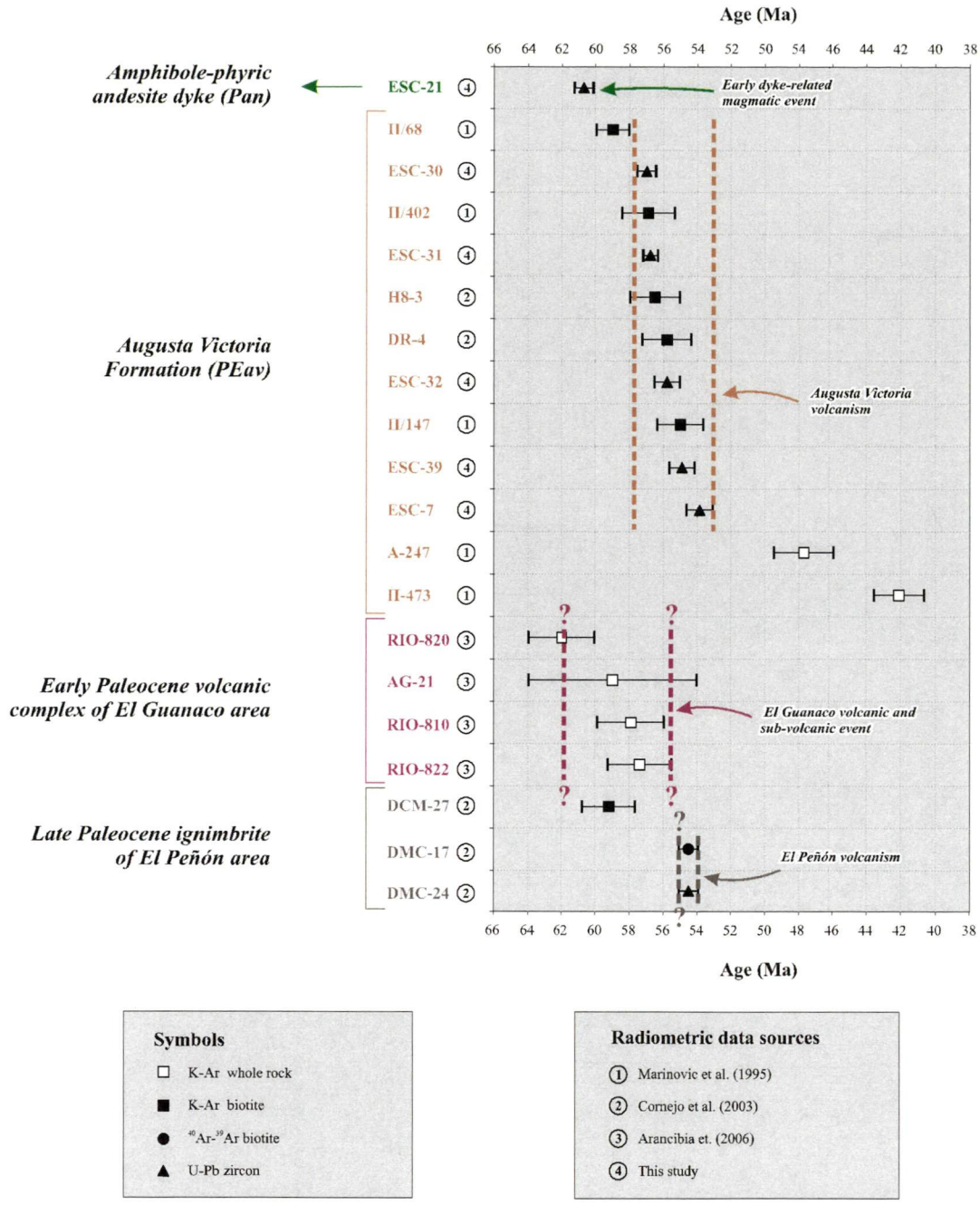

Figure 3.30 Age distribution for late Paleocene-early Eocene igneous units in La Escondida district and adjacent sectors. Analytical details provided in Appendix 6.

Escondida district is the abundance of coarse-grained volcaniclastic and clastic deposits in the lowest part of the stratigraphic section exposed to the west of Ferrocarrill fault. They are interpreted to be products of terrestrial mass-flow processes (i.e., Suthren, 1985; McPhie et al., 1993) that occurred pre- and most likely syn-volcanism. Previous studies have divided the Augusta Victoria Formation and equivalent sequences into a number of subaerial volcanic complexes. These are inferred to compose trapdoor calderas, domes and shield volcanos, and occurred between 24° and 26°S in a north-trending belt through

northern Chile (Marinovic et al., 1996; Cornejo et al., 2002).

3.4.2 Augusta Victoria Formation-related Intrusives *(PEdi)*

There are a number of elongate stocks, dykes and sills, composed of olive-coloured pyroxene-amphibole diorites, which have been emplaced into the Augusta Victoria volcanic rocks (Figure 3.25; Table 3.8). Gradational contacts have been locally observed. No age determinations have been done on these intrusions, but their close spatial association and compositional and textural similarities with the andesite country rocks imply coeval or near-coeval emplacement with the Augusta Victoria sequence.

3.4.3 Medium-grained Amphibole-phyric Andesite *(Pan)*

The amphibole-phyric andesite is a 4 km-long, <300 m-wide, north-trending dyke (Figure 3.25; Table 3.8). It has intruded monzonites of the 77-72 Ma Cerro Bayo plutonic complex. A LA-ICP-MS U-Pb zircon date yielded an age late Paleocene age (60.7 ± 0.6 Ma) for this dyke (Table 3.9; Appendix 6), indicating that it is an immediate precursor to the Augusta Victoria volcanic episode (ca. 57-53 Ma; Figure 3.30).

3.4.4 Summary of Late Paleocene-Early Eocene

The Augusta Victoria Formation volcanic rocks form part of a regionally extensive suite of subaerial bimodal intermediate to acid volcanic rocks, including domes and calderas, that define the late Paleocene-early Eocene magmatic arc (Chapter 2). The main arc zone was located slightly to the west of La Escondida district. It included numerous individual volcanic complexes that define a 1000 km-long magmatic front, and which host important high- and low-sulfidation gold and silver deposits (i.e., El Peñón, El Guanaco, Vaquillas, Cachinal de la Sierra; Cornejo et al., 2003; Warren et al., 2003). A major contractional deformation event, the Incaic tectonic phase (Coira et al.,1982), affected the Augusta Victoria volcanic sequence and associated intrusions during the middle-late Eocene (Chapter 4). In La Escondida area, significant alluvial clastic and volcaniclastic sedimentation occurred contemporaneously with volcanism, especially during the early stages in the eastern part of the arc, adjacent to the Domeyko Cordillera orogen.

3.5 MIDDLE EOCENE-EARLY OLIGOCENE

The middle Eocene-early Oligocene was the most important metalliferous period in the geological evolution of northern Chile due to widespread porphyry copper magmatism and mineralisation. Eocene-Oligocene magmatic activity in La Escondida district can be

separated into three major intrusive pulses (Figures 3.31 and 3.33): (1) a middle Eocene mesozonal-epizonal igneous complex known as the Cerro Rincones plutonic complex; (2) clusters of hypabyssal intrusions that form the middle-late Eocene La Escondida and Escondida Norte-Zaldivar porphyry copper deposits (Boric et al., 1990; Richards et al., 1999; Monroy, 2000; Padilla et al., 2001; Quiroz-Luna, 2003; Padilla-Garza, 2003); and (3) post-mineralisation dioritic, and andesitic to rhyolitic dykes, which were the last pulse of intrusive activity in the district.

A new stratigraphic unit, the uppermost middle-late Eocene San Carlos strata, has been identified in the current study. This volcano-sedimentary packages records middle-late Eocene subaerial sedimentation and volcanism, which has not been documented previously in this portion of the Domeyko Cordillera.

3.5.1 Cerro Rincones Plutonic Complex *(Eocr)*

The Cerro Rincones plutonic complex includes a series of medium- to large-sized, multi-stage stocks that have a pre-mineralisation timing with respect to the major porphyry copper deposit. This unit crops out over more than 45 km^2, and outlines an overall sub-circular area covering the northern half of La Escondida district (Figure 3.31). This sub-circular plan view is also apparent in regional-scaled magnetic images from La Escondida district (Chapter 4; Figure 4.22). The plutons are typically fine- to medium- grained and porphyritic. They range compositionally from diorite and monzodiorite to granite (Table 3.10). The plutons have produced well developed skarn and hornfels zones in the Mesozoic El Profeta-Santa Ana sequences and the Augusta Victoria Formation, respectively (Chapter 5). Field relationships, petrography and geochronological data suggest that the plutonic complex consists at least of nine mesozonal to epizonal intrusive phases that were emplaced between 43 and 41 Ma (Table 3.11; Appendix 6). Brief summaries of the most relevant features and age distributions of this unit are provided in Table 3.10 and Figure 3.40, respectively.

3.5.1.1 Fine- to Medium-grained Diorite and Monzodiorite, and Subordinate Quartz Monzodiorite *(Eocr1)*

This is the largest intrusive body in the complex, cropping out over 26 km^2 (Figure 3.31). It is associated with a number of small apophyses. The dominant rock types are fine- to medium-grained, equigranular to porphyritic pyroxene-bearing hornblende diorite and monzodiorite, which grade locally into quartz monzodiorite and quartz diorite.

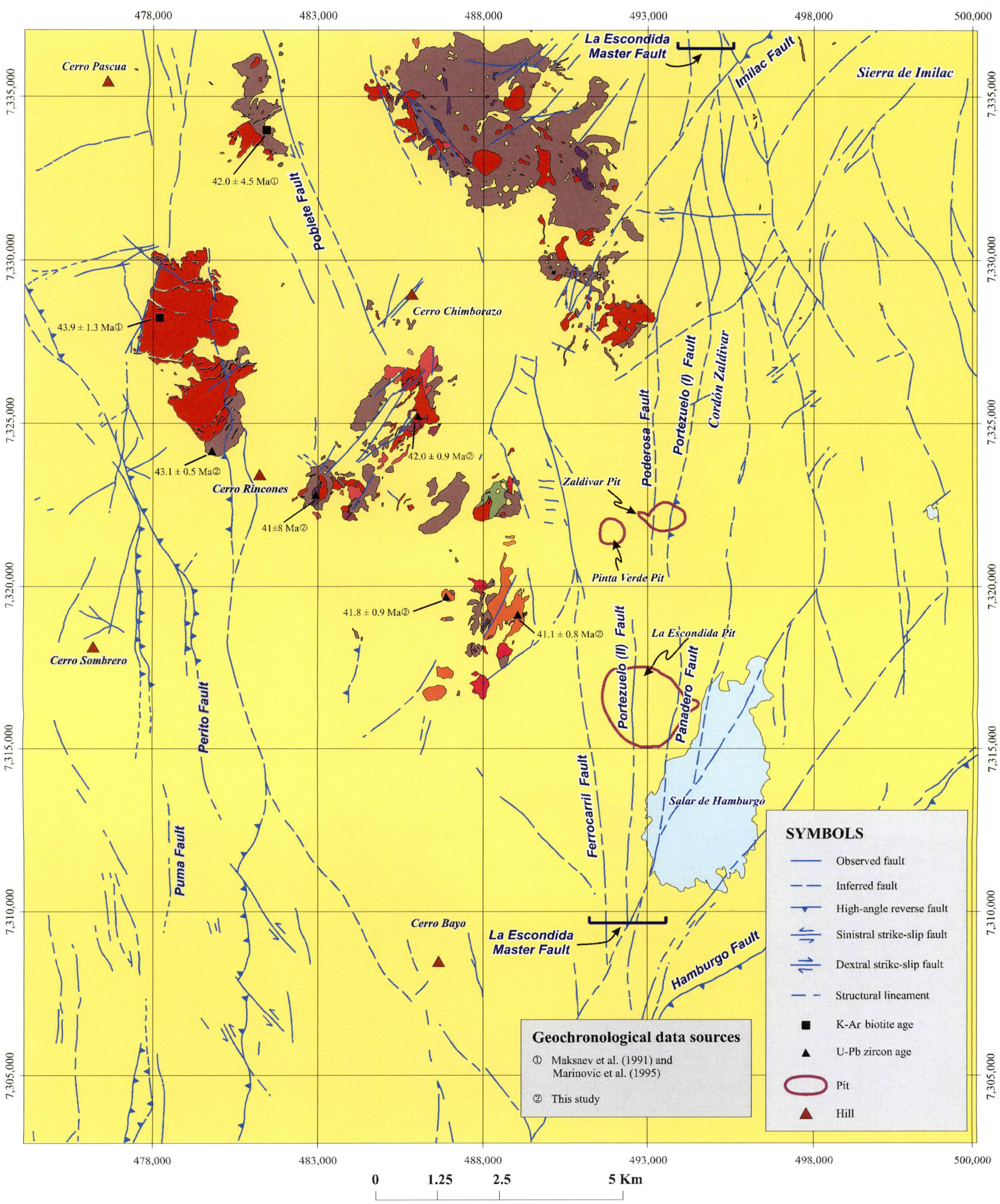

LEGEND

Cerro Rincones plutonic complex (middle Eocene; ~ 43-41 Ma)

- Eocr5 Coarse-grained, porphyritic monzonite and quartz monzonite (■ 43.9 ± 1.3 Ma①; ▲ 42.0 ± 0.9 Ma②)
- Eocr4 Fine to medium-grained, microaplitic quartz monzonite
- Eocr3 Medium-grained, porphyritic granodiorite and quartz diorite
- Eocr2 Metamorphosed porphyritic monzonite
- Eocr1 Fine- to medium-grained, diorite and monzodiorite, and quartz monzodiorite (▲ 43.1 ± 0.5 Ma②; ■ 42.0 ± 4.5 Ma①)
- Eocr9 Biotite-amphibole-pyroxene-phyric monzodiorite and quartz diorite (▲ 41.8 ± 0.9 Ma②, ▲41.1 ± 0.8 Ma②)
- Eocr8 Quartz-feldspar-phyric micromonzonite and microgranite (▲ 41±8 Ma②)
- Eocr7 Microaplitic and porphyrytic leucocratic quartz monzonite
- Eocr6 Medium- to coarse-grained, granodiorite and granite porphyries
- Modern cover and omitted outcrops of non-lowermost Middle Eocene rock units

Figure 3.31 Simplified distributions of middle Eocene intrusive units in La Escondida district.

Table 3.10 Summary of middle Eocene intrusive complexes exposed in La Escondida district.

Unit (Abbreviation)	Age	Regional Description Contact relationships and lithology	La Escondida District Contact relationships and lithology	References
Cerro Rincones plutonic complex *(Eocr)*	middle Eocene (~43-41Ma)	This complex comprises several composite plutons in the Domeyko Cordillera and Intermediate Depression. There are three particularly well-documented magmatic centres· - Monzodiorites and diorites of Cerro Paisaje-Anillo (ca. 48-42 Ma), which intruded the Augusta Victoria Formation. They crop out < 30 km to the west of La Escondida district. They host the Anillo Au-Cu porphyry system (see also Chapter 6). - Cerro Juncal Plutonic Complex (45-40 Ma), in the Sierra Exploradora region (25°45'S). Includes diorites, monzonite, monzodiorites and granitic porphyries, with Ag, Cu and Au mineralisation in hornfels developed in the Pampa Rubia volcanic sequences (55-48 Ma) - The granodiorites and monzodiorites of the Cerro Vicuña and the Quebrada La Ciénaga (ca 48-43 Ma) in El Salvador region.	- Has intruded the calcareous and clastic rocks of the Mesozoic El Profeta and Santa Ana Formations and the Late Paleocene-Early Eocene Augusta Victoria volcanic sequence - Large, composite intrusive that is strongly heterogeneous, composed of fine- to medium-grained and porphyritic facies of diorite and monzodiorite, through granodiorite and monzonite, to granite porphyry Large skarn zones and polymetallic Cu-Ba-Pb vein systems are present, as well as minor tourmaline breccia dykes with anomalous Cu-oxides Spatially associated with the secondary enriched high sulfidation Cu vein at Chimborazo	Cornejo et al (1993) Marquardt et al. (1994) Mpodozis et al (1993a) Marinovic et al. (1995) Cornejo and Mpodozis (1996) Richards et al (2001)

LA-ICP- MS U-Pb zircon dating of this unit has provided an age of 43.1 ± 0.5 Ma (Table 3.11), overlapping with the 42 ± 4.5 K-Ar age reported by Marinovic et al. (1995).

3.5.1.2 Metamorphosed Porphyritic Monzonite *(Eocr2)*, Medium-grained Granodiorite and Quartz Diorite *(Eocr3)*

Several poorly exposed minor stocks (<1 km^2) have intruded the Augusta Victoria and El Profeta Formations (Figure 3.31). Moderate deuteric alteration and metamorphic recrystallization are observed in a hornblende-pyroxene-phyric quartz diorite from the *Eocr3* sub-unit. Numerous micro-aplitic veins are present in these intrusive bodies. No unequivocal contact relationships with other intrusive phases of the Cerro Rincones plutonic complex have been recognized, but a porphyritic monzonite from the *Eocr2* sub-unit has been intruded by monzonite and quartz monzonite from the *Eocr5* sub-unit, which has yielded ages of 43.9 ± 1.3 (K-Ar biotite, Marinovic et al., 1995) and 42.0 ± 0.9 Ma (U-Pb zircon; this study). No radiometric studies have been completed on the *Eocr2* and *Eocr3* sub-units, but they are considered here to be early phases of the Cerro Rincones complex.

3.5.1.3 Fine- to Medium-grained, Micro-aplitic Quartz Monzodiorite *(Eocr4)*

North-northeast-trending intrusions (100-200 m wide) of quartz monzodiorite are poorly exposed on the outer margins of the Cerro Rincones complex (Figure 3.31). A typical quartz monzonite from *Eocr4* is slightly porphyritic, with pyroxene and amphibole phenocrysts dominant, and with a micro-aplitic groundmass. It has undergone contact metamorphism to hornfels, producing a characteristic light green-grey colour.

3.5.1.4 Coarse-grained Porphyritic Monzonite and Quartz Monzonite *(Eocr5)*

These rocks have the second largest surface area of any facies exposed within the Cerro Rincones complex (Figure 3.31). The *Eocr5* sub-unit consists of a large stock that covers an area of over 12 km^2 (Figure 3.32a). It is surrounded by other minor stocks and plugs that are only a few meters wide. The main intrusion is a heterogenous body that has a coarse-grained core, grading outwards to a medium-grained and porphyritic variant of similar composition; all cross cut by common leucocratic veins and thin dykes of felsic composition. The previous K-Ar biotite age for this unit of 43.9 ± 1.3 Ma (Marinovic et al., 1995) has been refined during the present study with a LA-ICP-MS U-Pb zircon date of 42.0 ± 0.9 Ma (Table 3.11; Appendix 6).

3.5.1.5 Medium- to Coarse-grained Granodiorite and Granite Porphyries *(Eocr6)*

Small tabular granodiorite and granite porphyry bodies are associated spatially and temporally with the *Eocr5* sub-unit (Figure 3.31). The rocks have a characteristic reddish pink colour and local occurrences of embayed quartz phenocrysts. The strongly porphyritic texture includes glomerocrysts of feldspars, quartz and biotite set in an epidotised, granophyric feldspar and quartz-bearing groundmass. The *Eocr6* sub-unit is inferred to be a late facies of *Eocr5*. The textural characteristics are suggestive of hypabyssal emplacement. No radiometric studies have been completed on *Eocr6*.

3.5.1.6 Micro-aplitic and Porphyritic Leucocratic Quartz Monzonite *(Eocr7)*

These small (<0.3 km^2) and intensely bleached plugs contain subangular monzonitic xenoliths derived from the Late Cretaceous Cerro Bayo plutonic complex and the Mesozoic sedimentary sequences. Petrographically, the leucocratic quartz monzonite contains glomerophenocrysts of plagioclase and rare K-feldspars altered to albite, sericite and clays minerals. It is locally associated with igneous- and tourmaline-cemented breccia bodies less than 5 meters wide. A pre-*Eocr9* intrusion age is inferred for *Eocr7*.

3.5.1.7 Quartz-feldspar-phyric Micromonzonite and Microgranite *(Eocr8)*

These rocks are the smallest intrusive unit of the Cerro Bayo complex (Figure 3.31). The principal body is a small dyke 700 m in length and less than 300 m wide (Figure 3.32b), which is hosted by *Eocr5*. The rocks have an intense red stain caused by abundant limonite. Texturally they are characterised by anhedral to subhedral phenocrysts of quartz, plagioclase and K-feldspar set in a micro-aplitic groundmass. The age of this unit is poorly constrained by a 41 ± 8 Ma U-Pb zircon age. The poor quality of this age determination is due to the presence of abundant inherited zircons (Table 3.11; Appendix 6).

3.5.1.8 Biotite-amphibole-pyroxene-phyric Quartz Diorite and Diorite *(Eocr9)*

Exposures of a medium- to fined-grained quartz diorite and diorite define a relatively homogenous stock (<2 km^2) which is located in the margin south of the Cerro Rincones complex (Figure 3.31; Appendix 1B). They are associated with minor diorite-cemented intrusive breccias and tourmaline-cemented hydrothermal breccia. Two LA-ICP-MS U-Pb zircon ages of 41.1±0.8 Ma and 41.8±0.9 Ma have been obtained for this unit (Table 3.11; Appendix 6), confirming that it formed during the late stages of the Cerro Rincones plutonic complex.

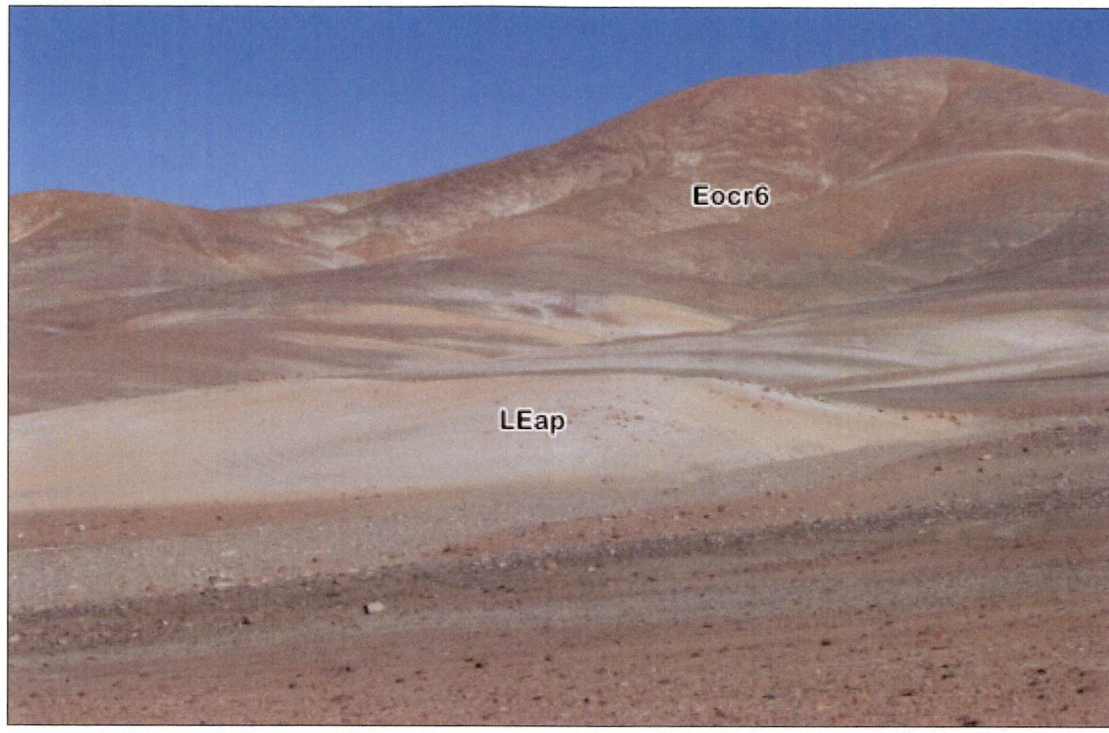

Figure 3.32a General view (looking south) of the outcrop patterns of monzonitic to quartz monzonitic facies of the *Eocr6* sub-unit (ca. 43-42 Ma) from the Cerro Rincones plutonic complex (ca. 43-41 Ma). Note the family of andesitic porphyry dykes (*LEap*; ca. 38-36 Ma) that have cut the intrusive complex. Northern flank of Cerro Rincones (7,328,000m N; 479,000m E).

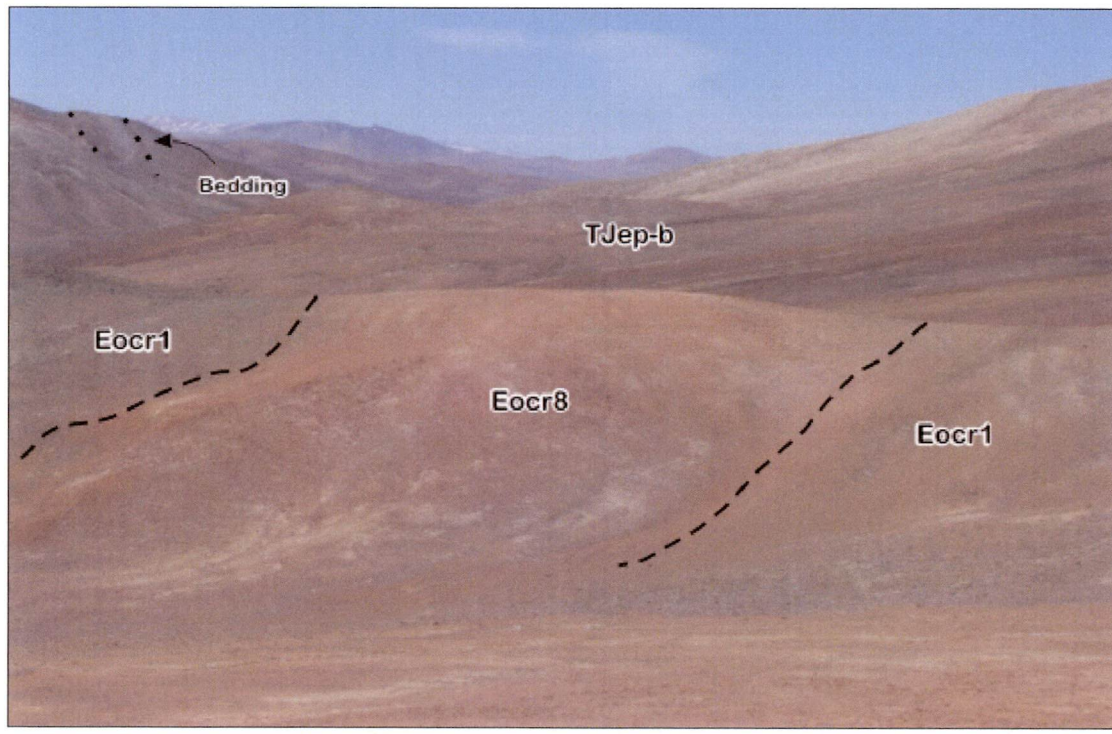

Figure 3.32b General view (looking south) of red-coloured and aplitic-textured microgranite dyke (*Eocr8;* ca. 41 ± 8 Ma) from the Cerro Rincones plutonic complex. It has intruded diorites and monzodiorites (*Eocr1* sub-unit; ca. 4 3-42 Ma). Note the steep dipping skarn-altered calcareous beds of the Mesozoic El Profeta Formation. Eastern flank of Cerro Rincones (7,323,100m N; 489,000m E).

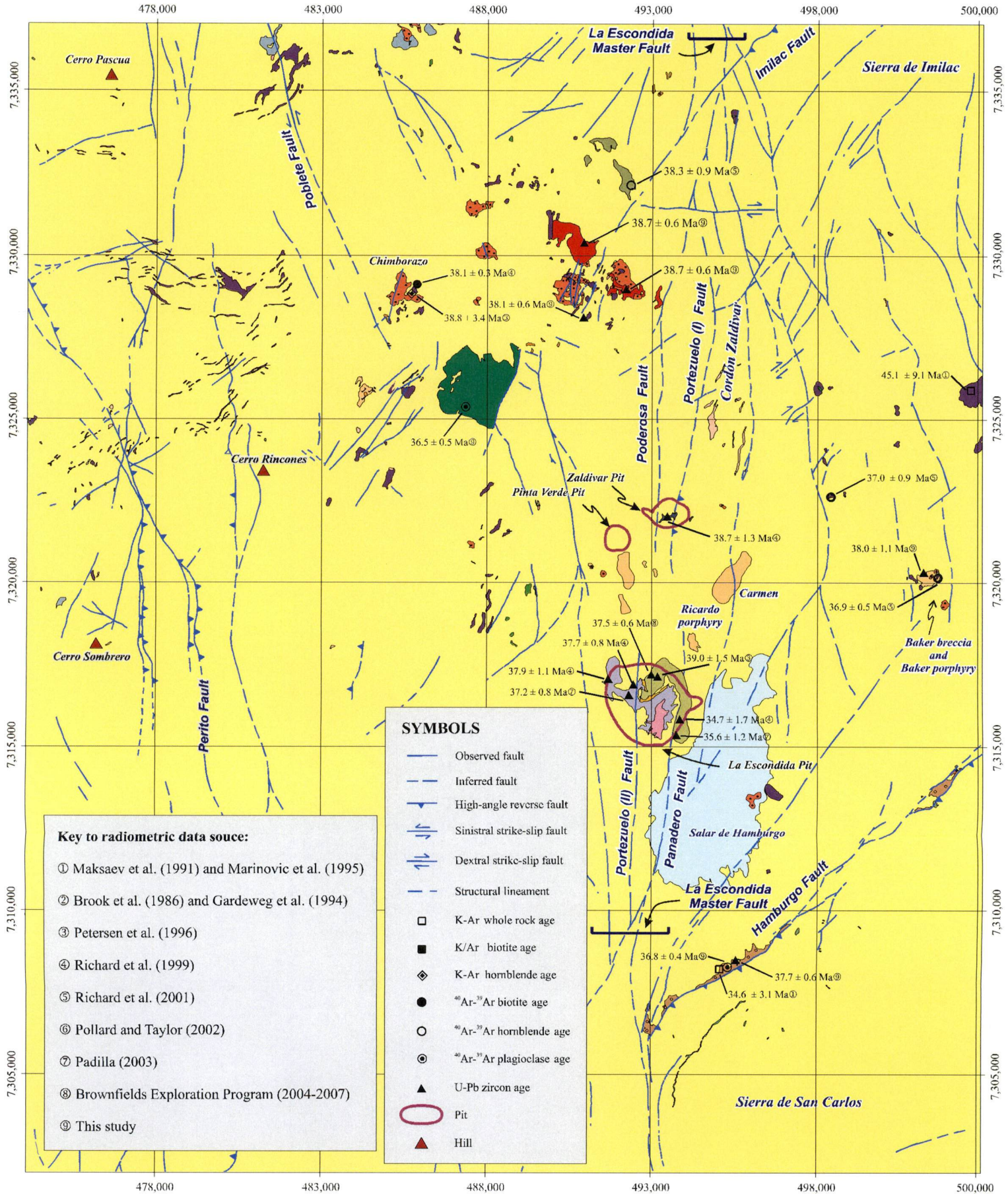

LEGEND

Intrusive rocks of middle Eocene-early Oligocene age

- Eodad — Dark greenish gray, fine-grained diorite and andesite dykes
- Eolda — Light olive brown, fine-grained dacite and andesite dykes
- Eooda — Grayish orange to yellowish orange, dacite and andesite porphyry
- Lepap — Grayish red, pyroxene andesite porphyry (◉ 36.5 ± 0.5 Ma⑨)
- Leap — Greenish gray to pale green, medium to coarse-grained, biotite-amphibole andesite porphyry and porphyric diorite (□ 45.9 ± 9.1 Ma②, ◈ 38.8 ± 3.4 Ma③, ● 38.1 ± 0.3 Ma④, ▲ 38.1 ± 0.6 Ma⑨, ○ 37.0 ± 0.9 Ma⑤, ○ 36.9 ± 0.5 Ma⑤)
- Eodpr — Altered and mineralised, medium to coarse-grained, dacite and rhyolite porphyry (e.g., Baker porphyry: ▲ 38.0 ± 1.1 Ma⑨)
- Plda — Altered, feldspar-phyric dacite of Paleogene age

Capella stocks (uppermost middle Eocene, ~39-38 Ma)

- Mecs — Pyroxene-phyric monzodiorite and quartz monzodiorite (▲ 38.8 ± 0.6 Ma⑨, ▲38.7 ± 0.6 Ma⑨)
- Medi — Fine-grained diorite (▲ 38.3 ± 0.9 Ma⑤)

La Escondida porphyry Cu complex

- Rhyolite porphyry (▲ 39.0 ± 1.5 Ma⑦, ▲ 37.5 ± 0.6 Ma⑧ ▲ 35.6 ± 1.2 Ma⑦, ▲ 34.7 ± 1.7 Ma④)
- Granodiorite- dacite porphyry
- Escondida porphyry (▲ 37.7±0.8 Ma)
- Colorado Grande porphyry (▲ 37.9 ± 1.1 Ma④, ▲ 37.2 ± 0.8 Ma⑦)

Escondida Norte-Zaldivar porphyry Cu complex

- Granodiorite-dacite porphyry complex of Escondida Norte (▲ 38.7 ± 0.4 Ma⑥, ▲ 37.5 ± 0.5 Ma⑥) Llamo porphyry of Zaldivar (▲ 38.7±1.3 Ma④, ○ 37.4 ± 0.2 Ma④)

- Silicified hydrothermal breccia
- Modern cover and omitted outcrops

San Carlos strata (uppermost middle-late Eocene, ~38-36 Ma)

- Eosc — Redbeds (conglomerate and sandstone), volcanic breccia and volcanic sandstone; autobrecciated lava flow of andesitic and dacitic composition (▲ 38.0 ± 2.1 Ma⑨, ▲ 37.7 ± 0.6 Ma⑨, ◉ 36.8 ± 0.4 Ma⑨, 34.6 ± 3.1 Ma①)

Figure 3.33 Simplified distributions of uppermost middle-late Eocene volcanic and intrusive units in La Escondida district.

Table 3.11 Summary of uppermost middle-late Eocene volcanic and intrusive units exposed in La Escondida district.

Unit (Abbreviation)	Age	Regional Description Contact relationships and lithology	La Escondida District Contact relationships and lithology	References
Capella stocks ***(MEcs)***	uppermost middle Eocene (~39 Ma)	They include the plutonic complex of La Fundición (ca 39-34 Ma) and the plutonic complex of Sierra del Jardín, in the region of Sierra Exploradora The latter complex includes monzonites, domes and dykes of rhyolitic composition, but is poorly dated at 40.7 ± 3.2 Ma (K-Ar whole-rock). This unit hosts the altered and weakly mineralised Sierra del Jardín dacitic porphyry of probable 38-32 Ma age (Cornejo and Mpodozis, 1996).	- Has intruded the Augusta Victoria Formation and Cerro Rincones plutonic complex and has been cut by andesitic dykes of the LEap (38-36 Ma). - Small stocks of pyroxene-phyric monzodiorite to quartz-monzodiorite (ca 39-38 Ma) spatially associated with the Capella hydrothermal alteration zone (Chapter 5).	Cornejo and Mpodozis (1996)
Fine-grained diorite (*MEdi*)	uppermost middle Eocene (38.3 ± 0.9 Ma)		- Some clustered plugs of fine-grained diorite have intruded the Cerro Rincones plutonic complex.	Marinovic et al (1995) Richards et al. (2001)
San Carlos strata ***(Eosc)***	uppermost middle-late Eocene (~38-36 Ma)	Several depocentres tectonically controlled by the Incaic deformation (ca 42-35 Ma) and filled by conglomerates and minor interbedded tuffs. The Loma Amarilla Formation occurs in the Salar de Atacama, whereas part of the Calama Formation crops out in the Chuquicamata District.	- A syn-tectonic succession of more than of 300 m of conglomerates, andesitic lavas and tuff, and minor volcanic sandstones and debris flows. Characteristic reddish brown colour of the massive beds In drill hole, this sequence has basal conglomerates that overlie the Augusta Victoria Formation (ca 57-53 Ma). Based on this relationship, a major unconformity is inferred, which is in agreement with the ages obtained for both units	Cornejo et al. (1993) Cornejo and Mpodozis (1996) May et al (1993) Blanco et al (2003) Mpodozis et al (2005) May et al (2005)

Table 3.12 Radiometric ages for middle Eocene rock units in La Escondida district and nearby areas.

Sample	Rock/Sub-Unit	Method (material)	Age & Error (Ma, 2 σ)	Source of Data (*)
Cerro Rincones plutonic complex (Eocr)				
ESC-34	Quartz monzodiorite */Eocr1*	U-Pb (zircon)	43 1 ± 0.5	2
II-220	Quartz monzodiorite */Eocr1*	K-Ar (biotite)	42.0 ± 4 5	1
II-231	Quartz monzodiorite */Eocr5*	K-Ar (biotite)	43.9 ± 1 3	1
ESC-15	Quartz monzodiorite */ Eocr5*	U-Pb (zircon)	42 0 ± 0.9	2
ESC-18	Quartz-phyric microgranite */Eocr8*	U-Pb (zircon)	41.0 ± 8 0	2
ESC-6	Pyroxene monzodiorite/*Eocr9*	U-Pb (zircon)	41.1 ± 0.8	2
ESC-25	Quartz monzodiorite */Eocr9*	U-Pb (zircon)	41 8 ± 0.9	2

(*) Source of data: (1) Maksaev et al (1991) and Marinovic et al (1995); (2) this study. Abbreviations: *Eocr1* = Fine- to medium-grained diorite and monzodiorite, and subordinate quartz monzodiorite; *Eocr5* = Coarse-grained, porphyritic monzonite and quartz monzonite; *Eocr8* = Quartz-feldspar-phyric micromonzonite and microgranite; *Eocr9* = Biotite-amphibole-pyroxene-phyric quartz diorite and diorite.

3.5.2 Other Altered Granodiorite, Dacite and Rhyolite porphyries (*Plda/ Eodp)*

These are several small shallow-level intrusions that crop out in the northern portions of the Cerro Rincones complex (Figure 3.31; Appendices 1A and B), whose ages are poorly constrained and which have undergone severe to moderate hydrothermal alteration. Whether they are associated with magmatism of early Eocene age or middle-late Eocene ages is yet to be determined. They are discussed further in Chapter 5.

3.5.3 Uppermost Middle-Late Eocene Intrusive and Volcanic Units

3.5.3.1 Capella Stocks *(MEcs)*

Two small, northwest-trending quartz-monzodiorite to pyroxene-phyric monzodiorite stocks (<0.8 km^2) have intruded the Augusta Victoria sequence and probably the Cerro Rincones plutonic complex (Figure 3.33; Table 3.12). Hand specimen is characterised by phenocrysts of plagioclase, orthopyroxene, clinopyroxene and subordinate biotite that has been altered to actinolite; all of them set in an interstitial groundmass of quartz, plagioclase and orthoclase. Minor cataclasitic domains and dioritic enclaves up to 3-4 mm long have been recognised in thin sections. The Capella stocks are spatially associated with the Capella alteration zone (Chapter 5), but the areal distribution of the outcrops and their contact relationships with Cerro Rincones complex are poorly constrained in the field (Figures 3.34a and b). Contacts are obscured by development of intrusion breccias,

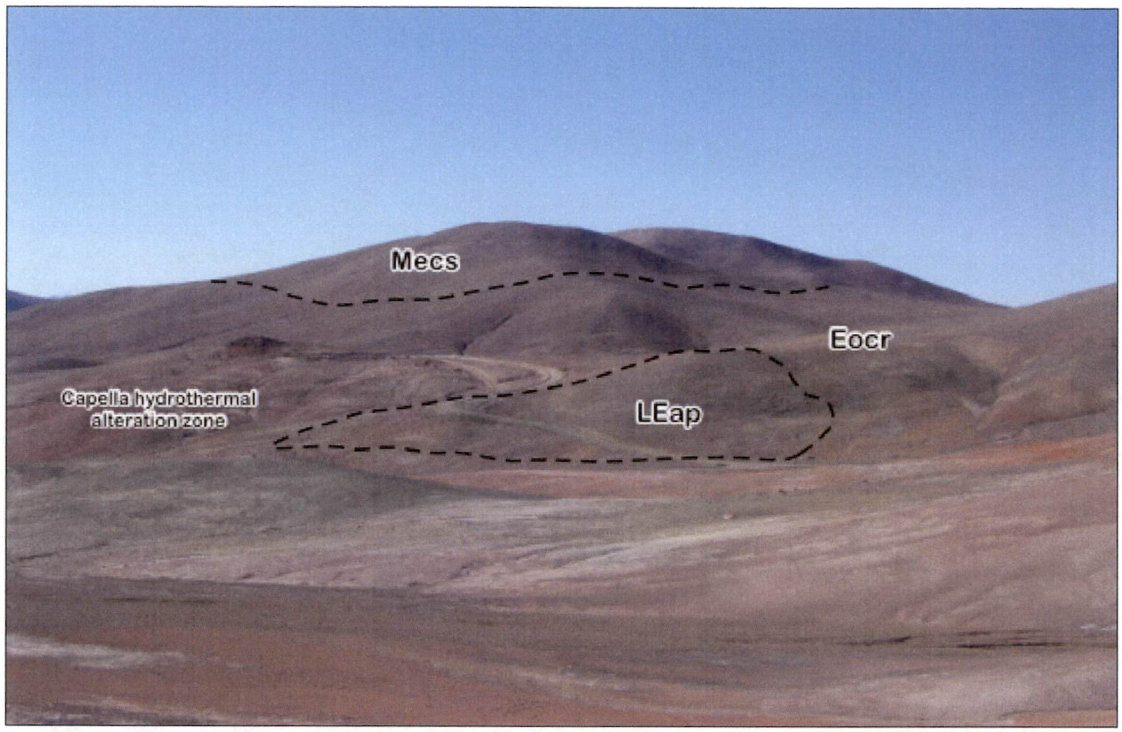

Figure 3.34a General view (looking north) of the main quartz monzodiorite body of the Capella stocks (*Mecs*; ca. 39-38 Ma), which have intruded the Cerro Rincones plutonic complex (*Eocr*; ca. 43-41 Ma) and has been cut by the dacite porphyries (*LEap*; ca. 38-36 Ma). Capella project sector (7,329,000m N; 490,400m E).

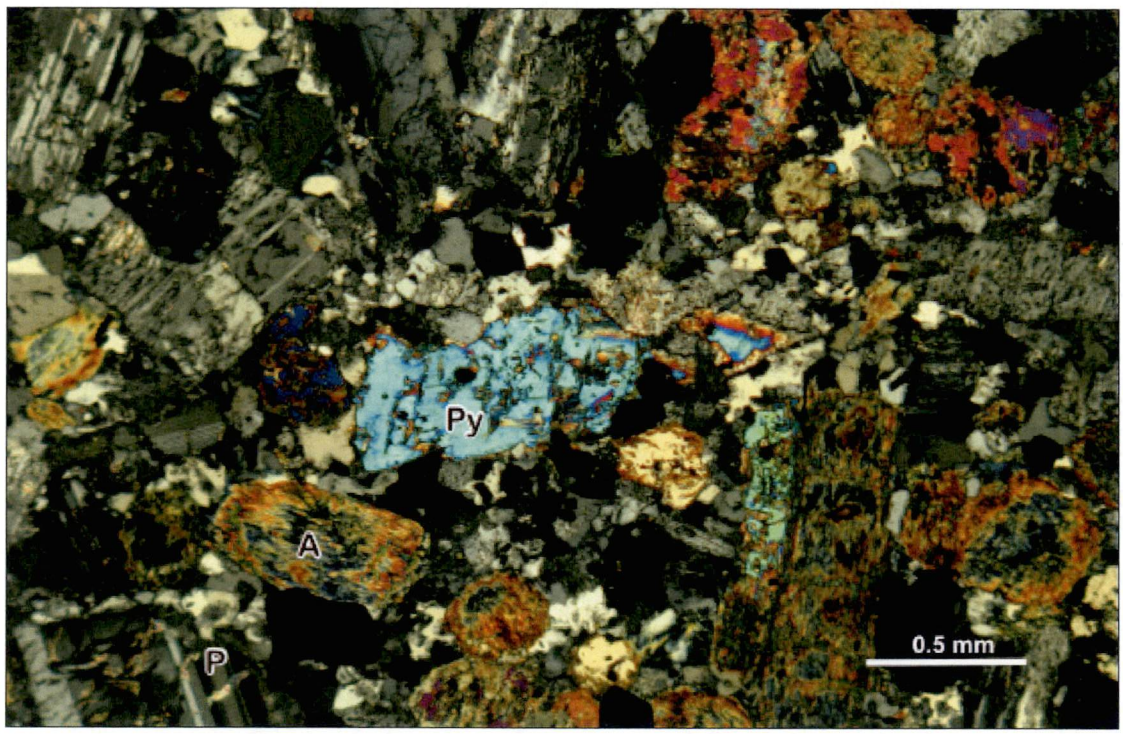

Figure 3.34b Photomicrograph (crossed nicols) of a weakly porphyritic quartz monzodiorite from the Capella stocks. Strongly actinolized pyroxenes (**Py**) and amphibole (**A**) occur with fractured plagioclase (**P**), which has been altered to albite and rare sericite. Note the quartz and feldspar-bearing intercrystalline groundmass. Sample ESC 10 (7,330,321m N; 490,956m E).

Table 3.13 Radiometric ages for uppermost middle Eocene syn-porphyry Cu intrusive and volcanic units in La Escondida district and adjacent sectors.

Sample (*)	Rock	Method (material)	Age & Error (Ma, 2 σ)	Source of Data (*)
Capella stocks ***(MEcs)***				
ESC-23	Monzonite	U-Pb (zircon)	38.8 ± 0.6	3
ESC-10	Quartz monzodiorite	U-Pb (zircon)	38 7 ± 0.6	3
Fine-grained diorite ***(MEdi)***				
IM- 110	Hornblende-phyric diorite	^{40}Ar-^{39}Ar (hornblende)	38 3 ± 0 9	2
San Carlos strata ***(Eosc)***				
ESC-46	Feldspar-phyric andesite	U-Pb (zircon)	38.0 ± 2.1	3
ESC-1	dacitic volcanic breccia	U-Pb (zircon)	37.7 ± 0.6	3
ESC-1	Amphibole-phyric dacite breccia	$^{40}Ar/^{39}Ar$ (plagioclase)	36.8 ± 0.4	3
REG-10	Amphibole-phyric dacite breccia	K-Ar (whole rock)	34.6 ± 3.1	1

(*) Source of data. (1) Maksaev et al. (1991) and Marinovic et al (1995); (2) Richards et al. (2001); (3) this study.

north-trending faulting and pervasive high-sulfidation hydrothermal alteration.

Two LA-ICP-MS U-Pb zircon ages of 38.7 ± 0.6 Ma and 38.8 ± 0.6 Ma were obtained for this unit (Table 3.13; Figure 3.40; Appendix 6), supporting an uppermost middle Eocene age for the intrusion. The Capella stocks (ca. 39-38 Ma) are therefore concluded to be somewhat younger than the Cerro Rincones plutonic complex (ca. 43-41 Ma) and are coeval with the start of the middle Eocene-early Oligocene porphyry Cu-related magmatic event (Figure 3.40; Appendix 6). However, field relationships indicate that they predate the blind porphyry associated with Capella alteration system (La Escondida brownfields exploration program, 2003-2007; this study).

3.5.3.2 Fine-grained Diorite *(MEdi)*

Plugs of fine-grained diorite have intruded the diorite to quartz monzodiorite unit *(Eocr1)* of Cerro Rincones complex and La Tabla Formation, at the northeastern extremity of the Cordon Poblete (Figure 3.33; Table 3.12). The fine-grained diorite plugs have a micro-granular texture that is locally microporphyritic. The plugs appear unaltered in outcrop. They were dated by Richards et al. (2001) at 38.3 ± 0.9 Ma (^{40}Ar-^{39}Ar), the same age as the Capella stocks *(Mecs)* (Figure 3.40). These fine-grained diorites are time equivalent with the following magmatic units mapped in the region (Figure 3.40): (1) the andesite to dacite porphyry suite *(LEap)*; and (2) the diorites and dioritic porphyries along the eastern border of La Escondida district (*Tdio* unit of Richards et al., 2001) grouped herein within the greenish grey to pale grey andesite porphyry unit *(LEap)*.

3.5.3.3 San Carlos Strata *(Eosc)*

The San Carlos strata is an informal name employed herein to describe a newly recognised continental sequence of andesitic volcaniclastic rocks and interbedded red beds, with a thickness of approximately 300 m (Figure 3.33; Table 3.12). Isolated exposures of this unit have been found in structurally-controlled slivers on the western foothills of the Sierra de San Carlos, where the west-vergent reverse Hamburgo Fault has juxtaposed Late Paleozoic crystalline basement against the San Carlos strata (Figure 3.35a). The base of the strata is not exposed due to the presence of recent alluvial cover, which prograde towards the Salar de Hamburgo (Appendices 1 and 2). Borehole logging has revealed that the strata continue beneath the salt pan (Figure 3.35b), for at least 300 m under the Recent gravels, and unconformably overlie the 57-53 Ma Augusta Victoria Formation (Appendices 2C and D).

The unit comprise a crudely layered and moderately consolidated succession of andesitic to dacitic volcanic breccia, coarse- to fine-grained lapilli-tuff, volcaniclastic sandstones and mudstones, with interbedded pebbly conglomerates (Figures 3.36a to 3.39a). Strong oxidation of fragments and matrix and ferricrete levels have imparted a characteristic red colour to these rocks, which is obvious in surface exposures, and drill core (3.39b).

Two ages were obtained for a volcanic breccia of the San Carlos strata, yielding a $^{40}Ar/^{39}Ar$ age of 36.8 ± 2.0 Ma, and an LA-ICP-MS U-Pb zircon age of 37.7 ± 0.6 Ma (Table 3.13; Figure 3.40; Appendix 6). A sample of tuffaceous sandstones from drill hole MRC-3215: 210-212 m gave an LA-ICP-MS U-Pb zircon age of 38.0 ± 2.1 Ma (Table 3.13; Figure 3.40; Appendix 6). These data place the San Carlos strata in the uppermost middle-late Eocene (38-36 Ma). The most probable depositional environment of the San Carlos strata is envisaged to be similar to that proposed for the Calama Formation (May et al., 1993; Blanco et al., 2003; May et al., 2005), and Sichal Formation (Blanco and Tomlinson, 2006): proximal alluvial fans and/or braidplain deposits in an endorheic, tectonovolcanic basin.

3.5.4 Middle Eocene-Early Oligocene Intrusives Related to Porphyry Cu Mineralisation

This group includes the mineralised hypabyssal intrusive complexes of the Escondida and Escondida Norte-Zaldivar porphyry copper systems, along with other mineralized systems known to be associated spatially and temporally with them (i.e., Pinta Verde,

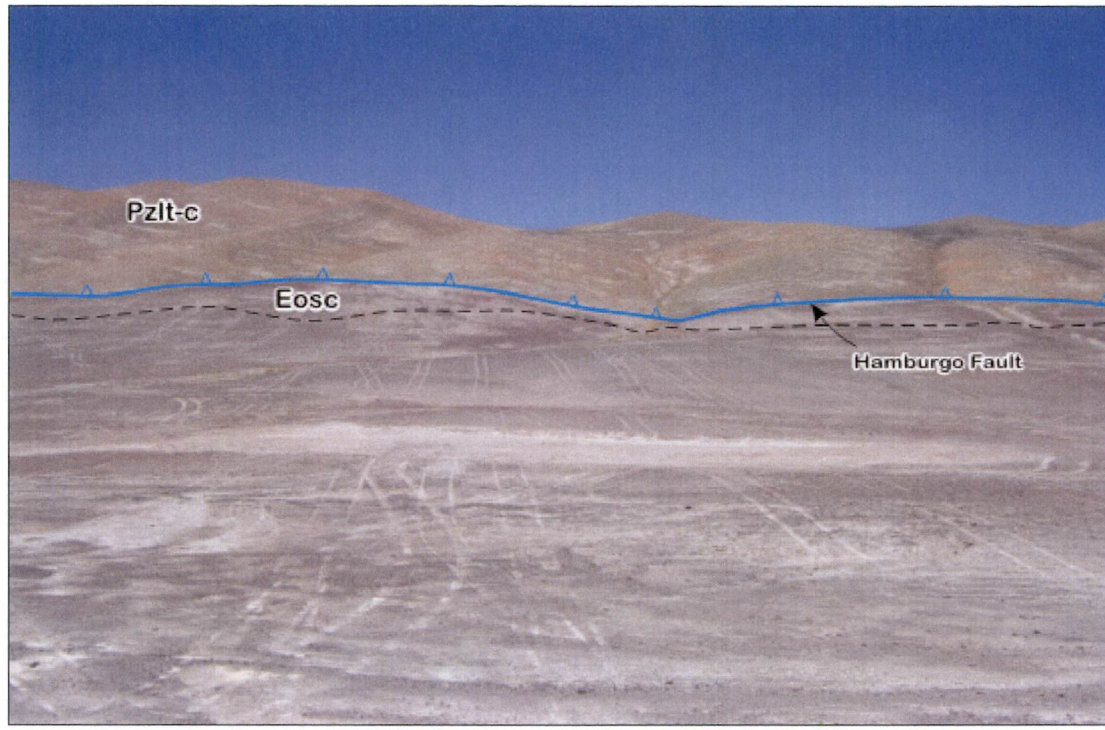

Figure 3.35a General view (looking east) of poorly exposed volcaniclastic rocks of the San Carlos strata (*Eosc*; ca. 38-36 Ma) in faulted contact through the reverse Hamburgo fault with the Eastern volcanic sub-unit *(Pzlt-c)* of La Tabla Formation (Late Carboniferous-Permian). Sierra de San Carlos (7,308,200m N; 495,000m E).

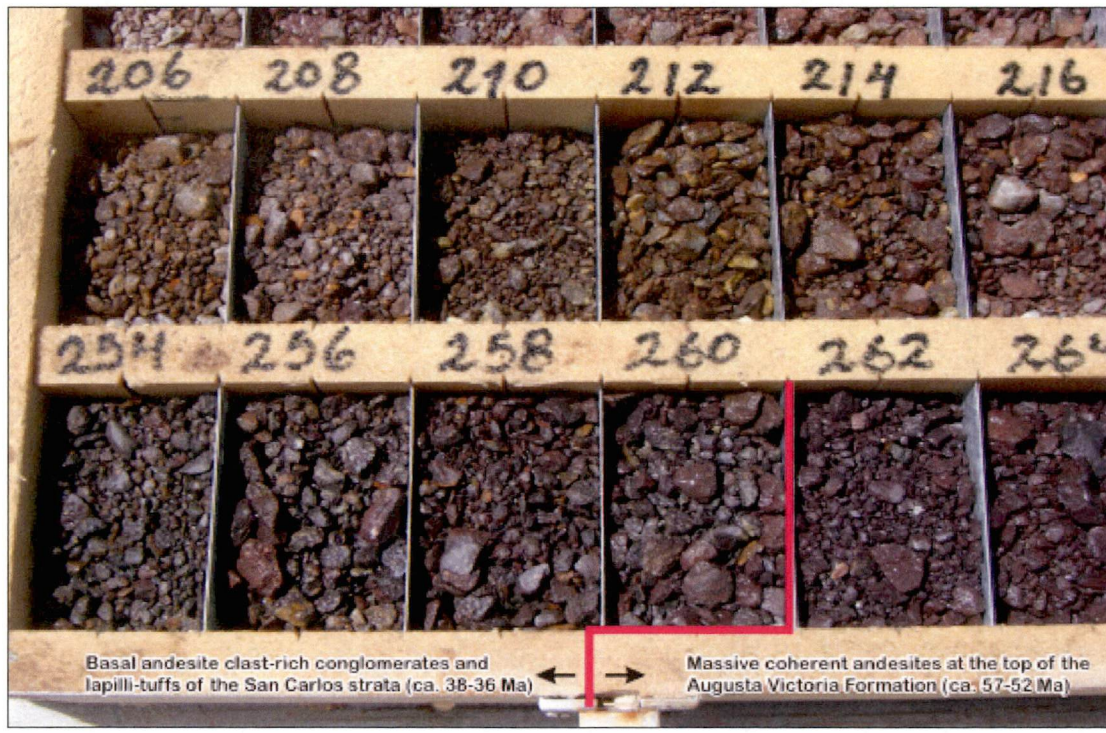

Figure 3.35b Borehole showing the lapilli-tuffs and volcaniclastic fine-grained conglomerates of the San Carlos strata (ca. 38-36 Ma) covering, with basal conglomerates, andesites of the Augusta Victoria Formation (ca. 57-53 Ma). RC-3007 borehole (Appendix 5), endorheic basin of Laguna Seca.

Figure 3.36a General view (looking north) of the gently dipping sequence of crudely stratified volcanic breccia and volcanic sandstones from the San Carlos strata. These outcrops occur about 300 m from the trace of the Hamburgo Fault. Western foothill of Sierra de San Carlos (7,308,200m N; 495,000m E).

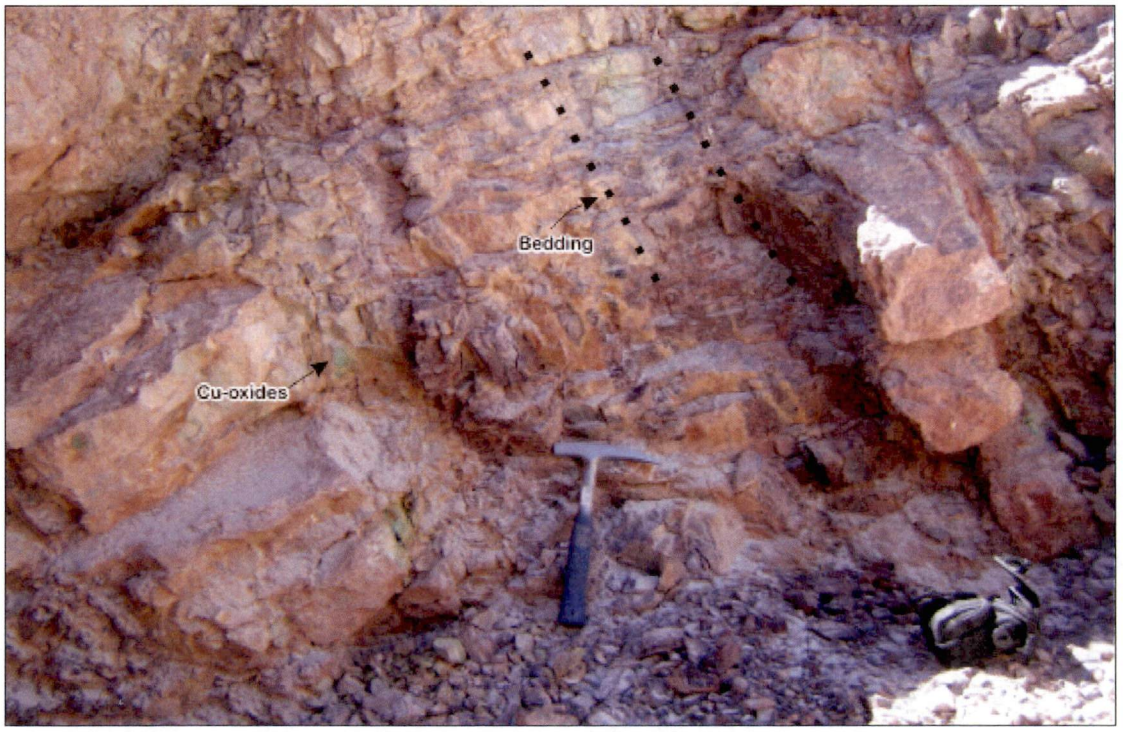

Figure 3.36b Volcaniclastic beds of the San Carlos strata close to the trace of the Hamburgo Fault. Note the steep dip (overturned?) of the stratified rocks as well as the occurrence of Cu-oxides. Western flank of Sierra de San Carlos (7,307,000m N; 493,700m E).

Figure 3.37a Massive and poorly sorted andesitic volcanic breccia of the San Carlos strata. Note the large lithic clast of andesitic composition and the coarse-grained matrix rich in lithic fragments of similar composition, together with broken feldspar crystals. Western flank of the Sierra de San Carlos (7,308,200m N; 495,000m E).

Figure 3.37b Detail of the coarse-grained matrix of the volcanic breccia of the San Carlos strata shown in Figure 3.33b. Note the finely laminated thin epiclastic bed overlying the breccia. Western flank of the Sierra de San Carlos (7,308,200m N; 495,000m E).

Figure 3.38a Finely laminated tuffaceous sandstones and mudstones, and fine-grained vitric tuffs of the San Carlos strata (ca. 38-36 Ma). Note the irregular and contorted laminations and the angular rip-up volcanic clasts. Western flank of the Sierra de San Carlos (7,307,000m N; 493,700m E).

Figure 3.38b Borehole showing the lapilli-tuffs and basal volcaniclastic conglomerates of the San Carlos strata under the Recent endoreic basin of Laguna Seca. Note the hematitic clasts and ferricrete that occur within the sequence. RC-3004 borehole, 238 to 294 m (Appendix 5).

Table 3.14 Selected radiometric crystallisation ages for La Escondida and Escondida Norte-Zaldivar porphyry copper deposits and Baker breccia.

Sample	Rock/Sub-Unit	Method (material)	Age & Error (Ma, 2 σ)	Source of Data (*)
La Escondida intrusive complex				
ESC4	Rhyolite/rhyodacite porphyry	U-Pb (zircon)	39.0 ± 1 5	1
ESC-3	Dacite/Colorado Grande porphyry	U-Pb (zircon)	37.9 ± 1.1	2
ESC2	Granodiorite/ Escondida porphyry	U-Pb (zircon)	37.7 ± 0.8	1
ESC1	Granodiorite/Colorado Grande porphyry	U-Pb (zircon)	37.2 ± 0.8	1
ESC6	Rhyodacite/rhyolite porphyry	U-Pb (zircon)	35.6 ± 1.2	1
ESC-1	Rhyodacite/rhyolite porphyry	U-Pb (zircon)	34.7 ± 1.7	2
6789	Rhyodacite/rhyolite porphyry	U-Pb (zircon)	37.5 ± 0.6	5
Escondida Norte-Zaldivar intrusive complex				
ZAL1	Dacite/Llamo Porphyry (Zaldivar operation)	U-Pb (zircon)	38.7 ± 1.3	2
ZERD-345	Dacite porphyry (Escondida operation)	U-Pb (zircon)	38.7 ± 0.4	4
ZERD-344	Granodiorite porphyry (Escondida operation)	U-Pb (zircon)	37.5 ± 0.5	4
05	Dacite/Llamo Porphyry (Zaldivar operation)	^{40}Ar-^{39}Ar (biotite)	37.7 ± 0.4	3
ZAL1	Dacite/Llamo Porphyry (Zaldivar operation)	^{40}Ar-^{39}Ar (biotite)	37 4 ± 0.2	2
06	Dacite/Llamo Porphyry (Zaldivar operation)	^{40}Ar-^{39}Ar (biotite)	37.1 ± 0.5	3
40	Dacite/Llamo Porphyry (Zaldivar operation)	^{40}Ar-^{39}Ar (biotite)	36.6 ± 0.4	3
30	Dacite/Llamo Porphyry (Zaldivar operation)	^{40}Ar-^{39}Ar (biotite)	36.6 ± 0.9	3
11	Dacite/Llamo Porphyry (Zaldivar operation)	^{40}Ar-^{39}Ar (biotite)	36.5 ± 0.5	3
16	Dacite/Llamo Porphyry (Zaldivar operation)	^{40}Ar-^{39}Ar (biotite)	36.0 ± 0 3	3
03	Dacite/Llamo Porphyry (Zaldivar operation)	^{40}Ar-^{39}Ar (biotite)	35.5 ± 0.7	3
Baker porphyry				
ESC-38	Dacite porphyry	U-Pb (zircon)	38.0 ± 1.1	6

(*) Source of data: (1) Padilla-Garza (2003); (2) Richards et al. (1999); (3) Campos (2002); (4) Pollard and Taylor (2002); (5) Sepulveda (written comm.); (6) this study

Carmen, Ricardo and Baker; Figure 3.33). The characteristics of each hydrothermal system are described in Chapter 5. The Baker dacite porphyry, a mineralised system peripheral to La Escondida deposit (Figure 3.33), has yielded a LA-ICP-MS U-Pb zircon age of 38.0 ± 1.1 Ma (Table 3.14; Figure 3.40; Appendix 6). Therefore, it lies within the range of previously reported ages (39-34 Ma) for the multiple intrusive phases at La Escondida (Richards et al., 1999; Padilla et al., 2001; Padilla-Garza, 2003; Table 3.14; Figure 3.40; Appendix 6) and the Escondida Norte-Zaldivar system (Richards et al., 1999; Richards et al., 2001; Campos, 2002; Campos et al., 2003; Pollard and Taylor, 2002; Sepúlveda, written

comm.,2007; Table 3.14; Figure 3.40; Appendix 6).

3.5.5 Middle-Late Eocene Dykes (post-mineralisation)

3.5.5.1 Greenish Grey to Pale Grey Andesite Porphyry *(LEap)*

This unit comprises a large swarm of dykes and minor plugs of dominantly andesitic composition, up to 15-20 m wide and several hundred meters long (Figures 3.33; Table 3.15). They are broadly distributed throughout the region, have diverse orientations (Chapter 4) and have been subdivided into several facies at Chimborazo (granodiorite porphyry, Palma, 1993; diorite dyke, Petersen et al., 1996; rhyodacite porphyry, Pritting, 2002; diorite dyke, Richards et al., 1999 and Richards et al., 2001). They postdate the altered and mineralised systems of Escondida, Escondida Norte-Zaldivar, Baker porphyry, Chimborazo and Capella. Several fingers of andesite porphyry have been identified during the present study in drill core from La Escondida, Escondida Norte and Chimborazo. The dominant lithology of the *LEap* unit is a greenish grey, medium- to coarse-grained andesitic porphyry, with characteristic phenocrysts of amphibole, biotite and rare quartz, set in a microcrystalline groundmass (Figure 3.39a). Part of these dykes from Capella and Chimborazo sectors has significant microcrystalline fracturing and brittle comminution (Figure 3.39a), as well as mesoscopic faulting and shearing in core (e.g., RC-976; Appendix 5) and outcrops (e.g., Zanjas prospect; Chapter 5). Subordinate medium-grained diorite and dacite are also present locally. When K-Ar age determinations from plagioclase are included, the radiometric dataset for these rocks shows a range of ages distributed between 46 and 34 Ma (Table 3.16; Figure 3.40; Appendix 6). However, when only the ^{40}Ar-^{39}Ar and LA-ICP-MS U-Pb zircon dates are considered (Richards et al., 1999; Richards et al., 2001; this study), it is apparent that the rocks formed around 38-36 Ma (middle-late Eocene; Figure 3.40). Problems with the plagioclase K-Ar ages are described comprehensively in Appendix 6.

3.5.5.2 Greyish Red Pyroxene Andesite Porphyry *(LEpap)*

This poorly exposed homogenous body has a surface area of approximately 2 km^2. Contact relationships are poorly constrained due to poor exposures (Figure 3.33, Table 3.15). Petrographically the *LEpap* unit is composed of an amphibole-bearing pyroxene-phyric andesite. The porphyry is recognised in the field by its distinct greyish red colour and coarse-grained porphyritic texture (Figure 3.39b), which contrasts with the surrounding, crudely stratified, greenish fine-grained andesite and sandstone of the Augusta Victoria Formation. One $^{40}Ar/^{39}Ar$ plagioclase age determination for this

Table 3.15 Summary of middle-late Eocene intrusive rocks exposed in La Escondida district.

Unit (Abbreviation)	Age	Regional Description Contact relationships and lithology	La Escondida District Contact relationships and lithology	References
Greenish grey to pale grey andesite porphyry *(LEap)*	middle-late Eocene (~38-36 Ma)	No regional description	- Regionally extensive dykes swarm plus minor plugs These have intruded all Paleozic to Paleogene sedimentary and magmatic units, and also the mineralized systems at Capella, Chimborazo, and Baker porphyry. Medium- to coarse-grained andesitic porphyry, with characteristic phenocrysts of amphibole, biotite and rare embayed quartz. Subordinate medium-grained diorite and dacite are also present in places	Palma (1993) Petersen et al (1997) Richards et al. (1999) Richards et al. (2001) Pritting (2002)
Greyish red coloured pyroxene andesite porphyry *(LEpap)*	lowermost late Eocene (36 5 ± 0.5 Ma)	No regional description	- Has intruded the Late Paleocene-Early Eocene Augusta Victoria Formation volcanic rocks. A distinct greyish red colour, coarse-grained porphyritic textured pyroxene-plagioclase-phyric andesite, contrasting with the surrounding greenish fine-grained andesite and sandstone country rocks.	
Greyish orange to yellowish orange dacite and andesite porphyries *(EOoda)*	middle-late Eocene	No regional description	- Orange coloured dacitic and andesitic dykes which exhibit local bleaching Small crystals of pyrite partially altered to Fe-oxides. The dykes commonly reach up to 3-5 m wide and a few tens of meters length Other plugs occur at the northern border of the study area in Sierra Poblete, where they are hosted by the Augusta Victoria Formation	

Table 3.16 Radiometric ages for middle-late Eocene andesitic to dacitic rock units (post-mineralisation), in La Escondida district and contiguous areas.

Sample	Rock	Method (material)	Age and Error (Ma, 2 sigma)	Source of data (*)
Greenish grey to pale grey andesite porphyry *(LEap)*				
SAM-5	N.D.	K/Ar (whole rock)	45.9 ± 9.1	1
CHIM-1	Amphibole diorite	K/Ar (hornblende)	38 8 ± 3.4	3
IM-154	Feldspar-biotite-quartz porphyry	^{40}Ar-^{39}Ar (biotite)	38.1 ± 0.3	4
ESC-9	Biotite-amphibole andesite porphyry	U-Pb (zircon)	38 1 ± 0.6	5
IM-46	Hornblende diorite	^{40}Ar-^{39}Ar (hornblende)	38.3 ± 0.3	2
IM-47	Hornblende diorite	^{40}Ar-^{39}Ar (hornblende)	37.9 ± 0.3	2
IM-70	Hornblende diorite	^{40}Ar-^{39}Ar (hornblende)	37 9 ± 0.3	2
IM-90	Dacite porphyry	^{40}Ar-^{39}Ar (hornblende)	37.0 ± 0.9	2
IM-79	Andesite dyke	^{40}Ar-^{39}Ar (hornblende)	36.9 ± 0.5	2
SAM-2	N.D.	K/Ar (whole rock)	34.3 ± 6.1	1
Greyish red pyroxene andesite porphyry *(LEpap)*				
ESC-8	Pyroxene andesite porphyry	$^{40}Ar/^{39}Ar$ (plagioclase)	36.5 ± 0 5	5

(*) Source of data: (1) Gardeweg et al. (1994); (2) Richards et al. (2001); (3) Palma (1993) and Petersen et al (1996); (4) Richards et al. (1999); (5) this study. Abbreviations: N.D. = Not described.

intrusion has provided an age of 36.5 ± 0.5 Ma (Table 3.16; Figure 3.40; Appendix 6).

3.5.5.3 Greyish Orange to Yellowish Orange dacite and Andesite Porphyries *(EOoda)*

A series of discontinuous, bleached orange dacitic and andesitic dykes (< 3-5 m thick) have mostly intruded the volcanic rocks of La Tabla and Augusta Victoria Formations. A north-northeast-orientated group of dacite dykes commonly contain small crystals of partially oxidised pyrite, and have undergone weak argillization at Escondida Norte-Zaldivar deposit. Other andesite plugs recognised at the northern end of the study area are strongly altered to clays, epidote and calcite. Late Eocene-Oligocene age is suggested for the dykes, based on the intrusive contact with the Augusta Victoria Formation.

3.5.5.4 Other Late Eocene-Early Oligocene Dykes *(Eodad/Eold)*

Relatively sparse, thin dykes (<1-2m) are hosted by the previous sedimentary, volcanic and intrusive rocks exposed in the region. The dykes are readily mappable in the field (Appendix 1), but they are not obviously linked to any of the major magmatic events described above. The dykes include: (1) fine-grained diorite and andesite dykes *(EOdad)*; and (2) fine-grained dacite and andesitic dykes *(EOld)*. No detailed work was done on these dykes during the current study due to their restricted distribution.

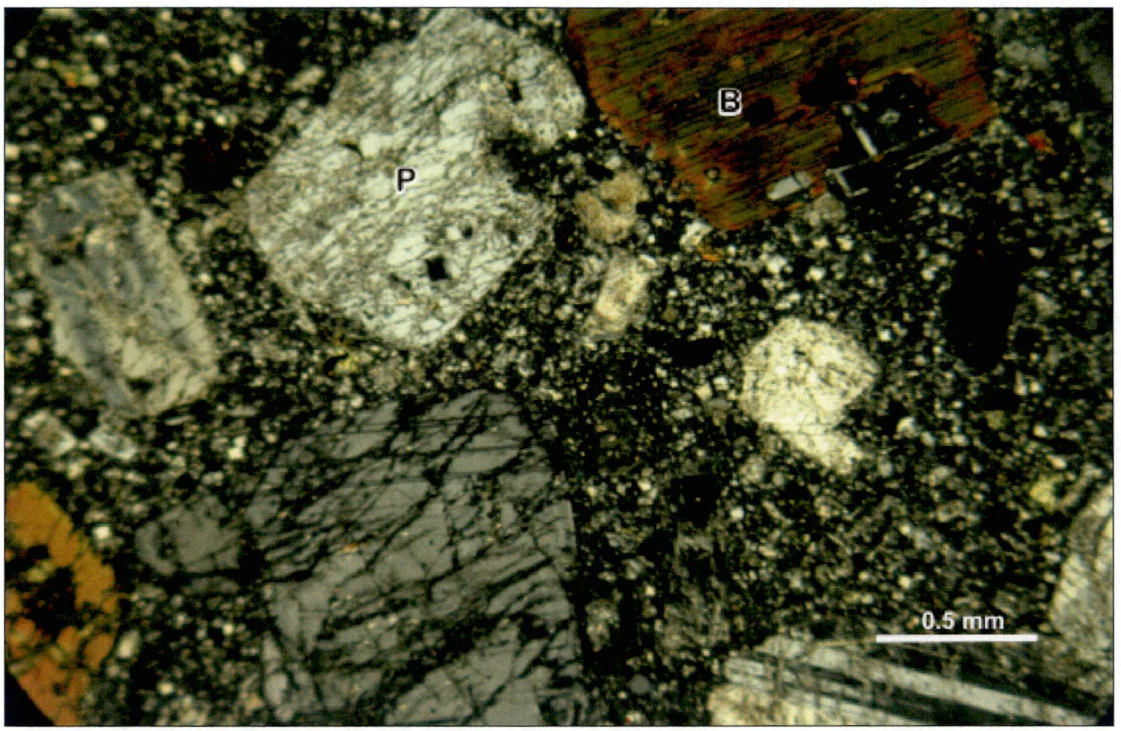

Figure 3.39a Photomicrograph (crossed nicols) of a medium-grained andesite porphyry of the *LEap* unit (ca. 38-36 Ma). Note the intense fracturing of the plagioclase (P) phenocrysts, along with unaltered biotite (B) in a microgranular groundmass. Sample ESC-9 (7,328,115m N; 491,057m E).

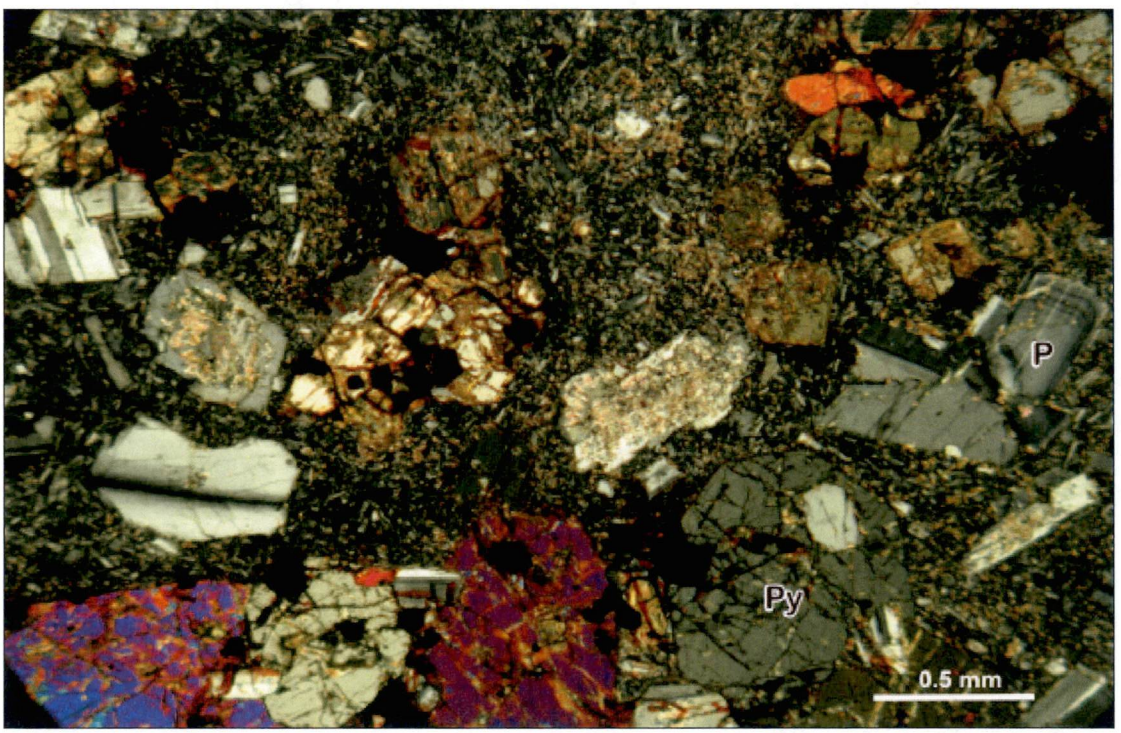

Figure 3.39b Photomicrograph (crossed nicols) of a medium-grained pyroxene-phyric andesite porphyry (*LEpap*; 36.5 ± 0.5 Ma). Relatively unaltered plagioclase (**P**) and pyroxene (**Py**) phenocrysts supported by a pilotaxitic groundmass rich in microlites. Sample ESC-8 (7,325,370m N; 487,316m E).

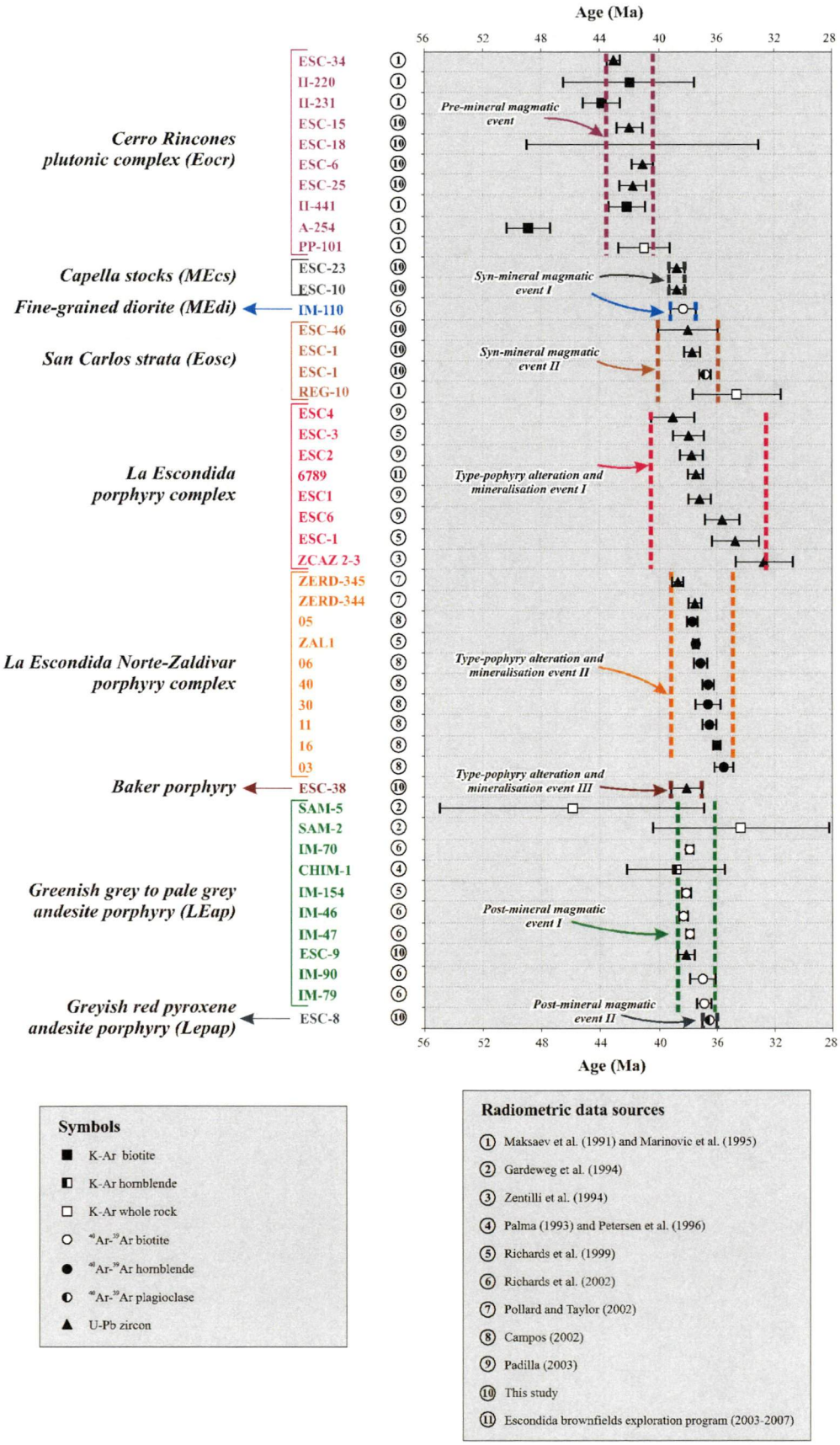

Figure 3.40 Age distribution for middle-late Eocene intrusive and volcaniclastic units in La Escondida district, referred to as pre-, syn- and post-mineralisation, with respect to the Eocene porphyry Cu-style magmatism and mineralisation. Analytical details provided in Appendix 6.

3.5.6 Geological Summary of Middle Eocene-Early Oligocene

The Cerro Rincones plutonic complex (43-41 Ma) is comparable to similar magmatic centres described from other porphyry districts of northern Chile, such as at El Salvador-Potrerillos (48-42 Ma) and Sierra Exploradora (48-40 Ma), described by Cornejo et al. (1993) and Cornejo and Mpodozis (1996) respectively. These authors argued that these clusters of intrusives constitute magmatic centres separated by a distance of ca. 100 km along the Domeyko Cordillera, coinciding with areas of porphyry copper mineralisation (i.e., El Salvador, Sierra Exploradora, and La Escondida). This magmatism pre-dated the Eocene Incaic deformation phase in El Salvador-Potrerillos and Sierra Exploradora regions (Mpodozis et al., 1994; Cornejo and Mpodozis, 1996; Cornejo and Matthews, 2001), which diachronously affected a large part of the Andean margin between 45 Ma and 35 Ma (e.g., Maksaev, 1990; Reutter et al., 1991; Mpodozis and Ramos, 1991; Cornejo et al., 1993; Chapter 4). However, field mapping in La Escondida district has not provided conclusive argument in favour of a pre-tectonic emplacement for the Cerro Rincones complex. Its diverse intrusive phases are characterised by a lack of mesoscopic and microscopic deformational fabrics. Early phases of the complex have also intruded the cores of anticlines in the Santa Ana and Augusta Victoria Formations (Appendix 1A), without any evidence of strain, and also a pre-deformation timing is inferred. In contrast, a syn-tectonic timing is suggested for the greenish grey to pale grey andesite porphyry dykes *(LEap)*. The dykes locally exhibit considerable mesoscopic and microcrystalline deformation (Figure 3.39a) and marked NE and WNW elongation in outcrop (Figure 3.33). Other syn-tectonic intrusions includes the monzodiorites of Capella (39-38 Ma), the mineralised porphyries of Escondida and Escondida Norte-Zaldivar copper deposits (39-34 Ma; Figure 3.40) and Baker porphyry, which were all emplaced along large faults (Appendixes 1A and B; Chapter 4).

Numerous previous workers have highlighted for this part of the Domeyko Cordillera the quiescence in volcanism from the middle Eocene to the present (Mpodozis et al., 1993a; Marinovic et al., 1995; Richards et al., 2001; Padilla-Garza, 2003). However, the current study has identified localized volcanic activity in the form of the 38-36 Ma San Carlos strata. This small volume volcanic event is believed to have been associated with terrestrial sedimentation in a small tectonovolcanic basin limited by the Hamburgo and Escondida faults (Figure 3.30). The basin most likely formed during the Incaic orogeny, and its boundary faults have a complex history of movement (Chapter 4).

3.6 LATE CENOZOIC

Late Cenozoic gravels and associated evaporite deposits cover approximately 45% of the mapped surface area (Appendices 1A and B). The unconsolidated geological units include the late Oligocene-middle Miocene Pampa Mulas Formation *(LTpm)*, the Pliocene-Holocene alluvial deposits *(Qa)* and Recent pyroclastic flows *(Qpy)* and evaporites *(Qe)* (Chong, 1973; Marinovic et al., 1995). Brief summaries of the most relevant features of these units are provided in Table 3.17.

3.7 SUMMARY

The Phanerozoic history of La Escondida district records a number of major geological events. The most relevant aspects to this study are as follows:

- The Late Paleozoic basement consists of a basic to silicic volcanic sequence (La Tabla Formation) and cogenetic intermediate to felsic plutons of the Imilac plutonic complex, which host altered dacite and rhyolites porphyries of Late Triassic age.
- A thick, mixed siliciclastic-calcarous sequence was deposited from the Late Triassic to the Neocomian. The interaction of terrestrial, transitional and marine sedimentary environments was the setting for a transgression-regression cycle registered by El Profeta and Santa Ana Formations. No evidence for magmatism has been observed in these sequences.
- After the Late Cretaceous Peruvian contractional tectonic phase, plutonism and volcanism occurred in the uppermost Late Cretaceous and lowermost early Paleocene. A series of compositionally diverse and preferentially north-elongated, small plutonic complexes (i.e., Torcaza, Cerro Bayo, Sombrero) were emplaced at 81-64 Ma. Subaerial deposition of a volcaniclastic and volcanic unit and intrusion of coeval dyke swarms, also occurred during this time (ca. 70-66 Ma).
- After the K-T contractional tectonic phase occurred at 64-62 Ma (Cornejo et al., 2003), an episode of intermediate to silicic explosive volcanism covered a large part of the region between 57 Ma and 53 Ma, resulting in the deposition of the Augusta Victoria Formation.
- From the middle Eocene onwards, several geological events preceded or occurred contemporaneously with emplacement of the porphyry copper mineralised systems during the Incaic deformation phase (ca. 45-35 Ma). The most relevant magmatic and sedimentary episodes were:

1. The intrusion of the pre-mineralisation Cerro Rincones plutonic complex (ca. 43-41 Ma), the largest plutons of La Escondida district.
2. The intermediate intrusive complex linked to La Escondida and Escondida Norte-Zaldivar porphyry copper clusters (ca. 39-34 Ma).
3. Few and small monzonitic stocks emplaced in the Capella sector around 39 Ma (uppermost middle Eocene), which can be interpreted as pre-mineralisation intrusions.
4. A post-mineralisation swarm of diorite and andesite dykes of middle-late Eocene age (ca. 38-36 Ma).
5. Deposition of a volcaniclastic sequence (ca. 38-36 Ma), the San Carlos strata, in a terrestrial tectonovolcanic basin that developed contemporaneous with the intrusion of the porphyry copper clusters.
6. Substantial volumes of gravels of Pampa Mulas Formation, almost 300 m thick underneath the Salar de Hamburgo (salt pan), record denudation and uplifting between the late Oligocene and middle Miocene.
7. Post-Miocene fossilisation of the landscape due to hyper- to semi-aridity, which has continued to Recent times.

Table 3.17 Summary of Late Cenozoic sedimentary units exposed in La Escondida district.

Unit (Abbreviation)	Age	Regional Description Contact relationships and lithology	La Escondida District Contact relationships and lithology	References
Pampa Mulas Formation *(LTpm)*	late Oligocene-middle Miocene	These are the well known Atacama Gravels and Tambores Formation, along with other stratigraphically equivalent gravel deposits as the Pampa de Tamarugal gravels in the Central Depression province. They are considered to be the product of an important peneplanisation event in northern Chile.	- Coarse-grained sequence of polymictic gravels, breccias and gravely sands, poorly consolidated and crudely stratified, which occur above a sub-horizontal unconformity over the older stratified and intrusive rocks exposed in the region Its maximum thickness in La Escondida, based on drill core information is probably in the order of 300-350 m.	Dingman (1963) Chong (1973) Mortimer (1973) Mpodozis et al. (1993a) Gardeweg et al (1994) Marinovic et al (1995) Marinovic et al (1996)
Alluvial deposits *(Qa)* and Recent pyroclastic flow *(Qpy)*	Pliocene-Holocene	They are widely recognised along northern Chile as significant aggradational components of the present landform	- This is the largest areal component of the Cenozoic alluvial cover. It includes old deposits that define piedmont aprons, alluvial plains, and subordinately, the marginal facies of closed basin that content salt pans and ephemeral lakes. Their thickness is up to 80-100 m in tectonically active areas, where talus deposits occur in fault-bounded ranges and beneath the endorheic basins	Marinovic et al. (1995)
Evaporites *(Qe)*	Pleistocene-Holocene	Relatively thick evaporite successions deposited in restricted basin elongated within the pre-Cordillera morphotectonic province in northern Chile. (e.g , Salar de Atacama and Salar de Punta Negra)	- Deposits composed of sulphates, chlorides and minor carbonates, with common interbedded salty silt and fine sand levels, which accumulated in confined intermountain basins that host ephemeral saline lakes, such as the Salar de Hamburgo salt pan and Laguna Seca dry mudflat (playa) Their thickness, defined by drill hole in Salar de Hamburgo, is on the order of 4-5 m.	Chong (1994) Marinovic et al. (1995) Henríquez (oral comm , 2003)

CHAPTER 4
Structural Geology

La Escondida district is located in the Domeyko Cordillera, an overall north-trending Cenozoic orogen intimately linked with the evolution of the Domeyko Fault System (DFS). The DFS was active in the Eocene and has remained so into the Holocene, providing the main control on the structural grain of the region (Maksaev, 1990; Coira et al., 1982; Reutter et al., 1991; Scheuber et al., 1994; Mpodozis et al., 1993a, 1993b; Tomlinson and Blanco, 1997a, 1997b). Structural studies have divided the orogen into four principal segments (Maksaev, 1990; Cornejo and Mpodozis, 1995; Figure 4.1) with varying kinematic histories. The study area occurs in the Limón Verde-Punta Negra segment, which includes crystalline and sedimentary rock units ranging from the Paleozoic to Early Cenozoic in age (Figure 4.2). These rocks experienced complex translations and rotations mostly before the Miocene (Mpodozis et al., 1993b; Arriagada et al., 2003). The contraction and extensional tectonic episodes that have affected the region since the Paleozoic are provided in Figure 2.1.

This chapter outlines the history of deformation for La Escondida region based on study of 27 key localities that provided information on the different deformation episodes. This study has involved field mapping, borehole logging, cross sections construction, radiometric dating, and kinematic measurements. Major limitations in the regional structural and paleostress analyses are: (1) the small number of measurements obtained due to the poorly exposed outcrops, with the exceptions of the Zaldivar and La Escondida open pits (Padilla-Garza, Niemeyer, and Delgado, 1997; Véliz and Padilla, 1997; Vergara, 2002); and (2) the complexity of the structural evolution observed in diverse structural blocks, particularly in those that record the effects of the Tertiary and earlier deformational history. Consequently, there are uncertainties intrinsic to the kinematic data and their significance at regional and/or local scales. Attempt to reduce these have been made incorporating all available structural information (e.g., dyke orientations, magmatic flow banding, cleavage, bedding, fault-striae, etc). Unpublished kinematic data (12 locatities) from H. Niemeyer (1996) have been incorporated into the data analysis. The structural stations of H. Niemeyer are discriminated by roman

numerals, whereas those of the current study are labeled by capital letters on Figure 4.3. Location of structural stations, measurements and all other relevant data are presented in Appendix 7.

4.1 Structural domains

Two principal fault-bounded structural domains have been identified on the basis of rock types, folding styles, structural orientations and ages (Figure 4.3). The Escondida master fault, a segmented and curvilinear eastern branch of the DFS, forms the boundary between the eastern and western domain (Figure 4.3).

4.1.1 Eastern Domain

This domain contains Late Paleozoic intrusive, volcanic and minor sedimentary basement units which are slightly deformed. It dominates the eastern flank of the Domeyko Cordillera, extending east as far as the Salar de Punta Negra pan (Figure 4.2). The latter is an intermontane basin that separates the Domeyko Cordillera from the Neogene volcanic chain located farther to the east (Figure 1.2). To the east, the eastern domain units have been thrusted over redbeds of the Late Cretaceous-Early Tertiary Purilactic foreland basin (Reutter et al., 1991; Scheuber and Reutter, 1992; Mpodozis et al., 1993a, 1993b; Marinovic et al., 1995; Mpodozis et al., 2005; this study) and the time-equivalent volcaniclastic rocks exposed at the latitude of La Escondida district (24°20'S). Two principal structural blocks (Imilac and San Carlos) have been defined within the eastern domain based on the dominant internal stratigraphic arrangement, deformation style and bounding faults (Figure 4.3).

4.1.2 Western Domain

This domain contains tightly folded Mesozoic platform carbonate-siliciclastic sequences and Late Cretaceous-Early Tertiary intrusive and volcanic units. Steep, west- and east-vergent, north-striking reverse faults have juxtaposed narrow discontinuous panels of Late Paleozoic volcanic basement against the folded and reverse-faulted Mesozoic mixed clastic-calcareous sequences. To the west, the western domain is bounded by the Sierra de Varas master fault, another large and curvilinear branch of the DFS (Figure 4.3), giving the domain the appearance of a mega-lens (Mpodozis et al., 1993a, 1993b). The principal structural blocks defined in the western domain include Poblete, Oxidos, Rincones, Puma W, Puma E, Bayo Pascua-Curvas, Perito, Sombrero and Cerro Campamento (Figure 4.3).

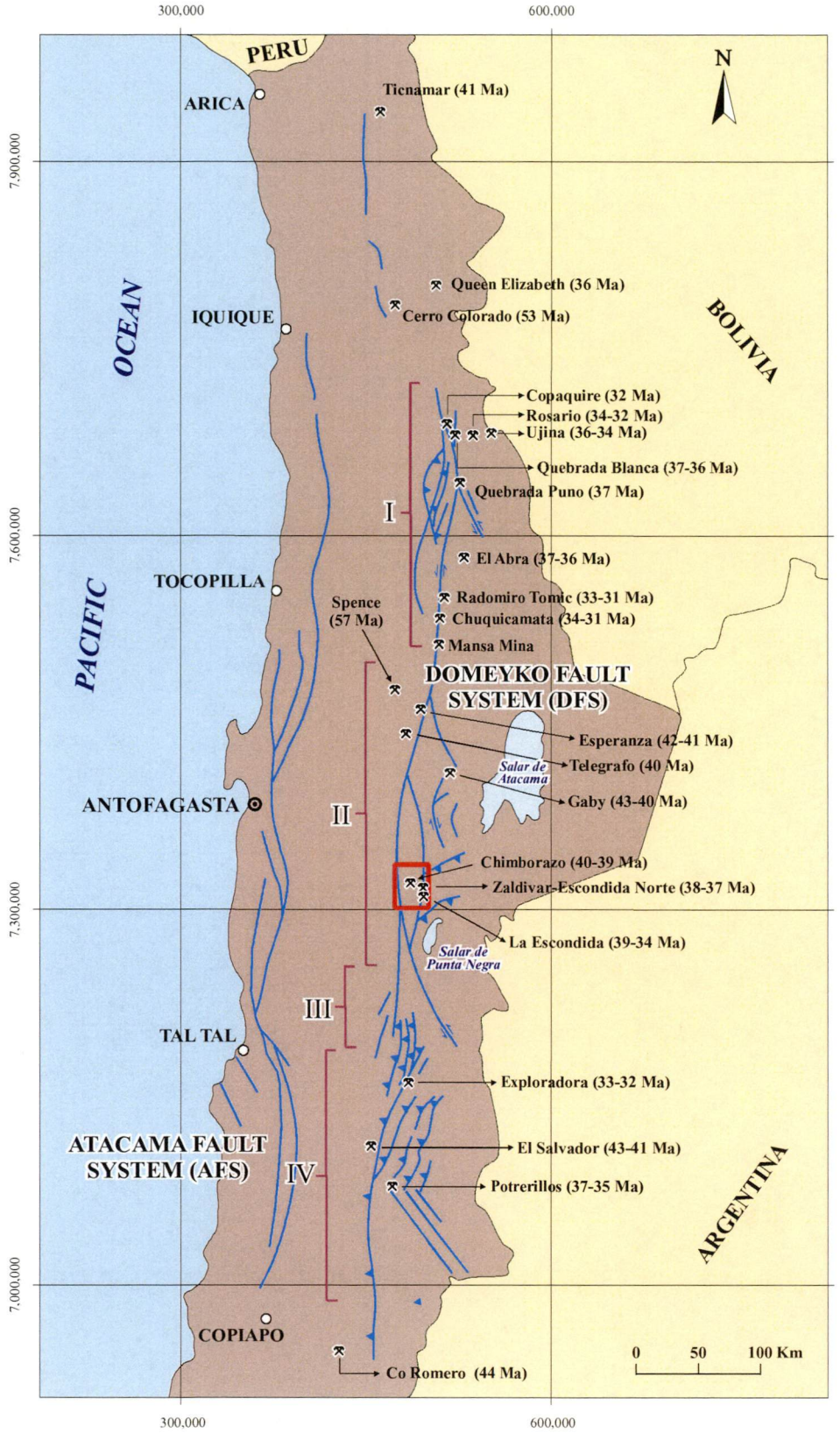

Figure 4.1 The Domeyko Fault System (DFS) in northern Chile, indicating the principal porphyry Cu deposits and the main structural segments (adapted from Maksaev, 1990 and Mpodozis et al., 1993a). The four principal segments of the DFS are: (I) Quebrada Blanca-Chuquicamata; (II) Limón Verde-Punta Negra; (III) Vaquillas-Sierra de Varas; and (IV) El Salvador-Quebrada Carrizalillo.

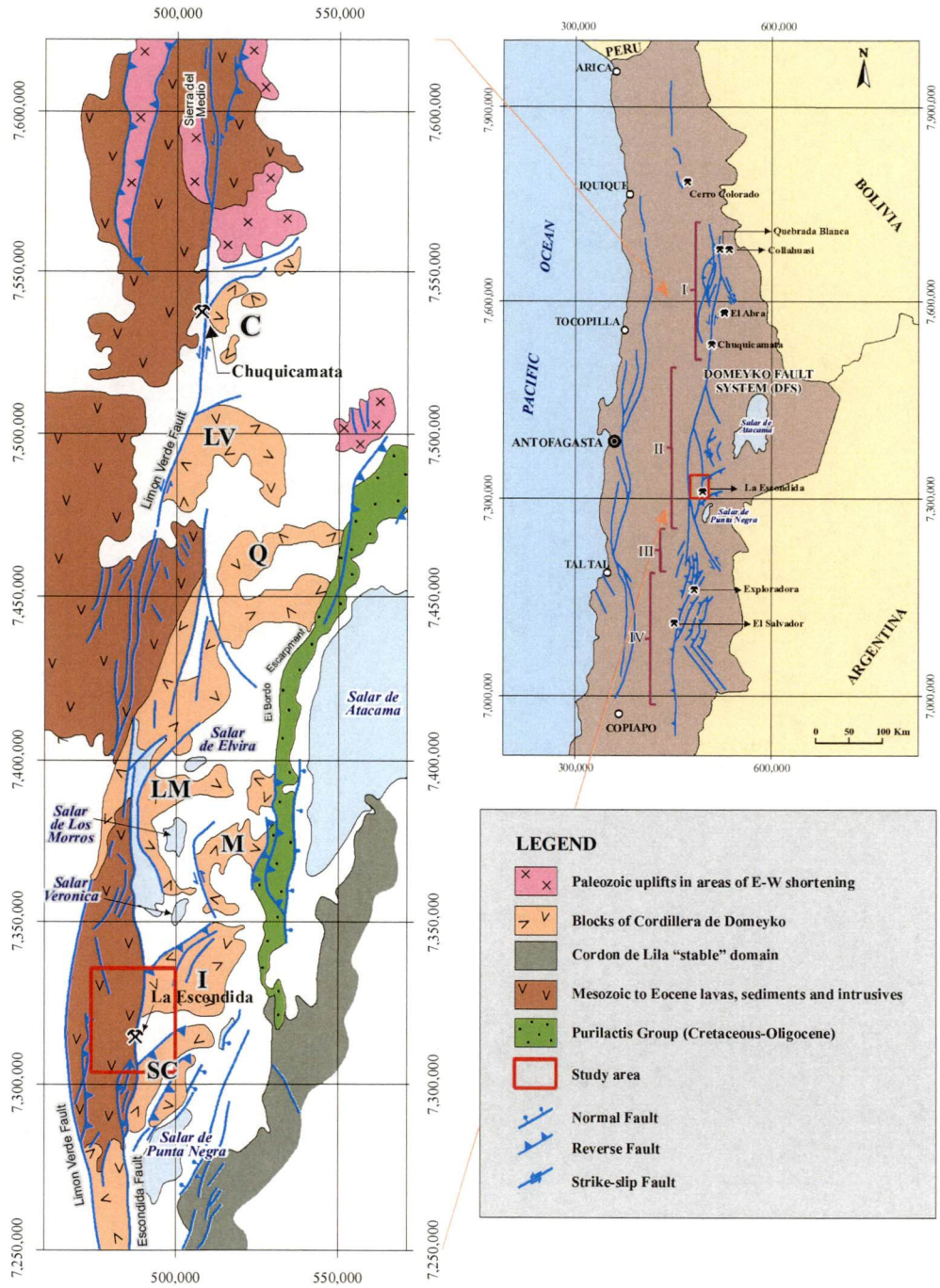

Figure 4.2 Schematic structural domains of the Cordillera de Domeyko in segment II: Limón Verde-Punta Negra, C, Cerros de Chuquicamata; LV, Limón Verde; Q, Quimal; LM, Los Morros; M, Mariposas; I, Imilac; SC, San Carlos basement blocks; LE, La Escondida Shear Lens (adapted from Mpodozis et al., 1993a, 1993b; Tomlinson and Blanco, 1997a, 1997b; Arriagada et al., 2003).

4.2 LATE PALEOZOIC-TRIASSIC DEFORMATION

Limited information has been obtained for the earliest recognized deformation events. The data come from the Late Carboniferous-Permian La Tabla Formation, which is exposed in the San Carlos and Imilac blocks (eastern domain). Here La Tabla strata are

Figure 4.3 Structural framework of the Domeyko Cordillera in La Escondida district, northern Chile (adapted from Maksaev, 1990; Mpodozis et al.,1993a and b; Palma, 1993; Gardeweg, 1994; Marinovic et al., 1995; Niemeyer, 1996; Urzúa, 2001a; Amilibia, 2002; this study).

gently folded and generally form homoclinal structures that extent largely to the east. Two first-order folds were observed in the Imilac block (Figure 4.4a). They are open to gentle synforms (interlimb angle > 100°), with wavelengths of a few km. Two regional scale NNW- to NW-trending fold axes plunge shallowly to the NW and SE (Appendix 1B). However, other N- to NNE-oriented folds have been recognized to the east of La Escondida district.

4.2.1 Stereonet Data

The limited amount of bedding observed in La Tabla Formation dips gently to the SW (Figure 4.4b). Spaced and anastomosing cleavage occurs locally in conglomerates and sandstones of the Central volcano- sedimentary sub-unit (*Pzlt-b*) (structural station A, Imilac block; Figure 4.3). At station A, there is a homoclinal structure with poorly defined bedding (Figure 4.5a) and the folding is almost negligible. The cleavage planes dip steeply ENE, whereas the cleavage-bedding intersection lineations (CBIL) plunge consistently towards SSE, with 35°-43° (Figure 4.5b). No appropriate bedding planes were found in the outcrops to establish whether the cleavage is an axial plane cleavage.

4.2.2 Age and Significance of the Deformation

There are few constraints on the age of the deformation observed in the Late Carboniferous-Permian (ca. 294-282 Ma) La Tabla Formation in the eastern structural domain. The folding style that affects La Tabla is very different to the lowermost Late Cretaceous folds observed in the Mesozoic sedimentary cover. The former consists of open folds with large wavelengths and low amplitude, in contrast to the tightly and locally disharmonic folds developed in El Profeta and Santa Ana Formations (Section 4.4). Previous studies in adjacent areas have demonstrated that Late Paleozoic NW-trending structural trends have been overprinted by N-striking Late Mesozoic and Cenozoic Andean structural trends (i.e., Sierra de Almeyda, Niemeyer and Crignola, 2003; Sierra de Varas, Niemeyer et al., 2004). However, the data collected in the Imilac block are insufficient to compare the structure orientation (i.e., fold axis, CBIL, bedding) with other similar rock units exposed along the Domeyko Cordillera.

4.3 TRIASSIC-EARLY JURASSIC EXTENSION

A Triassic-Early Jurassic extension in northern Chile has been demonstrated in numerous stratigraphic studies of the middle-late Triassic terrestrial volcaniclastic sequences and the Late Triassic-Neocomian Tarapacá back-arc basin (Suarez and Bell, 1985; Cornejo and

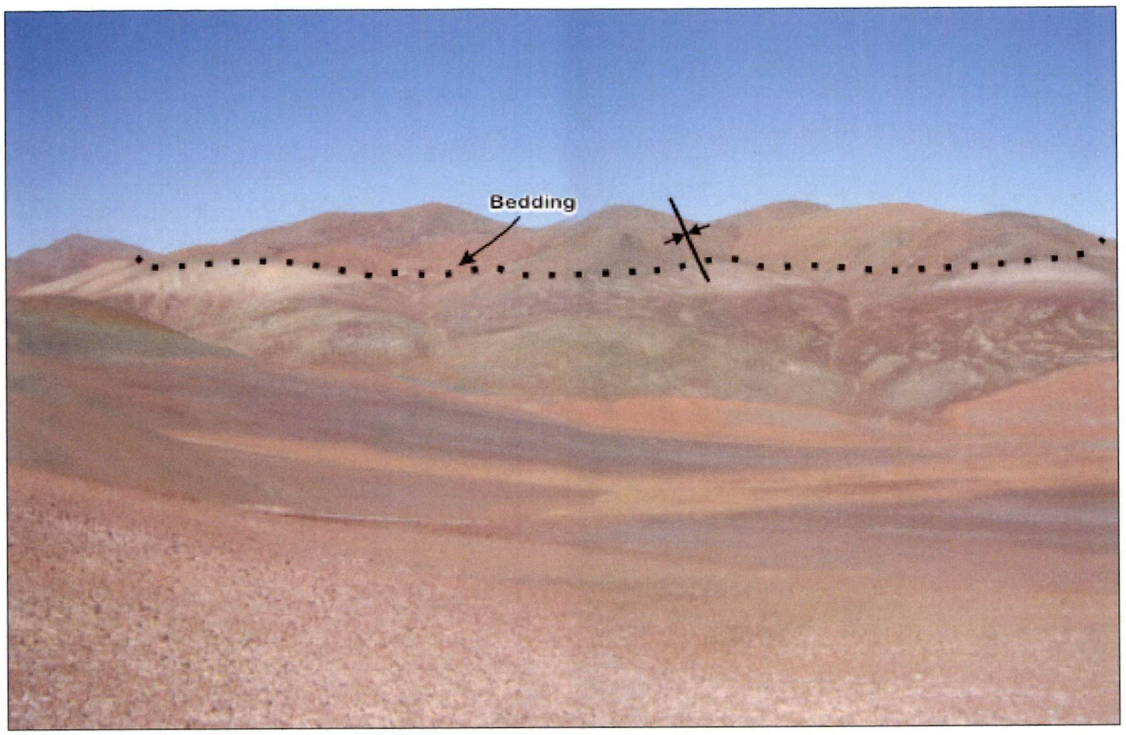

Figure 4.4a General view (looking to southeast) of a first-order open synform fold in the Late Carboniferous-Permian La Tabla Formation. It is defined by interbedded light gray tuffs, limestones and dark brown andesitic lava flows. Imilac structural block (7,329,200m N; 501,500m E).

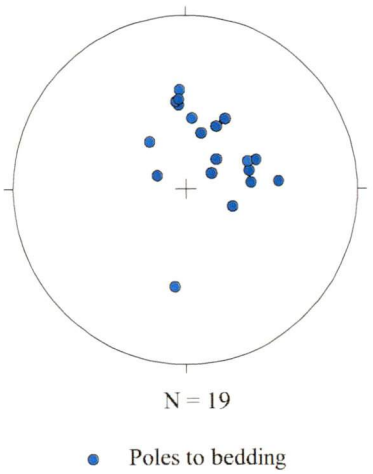

Figure 4.4b Graphic orientation for bedding in the Central volcano-sedimentary sub-unit *(Pzlt-b)* of La Tabla Formation. Note the low angle dip (40°-21°) of the beds. Sierra de Imilac block.

Mpodozis, 1995; Ardill et al., 1995; Vicente, 2006, and references therein). There is no direct structural evidence for this extensional event in La Escondida district, although there are marked changes in the thickness of the Late Triassic basal portion of El Profeta Formation. In particular, the thickness of the Lower Member (*TJep-a*) of El Profeta Formation changes considerably, from east to west. At the southern end of the western

Figure 4.5a Cleavage in sandstones (looking south) from the Central volcano-sedimentary sub-unit *(Pzlt-b)* of La Tabla Formation. Medium-scale bedding is poorly defined by 15-30 cm-thick beds that dip 40°-50° to the SW. Structural station A, Imilac block (7,324,573m N; 508,120m E).

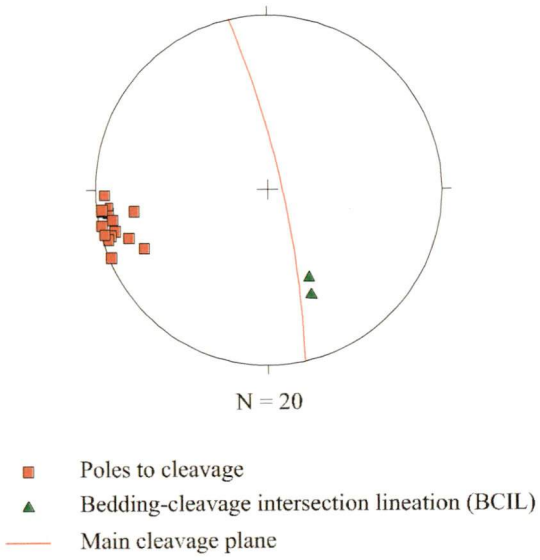

Figure 4.5b Orientation of cleavage and bedding-cleavage intersection lineation (BCIL) in sandstones of the Central volcano-sedimentary sub-unit *(Pzlt-b)* of La Tabla Formation. Structural station A, Imilac block (7,324,573m N; 508,120m E).

domain (Puma W block; Figure 4.3), this member is over 500 m thick and consists of boulder conglomerates and sandstones that unconformably overlie the Paleozoic La Tabla Formation (Appendix 1A). A few km to the west, similar conglomerate facies of *TJep-a* are less than 100 m thick, and are overlain by thousands of meters of platform coral-bearing

limestones of the Early Jurassic-Kimmeridgian Upper Member (*TJep-b*) (Appendix 1A). The conglomerates thin abruptly onto elevated basement blocks. The thickness change in the lower El Profeta conglomerates is the only direct evidence for an extensional deformation phase between the Late Triassic and Early Jurassic. Renewed syn-depositional extension affected some stratigraphic levels of the Upper Member (*TJep-b*) of El Profeta Formation (Figures 4.6a and b). Similar syn-depositional deformation has been observed in Toarcian calcareous strata from the Tarapacá Basin in the northern portions (20°-22°S) of the Domeyko Cordillera (Lira, 1991; Orrego, 1992).

4.4 LOWERMOST LATE CRETACEOUS COMPRESSION PERUVIAN TECTONIC PHASE, ~100-80 Ma)

On the basis of mechanical stratigraphy (*sensu* Mitra, 2002), rock units affected by the lowermost Late Cretaceous shortening event can be divided into four main structural packages. From oldest to youngest these are: (1) Late Paleozoic-Triassic crystalline basement consisting of La Tabla Formation massive ignimbritic flows and granitoids; (2) thick-bedded conglomerates of the Late Triassic-Early Jurassic Lower Member (*TJep-a*) of El Profeta Formation; (3) thin- to medium-stratified calcareous mudstones, limestones and interbedded evaporites of the Early Jurassic-Kimmeridgian Upper Member (*TJep-b*) of El Profeta Formation; and (4) laminated to thinly bedded redbed of the Late Jurassic Neocomian Santa Ana Formation.

The regional structural trends (folds and faults) in the Mesozoic clastic-calcareous units suggest a deformation style involving the Paleozoic basement blocks (Figure 4.7; Appendices 2A-D). Thick-skinned deformation has elevated narrow basement blocks against folded Mesozoic cover blocks (Cornejo and Mpodozis, 1993; Amilibia, 2002; Skarmeta et al, 2003). The eastern limit of the fold and thrust belt is defined by the Escondida master fault. To the west, it is partially exposed in a structural window within the Tertiary Augusta Victoria volcanic pile (Appendix 1A).

First-order reverse faults (i.e., Puma and Perito faults) consist of a number of fault segments that range from less than 1 km to 25 km length (Figure 4.7). They display complex geometry and individual strands are characterized by planar to curved traces (Figure 4.7; Appendices 1A and B). Most of these regional faults dip steeply east or west. Stratigraphic offsets observed across the major faults are consistent with a dominance of

"older-on-younger" reverse faults. The Perito fault in contrast, is an example of a "younger-on-older" reverse fault (Cornejo and Mpodozis, 1995; Amilibia, 2002). The latter structure uplifted Early Jurassic-Kimmeridgian limestones over Late Triassic conglomerates and Late Carboniferous-Permian ignimbrites (Structural Section B-B', Appendix 2B). This interpretation is consistent with reactivation of pre-existing normal faults, as proposed by Cornejo and Mpodozis (1996) and Amilibia (2002), where older extensional displacement was greater that the reverse reactivation displacement. Shortening has resulted in large-scale pop-up structures within the Late Paleozoic basement from the western domain (Cerro Campamento block; Figure 4.7; Appendix 1A) and associated fold trends that developed in the Mesozoic sedimentary sequences. Mesoscopic pop-up and duplex systems are spectacularly exposed in sections of interbedded limestones and shales, which are currently being mapped by H. Niemeyer about 5 km to the north of the La Escondida district (Figures 4.8a and b). Some packages of limestones and shales appear to have been backthrusted, with E or W vergence. Hypothetical relationships between basement and cover are illustrated in Figure 4.9, adapted from Coward et al. (1991). A family of NNW- to NW-striking sinistral strike-slip has caused displacements of less than 500 m across the N-striking reverse faults of the fold-thrust system (Puma W structural block; Figure 4.7; Appendix 1A). They probably correspond to transfer faults that formed during continued shortening.

A regional E-W structural section of Amilibia (2002) that is parallel to the Cross-section C-C' (Appendix 2C) proposes the occurrence of a deep basal thrust fault (decollement) and upward imbricated splays that affect the Paleozoic crystalline basement and Mesozoic sedimentary cover. This basal thrust is the most probable geometric interpretation to elucidate the folding style present in the surface (i.e., Cross-section D-D'; Appendix 2D). However, construction of balanced structural sections is beyond the aims of the present study.

Large folds are concentric to subangular, locally disharmonic, and generally asymmetric with an overturned short-limb (Figure 4.10a). The axial surfaces dip to W or E. They typically show sub-horizontal fold axes and wavelengths up to 2-3 km. The folds are close to tight, and both symmetric and asymmetric examples have been observed. Wavelengths and amplitude are up to tens of meters. Fault-propagation folds, drag folds and fold-accommodation faults (*sensu* Mitra, 2002) are common. Chevron folds are well exposed in the Puma E panel (Figure 4.10b; Cross-section D-D', Appendix 2D). Mesoscopic

Figure 4.6a Mesoscale intraformational breccias (looking south) in the Early Jurassic-Kimmeridgian Upper Member *(TJep-b)* of El Profeta Formation. Angular limestone clasts and broken layers occur within a folded calcareous matrix. Strata exposed 10 km north of the study area (7,348,600m; 488,900m E).

Figure 4.6b Intraformational breccias (looking south) within the Early Jurassic-Kimmeridgian Upper Member *(TJep-b)* of El Profeta Formation. Broken limestones bed supported by calcareous matrix. Strata exposed 10 km north of the study area (7,348,600m; 488,900m E).

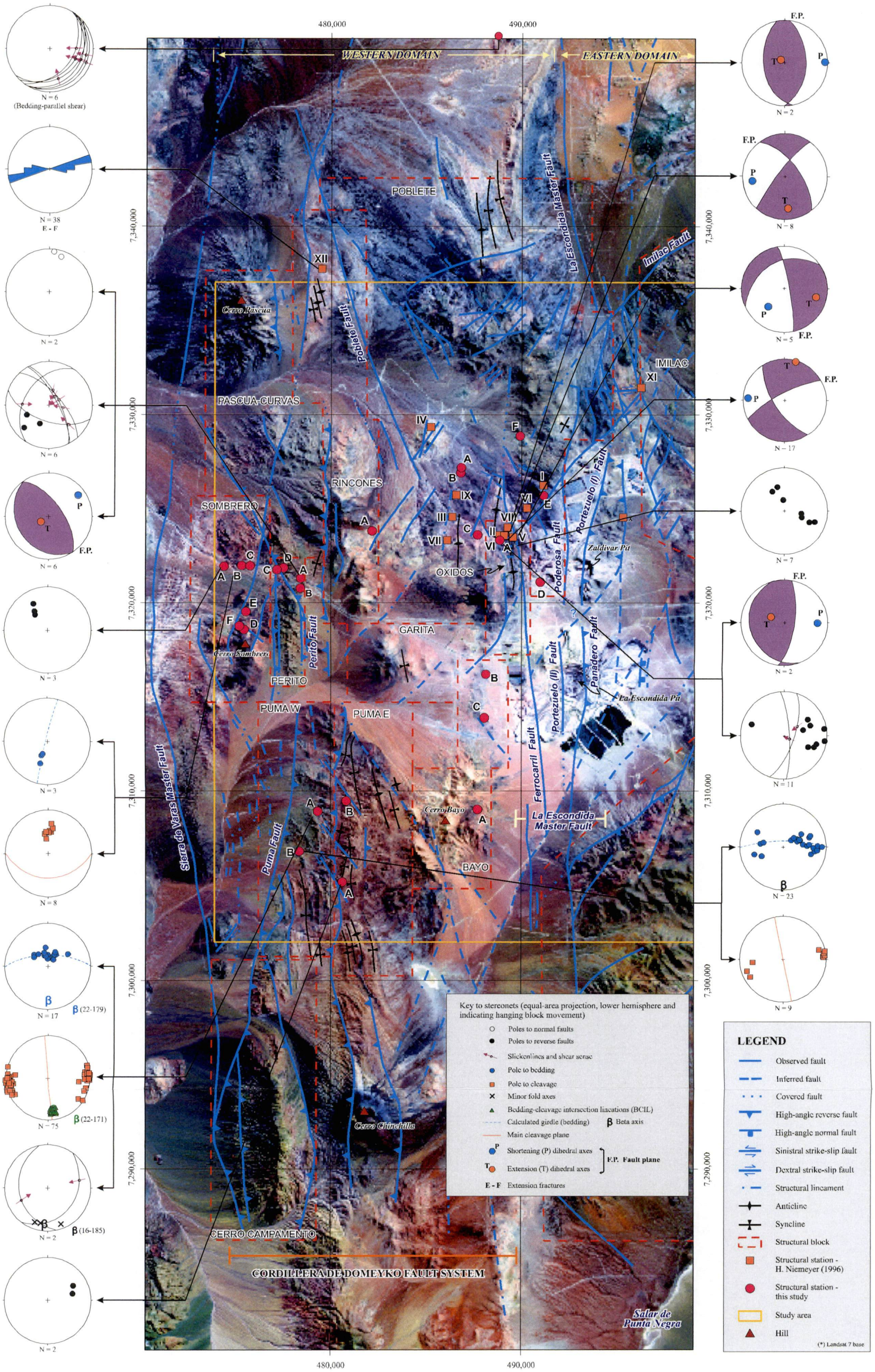

Figure 4.7 Graphic representation of kinematic data for the Late Triassic-Neocomian El Profeta and Santa Ana Formations in La Escondida district, which were affected by the lowermost Late Cretaceous positive tectonic inversion ("Peruvian" tectonic phase).

duplexes, thrust-bound horsts and triangular zones of considerable structural complexity are localized near the large faults (Figures 4.11a and b; Cross-section C-C', Appendix 2C), contrasting with the more harmonic deformation in those strata distant from major faults. Offsets on mesoscopic reverse faults range from a few centimeters to tens of meters.

4.4.1 Stereonet Data

In the following sections, the geometric and kinematic characteristic of structures (bedding, fold axis, cleavage and fault) observed in each structural block restricted to the western domain are summarized and interpreted (Figure 4.7). Accurate identification of structures and families of structures formed synchronous with or subsequent to the folded and reverse-faulted belt has been uncertain due to: (1) significant reactivation of faults related to younger deformation episodes; (2) poor exposure of major fault traces and key structural sections; and (3) the highly dynamic structural evolution of the region.

4.4.1.1 Bedding and Folds

Figures 4.12 and 4.13 show the results of orientation measurements of all bedding, map-scale regional faults and second- to third order (parasitic) fold axes in the Mesozoic sedimentary units. They are organized for each structural block of the western domain. In the Puma W and Pascua-Curvas blocks, where conglomerates are the dominant lithology, the poles to bedding are characteristic of overall broad and rounded folds (Figure 4.12). In contrast, interbedded limestones and shales from Puma E, Bayo, Rincones and Garita blocks, have folds with more angular axial zones due to variations of layer thickness and rheology (Figure 4.13).

4.4.1.2 Fault, Cleavage and Extensional Veins

In general, the dominant mesoscopic faults in the sedimentary sequences include (1) low- to high-angle, reverse faults that crosscut strata, and are characterized by non-cohesive fault breccia of few centimeters of thickness; and (2) a well-developed set of bedding-parallel reverse faults and related slickenlines. All of these mesoscale structural features are summarized in Figure 4.7. They occur in each structural block as follows:

Puma W block. A moderately spaced and anastomosing (Figures 4.14a and b), NNW- to NNE-striking cleavage, interpreted as an axial planar cleavage, occurs locally in conglomerates of the Lower Member from El Profeta Formation at structural station A (Figure 4.7). Similarly, weakly developed, steeply dipping slaty cleavage has been observed

in mudstones and siltstones of this member at station B (Figure 4.7). Main cleavage-bedding intersection lineation (171°-22°) and cleavage plane (89°/267°) in conglomerates exhibit a minor amount (ca. 7°) of apparent anticlockwise transection with the regional fold axes (station structural A, Figure 4.7). This apparent anti-clockwise transection is greater (ca. 15°) when compared to the mean cleavage-bedding intersection lineation (CBIL) and fold axis line (Figure 4.7). Elsewhere there are not enough data to comment on cleavage transection (station A, Sombrero block; Figure 4.7).

Two small bedding-parallel reverse fault planes contain slickenlines that lie at broadly variable angles (pitch: 46°-80°) (station A, Figure 4.7). A more regular kinematic relationship has been documented with other slickenline-bearing reverse faults (pitch: 74°-78°; Figure 4.7) observed at station A of Oxidos block, and at another imbricate block further north of the study area (pitch: 62°-80°; Figure 4.7; Appendix 7). These patterns are consistent with flexural slip folding, but with a considerable oblique component (Ramsay, 1967). All data (small bedding-parallel faults, first- and second order faults, cleavage and CBIL; Figures 4.7 and 4.12) are consistent with an overall ENE-WSW shortening for the Puma W block in a present-day reference frame. However, this inferred ENE-WSW tectonic shortening is poorly supported at this time by the scarce amount of measurements. It may be not representative of regional deformation.

Rincones Block. Niemeyer (1996) documented NNE-striking extensional calcite veins associated with regional N- to NNW-trending fold axes in the Rincones block (station XI, Figure 4.7). The data are consistent with E-W shortening for that part of the Rincones block, which appears to have been unaffected by younger tectonic activity (section 4.7).

Oxidos block. Stations A, II, V, VI and VIII are located along a section roughly perpendicular to hinge zones within the major NNE-striking anticline in the Santa Ana redbeds and overlying late Paleocene-early Eocene Augusta Victoria volcanic sequence. Fault striation datasets from stations A and VIII in Santa Ana unit are consistent with a local E-W to NW-SE shortening direction in a present-day reference frame (Figure 4.7). However, the other three stations (II, V and VI) which are located in the same unit contain NW-striking sinistral reverse faults. Niemeyer (1996) considered that the reverse component of these oblique slip faults was caused by proximity to the axial zone of the large anticline, which appears to have formed during the Eocene Incaic tectonic phase.

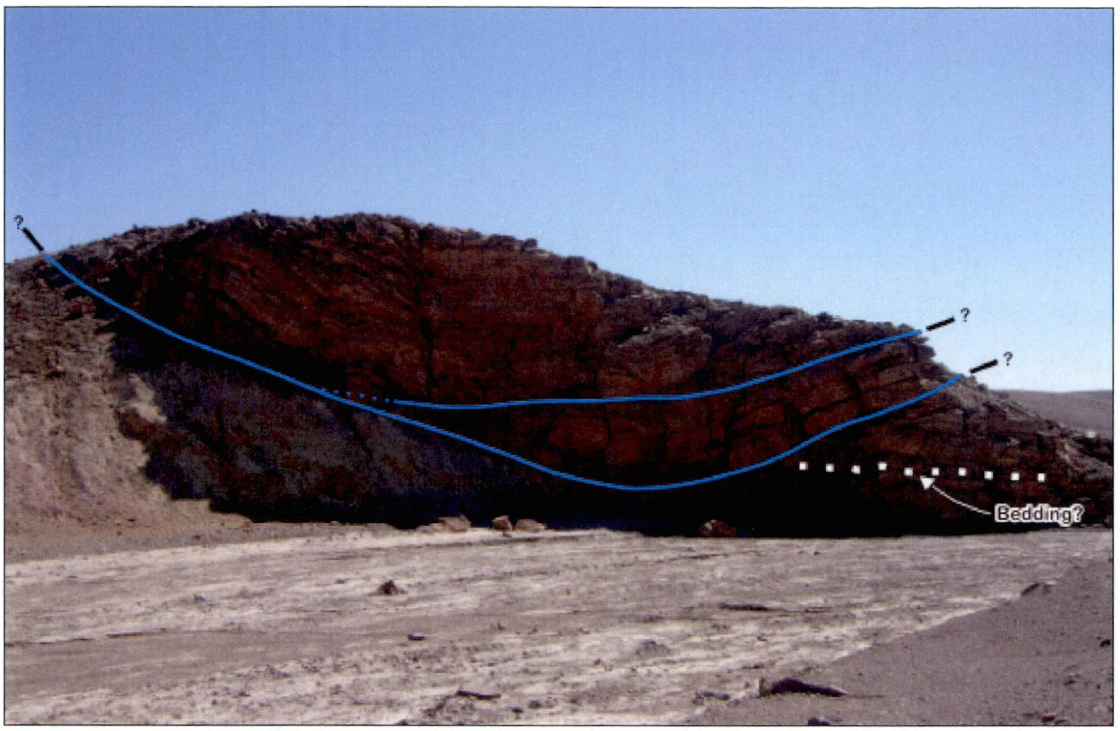

Figure 4.8a General view (looking southwest) of a detached synformal fold in limestones of the Lower Jurassic-Kimmeridgian Upper Member *(TJep-b)* of El Profeta Formation. Slickenlines indicate no sense of displacement. Strata exposed 10 km to north of the study area (7,348,604m N; 488,922m E).

Figure 4.8b E-vergent thrust-bound horses (looking south) within a contractional duplex in limestones of the Lower Jurassic-Kimmeridgian Upper Member *(TJep-b)* of El Profeta Formation. Similar outcrops as above (7,348,493m N; 488,424m E).

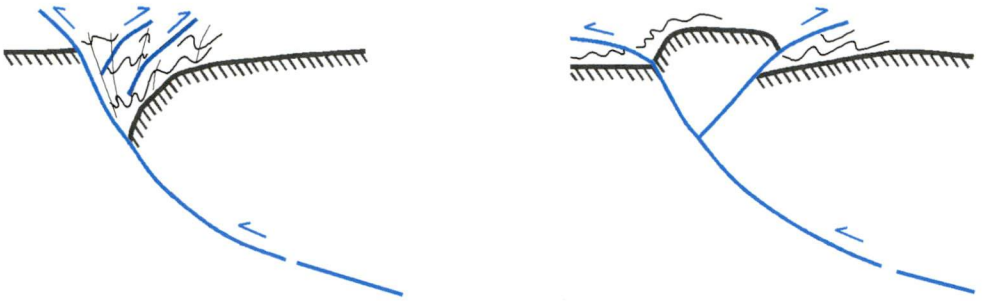

(a) Reactivation of normal fault with sedimentary cover backthrusting

(b) Pop-up structure

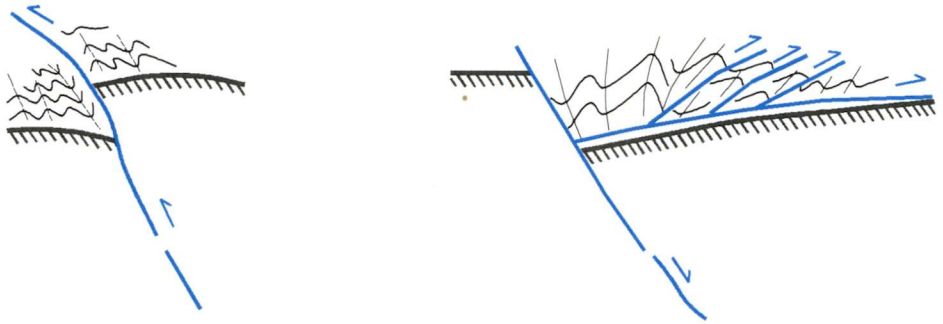

(c) Hanging wall ramps over footwall sedimentary cover

(d) Normal faults acts as a stress riser

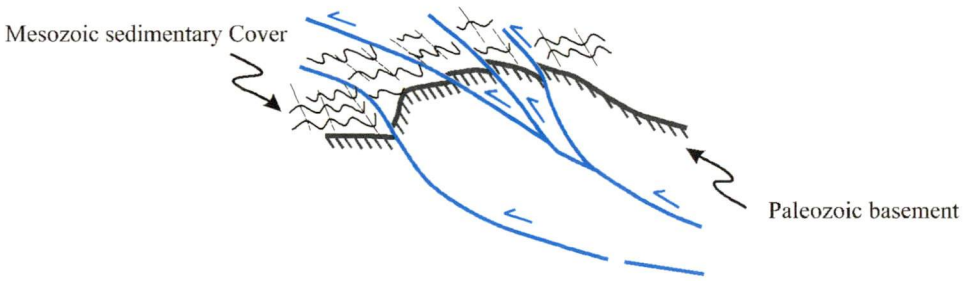

(e) Break- back thrust faults change in transport direction

Figure 4.9 Schematic illustrations of hypothetical inversion geometries that may have formed within the Mesozoic back-arc El Profeta and Santa Ana sequences during positive tectonic inversion in the lowermost Late Cretaceous (adapted from Coward et al., 1991).

This interpretation appears reasonable considering that folding affected beds of the late Paleocene-early Eocene Augusta Victoria Formation (Section 4.7).

Sombrero block. Reverse faults occur in limestones, shales and sandstones of El Profeta and Santa Ana units across the Sombrero block (structural cross-section B-B',Appendix 2B). At structural station A, a few of the reverse faults are NE-striking, but unfortunately

Figure 4.10a Asymmetric folds (looking northwest) with an overturned short-limb in limestones of the Lower Jurassic-Kimmeridgian Upper Member *(TJep-b)* of El Profeta Formation. Puma W block, western structural domain (7,206,100m N; 481,300m E).

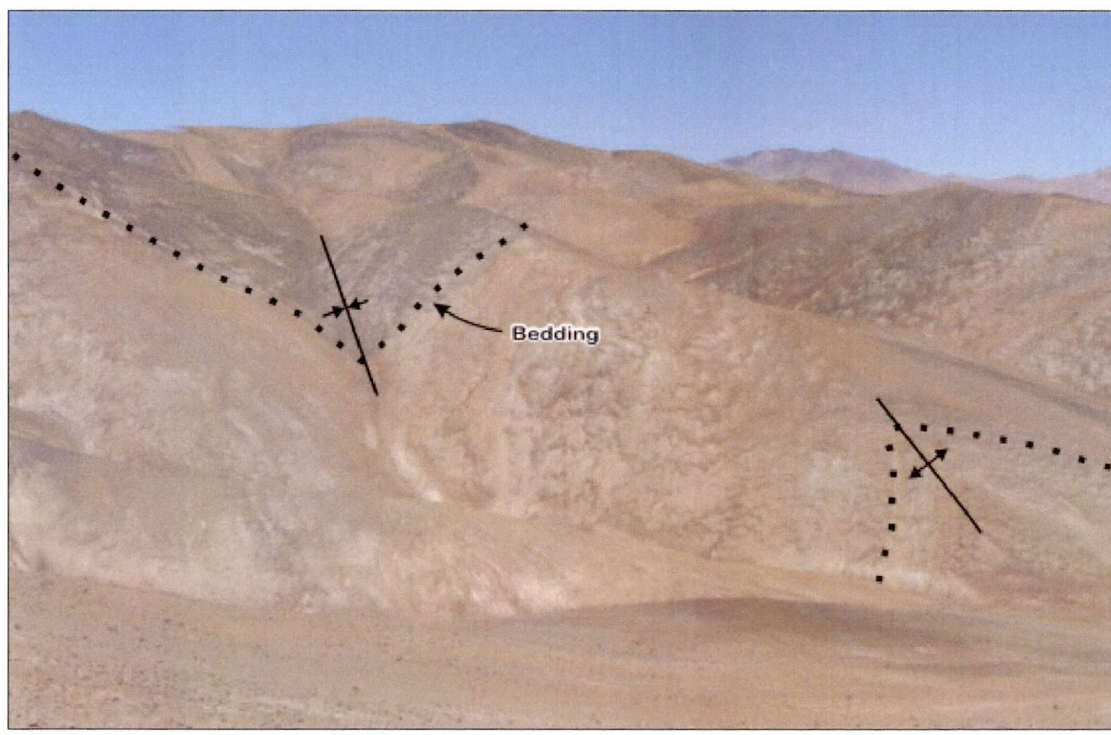

Figure 4.10b General view (looking south) of part of the structural cross-section D-D' (Appendix 2D) showing large scale anticlinal-synclinal pair of chevron folds in the Lower Jurassic-Kimmeridgian Upper Member *(TJep-b)* of El Profeta Formation. Puma W block, western structural domain (7,309,900m N and 481,700m E).

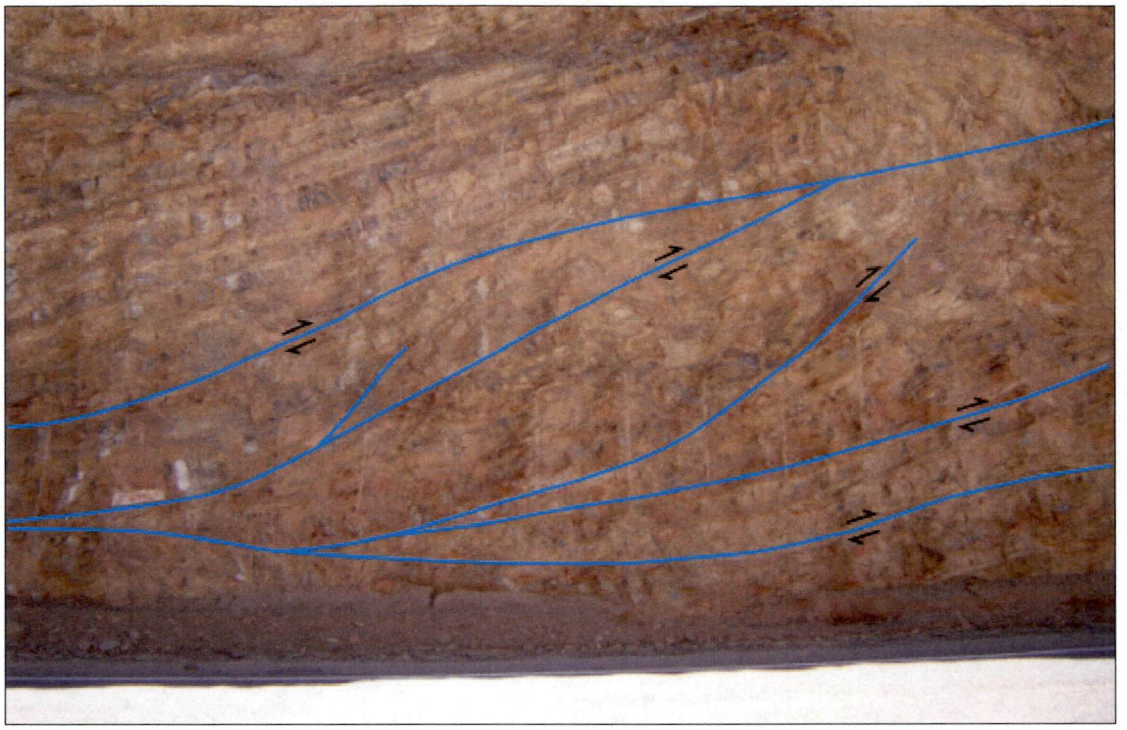

Figure 4.11a Mesoscale imbricate horses (looking north) in a contractional duplex system developed in well-bedded limestones of El Profeta Formation (Late Triassic-Kimmeridgian). Note the regular E vergence in each individual horse associated with a flat floor fault (Geological cross-section B-B', Appendix 2B). Paved road to La Escondida operation (7,322,375m N; 479,495m N).

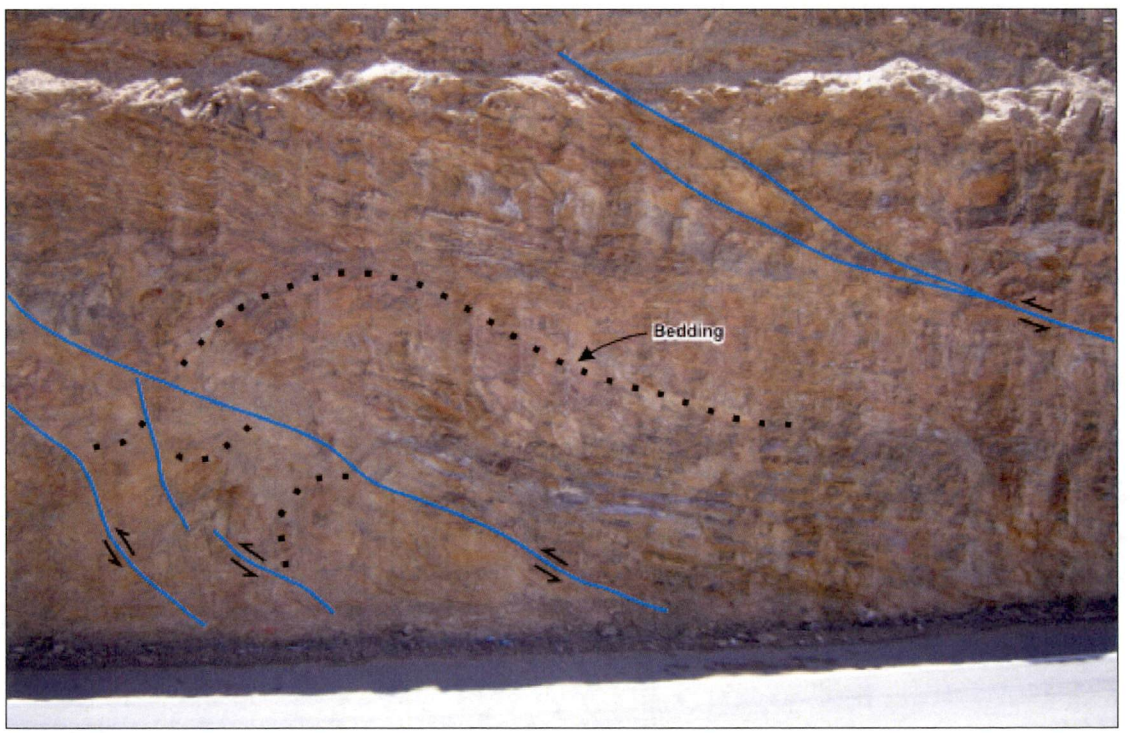

Figure 4.11b Intensely folded limestones (looking north) of the El Profeta Formation (Late Triassic-Kimmeridgian). Note the set of W-vergent reverse faults and the complex accommodation zones (Geological cross-section B-B', Appendix 2B). Paved road to La Escondida operation (7,322, 375m N; 479,495m N).

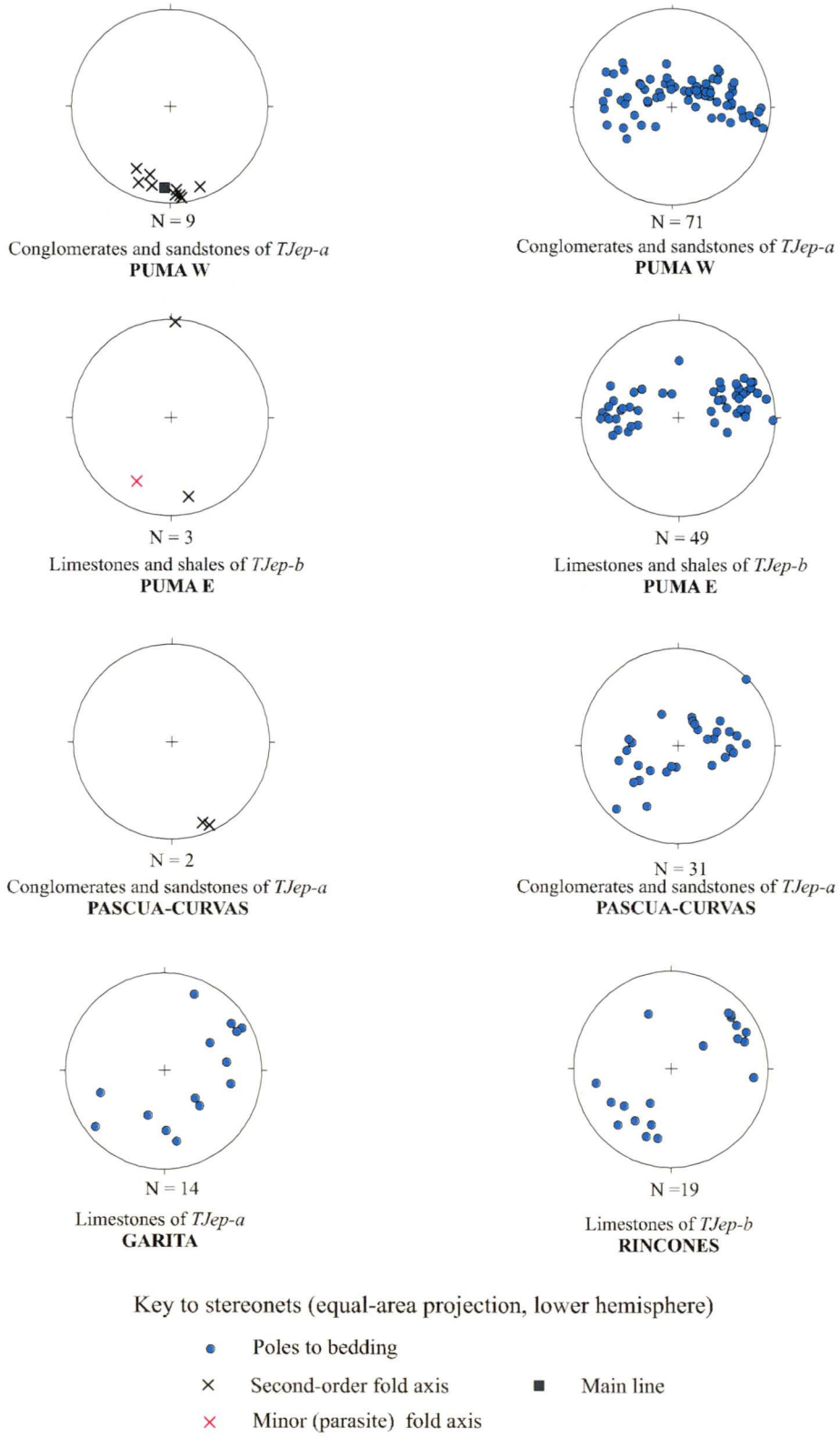

Figure 4.12 Orientation of bedding and fold axes for Mesozoic El Profeta and Santa Ana sedimentary sequences in diverse structural blocks of the western structural domain.

fault-striae features were not found on these structures (Figure 4.7). Slaty cleavage is well developed in siltstones and mudstones of the Santa Ana Formation (station B, Sombrero

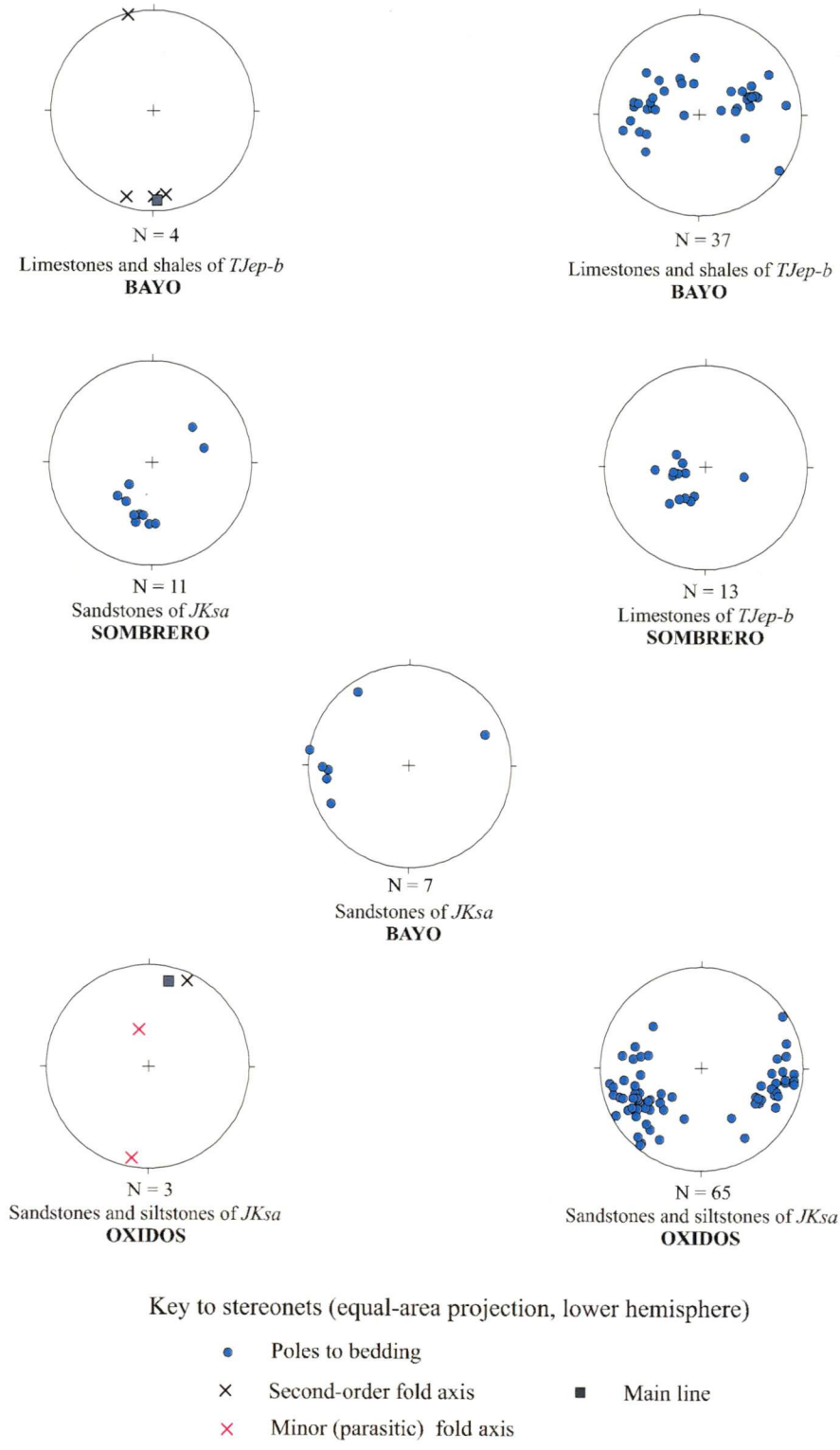

Figure 4.13 Orientation of bedding and fold axes for Mesozoic El Profeta and Santa Ana sedimentary sequences in diverse structural blocks of the western structural domain.

block; Figure 4.7); relationship between cleavage measurements and fold axis was not observed. The local folds at station B are probably not related to regional folds, instead, they are inferred to have formed in response to local deviation from the field-far regional

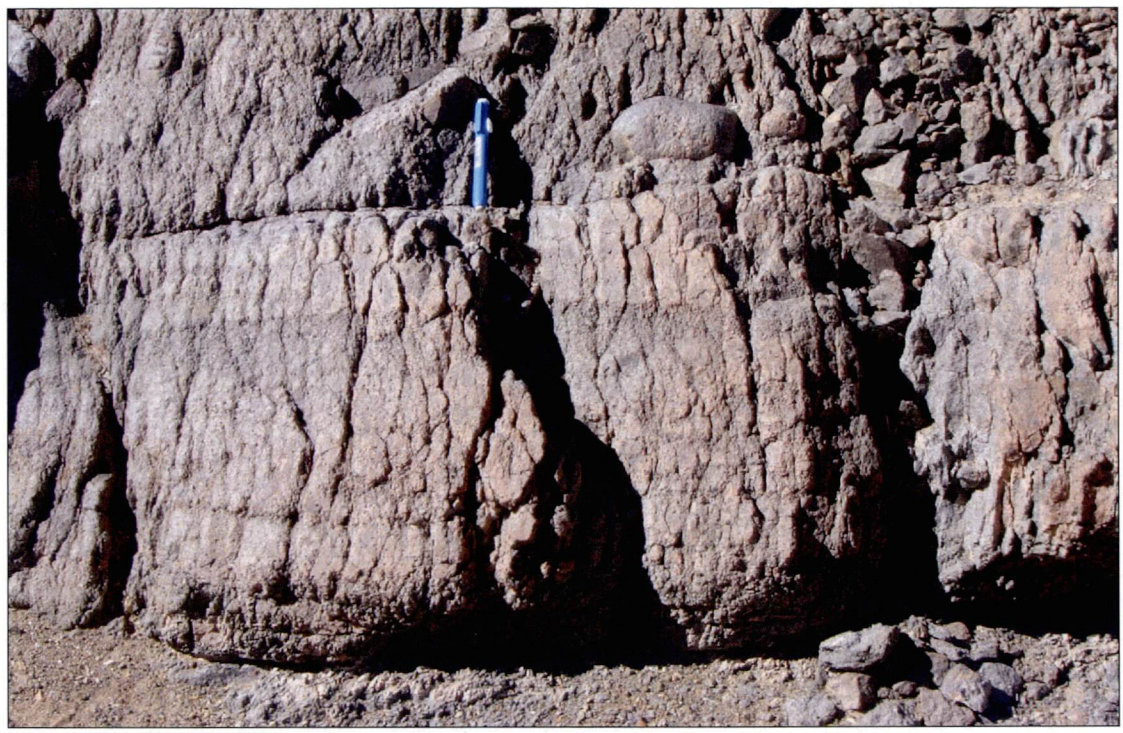

Figure 4.14a Axial planar cleavage (looking south) developed in beds of conglomerates and conglomeratic sandstones of the Late Triassic-Lias Lower Member from El Profeta Formation. Note the rounded cobble in the upper bed. Structural station B, Puma W block (7,309,279m N; 480,080m E)

Figure 4.14b Lineations (as indicated by the pen, CBIL) of intersection between cleavage and bedding planes (looking northeast). Lower Member (Late Triassic-Lias) of El Profeta Formation. Structural station B, Puma W block (7,309,279m N; 480,080m E).

stress regime. A significant geological feature of the Sombrero block is the reverse faults that have offset a family of amphibole-bearing andesite dykes dated at 82 + 4 Ma (U-Pb zircon; Table 3.7; Appendix 6), which have been tentatively interpreted as early intrusions of Las Torres igneous complex (Section 3.4.3). Segments of these dykes have been displaced and folded by the reverse faults (Figure 4.15b), confirming their pre- to syn-kinematic emplacement. Other younger dykes (ca. 66-65 Ma; Section 3.4.3) of Las Torres igneous complex were not offset by this family of reverse faults.

Perito block. In an extremely structurally complicated section of El Profeta sandstones and siltstones, station A contains medium- to small-scale, NW-striking reverse faults. Some of these faults are clearly bedding-parallel faults, with slickenlines at high angles (pitch: 74°-86°) to the strike of the bedding and, therefore, possibly related to flexural-slip folding (Ramsay, 1967). Kinematic indicators define a NE-SW compression direction (Figure 4.7). A few WNW-trending normal faults with centimeter- scale displacements are have been observed in thinly-bedded siltstones (station A, Perito block; Figure 4.7). These normal faults have been cut by the reverse faults.

4.4.2 Timing and Significance of Deformation

The similar northerly trends of regional faults and fold axes suggest that faulting and folding developed contemporaneously during the formation of the E- and W-vergent fold and thrust belt (Muñoz et al., 2005). The data collected from mesoscale structures (bedding, axial plane cleavage, CBIL, fold axe, faults and slickenlines) are mostly consistent with flexural-slip folding (Ramsay 1967), with a minor oblique component, during far-field E-directed shortening. Subordinate NE- and NW-directed shortening indicates variations probably caused by local stress regimes. Shortening was most likely achieved by coupled deformation of both the basement and sedimentary cover, including inversion of Triassic-Early Jurassic extensional faults (Cornejo and Mpodozis, 1995; Amilibia, 2002; Muñoz et al, 2005). Buckling of thickly-bedded conglomerates produced relatively rounded folds whereas more thinly-bedded alternations of shales, limestones and siltstones had angular folds. The competent rhyolitic basement has relatively weak penetrative deformation with the strain focused into block-bounding high-angle reverse faults and detachment folding of the sedimentary cover (Cornejo and Mpodozis, 1995). Compressional deformation was active after the deposition of the Late Jurassic-Neocomian Santa Ana Formation, and also affected the early (82 ± 4 Ma) andesite dykes

Figure 4.15a Mesoscale reverse faults (looking north) crosscutting the Upper Member of El Profeta Formation *(TJep)*, which has produced a drag-fold in the calcareous beds. Puma W block (7,322,346m N; 475,672m E).

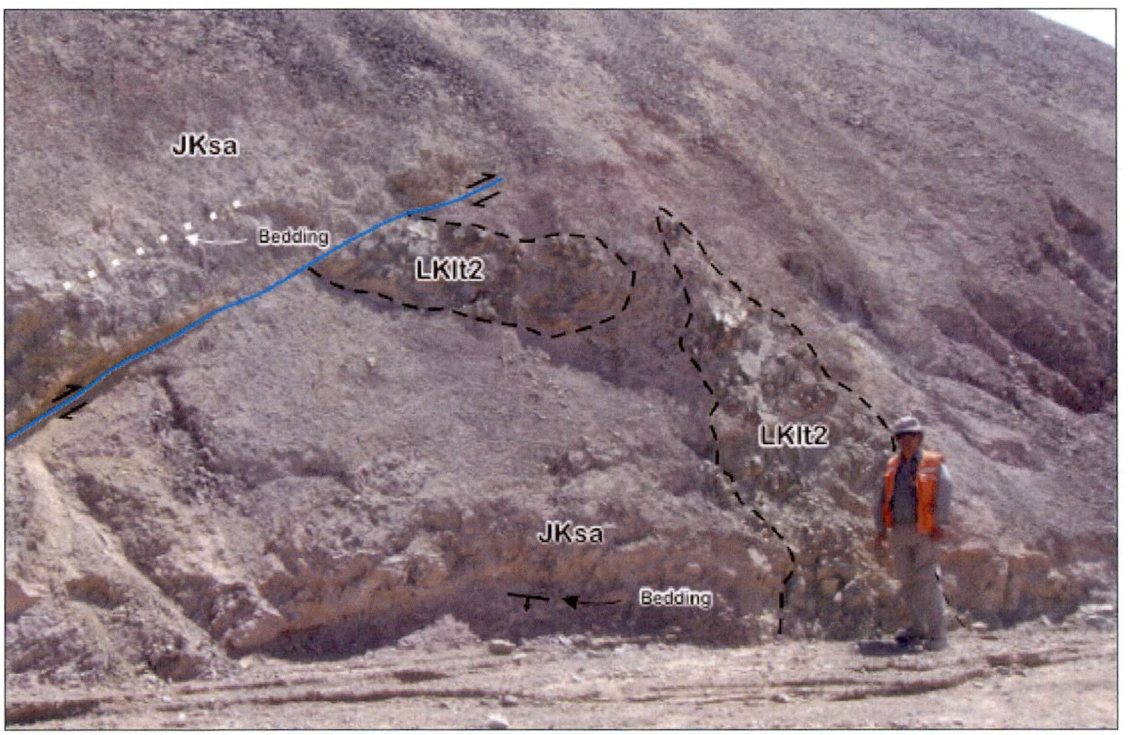

Figure 4.15b Set of mesoscale reverse faults (looking south) (143°/45°) cross-cutting red beds of the Late Jurassic-Neocomian Santa Ana Formation *(JKsa)* and an early andesite dyke *(LKlt1)* of Las Torres igneous complex, which has been dated at 82 ± 4 Ma. Paved road to La Escondida operation, Sombrero block (7,322,346m N; 475,672m E).

of Las Torres igneous complex (Chapter 3; Appendix 6). The deformation must therefore has been post-Neocomian (<100 Ma) and is likely to have been active at 80 Ma (Campanian).

The age for tectonic inversion of the Mesozoic Tarapacá Basin has been constrained previously to the lowermost Late Cretaceous (Cornejo and Mpodozis, 1996; Amilibia, 2002). A similar timing of deformation has been established for Jurassic-Early Cretaceous sequences in the Sierra de Moreno (Ladino et al., 1999) and in the Sierra El Buitre (Marinovic et al., 1996), which has been correlated by Cornejo and Mpodozis (1996) with the Peruvian tectonic phase (Mégards, 1987). The timing of Peruvian deformation event in La Escondida district is therefore concluded to have been lowermost Late Cretaceous.

The tectonic model proposed for the Late Cretaceous period by Cornejo and Mpodozis (1996) involved oblique tectonic inversion of the back-arc Tarapacá Basin in the Sierra Exploradora region. In contrast, field observations from La Escondida region during the current study indicated mainly coaxial contraction, with a minor oblique component, supporting in part the overall margin-normal inversion model proposed by Amilibia (2002), Skarmeta et al. (2003) and Muñoz et al. (2005). Strain partitioning (Chemenda et al., 2000) in response to oblique SE-oriented oblique subduction along convergent plate margins for the Late Cretaceous (Figure 2.1) is consistent with these observations. This model requires: 1) sinistral strike-slip faulting in the Jurassic-Cretaceous arc zone (Grocott and Taylor, 2002); and 2) mostly orthogonally shortening experienced by the back-arc Tarapacá basin during lowermost Late Cretaceous tectonic inversion (Grocott and Taylor, 2002; Mpodozis et al., 2005; Muñoz et al., 2005).

4.5 LATE CRETACEOUS EXTENSION (~74-64 Ma)

Regional studies have highlighted the importance of transtensional displacements along NNE-striking faults associated with the Late Cretaceous arc/back-arc pair of northern Chile (Marinovic et al., 1996, Tomlinson et al., 2002; Cornejo et al., 2003). In La Escondida district, there was only a small and poorly exposed volcaniclastic component that was deposited during this period (section 3.4). In contrast, volumetrically significant basic to silicic magmatism occurred in the Late Cretaceous-lowermost early Paleocene, resulting in the emplacement of shallow-level intrusive complexes at Torcaza, Las Torres, Cerro Bayo and Sombrero, from 81 Ma to 64 Ma (Table 3.7; Appendix 6). All of these complexes crop out west of La Escondida master fault (Appendices 1A and B).

4.5.1 Stereonet Data

Field mapping of the Late Cretaceous plutonic centers has revealed a general N- to NNE-trending structural pattern for the predominantly tabular and sheeted stocks, dykes and sills (Figure 3.14). The mesoscale structures that have developed in these intrusive complexes range from magmatic layering, through fracture cleavage and joints to post-emplacement faults. However, the low number of fault-striae observed in the intrusive rocks provides inadequate constraints with regards paleo-stress directions during and after the emplacement of plutons. In addition, important shear zones occur in the Mesozoic sedimentary rocks. Field observations indicate that the shear zones crosscut dip-slip reverse faults linked with the lowest Late Cretaceous tectonic inversion (Peruvian tectonic phase; Mégards, 1987).

4.5.1.1 Magmatic Layering, Flow-banding, Dykes and Veins, and Joints

Data from these structural features are summarized in Figure 4.16. Results from each structural block are as follows:

Bayo block. At station A (Figure 4.16), magmatic layering is preserved in gabbros of the Cerro Bayo complex (77-74 Ma *LKcb2*; Table 3.7; Appendix 6). The layers are mostly NW-striking (Figures 4.17a). These layers are parallel to spaced fractures and joints in the gabbros and also to flow-banding in vesicular aplites (73-72 Ma *LKcb8*; Table 3.7; Appendix 6).

Puma E block. At station B (Figure 4.16), a group of dioritic to gabbroic sills of the Cerro Bayo complex (77-74 Ma *LKcb2*; Table 3.7; Appendix 6) mimic the fold geometry in El Profeta calcareous rocks (Figure 4.17b). They have centimeter-scale layering, distinctive sharp contacts and well-developed internal chilled margins (Figures 4.18a and 4.18b). Although these sills are cut by a relatively close-spaced orthogonal jointing, they have been interpreted to be post-kinematic relative to the folding of El Profeta strata, which has been inferred here to be linked with the lowermost Late Cretaceous tectonic inversion.

Sombrero block. The principal intrusive phase of 70-66 Ma Las Torres igneous complex (*LKlt2*) consists of NNE-striking andesite-diorite, monzodiorite and gabbro dykes (structural station C and D; Figure 4.16). They were not deformed by the lowermost Late Cretaceous tectonic inversion (Figure 4.19a). Conversely, the dykes have been affected by

younger, high-angle faults, with multiple slickenline sets that show kinematic patterns typical of Tertiary deformation (Section 4.6). Monzogranites of the Sombrero intrusive complex (66.2 ± 0.8 Ma *TPsb4*; Figure 4.19b) contain NW-striking joints (station E, Figure 4.16). A subordinate number of Fe- and Cu-rich gossanous veins associated with the Late Cretaceous intrusions at Sombrero skarn (station F, Figure 4.16) and Alicia mine (station G, Figure 4.16) also strike dominantly NE.

4.5.1.2 Shear Zones

Perito block. At structural station B (Figure 4.16), thinly-bedded limestone and siltstone packages have been crosscut by conspicuous extensional S-C shear zones of E-strike (Figures 4.20a and 4.20b). The C- planes in the shear zones contain NNE- to NE-plunging slickenlines (mean line: 32°-035°; Figure 4.16). Field relationships indicate that these shear zones have been cut by Paleocene (?) or younger, high-angle reverse faults (Figure 4.20a; Section 4.7).

4.5.2 Timing and Significance of Deformation

The N- to NNE-strike of tabular stocks, dykes and sills of Cerro Bayo and Las Torres igneous complex (Figure) implies regional E-W to ESE-WNW extension during their emplacement. Based on the northeast orientation and shapes of the Cerro Bayo gabbros (77-74 Ma *LTcb2* sub-unit; Table 3.7; Appendix 6), Richards et al. (2001) interpreted a similar NW-oriented minimal (σ_3) stress. These authors assumed that the *LTcb2* sub-unit postdates the monzonites (ca 74-72 Ma *LKcb6-LKcb8* sub-units; Table 3.7; Appendix 6) and a family of north- and west-northwest-trending faults that affected them. They therefore concluded that the faults are older than 77-74 Ma, the age of the gabbros. This reasoning is in conflict with the new radiometric ages and field observations completed during the present study, specifically: (1) the monzonites have intruded the gabbros; and (2) the northwest-trending faults cannot be found in the available outcrops. The Sombrero plutonic complex (ca. 67-64 Ma; Table 3.7; Appendix 6) is oriented parallel to the Cerro Bayo and Las Torres dykes (Figure 3.14; Appendix 1A), implying that the field-far regional stress regime did not undergo any significant changes over a 10 m.y. period. The similar NE strike of the later gossanous veins spatially and genetically linked to the Late Cretaceous plutonic complexes support in part this assertion. The ESE-striking shear zones, which have also undergone normal-oblique extension after folding of the Mesozoic sedimentary rocks, could be related to the Late Cretaceous transtensional regime inferred by Marinovic et al. (1996), Cornejo and Mpodozis (1996), Cornejo et al. (2003) and

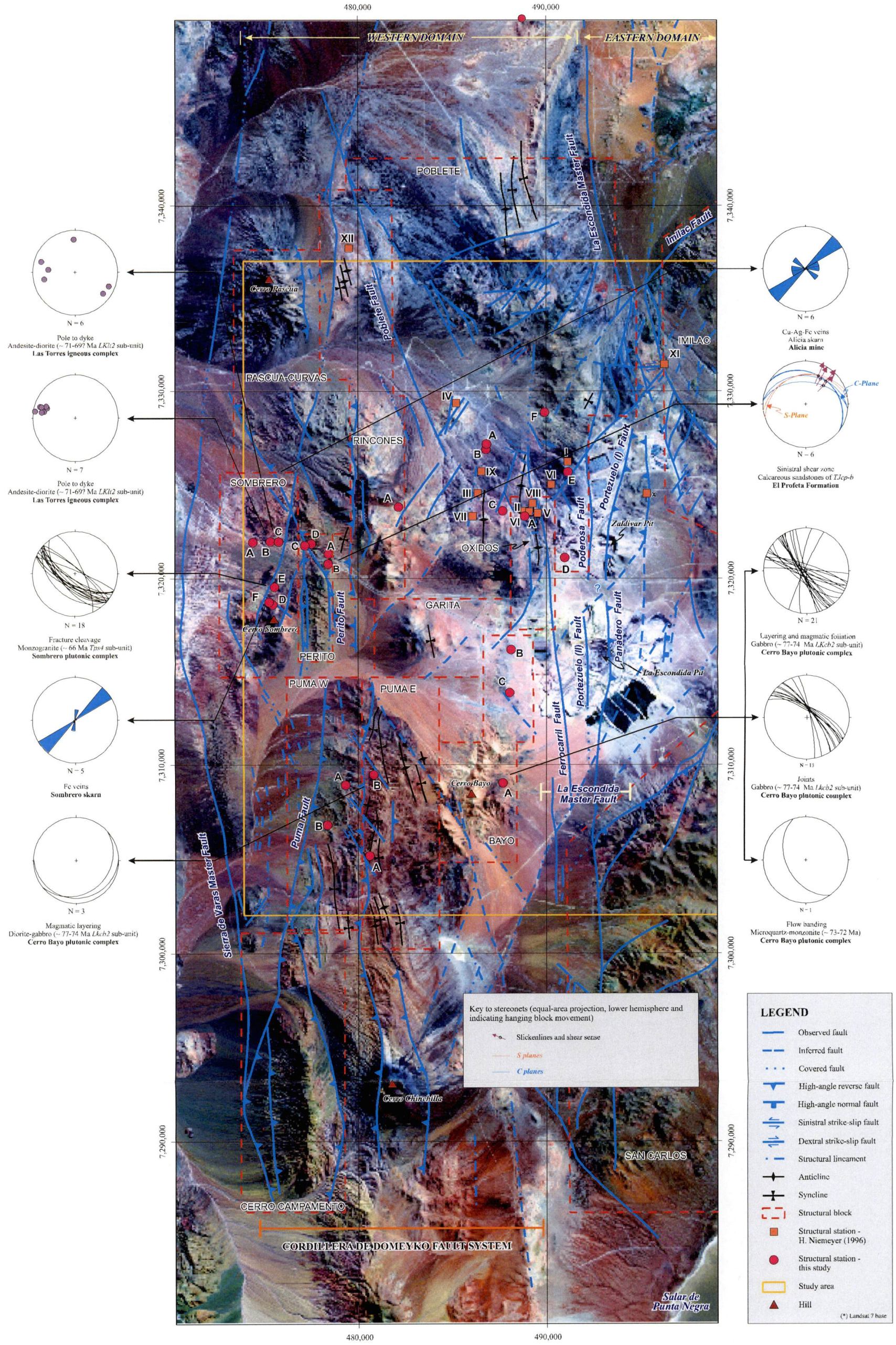

Figure 4.16 Simplified graphic representations of syn-magmatic structural features for the Late Cretaceous intrusions of La Escondida district, together with fault-striae kinematics from sinistral shear zones of post-mid Cretaceous age, dykes and veins orientations that are inferred to be linked to the Upper Cretaceous extensional regime.

Figure 4.17a Centimeter-scale magmatic layering in gabbros and monzogabbros (*LKcb*; ca. 77-74 Ma) of the Cerro Bayo plutonic complex. Structural station A, Bayo structural block (7,308,920m N; 487,780m E).

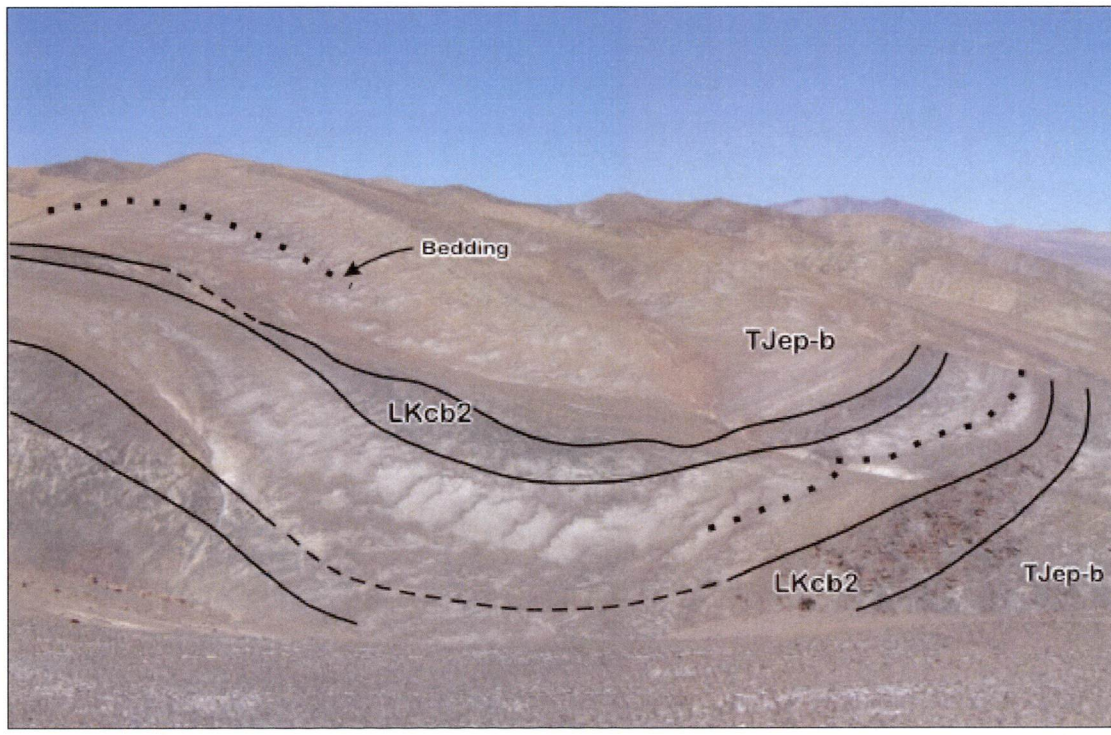

Figure 4.17b View (looking to south) of banded diorite to gabbro sills (*LKcb*; ca. 77-74 Ma) of the Cerro Bayo plutonic complex that are emplaced concordantly with limestones and siltstones of the Early Jurassic-Kimmeridgian Upper Member *(TJep-b)* of El Profeta Formation. Puma E structural block (7,309,730m N; 481,286m E). The sills have been interpreted as post-kinematic in relation to folding of the sedimentary rocks.

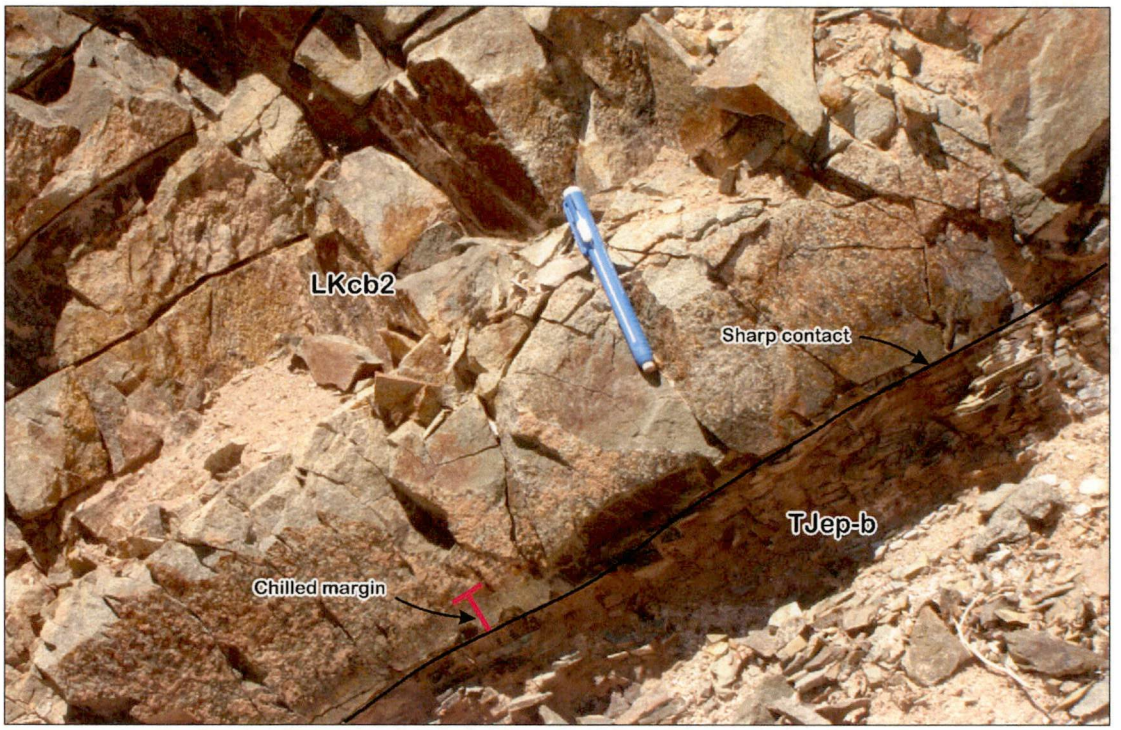

Figure 4.18a Sharp contact and chilled margin (looking west) of banded diorite to gabbro sills (*LKcb*; ca. 77-74 Ma) of the Cerro Bayo plutonic complex with limestones and siltstones of the Early Jurassic-Kimmeridgian Upper Member *(TJep-b)* of El Profeta Formation. Puma E structural block (7,309,730m N; 481,286m E).

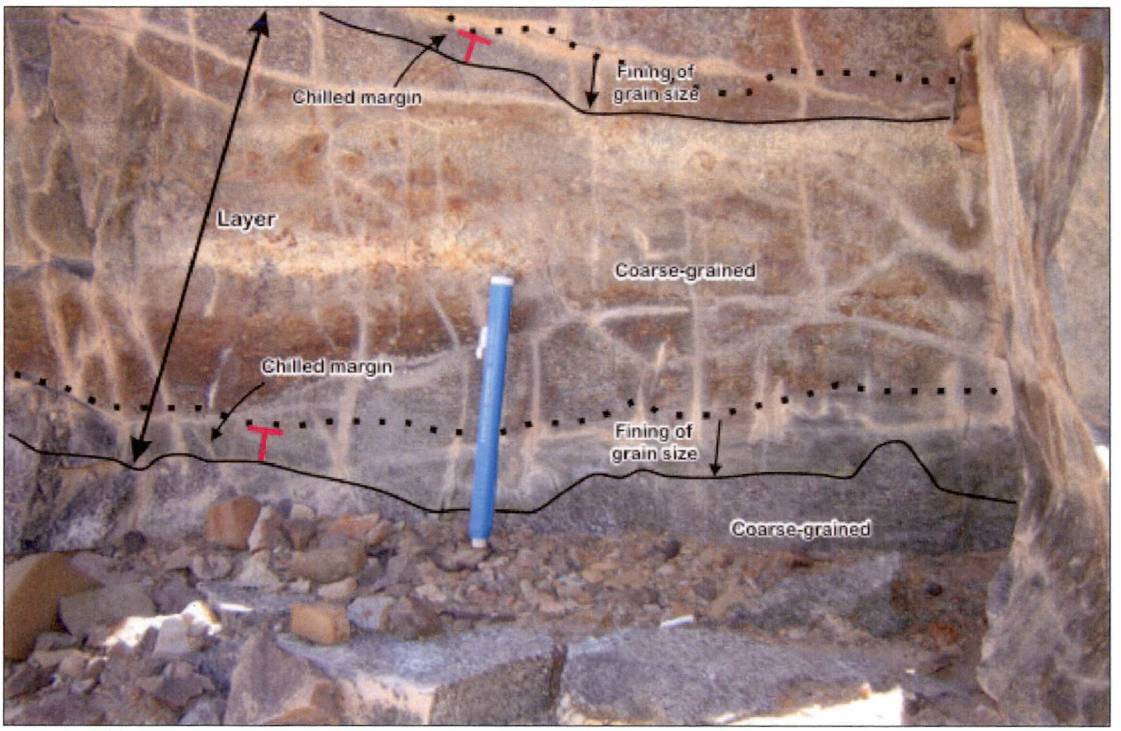

Figure 4.18b Magmatic layering (looking east) in diorite to gabbro sills (*LKcb2*; ca. 77-74 Ma) of the Cerro Bayo plutonic complex. Notice the successive pulses with centimeter-scale chilled margins, which suggest considerable cooling of the layer before the emplacement of the next. Puma E structural block (7,309,730m N; 481,286m E).

Figure 4.19a A complex association of sheeted dykes (looking northeast) of pyrite-bearing andesite-diorite (*LK/t1*; ca. 70-66 Ma), with bleached zones and strongly faulted and fractured interiors (left). A later monzodiorite dyke (right) is clearly identified by its sharp borders and undeformed interior. Paved road to La Escondida operation. Structural station B, Sombrero block (7,322,391m N; 475,442m E).

Figure 4.19b Close-spaced jointing in monzogranites (*TPsb4*; 66.2 ± 0.8 Ma) of the Sombrero plutonic complex. Structural station F, Sombrero block (7,320,015m N; 475,870m E).

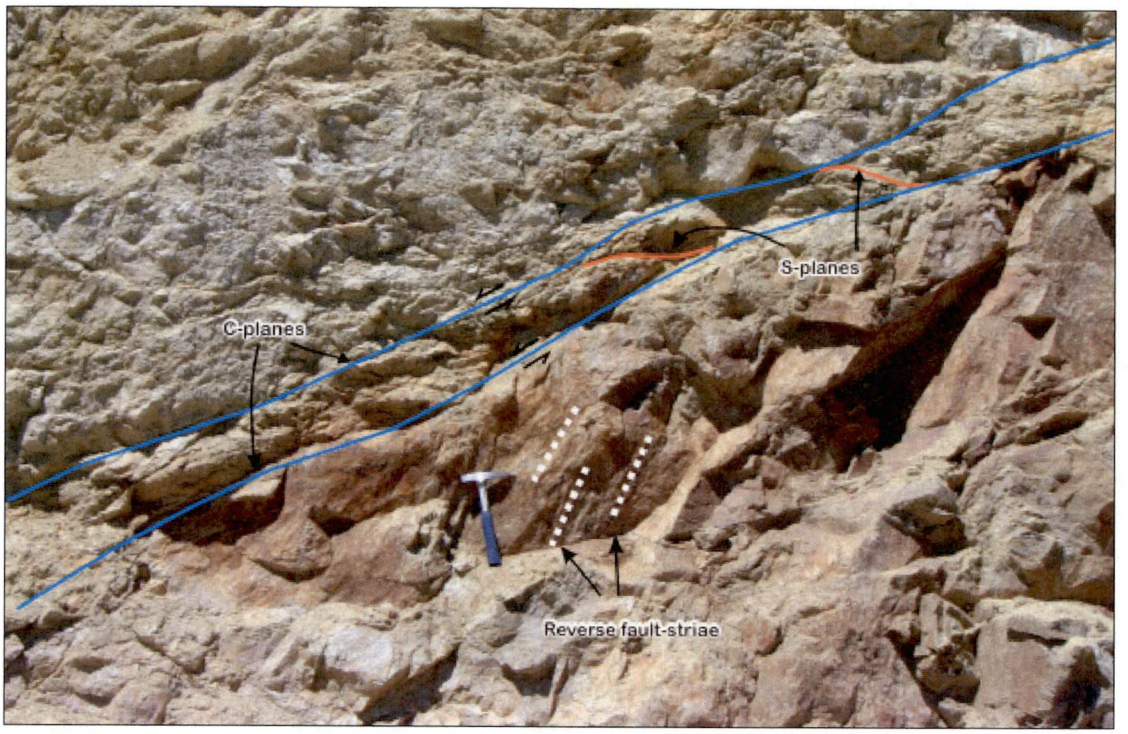

Figure 4.20a Mesoscopic-scale extensional shear zone, with well defined S-C planes, cutting limestones of the Early Jurassic-Kimmeridgian Upper Member *(TJep-b)* of El Profeta Formation. Notice the steeply plunging slickenlines of the reverse fault that crosscuts the shallow-dipping shear zone. Structural station B, Perito block (7,321,121m N; 479,237m E).

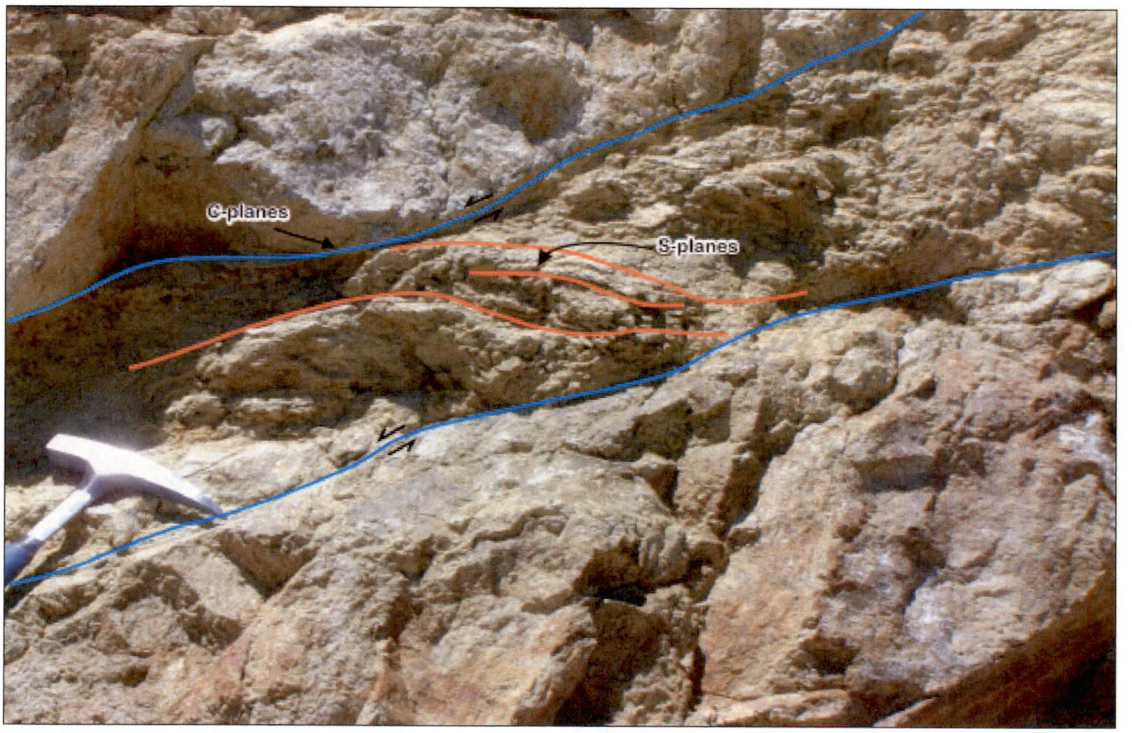

Figure 4.20b Detailed view (looking south) of the S-C planes from the shallow-dipping shear zone illustrated in Figure 4.20a. Structural station B, Perito block (7,321,121m N; 479,237m E).

Mpodozis et al. (2005) for the intra-arc tectonovolcanic basins (Figure 3.23). However, additional collection of kinematic data is necessary to better assess the regional geological significance of the extensional shear structures recognised in La Escondida district.

4.6 EARLY PALEOCENE COMPRESSION (K-T TECTONIC PHASE, ~64-62 Ma)

The Late Cretaceous volcanic and volcaniclastic sequences that are exposed in the Central Depression and part of the Domeyko Cordillera were folded by a transpressional episode in the lowest Paleocene (65-62 Ma "K-T" tectonic phase; Cornejo et al., 2003). These authors envisaged the tectonic phase as a short-lived but intense event. There are no structural features in the rock units within La Escondida district that can be linked unequivocally with the K-T tectonic phase. Systematic analyses of fault-striae data from structures that cut the Late Cretaceous-Lower Tertiary rock units suggest complex kinematic patterns related to multiple reactivations. It appears prudent to discuss these data under the perspective of the Eocene deformation (Section 4.7) due to the compatibility of the kinematic data with the dominant strike-slip deformation associated with the strongest Eocene Incaic tectonic phase (Maksaev, 1990; Boric, 1990; Reutter et al, 1991; Mpodozis and Ramos, 1991; Ramos and Alemán, 2000). At the present, there are no data that can establish unequivocally if the deformation observed in these dykes is as young as Tertiary.

The K-T tectonic phase in the study area has caused a marked angular and erosive discordance between the volcaniclastic packages of the Augusta Victoria Formation (57-53 Ma; Table 3.9) and the underlying redbeds of the Late Jurassic-Neocomian Santa Ana Formation. The Augusta Victoria magmatism was initiated with the emplacement of an andesitic dyke (60.7 ± 0.61 Ma *Pan* unit; Table 3.9) hosted by the Cerro Bayo complex (Section 3.5). The K-T deformation should therefore be older than 60.7 Ma and younger than the 74-64 Ma Cerro Bayo, Torcaza and Las Torres igneous complexes (Table 3.7). These radiometric constraints provides a probable age of 64-62 Ma for the K-T deformation in La Escondida district, which overlaps roughly with the 65-62 Ma age documented by Cornejo et al. (2003) along the Central Depression.

4.7 EOCENE COMPRESSION AND TRANSPRESSION (INCAIC TECTONIC PHASE; ~45-35 Ma)

The time-span encompassing the middle Eocene and early Oligocene is probably one of the most studied and debated period in the Cenozoic history of the Central Andes. The conjunction of diverse structural, magmatic and metallogenic processes lead to the formation of the world-class Eocene porphyry Cu belt along the Domeyko Cordillera.

The Incaic tectonic phase was preceded by significant silicic-intermediate explosive volcanism. This is preserved as the Augusta Victoria volcaniclastic sequence (ca. 57-53 Ma; Table 3.9; Appendix 6) and associated andesitic dykes (60.7 ± 0.61 Ma; Table 3.9; Appendix 6), in La Escondida region. These units formed in an extensional setting (Marinovic et al., 1996; Cornejo et al., 2003).

4.7.1 The Domeyko Fault System (DFS)

The Domeyko Fault System (DFS as defined by Maksaev, 1990) is a major 1000 km-long fault system that can be traced from Collahuasi to El Salvador (Maksaev, 1990; Boric, 1990; Reutter et al, 1991; Mpodozis and Ramos, 1991; Cornejo et al., 1993; Marinovic et al., 1995; Cornejo and Mpodozis, 1996; Tomlinson et al., 2001a; Figure 4.1). There has been significant progress over the past 15 years regarding the understanding of the history of the Domeyko Fault System and its role in the formation of the giant Eocene-Oligocene porphyry Cu belt of northern Chile, but the complex fault architecture and evolution remain controversial with at least two competing views. A number of regional studies highlighted the strong temporal and spatial relationship between porphyry Cu deposits and faulting activity along the DFS (Coira et al., 1982; Maksaev, 1990; Boric et al., 1990; Reutter et al., 1991). These investigations suggested that the DFS is a long-lived transpressional strike-slip system that was active between ca. 45 Ma and ca. 15 Ma, associated with a complex framework of strike-slip faults, and fold and thrust belts (i.e., Reutter et al., 1991; Scheuber and Reutter, 1992; Tomlinson et al., 1993; Tomlinson and Blanco, 1997a, 1997b). More recently the DFS has been modeled as an orogen controlled by tectonic inversion due to a strictly compressional regime since the Late Cretaceous (Amilibia, 2002; McClay et al., 2002; Skarmeta et al., 2003; Muñoz et al., 2005).

4.7.2 Segmentation of the Domeyko Fault System (DFS)

Available geological information currently permits the division of the DFS into four structural segments (Figure 4.1), each defined by relatively consistent structural patterns and styles, basement compositions and deformation history (Maksaev, 1990; Reutter et al., 1991; Mpodozis et al., 1993a; Cornejo and Mpodozis, 1996; Tomlinson et al., 2001a).

4.7.2.1 Segment I - Quebrada Blanca-Chuquicamata

The Sierra de Moreno and Sierra del Medio constitute pop-up blocks bounded by opposing vergence high-angle reverse faults named collectively Pre-Cordillera fault system (PFS), which is a northern expression of the DFS (Figure 4.2; Reutter et al., 1991; Tomlinson and Blanco, 1997a, 1997b; Tomlinson et al., 2001a; Amilibia and Skarmeta, 2003). The West fault is a branch of the PFS that played a key role in the history of the Chuquicamata porphyry Cu-Mo deposit. Important geochronological and kinematic information have been presented by Tomlinson and Blanco (1997a, 1997b) and Tomlinson et al. (2001a) for this structural segment and particularly for the West fault. The chronology of the deformation and the major movement history can be summarized as follows:

- Middle Eocene shortening involving reverse faulting constrained between ca. 44 Ma and 37 Ma.
- Late Eocene dextral transpression with strike-slip faults dated as post-39 Ma.
- Late Eocene-early Oligocene reversion from sinistral to dextral of the strike-slip movements at ca. 35-34 Ma.
- Early Oligocene dextral syn-mineralisation activity at ca. 34-33 Ma, inclusive up to 31 Ma. This corresponds to the West fault itself.
- Early Oligocene-early Miocene sinistral post-mineral movements between at least 31 and 25 Ma, and probably reaching 23-19 Ma, but before 16.5 Ma. Estimated offset on the order of the 35 km.
- Last movements on the West fault are reverse, dextral-slip and normal faults in Pleistocene-Holocene gravels as young as 0.5 ± 0.5 Ma.

4.7.2.2 Segment II - Limón Verde-Salar de Punta Negra

The Limón Verde- Salar de Punta Negra segment of the DFS includes La Escondida district. At the regional scale, this segment consists of a complex association of subsidiary and second-order faults linked to two master faults: La Escondida and Sierra de Varas (Figures 4.1-4.3). Mpodozis et al. (1993a, 1993b) proposed a tectonic model that considers the Domeyko Cordillera as part of a rotated sinistral orogen, bounded to the east by a set of listric normal faults (Barrancas Blancas and Quimal faults), from the thick red bed sequences of the Late Cretaceous to Lower Tertiary Purilactic Group (Reutter et al., 1991; Mpodozis et al., 2005) and from the Early Paleozoic Cordón de Lila block. To the west, the tectonic limit is considered to be the Sierra de Varas fault with the Mesozoic to

Paleocene volcanic and sedimentary cover. This model incorporates the following structural elements (Figure 4.2):

- The Domeyko Cordillera, which comprises a series of discrete basement block separated by small, closed basins (the salars of Elvira, Los Morros, Verónica Hamburgo and Punta Negra).
- Deformation in the Purilactic Group, which is particularly strong at the contact with the basement blocks.
- Five clockwise-rotated rhombohedral blocks. From north to south, they are the Quimal, Los Morros, Mariposa and San Carlos blocks (Figure 4.2). These blocks are bounded by strongly curved sinistral strike-slip faults in the south and by NNE-striking faults in the north.
- The Escondida shear lens (*sensu* Ringebach et al., 1992), which is limited to the west by the Sierra de Varas fault and to the east by the Escondida-Punta Negra Fault. This shear lens is interpreted to be a positive flower structure generated by a sinistral tranpressional regime (Sanderson and Manchini, 1984).

Mpodozis et al. (1993a, 1993b) and Marinovic et al. (1995) proposed that deformation in the region started at around 45-40 Ma and was associated with sinistral strike-slip movements that transported the basement blocks northward. The movements were buttressed against the Limón Verde block and subsequently transferred to the east (Purilactic basin), along curved NE-striking faults. More recent investigations propose that the rigid buttress occur on the Sierra del Medio, approximately 150 km to the north of Limón Verde (Figure 4.2). This is because of the structural continuity of the Domeyko Fault System up to the Sierra del Medio in Segment I (Tomlinson and Blanco, 1997a). A large scale N-striking sinistral transpressional system has been proposed by Niemeyer et al. (2000a) and Tomlinson et al. (1993) in this portion of the orogen.

4.7.2.3 Segment III - Vaquillas-Sierra Exploradora

The Sierra Exploradora pluton (ca. 35 Ma) and the Exploradora porphyry-Cu system (ca. 32 Ma) have been deformed by dextral transpression along of the Sierra del Castillo fault system during the late Eocene-early Oligocene (Cornejo and Mpodozis, 1996). Kinematic data suggest complex movement history composed of an early E-W shortening, which was followed by a NNW-SSE shortening roughly parallel with the fault (Niemeyer, 1999). A clockwise rotation of 65° was inferred for the principal stress direction by Niemeyer

(1999) to explain this change. In addition, multiple normal reactivations of the faults have been recorded by minor scarps in the Miocene ignimbrite and Recent gravels (Cornejo and Mpodozis, 1996; Niemeyer, 1999).

4.7.2.4 Segment IV - El Salvador-Quebrada del Carrizalillo

A large scale N-striking sinistral transpressional system has been proposed by Cornejo et al. (1993), Tomlinson et al. (1993) and Tomlinson et al. (1994) in this portion of the orogen. The sinistral Riedel shear model incorporates the following structural elements: (1) the fold-thrust belt of Potrerillos; (2) a series of conjugate dextral and sinistral faults; and (3) the Sierra del Castillo-Agua Marga as a master fault. The structural architecture was developed between 42 and 39 Ma and was accompanied by the emplacement of syn-tectonic mineralized intrusions at El Salvador and Potrerillos.

4.7.3 Domeyko Fault System - La Escondida Region (southern portion of structural segment II)

As mentioned previously, the Domeyko Fault System comprises two first order structural elements in La Escondida region, the Sierra de Varas and La Escondida master faults. The Sierra Varas is the major discontinuity in the orogen. It has a NNW-strike in the south and a NNW- to N-trending strike in the north, defining a curvilinear trace (Figures 4.2 and 4.3). Eocene-Oligocene strike-slip movements have been inferred on the Sierra de Varas fault (Marinovic et al., 1995; Niemeyer, 1996; Niemeyer et al., 2000a; Section 4.7.7). La Escondida master fault consists of several N-S-striking strands and splays with a complex geometric arrangement. Younger motions on this fault appear to be consistent with a conjugated strike-slip model (Marinovic et al., 1995; Mpodozis et al., 1993a, 1993b; Section 4.7.7).

Mpodozis et al. (1993a, 1993b) and Marinovic et al. (1995) determined that the Sierra de Varas and La Escondida faults bound a shear lens within the western domain that includes the folded Mesozoic sedimentary and Tertiary plutono-volcanic units (western structural domain). High-angle NNE and NNW faults, and subordinate ENE-striking fractures, have been developed within the shear lens (Figure 4.21). A series of E-striking dextral strike-slip faults postdate the other faults that occur in the mega-lens including a strand of La Escondida fault itself (Figure 4.21). A few tens of meters of relative displacements have been estimated for these later E-striking faults in the northern part of the area.

4.7.4 Stereonet Data

The mesoscopic faults have been grouped broadly into two main populations: (1) early-stage reverse faults of uncertain, but post-Late Cretaceous age; and (2) strike-slips faults associated with Eocene deformation. These grouping have been based on the age of the rock units affected by faulting, and in the cross-cutting relationships observed between the fault populations.

4.7.4.1 Early-stage Reverse Faults

Conspicuous reverse faults have been observed in diverse structural blocks that contain the Late Cretaceous intrusive complexes, Late Triassic-Kimeridgian El Profeta and Late Paleozoic La Tabla Formation (Figure 4.21). Steeply-dipping reverse faults have crosscut older reverse dip-slip faults related to the lowermost Late Cretaceous tectonic inversion and the dextral extensional shear zones of Late Cretaceous age (Figure 4.19a). These steeply-dipping reverse faults are associated with crudely foliated fault breccia and gouge, and the faults have relatively wide damage zones (<1.5 m) and abundant limonite-calcite-ankerite alteration. Evidences for later strike-slip reactivations (principal-stage strike faults) are common on the fault planes (Figure 4.26b).

Puma E block. At station B, a NW-striking set of minor reverse faults has affected the dioritic to gabbroic sills of the Cerro Bayo plutonic complex (*LKcb2*; ca. 77-74 Ma; Table 3.7; Appendix 6). The local shortening direction is inferred to have been oriented NE-SW orientation based on slickenline analysis (Figure 4.21).

Bayo block. The monzonites and quartz-monzonites of the Cerro Bayo plutonic complex (*LKcb6*; ca. 74 Ma; Table 3.7; Appendix 6) contain well developed set of NE-striking reverse faults at station B (Figure 4.22) and NW-striking reverse faults at station C (Figure 4.23). Maximum paleostress directions are inferred to have been NW-SE and NE-SW respectively. Slickenline kinematics data at both stations are consistent with later dextral (transtension) and sinistral (transpression) strike-slip reactivations, in rare cases followed by still younger reverse movements (Figures 4.22 and 4.23).

Sombrero block. At station B, andesite-diorite dykes of Las Torres igneous complex (*Lklt2*; ca. 70-66 Ma) are cut by conjugate sets of NE-striking reverse faults (Figure 4.21). The reverse faults have been overprinted in turn by NE- and WNW-striking strike-slip faults, with equivocal shear sense indicators (Figures 4.24a to 4.26a).

Perito block. At station B, a family of WNW- to WSW-striking reverse faults has cut the Late Cretaceous age extensional shear zones (Figure 4.19a). Kinematic indicators from the reverse faults indicate a NNE-SSW principal maximum stress orientation (Figure 4.21). The age of these reverse faults is unknown, but must be later than the Late Cretaceous extensional event.

A more complicated structural history has been determined at station C, proximal to the Perito fault (Figure 4.21). Here, NW-striking reverse faults have been reactivated with NW and NE strike-slip movements (Figures 4.26b and 4.28). Kinematic indicators on early reverse faults are consistent with a NE-SW shortening (Figures 4.21 and 4.27). No shear sense indicators were observed along the strike-slip fault planes.

Remarks. Faults and associated slickenlines indicate the occurrence of reverse faulting, herein named early-stage reverse faults, which affected the Paleozoic and Mesozoic rock units. There is no significant correlation of the paleo-stress directions obtained from them, and these paleo-stress directions are anomalous with regards a probable E-trending regional contraction. They are therefore considered to reflect local stress variations and are not representative of the regional stress regime. Reverse faulting probably correlates with either the early Paleocene K-T transpressive deformation phase (Cornejo et al., 2003) or the Eocene coaxial-transpressive Incaic deformation phase (Maksaev, 1990 Reutter et al., 1991). Further refinement on timing constraints are required to resolve which of these events was responsible for the early-stage reverse faults. These faults exhibit evidence of reactivation and overprinting by dextral and sinistral strike-slip faults (principal strike-slip faults) of probable Eocene age.

4.7.4.2 Bedding and Folds

The crudely stratified volcano-sedimentary rocks of the Augusta Victoria Formation (ca. 57-53 Ma; Table 3.9) have been deformed into open to tight folds (wavelength>500 m; Figure 4.28a). The map-pattern indicates regional folds that plunge gently to the north and south (Figure 4.21), and are sub-parallel to major Eocene reverse faults such as Portezuelo I fault (Section 4.7.7; Figures 4.21 and 4.29). In the Poblete structural block, the cores of the anticlines include refolded beds of the Mesozoic Santa Ana and El Profeta Formations. Bedding is scattered (Figure 4.28b) and measured fold hinges are also scattered.

Remarks. The structural relationships described above indicate that the deposition of the Augusta Victoria Formation was followed by a major compressional deformation event, which occurred after 53 Ma. The sub-horizontal and parallel pattern defined by the regional fold axes is consistent with an origin by reactivation and tightening of earlier folds (type O interface). Niemeyer (1996) considers it highly unlikely that these folds were originated by sinistral movements of the Domeyko Fault System, as originally proposed Reutter et al. (1991). Post-Augusta Victoria shortening has been documented along the Central Depression, where other similar volcanic units of the late Paleocene-early Eocene magmatic arc have been folded. Unfortunately no structural data are available to compare the folding styles.

4.7.4.3 Principal-stage Strike-Slip Faults

Principal-stage strike-slip faulting is the most widespread deformation that has occurred in La Escondida district. This deformation phase has largely obliterated evidence for Paleozoic and Mesozoic deformations. Fault-striae measurements of post-early Eocene faults have been collected principally from the folded Augusta Victoria Formation, and from the El Profeta Formation. The kinematic data are summarized in Figure 4.29.

Perito block. At station D, thick packages of conglomerates from the Lower Member (*TJep-a*) of El Profeta Formation have been crosscut by two well-defined sets of dextral strike-slip faults oriented ENE to NE. The striae-data set suggest a maximum principal stress oriented NW (Figures 4.30). The strike-slip faults have been crosscut by a conjugate set of WNW- and NW-striking normal faults of possible post-Eocene age (Figures 4.29 and 4.30).

Poblete block. Stations A, B, C, E, I and IX contain examples of NNE- to NE-striking strike-slip and oblique-slip faults (Figures 4.29). Kinematic indicators provide evidence of later strike-slip and normal dip-slip reactivations along the fault-planes (Figures 4.32 to 4.37). The fault data are also consistent with an overall dextral transpressive regime of NNE- to ENE-orientation (Figure 4.29). At stations D and XI, however, there are sets of NW-striking reverse faults, which have orientations consistent with NE-trending shortening (Figure 4.29). These reverse faults are inferred to be early-stage reverse faults, rather than principal-stage strike-slip faults related to the main Eocene deformation.

Remarks. Kinematic data have provided evidence for poorly preserved reverse faulting

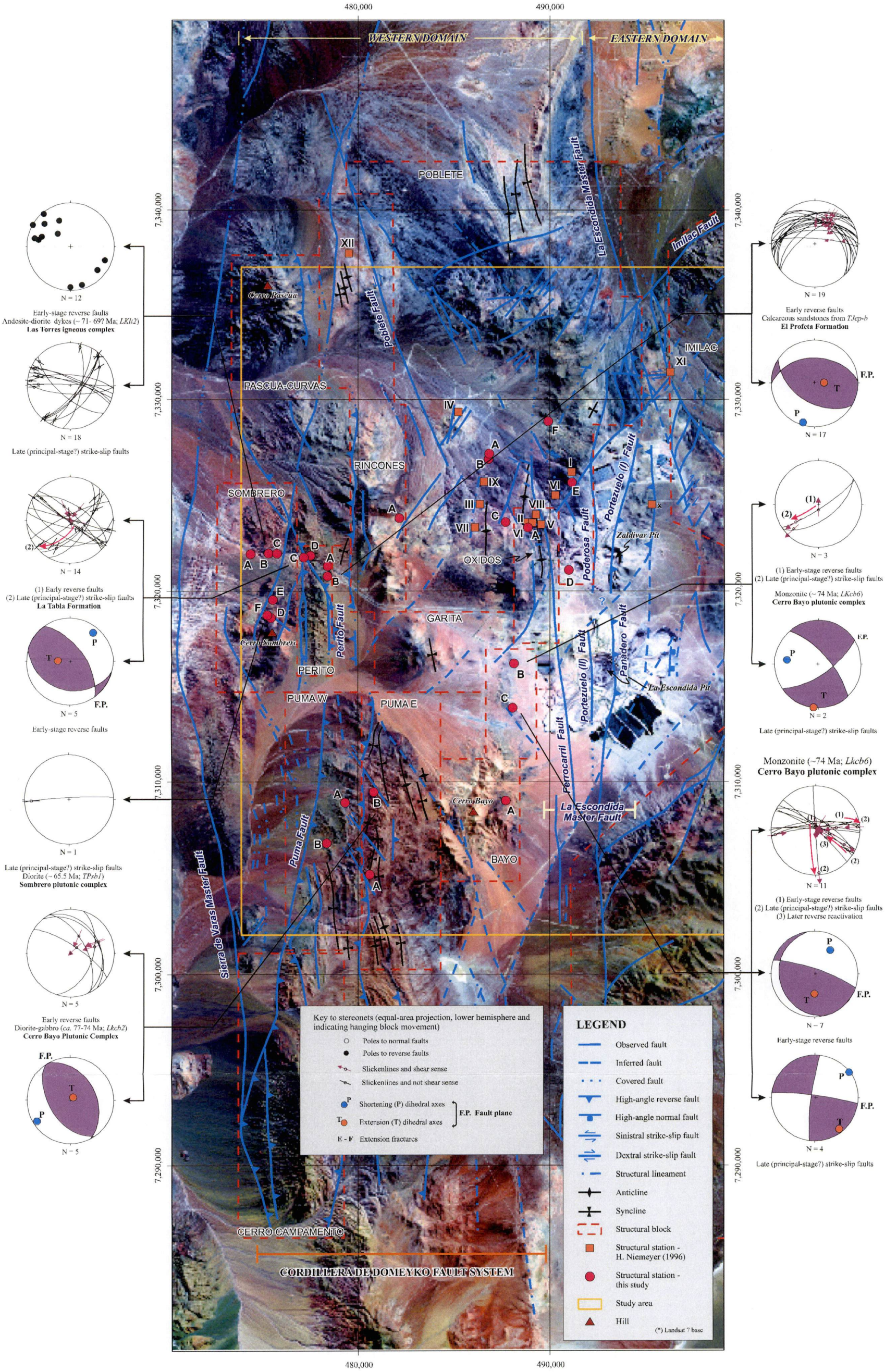

Figure 4.21 Simplified graphic representation of fault-striae kinematics of early-stage reverse faults and late (principal stage) strike-slip faults for the El Profeta and Santa Ana Formations (Late Triassic-Neocomian), and the Late Cretaceous intrusive complexes of La Escondida district.

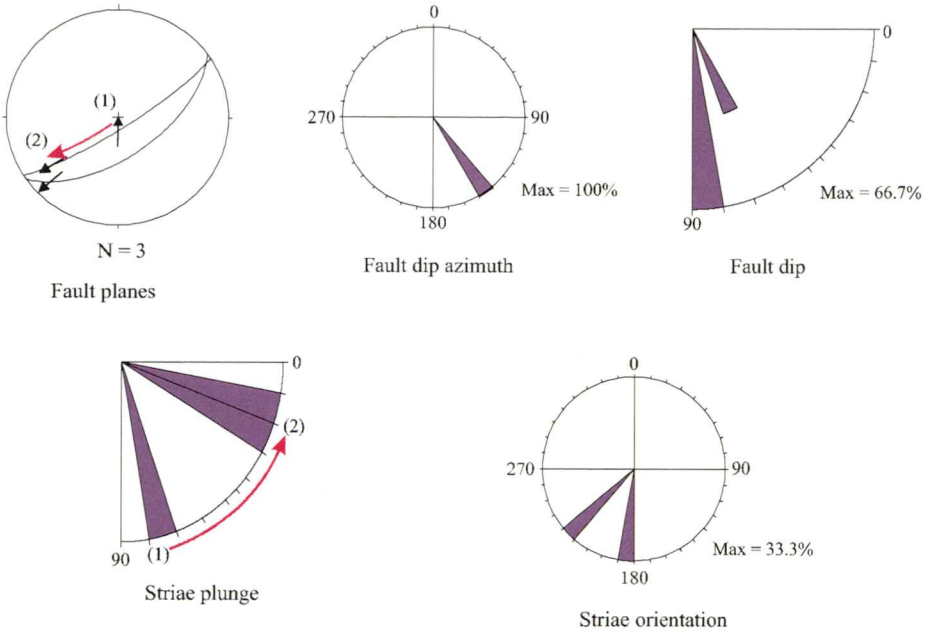

Figure 4.22 Orientation and kinematics of mesoscopic structures in quartz monzonites (*LKcb6*; ca. 74 Ma) of the Cerro Bayo plutonic complex (ca. 77-72 Ma). Fault-striae data indicating predominant NE-striking dextral strike-slip faults (principal-stage strike-slip faults?), which postdate earlier NE-striking reverse fault (early-stage reverse faults). Fault reactivations are indicated as (1) to (2).

interpreted to be related to folding of the Augusta Victoria Formation after 53 Ma and probably before 43 Ma (Sections 4.7.5 and 4.7.6). The kinematic data have also confirmed a major strike-slip faulting event, together with evidence for fault inversion and reactivation, that most probably coincides with the main period of porphyry Cu emplacement (ca. 39-37 Ma; Tables 3.14). The movement indicators are not adequate for determining the evolution of strike-slip movements from dextral to sinistral or vice versa. Field relationships are partly obscured by normal faults of post-Eocene age. Therefore, the interpreted regional paleo-stress regimes based on these fault-striae data should be treated with some caution, although there is a general correlation between these measurements with others obtained in the Zaldivar and Escondida open pits (e.g., Padilla et al., 1997; Véliz and Padilla, 1998; Vergara, 2003; Section 4.7.6).

4.7.5 Cerro Rincones Plutonic Complex (ca. 43-41 Ma) and Veins

The Cerro Rincones plutonic complex (ca. 43-41 Ma; Table 3.11; Appendix 6) crops out

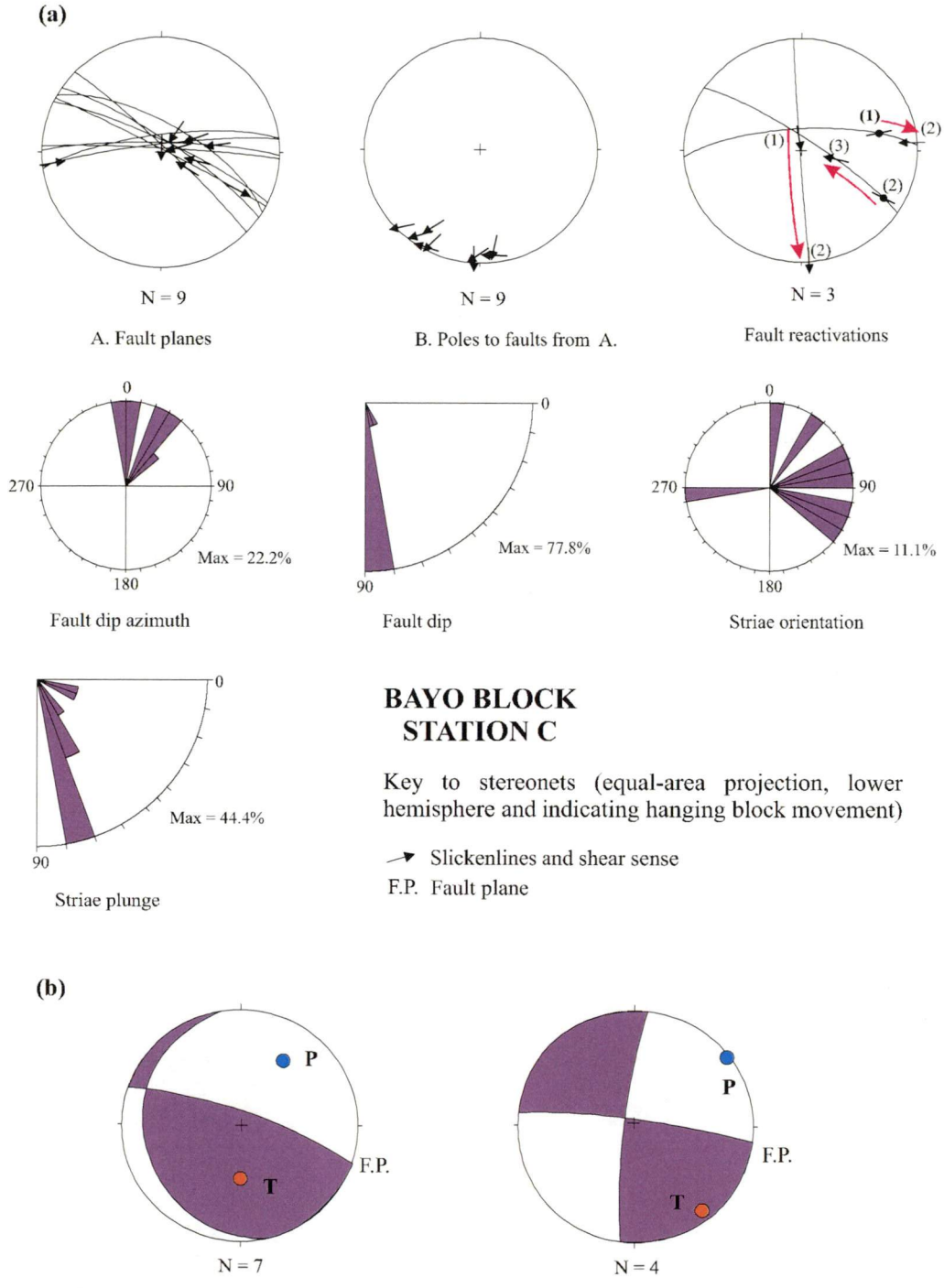

Figure 4.23 Orientation and kinematics of mesoscopic structures in quartz monzonite (*LKcb6*; ca. 74 Ma) of the Cerro Bayo plutonic complex (ca. 77-72 Ma). (a) Orientation of mesoscopic reverse and dextral strike-slip faults showing a dominant NNE-SSW local maximum stress. Striations indicate fault reactivations (1 to 2) from dextral strike-slip to reverse and vice-versa movements (2 to 3). (b) Kinematics for the minor reverse and later strike-slip faults, which show significant changes of local stress directions. Shortening (P) and extension (T) dihedres, indicating their respective axes, determined for the reverse faults (N=7) and the sinistral strike-slip faults (N=4).

in a subcircular shape (Appendix 1A), and is apparent in magnetic images as a highly magnetic ring structure that cuts the trace of the Ferrocarril Fault (Figure 4.38). Monzonitic facies of this intrusive complex host the quartz-limonite-Cu-oxides-galena-

Figure 4.24a Mesoscopic faults set of the early-stage reverse faults that have affected the Late Jurassic-Neocomian Santa Ana Formation redbeds *(JKsa)* and the diorite dykes (ca. 70-66 Ma) of Las Torres igneous complex. Notice the white-coloured limonite-calcite-ankerite zone associated with the faulted dykes. Paved road to La Escondida operation. Structural station B, Sombrero block (7,322,391m N; 475,442m E).

Figure 4.24b Reverse faulted andesitic dyke within a sheeted dyke complex (*LKlt1*; ca. 701-66 Ma) of Las Torres igneous complex. Paved road to La Escondida operation. Structural station B, Sombrero block (7,322,391m N; 475,442m E).

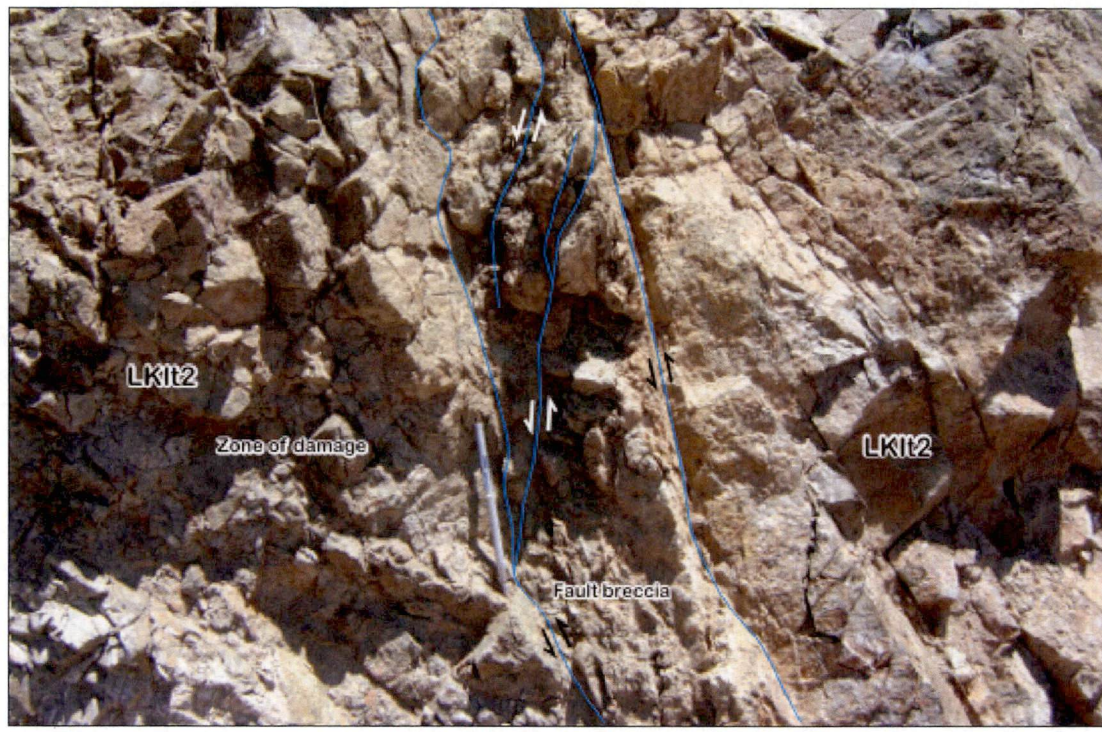

Figure 4.25a Steep reverse shear zone developed within a diorite dyke (*LKlt1*; ca. 70-66 M) of Las Torres igneous complex, with crudely small reverse faults within a fault-breccia. The margins of the dyke are also faulted, which suggest a post-emplacement deformation. A zone of damage is also observed to the left. Paved road to La Escondida operation. Structural station B, Sombrero block (7,322,391m N; 475,442m E).

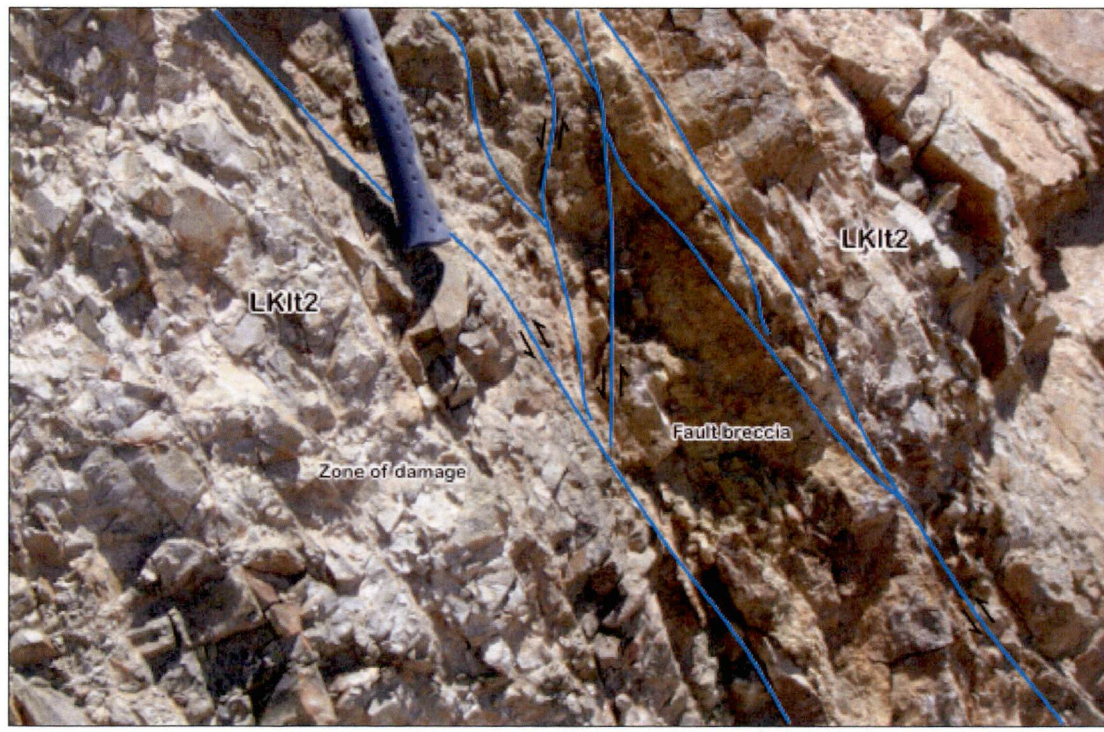

Figure 4.25b Complex net of internal reverse faults within a steeper mesoscale reverse fault zone. Limonite-rich fault-breccia and zone of damage are clearly recognized. Paved road to La Escondida operation. Structural station B, Sombrero block (7,322,391m N; 475,442m E).

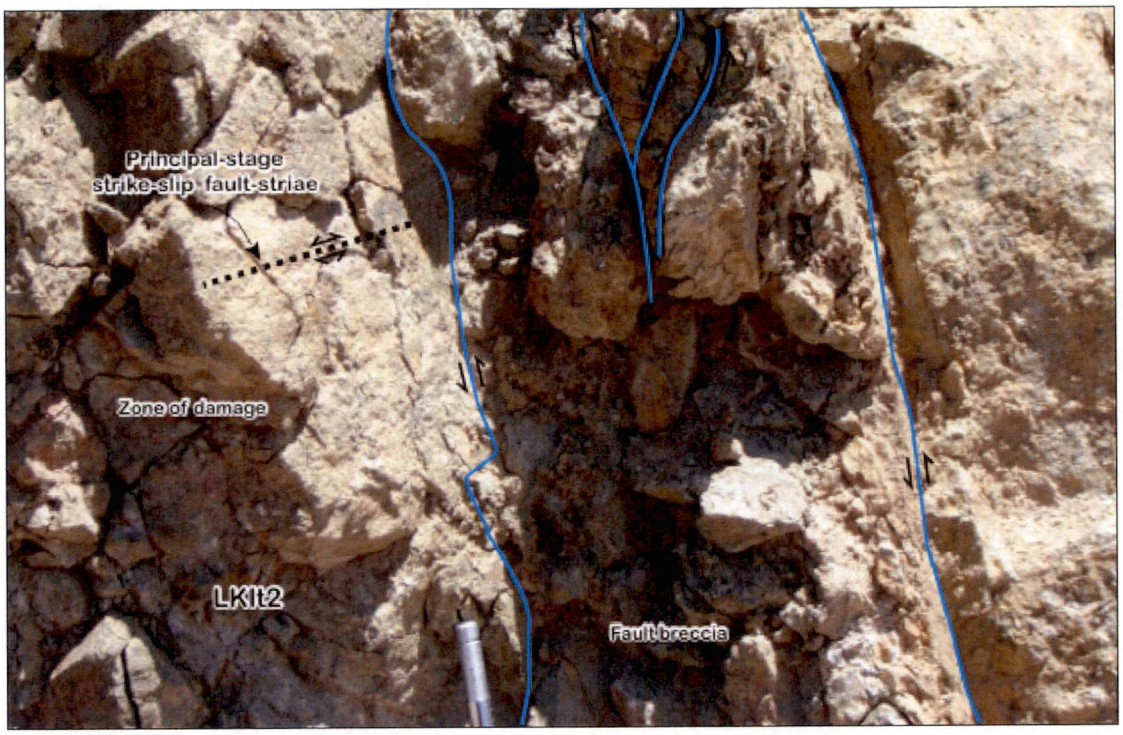

Figures 4.26a A steeper fault from the set of early-stage reverse faults, which has been reactivated with strike-slip displacement, within sheeted dykes of the *LKlt1* (70-66 Ma). Paved road to La Escondida operation. Structural station B, Sombrero block (7,322,391m N; 475,442m E).

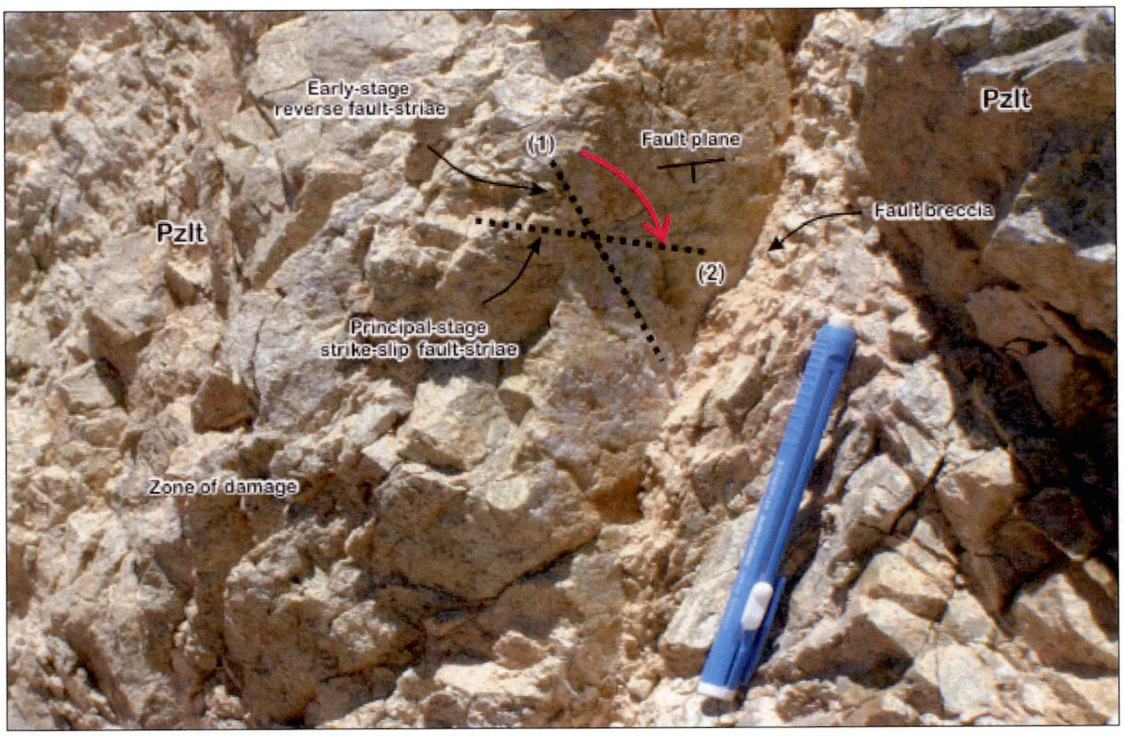

Figures 4.26b A reverse fault from the set of early-stage reverse faults that has been reactivated in a dextral strike-slip sense. In this example, the country rocks are rhyolites from La Tabla Formation (Late Carboniferous-Permian). Paved road to La Escondida operation. Structural station C, Sombrero block (7,322,009m N; 477,700m E).

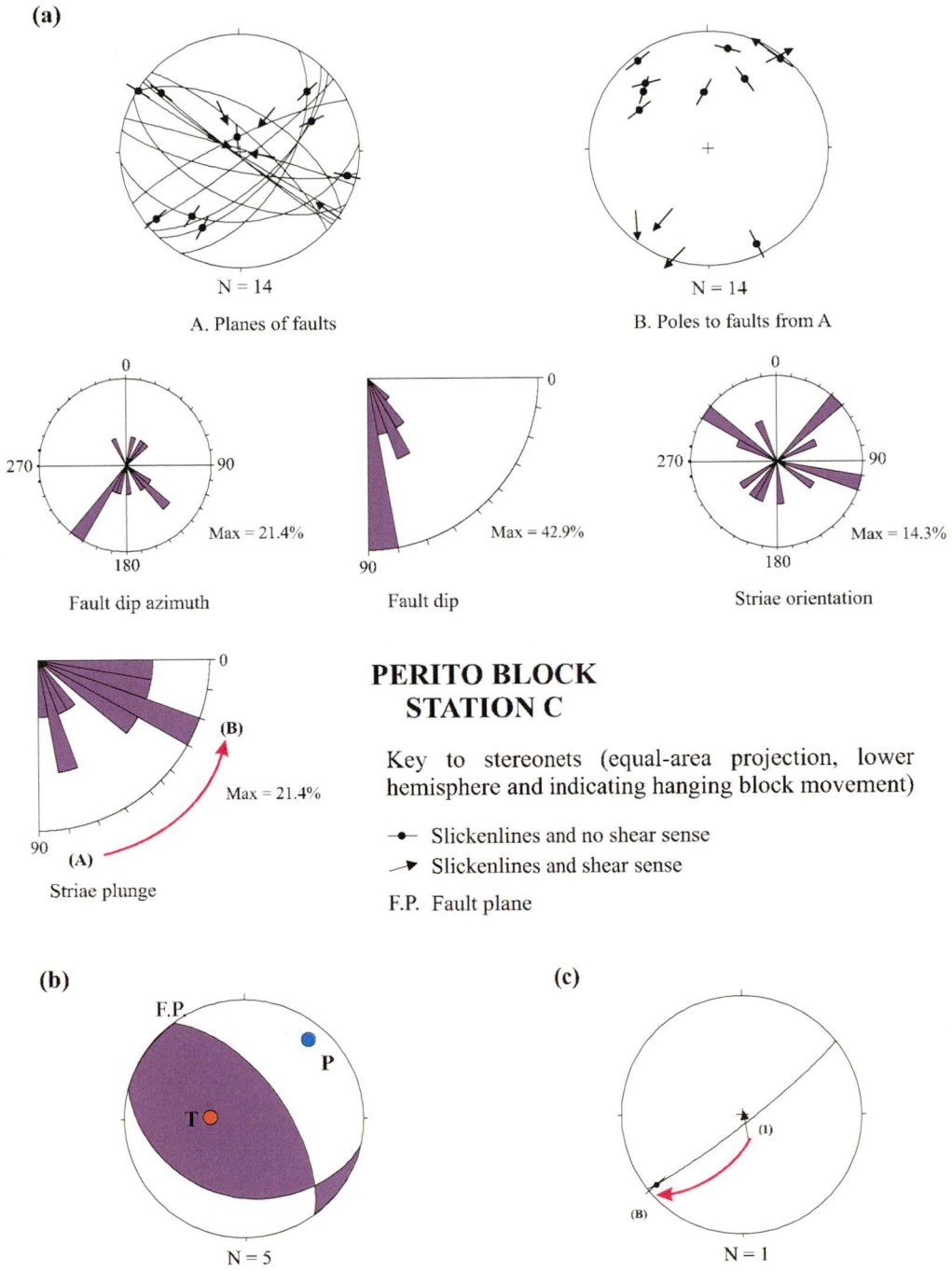

Figure 4.27 Graphical representation of fault-striae data for rhyolitic tuff of La Tabla Formation (Late Carboniferous-Permian), contiguous to the Perito fault. Structural station C, Perito block. (a) Fault-striae data suggesting three main families of faults: a northwest-trending reverse (early-stage reverse faults) and two northeast- and northwest-trending strike-slip types (principal-stage strike-slip faults?). Dip-slip movement was postdated by the strike-slip movements; (b) Shortening (P) and extension (T) dihedres for the reverse faults (their respective axis are indicated); and (c) Stereonets representation of fault plane reactivation from dip-slip to strike-slip directions.

barite-calcite veins near the Cerro Rincones skarns (Figure 4.29; Appendix 7), and also the enargite-pyrite-chalcocite veins at Chimborazo. The mineralized structures include two sets of tensional veins, with a principal component NE-striking and a secondary

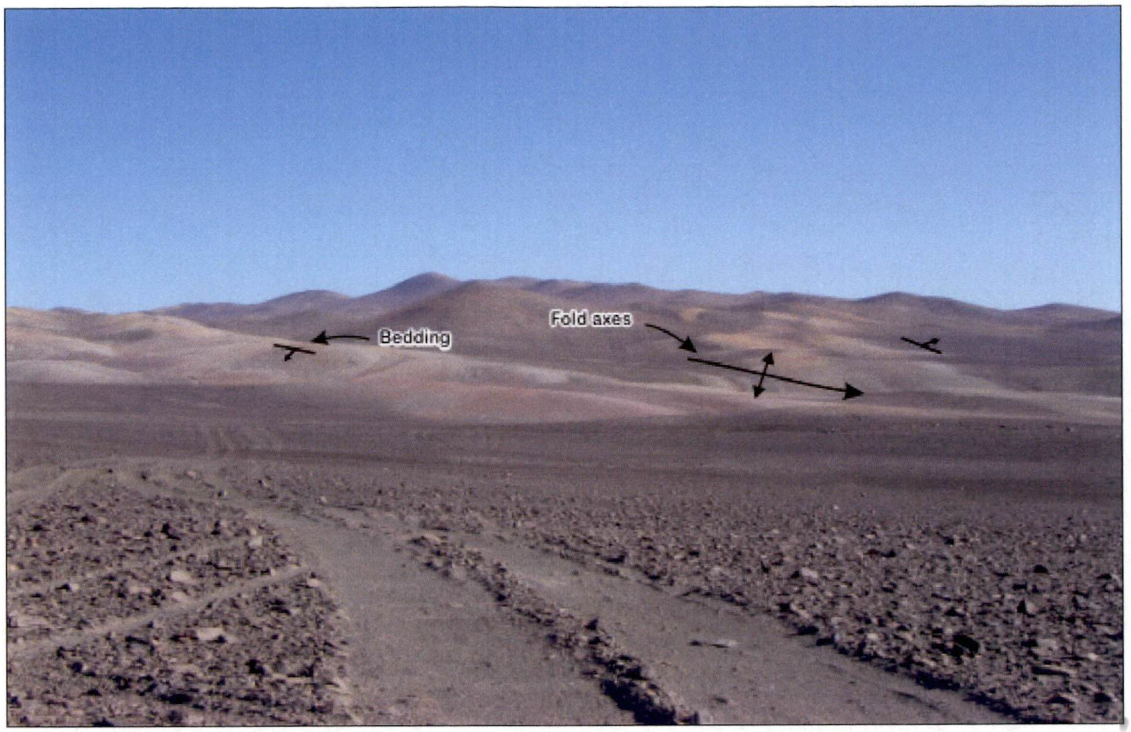

Figures 4.28a General view looking to SSW of a large-scale fold defined by interbedded white ignimibrites, volcanic sandstones, conglomerates and andesite lava flows of the Augusta Victoria Formation (ca. 57-53 Ma). The fold-axis plunges to the NNE. Chimborazo sector (7,327,000m N; 489,200m E).

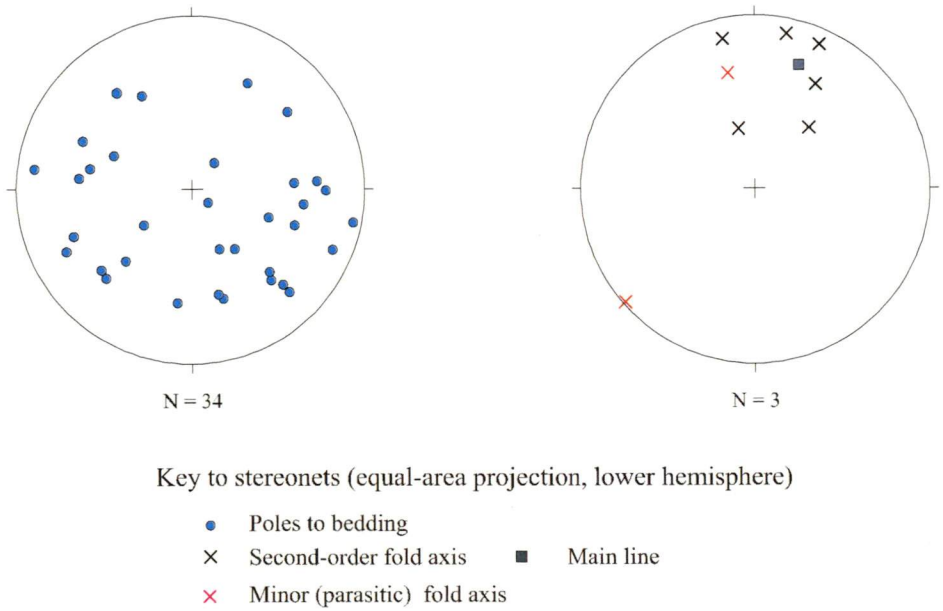

Figures 4.28b Orientation of bedding and fold axes for the late Paleocene-early Eocene Augusta Victoria Formation in the Poblete and Oxidos structural blocks.

component striking ENE (Figure 4.29). The principal geological features at Chimborazo (veins, hydrothermal bodies, faults and the post-mineral ca. 38 Ma andesitic dykes; Table 3.16) also have NNE- to NE-trends (Petersen et al., 1996; Figure 4.29). Moreover, the

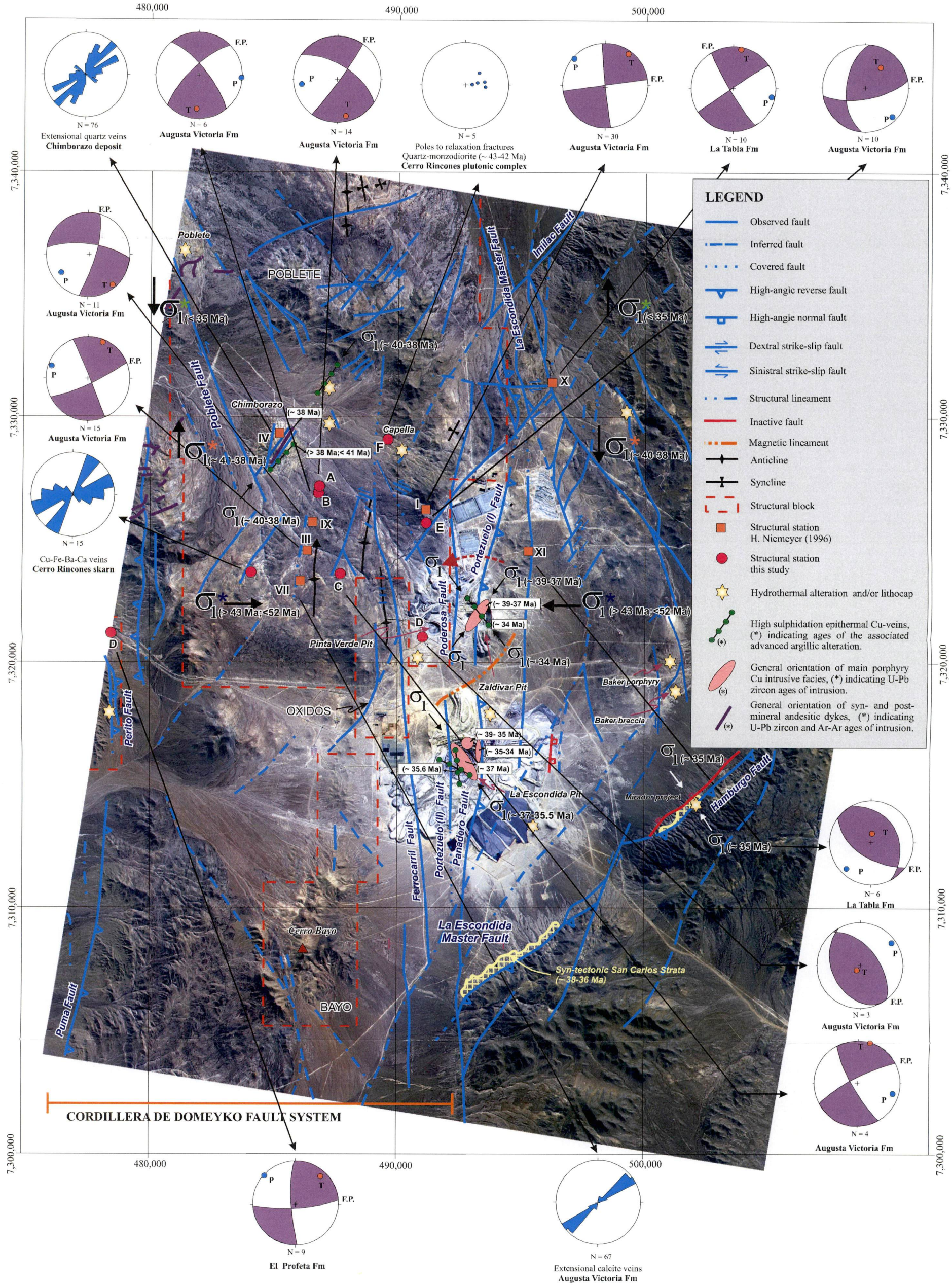

Figure 4.29 Graphic representation of the structural features for the period middle Eocene-early Oligocene including: (1) the late Paleocene-early Eocene (~57-52 Ma) Augusta Victoria Formation; (2) the Cerro Rincones plutonic complex (~43-41 Ma); (3) the high-sulfidation epithermal Cu-veins of Chimborazo (~41-39 Ma); (4) the Eocene intrusive complexes of La Escondida (~39-37 Ma) and Escondida Norte-Zaldivar (~39-37 Ma) deposits; (5) the middle-late Eocene (~38-36 Ma) syn-tectonic San Carlos strata; and (5) La Escondida master fault. Fault-striae kinematics and possible kinematic evolution are indicated.

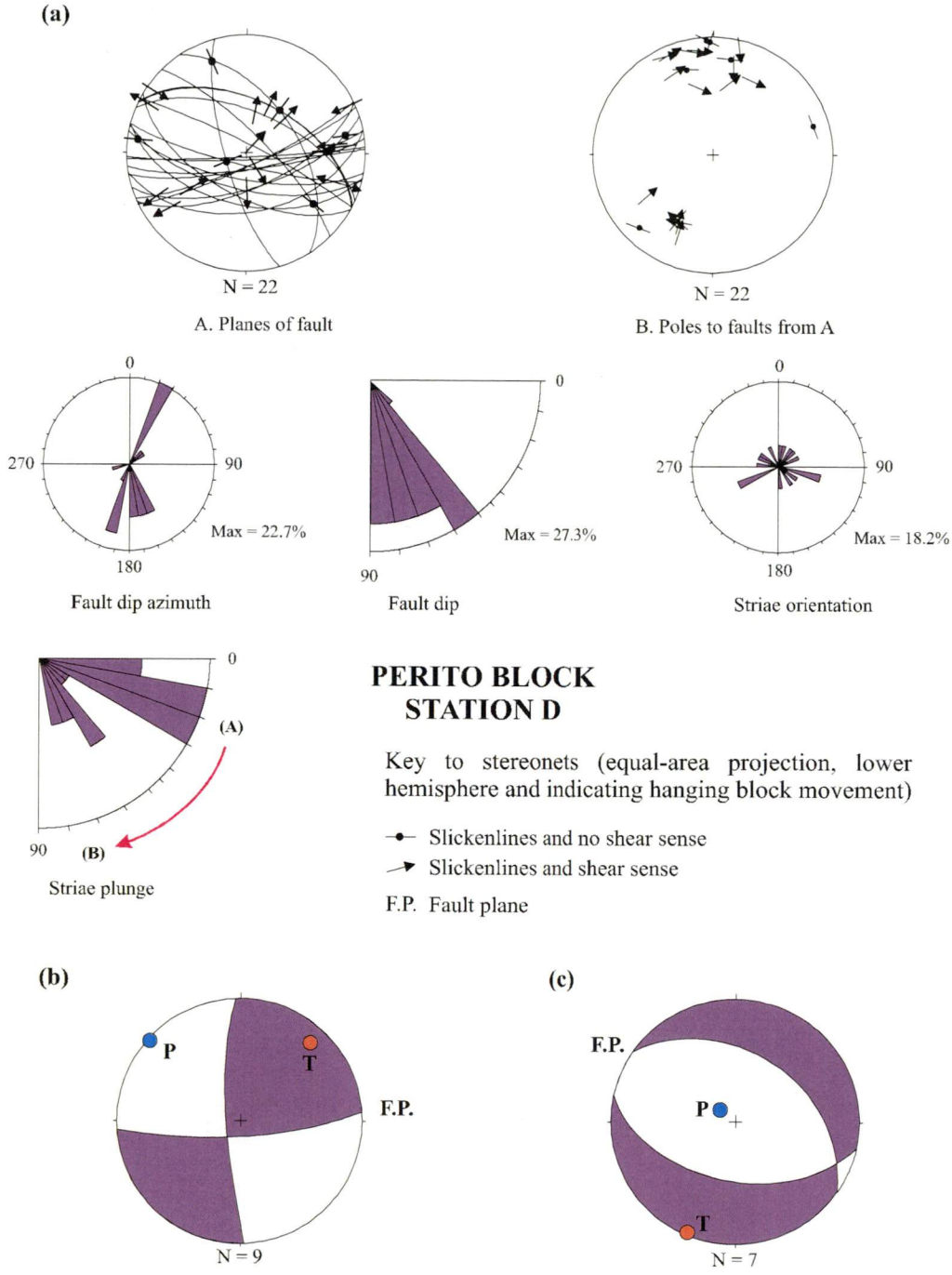

Figure 4.30 Graphical representations of fault-striae data for conglomerates of El Profeta Formation (Late Triassic- Jurassic), contiguous to Perito fault. Structural station D (7,322,150m N; 477,900m E). (a) Fault-striae data suggesting two main families of faults: east-northeast- and east-southeast-trending dextral strike-slip faults (A: principal-stage strike-slip fault). Late (post-Eocene?) and steeper, northwest-striking normal faults (B) crosscut the dextral strike-slip faults; (b) Shortening (P) and extension (T) dihedral for the strike-slip faults (their respective axis are indicated); and (c) Shortening (P) and extension (T) dihedral for the late normal faults (their respective axis are indicated).

syn-mineralisation NNE-striking tensional quartz veins at Chimborazo have been also documented at structural station V by Niemeyer (1996). A local principal maximum stress direction of NNE- to NE-orientation is therefore proposed for this sector at 40-38 Ma

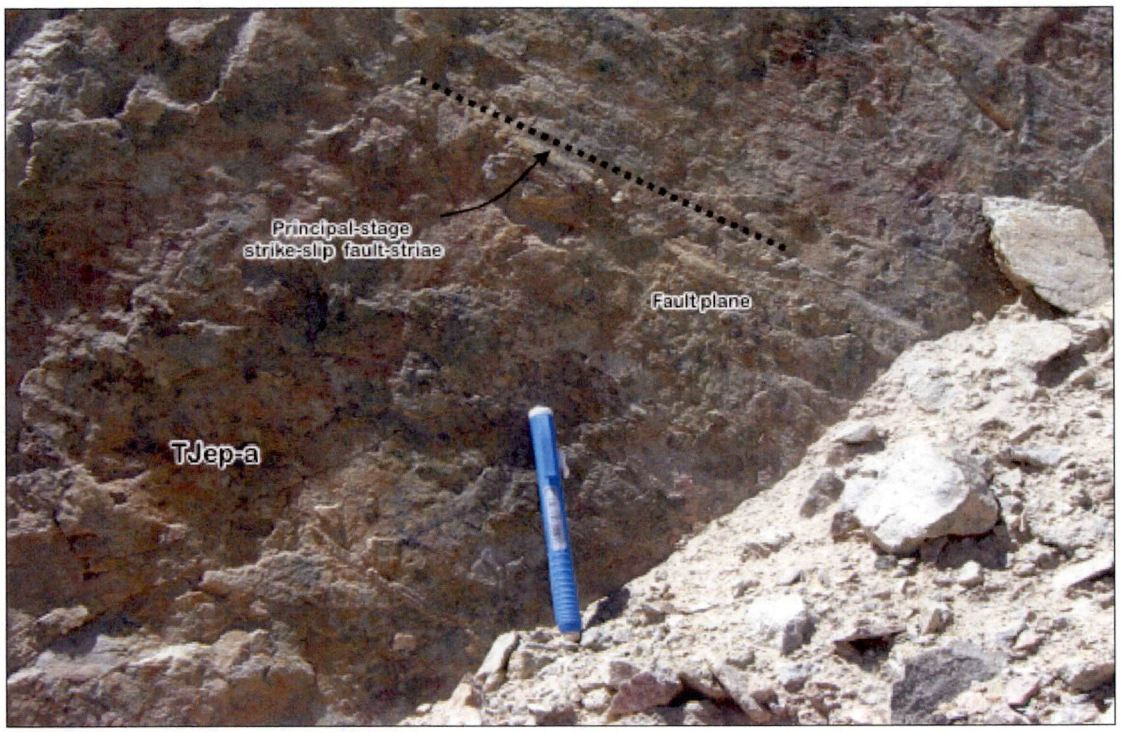

Figure 4.31a Well defined slickenlines on plane of dextral strike-slip fault of the principal stage. Paved road to La Escondida operation. Structural station D (7,322,150m N; 477,900m E).

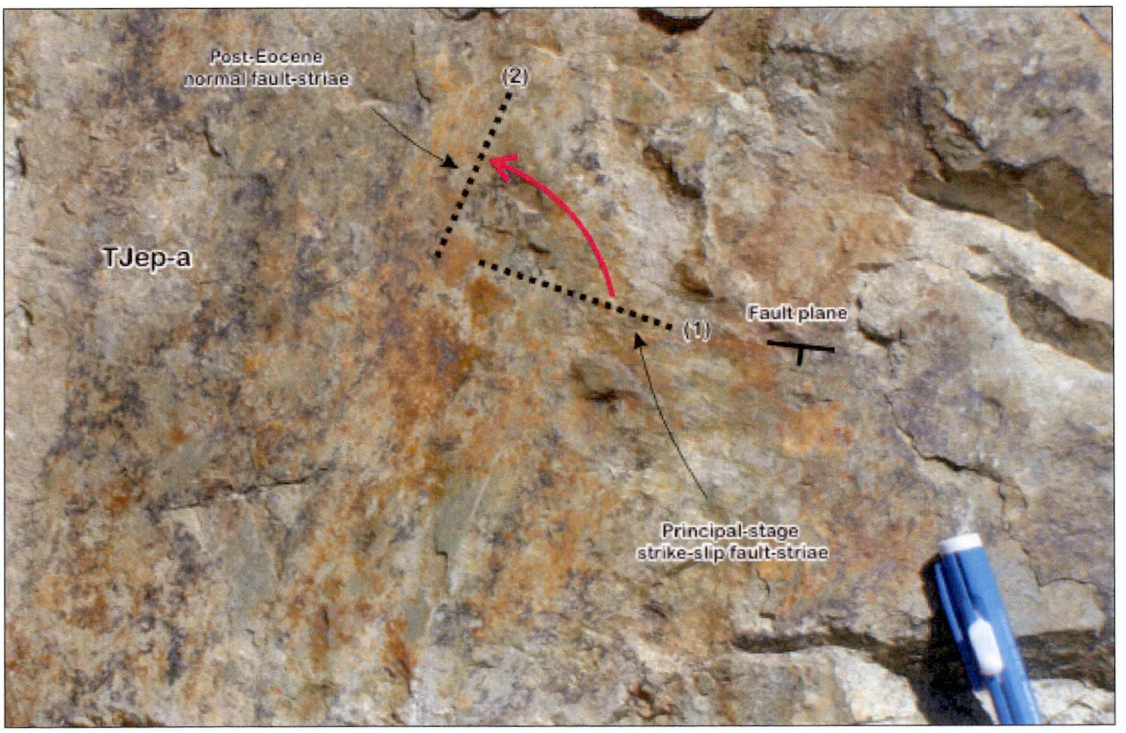

Figure 4.31b Clear reactivation of a dextral strike-slip fault of the principal-stage by a post-Eocene normal fault. Paved road to La Escondida operation. Structural station D (7,322,150m N; 477,900m E).

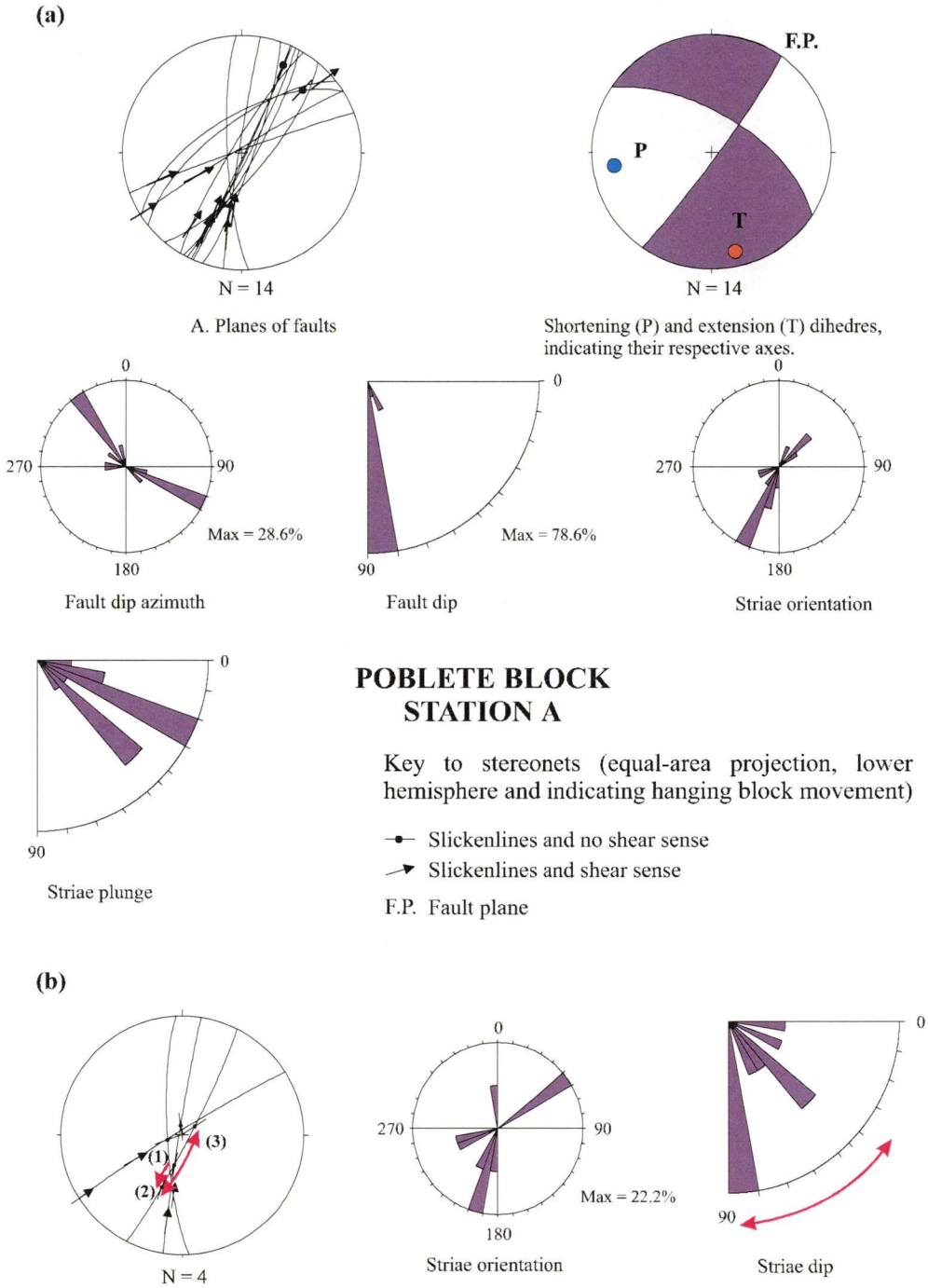

Figure 4.32 Graphical representations of fault-striae data for shallow-level diorite intrusions cogenetic with the Augusta Victoria Formation (late Paleocene-early Eocene). (a) Orientation and kinematics of faults; and (b) Striae data indicating multiple reactivations of faults.

based on the ages of the pre-mineralisation Cerro Rincones intrusion and post-mineralisation andesitic dykes (Figure 4.29). The NNE- to NE-striking of the tensile mineralized veins strike-slip faults (principal strike-slip faults) are similar to the pattern proposed in the dextral Riedel model (Tchalenko, 1970), implying major N-trending dextral transpression during this period (ca. 40-38 Ma). Transpression probably occurred

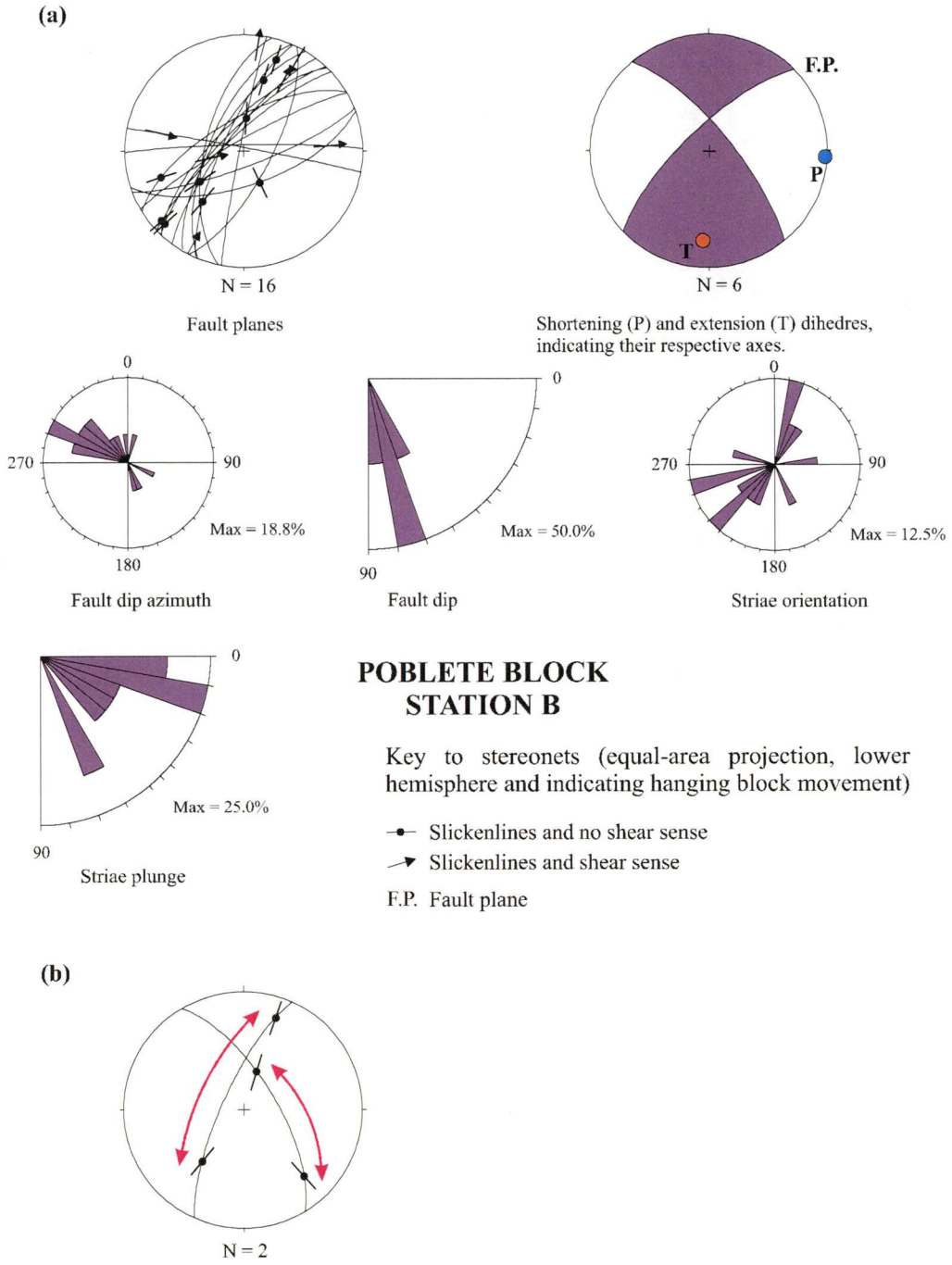

Figure 4.33 Graphical representations of fault-striae data for andesites of the Augusta Victoria Formation (late Paleocene-early Eocene). (a) Orientation and kinematics of faults; and (b) Striae data indicating multiple reactivations of faults.

along the major regional-scale faults (i.e., Sierra de Varas and La Escondida faults).

4.7.6 La Escondida and Escondida Norte-Zaldivar Porphyry Cu Deposits

Significant kinematic information has been collected recently in La Escondida and Pinta Verde pits (Padilla et al., 1997; Véliz and Padilla, 1998; Padilla-Garza, 2003; Vergara, 2003). These authors have documented dominant fault-striae data linked to NW-striking

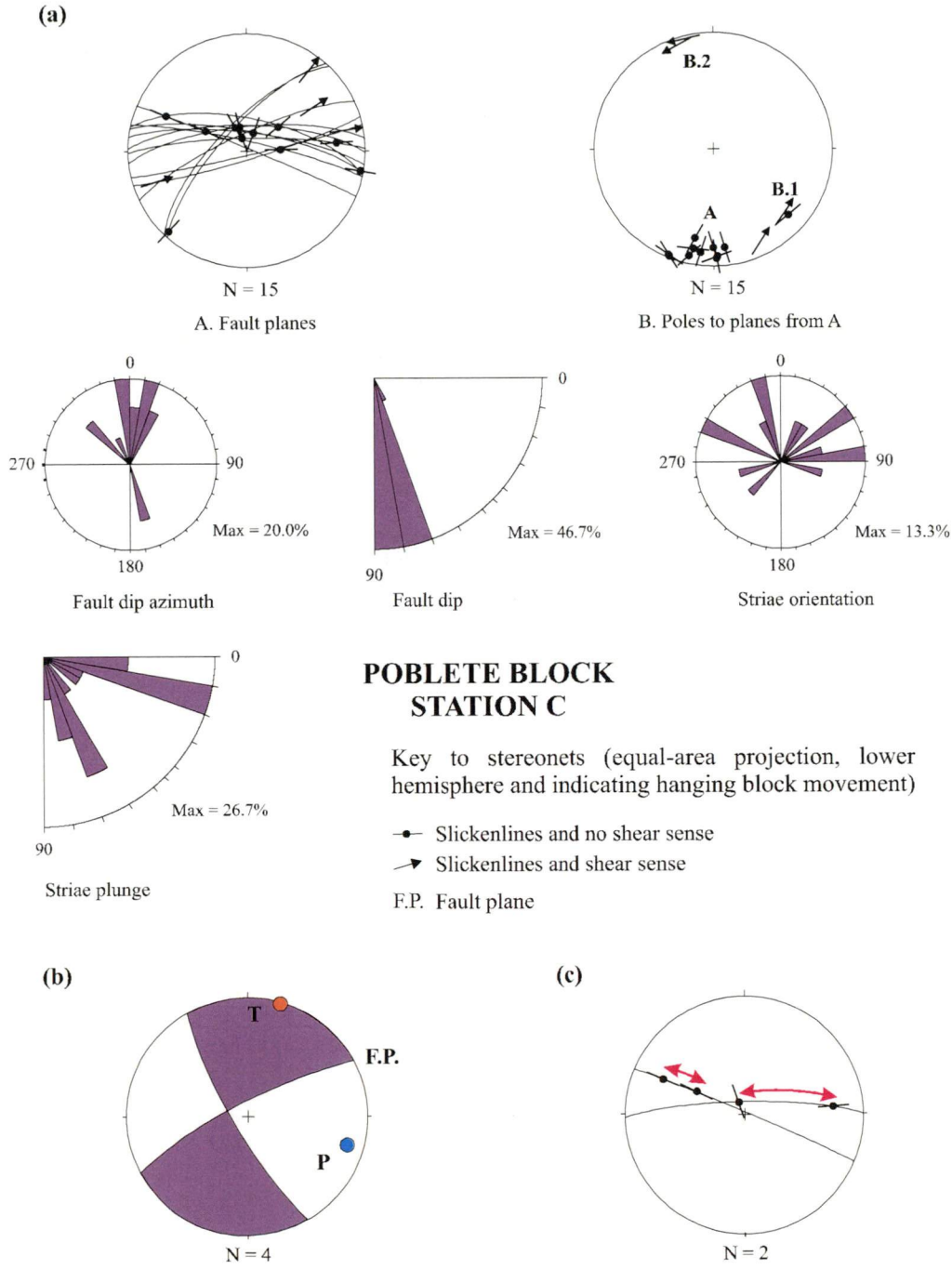

Figure 4.34 Graphical representations of fault-striae data for andesites of the Augusta Victoria Fomation (late Paleocene-early Eocene). See text for discussion. (a) Orientation and kinematics of faults; (b) Shortening (P) and extension (T) dihedres for the dextral strike-slip faults (their respective axis are indicated); and (c) Stria data indicating multiple reactivations of faults.

strike-slip faults in both of the ore deposits. A schematic distribution of the mineralized porphyry bodies for these deposits is presented in Figure 4.29, as well as the ages for individual intrusive phases and alteration-mineralisation events. The geochronological data on the multiple alteration-mineralisation events recognised in La Escondida district are discussed in detailed in Chapter 5.

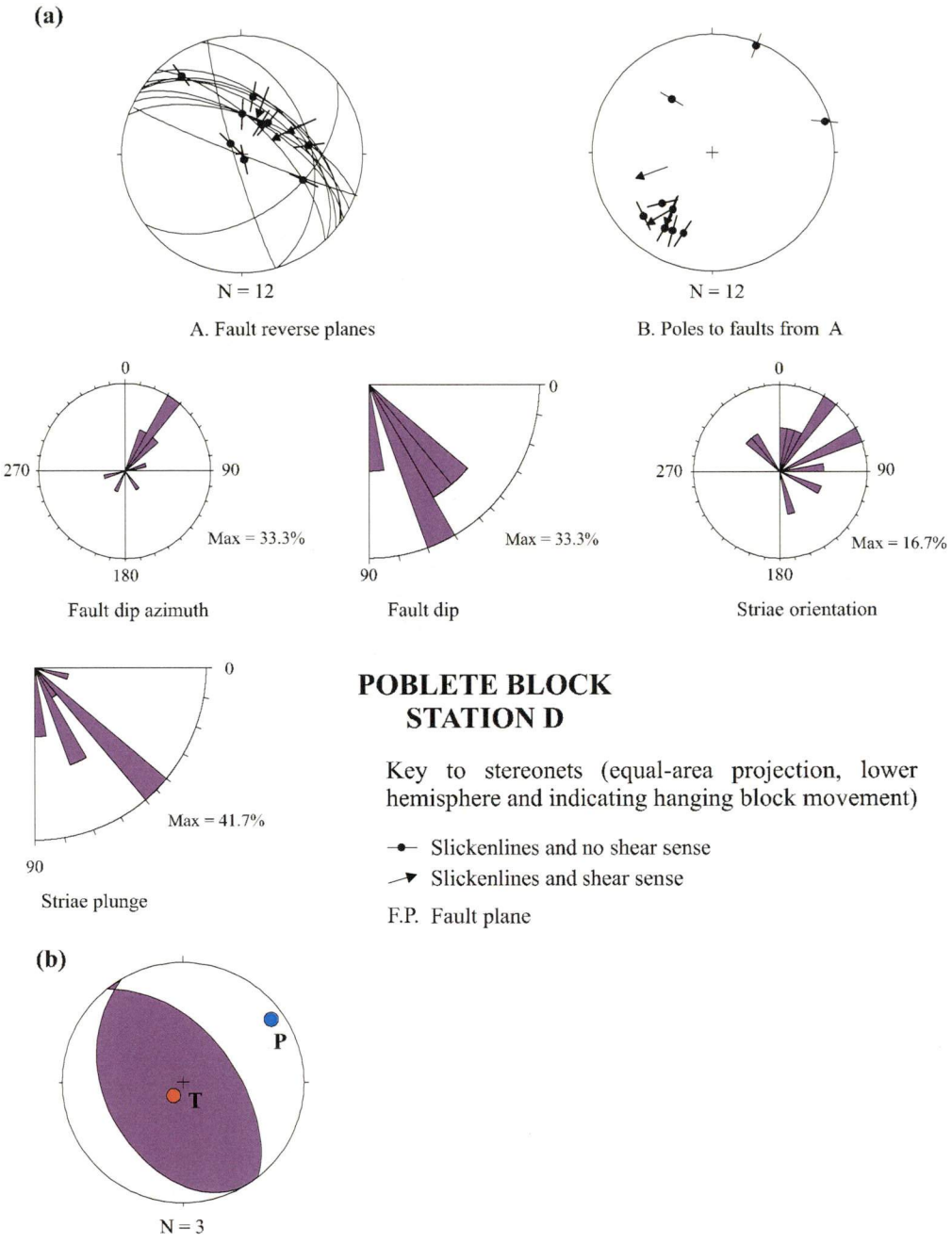

Figure 4.35 Graphic representations of fault-striae data for andesites of the Augusta Victoria Formation (late Paleocene-early Eocene). Structural data show dominant NE-oriented shortening.

The Escondida Norte-Zaldivar deposit is characterized by tabular quartz-monzonite bodies striking NNE-SSW, intruded at 39-37 Ma (Table 3.14). Porphyry-style sericitic alteration has been dated at 37-36 Ma (Pollard and Taylor, 2001; Table 3.14), whereas later advanced argillic associated with NNW-striking high sulfidation veins has been dated at 32 Ma (Pollard and Taylor, 2001; Chapter 5). Fault-striae measurements at Zaldivar pit by Padilla et al. (1997) suggest the following deformational history:

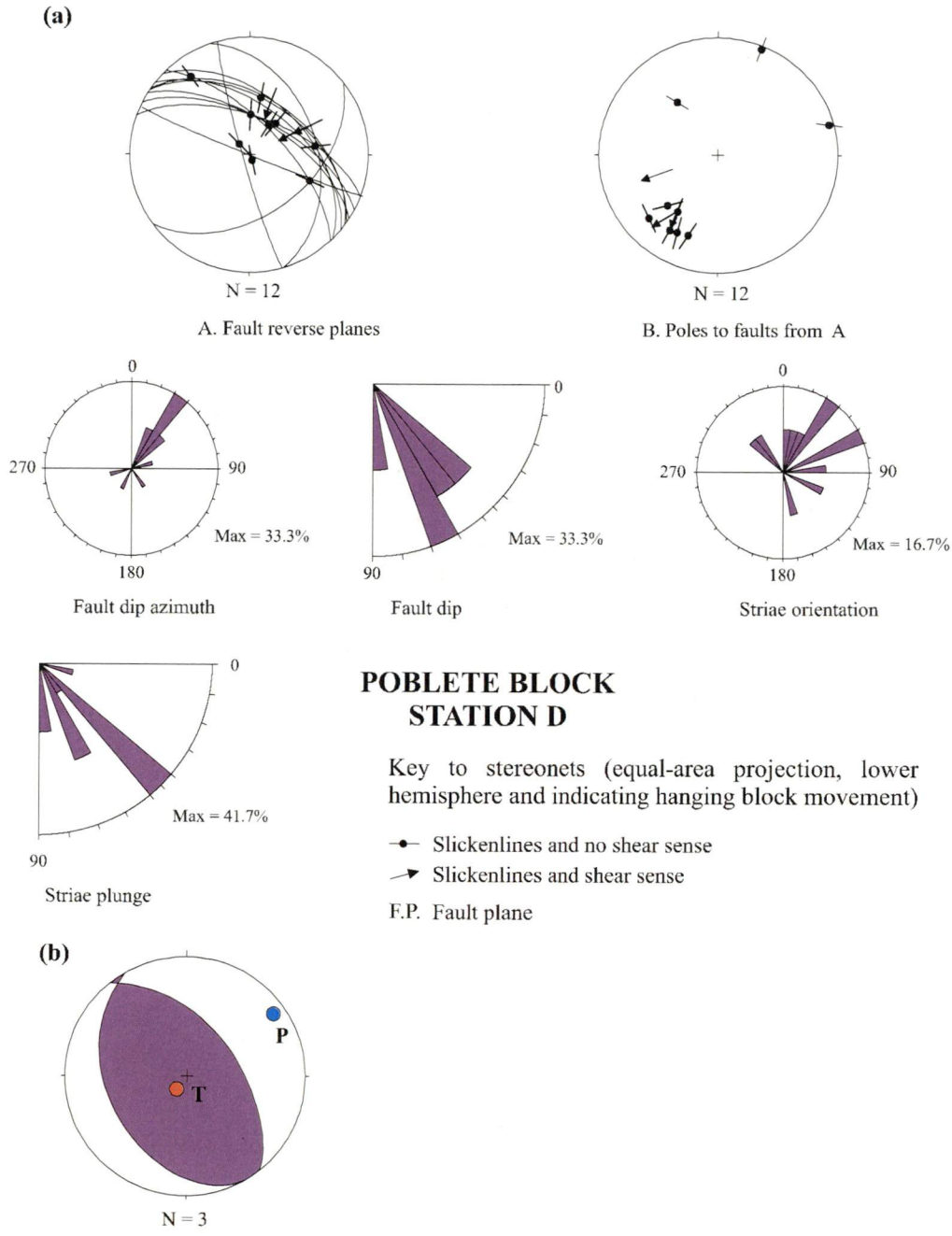

Figure 4.36 Graphic representations of fault-striae data for andesites of the Augusta Victoria Formation (late Paleocene-early Eocene). The structural data suggest dominant dextral and sinistral strike-slip movements preceded and followed by dip-slip movements. (a) Orientation and kinematics of faults; and (b) Striae data indicating at least three reactivations from dip-slip (1) to strike-slip (2) and dip-slip again (3).

- An early E-trending strike-slip fault, with sinistral and dextral movements.
- The N-striking Portezuelo (I) faults, which acted as principal sinistral Riedel shear surface.
- A NW-striking sinistral fault system, interpreted as synthetic R fractures with

Figure 4.37a Typical principal-stage dextral strike-slip fault developed in andesites of the Augusta Victoria Formation. Antofagasta-Salta railway. Structural station E (7,326,119m N; 492,161m E).

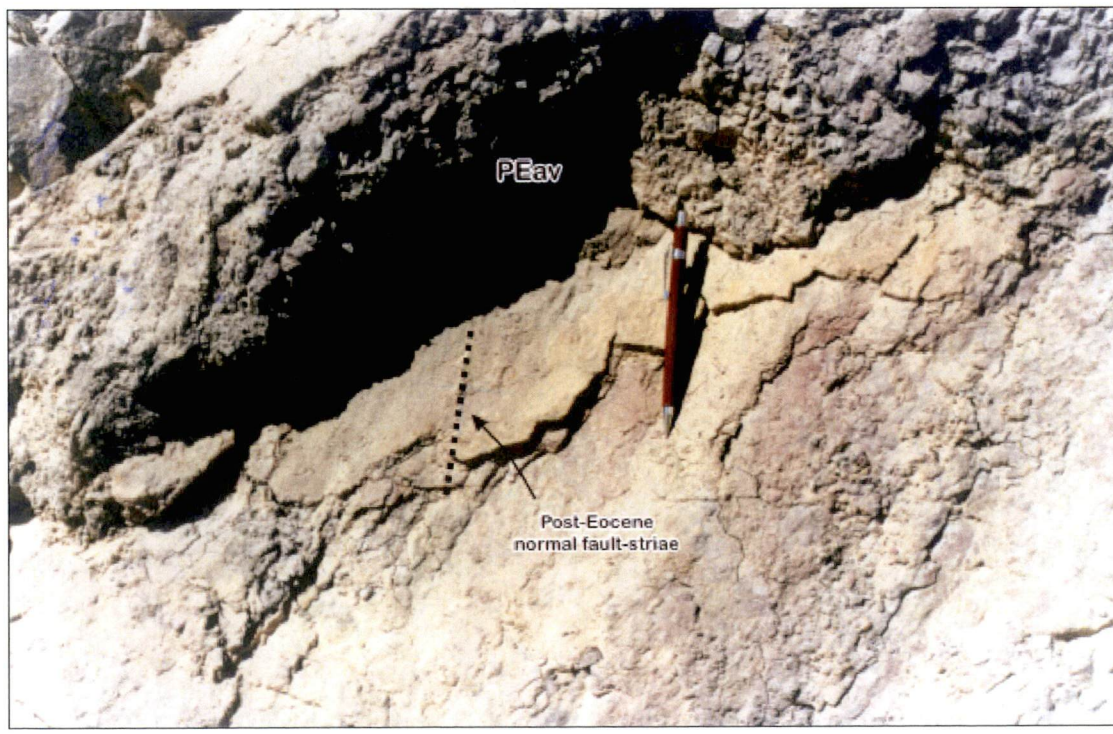

Figure 4.37b Young normal fault of post-Eocene age, with associated fault microbreccia and gouge. Antofagasta-Salta railway. Structural station C (7,326,362m N; 487,134m E).

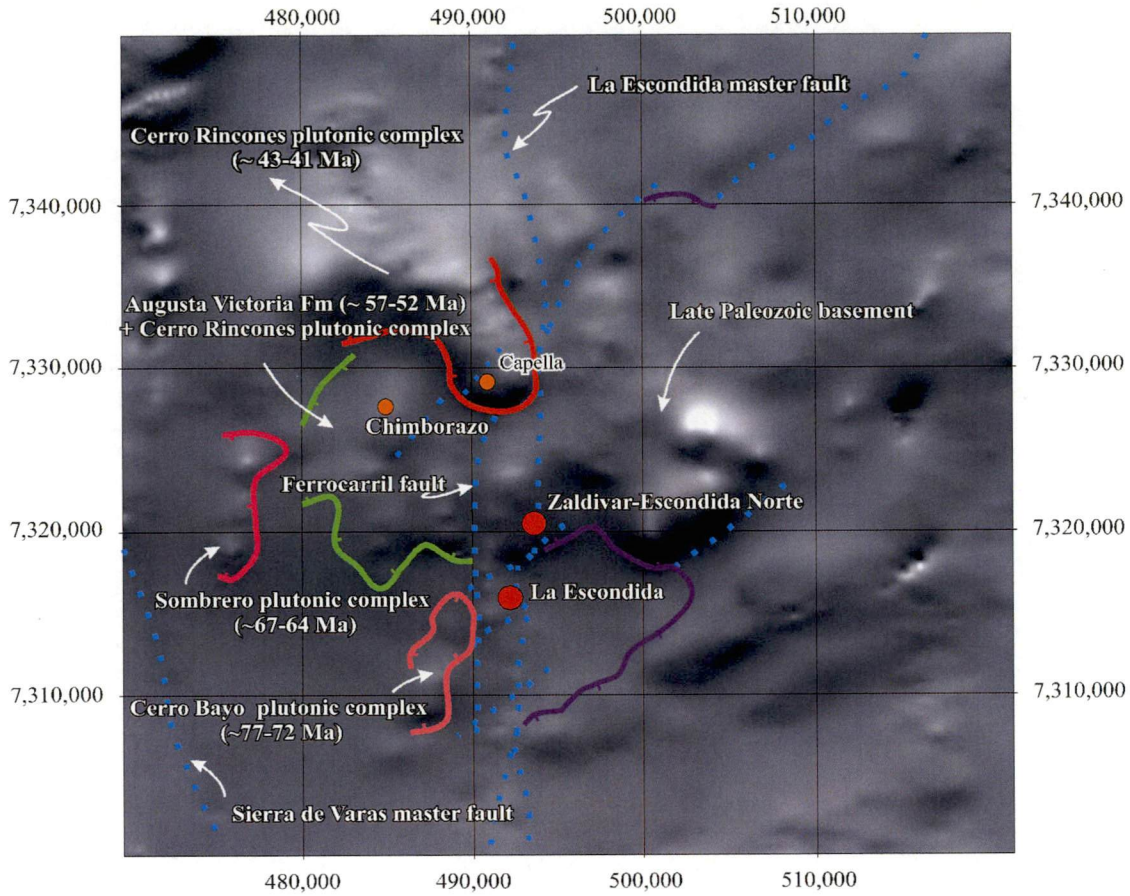

Figure 4.38 Regional total-field magnetic image of the Cordillera de Domeyko for La Escondida district, showing selected structural features of the study area.

respect to the Portezuelo (I) fault.

- A system of NNW- to NW-striking epithermal veins that have a tensional relationship to the Portezuelo (I) fault.
- A WNW-striking dextral strike-slip fault system which is interpreted as antithetic R' fractures that occur at high angles to the sinistral Portezuelo (I) fault.
- NE-striking dextral strike-slip faults that post-date the Portezuelo (I) fault.
- Normal faulting of post-Eocene age.

La Escondida porphyry clusters consist of a NW-trending intrusive complex (Véliz and Camacho, 2003). Local granodioritic phases have N- and NE-elongations (Quiroz, 2003). The reported intrusion ages for the Escondida pluton are similar to Escondida Norte-Zaldivar, ranging between 38-37 Ma (Richards et al., 2001; Table 3.14). In contrast, advanced argillic alteration related to NW-striking high-sulfidation veins is slightly older (ca. 35.6 Ma; Richards et al., 2001; Padilla-Garza, 2003) than the advanced argillic alteration at Escondida Norte-Zaldivar (ca. 32 Ma; Pollard and Taylor, 2001). NW-trending post-mineral dacitic-andesitic dykes have been dated at 36-35 Ma (Richards et al.,

1999; Richards et al., 2001; Tables 3.14). The fault-striae measurements of Vergara (2003) from La Escondida open pit suggest the following deformational history:

- Initial dextral displacements along major N-trending faults.
- Subsequent sinistral displacement due to reactivation of the N-striking faults.
- A third event of normal displacement on NW-striking conjugate normal faults of post-Eocene age.

Remarks. Several important implications result from integration of the available structural and geochronological information (Figure 4.29):

- The hypabyssal stocks of the Escondida Norte-Zaldivar deposit could have been emplaced under a local NNE-directed principal maximum stress regime around 39-37 Ma, based on crystallization ages (Pollard and Taylor, 2001; Table 3.14). At La Escondida, the intrusion ages are similar (Richards et al., 1999; Richards et al., 2001; Padilla-Garza, 2003; Table 3.14) but stress conditions remain unclear due to the poorly understood morphologies of the intrusions.
- An important change in the paleo-stress direction has been recognised at Escondida Norte-Zaldivar, after 37 Ma and before 34 Ma, based on the difference in orientation between tabular intrusives (ca. 39-37 Ma) and the high-sulfidation Cu-Fe-As veins (ca. 34 Ma). The veins have been interpreted as tensional fractures related to the N-striking Portezuelo (I) faults with sinistral movement (Padilla et al., 1996). This probably occurred after 35 Ma.
- Polymetallic Cu-Fe-As veins at La Escondida were emplaced in a stress regime with a principal maximum stress of NNW- to NW-orientation around 35 Ma (Chapter 5). The structural conditions before 35 Ma remain unclear.

4.7.7 Activation, Reactivation and Kinematics of Major Faults

4.7.7.1 Sierra de Varas Master Fault

This fault has been described by Marinovic et al. (1995), Niemeyer (1996) and Niemeyer et al. (2000a, 2004) in the Aguada de Varas sector, 25 km to south of La Escondida (Figure 4.2). Niemeyer et al. (2000a) proposed a Riedel geometry with a sinistral displacement of 15.4 km for the N-striking master fault, based on offset of Paleozoic plutons and kinematic indicators observed on secondary faults. A middle-late Eocene age was suggested for this sinistral movement. The Sierra de Varas fault experienced a dextral reactivation of unknown age and displacement (Niemeyer, 1996; Niemeyer et al., 2000a).

4.7.7.2 La Escondida Master Fault

The north-striking strands of La Escondida master fault, including the Panadero, Portezuelo I, Portezuelo II and Ferrocarril faults, dip steeply to the W or E, and have uplifted Late Paleozoic basement against the ca. 57-53 Ma Augusta Victoria Formation (Appendices 2B and 2C). The stratigraphic juxtaposition of older rocks on younger rocks is consistent with reverse faulting. Multiple strike-slip reactivations have obscured the early kinematic histories of the thrusting.

The kinematic data of Niemeyer (1996) from station XI is consistent with a NE-striking contractional stress regime (Figures 4.29 and 4.39). In contrast, at station X, Niemeyer's (1996) measurements indicate a sinistral sense of displacement for minor NNW-striking strike-slip faults spatially associated with the trace of the first-order structure (Figures 4.28). The interpreted movement history therefore involves: (1) an early reverse movement of the fault branches contemporaneously with Augusta Victoria folding; (2) fault reactivation with dextral strike-slip motions followed by a reactivation with sinistral movement; and (3) normal faulting of post-Eocene age.

4.7.8 Middle-Late Eocene San Carlos Strata and the Hamburgo Reverse Fault

The San Carlos strata (ca. 38-36 Ma; Table 3.13) are a volcaniclastic succession deposited synchronous with the intrusion of La Escondida and Escondida Norte-Zaldivar porphyry complexes (ca. 39-35 Ma; Table 3.14). The Paleozoic San Carlos basement block has been uplifted over the San Carlos strata by the oblique NE-striking Hamburgo reverse fault (Figure 3.35a), which dips to the SE (ca. 70°, as determined the 2006 drilling program). Therefore, the drilling results invalidated the previous interpretation given by Mpodozis et al. (1995a, 1995b) that the Hamburgo fault is a low-angle. In the foothills of the San Carlos Range, the Hamburgo Fault was the focus of minor high-sulfidation epithermal mineralisation during the Eocene (Chapter 5). The fault is a subsidiary branch of La Escondida fault, and is oriented oblique to the main N-trending strand (Figures 4.29 and 4.39). After 36 Ma, the principal motions of the Hamburgo fault were probably reverse within a contractional bend setting during the principal sinitral strike-slip motions of La Escondida master fault (Figure 4.39).

4.7.9 Cenozoic Paleomagnetic Rotation on Vertical Axes

Numerous paleomagnetic studies on the Late Cretaceous Quebrada Mala sequence and

Late Cretaceous-Paleocene Purilactic basin suggest that the structural panels have undergone rotation about vertical axes in a clockwise sense by up to 65°. Generally this rotation is estimated to be about 15°-20° for the blocks nearest to La Escondida region (Somoza and Tomlinson, 2002; Arriagada et al., 2000; Arriagada et al., 2003; Roperch, oral comm., 2002). These workers estimated an Eocene-early Oligocene age for much of the clockwise rotation associated with sinistral displacements in the Andean orogen, during the Incaic deformation. They conclude that some of the rotation could have occurred in the lowermost early Paleocene (K-T tectonic phase) or even the Late Cretaceous.

4.7.10 Age and Significance of Deformation

The first phase of the evolution of the Domeyko Fault System was characterized by folding and faulting of the 57-53 Ma Augusta Victoria Formation and thrusting of the Paleozoic blocks along high-angle reverse faults (i.e., La Escondida, Sierra de Varas; Figures 4.3 and 4.29). Compression was essentially E-W, with a local NE-SW shortening direction, based on the kinematic data. This older compressional regime most likely prevailed from 50 to 44-43 Ma. Some phases of the 43-41 Ma Cerro Rincones plutonic complex were preferentially intruded as sub-tabular bodies along the axial zones of the large scale folds developed in the Augusta Victoria sequence (Appendix 1A).

A dextral transpressional regime developed along the N-trending faults, which generated NNE- to NE-trending transfer faults that connected the diverse strands of La Escondida master faults. These transfer faults were the loci for emplacement for La Escondida Norte-Zaldivar and eventually La Escondida intrusions. In addition, the high sulfidation epithermal Cu-Fe-As veins of Chimborazo were emplaced under this regime some 10 km NW of Escondida Norte. The age of the dextral displacement along the N-trending faults is constrained to around 40-38 Ma, based on alteration age (Chapter 5).

A significant inversion to a sinistral sense of displacement is inferred to have occurred on La Escondida master fault at 35 Ma. This controlled: (1) the reverse movement of the Hamburgo Fault; (2) the emplacement of high sulfidation Cu-Fe-As veins at Escondida; and (3) the subsequent formation of the high sulfidation Cu-Fe-As veins at Escondida Norte. It is likely that the Sierra de Varas master fault also underwent reverse movement at this time. In general terms, this first phase of evolution of the Domeyko Fault System coincides with the schematic structural model proposed by Richards et al. (2001) in the development of a dextral sense of movement on La Escondida master fault and its

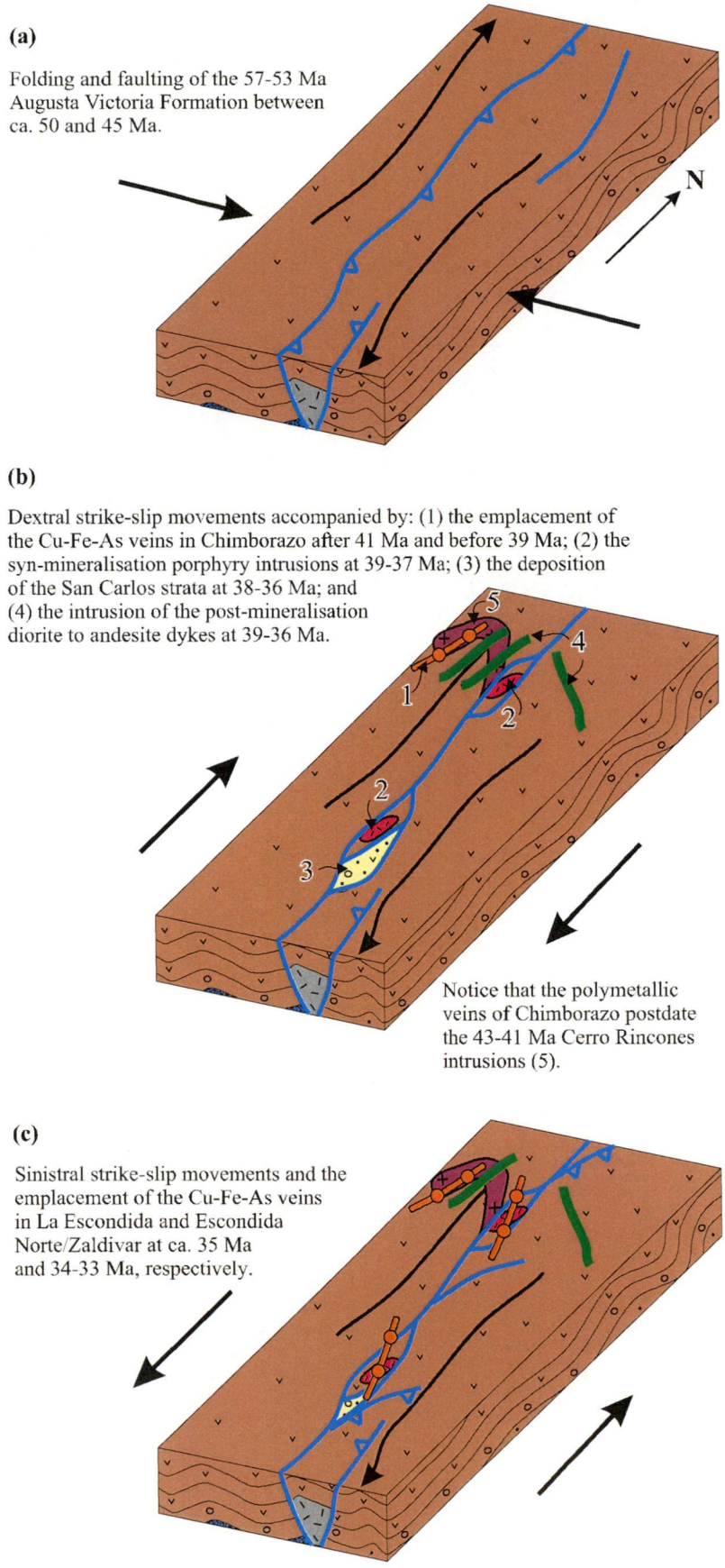

Figure 4.39 Schematic structural evolution of La Escondida district for the middle-late Eocene period (not at scale).

subsequent reversion to a sinistral sense of displacement. This model precludes role in deformation, as attributed by Richards et al. (2001), to the northwest-oriented Archibarca lineament (Salfity, 1985). Exhaustive mapping has been conducted along this hypothetical northwest-oriented structural corridor during the present study, encompassing the western border of the Salar de Punta Negra and Cerro Pascua (Figure 4.3). There is notable stratigraphic continuity of the rock units between the northeast and southwest domains that should be separated by the Archibarca lineament. The distribution of the Late Paleozoic La Tabla Formation and late Paleocene-early Eocene Augusta Victoria Formation, which are shown to have been displaced by northwest-elongated faults in the structural model presented by Richards et al. (2001), is in conflict with the district scale-geological mapping from the current study (Appendices 1A and B) and other more detailed studies completed in the Imilac block (Sepúlveda et al., 2006; this study). It is therefore concluded that the Archibarca lineament had no discernible effect on the distribution of the Late Paleozoic to Tertiary rock units in La Escondida district, as currently exposed. Therefore, its role in the location of La Escondida porphyry copper clusters is also debatable.

Regional studies have documented large-scale sinistral displacement of the Domeyko Fault System in two localities, SW of Punta Negra, and at Chuquicamata (Figure 4.2). These displacements are estimated to have occurred during the middle-late Eocene and early Oligocene-early Miocene, respectively. Offsets of 15.4 km and 35 km were inferred by Niemeyer et al. (2002a) and Tomlinson et al. (1997b) from these localities. Campbell et al. (2006) provided supporting data for the sinistral offset on the West fault at Chuquicamata. In contrast, no field evidence has been observed in La Escondida district for any displacement of comparable magnitude to those documented by these authors in the Punta Negra and Chuquicamata regions. Strike-slip deformation recognised in La Escondida has only caused displacements on individual faults of a few tens of metres, although the strike-slip faults are closely spaced and persistent areally. There is evidence for multiples reversals movements along strike of individual faults. Transfer, dissipation or attenuation of offset can occur towards the end of strike-slip faults and segmented rift systems, especially near tear or transfer zones between strands and/or segments (Rowland and Sibson, 2004; Mouslopoulou, 2006; Storti et al., 2008). This may explain the nature of the Domeyko Fault System in La Escondida district during part of the Eocene and Oligocene periods. The ore deposits may have formed at the terminus of strands of the

DFS, without the interaction of the northwest-oriented Archibarca lineament, in response to movements on localised northeast-oriented dextral strike-slip transfer faults.

Despite the abundant structural, geochronological, thermochronological (Section 4.9) and stratal architectural information available it remains difficult to constrain the age of the Eocene Incaic deformation phase in La Escondida district precisely. The history of the Eocene deformation is complex in the study area, and appears to have included several successive conpressional and strike-slip events punctuated by periods of relative tectonic quiescence since 50 Ma. The folding of the Augustà Formation occurred after 53 Ma and before the intrusion of the 43-41 Ma Cerro Rincones plutonic complex. This conpressional event is widely recognised in northern Chile. It produced a particular structural style (i.e., synform-antiform fold open limbs, large wavelength, short amplitude, absence of cleavage) on the late Paleocene-early Eocene volcanic successions equivalent to the Augusta Victoria Formation. It is unclear if this shortening was part of the Incaic tectonic phase which, in that case, should be considered a poly-phase tectonic deformation that extended between ca. 50 and 36 Ma. In La Escondida district, the 43-41 Ma Cerro Rincones plutons do not have field or microscopic evidence for deformation during their emplacement. Therefore a gap of ca 3 m.y. may have occurred during progression of the deformation event. The minimum age of deformation is provided by post-mineralisation dykes (the 38-36 Ma greenish grey to pale grey andesite porphyry - *LEap*) and a small 36.5 ± 0.5 Ma greyish red pyroxene andesite porphyry (*LEpap*). *LEap* occurs as consistently NE and WNW-oriented dykes with intense micro-crystalline deformation. The style contrasts with the undeformed sub-circular body of *LEpap* (Appendices 1A and B; compare Figures 3.39a and b). It suggests that the Incaic phase ceased prior to the emplacement of *LEpap*, but during and/or slightly after *LEap*. This interpretation is inconsistent with a previous thermochronological study in Chuquicamata (McInnes et al., 1999) and new data obtained in La Escondida (Section 4.8), which suggest the deformation continued up to 20 Ma. The results of the present study suggest that the Incaic tectonic phase occurred between 50 Ma (post-Augusta Victoria volcanic event) and 36-35 Ma (pre-greyish red pyroxene andesite porphyry intrusion).

4.8 LATE CENOZOIC DEFORMATION: The 18-10 Ma Quechua Compressive Tectonic Phase and Later Events

During the Late Cenozoic, compressive tectonic activity migrated eastwards (Mpodozis et

al., 2005). A thin-skinned fold and thrust belt developed within a post-Miocene back-arc setting in northwestern Argentina, whereas the Domeyko Cordillera now occupied a fore-arc setting and experienced extensional activity (Somoza and Tomlinson, 2002; Muñoz et al., 2005). The timing of the Quechua compressive phase has been constrained to 18-10 Ma, based on Late Cenozoic filling of the Salar de Atacama basin (Mpodozis et al., 2005); and to 12-10 Ma on the Calama basin stratigraphy (May et al., 2005). Local effects of this regional event have not been documented in La Escondida district.

Pliocene-Holocene reactivation of the Mesozoic and Tertiary faults produced scarps in the late Oligocene-middle Miocene Pampa Mulas Formation and Recent alluvium. This reactivation seems to have been mainly extensional, with net-slip of 20 m in the southern extension of the Sierra de Varas master fault (Niemeyer et al., 2002). The Recent alluvial deposits provide evidence of normal reactivation of regional faults on the order of 0.5-2 m. Drill holes in the Escondida sector determined normal displacement of the gravels on the order of 20-40 m (Appendix 2C).

Isopach modeling of the Late Cenozoic sediments, the Pampa Mulas Formation and the Holocene gravels of the Hamburgo Salar basin has been completed using the subsurface drill hole information of the unconsolidated overburden (Figure 4.40). The contouring of gravels from about 1,500 holes indicates:

- The thicknest gravels (> 300 m) are concentrated in those holes located against the Hamburgo fault. This information is consistent with a post-early Oligocene normal movement on this fault. A series of NNE- to NE lineaments seem to have controlled the gravel thicknesses locally.
- A SW and NNE- to NW network of paleo-streams in the pre-Pampa Mulas basement implies a SW paleo-slope and a series of blocks tilted by the NNE- to NE-striking faults. The land surface changed to the NE, along the western half ofthe Hamburgo basin.
- When the pre-Pampa Mulas Formation basement is compared with the most recent Holocene streams, it is inferred that the SW slope of the Hamburgo basin probably formed in a sinistral releasing bend developed by transtensional activation of La Escondida master fault after the early Oligocene, and probably during the early Miocene.
- Displacements of modern alluvial fans suggest dextral inversions of the strike-slip

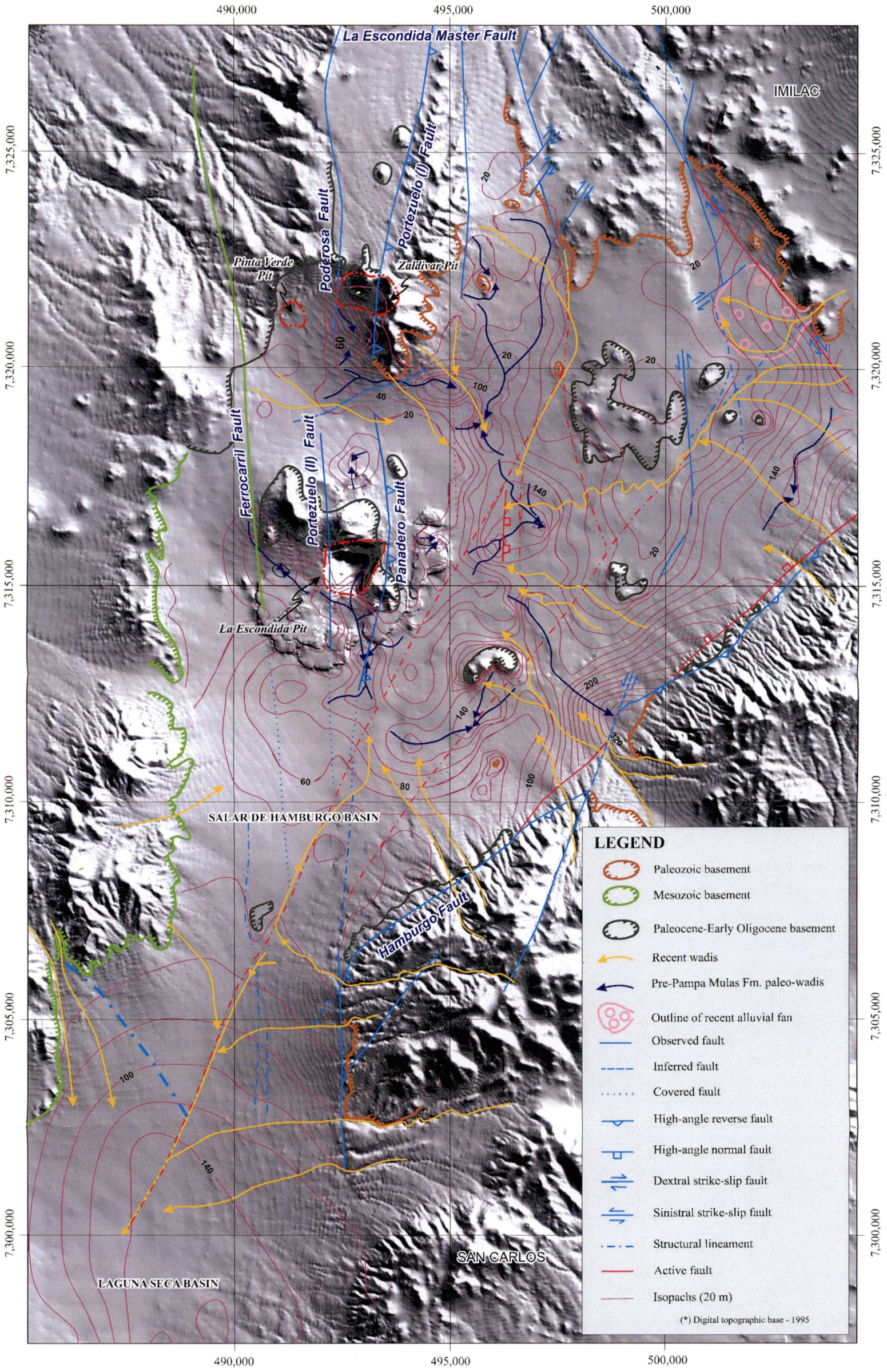

Figure 4.40 Isopach map of the Pampa Mulas Formation gravels (late Oligocene-middle Eocene) and Recent alluvial-evaporitic sediments (Pliocene-Holocene) of the Salar de Hamburgo basin (*), in La Escondida district. Isopachs based on data of sedimentary cover thickness from about 1,500 drill holes.

faults that bound the north-eastern border of the Salar de Hamburgo basin, which were controlled by the releasing bend in the Escondida master fault. The apparent strike-slip displacements are a few tens of meters.

Remarks. La Escondida region experienced significant extension and sinistral transtension from the late Oligocene through the early Miocene. During this period, La Escondida master fault generated the triangular basin of the Salar de Hamburgo, which was probably dissected by NNE-striking short-cut faults. The basin consisted of southeast-tilted fault blocks that formed a series of relatively flat bottomed half-grabens of roughly NNE- to NE-elongation. Displacement of alluvial plains and alluvial fans records activity of Recent normal and strike-slip faults as well as reactivation of older faults (Figure 4.39).

4.9 EXHUMATION

During the past fifteen years, there has been considerable multidisciplinary effort to understand the Neogene climatic evolution of the Atacama Desert and the uplift of the Altiplano-Puna plateau (Adriessen and Reutter, 1994; Jordan et al., 1997; Tomlinson et al., 2001b; Hartley, 2003; Yang and Liu, 2003; Victor et al., 2004; Haschke et al., 2005; Schildgen et al., 2006). Among the techniques employed, the thermal history of the late Eocene-early Oligocene porphyry Cu-type intrusions has been assessed by thermochronological studies of zircon fission track and low-temperature (U-Th)/He zircon and apatite dating a few deposits (Chuquicamata and El Savador; Maksaev, 1990; McInnes et al., 1999; Maksaev and Zentilli, 1999).

New (U-Th)/He zircon (ZHe) and apatite (AHe) thermochronologic data for five Late Cretaceous-Eocene intrusions and one volcanic unit from La Escondida district are presented in Table 4.1 and Figure 4.41. There is a significant limitation on the reliability of this group of ages, because no analytical details have been provided by the CSIRO thermochronological laboratory (Perth, Australia) who conducted the analysis, despite numerous requests. This prevents any detailed analysis of the data quality. The data provided here for sake of completeness, but the reader is advised to treat the results with caution, since the quality of the analyses cannot be verified.

Sampling was not specifically designed for a U-Pb-He triple-dating study, and this reduced

the number of successful ages considerably (McInnes, written comm., 2003). There are inconsistencies between some ages and the host rock ages determined by U-Pb zircon analysis (Chapter 3; Appendix 6). The 42.5 ± 1.3 Ma and 41.3 ± 1.2 Ma (U-Th)-He zircon ages for the greenish grey to pale grey andesite porphyry (ESC-9) are slightly older than and do not overlap with the 38.1 ± 0.6 Ma U-Pb crystallisation age for this unit. The Cerro Rincones plutonic complex (ESC-25) yield a 34.9 ± 1.2 Ma (U-Th)/He apatite age determination which is older than the 30.5 ± 1.2 Ma (U-Th)-He zircon age. This type of discrepancy has been interpreted in other studies as result of He retentivity increases in apatite, which can lead to anomalously old AHe ages (Farley, 2000; Flowers et al., 2006a; Rainers and Brandon, 2006; Shuster et al., 2006) or thermal resetting of the ZHe ages. Unfortunately, no analytical data have been provided by CSIRO to evaluate these possibilities for sample ESC-25. Thermal resetting of the 30.5 ± 1.2 Ma ZHe age is estimated to have been more likely considering their clustering along with another anomalously young ZHe age discussed in next section (samples ESC-38; Table 4.1), and the large hydrothermal activity focused in La Escondida district between 35 and 30 Ma (Chapter 5).

Resetting of ZHe ages by later thermal event seems to have been significant for the tuffaceous sample (ESC-38) obtained 20 m above from the base of the Augusta Victoria Formation (McInnes, written comm., 2003). Crystallisation ages of 57-53 Ma for these volcanic rocks are substantial older than the 33.6 ± 1.0 (U-Th)/He obtained for a tuff. Considering that magmatism ceased in the region with the andesite porphyry dykes around 38-36 Ma (Chapter 3), the probable origin for this anomalously younger ZHe age could be hydrothermal activity associated with the Pinta Verde Cu system, which was active from 37 to 33 Ma (Chapter 5). The distance between sample ESC-25 and the Pinta Verde porphyry is less than 2 km (Figure 4.41; Appendix 1B).

The remaining U-Pb zircon and (U-Th)-He zircon and apatite cooling ages have been plotted against their respective closure temperatures (Figure 4.42a) and elevation (Figure 4.42b). Analysis of these plots suggests La Escondida district has experienced a complex history of regional exhumation (*sensu* Molnar and England, 1990) history since the Late Cretaceous. This means that additional detailed sampling transects for (U-Th)-He dating is evidently required to fully research the history of exhumation for La Escondida district. The intrusive rocks do not share a common unroofing history. It is more likely that they were exhumed independently within their respective structural domain/panel.

Table 4.1 Single-grain (U-Th)/He zircon and apatite radiometric age determinations for selected samples of post-Paleozoic intrusive and volcanic units from LaEscondida district.

Sample	Rock/Sub-Unit	Structural block	Material	Age & Error (Ma, 2 σ)	Source Data (*)
Cerro Bayo plutonic complex *(LKcb)*					
ESC-12	Quartz monzonite /*LKcb6*	**Bayo**	Zircon	Failed	
	(exposed section: 3 x 1.3 km)		Apatite	60.3 ± 1.4	1
Sombrero plutonic complex *(EPcs)*					
ESC-17	Granodiorite/*TPsb6*	**Sombrero**	Zircon	53.2 ± 1.5	1
ESC-17	(exposed section: 1.5 x 0.4 km)		Apatite	19.1 ± 1.3	1
Medium-grained amphibole-phyric andesite dyke *(Pan)*					
ESC-21	Amphibole andesite	**Bayo**	Zircon	51.6 ± 1.5	1
ESC-21	(exposed section: 3 x 0.3 km)		Apatite	32.3 ± 1.4	1
Augusta Victoria Formation *(PEav)*		**Oxidos**			
ESC39	Vitric tuff		Zircon	33.6 ± 1.0 (†)	1
ESC39	(few metres above the base, less than 20 m)		Apatite	34.4 ± 2.0	1
				30.3 ± 4.5	1
Cerro Rincones plutonic complex (Eocr)					
ESC-25	Quartz monzodiorite /*Eocr9*	**Garita**	Zircon	30.5 ± 1.2 (†)	1
ESC-25	(exposed section: 0.4 x 0.4 km)		Apatite	34.9 ± 1.2	1
Greenish grey to pale grey andesite porphyry *(LEap)*					
ESC-9	Biotite-amphibole	**Poblete**	Zircon	42.5 ± 1.3 (¤)	1
	andesite porphyry			41.3 ± 1.2 (¤)	1
ESC-9	(exposed section: 80 x 30 m)		Apatite	25.3 ± 1.4	1

(*) Source of data: (1) this study. ¤ = too old; † = thermal resetting. No analytical details have been provided.

Although the data are scarce, no clear slope or trend is apparent for the AHe ages (some of them projected) on the E-W transect plotted in Figure 4.43. This implies that some of the principal N- to NNE-trending faults should have tilted and uplifted discrete structural panels, giving a differential exhumation and cooling history. The youngest AHe age (ca. 20 Ma) is given by the Late Cretaceous (ca. 67-64 Ma) Sombrero plutonic complex, located at the western end of the E-W transect and at a lower elevation than other samples (compare Figures 4.42b and 4.43). This suggests that apatites reached the partial retention zone (PRZ, *sensu* Reiners and Brandon, 2006) ca. 6-7 m.y. later than the Eocene rocks, implying that a deeper crustal level has been exposed along the wester part of the district. To the east, in contrast, the structurally higher rock samples cooled earlier,probably due to higher denudation rates associated with activation of some of the major faults (i.e., Perito, Ferrocarril and La Escondida; Appendices 1A and B; Figure 4.41).

A simple age-elevation relationship (AER, Reiners and Brandon, 2006) for the AHe ages suggests an eroded column of rocks of ca. 580-600 m between ca. 35 and 19 Ma, giving an

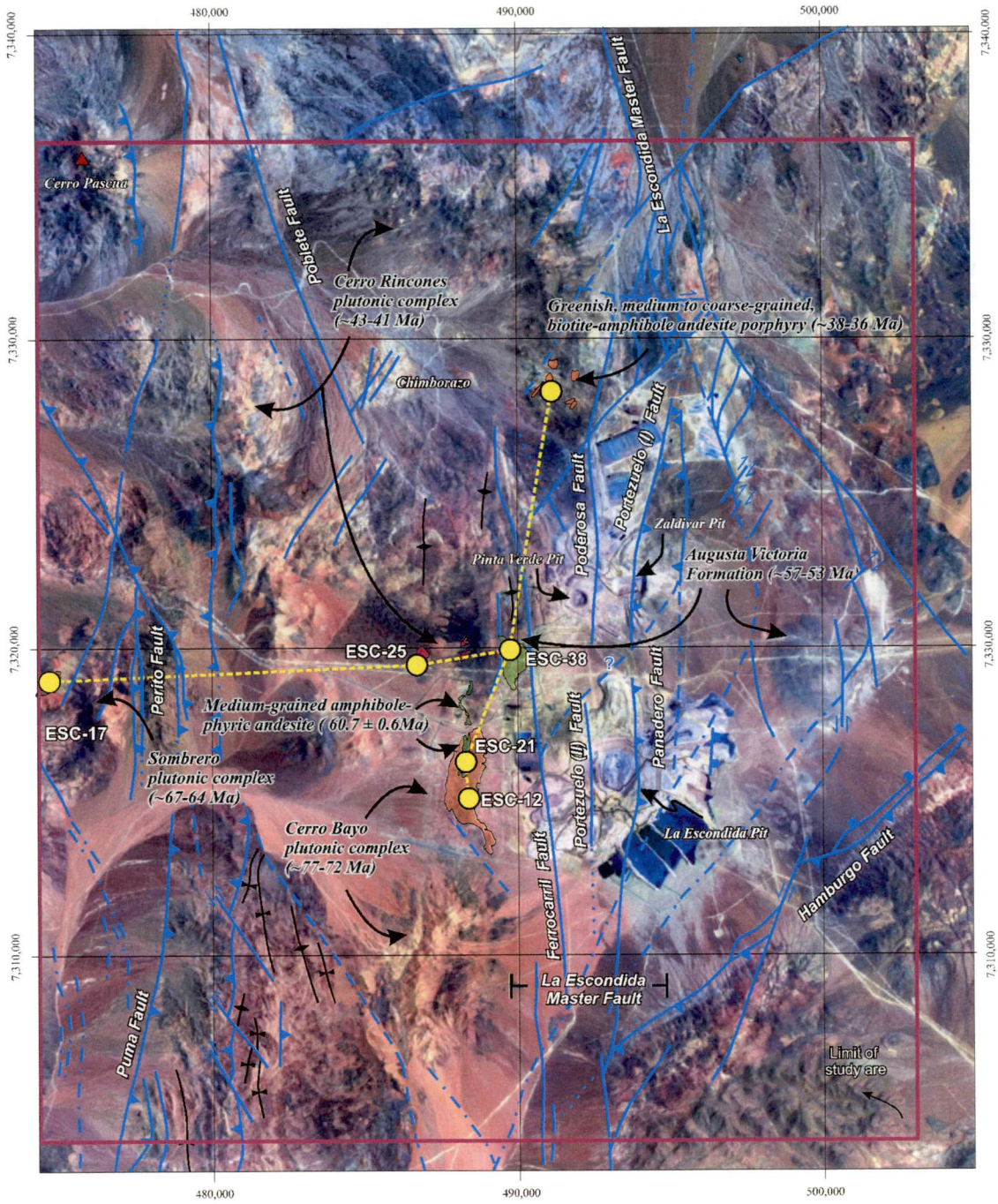

Figure 4.41 Location of low-temperature (U-Th)/He zircon and apatite geochronology for selected samples of Late Cretaceous-Eocene igneous units in La Escondida district. Notice the proximity between the sample ESC-38 and Pinta Verde pit.

erosion rate of 0.03 km/m.y. (Figure 4.42b). This type of analysis is based on an assumption that the erosion rates were the same for all samples involved in the AER slope, and that there was a flat closure isotherm at the time of closure (Reiners and Brandon, 2006). The first assumption is not supported by the E-W transect data (Figure 4.43) that suggest diachronic tectonic uplifting of structural blocks. Similarly, a flat closure isotherm is highly improbable given the multiple intrusive events and probably complex

cooling history experienced by the region since approximately 40 Ma. A more refined treatment of the AHe ages following the approach of Reiners and Brandon (2006) and using the computer program AGE2EDOT of Brandon (2007) predicts an eroded column (z) of ca. 1.4 km and 2.1 km for geothermal gradients of 30°C/km and 20°C/km, respectively. These results are based on an average cooling age (τ_m) of ca. 27 Ma at present local mean elevation of 2,900 m (Figure 4.42b). Using typical geothermal parameters applied by Schildgen et al. (2007) in the Peruvian Central Andes (i.e., thermal diffusivity: 30 km^2/my; internal heat production: 8°C/km; surface temperature: 10°C), and a crustal thickness of 50 km, the calculated average exhumation rate for La Escondida district since 27 Ma is about 0.05 km/m.y. and 0.08-0.07 km/m.y., for geothermal gradients of 30°C/km and 20°C/km respectively.

The AHe ages for La Escondida district are similar to those reported by McInnes et al. (1999) for Chuquicamata, where an age range of ca. 34-17 Ma was determined. They are supported by the fission track analyses of Maksaev and Zentilli (1999) from Chuquicamata and El Salvador, which suggest low rates of exhumation of ca. 0.05 km/m.y. for the orogen since 30 Ma. These authors proposed that major uplifting of the Domeyko Cordillera occurred between ca. 50 and 30 Ma, during the Incaic tectonic phase.

The new (U-Th)/He zircon age determinations obtained during the present study in La Escondida district suggest less lower cooling rates between ca. 72 and 50 Ma (Figure 4.42a). These data are compatible with a $^{40}Ar/^{39}Ar$ amphibole age determination for Cerro Bayo plutonic complex (Figure 4.42b). Unfortunately younger ZHe ages from the Augusta Victoria Formation have been thermally reset and the cooling history between ca. 50 and 35 Ma cannot be appropriately constrained with the available ages. AGE2EDOT calculations for data obtained from a medium-grained amphibole-phyric andesite dyke *(Pan)* sample (ESC-21), with an individual-grain (U-Th)/He zircon age of 53.2 ± 1.5 Ma, predicts depths on the order of 5 km and 8 km for 30°C and 20°C, respectively; with a closure temperature (τ_c) of about 172°C. These data suggest erosion rates of 0.1-0.2 km/m.y., assuming a crustal thickness of 30 km and other normal thermal parameters (thermal diffusivity: 30 km^2/my; internal heat production: 8°C/km; surface temperature: 10°C) given by Reiners and Brandon (2006).

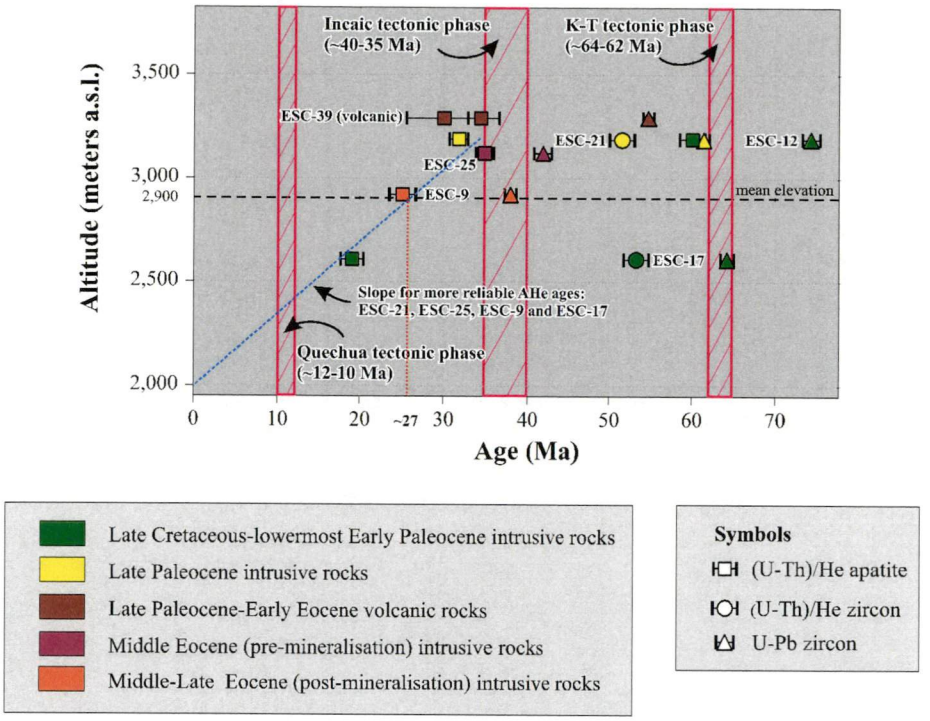

Figure 4.42a Distribution of single-grain (U-Th)/He zircon and apatite ages versus altitude for selected post-Paleozoic igneous units from La Escondida district. Each sample includes their respective crystallisation U-Pb zircon age (adapted from Reiners and Brandon, 2006).

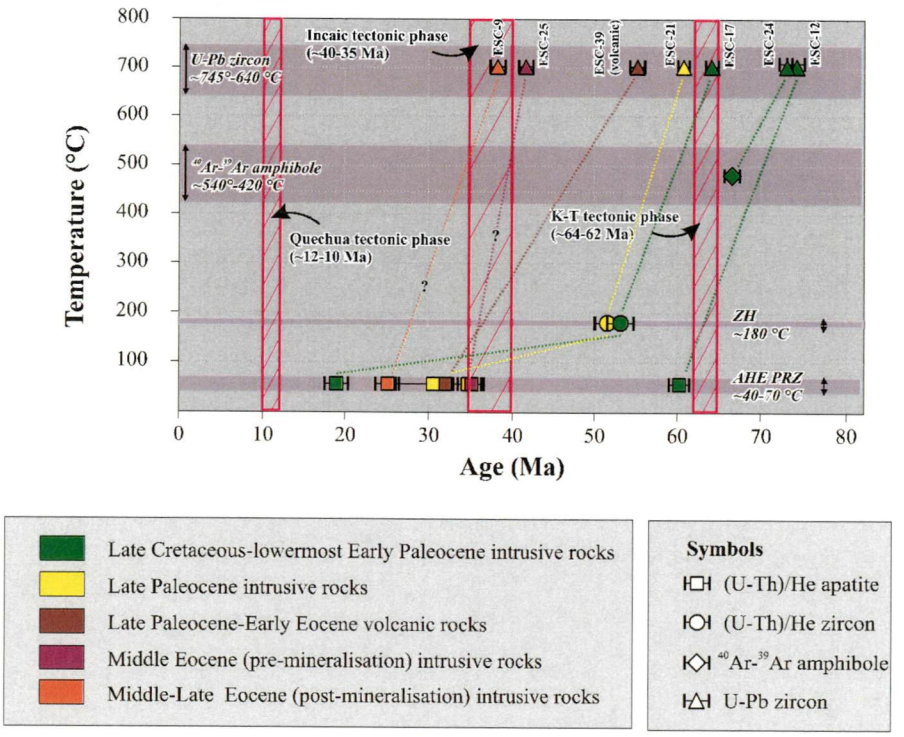

Figure 4.42b Distribution of single-grain (U-Th)/He zircon and apatite ages versus closure temperatures for selected post-Paleozoic igenous units from La Escondida district. Each sample includes their respective U-Pb zircon age. Some ^{40}Ar-^{39}Ar amphibole ages for from the same magmatic unit have been plotted for comparative purposes. Closure parameters and closure temperatures from Farley (2000), Reiners et al (2004), Rainers (2005) and Rainers and Brandon (2006). Abbreviation: PRZ = partial retention zone.

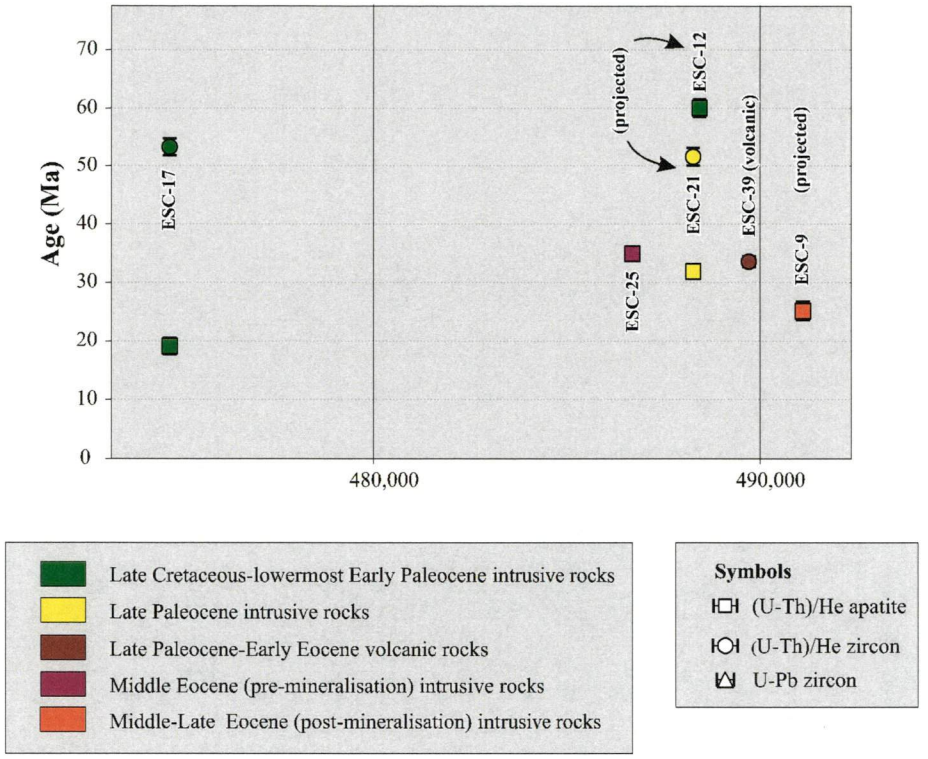

4.43 Distribution of single-grain (U-Th)/He zircon and apatite ages along a roughly E-W transect for selected post-Paleozoic intrusive and volcanic units from La Escondida district.

4.9 SUMMARY

The structural evolution of La Escondida district has been dynamic, with a complex history of multiple reactivations since the Triassic.

- Late Paleozoic-Early Triassic deformation produced minor folding of La Tabla Formation, along NW-striking fold axes.
- Late Triassic-Early Jurassic extension is recorded by local thickening of conglomerates of El Profeta Formation. Renewed tectonic activity during the Late Jurassic caused slumping of platform limestones.
- Positive tectonic inversion occurred by the lowermost Late Cretaceous, when a thick-skinned fold and thrust belt formed in the Mesozoic sedimentary units. Some Late Triassic-Early Jurassic extensional faults were reactivated as reverse faults during this tectonic inversion.
- A transtensional to extensional setting was dominant during the rest of the Cretaceous (ca. 74-64 Ma). NNE-trending bimodal intrusive complexes were emplaced during this period.
- An important but brief compressional to transpressional tectonic event (K-T tectonic phase) faulted and folded Mesozoic and older units in the region.

Evidence for this event is provided by the well-developed unconformity between the Augusta Victoria Formation and underlying Mesozoic sedimentary units. Radiometric constraints suggest a lowermost early Paleocene age (ca. 64-62 Ma).

- The first phase of the Eocene evolution of the Domeyko Fault System was characterized by folding of the late Paleocene-early Eocene Augusta Victoria Formation and high angle reverse faulting of the Paleozoic blocks along submeridian regional faults (i.e., La Escondida and Sierra de Varas). The age of this compressional regime is inferred to be between 50 Ma and 41 Ma. It was followed by a dextral transpressional regime that activated the principal N-striking faults. The Escondida Norte-Zaldivar porphyry system and the high sulfidation epithermal Cu-Fe veins of Chimborazo were emplaced along NNE- to NE-striking tensional fractures of this transpressive Riedel geometry. The age of dextral displacement along the N-striking master faults is constrained to 40-37 Ma. A significant reversion to sinistral movement is inferred to have occurred along La Escondida master fault after 36 Ma. This controlled the emplacement of high sulfidation Cu-Fe-As veins at La Escondida and subsequently at Escondida Norte-Zaldivar ore bodies. It is highly likely that reverse movements also occurred on the Sierra de Varas master fault.
- La Escondida region experienced significant extension and sinistral transtension from the late Oligocene to the early Miocene. Movements on La Escondida master fault produced the triangular pull-apart basin of the Salar de Hamburgo. Dissection of the Hamburgo basin during the early Miocene was caused by NNE-striking faults.
- Successive normal and minor dextral strike-slip faulting and reactivation of some of the more significant faults that bound the Hamburgo basin are recorded by minor displacement of the Recent alluvial plains and alluvial fans, respectively.
- The protracted history of the Domeyko Fault System in the study area fits relatively well with the kinematic evolution inferred from other segments of the Domeyko Fault System at Quebrada Blanca-Chuquicamata (Tomlinson and Blanco, 1993a), Sierra Exploradora and El Salvador-Potrerillos (Niemeyer, 1996), for the period encompassing the middle Eocene to the early Oligocene. However, the structural evolution of La Escondida district since the middle Oligocene is not consistent with the tens of kilometres of sinistral motion inferred for other regions such as Chuquicamata (Tomlinson and Blanco, 1993b) and Sierra de Varas (Niemeyer et al.,

2000b). This suggests a partitioned or compartmented history of the Domeyko Faults System along their diverse segments and significant attenuation of strike-slip offset focused on tear or transfer zones and the ends of N-S-striking strands.

- New (U-Th)/He apatite age determinations for Late Cretaceous-Eocene intrusive units suggest comparatively low exhumation rates (> 0.05 km/m.y.) after 33-32 Ma; whereas more rapid cooling and unroofing rates (0.1-0.2 km/m.y.) are documented by (U-Th)/He zircon and ^{40}Ar-^{39}Ar hornblende ages for the Late Cretaceous and early Paleocene intrusions between ca 72 Ma and 50 Ma.. No data are available to constrain exhumation rates between 50 Ma and 35 Ma.

CHAPTER 5
Hydrothermal Systems of La Escondida District

This chapter describes the major hydrothermal alteration and mineralization zones of La Escondida district and surrounding sectors (Figure 5.1; Appendices 3A and B). The hydrothermal systems are discussed within the context of regional metallogenic events and, in particular, with respect to the geological units with which they are thought to be associated. Emphasis is placed on the ages of hydrothermal alteration and mineralisation, in order to help constrain the metallogeny of the district. Descriptions are based on public geological information, confidential reports of several mining and exploration companies, field mapping results from the current study, as well as the personal exploration experience of the author in this part of the Domeyko Cordillera.

It is important to note that these alteration zones represent targets that have been intensely explored and drilled over at least two decades. The key exploration tools have been two models: (1) the lithocap model for the top of porphyry copper deposits (Sillitoe and Gappe, 1984; Sillitoe, 1985; Sillitoe, 1995; Corbett and Leach, 1998); and (2) the precious metal-rich high sulfidation epithermal system (Hedenquist, 1987; White and Hedenquist, 1990; White, 1991). The term lithocap was coined by Sillitoe (1995) to described *"topographically prominent zones of advanced argillic and argillic alteration that are located between the subvolcanic intrusive and the paleosurface, where they commonly constitute the upper part of a porphyry copper system"*.

Geochronology is used in this chapter to help correlate mineralisation events with the geological units of La Escondida district. Details of the new U-Pb, K-Ar and ^{40}Ar-^{39}Ar analyses are provided in Appendix 5. UTM coordinates of rock samples are presented in Appendix 4.

5.1 LATE PALEOZOIC-TRIASSIC

Late Paleozoic-Triassic copper mineralisation and hydrothermal alteration assemblages in La Escondida district can be broadly grouped into four types: (1) volcanic-hosted Cu mineralisation; (2) epithermal veins and associated porphyry Cu mineralisation; (3)

porphyry Cu associated with tourmaline-quartz-cemented hydrothermal breccia; and 4) greisens, pegmatites and associated massive quartz-veins. Most of these mineralised occurrences are hosted by La Tabla Formation within the Imilac and San Carlos structural blocks (Figure 5.1), along the eastern portion of the district.

5.1.1 Volcanic-hosted Cu Mineralisation

During the current mapping program, Cu silicates and oxides (chrysocolla and cuprite, respectively), native copper and hematite have been observed locally as amygdule-fill, disseminations and impregnations within basic to intermediate lava flows of the central volcano-sedimentary sub-unit *(Pzlt-b)* at La Tabla Formation. Rare centimetre-thick quartz veins with Cu-oxide coating have recognized in the volcanic rocks. Several prospects of this mineralisation style, including Chinchilla (Peri and Palma, 1997), Isabel east and Isabel west (Matthews et al., 2004; Sepulveda, 2006), have been identified to the south and east of the study area (Figure 5.1). The volcanic rocks have undergone moderate intensity alteration to chlorite, magnetite and montmorillonite, with minor albite and zeolites (Peri and Palma, 1997; Sepulveda, 2006). A 147 Ma K-Ar (whole rock) age has been reported by Peri and Palma (1997) for the host rocks from Chinchilla. This volcanic-hosted Cu mineralisation is comparable to Michigan-type native copper deposits (Brown, 1992; R. Sillitoe, oral comm., 2006).

5.1.2 Epithermal Veins and Associated Porphyry Cu Mineralisation

Relatively broad advanced argillic hydrothermal alteration zones (>1 km^2) occur in volcanic rocks of the central volcano-sedimentary sub-unit (Pzlt-b) of La Tabla Formation. These are characterised by marked colour anomalies and the common occurrence of vuggy quartz ledges. There is a strong stratigraphic control, with alteration best developed within the more permeable volcaniclastic horizons (i.e., San Pablo prospect; Figure 5.2a). In contrast, a structural control is evident at the Isabel del Carmen prospect (Figure 5.1), where the host rocks are strongly altered to quartz-alunite-kaolinite-pyrophyllite-barite-jarosite (Figure 5.2b). Minor scorodite- and pyrite-bearing vuggy quartz ledges occur at San Pablo (Urzúa, 2005a), Chimalén (Sepúlveda, 2005; Figures 5.3a and b), Isabel del Carmen (Matthews 2004; Urzúa 2005b) and Elita (Palma, 1993). Siliceous multi-stage hydrothermal breccias have been described at Tambo (Matthews et al., 2004) and Isabel del Carmen (Matthews 2004, Urzúa 2005b). The advanced argillic lithocaps at Isabel del Carmen and Chimalén have been linked to blind, pyrite-bearing porphyritic dacite intrusions by drilling (La Escondida brownfields

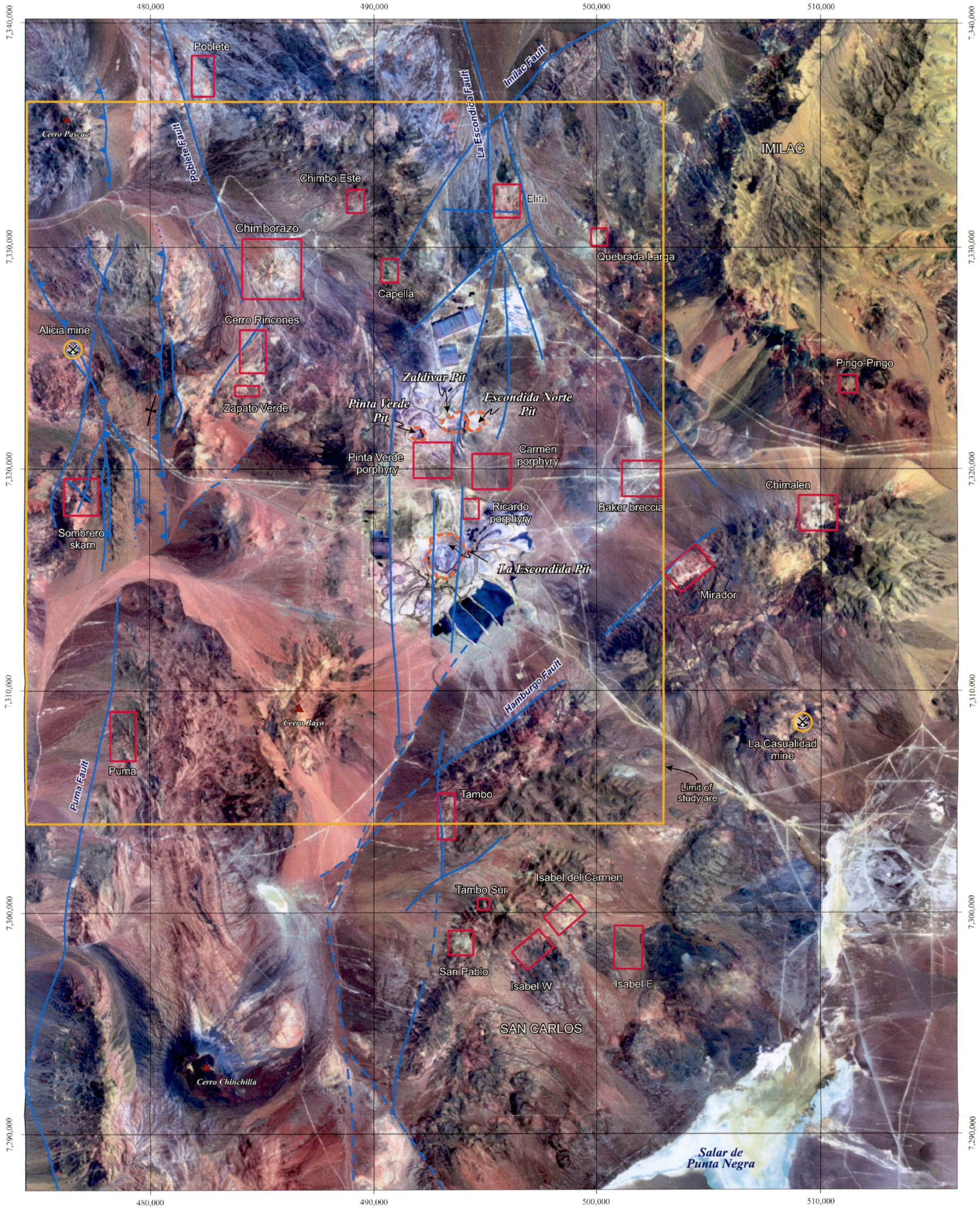

Figure 5.1 Selected locations of the hydrothermal alteration systems and mineral occurrences in La Escondida district.

exploration program, 2003-2007; Sepúlveda, 2006), with traces of secondary chalcocite. Petrographic and spectral analyses of drill core have identified that quartz-illite-kaolinite-montmorillonite is the dominant alteration assemblage. Relict secondary biotite and K-feldspar have been also recognised microscopically.

Rare low-sulfidation style pyrite-chalcopyrite-bearing quartz-barite-calcite-veins have been recognised recently in the Imilac block (Pingo-Pingo prospect; Figure 5.1). They are hosted by cross-bedded conglomerates and conglomeratic sandstones that have been intensely altered to pyrophyllite and subordinate alunite (Figure 5.4a). No porphyry-type intrusion has been identified in this area.

5.1.2.1 Geochronology

Consistent K-Ar (whole rock) ages of 280 ± 9 Ma and 281 ± 9 Ma for quartz-sericite altered pyroclastic rocks from La Tabla sequence have been obtained from Isabel del Carmen (RC-3617) and Chimalén (RC-3627) prospects respectively (La Escondida brownfields exploration program, 2003-2007; Table 5.1; Figure 5.5). They agree, within uncertainty, with the Late Paleozoic (ca. 283-281 Ma) porphyry-style alteration and mineralisation events documented from other parts of the Domeyko Cordillera (i.e., Cornejo et al., 2006; and references therein; Figure 5.5).

A quartz-sericite altered groundmass from pyroclastic rocks at the Tambo Sur prospect has provided a younger K-Ar whole rock age of 267 ± 8 Ma (La Escondida brownfields exploration program, 2003-2007; Table 5.1; Figure 5.5). Another unnamed, small quartz-sericite alteration zone linked to a feldspar-phyric intrusion located a few kilometres east of Escondida Norte has been dated during the present study at 216 ± 7 Ma (K-Ar whole rock age; Table 5.1; Figure 5.5; Appendix 5). U-Pb zircon dating (LA-ICP-MS technique) on the intrusion yielded a crystallisation age of 227 ± 3 Ma (Table 5.1; Figure 5.5). Based on the uncertainty ranges, both of the ages overlap with a Late Triassic (ca. 218-203 Ma) magmatic event known to be related with porphyry Cu-Mo mineralisation elsewhere in the Cordillera (Cornejo et al., 2006; and references therein). A similar 223 ± 4 Ma U-Pb zircon age has been determined during the present study for a quartz-sericite altered dacitic porphyry dyke intercepted by a borehole in the Hamburgo basin (Table 5.1; Figure 5.5; Appendices 2C and 7). An age of 129 ± 1.3 Ma (^{40}Ar-^{39}Ar method) has been obtained for quartz-sericite altered tuffs at Sierra de San Carlos (Appendix 3B; Table 5.1; Figure 5.4). However, the validity of this age determination has been questioned by Pérez de

Table 5.1 Radiometric ages determination of hydrothermally-altered rocks associated with Late Paleozoic-Triassic units in La Escondida district and adjacent areas.

Sample (*)	Rock/Unit	Method (material)	Age & Error (Ma, 2 σ)	Area Prospect
N D (1)	N.D. / Imilac plutonic complex	K-Ar (sericite)	298 ± 7	La Casualidad
RC-3627 (3)	Quartz-sericite-altered tuff / La Tabla	K-Ar (whole rock)	281 ± 9	Chimalén
RC-3617 (3)	Quartz-sericite-altered tuff / La Tabla	K-Ar (whole rock)	280 ± 9	Isabel del Carmen
TAMBO S (3)	Quart-sericite-altered tuff / La Tabla	K-Ar (whole rock)	267 ± 8	San Carlos
ESC-51 (4) (†)	Feldspar porphyry / Dacite porphyry (Trdp)	U-Pb (zircon)	227 ± 3	E of Escondida Norte
ESC-52 (4)	Feldspar porphyry / Dacite porphyry (Trdp)	U-Pb (zircon)	223 ± 4	Hamburgo basin (Hole RC-3292)
ESN0 (4) (†)	Feldspar porphyry / Dacite porphyry (Trdp)	K-Ar (whole rock)	216 ± 7	E of Escondida Norte
N.D. (2)	Basaltic andesite / La Tabla	K-Ar (whole rock)	147 ± N D.	Isabel Este
FU-469 (4)	Quartz-sericite-altered crystal tuff /La Tabla	^{40}Ar-^{39}Ar (sericite)	129.4 ± 1.3	SE of Escondida

(*) Source of data (1) Davidson et al. (1985) and Brook et al. (1986); (2) Peri and Palma (1997); (3) La Escondida brownfields exploration program (2003-2007); (4) this study. † = Same outcrop. Abbreviations: N.D. = Not described.

Arce and Matthews (written comm., 2004; Appendix 5) due to: (a) a complex interaction of excess Ar from the older protolith; (b) ^{39}Ar recoil from fine-grained sericite and Ar loss (Figure 5.6a); (c) an isochron with elevated MSWD value (0.62); and (d) a ^{40}Ar-^{39}Ar intercept (717 ± 15) indicative of excess Ar (Figure 5.6b). Therefore, the 129 ± 1.3 Ma ^{40}Ar-^{39}Ar age is discarded from further discussion due to its analytical problems and geologically meaningless result.

5.1.3 Porphyry Cu Mineralisation Associated with Tourmaline-quartz-cemented Hydrothermal Breccia

This group of prospects are the most conspicuous Late Paleozoic-Triassic copper systems recognised in La Escondida district. Some of the prospects have been mined at a small scale (Figure 5.1). La Casualidad mine consists of a series of Cu-oxide-bearing faults and veins that have cut small tourmaline-quartz-cemented hydrothermal breccias bodies and associated granodiorite-dacite porphyries (Matthews et al., 2004). Supergene copper minerals are also hosted by tourmaline-quartz-cemented breccias (Figure 5.4b). The intrusive rocks have undergone incipient K-silicate alteration, where secondary biotite has replaced primary ferromagnesian minerals. Sericite from La Casualidad mine has provided a K-Ar age of 298 ± 7 Ma (Davidson et al., 1985; Brook et al., 1986; Table 5.1; Figure 5.5). No data on Cu grade and tonnage are available for La Casualidad mine, but the potential to find a significant copper ore body is very low.

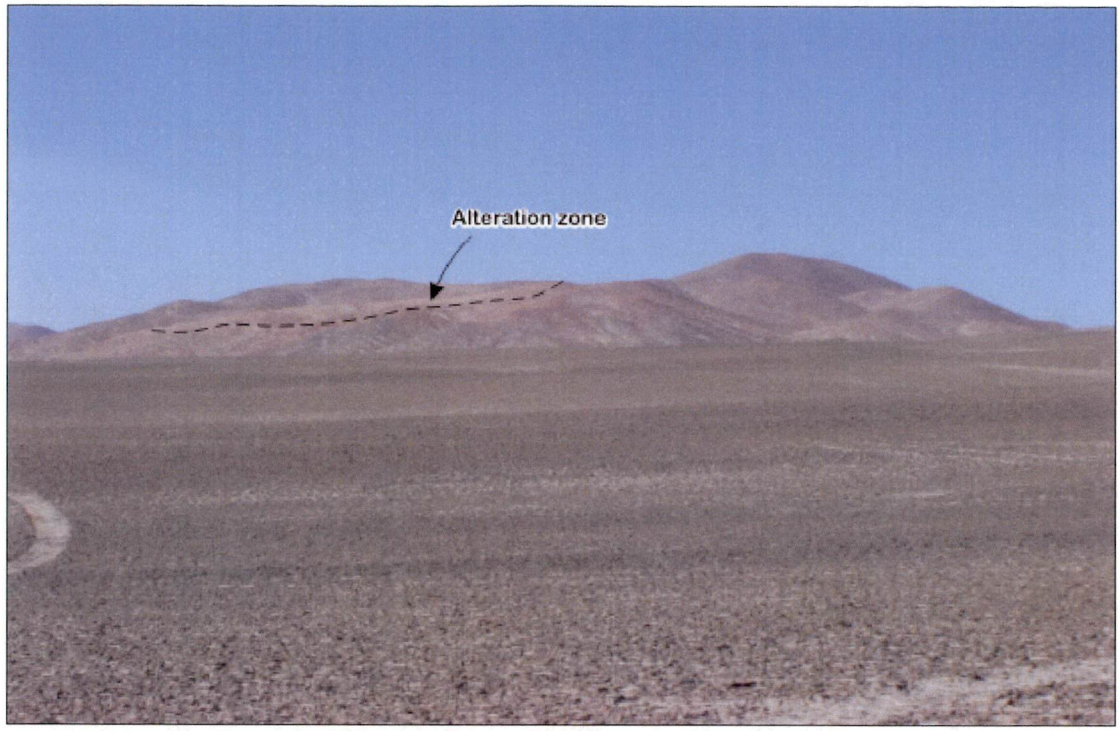

Figure 5.2a General view (looking north) to the San Pablo alteration zone, which formed within coarse-grained rhyolitic ignimbrites of the eastern volcanic sub-unit of La Tabla Formation (Late Carboniferous-Permian). The alteration zone is elongated sub-parallel with the dip-slope. Western flank of San Carlos block (7,298,679m N; 494,129m E).

Figure 5.2b General view (looking northeast) to the lithocaps at Isabel del Carmen prospect. The lithocaps occur in coarse-grained rhyolitic ignimbrites of the central volcano-sedimentary sub-unit of La Tabla Formation. The alteration zone is largely elongated in a NE-direction. Eastern flank of San Carlos block (7,299,750 m N; 498,900m E).

Figure 5.3a General view (looking west) to the Chimalén prospect, which consists of a large domain of quartz-sericite and argillic alteration. The surrounding country rocks are the volcaniclastic and sedimentary beds from La Tabla Formation (Late Carboniferous-Permian). Northern flank of San Carlos block (7,317,800m N; 510,400m E).

Figure 5.3b General view (looking east) to a meter-wide quartz ledge at Chimalén prospect, which consists of cryptocrystalline quartz, brecciated in some places, along with minor scorodite and hypogene alunite. The surrounding country rocks are argillised volcaniclastic beds from La Tabla Formation (Late Carboniferous-Permian). Northern flank of San Carlos block (7,318,200m N; 509,600m E).

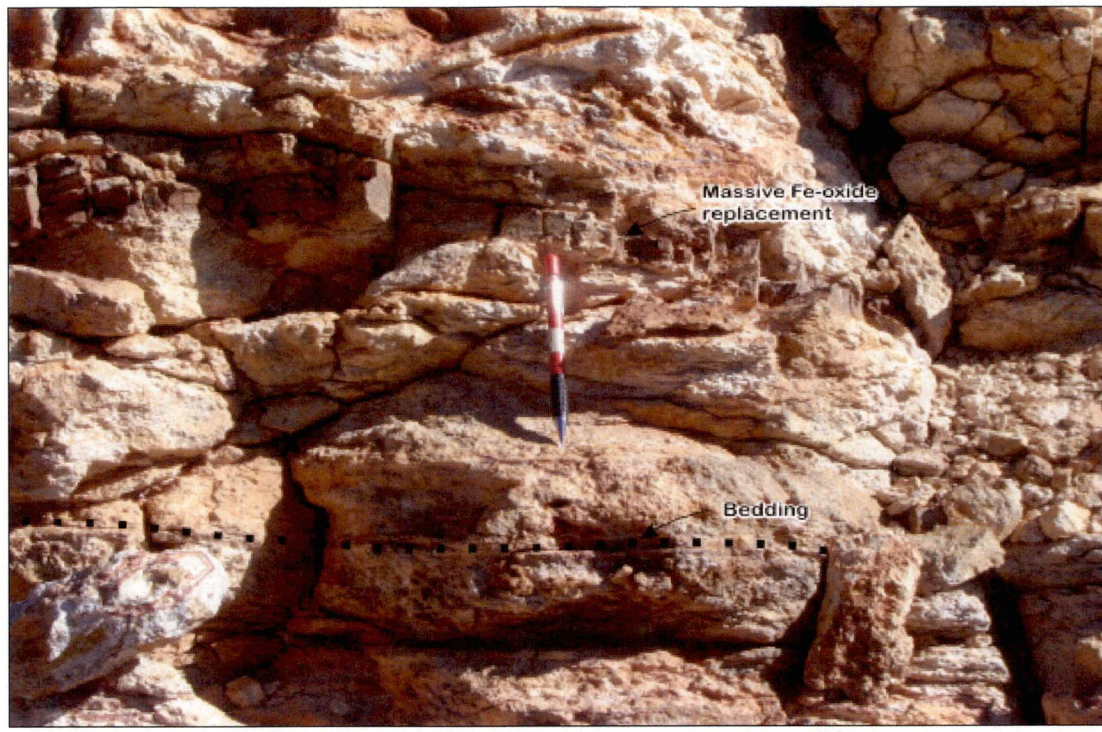

Figure 5.4a Cross-bedded conglomerates and sandstones of La Tabla Formation in Pingo-Pingo prospect, which have been strongly altered to pyrophyllite and minor alunite. Thin beds have been replaced by Fe-oxide. Eastern flank of Imilac block (7,325,595m N; 508,120m E).

Figure 5.4b Tourmaline-quartz-cemented hydrothermal breccia of La Casualidad mine. These small Cu-oxide-bearing breccia pipes are associated with a dacite porphyry intrusion, which occur as clasts within Late Triassic conglomerate. Note the similarity with the clasts of similar composition shown in Figure 5.7b). Eastern flank of San Carlos block (7,313,650m N; 510,600m E).

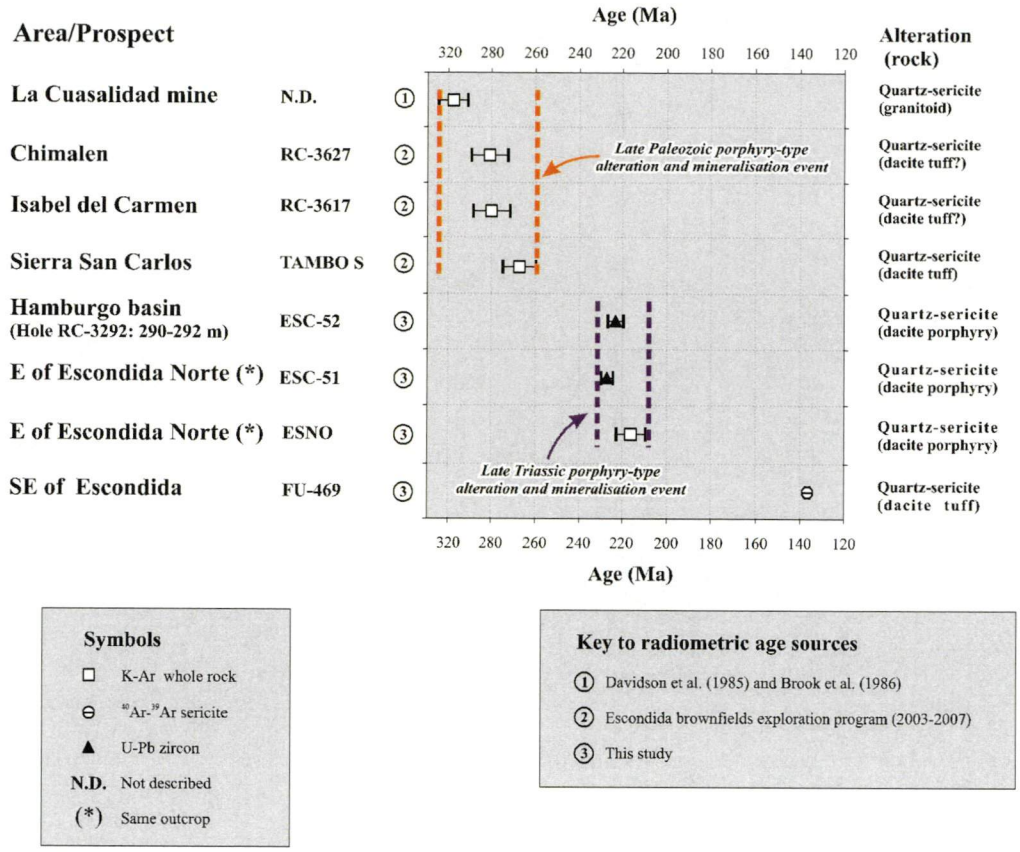

Figure 5.5 Selected radiometric ages for Late Paleozoic-Triassic hydrothermal systems at La Escondida district

5.1.4 Greisens, Pegmatites and Associated Massive Quartz-Veins

Small greisen-type alteration zones occur in quartz diorites of the Late Paleozoic Imilac intrusive complex (Figure 5.1). The greisens consist of an assemblage of coarse-grained muscovite, sericite, chlorite and quartz, with abundant pyrite (Appendix 3A). The rhyolitic wall rocks (La Tabla Formation) have been intruded by massive bodies of pegmatitic quartz, which occur close to the contact with the Late Paleozoic plutons, particularly in the San Carlos block (Figure 5.1; Appendix 3B). Small-scale exploitation of these pegmatite veins was undertaken a few decades ago.

The Altair prospect is a small zone of structurally controlled quartz veins hosted by tuffs from La Tabla sequence and surrounded by narrow domains of argillisation, silicification and limonitisation (Appendix 3B). The veins contain traces of pyrite, chalcopyrite and covellite (Sandoval, 2001a; this study). A few of trenches and drill holes programmed in this prospect by La Escondida brownfields exploration program (2000-2002) have confirmed its little economical potential.

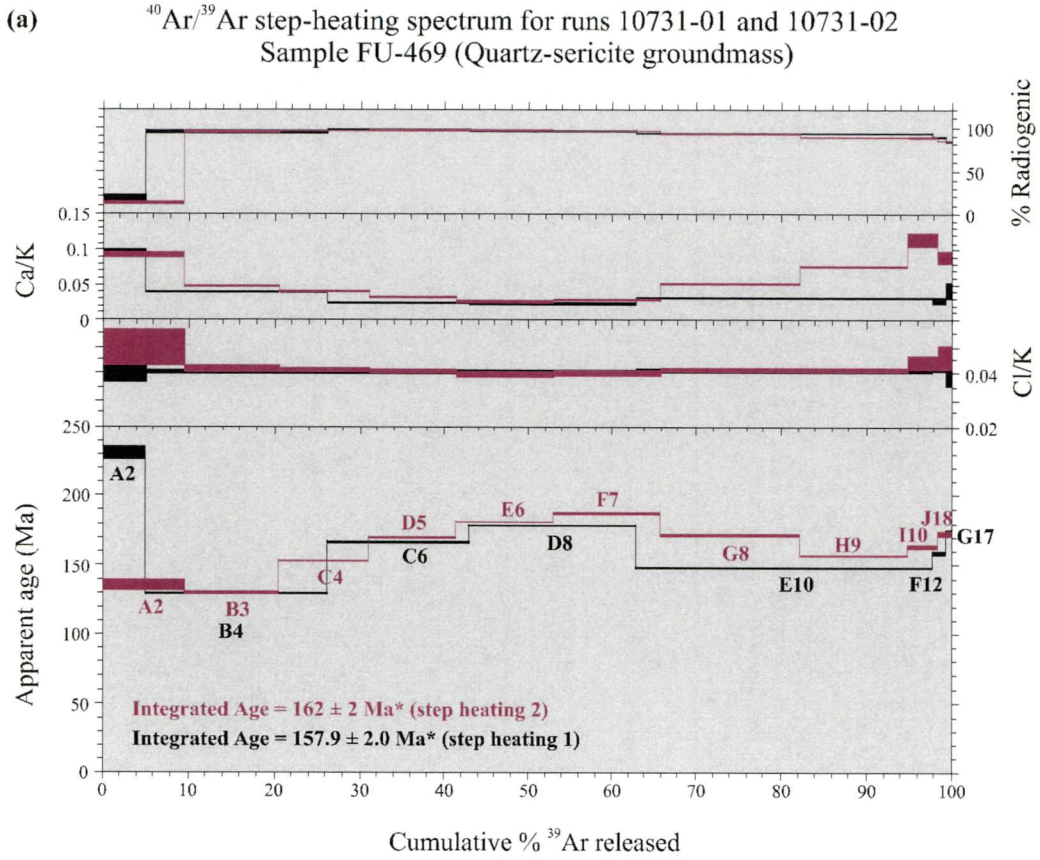

Figure 5.6 Disturbed ^{40}Ar-^{39}Ar age spectrums (a) and inverse isochron obtained by combining the highest temperature steps (b) from two runs on an altered dacitic tuff (sample FU-269;*: 2σ; **: inside 95% confidence interval; modified from Pérez de Arce and Matthews, written comm., 2004). An apparent minimal age of 129.4 ± 1.3 Ma is suggested by high-temperature steps (N=5). However, the analytical results suggest excess Ar, ^{39}Ar recoil, Ar loss and heterogeneity given by the inclusions (high Ca/K ratio at high temperature steps; samples degassed at two peaks) making the 129.4 ± 1.3 Ma combined Ar isochron age unreliable.

5.2 LATE TRIASSIC-JURASSIC

Conglomerates of the Lower Member (*TJep-a*) of El Profeta Formation host Cu-oxide mineralisation at the Puma prospect (Figure 5.1; Appendix 3A). Mineralization is dominated principally by chrysocolla, copper-wad (neotocite) and amorphous Mn- and Cu-bearing clays, which have coated fractures and impregnated clasts and matrix within the conglomerates (Figure 5.7a). Pebbles and cobbles have been observed that consist of quartz-tourmaline-cemented hydrothermal breccia, and also quartz-diorite porphyry (Figure 5.7b) with incipient K-silicate (secondary biotite and K-feldspar) and propylitic (chlorite, epidote and calcite) alteration assemblages. This presumably indicates erosion of the Late Paleozoic-Late Triassic porphyry systems. The mineralised clasts contain traces of pyrite, chalcopyrite and chalcocite, along with supergene chrysocolla, malachite, tenorite, neotocite and copper-wad. Transported supergene Cu mineralisation is interpreted to have been formed by *in situ* remobilization and reconcentration of copper from the clasts of eroded Late Paleozoic-Middle Triassic porphyry copper systems.

Detailed investigation of the mineralised zone has delineated several concentrations of mineralised clasts and related Cu-oxide-bearing fractures, over a surface area of 8 km^2 (Figure 5.1; Appendix 3A). The sequence lacks unidirectional tractional sedimentary structures (i.e. cross-bedding or clast imbrications) that would allow the provenance region to be determined. However, more than ten holes have been drilled by La Escondida exploration program (2003-2007) on the alluvial plain extended along the western border of the Puma prospect (Appendix 1A). They were programmed to test the occurrence of an "exotic" blanket of transported secondary copper; however the drilling results were inauspicious.

5.3 LATE CRETACEOUS- EARLY PALEOCENE

5.3.1 Gossanous Veins Associated with Skarn

Broad zones of calc-silicate alteration, including skarn, are associated with the Late Cretaceous intrusive complexes (Cerro Bayo, Torcaza and Sombrero plutons; Figure 5.1; Appendices 1A and 3A). Calc-silicate alteration occurs mostly in calcareous strata of the Mesozoic El Profeta and Santa Formations. Limited zones of endoskarn are also present in the adjacent plutons. No study of skarn zonation has been attempted, but abundant wollastonite, diopside, garnet, amphibole, epidote, calcite, magnetite and minor scapolite have been recognised during the current study. Numerous Fe-oxide and gossanous veins

Figure 5.7a Minor occurrence of transported **supergene copper mineralisation** (mainly chrysocolla) in clasts and matrix of a monomictic conglomerate of the Late Triassic-Early Jurassic Lower Member *(TJep-a)* of El Profeta Formation. Puma sector (7,306,920m N; 479,900m E).

Figure 5.7b Pebble of tourmaline-quartz-cemented hydrothermal breccia within a Late Triassic-Early Jurassic conglomerate of El Profeta Formation. Puma sector (7,306,920m N; 479,900m E).

Figure 5.8a Limonite-rich, gossanous vein associated with skarn near the Sombrero plutonic complex (ca. 67-64 Ma). Cerro Sombrero sector (7,318, 990m N; 476,100m E).

Figure 5.8b General view to south of low-relief outcrops of advanced argillic alteration associated with a rhyolite porphyry (TPsb7) that is nested within a coarse-grained granodiorite (*TPsb6*; ca. 64 Ma) of the Sombrero plutonic complex. Cerro Sombrero sector (7,319,100m N; 475,750m E).

are associated with the skarn zones (Figure 5.8a). They have a pronounced NNE-trending orientation at the Cerro Bayo and Sombrero plutonic complexes (Figure 4.16). The veins contain limonite, martite, magnetite and traces of pyrite. No Cu-oxide and sulphide occurrences have been recognised during the current study; and no economic potential has been assessed for the ferruginous veins. Based on the closed spatial relationships of the skarns with the Late Cretaceous and Eocene intrusions, similar ages are proposed.

5.3.2 Advanced Argillic Alteration Zones

The <0.8 km^2 Sombrero alteration zone (Figure 5.1; Appendix 3A) is associated with late stage granodiorite and granite porphyry (*TPs7*) of the Sombrero plutonic complex (*ca.* 67-65 Ma). The granite porphyry has been pervasively altered to an assemblage of quartz, kaolinite, traces of sericite and alunite, which is surrounded by narrow haloes of chlorite-montmorillonite-calcite±epidote alteration association (Figure 5.8b). Barren quartz-stockworks are present, as are transported limonites (jarosite and goethite) and oxidised pyrite disseminations. No further economical potential has been assessed in the Sombrero alteration system during the present study due to occurrence of a goethitic-jarositic leached zone, which is usually diagnostic of a pyrite-rich porphyry system at depth (Anderson, 1982; Gilmour, 1995; Sillitoe and McKee, 1996)

5.3.3 Polymetallic Fe-Cu-Ag Veins

Mineralised veins and faults at Alicia mine are polymetallic structures hosted by skarn-altered calcareous sandstones of Jurassic-Neocomian age. The mineralised bodies are less than 2 m width and 300 m length, with a pronounced NNE-trending orientation (Figure 4.16). They were exploited at a small scale probably during the 1960s and 70s, but the access shafts and declines have now collapsed. Primary mineralisation comprises pyrite, galena, digenite and chalcopyrite. Secondary Ag and Cu minerals are also present (Boric et al., 1990). In a small dump, the gangue mineralogy consists of quartz, siderite, limonite, siderite and calcite. No data on Cu grade and tonnage are available.

5.4 MIDDLE EOCENE

A well-defined system of northeast- and northwest-trending faults and veins occur to the east of Cerro Rincones (Figures 5.1 and 4.29; Appendix 3A). The mineralised structures contain an association of quartz, limonite, Cu-oxide, galena, barite, calcite and siderite (Pritting, 2001, 2002; this study). They are a few tens of meters long and 20-70 cm thick.

Table 5.2 Characteristics of the Middle-Late Eocene intrusives related to porphyry Cu mineralisation in La Escondida district.

Deposit	Intrusion Age	Description / Contact relationships and lithology	References
La Escondida	Middle-Late Eocene	La Escondida intrusive complex consists of four main facies that were emplaced along a structural contact (Panadero Faults) between two contrasting geological domains the La Tabla Formation (Late Carboniferous-Permian) to the east and the Augusta Victoria volcanic sequence (Late Paleocene-Early Eocene) to the west Early monzodiorite porphyry has been intruded by syn-mineralisation quartz-monzodiorite and granodiorites A numbers of intrusive breccia bodies containing xenoliths of both lithologies were also emplaced, especially in the southeastern portion of the deposit, exhibiting a characteristic subvolcanic groundmass and epithermal alteration in the upper level of the mineralised system Several generations of large bodies of hydrothermal breccias are also present Late rhyolites to rhyodacite domes, probably including more than two intrusions, have crosscut the earlier units Post-mineral dykes of dacitic to andesitic composition are correlated with similar dykes observed elsewhere the district.	Ojeda (1986) Alpers and Brimhall (1988) Richards et al (1999) Richards et al. (2001) Padilla et al. (2001) Quiroz (2003) Padilla (2003) Véliz and Camacho (2003)
Escondida Norte-Zaldivar	Middle-Late Eocene	The Escondida Norte-Zaldivar deposit contains a multi-stage intrusive complex with marked north-northeast orientation, comprising at least three principal pulses related to copper mineralisation They correspond to the coarse-grained porphyries that are from oldest to youngest, the rhyolite, granodiorite and diorite bodies, which were emplaced along and are cut by a major structural weakness (Portezuelo Fault) that again separates an eastern Upper Paleozic block (La Tabla rhyolitic tuffs) from a western Lower Tertiary andesitic volcanic (Augusta Victoria Formation).	Maturana and Saric (1991) Richards et al (1999) Monroy (2000) Richards et al. (2001) Pollard and Taylor (2002) Williams et al (2002) Williams (2003)
Pinta Verde	Middle-Late Eocene	Pinta Verde is a primary Cu-Fe sulphide and Cu-oxide deposit hosted by andesites of the Augusta Victoria Formation (Late Paleocene-Early Eocene) with biotite (K-silicate), propylitic and phyllic alteration assemblages. A northwest orientation was determined for the mineralizing diorites	Sandoval (2002b)
Carmen	Middle-Late Eocene	The blind Carmen porphyry system, located between the Escondida Norte and the La Escondida deposits, occurs beneath a gravel cover 60-90 m thick. Saldoval (2002) described granodiorite fingers that have been affected by biotite and quartz-sericite alteration, and low-grade primary Cu mineralisation	Sandoval (2002c)
Chimborazo	Middle-Late Eocene	The Chimborazo deposit occurs within andesitic to dacitic volcanic rocks of Augusta Victoria Formation which are intruded by the Cerro Rincones plutonic complex (43-41 Ma). Early alteration and mineralisation consist of a K-silicate and propylitic assemblage accompanied by chalcopyrite, pyrite and bornite. A series of NE-trending hydrothermal breccia bodies were emplaced later, along with large domains of advanced argillic alteration, silicification and sericitisation Associated mineralisation included mainly pyrite, enargite and chalcocite. Supergene Cu enrichment processes developed a low-grade blanket up to 200 m thick. Small supergene copper occurrences are associated with exotic-type mineralisation in the surrounding gravel cover and Fe-Cu veins at the northern foothill of Chimborazo Hill	Palma (1993) Petersen et al. (1996) This study

The host rocks are the calcareous and volcanic strata of the El Profeta and Augusta Victoria Formation, respectively, which have been intruded by multiple phases of the Cerro Rincones plutonic complex (*ca.* 43-41 Ma). Minor exploitation of gold and copper commodities was developed probably during the second part of the past century. The veins appear to have no significant economical potential.

5.5 MIDDLE-LATE EOCENE

The middle-late Eocene metallogenetic event was the most important economically in the district. It produced the large mineralised hypabyssal intrusive complexes of the Escondida and Escondida Norte-Zaldivar porphyry copper deposits, along with a series of altered and mineralised small plugs that are temporally and spatially associated with them. The porphyry deposits have been the subject of intensive previous studies. Consequently, only brief descriptions are provided here, as further documentation of detailed deposit geology for such thoroughly studied systems is outside of the scope of this PhD thesis. Descriptions of the magmatic, mineralisation and alteration features are provided by Ojeda (1986), Padilla et al. (2001), Padilla (2003), Quiroz (2003) and Véliz and Camacho (2003), for Escondida; whereas Maturana and Saric (1991), Monroy (2002), Williams et al. (2002) and Williams (2003) described features of Escondida Norte-Zaldivar. The key geological elements of these deposits are summarised in Table 5.2.

5.5.1 La Escondida

In broad terms, La Escondida is an intrusive complex composed of four main phases that were emplaced along a structural contact (Panadero fault) between two contrasting geological domains: La Tabla Formation (Late Carboniferous-Permian) to the east and the Augusta Victoria Formation (late Paleocene-early Eocene) to the west (Padilla et al., 2001; Quiroz, 2003; Figure 4.29; Appendices 1B and 2C; Figure 5.9a). An early facies of fine- to medium-grained monzodioritic porphyry was intruded by syn-mineralisation quartz-monzodiorite and granodiorite (Quiroz, 2003). Five U-Pb zircon determinations suggest intrusion ages of 38-34 Ma for syn- to slightly post-mineralisation intrusive phases of La Escondida complex (Richards et al, 1999; Padilla 2003; Table 3.14). There are several epizonal intrusive breccia bodies that contain clasts of monzodiorite and granodiorite. Several of these breccias were emplaced in the southeast part of the deposit, and are characterised by a dacitic groundmass and intense advanced argillic alteration (Urzúa et al., 2001). There are also a series of matrix-rich hydrothermal breccias. Early rhyolitic (39 ±

1.5 Ma U-Pb zircon) and late rhyodacitic (34.7 ± 1.7 Ma U-Pb zircon) domes have cut the older intrusive facies (Ojeda, 1986; Richards et al., 1999; Richards et al., 2001; Padilla, 2003; Table 3.14). Post-mineral (35.6 ± 1.2 Ma U-Pb zircon) dykes of dacitic and andesitic composition are also present (Richards et al., 1999; Richards et al., 2001; Padilla, 2003; Quiroz, 2003; Table 3.14). The cluster of mineralised porphyries are elongated in a northwest direction, as well as the overprinting high-sulfidation epithermal Cu veins and secondary Cu-enrichment blanket (Padilla et al., 2001; Padilla, 2003; Quiroz, 2003; Camacho and Véliz, 2003; Vergara, 2004; Figure 4.29; Appendix 1B). There is also a preferred north- to northeast-orientation for some intrusive facies exposed in the pit, based on mapping of Quiroz (2003; Figure 4.29; Appendix 1B). Hypogene alteration and mineralisation ages are summarised in Table 5.3 and Figure 5.12. Lixiviation and supergene enrichment processes gave origin to a thick blanket of secondary chalcocite and, in minor proportion, covellite, of at least 250 m of average thickness (Ojeda, 1986; Padilla, 2003; Camacho and Véliz, 2003). Supergene mineralisation formed around 18-15 Ma (Alpers and Brimhall, 1988).

5.5.2 Escondida Norte-Zaldivar

Escondida Norte-Zaldivar is associated with a multi-stage, northeast-elongated intrusive complex (Figure 4.29). At least three intrusive phases are known to be related to copper mineralisation (Monroy, 2000; Williams et al., 2002; Williams, 2003; Figure 5.9b). From oldest to youngest, the coarse-grained mineralised porphyries have rhyolite, granodiorite and diorite compositions (Williams et al. 2002). They have been named collectively as the Llamo porphyry at Zaldivar (Monroy, 2000). All three phases were emplaced along, and then cut by, the Portezuelo (I) fault (Figure 4.29; Appendices 1B and 2B). This fault also separates Late Paleozic La Tabla Formation to the east from late Paleocene-early Eocene Augusta Victoria Formation to the west (Figure 4.29; Appendix 2B). Similar to La Escondida, the Escondida Norte-Zaldivar deposit is cut by late high-sulfidation Cu-veins that have a dominant north- to northwest-orientation (Monroy, 2000; Williams et al., 2002). Three U-Pb zircon and one ^{40}Ar-^{39}Ar age determination indicate intrusion ages of 38-37 Ma (Richards et al., 1999; Pollard and Taylor, 2002). However, Campos (2002) and Campos et al. (2003) expressed concerns over the sample coordinates reported by Richards et al. (1999), for samples collected within Zaldivar pit, thereby raising questions as to whether the mineralising intrusive phase was actually sampled. Consequently, these questions have diminished the geological meaning of age determinations of Richards et al.

(1999), which are therefore used with caution in the current study (Appendix 5). Alteration ages are listed in Table 5.3 and Figure 5.13.

5.5.3 Other Porphyry Cu Systems

Apart from La Escondida and Escondida Norte porphyry clusters, other Eocene alteration systems in the district include the Ricardo porphyry and Baker breccia lithocap (Figure 5.1; Table 5.2). The Baker breccia lithocap is partially covered by gravels of the Salar de Hamburgo basin (Figure 5.10a). Outcrops of conspicuous advanced argillic alteration and phreatomagmatic hydrothermal breccia are hosted by strongly altered dacitic porphyry and ignimbrites from the late Paleocene-early Eocene Augusta Victoria Formation (Chapter 3). An advanced argillic alteration assemblage of quartz, alunite, dickite, kaolinite and minor sericite has destroyed primary textural features in the porphyry. Minor quartz stockworks are present locally (Figure 5.10b). The Baker breccia is inferred to have been a pyritic system based on the occurrence of a jarositic-goethitic leached cap (i.e., Anderson, 1982; Gilmour, 1995; Sillitoe and McKee, 1996; Chavez, 2004). The hydrothermal breccia is clast-supported (Figure 5.10b), contains a small amount of silicified matrix and has rounded to subrounded clasts of altered dacite porphyry that locally contain truncated quartz veinlets (Figures 5.11a and b). Minor vuggy quartz ledges are also present. A crystallisation age (U-Pb zircon) of 38.0 ± 1.1 Ma was obtained for the dacite intrusion associated with the Baker breccia (Table 3.14; Appendix 5) during the current study. Drill holes have intercepted incipient secondary chalcocite mineralisation, but Cu grade and tonnage data are not available.

5.5.3.1 Carmen

The Carmen porphyry, located between Escondida Norte and Escondida deposit, is covered by up to 90 m of gravels (Figure 5.1). It is composed of a group of granodiorite dykes that had been altered to produce a classic porphyry-type zoning patterns of biotite, intermediate argillic, quartz-sericite and propylitic alteration assemblages (Saldoval, oral comm., 2002), and were associated with primary and secondary Cu mineralisation with grades over 0.5% CuT (Base Metals Development-BHPBilliton, 2003). No ages are available for the Carmen porphyry. Results of recent deep drilling suggest that there is high potential for economic occurrences of chalcopyrite-bornite, along with interesting gold values (Sepúlveda, oral comm., 2007).

Table 5.3 Radiometric age determinations of hydrothermal alteration and mineralisation from the eastern sub-belt of Eocene hydrothermal alteration systems.

Sample	Rock	Method (material)	Age & Error (Ma, 2 σ)	Source of Data (*)
La Escondida intrusive complex				
ESC8	Biotite vein cutting andesite	^{40}Ar-^{39}Ar (biotite)	34.8 ± 0.2	1
ESC28	Alunite from a halo of a polymetallic vein cutting the rhyolite dome	^{40}Ar-^{39}Ar (alunite)	35.4 ± 0.2	1
ESC29	Alunite from a halo of a polymetallic vein cutting the rhyolite dome	^{40}Ar-^{39}Ar (alunite)	35.2 ± 0.2	1
ESC14	Pyrite-chalcopyrite-covellite-molybdenite vein	Re-Os (molybdenite)	33.7 ± 0.3	1
Escondida Norte-Zaldivar intrusive complex				
ZED20 (265.8 m)	Albite-biotite alteration on andesite and granodiorite porphyry	^{40}Ar-^{39}Ar (biotite)	37.3 ± 0.1	3
N.D.	Quartz-sericite alteration associated with pyrite-chalcopyrite-molybdenite-quartz vein cutting granodiorite porphyry	^{40}Ar-^{39}Ar (sericite)	37 0 ± 0.6	2
ZEHD297 (114.4 m)	Quartz-sericite alteration associated with pyrite-chalcopyrite-molybdenite-quartz vein cutting granodiorite porphyry	^{40}Ar-^{39}Ar (sericite)	36.8 ± 0.1	3
N.D.	Advanced argillic alteration	^{40}Ar-^{39}Ar (sericite)	33. 8± 1 1	2

(*) Source of data: (1) Padilla (2003); (2) Pollard and Taylor (2001); (3) Pollard and Taylor (2002). Abbreviations: N.D. = not described.

5.5.3.2 Pinta Verde

Pinta Verde contains hypogene primary Cu-Fe sulphides and oxidised Cu minerals. The deposit is associated with dacite porphyry that has intruded andesites of the Augusta Victoria Formation. Hydrothermal alteration domains include biotite (K-silicate), sericite-clay-chlorite (*sensu* Sillitoe and Gappé, 1984; also known as intermediate argillic alteration),and quartz sericite and propylitic assemblages (Sandoval, 2002b). No ages are available for Pinta Verde. Data on Cu grade and tonnage have been not published yet.

5.5.4 Minor Altered Dacitic to Rhyolitic Porphyries *(Eodrp)*

The western part of La Escondida district contains a belt of hydrothermal centres whose ages are poorly constrained. The prominent features are lithocaps (i.e., Chimborazo and Capella; Figure 5.1) and large advanced argillic alteration zones (i.e., Poblete and Chimbo Este prospects; Figure 5.1) that occur within tuffs and minor andesitic lava flows of the Augusta Victoria Formation. These alteration systems have been explored intensely

during the last 20 years based on their association with a series of blind, shallow-level intrusions. The best intersections show that they are poorly mineralised, with traces of secondary chalcocite and abundant pyrite. It remains unclear whether magmatism occurred in the middle Eocene or middle-late Eocene. Lithologically, these intrusions include a series of dacitic to rhyolitic porphyries that have been intensely altered to alunite, dickite, pyrophyllite, quartz, sericite and limonites. Narrow vuggy quartz ledges are closely associated with the hydrothermal alteration zones that have large spatial extents, up to 3 by 1 km area (Figure 5.1; Appendices 3A and 3B). Previous drilling, relict sulphide studies and the occurrence of goethitic-jarositic leached cappings (Anderson, 1982; Gilmour, 1995; Sillitoe and McKee, 1996) suggest limited economic potential for all of these alteration systems.

5.5.5 Chimborazo

The Chimborazo lithocap covers a surface area of almost 1 km^2 (Figure 5.1) and has been described previously by Petersen et al. (1996). Mineralisation consists of a series of enargite veins with north-northeast-trends (Figure 4.29). Weathering of the veins produced a weakly developed supergene blanket that contains chalcocite. The supergene zone was concealed by gravels up to 100 m thick (Petersen et al., 1996). Chimborazo Hill is capped by a prominent, visibly destructive advanced argillic alteration zone, with local intense silicification and pervasive domains of granular and cryptocrystalline quartz, alunite, pyrophyllite, clays, and minor diaspore and allophane (Petersen et al., 1996). Silicified hydrothermal breccias have been recognised from several drilling programs (Figure 5.12a). They contain abundant clasts of tuffs derived from the Augusta Victoria Formation. Dating of the alunite-altered tuffs provided a K-Ar (whole rock) age of 38.1 ± 1.4 Ma (Table 5.4), which is consistent with similar middle Eocene hydrothermal alteration occurrences (Palma, 1993; Petersen at al., 1996; Table 3.5). However, the application of the conventional K-Ar radiometric method to this heterogeneously altered sample produced a result that is undoubtedly highly inaccurate (McDougall and Harrison, 1999; Richards et al., 1999). A post-mineral andesite-diorite dyke (*LEap* unit; Chapter 3) has been dated at 38.8 ± 3.4 Ma (K-Ar on hornblende; Palma, 1993; Petersen at al., 1996) and 38.1 ± 0.3 Ma (^{40}Ar-^{39}Ar on biotite; Richards et al. 1999). Richards et al. (1999, 2001) suggested a similar age of formation for the Chimborazo, Escondida and Escondida Norte-Zaldivar deposits (Tables 5.3 and 5.4; Figure 5.14).

Figure 5.9a General view (looking to east-southeast) of La Escondida open pit. The Sierra de San Carlos and the Hamburgo fault along the foothill are observed behind. The Llullaillaco volcano (ca. 6,800 m of altitude) appears also at the back (March-2007; image provided by S. Pizarro).

Figure 5.9b View (looking to NE) of Escondida Norte open pit. (March-2008; image provided by O. Dominguez)

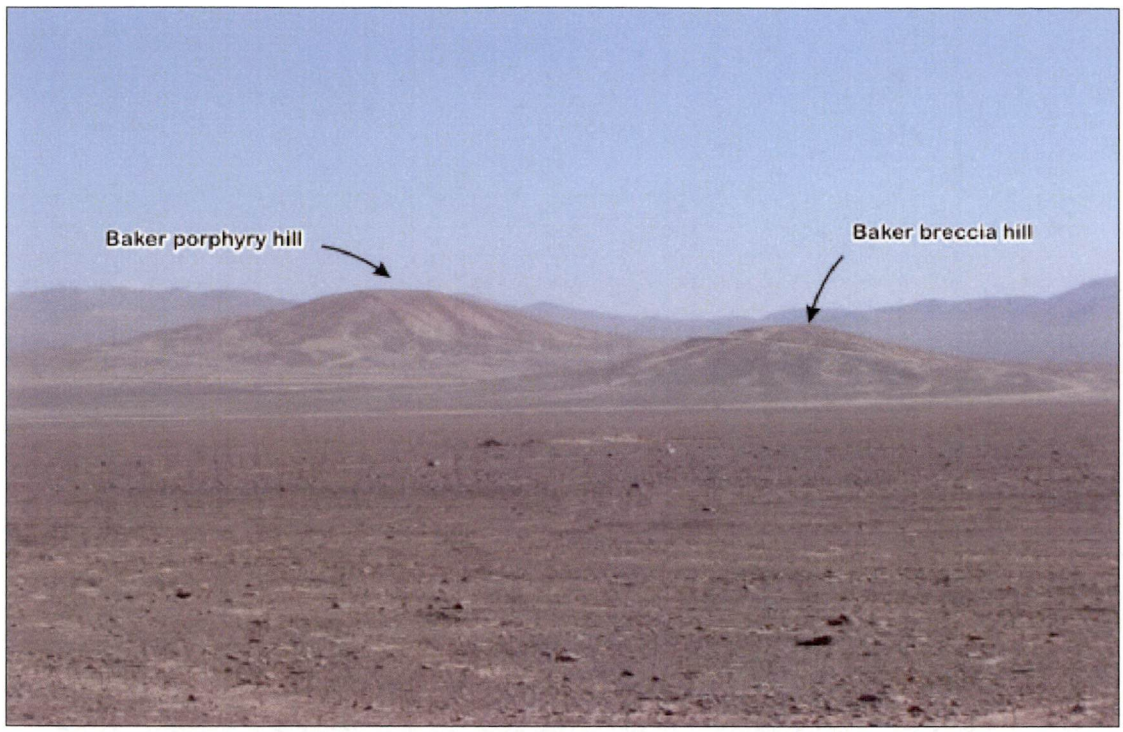

Figure 5.10 General view to northwest towards the lithocaps at Baker breccia. The lithocap forms a prominent hill with respect to the surrounding Salar de Hamburgo basin. Baker breccia hills (7,320,000m N; 502,000m E).

Figure 5.10 View (looking to NE) of the clast-supported hydrothermal breccia at the Baker breccia lithocap. The breccia is composed of cobble- and pebble-sized clasts of quartz-alunite-altered dacite porphyry. Baker breccia hills (7,320,000m N; 502,000m E).

Figure 5.11a Clast-supported hydrothermal breccia at the Baker breccia lithocap. The breccia is composed of subrounded clasts of quartz-alunite-altered dacite porphyry. Truncated quartz veins occur in some clasts. Baker breccia hills (7,320,000m N; 502,000m E).

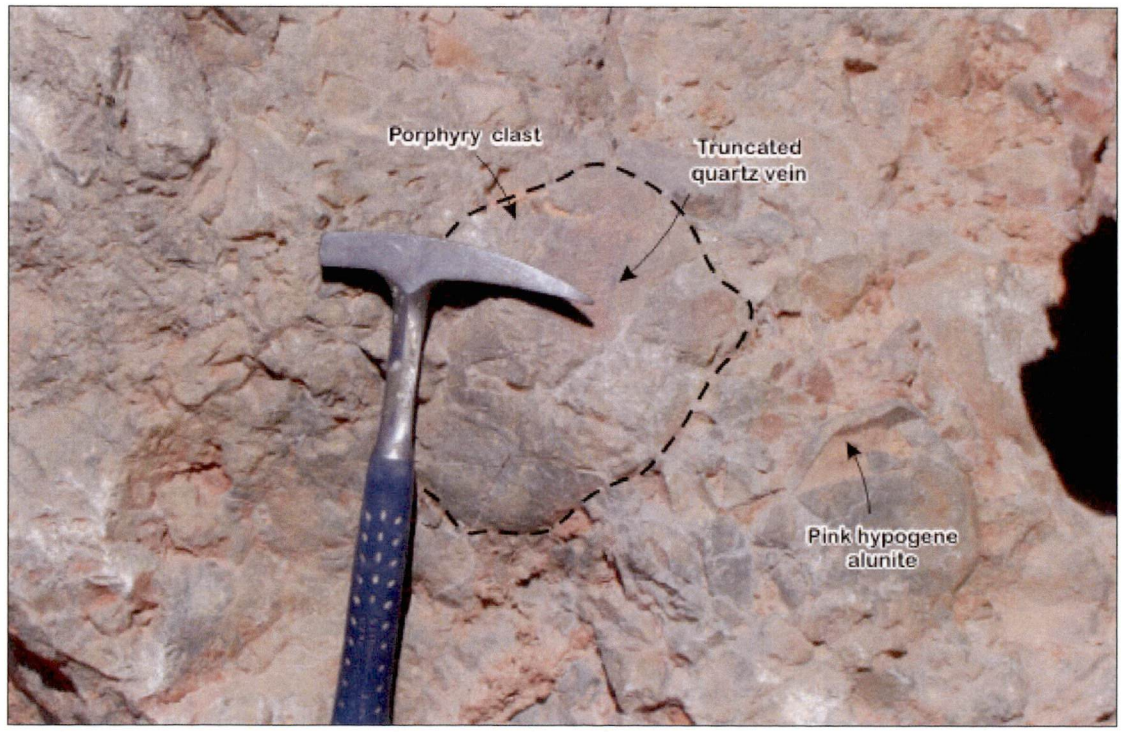

Figure 5.11b Clast-supported hydrothermal breccia at the Baker breccia lithocap. The breccia is composed of cobble- and pebble-sized clasts of altered dacite porphyry. The rock-flour matrix has been altered to quartz-alunite±clays. Baker breccia hills (7,320,000m N; 502,000m E).

Figure 5.12a General view (looking east-northeast) of Chimborazo Hill. This is capped by a zone of prominent advanced argillic and silicified alteration associated with high sulfidation enargite veins at depth. Chimborazo hill (7,328,900m N; 485,100m E).

Figure 5.12b Float of advanced argillic altered hydrothermal breccia, with clast-supported texture defined by subangular clasts of dacite porphyry. Note the poor occurrence of limonites and hydrothermal content, and almost total absence of quartz veinlets. Capella prospect (7,325,500m N; 487,250m E).

Table 5.4 Radiometric age determinations of hydrothermal alteration and associated intrusions along the western sub-belt of Eocene hydrothermal alteration systems in La Escondida district.

Sample (*)	Rock/Unit	Method (material)	Age & Error (Ma, 2 σ)	Area
6434 (1)	Diorite / Cerro Paisaje intrusive complex	K-Ar (biotite)	48.2 ± 1 3	Anillo (‡)
6433 (1)	Diorite porphyry / El Peñón intrusive complex	K-Ar (whole rock)	42.5 ± 1.7	Anillo (‡)
8249 (1)	Hydrothermal breccia / Anillo porphyry	K-Ar (alunite)	43.0 ± 2.3	Anillo (‡)
MP-01 (4)	Sericite-altered dacitic porphyry / Quebrada Larga porphyry (EOdrp)	K-Ar (whole rock)	67 ± 8	Quebrada Larga
RMP1 (2)	Sericite-altered tuff/ Augusta Victoria Fm	K-Ar (whole rock)	48.2 ± 3.5	Zapato Verde
RMP2 (2)	Sericite-altered tuff / Augusta Victoria Fm	K-Ar (whole rock)	45.4 ± 4.0	Zapato Verde
DCH-10 (3)	Alunite-altered tuff / Augusta Victoria Fm	K-Ar (whole rock)	38 1 ± 1.4	Chimborazo

(*) Source of data. (1) Marquardt et al. (1994); (2) Escondida brownfields exploration program (2003-2007), (3) Palma (1993) and Petersen et al. (1996); (4) this study. (‡) Anillo prospect is located 32 km to the west of La Escondida district.

5.5.6 Capella

The Capella lithocap has a surface area of <1.5 km² (Figure 5.1) and was formed within tuffs and andesites of the Augusta Victoria Formation. It includes two main alteration zones that trend north to north-northeast. There has been pervasive alteration of the host rocks to a quartz, clay, alunite, sericite and pyrophyllite-bearing assemblage, accompanied by goethite and jarosite. Microscopically minor gypsum and bassanite have been described (Kim, 2001). Several floats of quartz-alunite-cemented hydrothermal breccias have been found during the current study. They contain subrounded to angular clasts of altered dacite porphyry with barren quartz veinlets (Figure 5.12b). Minor tourmaline-quartz-cemented breccias are aligned with the north- to northeast-trending faults (Appendix 1A). Minor occurrences of supergene copper minerals are associated with the breccia bodies. The system has an epizonal alteration assemblage dominated by fine-grained granular quartz and cherty microgranular quartz in lenses or bands, together with tabular alunite grains. Only traces of secondary chalcocite are hosted by a quartz-sericite altered dacite porphyry intercepted by bore holes (La Escondida brownfield exploration program, 2003-2007). The Capella alteration system predates a series of north- to northeast-elongated andesite porphyry dated during the present study by U-Pb zircon method at 38.1 ± 0.6 Ma (*LEap* unit; Chapter 3; Appendix 5). Considering the drilling results to date, the hematite-jarosite leached cap and the scarcity of untested targets, the Capella prospect is considered to have only limited mineral potential.

5.5.7 Cerro Rincones

The Cerro Rincones prospect is a poorly exposed alteration zone located 1.5 km south of Chimborazo (Pritting, 2001, 2002; Figure 5.1; Appendix 3A). No data on grade and tonnage are available. Sub-crop exposures of a small (<0.5 km^2) north-northeast-elongated stock that is associated with the larger (2-2.5 km^2) NNE-trending alteration zone have been identified during the present study. Numerous float samples of advanced argillic-altered hydrothermal breccias and tuffs were also observed. Previous petrographic studies have identified brochantite-bearing granodiorite and rhyolite that have been altered pervasively to an assemblage of alunite, quartz, kaolinite, illite, sericite and rare smectite, along with diaspore (Pritting, 2001). The altered porphyry of Cerro Rincones has not been dated. Its age is inferred to be the same as the mineralising porphyries at Chimborazo (Pritting, 2001; this study). This is consistent with the presence of incipient secondary Cu enrichment (chalcocite) associated with enargite veins that have been cut by holes drilled recently by La Escondida brownfields exploration program (2003-2007). A review of drill core from Cerro Rincones prospect in the current study has identified the occurrence of propylitic alteration envelopes around the quartz-sericite and advanced argillic alteration domains. This relationship is similar to the overall hydrothermal alterations arrangement observed at Chimborazo Hill.

5.5.8 Zapato Verde

Zapato Verde is a quartz-sericite and advanced argillic alteration zone hosted by pyroclastic rocks of the Augusta Victoria Formation (Appendix 3A). Traces of supergene copper minerals and scarce limonite have been observed in outcrop, but no evidence of porphyry-style alteration in depth has been observed during the present study. Zapato Verde occurs almost 2 km south of Cerro Rincones prospect (Figure 5.1). Two altered rock samples from this system have been dated using the K-Ar (whole rock) method at 48.2 ± 3.5 Ma and 45.4 ± 4.0 Ma (F. Crignola and M. Hervé, written comm., 2004; Table 5.4; Figure 5.13). The difference in age relative to La Escondida (compare Tables 5.3 and 5.4; Figure 5.13) may imply that Zapato Verde is related to an older porphyry system than the La Escondida and Escondida Norte-Zaldivar systems. However, this hypothesis requires further testing because of the inaccurate dating method employed previously on Zapato Verde samples. Based on the current field mapping results, the likelihood of discovery of mineralisation at Zapato Verde hydrothermal alteration is considered to be minimal because of the absence of an altered lithocap. Recent drilling has reported negative results.

5.5.9 Poblete

Poblete is a north-northwest-elongated hydrothermal alteration zone less than 1.5 km^2 in surface area. It was formed within pyroclastic layers that are intercalated with andesitic lava flows of the Augusta Victoria Formation (Figure 5.1; Appendix 3A). Poblete is located about 7 km north-northwest of Chimborazo at the northern limit of the study area (Figure 5.1). The Poblete fault has controlled the distribution of hydrothermal alteration within the pyroclastic strata. Microscopically, the alteration assemblage consists of abundant quartz, cryptocrystalline alunite, minor kaolinite, allophane and pyrite (mostly oxidised to jarosite.) Hydrothermal breccia bodies have been pervasively silicified. They contain traces of sericite and minor adularia, along with abundant limonite. The silicified fragments are probably derived from andesitic to dacitic protoliths, based on relict igneous textures (Urzúa, 2001a). The results of previous drilling programs suggest that there is no Cu and Au mineralisation in the Poblete alteration zone. In summary, the geology intercepted by the bore holes consists of limonite-bearing of tuff packages altered to quartz, kaolinite and traces of alunite, which are interbedded within massive and brecciated andesite lavas moderately altered to an association of chlorite, montmorillonite, illite and smectite, in conjunction with pyrite.

5.5.10 Chimbo Este

Chimbo Este contains northeast-striking quartz veins, which occur over a surface area of almost 1 km^2 (Figure 5.1; Appendix 3A). Mapping of several trenches completed during the present study indicate that pervasive quartz, kaolinite, limonites, minor alunite and pyrophyllite are the main alteration minerals associated with veins less than 30 cm wide. Andesite-diorite dykes (*LEap* unit; Chapter 3) have intruded altered volcanic country rocks of the Augusta Victoria Formation, and have subsequently been faulted. A number of holes have been drilled here by various exploration companies. Their results indicate that there is little or no potential for Cu and Au mineralisation in the Chimbo Este alteration zone.

5.5.11 Quebrada Larga

At Quebrada Larga (Figure 5.1; Appendix 3B), a strongly altered feldspar-quartz porphyry is exposed, along with minor bodies of limonite-quartz-bearing hydrothermal breccias. The wallrock consists of tuffs and sedimentary rocks of La Tabla Formation (Late Carboniferous-Permian). A 67 ± 8 Ma K-Ar (whole rock) age has been obtained from a strongly sericitised feldspar porphyry sample from the Quebrada Larga alteration zone

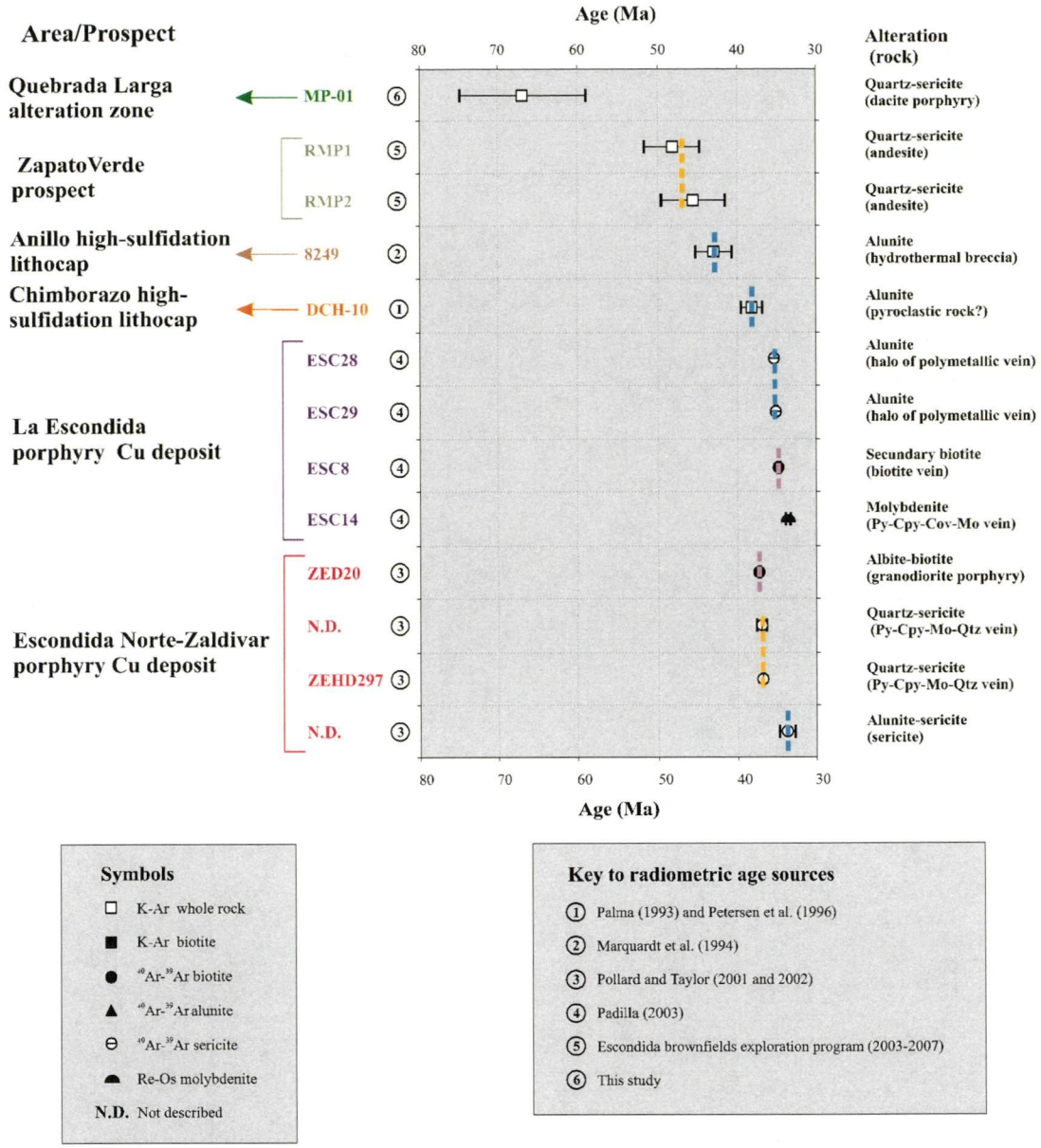

Figure 5.13 Selected radiometric ages for Eocene hydrothermal systems of La Escondida district.

(Table 5.4; Figure 5.12; Appendix 5). This age is considered unreliable due to the likely presence of excess argon (Appendix 5). No further economical potential is observed in the Quebrada Larga alteration system due to the limited occurrence of attractive limonites in the leached zone (Anderson, 1982; Gilmour, 1995; Sillitoe and McKee, 1996), lack of quartz-stockworks and scarce amount of relict Cu sulphides observed petrographically.

5.5.12 Mirador

A narrow zone of hydrothermal breccia with abundant lithic fragments occurs along the Hamburgo fault and is partially hosted by the San Carlos strata (38-36 Ma), on the eastern side of the study area (Figure 5.1; Appendix 3B). The breccia matrix includes sand- to

mud-sized lithic fragments that have been silicified pervasively and altered to alunite by multiple episodes of alteration (Urzúa, 2006). Locally abundant jarosite, hematite and goethite have been recognised in outcrops. A structural control is evident for these breccias. Several drill holes were drilled by La Escondida brownfield exploration program (2003-2007). They did not intercept Cu and Au mineralisation. At depth, the geology consists of volcaniclastic rocks moderately altered to montmorillonite-kaolinite-illite-smectite±zeolites, presumably of the late Paleocene-early Eocene Augusta Victoria Formation and Eocene San Carlos strata.

5.5.13 Discussion

Radiometric age determinations (Table 5.4; Figure 5.12) have confirmed that advanced argillic alteration and mineralisation occurred in the western sub-belt of La Escondida district both prior to and at the same time as the world-class middle-late Eocene porphyry deposits that formed in the eastern sub-belt. It is possible that some alteration of the western sub-belt occurred after 50 Ma and before 40 Ma as indicated by the K-Ar ages reported by Marquardt et al. (1994) for the Anillo porphyry Au prospect, located 32 km to the west of Las Escondida district. The lithocap at Chimborazo and the Capella alteration zones indicate that buried porphyry-style systems of middle Eocene age also occur in this sub-belt. However, these hydrothermal systems remain poorly understood in terms of the chronology of the intrusions, alteration and mineralisation.

Available intrusion, alteration and mineralisation ages for the eastern sub-belt suggest the occurrence of four advanced argillic alteration episodes of different ages (Pollard and Taylor, 2002; this study): 37.5 ± 0.3 Ma and 35.9 ± 0.4 Ma at La Escondida (Padilla, 2003), and a younger (33.8 ± 0.1 Ma) event at Escondida Norte-Zaldivar (Pollard and Taylor, 2001 and 2002; this study). Both La Escondida and Escondida Norte-Zaldivar systems are younger than the advanced argillic alteration domain associated with the Baker breccia, which is inferred to have formed between the Baker porphyry crystallisation age of 38.0 ± 1.1 Ma (U-Pb zircon; Chapter 3) and a post-mineral diorite dyke dated by Richards et al. (2001) at 36.9 ± 0.5 Ma (^{40}Ar-^{39}Ar amphibole; *LEap* unit; Chapter 3). These data determines a probable duration for the alteration and mineralisation events at Baker between ca. 1.7 and 0.5 m.y., which is in agreement with the 2 m.y. time span between crystallization of the syn-mineralisation intrusions and the cessation of the main hydrothermal events at Escondida Norte-Zaldivar mine (Campos, 2002; Campos et al., 2003).

5.7 SUMMARY

La Escondida district has a protracted and diverse history of hydrothermal alteration and mineralisation. The most relevant aspects of the Phanerozoic metallogenic history of the district are as follow:

- The Late Paleozoic-Early Triassic period produced a variety of copper mineralisation styles, including porphyry-related lithocaps, tourmaline breccia pipes, and volcanic-hosted copper occurrences. No economic examples of these weakly mineralised alteration systems have been discovered along the Domeyko Cordillera as yet. The chronology of intrusion, mineralisation and alteration events remain poorly known.
- The Mesozoic clastic and calcareous units have been intruded by Late Cretaceous-early Paleocene magmatic complexes, resulting in large skarn zones and some Cu-Au-bearing veins of minor economic interest.
- There are two north-trending sub-belts of Eocene hydrothermal alteration systems in the district. The western sub-belt consists of advanced argillic altered and silicified rocks (lithocaps at Capella and Rincones, and the Chimborazo high sulfidation Cu deposit). The low-precision K-Ar (whole rock) geochronological data cannot discriminate whether they form a distinct metallogenic belt (early or middle Eocene?), or are the same age as the highly mineralised eastern sub-belt of porphyries.
- The middle-late Eocene Cu deposits of La Escondida and Escondida Norte-Zaldivar deposits are world-class Cu porphyry clusters that define the eastern sub-belt, along with a number of peripheral mineralised intrusives (i.e., Baker breccia, Carmen, Pinta Verde, and Ricardo). Four spatially and temporally separated episodes of advanced argillic alteration occurred at La Escondida, Escondida Norte-Zaldivar and Baker, from 38-33 Ma. These deposits represent the culmination of hydrothermal activity in La Escondida district.

CHAPTER 6
Igneous Geochemistry

This chapter presents new geochemical data for the Late Paleozoic to Eocene igneous rock units from La Escondida district and integrates them into the framework of the magmatic evolution of northern Chile. Regional descriptions of the magmatism in northern Chile have been divided into two main geological events (i.e. Coira et al., 1982; Cornejo and Mpodozis, 1995; Haschke et al., 2006): pre-Andean (the Cambrian-Ordovician Ocloyic and Carboniferous-Triassic Gondwanian) and Andean (Jurassic to Recent). A previous geochemical study by Richards et al. (2001) provided useful data for the main igneous rock units recognised in La Escondida district. However, some of these analyses are reassigned here to different geological units on the basis of the results of the current mapping program and new radiometric age determinations. All geochemical data for the district are provided in Appendix 6.

6.1 SAMPLING AND ANALYTICAL PROCEDURES

New whole rock geochemical analyses were performed at the chemical laboratory of the Servicio Nacional de Geología y Minería (SERNAGEOMIN, Chile). Selected rock samples were crushed, ground, pulverized to less than 200 mesh to be analysed for major, trace and REE elements. A total of 40 samples were analysed as part of the current study.

6.1.1 Major oxide

Approximately 500 mg of pulverized sample was digested with a concentrated mixture of four acids (HCl, HNO_3, HF, H_2SO_4) at low temperature and atmospheric pressure. Al, Fe, Ca, Ti, Mg, Mn, Na and K determinations were performed by flame Atomic Emission Spectrophotometry (AAS-Flame; Equipment Perkin-Elmer 4000). Si and Al elements were also measured by flame AAS on fused 100 mg sample (glass beads) prepared using a 1:4 mixture of lithium tetraborate and sodium carbonate flux. Phosphorous was determined by UV-visible spectrophotometry. Direct determinations in dry samples were completed as follow:

- Fe^{++} ferrous ion by oxidation with potassium chromate after reaction with a mixture of acid (H_2SO_4, HF, H_3PO_4).

- Carbon and sulfur by absorption in KOH and iodometry, respectively, on samples ignited in a high temperature furnace.
- CO_2 in carbonates by absorption of CO_2 in KOH after acid hydrolysis.
- Crystalline water (H_2O^+) was determined by the Penfield method (Llona, written comm., 2004).

6.1.2 Trace elements

Approximately 1 g of powdered sample was treated by acid dissolution (HCl, HNO_3, HF) obtaining a final volume of 50 ml. Cu, Pb, Ni, Co, Rb and Zn were analysed by AAS-Flame, with detection limits on the order of 1-5 ppm. Cr, Y, V, Sc, Ba, Sr, Nb, Zr, La, Ce and Nd were determined using inductively coupled plasma mass spectrometry (ICP-MS), with detection limits of 0.01 ppm, on fused glass beads prepared using a lithium tetraborate flux.

6.1.3 Rare-Earth Elements (REE)

To prepare samples for analysis, 0.1 g of powder was dissolved by standard acid attack (using HF and HNO_3), spiked by Re internal standard and run in a nitric acid matrix at 0.1 $g.l^{-1}$ concentrations of total dissolved solids. Determinations were completed by ICP-MS, with detection limits of 0.01 ppm.

6.2 ALTERATION AND ELEMENT INMOBILITY

Detailed petrographical studies indicate that all analysed samples have suffered variable degree of secondary alteration. Evidence of devitrification, low-grade metamorphism, and deuteric and/or hydrothermal alteration has been found in almost all of the lithological groups examined petrographically. A first approach to evaluate the effects of the sub-solidus alteration processes on the rocks composition has been to compare the plotting of the samples on the mobile total alkali-silica diagram (TAS, Le Bass et al., 1985) and on the immobile-element Zr/TiO_2 versus Nb/Y diagram (Winchester and Floyd, 1977) relative to the loss by ignition (LOI). The first diagram shows that only few samples with high LOI (> 4) are dispersed from the principal compositional range given by the mobile K_2O, Na_2O and SiO_2 (Figure 6.1a). This suggests that secondary remobilisation of the alkali and silica has occurred only in few samples that normally present elevated LOI. The Zr/TiO_2 versus Nb/Y graphic has restricted the compositional range for all of samples confirming the changes in these major oxides (Figure 6.1b). A second approach consisted of the co-

variation analysis of a selected group of immobile elements (Al_2O_3, P_2O_5, TiO_2, Nb and Zr), and is presented in Figure 6.2. In general, there is a weak correlation between major immobile oxides, but accompanied by a minor dispersion of Zr and Nb. This dispersion has been interpreted here as magmatic in origin and likely caused by the diverse concentrations of accessories minerals (i.e., zircon, rutile and titanomagnetite) in determined intrusive and volcanic lithological groups.

A relatively persistent scattering of major and trace elements observed in the Late Cretaceous-lowermost early Paleocene igneous suite (Figures 6.1 and 6.2) has been confirmed petrographically. A moderate to intense alteration of feldspar to albite, sericite and calcite, is observed whereas the ferromagnesian phases are replaced by an association of chlorite, epidote and biotite. Incipient levels of deuteric alteration have been also recognised microscopically in the Tertiary volcanic and intrusive suites, and their intensity and persistence were sufficient to have changed substantially the original composition of some samples. Two samples (one from Richards et al., 2001) from Cerro Rincones plutonic complex that show unusually depleted heavy rare elements (HREE) have been excluded from the following petrogenetic discussions (samples ESC18 and IM150).

In a third approach, it was intended to assess the effects of the alteration on the mobile large-ion lithophile elements (LILE) and immobile high-field strength lithophile elements (HFSE). Variation of Ba and Zr versus LOI has respectively validated enrichments and depletions of LILE only in those samples with LOI > 4 (Figure 6.3a and b). Therefore, on the basis of mobility of elements and LOI, one sample from the Triassic porphyry unit has been excluded from further analysis (ESC52). Another sample (ESC53) was rejected due to analytical problems presented during the radiometric dating that make their obtained age useless.

A series of Harker variation diagrams of major and trace elements versus silica for each magmatic suite are presented in the following sections. They display significant changes in alkali (K_2O, Na_2O), SiO_2, FeO and Fe_2O_3, and some LILE-element group (i.e., Ba and Rb) in determined samples. However, the rock classifications, tectonic discrimination plots and petrogenetic discussions are based fundamentally on immobile high field strength (HFSE) and rare earth (REE) element ratios with negligible remobilisation in the group of studied rocks.

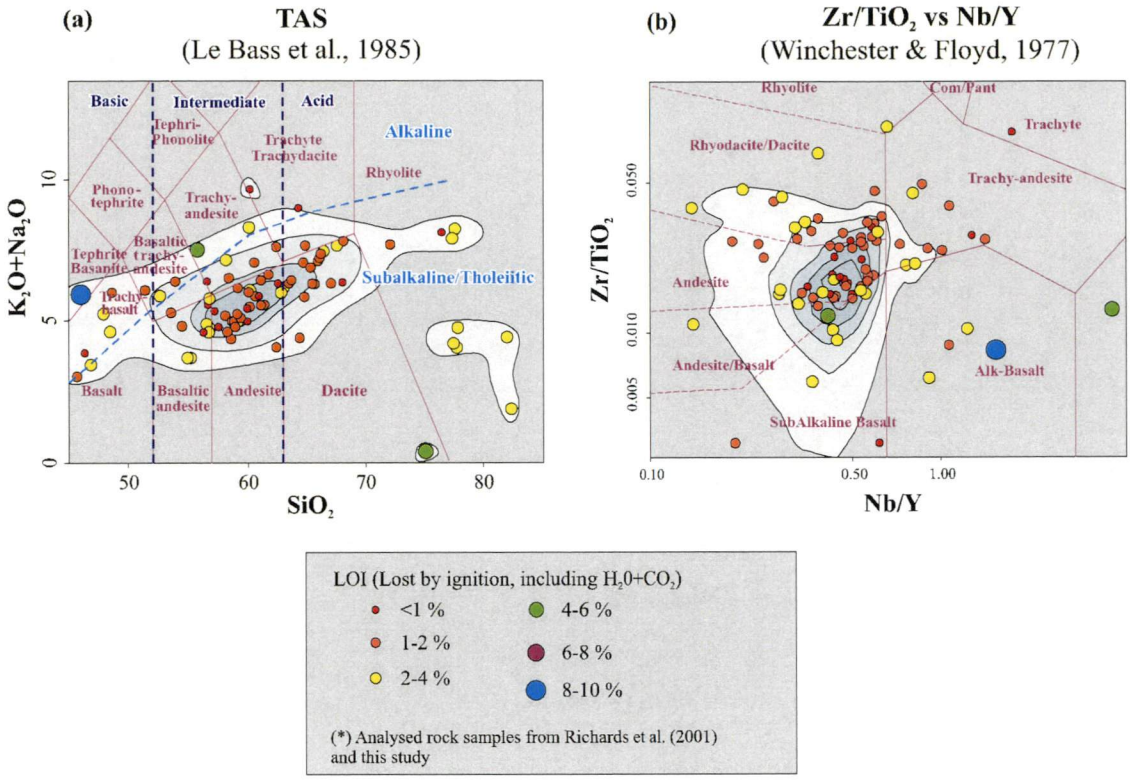

Figure 6.1 Distribution of the available geochemical analyses for volcanic and intrusive rocks of La Escondida district on (a) total alkali versus silica classification diagram (TAS, Le Bas et al., 1985), and (b) the Zr/TiO_2 versus Nb/Y (Winchester and Floyd, 1977) classification diagram discriminated by LOI. Major element data recalculated to 100 wt% volatile-free. Contours indicate sample distribution. Abbreviations: LOI = Lost by ignition; Com = Comendite; Pant = Pantellerite.

6.3 WHOLE ROCK GEOCHEMISTRY

6.3.1 Pre-Andean Magmatism (Gondwanian)

The compositions of the Late Paleozoic-Late Triassic volcanic and intrusive rocks have been plotted on the Zr/TiO_2 versus Nb/Y geochemical discriminating diagram (Winchester and Floyd, 1977). The samples fall within the andesitic basalt, andesite and rhyodacite/dacite fields (Figure 6.4a). Most of the samples are calc-alkaline, based on the graphic of FeOt/MgO versus SiO_2 plot (Miyashiro, 1974; Figure 6.4b). Harker variation diagrams for major elements show decreasing TiO_2, Al_2O_3, FeO_t, MgO and CaO contents with increasing SiO_2 (Figure 6.5). Similar trends have been observed for compatible transition metal elements (i.e., Cr, Ni, V, Sc), which are usually occur in low concentrations (Figure 6.6). K_2O contents increase sharply with SiO_2 and then decrease dramatically at 70 wt% SiO_2. The large-ion lithophile elements (LILE: Rb, Ba, Cs), high-field strength elements (HFSE: Zr, Y) and light rare elements (LREE: La, Ce) show

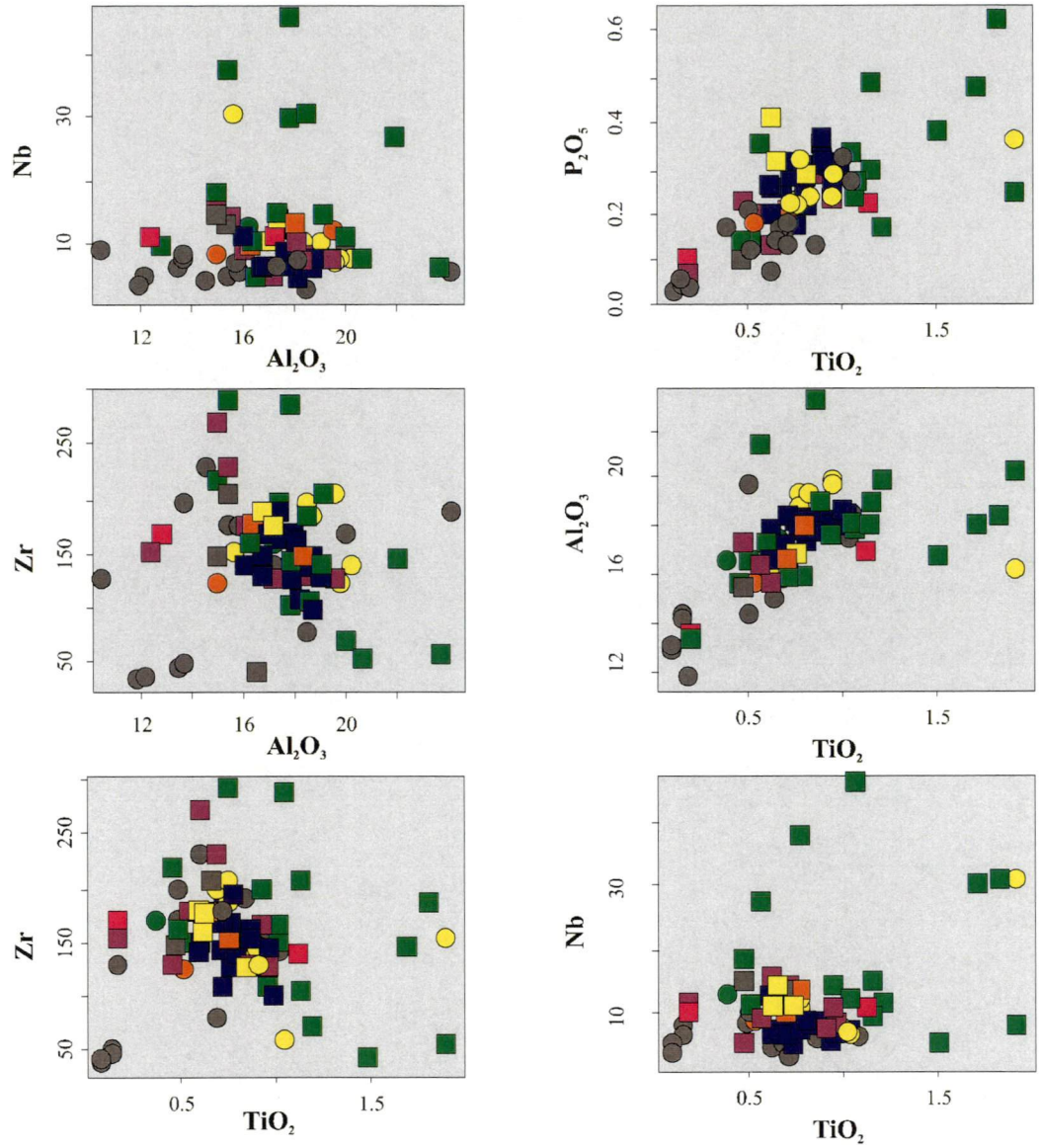

Figure 6.2 Variation of selected immobile elements for the igneous rock units exposed in La Escondida district. Samples from Richards et al. (2001) and this study.

similar behaviour, with concentrations increasing up to 73-75 wt% SiO_2, followed by depletions in more silicic rocks (Figure 6.6). Sr roughly decreases with CaO; whereas

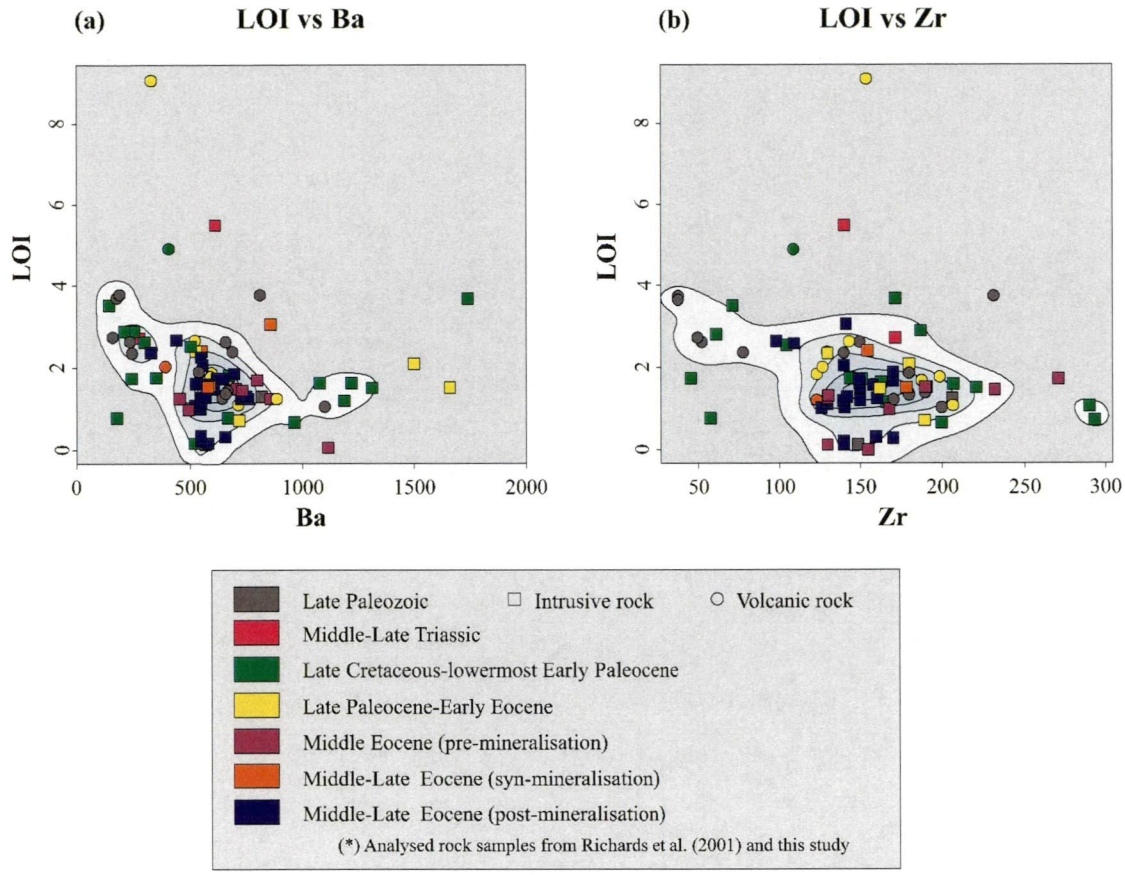

Figure 6.3 Plot of LOI versus (a) the mobile Ba and (b) the immobile Zr elements. Contours indicate sample distribution. Abbreviations: LOI = Lost by ignition.

Na_2O, K_2O and Rb are considerably scattered as result of secondary remobilisation. There is a distinct group of coarse-grained zircon-bearing rhyolites in La Tabla Formation that is restricted to the western volcanoclastic sub-unit *(Pzlt-a)* and to a determined stratigraphic level of the central volcano-sedimentary sub-unit. *(Pzlt-b)*. These zircon-bearing rhyolites are rich in Ba, Zr, La, Ce and ± Y compared to the fine-grained zircon-poor rhyolites of the central volcano-sedimentary sub-unit, which are depleted in these elements (Figure 6.6).

The less differentiated (SiO_2: 55-57 wt%), intermediate (SiO_2: 58-67 wt%), and evolved (SiO_2: 72-78 wt%) volcanic rocks of La Tabla Formation *(Pzlt)*, as well as a sample from the coeval dacite porphyry *(Pzda)*, are all marked by a typical spiky pattern on the primitive mantle-normalised trace element plot (Figures 6.7 and 6.8). There is enrichment in LILE (Cs, Ba, K, Rb and Sr) and U-group elements (U, Th and Pb), and significant troughs in the patterns defined by HFSE (i.e., Nb, P and Ti) and REE. However, the sharp LILE peaks observed in the intermediate rocks do not seem to be entirely magmatic in origin

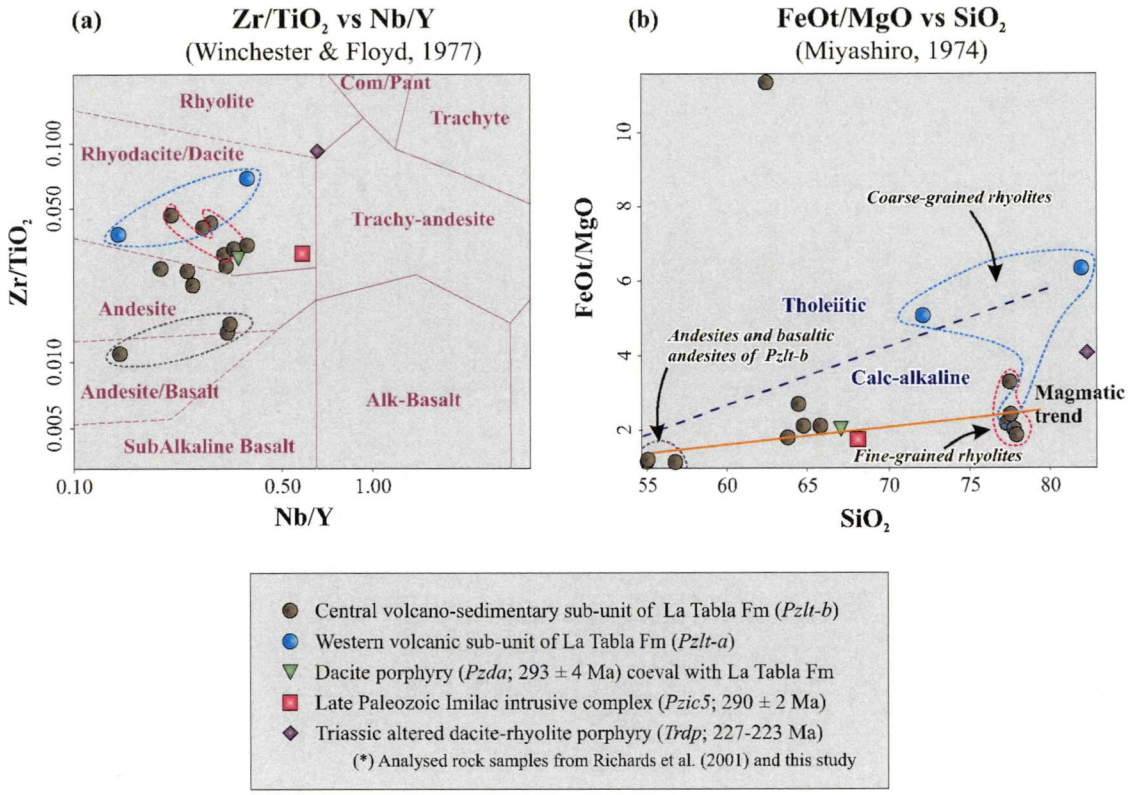

Figure 6.4 Classification diagrams of (a) Zr/TiO2 versus Nb/Y (Winchester and Floyd, 1977), and (b) FeO_t/MgO versus SiO_2 (Miyashiro, 1974) for Late Paleozoic-Triassic igneous rocks. Probable co-magmatism is indicated by magmatic trend line. Major elements data recalculated to 100% volatile-free. Abbreviations: Com = Comendite; Pan = Pantellerite; *Pzlt-b* = Central volcano-sedimentary sub-unit from La Tabla Formation.

(Figure 6.7b). They likely reflect minor secondary enrichment in these elements, as observed the feldspar alteration in the thin sections. The chondrite-normalized REE patterns have moderately steep slopes within the intermediate and silicic rocks being characterized by more pronounced upward concavity and a negative Eu anomaly (Figures 6.7 and 6.8). The sum of the REE increases 1.3 times in the silicic rocks compared to the basic rocks. La/Yb ratios and LREE fractionation also increase with increasing SiO_2 (Figures 6.7 and 6.8). The REE patterns for the coarse-grained zircon-bearing ignimbrites from the *Pzlt-a* and *Pzlt-b* are similar to the dacites and a common petrogenetic origin is inferred on the basis of the parallelism of the normalised element patterns. In contrast, the fine-grained zircon-poor ignimbrites from *Pzlt-b* have a flatter chondrite-normalised REE curve and an exceptionally strong negative Eu anomaly (Eu/Eu*: 0.19-0.25; Figure 6.8). Chondrite-normalised REE pattern for a sample from the dacite porphyry unit *(Pzda)*, which has been interpreted to be cogenetic with La Tabla Formation on the basis of field mapping and geochronology (Chapter 3), is similar to intermediate rocks from La Tabla Formation (Figure 6.7), and a common petrogenetic derivation is also proposed.

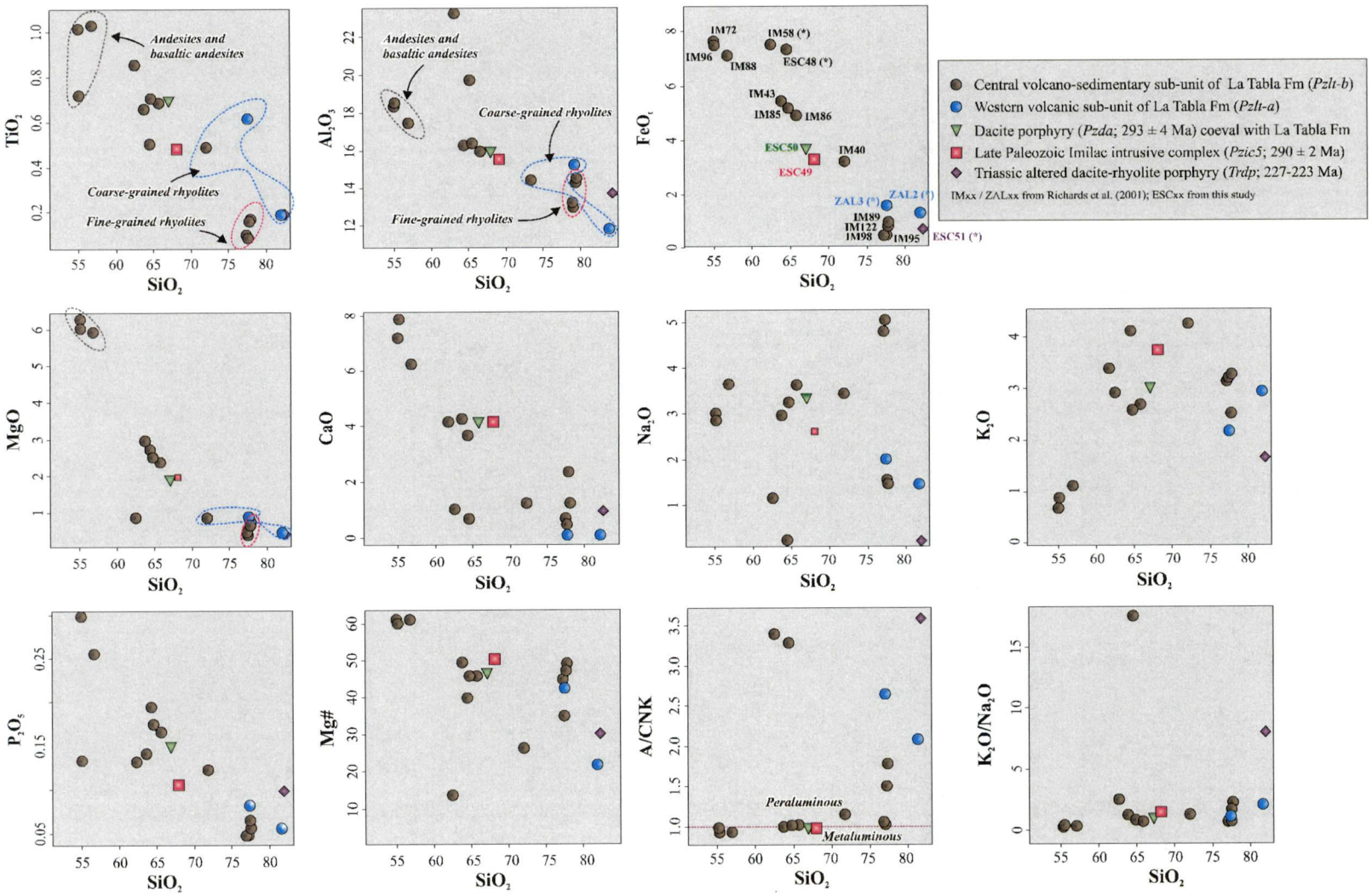

Figure 6.5 Variation of selected major elements (wt%) versus SiO_2 (wt%) for the Late Paleozoic-Triassic igneous rocks. Data recalculated to 100 wt% volatile-free.

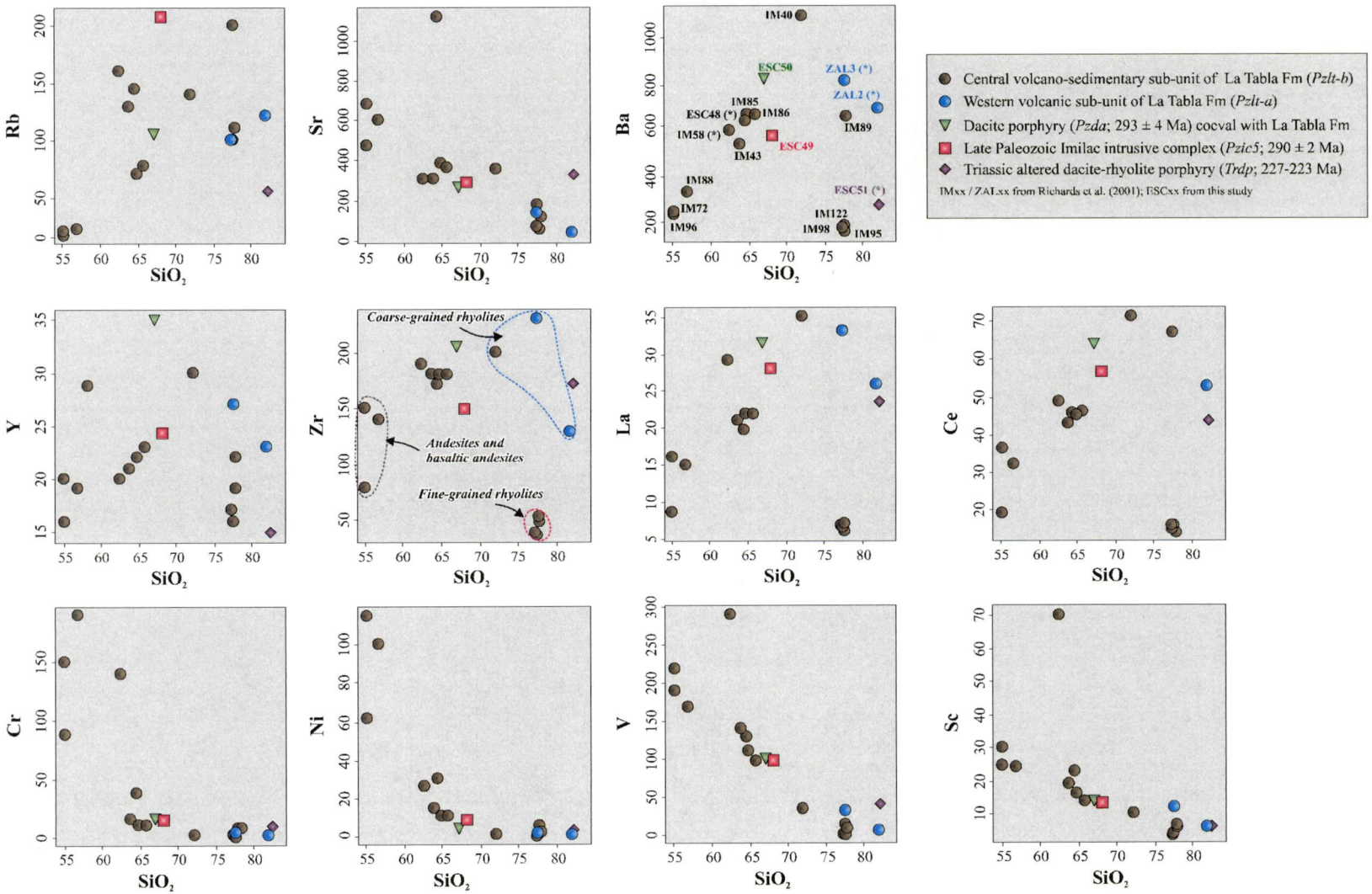

Figure 6.6 Variation of selected trace elements (ppm) versus SiO_2 (wt%) for the Late Paleozoic-Triassic igneous rocks.

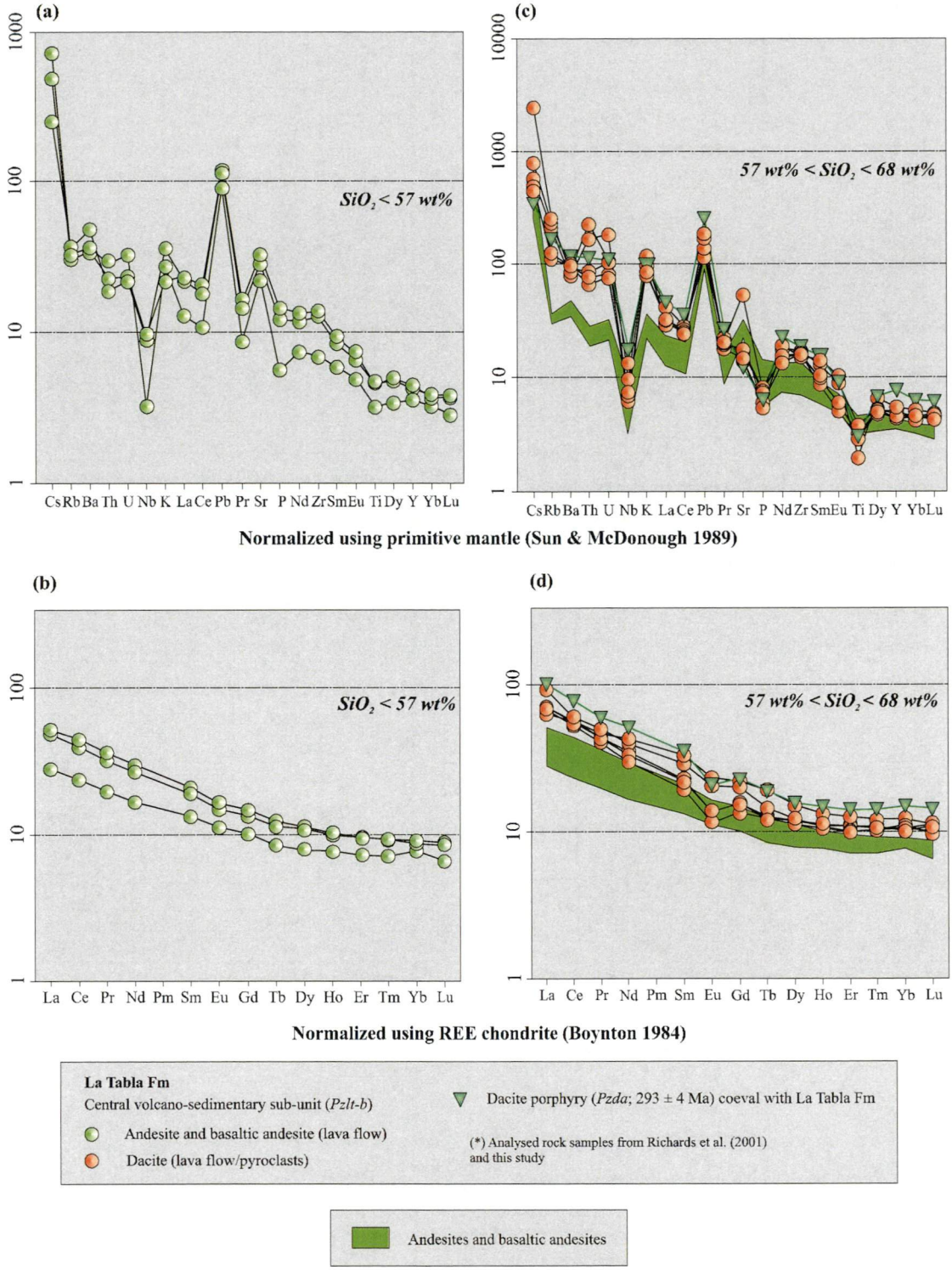

Figure 6.7 Primitive mantle-normalized trace elements (a, b) and chondrite-normalized REE (c, d) patterns for Late Paleozoic-Triassic mafic (SiO_2 < 57 wt%) and intermediate (57 wt% < SiO_2 <68 wt%) igneous rocks.

A monzonite from the Imilac plutonic complex *(Pzic)* has the major element chemistry of a slightly metaluminous I-series granodiorite using the criteria of Chappell and White (1974), with 68.1 wt% of SiO_2 and low Al_2O_3 (15.5 wt%). Their chondrite-normalized

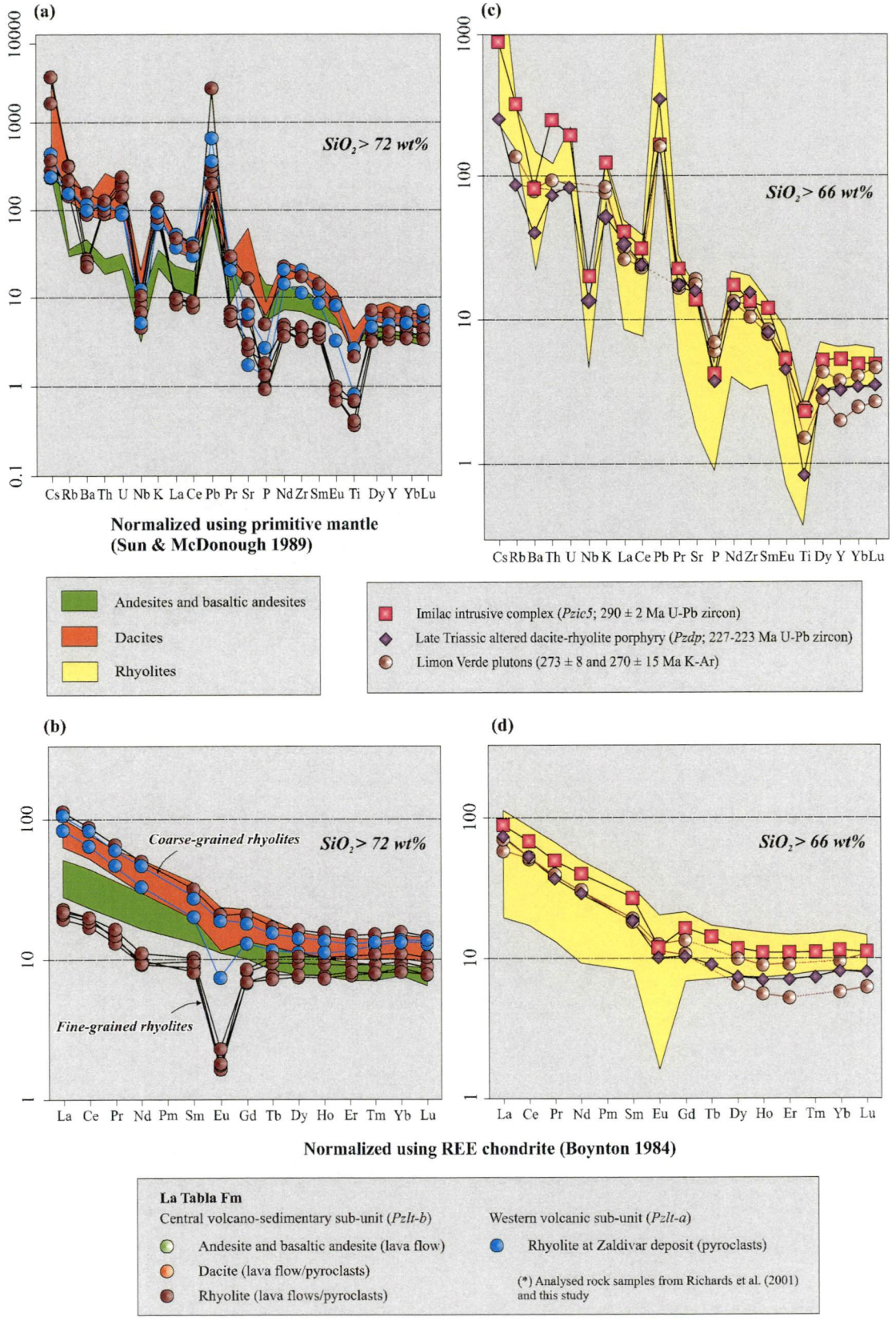

Figure 6.8 Primitive mantle-normalized trace elements (a, b) and chondrite-normalized REE (c, d) patterns for Late Paleozoic-Triassic felsic volcanic (SiO_2 > 72 wt%) and intrusive (SiO_2 > 66 wt%) rocks. Two Late Paleozoic granodiorite studied by Lucassen et al. (1999) from the Limón Verde region have been included for comparative purposes.

REE abundances overlap with the *Pzlt-a* ignimbrite field (Figures 6.8). There is also a parallelism in REE signatures between the Imilac granodiorite and the strongly altered rhyolite porphyry of the Middle-Late Triassic porphyry-style intrusions (Figure 6.8).

6.3.1.1 Discussion, Interpretation and Geodynamic Implication

The Late Paleozoic-Late Triassic volcanic and plutonic rocks all have calc-alkaline geochemical affinity (Richards et al., 2001; this study). Primitive- and chondrite-normalised elements patterns for basic to intermediate volcanic products suggest that fractionation of plagioclase, pyroxene, amphibole, opaque minerals and zircon can also explain the principal variations observed in the major and trace elements. The negative Eu anomalies observed in the plutonic and volcanic products have been usually considered to be indicative of plagioclase fractionation or retention of plagioclase in a garnet-free zone source regime due to preferential partitioning of Eu in that mineralogical phase (Rollinson, 1993; Richards et al., 2001; this study). This observation has been confirmed in the La/Sm versus Sm/Yb diagram (Kay and Kay, 1993; Kay et al., 1999; Figure 6.9d), which suggests that these magmas originated at relatively low pressure in the crust. The increase in La/Yb ratios (Figure 6.9a) and concave-upward MREE patterns indicate that amphibole fractionation played an important role during magmatic differentiation of fluid-rich (hydrous) parental magmas in the intermediate to silicic products. The most abundant ferromagnesian mineral phases are amphiboles, suggesting that the magmas were water-rich to stabilise this phase, likely due to slab dehydration (Pearce and Parkinson, 1993; Annen and Sparks, 2002).

The basaltic andesites and andesites (SiO_2 < 57 wt%) are the least fractionated rocks of La Tabla Formation. They represent magmas that have undergone fractionation and are not thought to be directly derived from primitive mantle-derived liquids, seeing their low Mg, Cr, Ni and V. The plotting of these less evolved rocks on the tectonic discrimination Th/Yb versus Nb/Yb diagram (Pearce and Peate, 1995) highlights a subduction zone signature and/or crustal contamination (Figure 6.9a). They have typical plate margin magmatic arc affinities, with enrichment of LILE and LREE and depletion of HFSE and HREE (i.e., Hawkesworth et al., 1993; Thirlwall et al., 1994). As occurs in modern lavas, the high ratios of Ba/La (>20) and Ba/Nb rations (>26), along with moderate to elevated Th/La (0.1-0.7) and Th/Nb (0.1-2.0), of more basic rocks from La Tabla Formation illustrate an important role for slab-derived fluid as source of mobile elements (Gill, 1981; Plank et al., 2002).

In Late Cenozoic Andean volcanism, Trumbull et al. (1999) have suggested that incompatible Ba/Zr and Th/Zr ratios are indicative of crustal contamination or assimilation of arc magmas because they are not affected by fractional crystallisation. The grade of contamination via fluid transport would result in variably elevated Ba/Zr at the same Th/Zr. In contrast, high Th/Zr associated with low values and a narrow range of Ba/Zr could be caused by a high degree of crustal assimilation. Following these criteria, the geochemical data for the Late Paleozoic rocks could indicate limited crustal contamination by fluid and/or by assimilation, considering the low ratios of Ba/Zr and Th/Zr ratios (Figure 6.9e). However, the available data set for the mafic rocks is very limited, and therefore limits the confidence that can be placed on this conclusion.

Another assessment of possible petrogenetic processes has been proposed by Nicolae and Saccani (2003) on the basis of Th/Nb ratios plotted against Zr concentrations (Figure 6.9f). These authors suggested that LILE/HFSE ratios will remain almost unaffected by fractional crystallisation, producing flat trends when plotted against an incompatible element that increases with fractionation. Basaltic andesites and andesites from La Tabla Formation are marked by similar Th/Nb ratios and are therefore diagnostic of fractional crystallisation as an important petrogenetic process.

The zircon-poor *Pzlt-b* ignimbrites are discriminated from the zircon-bearing *Pzlt-a* ignimbrites and other less evolved rocks of La Tabla Formation by lower contents of Ba, Zr, La, Ce and ± Y, and lower LREE/HREE ratios (Figures 6.6-6.9). A distinct crustal signature is suggested for the group of zircon-poor *Pzlt-b* ignimbrites, whereas the remaining mafic to silicic volcanic rocks seem to be linked by assimilation-fractional crystallisation (AFC, DePaolo, 1981).

The La Tabla Formation ignimbrites have relatively low La/Yb ratios (<15; Figure 6.9b). This is consistent with other Andean ignimbrite episodes, where low La/Yb ratios have been attributed to low pressure during the production of magma (Kay et al., 1999; Coira et al., 1999; Cornejo and Matthews, 2000; Cornejo and Matthews, 2001; Haschke et al., 2006). The La/Sm versus Sm/Yb diagram (Figure 6.9d) is currently considered to be a useful indicator of crustal thickness and residual mineral phases in the magma source region (Kay and Kay, 1993; Kay et al., 1999; Coira et al., 1999; Cornejo and Matthews, 2000). It is indicative of pyroxene (~30-35 km depth; Rapp and Watson, 1995) as the main residual mineral phase during the Late Paleozoic magmatism in La Escondida

district (Figure 6.9d).

Some silicic provinces, such as the Triassic-Jurassic Chon-Aiken silicic province in the Patagonia-Antarctic arc, are characterised by low Nb concentrations (<12 ppm) that are considered typical of rhyolites associated with a continental margin setting (Riley et al., 2001). In other large silicic volcanic episodes, higher Nb (~20 ppm) contents are typical of rhyolites erupted in a continental interior setting (Macdonald et al., 1992). La Tabla silicic rocks have low Nb contents (<13 ppm), consistent with a continental margin setting.

La Tabla Formation and contemporaneous granitoids are part of the Late Paleozoic El Choyoi silicic province (Kay et al., 1989; Chapter 2), which covers a vast region along the Chilean-Argentinean Andes (20°-26°S). The overall tectonic setting for this voluminous region of silicic magmatism is not clearly defined. Both continental crustal extension or proto-subduction at the Pacific margin of Gondwana have been proposed as alternative views (i.e., Mpodozis and Kay, 1990 and 1992; Breitkreuz and Zeil, 1994). For the plutonic components of El Choyoi province, Cornejo and Mpodozis (1996) documented flat REE patterns and low La/Yb (<13) in batholiths emplaced between 24° and 25°S. These authors argued for the absence of garnet as residual phase in the magma source coinciding with a thin crust. This interpretation is in agreement with the La/Yb and Sm/Yb ratios obtained in the Late Paleozoic-Triassic rocks exposed in La Escondida district (Figures 6.9b and d). The coexisting I-series tonalitic granitoids of arc signature and evolved rhyolitic porphyries of crustal affinity was also documented by Cornejo and Mpodozis (1996) in the Sierra Exploradora region, less than 200 km to the south from La Escondida district (Figure 4.1). This common occurrence of subduction-linked Late Paleozoic-Triassic granitoids and rhyolites associated with crustal extension was interpreted by these authors as signalling that the subduction signature for the period became indistinct to the north of 24°S, which coincides with the latitude of La Escondida district (24°15'S). Cornejo and Mpodozis (1996) inferred that the subduction changed northwards to a passive margin governed by an extensional tectonic regime (i.e., Maksaev, 1990; Lucassen et al., 1999a; Bahlburgh and Hervé, 2000). The enrichment of Rb, Th, U, Ta, Nb, Hf and Y and depletion in Ba,Sr, P, Zr and Ti, observed in normalised diagrams for the Late Paleozoic silicic rocks exposed in La Escondida district, attest to magmatism associated with subduction, in an arc system. The geochemical data for La Escondida district therefore do not support previous models for the tectonic transition from an

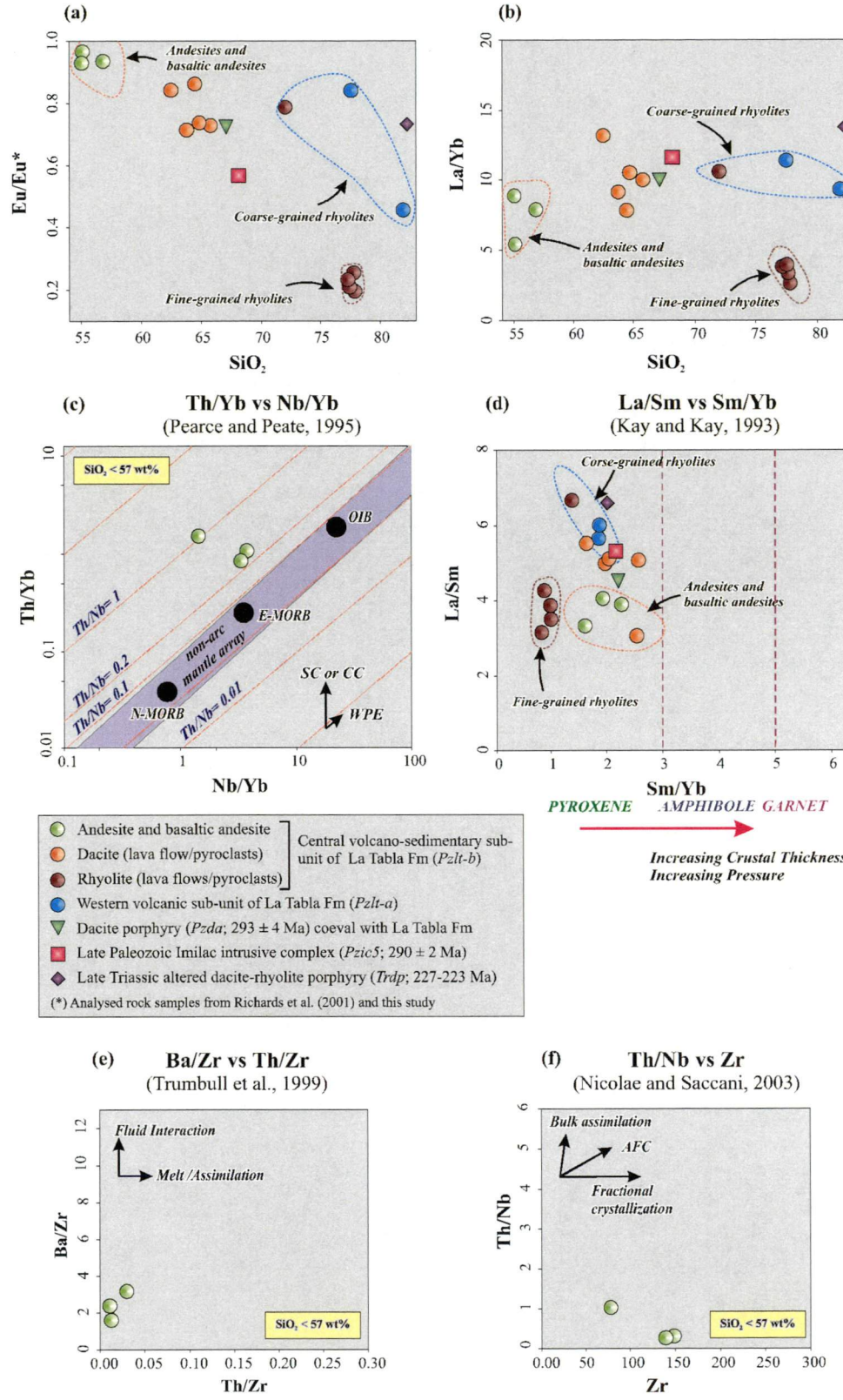

Figure 6.9 Geochemical discrimination diagrams of (a) E/Eu* versus SiO_2, (b) La/Yb versus SiO_2; (c) Th/Yb versus Nb/Yb (Pearce and Peate, 1995), (d) La/Sm versus Sm/Yb (Kay and Kay; 1993), (e) Ba/Zr versus Th/Zrb (Trumbull et al., 1999), and (f) Th/Nb versus Zr (Nicolae and Saccani, 2003) for the Late Paleozoic-Triassic igneous rocks. Abbreviation: N-MORB = Normal mid-oceanic ridge basalt; E-MORB = Enriched mid-oceanic ridge basalt; OIB = Oceanic island basalt; SC = Subducted crust; CC = Continental crust; WPE = Within plate; AFC = Assimilation and fractional crystallisation.

active plate boundary to a passive plate boundary at La Escondida latitude during the Late Paleozoic period. The hypothetical tectonic transition proposed by Cornejo and Mpodozis (1996) may be located further to north.

An isotopic study of the Late Paleozoic granitoids and the Early Paleozoic metamorphic basement completed by Lucassen et al. (1999a) in northern Chile, to the north of 24°S, included the Late Paleozoic intrusive rocks from the Limón Verde region. These rocks have similar geochemical signatures to the Imilac plutons from La Escondida district (Figure 6.8). This isotopic study has determined that all Late Paleozoic granitoids in northern Chile and northwestern Argentina were originated from crustal melting of Early Paleozoic felsic granulitic lower crust (Lucassen et al., 1999a; Figure 6.10). It is difficult to reconcile these isotopic data diagnostic of crustal melting with the clear subduction-linked geochemistry of La Tabla Formation volcanic rocks and coeval plutons (Saunders et al., 1980; Gill, 1981; Hawkesworth et al., 1993; Thirlwall et al., 1995; Richards et al., 2001; this study). However, it is possible that the geochemical results for all the Late Paleozoic igneous rocks from La Escondida district can be due to nature of source materials rather than the tectonic processes operating during magma emplacement (i.e., Arculus, 1987; Wilson, 1989; Thirlwall et al., 1993). The enormous volumes of silicic volcanism from La Tabla Formation and equivalent stratigraphic units in northern Chile (21°-25°S) must have involved crustal contamination and/or crustal melting associated with destructive plate margin (i.e., Mpodozis and Kay, 1990 and 1992; Breitkreuz and Zeil, 1994; Cornejo and Mpodozis, 1996; Richards et al, 2001; this study). A useful approach to appraise the grade of crustal contamination and/or crustal fusion in La Tabla Formation and granitoids magmatic suites involves investigating the occurrence of old crustal zircons inherited in these rocks as a signal of crustal assimilation. The data collected during the present geochronological study indicate minimal zircon inheritance of an older crust in the Late Carboniferous-Permian intrusive and volcanic rocks from La Escondida district (Appendix 5). In contrast, the Middle-Late Triassic dacite porphyry (*Trdp*) contains a significant amount of inherited zircons with ages range between 458 and 245 Ma (Late Ordovician to Early Triassic), but with a dominant population of zircon grains of ca. 260-300 Ma, (Appendix 5). Therefore, these Triassic magmas experienced contamination and/or interaction with an Early-Late Paleozoic upper crust.

A probable petrogenetic model for the Late Paleozoic La Tabla mafic and silicic magmatism has to incorporate a complex interaction of AFC (assimilation and fractional

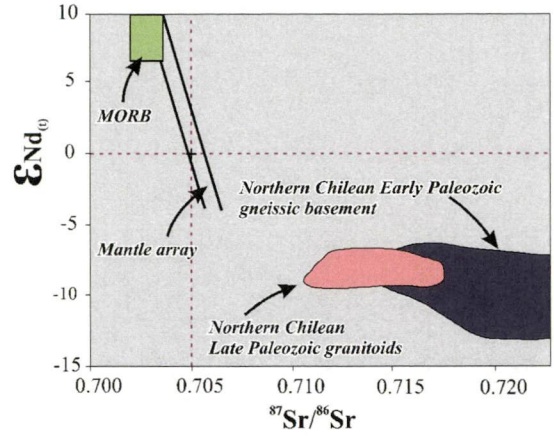

Figure 6.10 Summary of initial $^{87}Sr/^{86}Sr$ and E_{Nd} for Late Paleozoic granitoids and Early Paleozoic gneiss basement in northern Chile, but not including rock units from La Escondida district (adapted from Lucassen et al., 1999a). Abbreviations: MORB = Mid-oceanic ridge basalt.

crystallisation) or MASH (mixing, assimilation and homogenisation) of mafic magmas in the lower crust, crustal anatexis and hybridization (i.e., Riley et al., 2001; Caffe et al., 2002; Reagan, 2003). Annen and Sparks (2002) have proposed a petrogenetic model that includes: (1) the less differentiated products (basaltic andesites and andesites) derived by crystallization of hydrous, mantle wedge-derived basalt within a lower hot crustal zone (underplating in Zones I) in a volcanic arc, and accompanied by volumetrically lesser melting of crustal rocks; and (2) ascent and residence of hydrous andesitic magmas to shallow crustal levels (Zones II in upper crust) where they undergone extensive crystallization to form evolved volcano-feeding magma chambers and shallow plutons.

6.3.2 Andean Magmatism

The Andean magmatism in La Escondida district is divided herein into three main episodes, which were associated with two successive Late Cretaceous and Paleogene arcs (Chapters 2 and 3): (1) Late Cretaceous-lowermost early Paleocene (81-64 Ma) intrusions and subordinate intermediate volcanism; (2) late Paleocene-early Eocene (60-53 Ma) bimodal volcanism and associated intrusions of the Augusta Victoria Formation; and (3) a series of middle-late Eocene intrusions and volcaniclastic deposits of intermediate to silicic composition. The middle-late Eocene magmatic event is further subdivided into pre-, syn- and post-mineralisation events relative to the cluster of intrusions that host La Escondida and Escondida Norte-Zaldivar copper deposits (Chapters 3 and 5).

Immobile element plots can help to identify signatures in altered igneous rocks (i.e., McLennan, 1996). The variation of Nb and Ta against Zr plotted on Figures 6.11a to d

suggest the existence of two different magmatic trends during the Late Cretaceous-lowermost early Paleocene period: (1) the ca. 77-72 Ma Cerro Bayo plutonic complex *(LKcb)*; and (2) the ca. 70-66 Ma Las Torres igneous complex *(LKlt)* and 67-64 Ma Sombrero plutonic complex *(Tpsb)* units. The 81-79 Ma Torcaza pluton *(LKtp)* appears to have similar compositions to the Sombrero complex and presumably Las Torres igneous complex (Figures 6.11a and b). Younger rocks cannot be divided into separate magmatic suites on Figures 6.11c to e. The data show a decreasing trend in La/Yb, Nb/Zr and Ta/Zr ratios from the Late Cretaceous to late Eocene rock units.

6.3.2.1 Late Cretaceous-lowermost Early Paleocene Magmatism

The Cerro Bayo plutonic complex *(LKcb)* samples define an array extending across the gabbro, syenite and diorite, to granodiorite fields on the diagram of Cox et al (1989) for intrusive rocks (Figure 6.12a). Most of the samples plot on a tholeiitic trend on the FeO_t/MgO versus SiO_2 diagram (Figure 6.12b), although some scattering is caused by alteration. Samples from the Torcaza, Las Torres and Sombrero plutonic complexes have compositions that range from calc-alkaline gabbro and syenite to granite on Figure 6.12a and b, respectively. The occurrence of magnetite and phenocrysts of amphibole, pyroxene, biotite and plagioclase, along with their high Fe_2O_3/FeO ratios (0.5-2.9), indicate that these rocks are metaluminous I-type rocks (Chappell and White, 1994).

Major elements (TiO_2, Al_2O_3, Fe_2O_3, FeO, MgO and CaO) decrease with increasing SiO_2 (Figure 6.13). Na_2O correlates roughly with increasing SiO_2, whereas P_2O_5 is strongly scattered. Rb and Ba abundances correlate positively with K_2O as does Sr with CaO (Figures 6.13 and 6.14). Immobile and incompatible HFSE (i.e., Zr, Nb, Ta and Y) and LREE (La and Ce) are dispersed, but generally have higher concentrations in rock of intermediate compositions (63-65 wt% SiO_2) and lower abundances in more felsic samples (Figure 6.14). The normalized arrays for all rock compositions are roughly similar (Figures 6.15a and c), with peaks of LILE and U-series elements relative to depleted REE and HFSE, with respective troughs of Nb, P, Zr, Ti and La. Secondary enrichment of LILE has produced a diffused peak for K_2O in Torcaza and Las Torres samples (Figure 6.13). This is supported by petrographic observation that indicates alteration of feldspars to a sericite-calcite-albite association. On chondrite-normalised diagrams of Figures 6.15b and d, there is a slightly more pronounced upward concavity of MREE in the Sombrero and Las Torres suites (SiO_2: < 68 wt%), compared to the less evolved rocks of Cerro Bayo and Torcaza suites (SiO_2: < 63 wt%). The more fractionated character of Sombrero

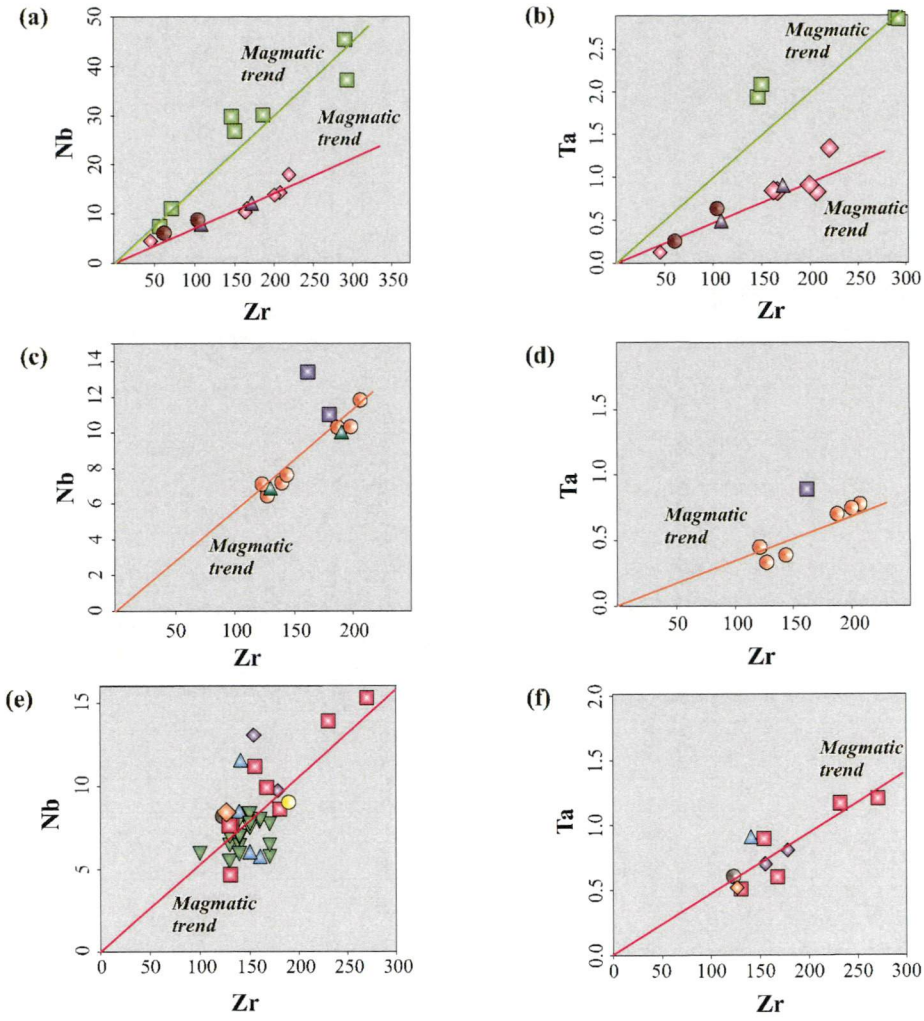

Late Cretaceous-lowermost Early Paleocene

- Cerro Bayo plutonic complex (*LKcb*; ~77-72 Ma U-Pb and ^{40}Ar-^{39}Ar)
- Torcaza pluton (*LKtp*; ~81-79 Ma U-Pb)
- Sombrero plutonic complex (*Tpsb*; ~67-64 Ma U-Pb)
- Las Torres igneous complex (*LKlt*; ~70-66 Ma)

(*) Analysed rock samples from Richards et al. (2001) and this study

Late Paleocene-Early Eocene

- Augusta Victoria Fm (*PEav*; ~57-53 Ma U-Pb zircon)
- Amphibole-phyric andesite (*Pan*; 60.7 ± 0.61 Ma U-Pb zircon)
- Diorite dyke and sill (*PEdi*) coeval with Augusta Victoria Fm.

(*) Analysed rock samples from Richards et al. (2001) and this study

Middle-Late Eocene

- Cerro Rincones Plutonic Complex (*Eocr*; ~43-41 Ma U-Pb and K-Ar) → ***Pre-mineralisation***
- Capella stocks (*MEcs*; ~39 Ma U-Pb)
- Diorite-microdiorite (*MEdi*; 38.3 ± 0.9 Ma ^{40}Ar-^{39}Ar)
- San Carlos strata (*Eosc;* ~38-36 Ma U-Pb)

→ ***Syn-mineralisation***

- Diorite-andesite of Richards et al. (2001) (*Tdi*; ~38-37 Ma ^{40}Ar-^{39}Ar)
- Andesite-diorite porphyry (*Leap*; ~38-36 Ma U-Pb and K-Ar)
- Andesite porphyry (*LEpap*; 36.5 ± 0.5 Ma ^{39}Ar-^{40}Ar)

→ ***Post-mineralisation***

(*) Analysed rock samples from Richards et al. (2001) and this study

Figure 6.11 Plots of Nb and Ta versus Zr for the Late Cretaceous to Eocene igneous rocks (adapted from McLennan, 1996). Probable co-magmatism is indicated by the magmatic trend line. Notice that Ta was not analysed in some samples.

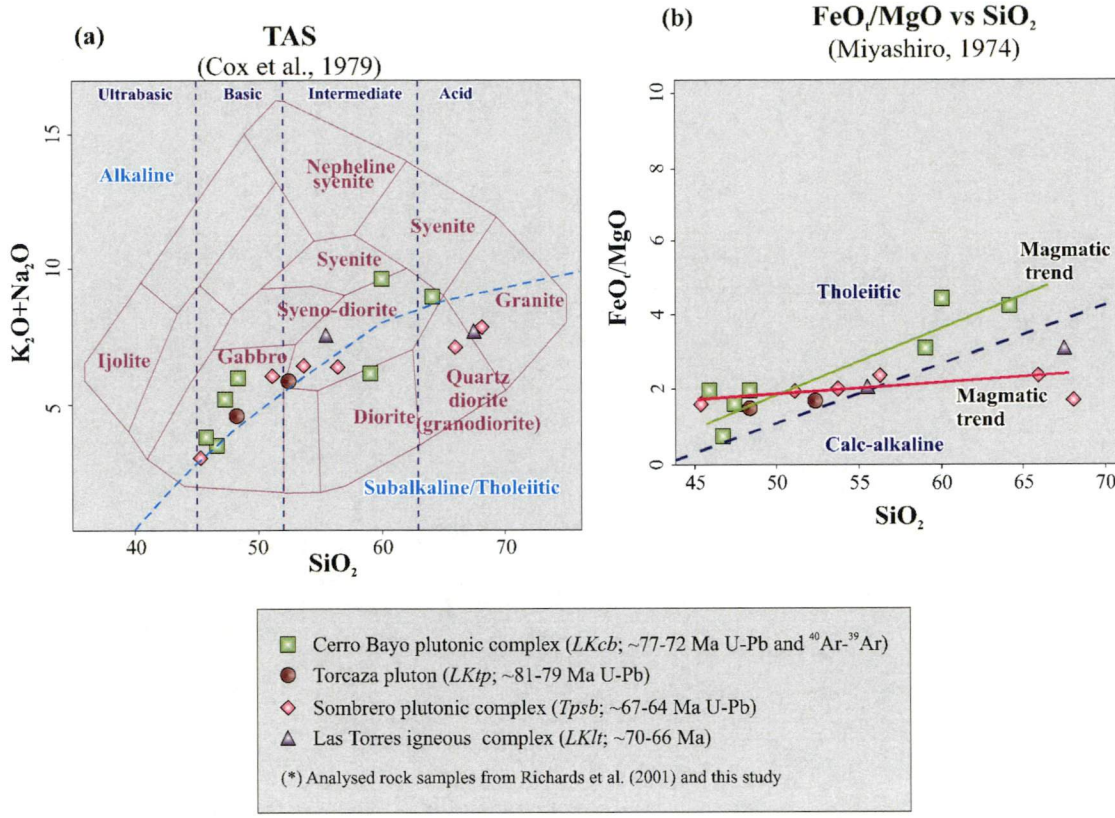

Figure 6.12 Geochemical discrimination diagrams (a) TAS (Cox et al., 1979); and (b) FeO_t/MgO versus SiO_2 (Miyashiro, 1974), showing igneous rocks of Late Cretaceous-lowermost early Paleocene age from La Escondida district. Notice the anomalous samples due to the hydrothermal alteration and minor low-grade metamorphism. Major elements data recalculated to 100% volatile-free.

and Las Torres suites is also expressed by higher LILE, HFSE, total REE contents. The Eu/Eu* anomalies are positive in Cerro Bayo and Torcaza plutons; whereas Sombrero and Las Torres samples have negative Eu/Eu* anomalies (Figure 6.16a). La/Yb ratios nearly overlap between Sombrero and Las Torres igneous complexes and Cerro Bayo and Torcaza plutons (Figure 6.16b).

The tholeiitic Cerro Bayo plutonic complex ranges in composition from gabbros to monzogranites and rhyolite porphyries, and a common evolution from differentiated magmas is inferred on the basis of low compatible HFSE abundances (eg., Ni, Cr, V and Sc). The mafic rocks have geochemical and petrographic evidence for plagioclase accumulation in the early stages of crystallisation, specifically the increasingly positive Eu anomalies with increase SiO_2 contents (Figure 6.16a). The lack of significant negative Eu anomalies, even in some of the more evolved samples, can be indicative of high oxygen fugacities (Cornejo and Matthews, 2000; Caffe et al., 2002).

The calc-alkaline Las Torres and Sombrero magmas would have experienced plagioclase and amphibole fractionation, based on their negative Eu anomalies and depleted MREE patterns, as well as by the increasing La/Yb ratios with SiO_2. There are notable differences between the Cerro Bayo plutonic complex and Sombrero and Las Torres igneous complexes on the Th/Yb versus Nb/Yb diagram, with within-plate- and/or upper crust-type or enriched mantle magmas sources suggested for Cerro Bayo complex, whereas both other units have slab subduction calc-alkaline affinities (Figures 6.16c and e).

The less evolved rocks of the Cerro Bayo intrusive complex have unusually elevated Nb and lesser Ti concentrations compared with other igneous suites. The immobile nature of Nb (HFSE element) precludes enrichment by slab-derived fluids (i.e., Hawkesworth et al., 1993; Pearce and Peate, 1995). Nb contribution from slab-melt to a modified mantle wedge has been proposed for adakite/TTG-like magmas with Nb anomalies, along the northern-central Andes Cordillera and elsewhere (Bourdon et al., 2003; Krammer et al., 2005; Zhang et al., 2005). However, adakitic signature for the Nb-bearing Cerro Bayo samples has been defined only by two samples on the Sr/Y versus Y discrimination diagram (Defant and Drummond, 1990; Figure 6.16f), and which have low concentrations of Al_2O_3 (< 15 wt%), MgO, Cr and Ni. Furthermore, the association of adakite/TTG-like rocks with slab melts contribution in arc-related magmas has been questioned recently by Coldwell et al. (2005) and Richards and Kerrich (2007). At the present, there is no other simple explanation for Nb addition to magmatic arcs than slab melts that have sank and mixed with metasomatised mantle peridotite to generate magma by partial melting (Bourdon et al., 2003; Krammer et al., 2005). High Nb abundances in alkaline basalts of Central America Cenozoic volcanic arcs have been explained as the result of residual rutile stabilized by a large ion lithophile element bearing slab-derived fluid in a heterogenous mantle (Reagan and Gill, 1989), but these petrological matters are beyond of the scope of the present thesis.

The La/Sm versus Sm/Yb plots for the Cretaceous-lowermost early Paleocene units are compatible with magma derivation in a pyroxene- to amphibole-stable regime of the lower crust (Kay and Kay, 1993; Kay et al., 1999; 6.16d), which is dominant at depths of about 40 km (Rapp and Watson, 1995). Therefore, these data do not suggest important pressure changes and/or high water concentration conditions for magma sources associated with the Cretaceous-lowermost early Paleocene igneous events.

Plots of petrogenetically important HFSE and LILE elements (i.e., Th, Nb, Zr, Ba and Y) for the less evolved rocks are presented on Figures 6.17a and b. Low and narrow Th/Nb (< 0.5) ratios across mafic components (increasing Zr abundance) suggest that fractional crystallization of magmas played an important role during the petrogenetic evolution of the Late Cretaceous igneous suites (*cf.* Nicolaes and Sacanni, 2003; Figure 6.17a). The high LILE (e.g., Ba, Rb, Cs) abundances in calc-alkaline volcanic rocks have been normally attributed to participation of slab-derived components (Hawkesworth et al., 1993; Pearce and Pearce, 1995). By contrast, HFSE (i.e., Nb, Ta) are not mobilised via hydrous fluid (deshydratation) into the mantle wedge (Hawkesworth et al., 1993; Pearce and Pearce, 1995). The Ba/Y versus Nb/Y diagram (Figure 6.17b) has been proposed by Nicolae and Saccani, (2003) to evaluate possible enrichment trend related to slab-derived hydrous fluids (high LILE/HFSE) or melt-derived processes. The analyses of the tholeiitic Cerro Bayo rocks do not provide evidence for a slab-derived fluid contribution (Figure 6.17b). On the contrary, the sample array suggests a pattern compatible with melting enrichment. Variations of Ba/Y, Nb/Zr and Ba/Zr ratios have also reinforced a major participation of slab fluids in magmas that sourced the Sombrero plutonic event (Figures 6.17a and b).

The mafic to intermediate rocks of the Cerro Bayo plutonic complex have OIB-type continental basalt to back-arc and/or within-plate alkaline compositions on diverse geotectonic discrimination diagrams (Figures 6.18a to d). In contrast, the mafic rocks of the Torcaza, Las Torres and Sombrero plutonic complexes are consistent with calc-alkaline basalts from a magmatic arc zone (Figures 18a to d). A back-arc and arc realm inferred for the Late Cretaceous magmatism along the main part of northern Chile remains poorly understood. However, the Late Cretaceous plutons of El Salvador-Petrerillos region (26°S) have been considered magmatic arc calc-alkaline suites (Cornejo and Matthews, 2000; Cornejo Matthews, 2001). They have intruded a 2000 m thick effusive counterpart of basaltic andesite to rhyolitic ignimbrite flows, with a geochemical signature transitional between calc-alkaline and intra-plate volcanism (Cornejo et al., 1999; Cornejo and Matthews, 2001). The Late Cretaceous plutons of El Salvador-Petrerillos differ from the Late Cretaceous intrusive rocks of La Escondida districts in their low Zr (< 100 ppm) and Nb (< 5 ppm) abundances (Cornejo and Matthews, 2000). To the north of La Escondida region, the Late Cretaceous Cerro Colorado shoshonitic intrusive complex is considered to be a typical magmatic arc granitoids, with elevated Sr (>1000 ppm), Al_2O_3 (>20 wt%) and moderate Zr (50-270 ppm) contents (Kojima et al., 2005). No Nb concentrations have been determined for these intrusions, but their isotopic

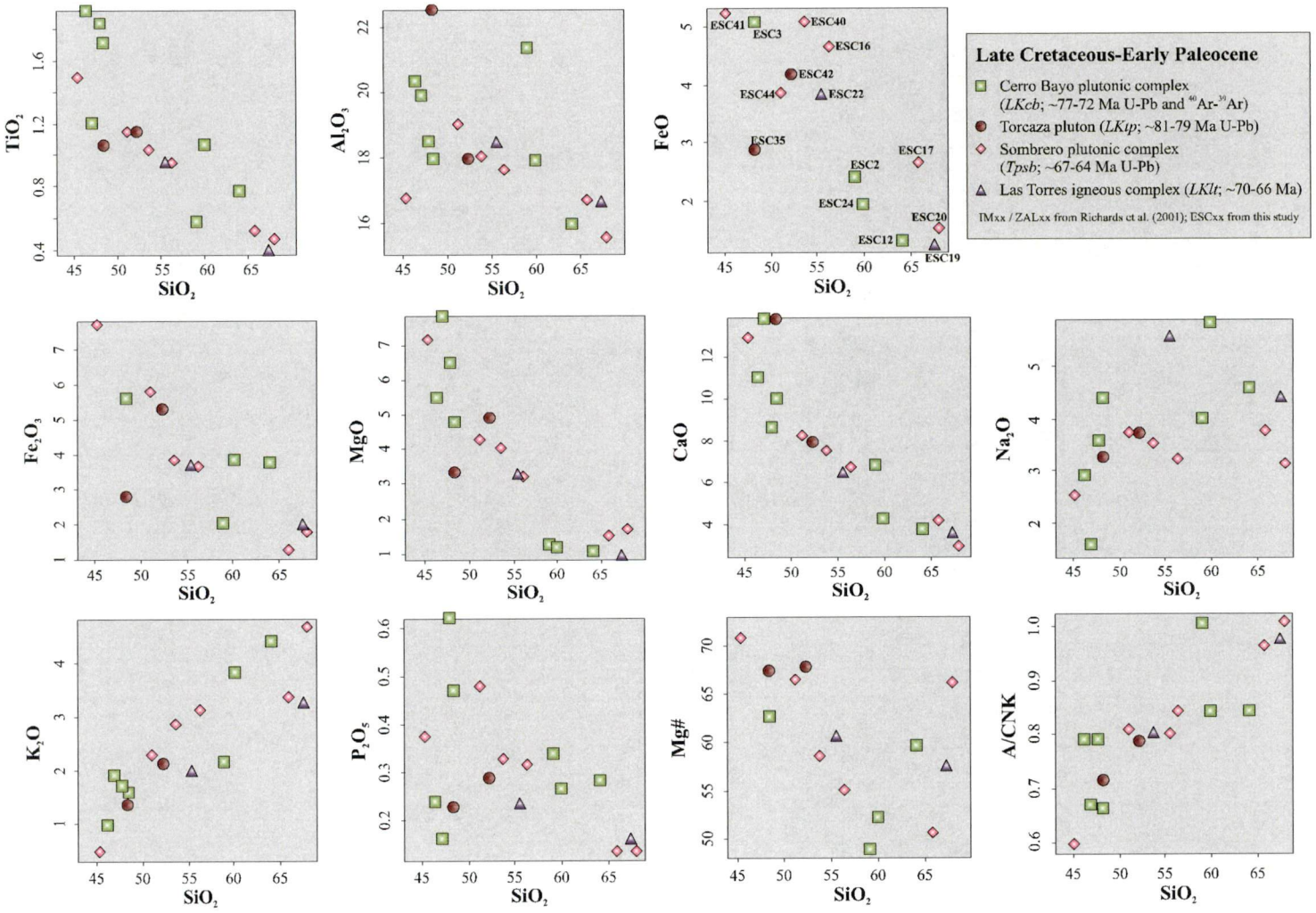

Figure 6.13 Variation of selected major elements (wt%) versus SiO_2 (wt%) for the Late Cretaceous-lowermost early Paleocene igneous rocks. Data recalculated to 100% volatile-free.

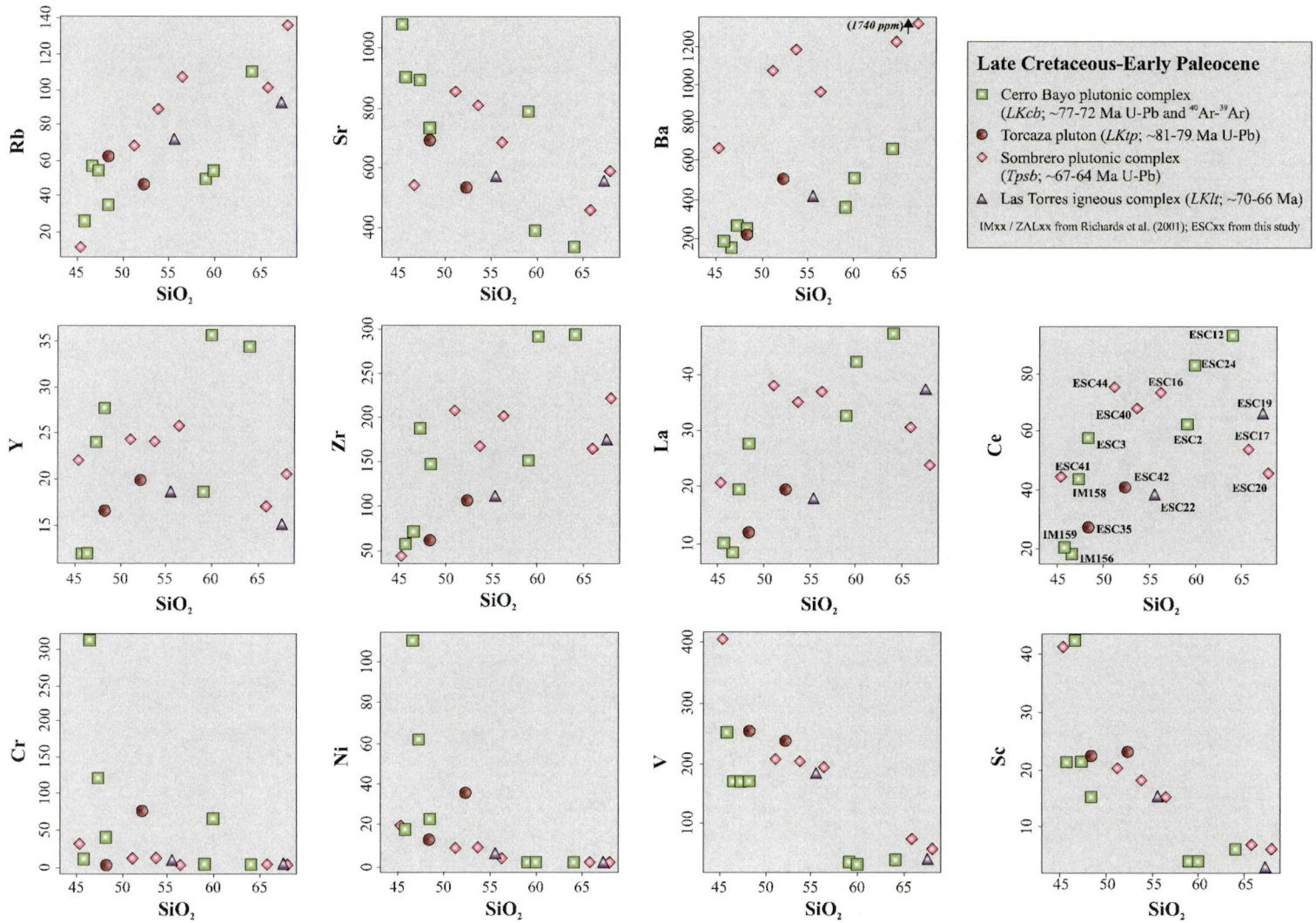

Figure 6.14 Variation of selected trace elements (ppm) versus SiO_2 (wt%) for the Late Cretaceous-lowermost early Paleocene igneous rocks.

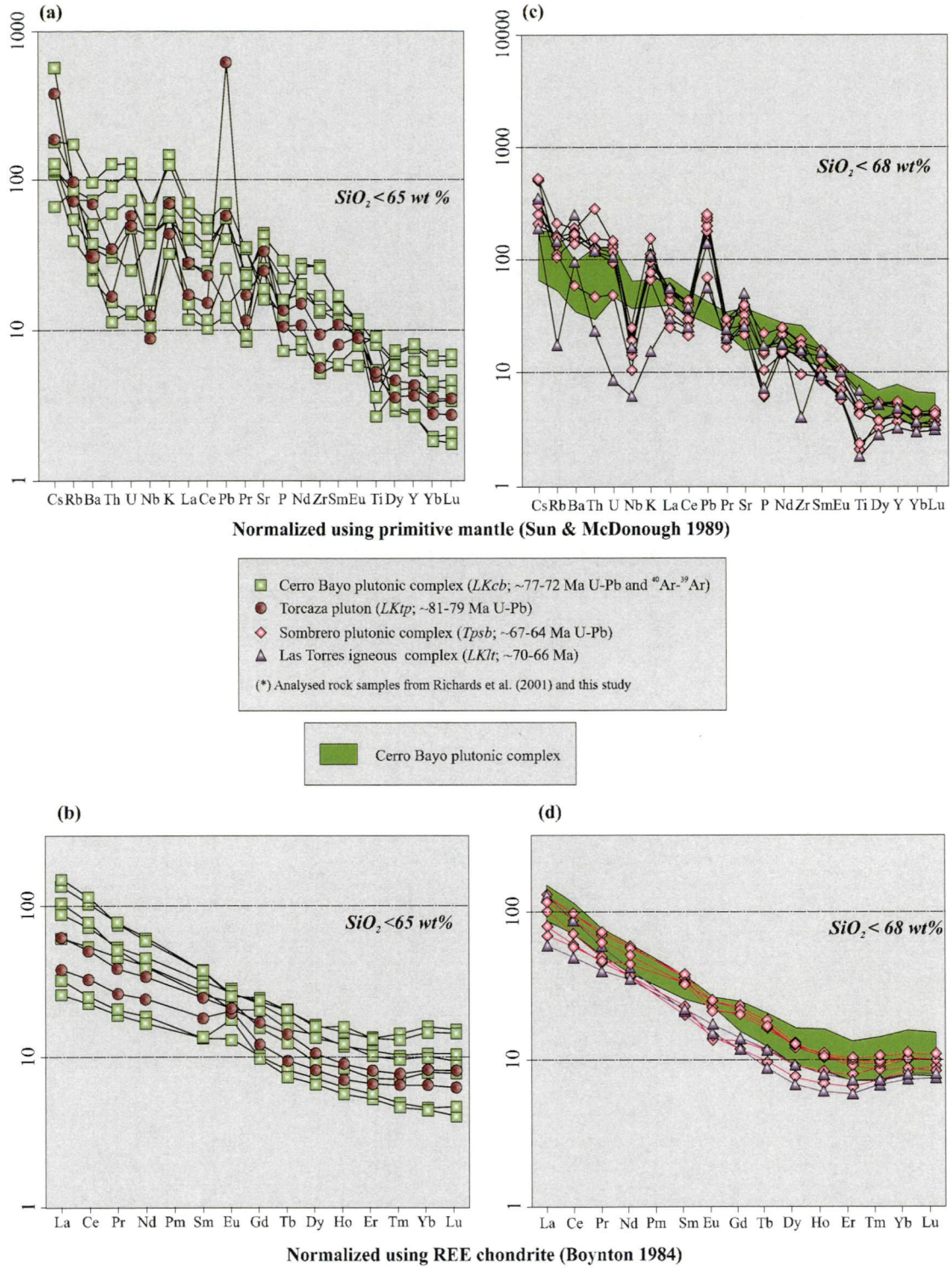

Figure 6.15 Primitive mantle-normalized trace elements (a, c) and chondrite-normalized REE patterns (b, d) for the Late Cretaceous-lowermost early Paleocene igneous rocks.

compositions are consistent with crustal derivation (Rogers and Hawkesworth, 1989). In contrast, in the Salar de Atacama region, the Late Cretaceous Cerro Quimal alkaline gabbros and diorites (Figure 3.24) and La Totola alkaline lavas are interpreted to have formed in a back-arc setting. A poorly depleted mantle origin is suggested for the Cerro

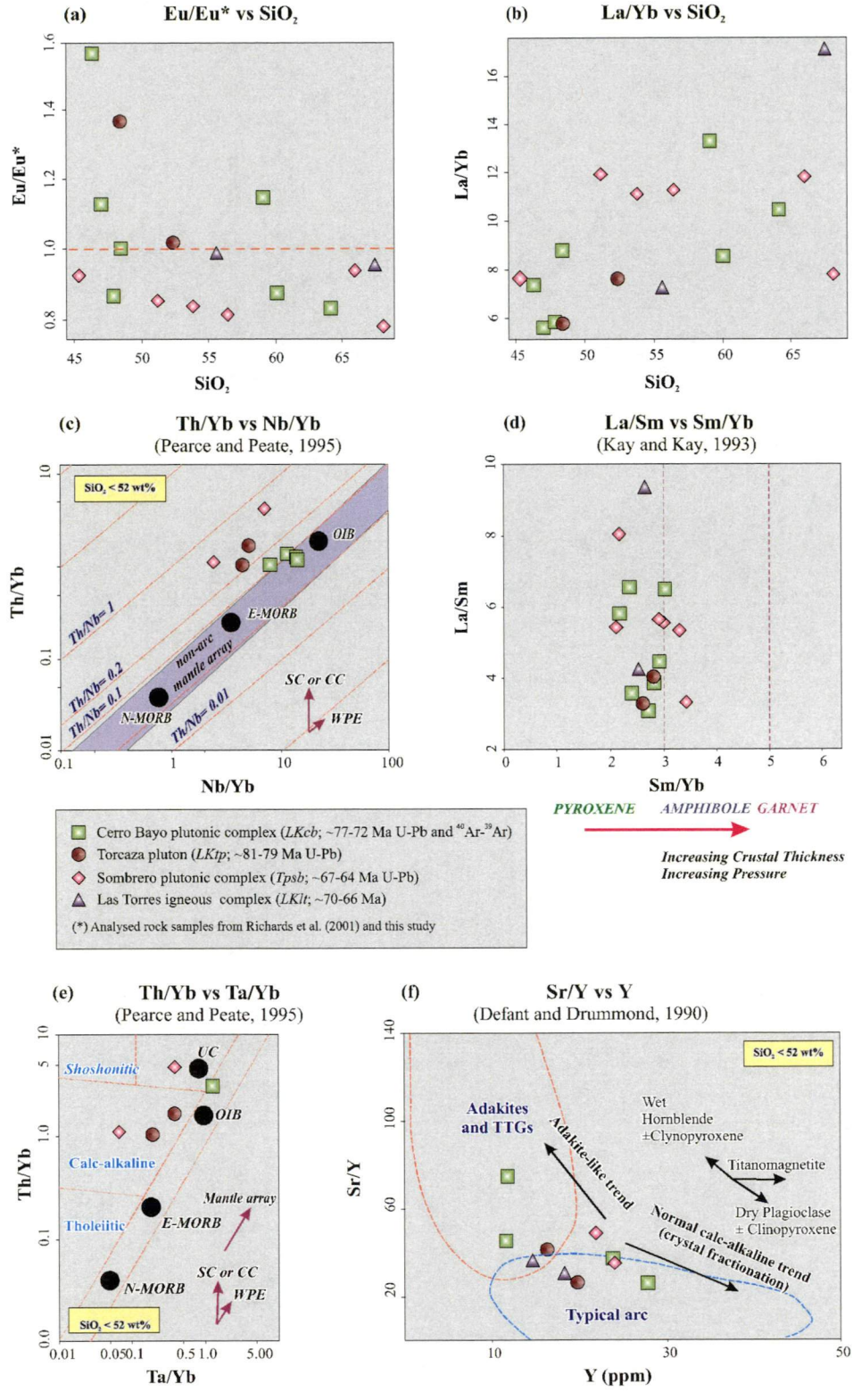

Figure 6.16 Geochemical discrimination diagrams of (a) Eu/Eu* versus SiO_2, (b) La/Yb versus SiO_2, (c) Th/Yb versus Nb/Yb (Pearce and Peate, 1995), (d) La/Sm versus Sm/Yb (Kay and Kay; 1993), (e) Th/Yb versus Ta/Yb (Pearce and Peate, 1995), and (f) Sr/Y versus Y (Defant and Drummond, 1990) for Late Cretaceous-lowermost early Paleocene igneous rocks. Abbreviations: N-MORB = Normal mid-oceanic ridge basalt; E-MORB = Enriched mid-oceanic ridge basalt; OIB = Oceanic island basalt; SC = Subducted crust; CC = Continental crust; WPE = Within plate; AFC = Assimilation and fractional crystallisation; TTGs = Tonalite, trodhjemite and granodiorite.

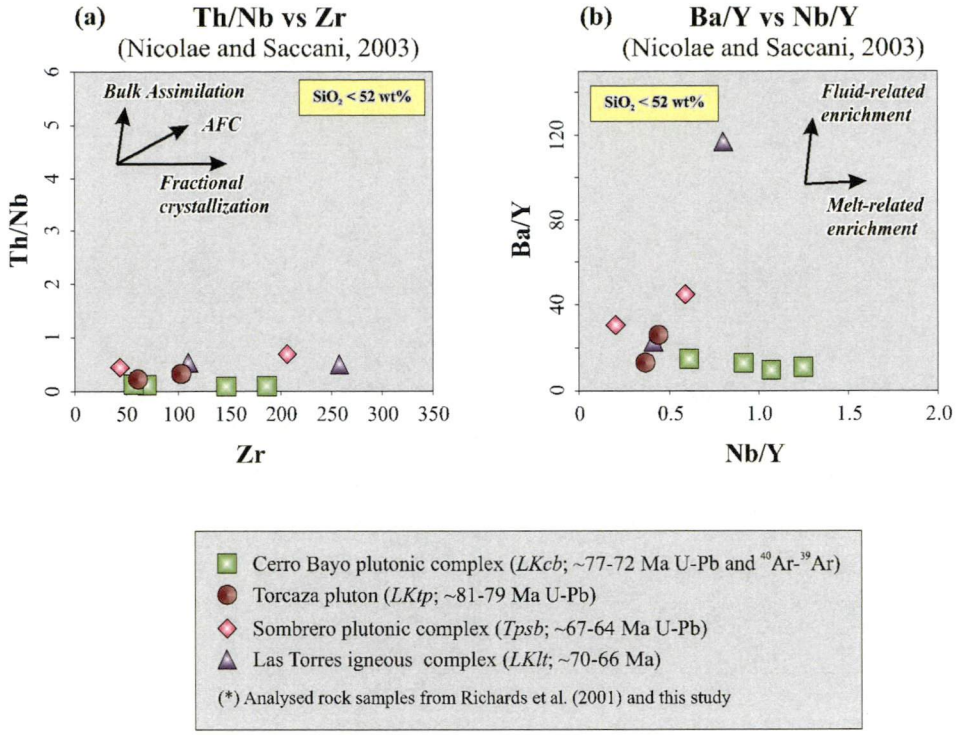

Figure 6.17 Geochemical discrimination diagrams of (a) Th/Nb versus Zr (Nicolae and Saccani, 2003) and (b) Ba/Y versus Nb/Y (Nicolae and Saccani, 2003) for the Late Cretaceous-lowermost early Paleocene igneous rocks. Abbreviations: AFC = assimilation and fractional crystallisation.

Quimal unit by their Sr and Nd isotopic compositions on Figure 6.19 (Haschke, 2002; Mpodozis et al., 2005). In consequence, a back-arc/arc tectonic environment appears to be well established for part of the Late Cretaceous magmatic centres along the Domeyko cordillera. But, their westward boundary with the Late Cretaceous arc front, which contained a series intra-arc volcanotectonic basins (i.e., Quebrada Mala and Llanta Formations; Marinovic et al., 1999; Cornejo and Matthews, 2001; Mpodozis et al., 2005), remains partially documented (Chapter 3; Figure 3.24).

Available Sr and Nd isotopic studies for Cretaceous igneous rocks in northern Chile are presented in Figure 6.19. They suggest a slightly depleted mantle origin for extrusive and intrusive rocks exposed to the north of 24°S (Rogers and Hawkesworth, 1989; Lucassen et al., 1999a; Haschke, 2002; Haschke et al., 2006). The only evidence for crustal assimilation and/or contamination of Late Cretaceous magmas in La Escondida district has been provided by the ca. 300-260 Ma (Late Carboniferous-Early Permian) older zircon grains found in andesites and monzodiorite from Las Torres and Sombrero igneous complex, respectively (Appendix 5). Zircons from the earlier Cerro Bayo and Torcaza units, in contrast, do not have older cores, suggesting that their magmas

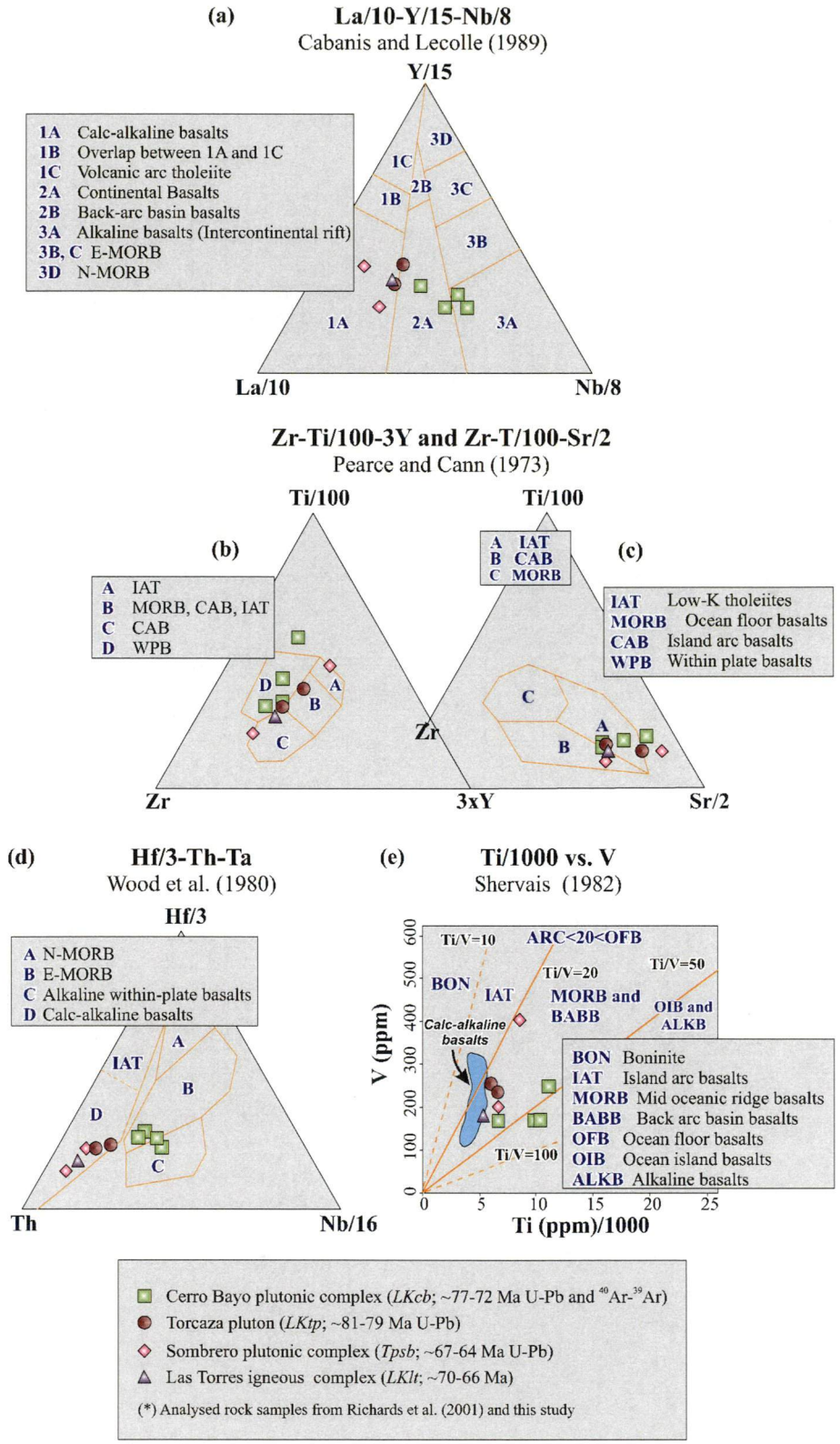

Figure 6.18 Tectonic discrimination diagrams of (a) La/10-Y/15-Nb/8 (Cabanis and Lecolle, 1989), (b) Zr-Ti/100-3Y, (c) Zr-T/100-Sr/2 (Pearce and Cann, 1973), (d) Th-Hf/3-Ta (Wood et al., 1980) and (e) V versus Ti/1000 (Shervais, 1992), for mafic rocks of the Late Cretaceous-lowermost early Paleocene igneous event. Abbreviations: N-MORB = Normal mid-oceanic ridge basalt; E-MORB = Enriched mid-oceanic ridge basalt; OIB = Oceanic island basalt; SC = Subducted crust; CC = Continental crust; WPE = Within plate; AFC = Assimilation and fractional crystallisation.

did not undergo any degree of crustal contamination (Appendix 5). There is a notable coincidence between inherited zircons and crustal contamination suggested by trace element geochemistry (high Th/Nb in Figure 6.17a) in Las Torres and Sombrero igneous complexes, as well as non-inherited zircon and reduced contamination (low Th/Nb ratios in Figure 6.17a) for Cerro Bayo and Torcaza igneous rocks. Note also that for samples that lack inherited zircons, it is not possible to exclude crustal contamination (R. Tosdal, written comm., 2008).

The available geochemical information for the Late Cretaceous-lowermost early Paleocene magmatism in La Escondida district outline the passage from the tholeiitic Cerro Bayo and calc-alkaline Torcaza plutonic episode, which occurred in a transitional/back-arc at ca. 81-72 Ma, to the calc-alkaline Sombrero and Las Torres intrusive and volcanic event of arc affinity that occurred between 70 and 64 Ma.

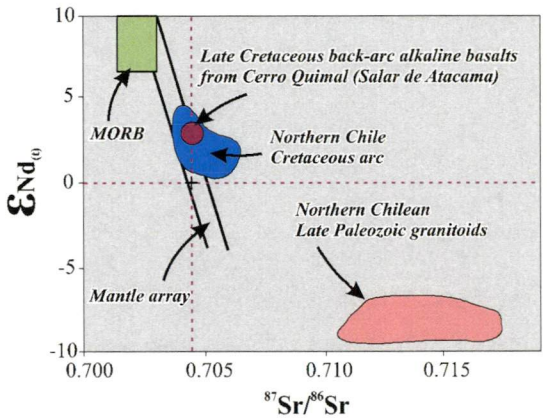

Figure 6.19 Summary of initial $^{87}Sr/^{86}Sr$ and E_{Nd} for Cretaceous igneous rocks in northern Chile ((adopted from Rogers and Hawkersworth, 1989; Lucassen et al., 1999a; Haschke, 2002; Kramer et al., 2005). Abbreviations: MORB = Mid-oceanic ridge basalt.

6.3.2.2 Late Paleocene-Early Eocene Magmatism

The late Paleocene-early Eocene Augusta Victoria Formation and associated intrusive rocks range from basaltic andesite and trachy-andesites to rhyodacite/dacite, and have calc-alkaline compositions (Figures 6.20a and b). In terms of their K_2O and SiO_2 concentrations, most of the samples belong to the medium-K or high-K calc-alkaline series (Figure 6.20c).

Major and trace element variations plots show regular decreasing patterns for TiO_2, Al_2O_3, FeO_t, MgO and CaO with increasing SiO_2 (Figures 6.21). Total alkali are significantly dispersed (4.6-8.2 wt%), in part due to weathering and hydrothermal alteration (Figures

6.22 and 6.23). P_2O_5 is appreciably scattered. Decreasing trends have been observed for compatible transition metal elements (Cr, Ni, V and Sc), which invariably are present in low concentrations (Figure 6.22). The mobile LILE (Rb, Sr and Ba) are dispersed due to alteration and LREE (La and Ce) abundances increase towards more differentiated rocks (Figure 6.22). The Sr is poorly coupled with CaO, but Rb with K_2O, show positive co-variation. The immobile incompatible HFSE elements (Zr, Nb and Ta) are also enriched in more evolved rocks (Figure 6.22). Primitive mantle- and chondrite-normalised element plots show the typical spiky and upward-concave patterns, respectively, that do not deviate significantly from the typical Andean-type arc magmatism (Figure 6.23).

The relatively coherent trends of major and trace elements on the Harker diagrams for the ca. 57-57 Ma Augusta Victoria Formation (*PEav*) and coeval intermediate intrusions (*Pedi*) are consistent with a common fractionation trend from the mafic to silicic rocks (Figure 6.22). Samples from the 60.7 ± 0.61 Ma andesite dikes (*Pan*), in contrast, have some differences from the Augusta Victoria Formation, including a small positive Eu anomaly (Eu/Eu* = 1.02 against Eu/Eu*= 0.71-0.98), higher total REE (Σ REE = 185.7-200.7 against Σ REE = 96.7-136.7), and higher LREE and HREE ratios. The andesite dikes of *Pan* are also more enriched in LILE, Sr, Nb, Zr, U and LREE elements than the Augusta Victoria volcanic rocks (Figure 6.22). Unfortunately, these geochemical features have been determined from only two samples. More data are necessary to demonstrate if *Pan* is part of a distinctive magmatic suite that predated the Augusta Victoria volcanic rocks by 2-3 m.y. (Chapter 3; Appendix 5).

A typical magmatic arc calc-alkaline geochemical signature has been documented for the Augusta Victoria Formation and equivalent rocks in northern Chile (i.e., Chile-Alemania and Cinchado Formations; Marinovic et al., 1994; Mpodozis et al., 1993a; Cornejo and Mpodozis, 1995; Marinovic et al., 1995). The Augusta Victoria Formation samples from La Escondida district studied herein are all consistent with a continental magmatic arc setting on the tectonic discrimination diagrams (Figure 6.24).

Geochemical changes from the andesite dikes to Augusta Victoria Formation are of major significance in the petrogenetic evolution of the late Paleocene-early Eocene magmatic event. The andesite dykes have the highest LREE/HREE ratios and steepest HREE slopes (Figure 6.25a), along with more elevated ratios of Th/Yb, Th/Nb, Ba/Nb, and Sm/Yb, relative to the Augusta Victoria Formation and related intrusions. These

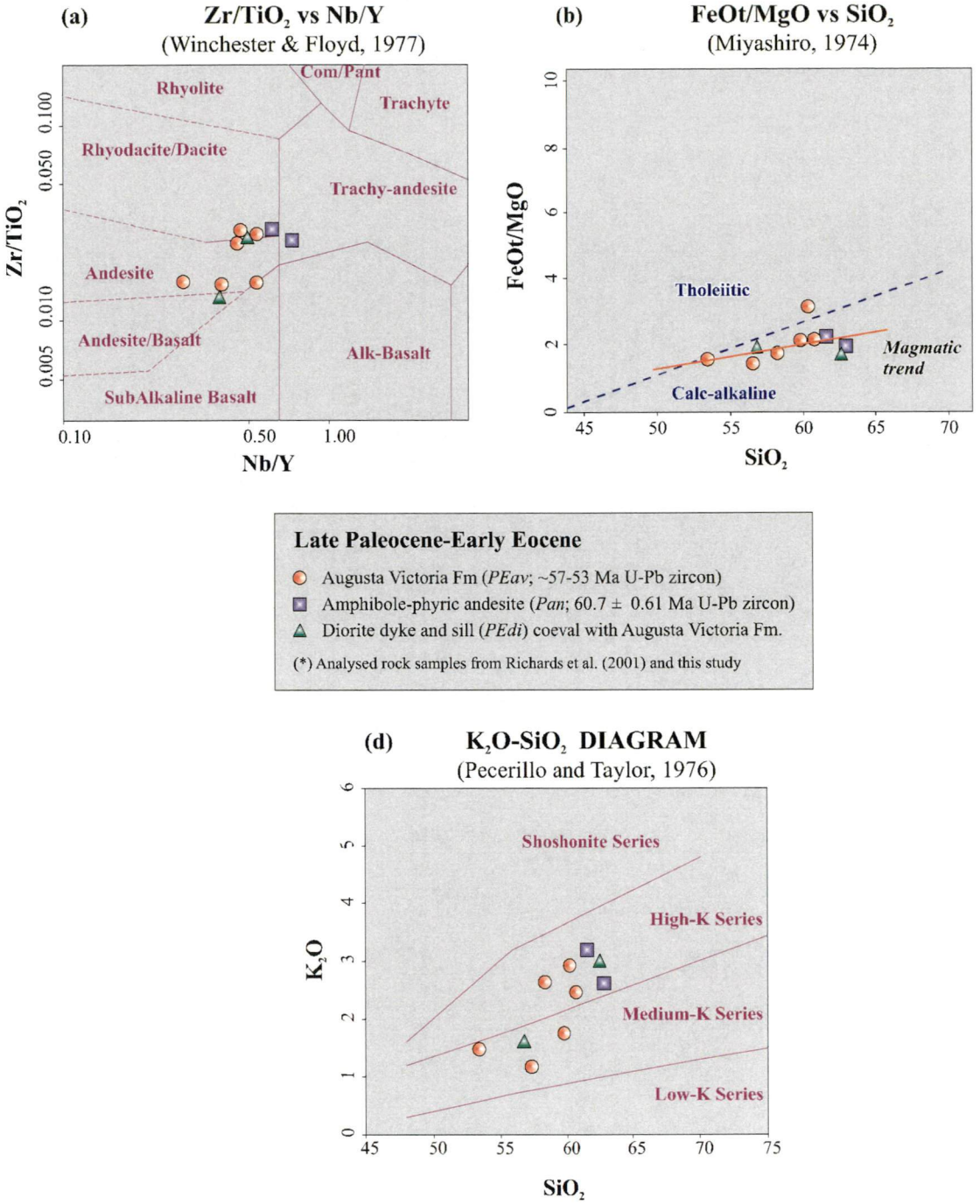

Figure 6.20 Geochemical classification diagrams of (a) Zr/TiO_2 versus Nb/Y (Winchester and Floyd, 1977), (b) FeO_t/MgO versus SiO_2 (Miyashiro, 1974), and (c) K_2O versus SiO_2 (TAS; Pecerillo and Taylor, 1976) for the late Paleocene-early Eocene igneous rocks. Abbreviations: Com = Comendite; Pant = Pantellerite.

elemental ratios are consistent with a parental magma sourced from a metasomatised asthenospheric mantle wedge largely modified by slab-fluid or crustal components. Although these data point to a common origin related with considerable slab-derived fluids participation and/or crustal contamination for both rock units (Figures 6.25c and d), the source zone for the andesite dykes magmas may have been localised in a deeper

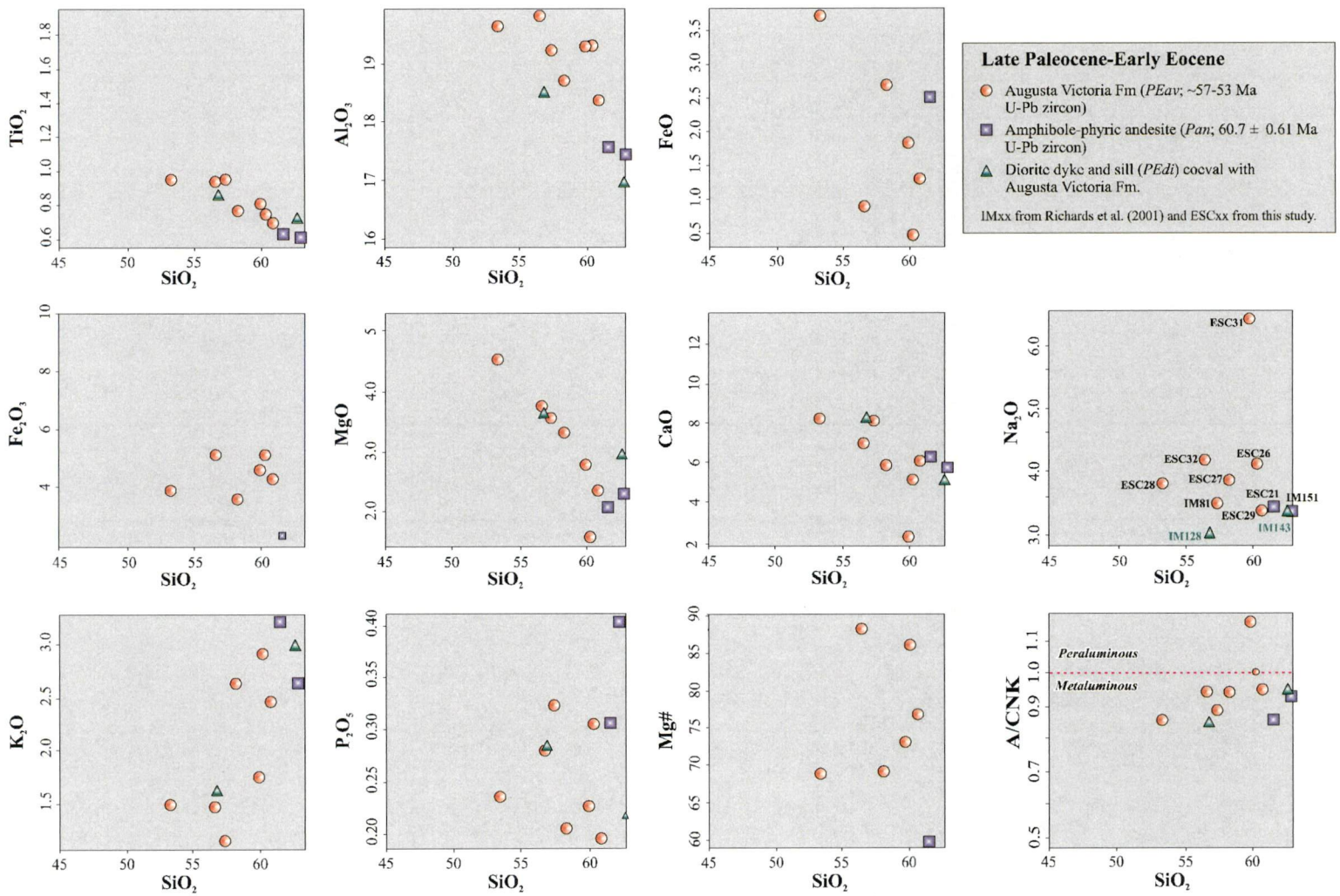

Figure 6.21 Variation of selected major elements (wt%) versus SiO_2 (wt%) for the late Paleocene-early Eocene igneous rocks. Major elements data recalculated to 100% volatile-free.

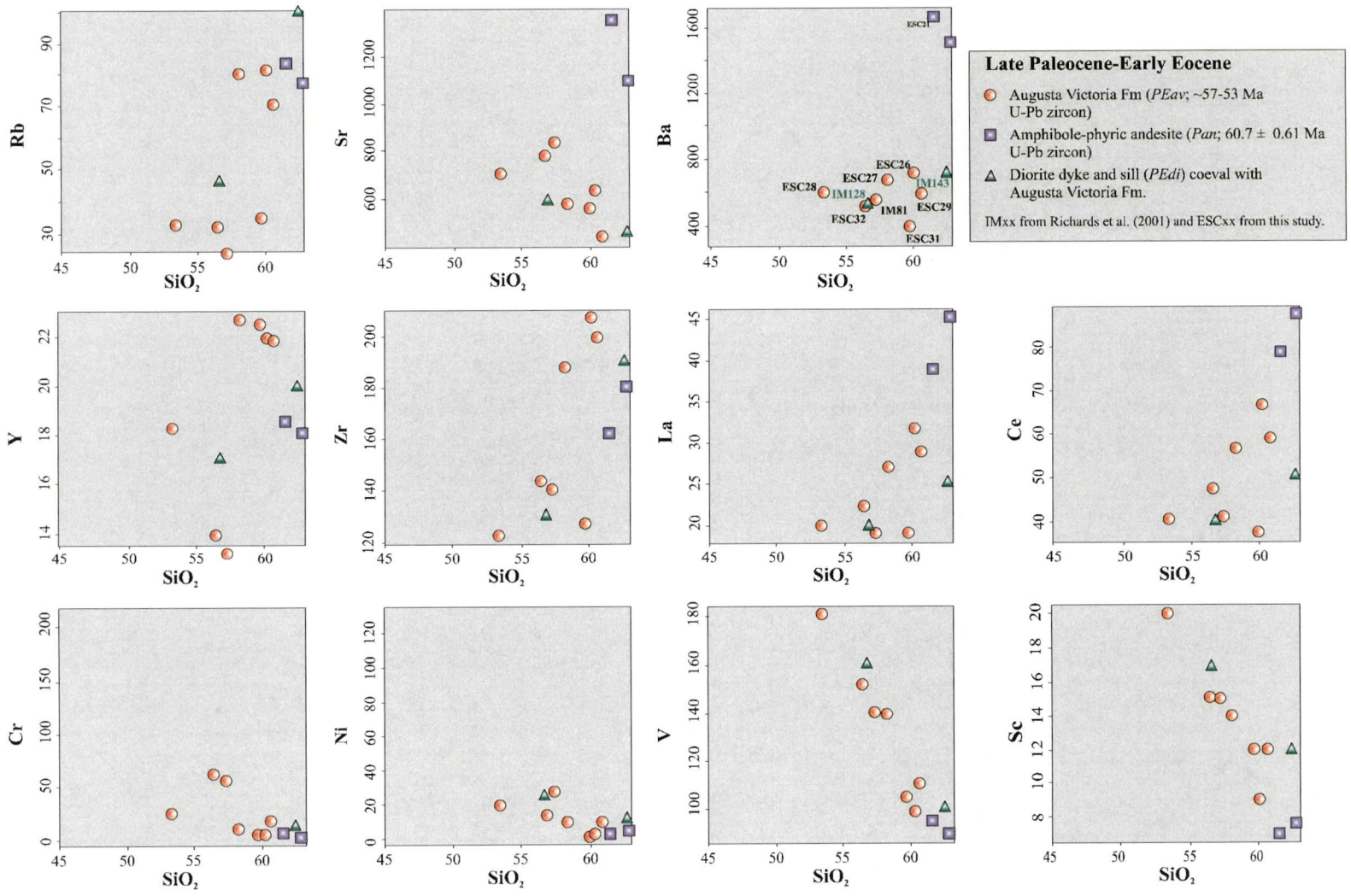

Figure 6.22 Variation of selected trace elements (ppm) versus SiO_2 (wt%) for the late Paleocene-early Eocene igneous rocks.

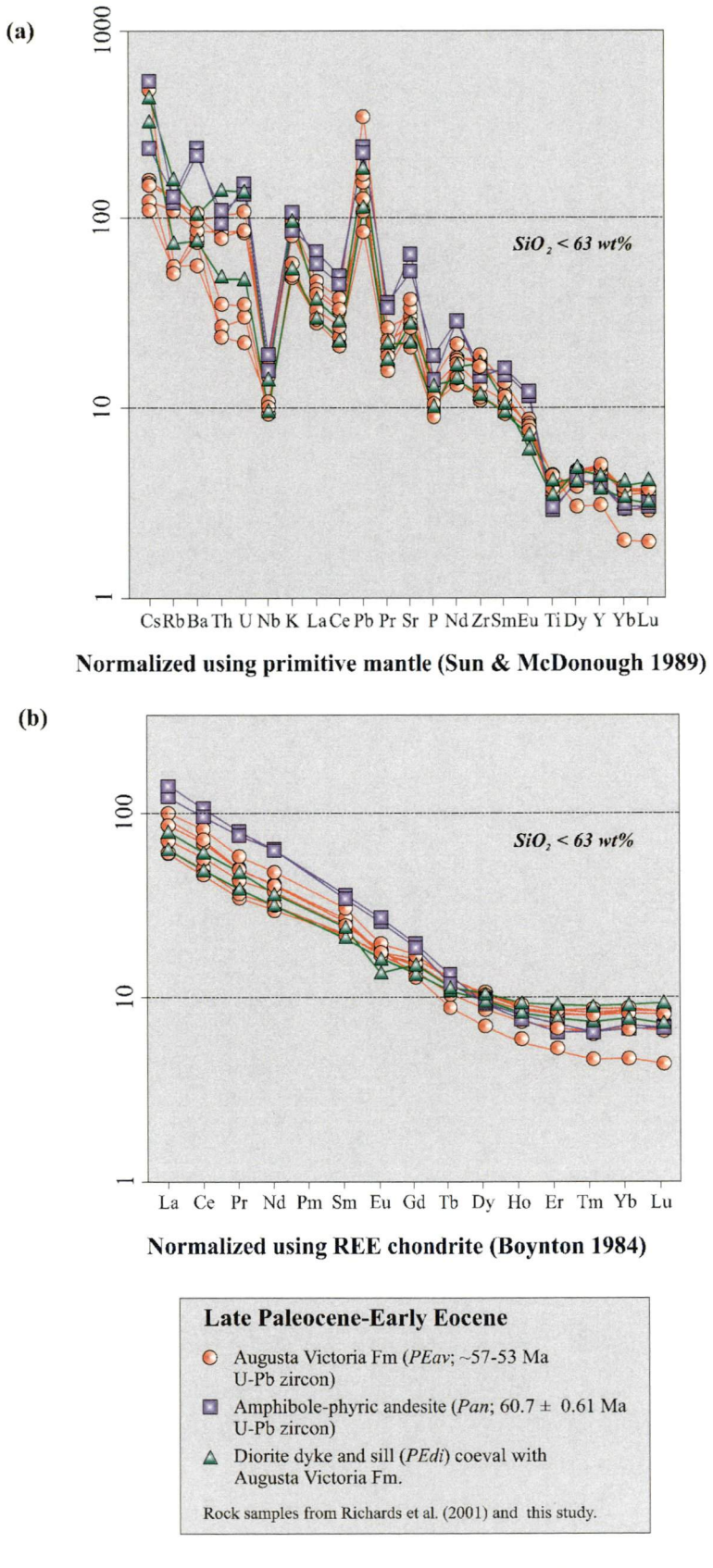

Figure 6.23 Primitive mantle-normalized trace elements (a) and chondrite-normalized REE (b) patterns for the late Paleocene-early Eocene igneous rocks.

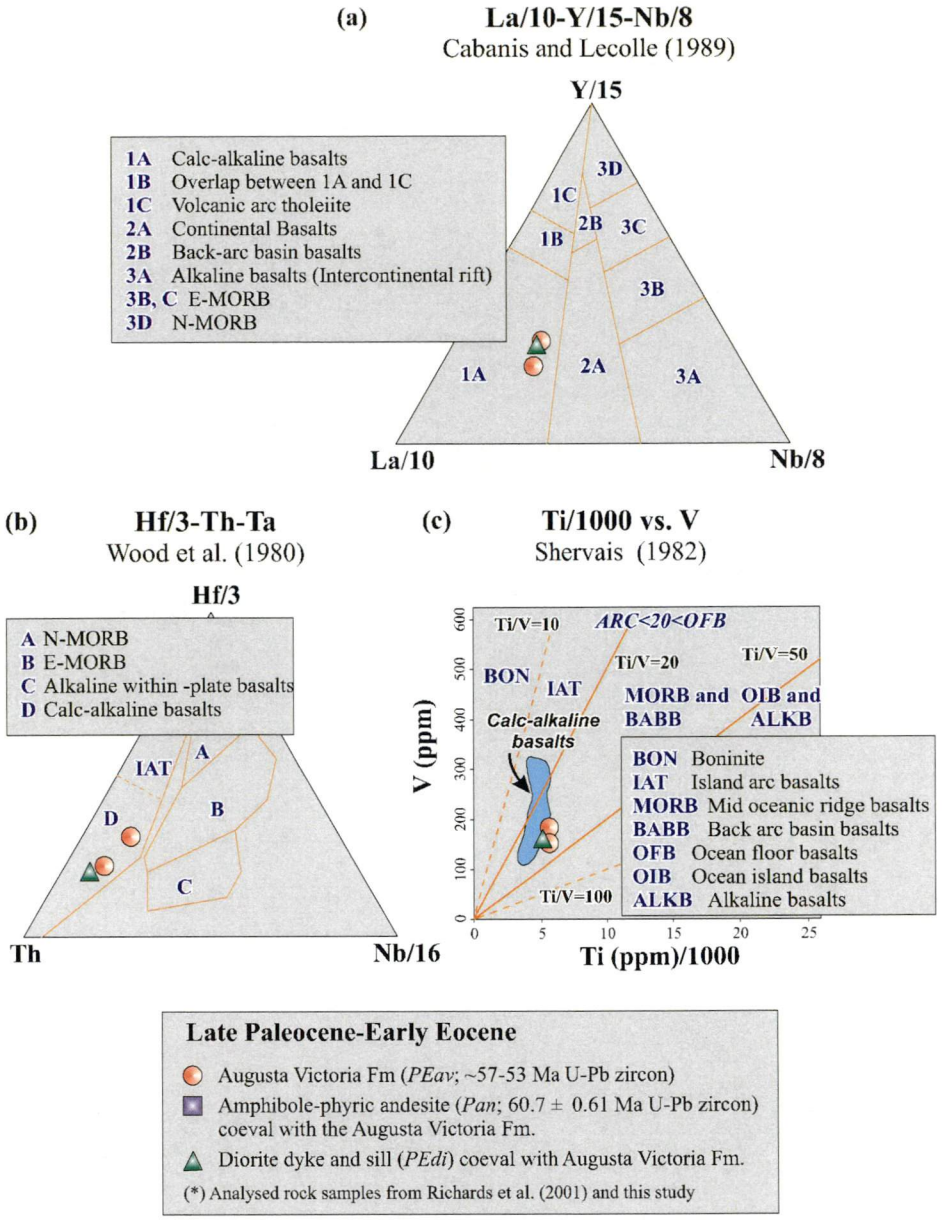

Figure 6.24 Tectonic discrimination diagrams of (a) La/10-Y/15-Nb/8 (Cabanis and Lecolle, 1989), (bThHf/3-Ta (Wood et al., 1980) and (c) V versus Ti/1000 (Shervais, 1992), for basic to intermediate rocks of the late Paleocene-early Eocene igneous rocks. Abbreviations: N-MORB = Normal mid-oceanic ridge basalt; E-MORB = Enriched mid-oceanic ridge basalt; OIB = Oceanic island basalt; SC = Subducted crust; CC = Continental crust; WPE = Within plate; AFC = Assimilation and fractional crystallisation.

level of the upper mantle-lithosphere based on the La/Sm and Sm/Nd ratios (Figure 6.25 b). Indeed, La/Sm versus Sm/Yb plots suggests a magma source for the andesite dykes at depths corresponding to the transition from amphibole-bearing amphibolite zone to garnet-bearing eclogite zone (≥ 45-50 km depth). This differs from the shallower pyroxene-stable to amphibole-stable domains (~35-40 km depth) suggested for magmas associated with the Augusta Victoria Formation (Kay and Kay, 1993; Rapp and Watson, 1995). This interpretation is reinforced by the occurrence of the 64-62 Ma

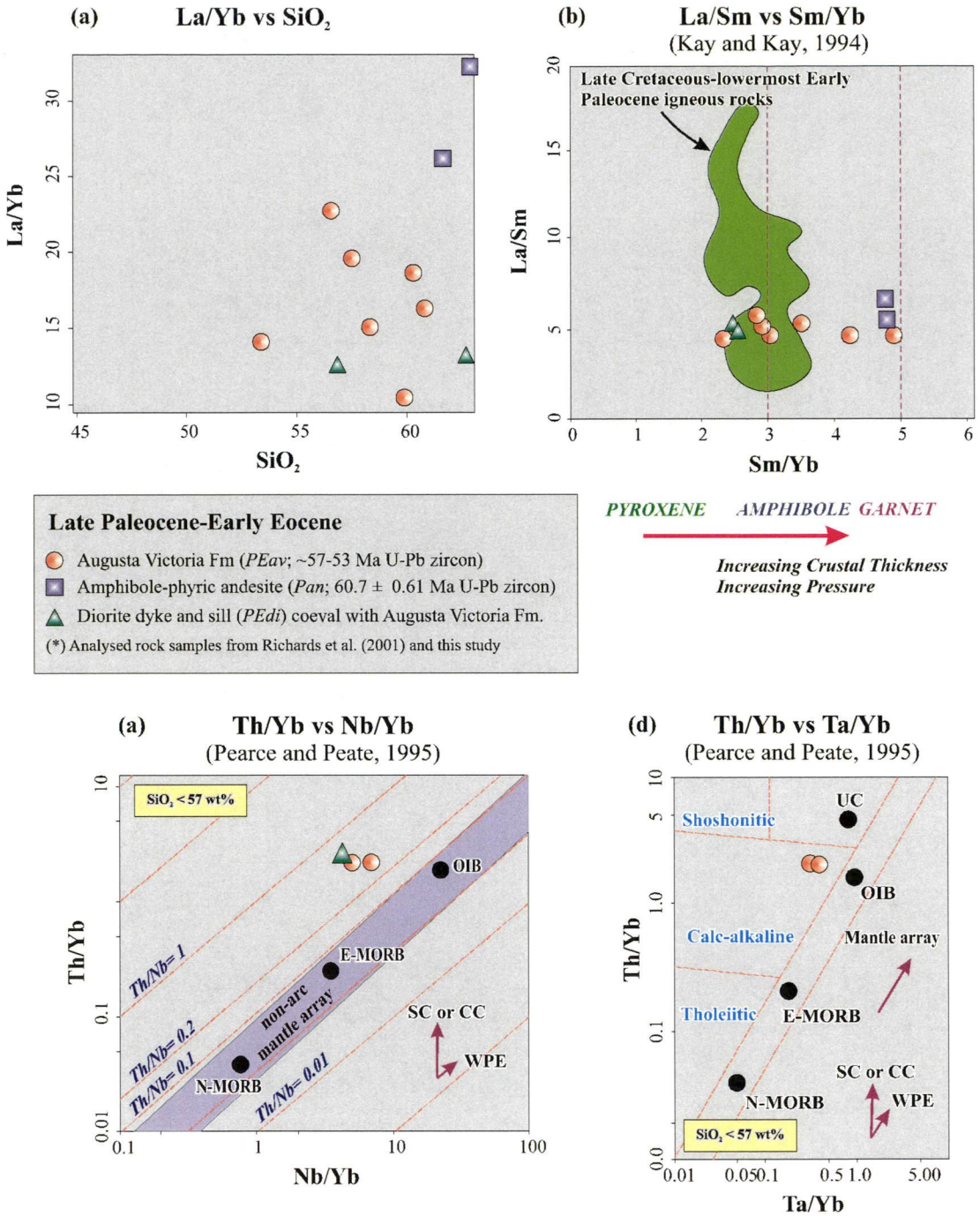

Figure 6.25 Geochemical discrimination diagrams of (a) La/Yb versus SiO_2, (b) La/Sm versus Sm/Yb (Kay and Kay, 1993), (c) Th/Yb versus Nb/Yb (Pearce and Peate, 1995), (d) Th/Yb versus Ta/Yb (Pearce and Peate, 1995) for the late Paleocene-early Eocene igneous rocks. Notice that Ta was not analysed in some samples. Abbreviations: N-MORB = Normal mid-oceanic ridge basalt; E-MORB = Enriched mid-oceanic ridge basalt; OIB = Oceanic island basalt; UC = Upper crust; SC = Subducted crust; CC = Continental crust; WPE = Within plate; AFC = Assimilation and fractional crystallisation.

K-T tectonic deformation phase that undoubtedly caused extensive crustal thickening prior to the intrusion of the ca. 60-61 Ma andesite dikes (Chapter 4). Based on the low Th/Nb Sr/Y ratios of Figure 6.26a, there is no convincing evidence for assimilation in the

petrogenesis of the more basic rocks of Augusta Victoria and coeval diorite intrusion. In contrast, slab-related fluid participation is suggested by relatively high Ba/Y (Figure 6.26b).

Inherited zircons in the Augusta Victoria Formation have ages of ca. 295-275 Ma and 230-220 Ma (Appendix 5). This inheritance is interpreted to indicate that the Paleocene magmas were contaminated by a Late Paleozoic crust as occurred for the Late Cretaceous intrusions. No evidence for zircon inheritance has been recognised for the andesite dikes from *Pan.*

Compilations of isotopic data encompassing volcanic sequences and plutonic bodies of Paleocene and Eocene ages in northern Chile have determined a depleted mantle source for magmas, along with subordinate crustal contamination (Rogers and Hawkesworth, 1989; Haschke, 2002; Figure 6.27). However, the data should be treated with caution as the late Paleocene-early Eocene (ca. 57-50 Ma) magmatism has been poorly assessed as a magmatic event limited by two major tectonic deformation events in northern Chile: the ca. 64-62 Ma "K-T" phase and ca. 40-35 Ma Incaic phase (Marinovic et al., 1999; Cornejo and Matthews, 2001; Cornejo et al., 2003; this study). It has been usually included, along with other Late Cretaceous and middle-late Eocene igneous events, within a larger Late Cretaceous-Eocene tectonomagmatic cycle in the Central Andes cordillera (i.e., Scheuber and Reutter, 1992; Scheuber et al., 1994; Haschke, 2002; Haschke et al., 2006).

There is a marked similarity between the syn-extensional calc-alkaline volcanism of the Augusta Victoria Formation and other Paleocene volcanic units that were described by Cornejo and Matthews (2001; and references therein) in El Salvador-Petrerillos region. These authors attributed a 2000 m thick sequence of basaltic andesite, andesite and dacite from El Salvador district to a complex combination of decompression and melting of the mantle lithosphere, entrapment of mafic magmas in the previously thickened crust, and extensive melting of upper crustal rocks.

6.3.2.3 Middle-Late Eocene Magmatism

The middle-late Eocene igneous rocks in La Escondida district constitute three distinctive tectonomagmatic events of particularly important metallogenetic connotations. Pre-, syn- and post-mineralisation rock units have been defined relative to the Eocene porphyry-style copper mineralising event (Chapter 5). They range in composition from gabbro to

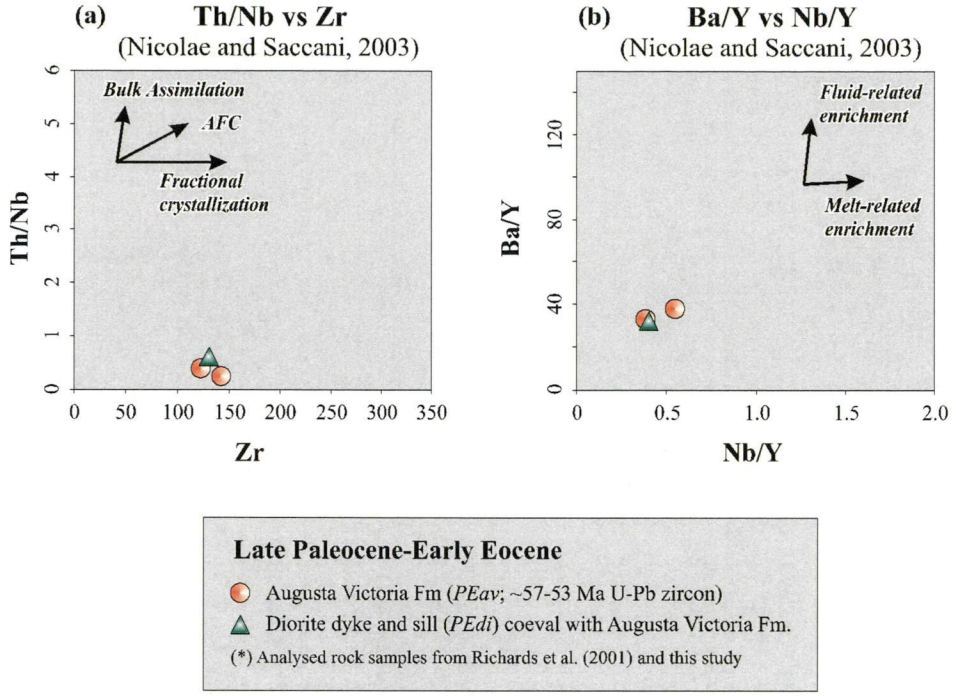

Figure 6.26 Geochemical discrimination diagrams of (a) Th/Nb versus Zr (Nicolae and Saccani, 2003), (b) Ba/Y versus Nb/Y (Nicolae and Saccani, 2003), (c) Nb/Zr versus N (Nicolae and Saccani, 2003), and (d) Zr/Yb versus Nb/Yb versus Sm/Yb (Pearce and Peate, 1995) for the late Paleocene-early Eocene igneous rocks. Abbreviations: AFC = Assimilation and fractional crystallisation.

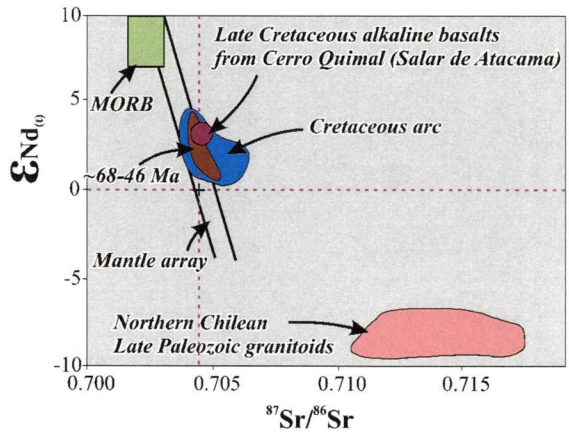

Figure 6.27 Summary of initial $^{87}sr^{86}Sr$ and ε_{Nd} for late Paleocene-early Eocene igneous rocks (Rogers and Hawkersworth, 1989; Lucassen et al., 1999a; Haschke, 2002a; Krammer et al., 2005). Abbreviations: MORB = Mid-oceanic ridge basalt.

granodiorite on the total alkali-silica diagram (Figure 6.28a) and from andesite to rhyodacite/dacite and subordinate trachy-andesite on the Zr/TiO_2 versus Nb/Y classification diagram (Figure 6.28b). All samples analysed are metaluminous, calc-alkaline I-type rocks (Chappell and White, 1994). Fe_2O_3/FeO ratios are available for some rocks; they distinguish the Cerro Rincones plutonic complex and Capella stock (0.6-1.4) from

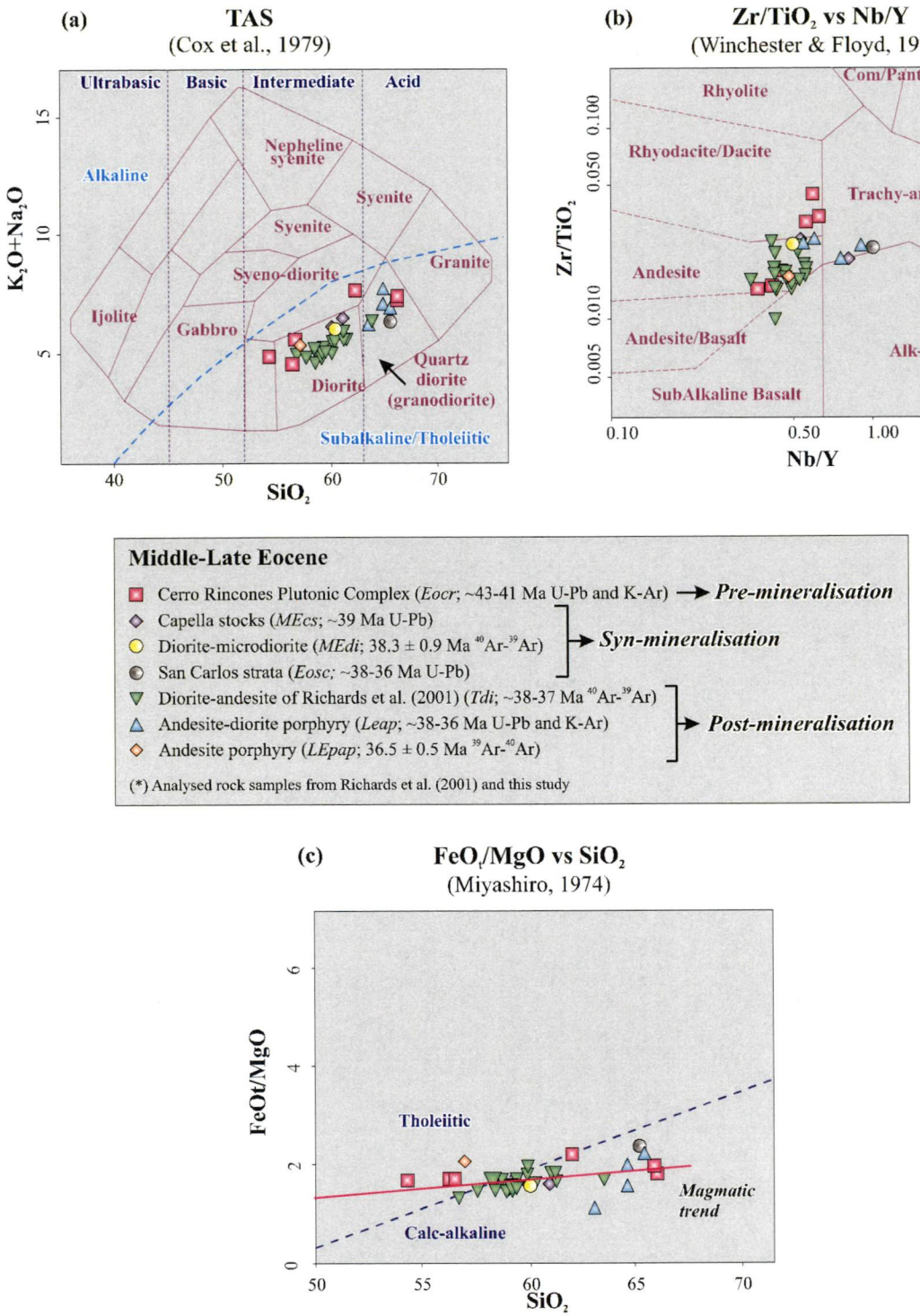

Figure 6.28 Geochemical classification diagram of (a) Zr/TiO_2 versus Nb/Y (Winchester and Floyd, 1977), (d) K_2O versus SiO_2 (Pecerillo and Taylor, 1976) and (b) FeO_t/MgO versus SiO_2 (Miyashiro, 1974) for middle-late Eocene igneous rocks. Abbreviations: Com = Comendite; Pant = Pantellerite.

the Fe-oxides-rich San Carlos strata volcanic rocks (11.5) and andesite and diorite porphyries (1.6-2.9). Harker variation diagrams for major elements show regular decreasing TiO_2, Al_2O_3, FeO_t, MgO and CaO contents with increasing SiO_2, (Figure 6.29),

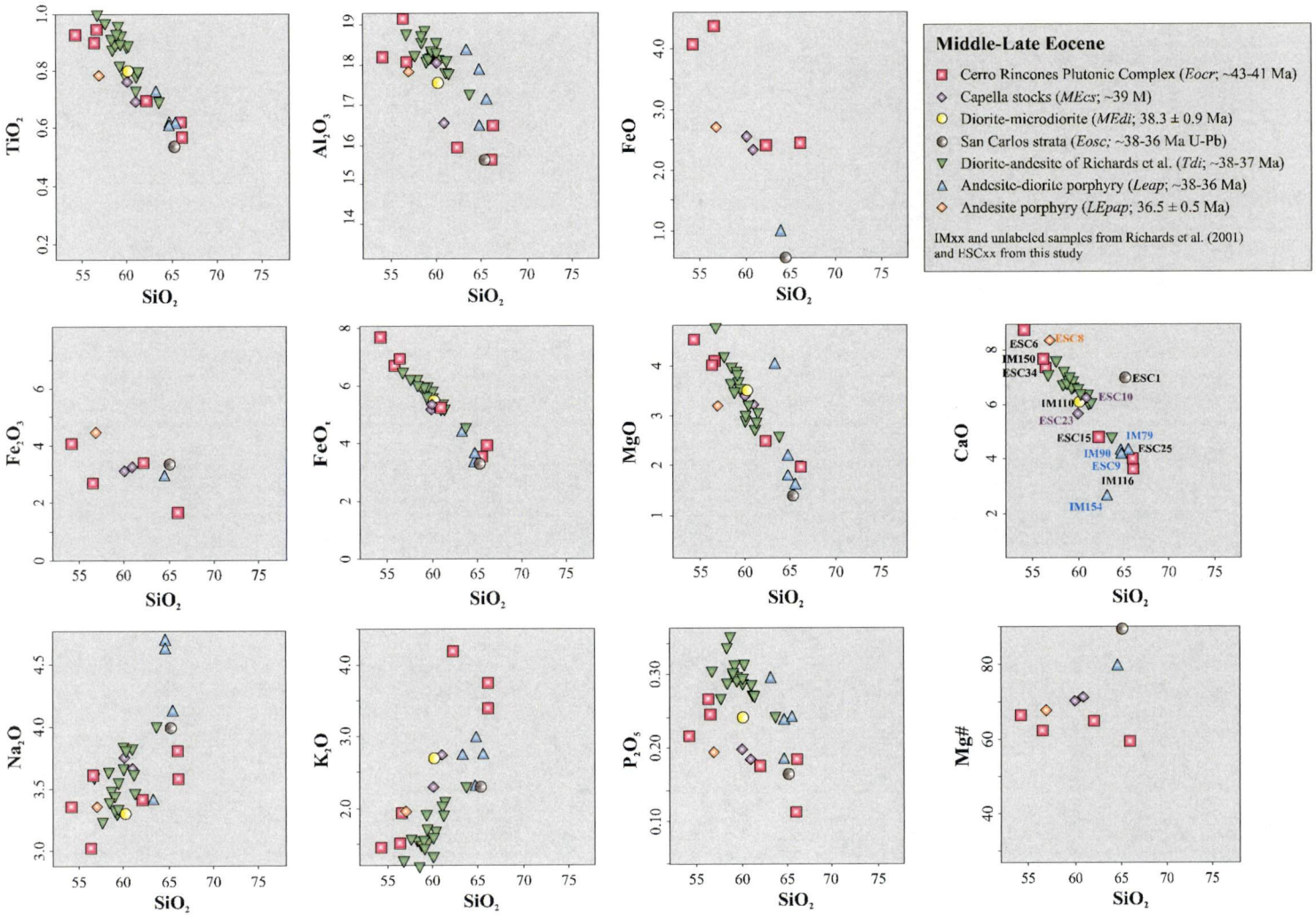

Figure 6.29 Variation of selected major elements (wt%) versus SiO_2 (wt%) for the middle-late Eocene igneous rocks. Major elements data recalculated to 100% volatile-free.

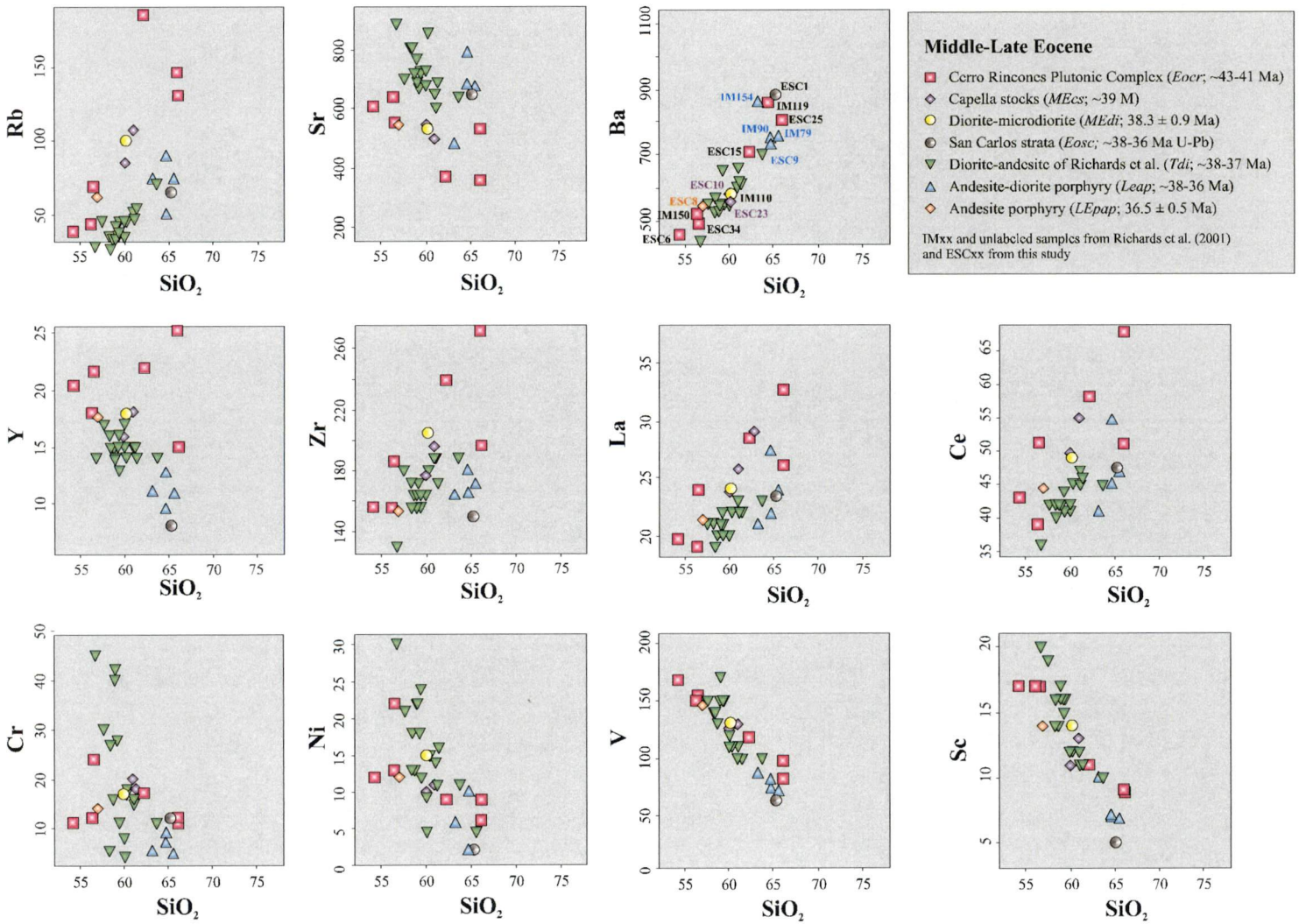

Figure 6.30 Variation of selected trace elements (ppm) versus SiO_2 (wt%) for the middle-late Eocene igneous rocks.

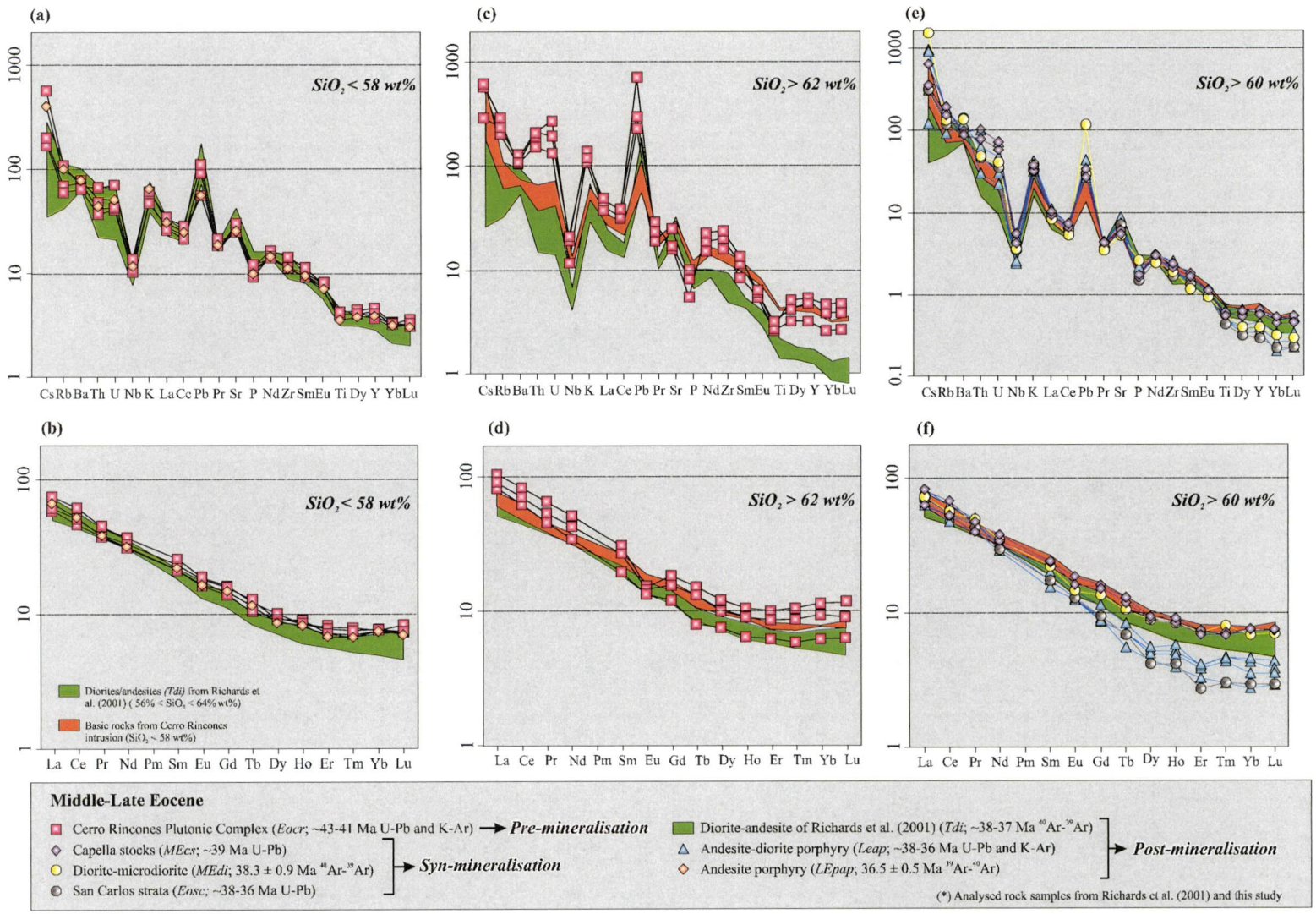

Figure 6.31 Primitive mantle-normalized trace elements (a) and chondrite-normalized REE (b) patterns for the middle-late Eocene igneous rocks.

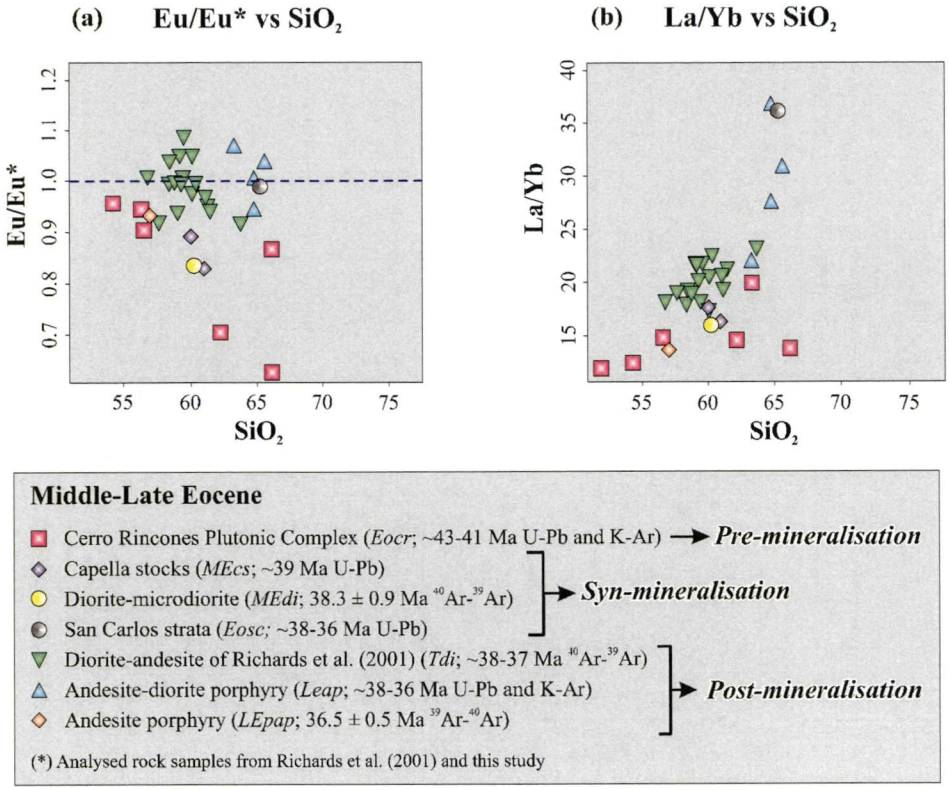

Figure 6.32 Geochemical discrimination diagrams of (a) E/Eu* versus SiO_2, and (b) La/Yb versus SiO_2 for the middle-late Eocene igneous rocks.

without distinctive trends separated from a principal array defined by all analysed samples. Trace element plots on Figure 6.30 indicate that the LILE (Rb and Ba) and HFSE (Zr, Nb and Ta) are enriched in more evolved rocks. Mantle-normalised element plots define spiky patterns that consist of peaks in LILE and Pb, and HFSE and REE troughs (Figure 6.31). Chondrite-normalised REE element plots display parallel convex arrays, with more increased REE fractionations and positive Eu/Eu* anomalies in the post-mineralisation andesite and andesite-diorite porphyries regarding to the pre- to syn-mineralisation Cerro Rincones and Capella stocks (Figures 6.31 and 6.32).

In the pre-mineralisation Cerro Rincones plutonic complex and slightly pre- to syn-mineralisation Capella stocks, the plotting of some HFSE (i.e., Th, Ta and Nb) and REE (i.e., La, Sm Yb) ratios on Figures 6.33a to c are consistent with derivation from a pyroxene- to amphibole-stable source regime (i.e., Kay and Kay, 1993) and significant contamination of parental magmas by subduction-slab fluid and/or crustal components. These interpretations are reinforced by the abundance of inherited zircon comparing with less crustally contaminated andesite and andesite-diorite porphyries samples that are poor in old zircons (Appendix 5). A non-adakitic affinity for Cerro Rincones plutonic complex

igneous suite is indicated by the Sr/Y versus Y diagram (Figure 6.33d) and an arc setting is highlighted by Ba/Nb ratios > 50 (Trumbull et al., 1999; Coira et al., 1999; Caffe et al., 2002).

The syn- to post mineralization magmatic episodes (i.e., San Carlos strata, andesite-diorite porphyry, diorite-microdiorite and andesite porphyry units) produced rocks that had undergone increased REE and LREE fractionation (Figures 6.32b and 6.33b), features compatible with a deeper source regime for their magmas. They were probably sourced from amphibole- to garnet-stable domains in an eclogitic lower crust (i.e., Kay and Kay, 1993; Kay et al., 1999). The andesite-diorite dyke of Richards et al. (2001) is the only unit that displays geochemical features similar to adakite or tonalite-trodhjemite series (Figure 6.33d). No data are available for basic rocks from other Eocene units exposed in La Escondida district. The pre-mineral Cerro Rincones and Capella intrusive rocks have pyroxene and subordinate amphibole as the principal ferromagnesian mineral phases. Main part of the remaining syn- to post-mineralisation volcanic and plutonic rocks (i.e., andesite-diorite porphyries from *Leap*, diorite-andesite intrusions from *Tdi* and San Carlos strata) contain hornblende and biotite as the main ferromagnesian minerals (Chapter 5). However, the andesite porphyry from *Lepap*, which is the youngest intrusive unit in La Escondida district, has pyroxene as the main ferromagnesian mineral. These petrographic differences are expressed by HFSE and LILE ratios plotted on Figures 6.32 to 6.34. Apparently the volatile-rich aqueous fluid phases played an important function in the geochemical characteristics of igneous suites and metal-transport (Cornejo and Matthews, 2001; Valente et al., 2006).

Middle-late Eocene magmatism occurred synchronous with a major tectonic deformation (Incaic phase) in northern Chile (Coira et al., 1982; Maksaev, 1990; Boric, 1990; Reutter et al, 1991; Marinovic et al., 1995; Chapter 4). The pre-mineralisation pyroxene-bearing Cerro Rincones plutonic complex is temporally equivalent to syn-tectonic and syn-mineralisation calc-alkaline intrusions described by Cornejo and Matthews (2001) in El Salvador-Petrerillos district. The latter intrusions have amphibole as the main ferromagnesian mineral, high MREE-HREE (Sm/Yb: 4-9) ratios, elevated Sr and Al contents, and lack significant negative Eu anomalies (Cornejo and Matthews, 2001). Such features have been interpreted as diagnostic of a derivation from TTG-type magmas at the amphibolite-eclogite transition in the lower crust (Cornejo and Matthews, 2001). The tonalitic magmas are inferred to have been contaminated by basaltic magmas during

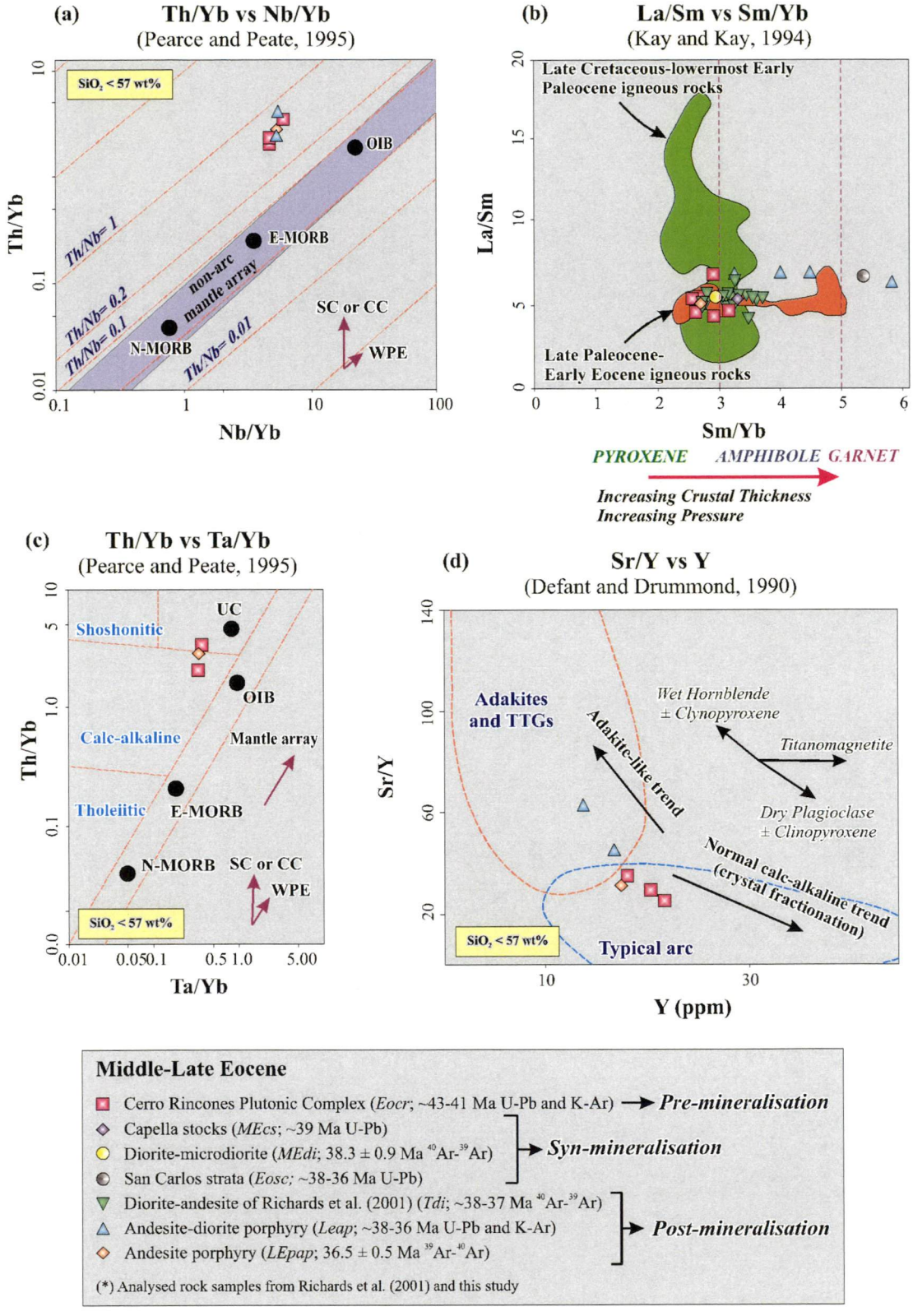

Figure 6.33 Geochemical discrimination diagrams of (a) Th/Yb versus Nb/Yb (Pearce and Peate, 1995), (b) La/Sm versus Sm/Yb (Kay and Kay; 1993), (c) Th/Yb versus Th/Zrb (Pearce and Peate, 1995), (d) Sr/Y versus Y (Denfant and Drummond, 1990) for the middle-late Eocene igneous rocks. Abbreviations: N-MORB = Normal mid-oceanic ridge basalt; E-MORB = Enriched mid-oceanic ridge basalt; OIB = Oceanic island basalt; UC = Upper crust; SC = Subducted crust; CC = Continental crust; WPE = Within plate; AFC = Assimilation and fractional crystallisation; TTGs = Tonalite, trodhjemite and granodiorite.

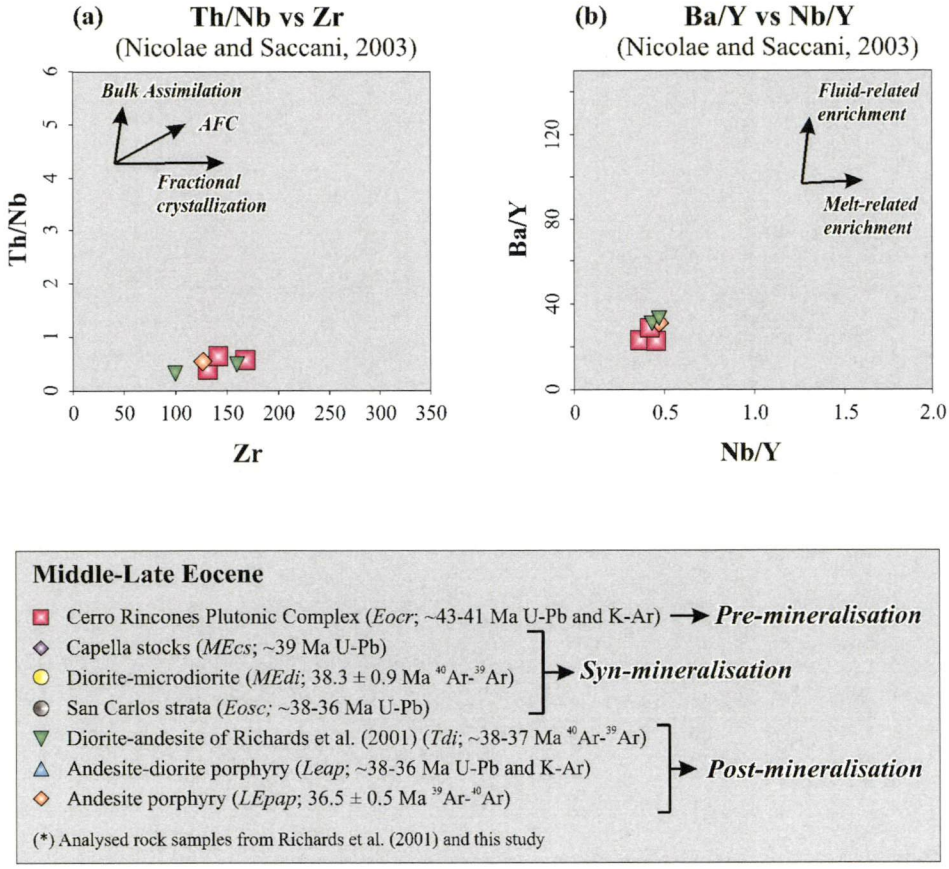

Figure 6.34 Geochemical discrimination diagrams of (a) Th/Nb versus Zr (Nicolae and Saccani, 2003), and (b) Ba/Y versus Nb/Y (Nicolae and Saccani, 2003) for the middle-late Eocene igneous rocks. Abbreviations: AFC = Assimilation and fractional crystallisation.

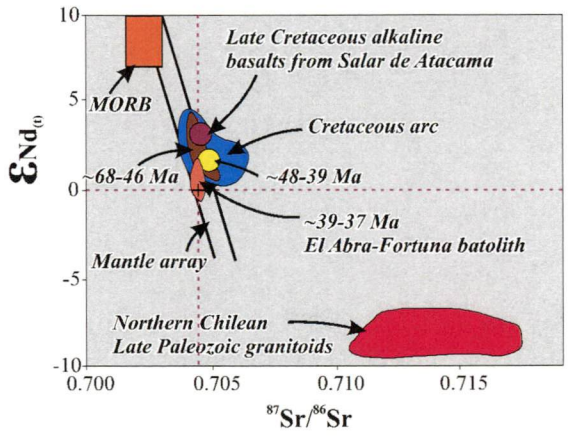

Figure 6.35 Summary of initial $^{87}sr^{86}Sr$ and ε_{Nd} for middle-late Eocene igneous rocks (adapted from Rogers and Hawkersworth, 1989; Lucassen et al., 1999a; Haschke, 2002a; Krammer et al., 2005). Abbreviations: MORB = Mid-oceanic ridge basalt.

ascent from the mantle. They have distinctive low initial $^{87}Sr/^{86}Sr$ ratios and $^{143}Nd/^{144}Nd$ isotopic ratios (Cornejo and Matthews, 2000). Richards et al. (2001) and Padilla et al.

(2001) arrived at similar conclusions for the porphyry copper-style intrusions in La Escondida district. The geochemical ratios plotted on Figure 6.34 suggest that assimilation and fractional crystallization processes (AFC), magma mingling, modification of the mantle wedge and crustal contamination occurred during the petrogenetic evolution of the Eocene igneous rocks. There are two first-order factors that apparently controlled the passage from the pre-mineralisation Cerro Rincones intrusions to the mineralising hypabyssal porphyritic intrusions and subsequent post-mineralisation dykes. First, there was a transition from a pyroxene/amphibole- bearing amphibolite domain to a garnet-bearing eclogitic domain in the lower crust (crustal thickening and fluid delivery by dehydration of amphibole). Second, the start of the Incaic deformational phase produced a strongly compressive regime, and caused subsequent changes in the rheology, pressure and temperature of the crust. Elsewhere in northern Chile, isotopic studies of Eocene intrusive and volcanic rocks have determined a slightly juvenile mantle source, with low initial $^{87}Sr/^{86}Sr$ ratios and positive E_{Nd} (i.e., Haschke, 2002; Figure 6.35).

At El Abra porphyry copper deposit, the Pajonal-El Abra mineralised suite of intrusions have been interpreted as upper crustal magmas that received periodic injection of new magma from the lower crust (Valente et al., 2006). The time encompassed by the evolution of the lower crustal magmatic chamber was estimated to be on the order of 11 m.y., between 45.1 and 34.5 Ma. It underwent varied processes, including assimilation, fractional crystallisation and magma mixing (Valente et al., 2006). The Pajonal-El Abra suite is inferred by these authors to define a single cooling trend, broadly divided into dry magma series (plagioclase/pyroxene-dominated fractionation) and wet magma series(amphibole-dominated fractionation).

The model of Valente et al. (2006) for El Abra has relevance in La Escondida district. The middle-late Eocene magmatic event occurred over at least 9 m. y. from 43 to 36 Ma (Chapter 3). It started with the pre-mineralisation Cerro Rincones and Capella stock (composition consistent with the dry magma series), through the syn-mineralisation andesite to diorite intrusions and contemporaneous volcanic deposits (wet magma series), to the post-mineral pyroxene andesite porphyry (Figure 6.33d).

Haschke et al. (2006) proposed a cyclic tectonomagmatic evolution of the Andean orogen (21°-26°S) that consists of three tectomagmatic events associated with successively eastwards-migrating arc axes. Jurassic (195-130 Ma), "*mid*"-Cretaceous (125-90 Ma), Late

Cretaceous-Eocene (78-38 Ma) and Neogene (26 Ma-Recent) arcs (characteristically referred to as magmatic cycles) recognised by these authors evolved individually as follows: (1) magmatism for 40-30 m.y., with increasing REE fractionation; (2) increasing crustal thickness and initial Sr and Nd isotopes with new each cycle; (3) early-stage, back-arc, alkaline magmatism; and (4) late-stage tectonic deformation of the mature arc, followed by mineralisation and a magmatic gap of 5-12 Ma.

The cyclic model of Haschke et al. (2006) is not consistent with detailed geological information collected from La Escondida district for the Late Cretaceous (~81 Ma) to Eocene (~35 Ma) rocks. A major discrepancy is the K-T tectonic phase, which separated the Late Cretaceous volcanic and intrusive rocks from the late Paleocene-early Eocene Augusta Victoria Formation. Rather than the hypothetical Late Cretaceous-Eocene arc, two major arcs are inferred here: (1) the Late Cretaceous-lowermost early Paleocene (81-64 Ma) magmatism and (2) the Paleogene (60-36 Ma) magmatic events. Both events are represented by a series of mappable rock units with different geochemical, structural and metallogenetic features.

6.4 SUMMARY

Geochemical sampling of outcrops in La Escondida district has provided the following conclusions:

- The pre-Andean (Gondwanian) magmatism started with the voluminous and dominantly siliceous magmatism of the Late Carboniferous-Permian La Tabla Formation and Imilac plutons. They correspond to a calc-alkaline suite that has geochemical signature of an active continental margin. The magmas probably originated at the pyroxene-stable zone in the lower crust, involving melting of metasomatised mantle wedge, underplating magmas and mingling.
- The Middle-Late Triassic porphyry-style intrusions ended the pre-Andean magmatic cycle. There are no significant geochemical differences between these intrusions and the more evolved products of La Tabla Formation and Imilac plutons. But, the Triassic intrusions contain evidences of crustal contamination, specifically by a group of inherited zircons of ca. 458 and 245 Ma.
- The Andean magmatism in LaEscondida district produced three main episodes of intrusions and volcanism of ca. 81-65Ma, 60-53 Ma and 43-35 Ma; all with

distinctive slab subduction geochemical affinities. The most relevant aspects of each event are as follows:

1. The Late Cretaceous-lowermost magmatic episode has two distinct geochemical trends: (1) early tholeiitic alkaline Cerro Bayo intrusions with transitional-back-arc affinity; and (2) late calc-alkaline Sombrero plutons that have frontal magmatic arc signatures. Two of these igneous suites, Torcaza pluton and Las Torres igneous complex, remain only partially characterised in their geochemistry and further analyses are required. However, the available samples of Las Torres unit suggest a co-magmatic relationship with the Sombrero intrusions. The magmas that produced all of these rocks were probably sourced from the amphibole-stable zone in the depleted upper mantle-lithosphere. Inherited zircons of ca. 300-260 Ma confirm the occurrence of some crustal contamination/assimilation in Las Torres and Sombrero intrusive rocks. In contrast, the Cerro Bayo and Torcaza plutonic complexes do not contain old zircon, suggesting no crustal contamination.

2. The late Paleocene-early Eocene Augusta Victoria Formation volcanic event started by intrusion of minor andesite dykes at ca. 60 Ma. They represent a magmatic episode related to a major crustal thickening event caused by the previous K-T deformation. The andesite dykes were sourced from a thicker crust (garnet-zone in an eclogitic lower crust-mantle), whereas the subsequent Augusta Victoria volcanic rocks were erupted in a crust thinned by extension and their parental magmas originated at shallower levels (amphibolite-zone in an amphibolite lower-middle crust).

3. The middle-late Eocene was a period of essentially continuous calc-alkaline magmatic activity that produced discrete intrusions. Magmatism was initiated with the emplacement of the pre-mineralisation Cerro Rincones plutonic complex, the largest pluton in La Escondida district. The transformation from this pre-mineralisation intrusion to the syn- to post-mineralisation and intrusions punctuated by explosive volcanism was marked by increases in pressure and depth of the magma source regime from an amphibole-stable zone crustal source, to an amphibole- to garnet-stable zone in an eclogitic lower crust-mantle. Evolution from dry magma (pre-mineralisation intrusions: Cerro Rincones, Capella and diorite microdiorites), through wet magma (syn-mineralisation intrusions and volcanism: andesite-diorite porphyry, diorite-andesite from Richards et al., 2001; San Carlos strata), and then to dry magma (post-mineralisation intrusion: pyroxene andesite porphyry) is inferred for the Eocene magmatic rocks of La Escondida.

CHAPTER 7
Conclusions and Recommendations

This chapter summarised the main geological observations and interpretations made during this Ph.D. study of La Escondida district, and comments on implications for future exploration activities. Four initial aims were originally established as the basis for this study: (1) 1:25,000-scale mapping of an area about 1,000 km^2 to determine the relationships and ages of Phanerozoic geological units (Appendix 1); (2) four 1:25,000-scale E-W geological cross-sections based on outcrops mapping and borehole logging (Appendix 2); (3) the structural evolution of the district to be determined based on kinematic measurements from the Mesozoic and younger rocks (Chapter 4), coupled with geochronological (Appendix 5) and geochemical characterization of the recognised intrusions (Chapter 6); and (5) to identify and characterise the alteration zones and other targets concealed by the Miocene to Recent sediments (Chapter 5; Appendix 3).

7.1 CONCLUSIONS

Andean magmatism is more complex in La Escondida district than conceived originally, in terms of composition and diversity of ages. Detailed mapping and geochronology have proven essential for separating the discrete magmatic events. High-precision LA-ICPMS U-Pb zircon dating proved a highly effective tool to assist district-scale mapping. Other, less accurate or reliable geochronological methods should be avoided as much as possible (i.e.; K-Ar whole rock on altered samples). Structural analysis has demonstrated that individual structural blocks in the district have complicated and unique deformational histories. Therefore, interpretations and models based only on kinematic studies are tentative and need further support by other analysis techniques (i.e., restored or balanced structural sections, geochronology of deformation). Major and trace element geochemistry has demonstrated a preponderance of arc-related magmatism throughout the history of La Escondida district. Mesozoic sedimentary, magmatic and mineralization processes occurred in the region, and were intimately linked with the tectonic evolution of the Domeyko Cordillera orogen and the Domeyko Fault System. The pre-Mesozoic tectonic history remains poorly understood.

7.1.1 Pre-Andean (Gondwanian) Cycle

During the Late Paleozoic, bimodal terrestrial volcanism in La Escondida district was largely dominated by rhyolitic ignimbrite eruptions and subordinate andesitic lavas and fluvio-lacustrine sedimentation. It probably occurred as calderas and domes and was part of the Late Paleozoic-Triassic El Choiyoi magmatic province. Products of El Choiyoi are recognised along the southern Central Andes, and represented in La Escondida region by La Tabla Formation. U-Pb zircon (SHIMP, conventional and LA-ICP-MS) dates have determined that La Tabla Formation was deposited between 300 and 280 Ma. It was followed shortly thereafter by the emplacement of granitoids at 340-260 Ma. High-precision geochronology has defined a tight distribution of ages that confirms the almost contemporaneous occurrence of the volcanism and mesozonal to epizonal intrusions. It has identified two major thermal events, with Late Paleozoic and Jurassic ages, that have perturbed some isotopic systematics of La Tabla succession. Therefore, radiometric dating techniques as K-Ar and ^{40}Ar-^{39}Ar are sensitive to disturbance and have provided ages of uncertain geological meaning for La Tabla Formation. There is no record of significant Early Mesozoic magmatic activity in the study area, but ca. 230-207 Ma plutons and rhyolite porphyries have been reported from the Imilac range (Davidson et al., 1985; Marinovic et al., 1995; Mpodozis et al., 1993a; Gardeweg et al., 1994), showing that Andean intrusive activity occurred in the Middle-Late Triassic.

Uneconomic porphyry copper systems, including porphyry-related lithocaps and tourmaline breccia pipes, were the last Paleozoic-Triassic igneous episode, most likely within a mature arc setting, at ca. 230-220 Ma. Regional correlations indicate that these porphyry systems appear to be related to a Middle-Late Triassic phase of mineralised intrusive activity along the Domeyko Cordillera (i.e., Cornejo et al., 2006). Michigan-style volcanic-hosted copper occurrences have been recognised in the lower stratigraphic sections of La Tabla Formation, although none have proven to be economic. The major and trace element geochemistry of the metaluminous, low-K calc-alkaline suites is consistent with a continental magmatic arc setting. The petrogenetic evolution of these suites involved melting of modified asthenospheric mantle wedge, lower crustal residence of magmas, mixing and contamination by mid-crustal material, and some products derived directly from crustal melting. The magmas probably originated in the pyroxene-stable zone in the lower-middle crust. Only the Middle-Late Triassic porphyry-style intrusions show evidence of crustal contamination, specifically a group of inherited zircons of Late

Paleozoic age. A poorly constrained deformation, but of probable Late Paleozoic-Early Triassic age, produced minor folding of La Tabla Formation.

7.1.2 Andean Cycle

A major extensional event affected the southwestern margin of South America as part of the fragmentation of Gondwana during the Late Triassic-Early Jurassic. This was recorded locally by thick basal packages of Mesozoic sedimentary rocks deposited in a rift setting. Andean subduction would have commenced shortly after this trans-continental extension. Much of La Escondida district was occupied by a Jurassic back-arc basin that closed during the Neocomian. Two successive magmatic arcs overprinted the basin, with three main episodes of intrusions and volcanism at ca. 81-65 Ma, 60-53 Ma and 43-34 Ma.

7.1.2.1 The Mesozoic Back-arc Tarapacá Basin

A thick, mixed siliciclastic-calcareous sequence was deposited within the Tarapacá back-arc basin from the Late Triassic to the Neocomian (i.e., Vicente, 2006). El Profeta and Santa Ana Formations represent sedimentation along the eastern border of the basin (Figure 7.1a). Distal, thin ash interbeds are the only record of incipient, early stage silicic explosive magmatism. The location of eruptive centres is unknown. Positive tectonic inversion caused by the Peruvian tectonic phase (Mégard, 1987) occurred during the lowermost Late Cretaceous. This compressive deformation formed a thick-skinned fold and thrust belt in the Mesozoic sedimentary rocks. Some Late Triassic-Early Jurassic extensional faults were reactivated as reverse faults during tectonic inversion. Minor occurrences of Cu-oxides occur in the matrix and as occasional mineralised (Cu-sulphide bearing) porphyry-type intrusive clasts within basal conglomerates of El Profeta Formation. The clasts are inferred to have been derived by erosion of pre-Mesozoic porphyry copper systems.

7.1.2.2 The Late Cretaceous-lowermost Early Paleocene Transpressional Arc-type Magmatism

After the Late Cretaceous Peruvian contractional tectonic phase, mafic to felsic plutonic complexes (i.e., Torcaza, Cerro Bayo and Sombrero) were emplaced in the Mesozoic clastic and calcareous sequences at 81-64 Ma (Figure 7.1b). Large skarn zones and some Cu- and Au-bearing veins of minor economic interest are associated with the largest intrusions. Early shallow-level intrusion of Las Torres igneous complex were followed by short-lived, explosive volcanic eruption, the Sombrero plutonic complex was almost

synchronous. The K-T tectonic phase faulted and folded the Mesozoic cover and older units in the region. Within the Late Cretaceous-lowermost magmatic episode, there are two distinct geochemical suites: (1) an early tholeiitic alkaline suite including the Cerro Bayo intrusions with a back-arc affinity; and (2) a late calc-alkaline suite including the Sombrero plutonic complex, which has a frontal magmatic arc geochemical signature. Two other igneous rocks, the Torcaza pluton and Las Torres igneous complex, remain poorly understood geochemically due to the small number of analyses. However, results from two analysed samples of Las Torres unit suggest a co-magmatic relationship with the Sombrero intrusions. The magmatic source regime for the two major Cretaceous igneous suites were probably localised at the amphibole-stable zone in depleted mantle-lower crust. Inherited zircons of ca. 300-260 Ma provide evidence for crustal contamination/assimilation in Las Torres and Sombrero rock units (Appendix 5).

7.1.2.3 The Late Paleocene-Early Eocene Extensional Volcanism

Shortly after the K-T tectonic phase, a new phase of arc-linked magmatism started with minor intrusion of andesite dykes at ca. 60 Ma. The andesite dykes were followed the deposition of the Augusta Victoria Formation between 57 Ma and 53 Ma. This major volcanic episode occurred in a renewed volcanic arc system in an extensional tectonic regime (Figure 7.1c). The REE geochemistry shows the existence of two discrete magmatic suites. The data indicate a decrease in the depth of the source region from a thicker crust (garnet-zone in an eclogite lower crust-mantle) for the andesite dykes to a thin crust (amphibolite-zone in an amphibolite lower-middle crust) for the Augusta Victoria volcanic rocks. Large zones of hydrothermal alteration are hosted by tuffaceous and lava packages of the Augusta Victoria sequence and strong structural and lithological controls influenced their locations. The Augusta Victoria Formation was folded and faulted by the Incaic tectonic that diachronically affected large portions of the Central Andes by the middle-late Eocene.

7.1.2.4 The Middle-Late Eocene Syn-tectonic Magmatism and Porphyry Cu-style Intrusions

During the Eocene period, magmatic activity was essentially continuous and contemporaneous with movements on the Domeyko Fault System (Figure 7.1c). It consisted of short-lived magmatic events that can be separated into pre-, syn- and post-mineralisation timing relative to the porphyry copper intrusions. The successive magmatic events are as follows:

- The intrusion of the pre-mineralisation Cerro Rincones plutonic complex at ca. 43-41 Ma. This large, metaluminouos, calk-alkaline suite of diorite, monzodiorite, monzonite and monzogranite was originated within pyroxene- to amphibole-stable zones of partial melting.
- The 39-38 Ma Capella monzonite stocks are interpreted as pre-mineralisation intrusions and show similar geochemical and magmatic features to the 43-41 Ma Cerro Rincones plutonic complex.
- The syn-mineralisation La Escondida and Escondida Norte-Zaldivar porphyry copper intrusive complexes (ca. 39-34 Ma) were emplaced syn-tectonically with the Incaic deformation phase (ca. 40-35 Ma).
- A syn- to post-mineralisation swarm of diorite and andesite dykes and a volcaniclastic sequence that is a few hundred metres thick were emplaced at ca. 38-36 Ma. They have geochemical compositions comparable with the adakite or tonalite-trodhjemite suites. The magmas were probably sourced from a higher pressure, deeper region of partial melting than the pre-mineralisation units, probable from amphibole- to garnet-stable zone in an eclogitic lower crust/mantle.

High denudation rates caused by uplift on the Domeyko Fault System have been suggested by preliminary low-temperature U-Th-(He) thermochronology on the Paleocene to Eocene volcanic and intrusive rock units. This is consistent with previous studies (Maksaev and Zentilli, 1999). A tentative chronology of the movements recognised on the Domeyko Fault System in the study area is as follow:

- A contractional deformation (ca. 50-41 Ma.) on the Domeyko Fault System (Figure 4.39a) was followed by a right-lateral transpressional regime that activated the principal N-striking faults, including the Sierra de Varas and La Escondida master faults, at ca. 40-37 Ma. The Escondida Norte-Zaldivar porphyry system and the high sulfidation epithermal Cu-Fe-As-Au veins of Chimborazo were emplaced along NNE- to NE-striking tensional fractures during the transpressive stage (Figure 4.39b).
- Reversion to left-lateral movement is inferred to have occurred along La Escondida master fault after 36 Ma (Figure 4.39c). This controlled the emplacement of high sulfidation Cu-Fe-As-Au veins at La Escondida and subsequently at Escondida Norte-Zaldivar ore bodies.
- La Escondida region experienced significant extension and sinistral strike-slip

transtension from the late Oligocene to the early Miocene (Figure 4.40). Movements on La Escondida master fault produced the rhomboidal pull-apart basin of the Salar de Hamburgo. Dissection of the Hamburgo basin occurred in the early Miocene by NNE-striking short-cut faults.

The large volumes of gravels of the Pampa Mulas Formation record uplifting and denudation of the Domeyko Cordillera, between the late Oligocene and middle Miocene (Figure 4.40). Development of major secondary enrichment zones at La Escondida and Zaldivar-Escondida Norte deposits required low denudation rates during the late Oligocene-middle Miocene (Sillitoe and McKee, 1996; Camus, 2003). Post-middle Miocene hyper- to semi-aridity and tectonic quiescence were optimal for the preservation of these world-class supergene-enriched copper deposits (Sillitoe and McKee, 1996; Camus, 2003).

The middle Eocene-early Oligocene Incaic deformational event largely affected the Mesozoic geological record and activated regional fractures. Strike-slip movements occurred on the Domeyko Fault System in La Escondida district are in agreement with principal movements recorded by the Domeyko Fault System in other segments such as Quebrada Blanca-Chuquicamata (Tomlinson and Blanco, 1997a, 1997b), Sierra Exploradora (Niemeyer, 1999) and El Salvador-Potrerillos (Cornejo et al., 1993). Athough some previous workers have argued for tens of kilometres of left-lateral motion inferred to have be occurred since the middle Oligocene for other regions (i.e., Chuquicamata and Sierra de Varas; Tomlinson and Blanco, 1997a, 1997b; Niemeyer et al., 2000a), no evidence for such large scale movements has been recognised in La Escondida district. Likewise, no field evidence for the hypothetical Archibarca lineament (Salfity, 1985), which Richards (2001) considered to have exerted a first-order control of the mineralisation loci at La Escondida district, could be found during the current study.

There are two north-trending sub-belts of Eocene hydrothermal alteration systems in La Escondida district. The eastern sub-belt contains the world-class middle-late Eocene Cu deposits of La Escondida and Escondida Norte-Zaldivar deposits and several marginal mineralised intrusives (i.e. Baker breccia, Carmen, Pinta Verde, and Ricardo). Three spatially and temporally separated episodes of advanced argillic alteration occurred at La Escondida, Escondida Norte-Zaldivar and Baker, from 37-33 Ma. These deposits represent the culmination of hydrothermal activity in La Escondida district. The more

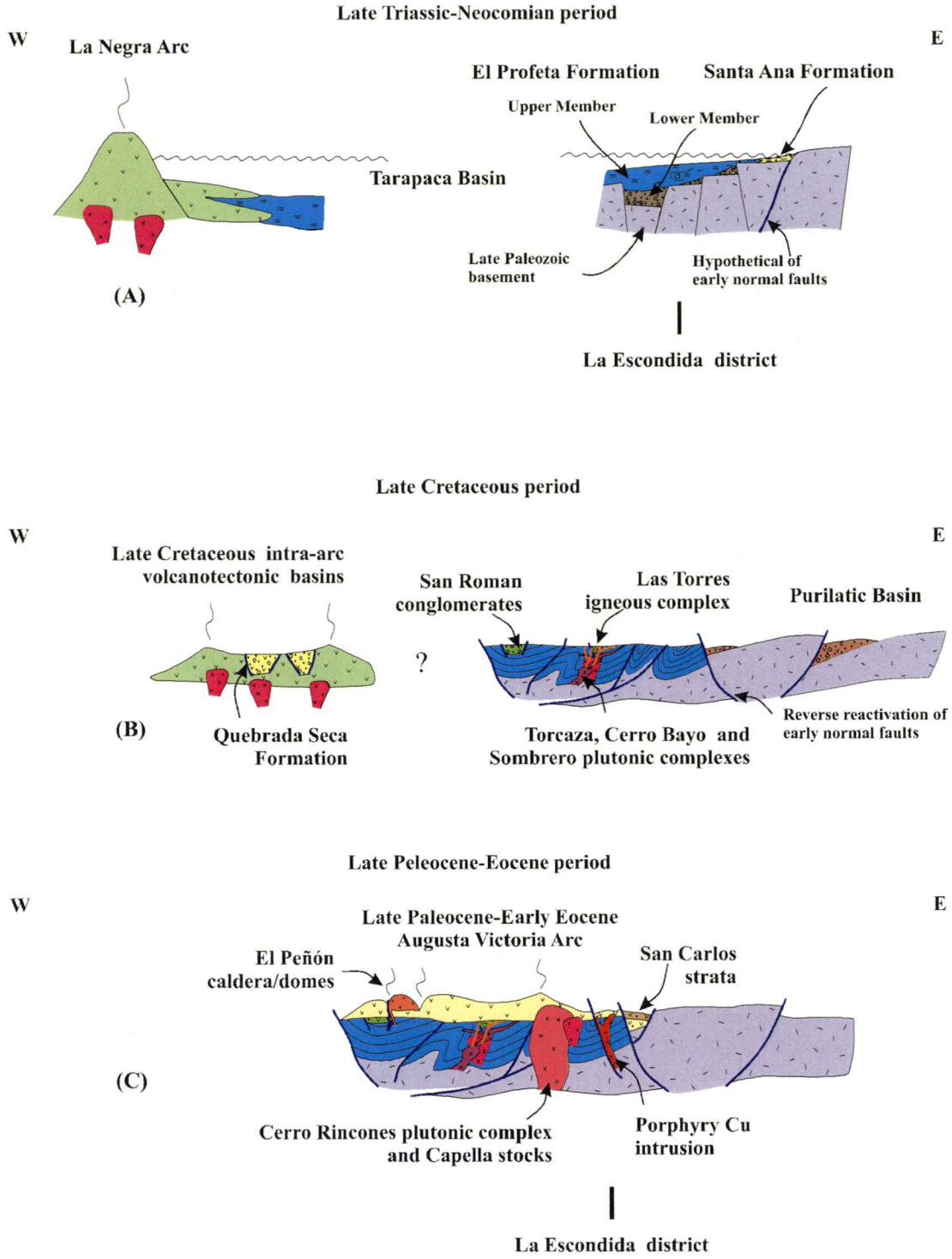

Figure 7.1 Schematic Mesozoic-Lower Cenozoic evolution of La Escondida district.

poorly defined western sub-belt consists of advanced argillic altered and silicified rocks (lithocaps at Capella, Rincones, Zapato Verde, Poblete, and the Chimborazo high sulfidation Cu deposit). However, the available low-precision geochronological data do not permit the western sub-belt to be defined as distinct metallogenic belt (early or middle

Eocene?). It is possible that both of sub-belts are the same ages based on the available data.

7.2 RECOMMENDATIONS

Future work that could help to improve the geological model of La Escondida district includes:

- Detailed facies analysis and geochronological investigation of Las Torres igneous complex, in order to decipher its evolution within the Late Cretaceous magmatic arc.
- High-precision radiometric dating of the western sub-belt of Eocene hydrothermal alteration systems. The sub-belt has been defined on the basis of poor quality K-Ar ages of uncertain merit, and it is a high priority to determine if this belt represents a discrete metallogenetic event in the district.
- Additional geochemical and geochronological investigations and detailed facies analysis of the San Carlos strata, would give significant insights into the evolution of this syn-mineralisation volcano-sedimentary depocenter.
- Extrapolation of the surface geology from the mine open pits (La Escondida and Escondida Norte) toward the bore hole-based subsurface geology that has been identified in Salar Hamburgo basin and adjacent covered sectors could help to find blind porphyry systems.
- Present and future brownfield exploration activity should focus on the eastern sub-belt of the Eocene hydrothermal alteration systems. Undiscovered ore bodies peripheral and/or marginal to the known large mineralised systems is conceived most likely along the north- and northeast-trending structural braches of La Escondida master fault system.
- The eastern sub-belt of the Eocene hydrothermal alteration systems has been highly explored with meagre results and a few small cover areas remain untested for marginal targets. No further potential is observed under the Recent gravels.

REFERENCES

Alfaro, J. (2001) Proyecto Chimborazo: Informe campaña sondajes Enero-Junio 2001. Escondida Brownfields Exploration Program. Minera Escondida Ltda., p. 1-64.

Allmendinger, R., Jordan, T., Kay, S., and Isack, B. (1997) The evolution of the Altiplano-Puna Plateau of the Central Andes. Annual Review of Earth and Planetary Sciences, v. 25, p. 139-174.

Alpers, C., and Brimhall, G. (1988) Middle Miocene climatic change in the Atacama Desert, northern Chile, evidence from supergene mineralization at La Escondida. Geological Society of America Bulletin, v. 100, p. 1640-1656.

Alpers, C., and Brimhall, G. (1989) Paleohydrologic evolution and geochemical dynamics of cumulative supergene metal enrichment at La Escondida, Atacama Desert, northern Chile. Economic Geology, v. 84, p. 229-255.

Amilibia, A., Sabat F., Chong, G., Muñoz, J., Roca, E., and Rodríguez-Pera, A. (1999) Evolution of Domeyko range, northern Chile. *In* Fourth International Symposium on Andean Geodynamics (ISAG), Goettingen, p. 25-29.

Amilibia, A. (2000) Inversión tectónica en la Cordillera de Domeyko, Andes del Norte de Chile. Tesis de Doctorado (Unpublished), Departament de Geodinàmica i Geofísica Universitat de Barcelona, Barcelona.

Amilibia, A., Sábat, F., Chong, G., Muñoz, J., Roca, E., and Gelabert, B. (2000) Criterios de Inversión Tectónica, Ejemplos de la Cordillera de Domeyko (II Región de Antofagasta). *In* Noveno Congreso Geológico Chileno, Puerto Varas, 2000, p. 548-552.

Amilibia, A., and Skarmeta, J. (2003) La inversión tectónica de la Cordillera de Domeyko en el norte de Chile y su relación con la intrusión de sistemas de pórfidos de Cu-Mo. *In* Décimo Congreso Geológico Chileno, Concepción, 2003, Sesión Temática 5, CD.

Anderson, J. (1982) Characteristics of leached capping and techniques of appraisal. *In* Titley, S. (ed.) Advances in Geology of Porphyry Copper Deposits, Southwestern

North America. University of Arizona Press, p. 275-295.

Andriessen, P., and Reutter, K. (1994) K–Ar and fission track mineral age determination of igneous rocks related to multiple magmatic arc systems along the 23°S latitude of Chile and NW Argentina. *In* Reutter, K., Scheuber, E., and Wigger P. (eds) Tectonics of the Southern Central Andes, Springer Verlag, Heidelberg, p. 141–153.

Annen, C, and Sparks, R. (2002) Effects of repetitive emplacement of basaltic intrusions on thermal evolution and melt generation in the crust. Earth and Planetary Science Letters, v. 203, p. 937-955.

Arabaz, W. (1971) Geological and geophysical studies of the Atacama fault zone in northern Chile. Ph.D. Thesis (Unpublished), University of California, California, p. 1-264.

Arancibia, G., Matthews, S., and Perez de Arce, C. (2006) K-Ar and $^{40}Ar/^{39}Ar$ geochronology of supergene processes in the Atacama Desert, northern Chile, tectonic and climatic relations. Journal of the Geological Society of London, v. 163, p. 107-118.

Ardill, J., Flint, S., Chong, G., and Wilke, H. (1998) Sequence stratigraphy of the Mesozoic Domeyko basin, northern Chile. Journal of the Geological Society of London, v. 155, p. 71-88.

Arriagada, C., Roperch, P., Mpodozis, C. (2000) Clockwise block rotations along the eastern border of the Cordillera de Domeyko, northern Chile (22°45'-23°30'S). Tectonophysics, v. 326, p. 153-171.

Arriagada, C., Roperch, P., Mpodozis, C., Dupond-Nivet, G., Cobbold, P., Chauvin, A., and Cortés, J. (2003) Paleogene clockwise tectonic rotations in the forearc of central Andes, Antofagasta region, northern Chile. Journal of Geophysical Research, v. 108(B1), 2032, doi: 10.1029/2001JB001598.

Bahlburg, H., and Hervé, F. (1997) Geodynamic evolution and tectonostratigraphic terranes of northwestern Argentina and northern Chile. Geological Society of America Bulletin, v. 109, p. 869-884.

Bahlburg, H., Moya, M., Zimmermann, U., Bock, B., Hervé, F. (2000) Paleozoic plate tectonic evolution of the western Gondwana margin in northern Chile and northwestern Argentina. *In* Zeitschrift Für Angewandte Geologie, SH 1 Geoscientific Cooperation with Latin America, 31st International Geological Congress, Rio de Janeiro, 2003, p. 345-353.

Basso, M., Marinovic, N. (2003) Antcedentes geocronológicos del volcanismo Triásico en la zona de los estratos del Bordo. *In* Décimo Congreso Geológico Chileno, Concepción, 2003, Sesión Temática 5, CD (poster).

Beck, S., Zandt, G., Myers, S., Wallace, S., Silver, P., and Drake, L. (1996) Cristal-thickness variation in the central Andes. Geology, v. 24, p. 407-410.

Bell, M. (1987) The origin of the Upper Palaeozoic Chañaral melánge of northern Chile. Journal of the Geological Society of London, v. 144, p. 599–610.

Black, L., Kamo S., Allen C., Aleinikoff, J., Davis, D., Korsch, R., and Foudoulis C. (2003) TEMORA 1: a new zircon standard for Phanerozoic U-Pb geochronology. Chemical Geology, v. 200, p. 155–170.

Blanco, N., Tomlinson, A., Mpodozis, C., Pérez de Arce, C., and Matthews, S. (2003) Formación Calama, Eocene, II Región de Antofagasta (Chile): Estratigrafía e implicancias tectónicas. *In* Décimo Congreso Geológico Chileno, Concepción, 2003, Sesión Temática 3, CD.

Blanco, N., and Tomlinson, A. (2006) Fm. Sichal: Sedimentación aluvial (Eoceno-Oligoceno) sintectónica al evento orogénico Incaico, II Región de Antofagasta, Chile. *In* Undécimo Congreso Geológico Chileno, Antofagasta, 2006, v. 2, p. 29-32.

Bock, B., Bahlburg, H. Wörner, G., Zimmermann U. (2000) Tracing crustal evolution in the southern Central Andes from Late Precambrian to Permian with geochemical and Nd and Pb isotope data. Journal of Geology, v. 108, p. 515-535.

Boric, R., Díaz, F., Maksaev, V. (1990) Geología y yacimientos metalíferos de la Región de Antofagasta. Servicio Nacional de Geología y Minería, Boletín No. 40, p. 1-246.

Bouzari, F., Clark, A.H. (2002) Anatomy, evolution and metallogenic significance of the supergene orebody of the Cerro Colorado porphyry copper deposit, I region, northern Chile. Economic Geology, v. 97, p. 1701–1740.

Brandon, M. (2005) Programs for illustrating closure, partial retention, and the response of cooling ages to erosion: Closure, AGE2EDOT, and resptime. htt: //ww.geology.yale.edu/~brandon.

Breitkreuz, C. (1991) Stratigraphic, volcanological and geochemical investigation of Late Carboniferous-Triassic volcanosedimentary successions in Chile, 20°-25°S: Geotectonic implications. *In* Sexto Congreso Geológico Chileno, Viña del Mar, 1991, p. 23-26.

Breitkreuz, C., Zeil, W. (1994) The Late Carboniferous to Triassic volcanic belt in northern Chile. *In* Reutter, K.-J., Scheuber, E. & Wigger, P. (eds) Tectonics of the Southern Central Andes, Springer Verlag, p. 277–292.

Brook, M., Shepherd, T., Spiro, B., Smelling, N., Swainbank, J., and Pandhurst, R. (1986) ANDCHRON: Andean geochronology and metallogenesis. British Geological Survey, p. 1-137.

Brown, M., Díaz, F., and Grocott, J. (1993) Displacement history of the Atacama fault system 25°-27°S, northern Chile. Geological Society of America Bulletin, v. 105, p. 1165-1174.

Brown, A. (1992) Sediment-hosted stratiform copper deposits. Geoscience Canada, v. 19, p. 125-141.

Cabanis, B., and Lecolle, M. (1989) Le diagramme La/10-Y/15-Nb/18: un outil pour la discrimination des series volcaniques et la mise en evidence des processus de melange et/ou de contamination crustale. C.R. Acad. Sci. Ser. II, v. 309, p. 2023-2029.

Caffe, P., Trumbull, R., Coira, B., and Romer, R. (2002) Petrogenesis of Early Neogene magmatism in the northern Puna; implications for magma genesis and crustal processes in the Central Andes plateau. Journal of Petrology, v. 43, p. 907-942.

Cahill, T., Isacks, B. (1992) Seismicity and shape of subducted Nazca Plate. Journal of Geophysical Research, v. 97, p. 17503-17529.

Campbell, I., Ballard, J., Palin, J., Allen, C., Faunes, A. (2006) U-Pb zircon geochronology of granitic rocks from the Chuquicamata-El Abra porphyry copper belt of Northern Chile: Excimer laser ablation ICP-MS analysis. Economic Geology, v. 101, p. 1327-1344.

Campos, E., Vis, R., Touret, J., Delgado, J. (2000) Microthermometry, raman and pixe microanalysis of extremely saline, magmatic fluid inclusions from Zaldivar porphyry copper deposit. *In* Noveno Congreso Geológico Chileno, Puerto Varas, 2000, p. 167-170.

Campos, E. (2002) Metal origin and fluid evolution in the Zaldivar porphyry copper deposit, Chile: An orthomagmatic model. Ph.D. Thesis (Unpublished) Vrije Universiteit Amsterdam, Amsterdam, p. 1-165.

Campos, E., Touret, J., Nikogosian I., and Delgado, J. (2002) Overheated, Cu-bearing magmas in the Zaldívar porphyry-Cu deposit, northern Chile: Geodynamic consequences. Tectonophysics, v. 345, p. 229– 251.

Campos, E. (2003) Compositional variability in the hydrotermal system at the Zaldívar porphyry copper deposit: A fluid inclusion approach. *In* Décimo Congreso Geológico Chileno, Concepción, 2003, Simposium 2: Metalogénesis Andina, CD.

Camus, F. (2003) Geología de los sistemas porfíricos en los Andes de Chile. Servicio Nacional de Geología y Minería, p. 1-267.

Charrier, R. (1979) El Triásico en Chile y regiones adyacentes de Argentina: Una reconstrucción paleogeográfica y paleoclimática. Universidad de Chile. Comunicaciones, No. 26, p. 1-37.

Chávez, W. (2000) Supergene oxidation of copper deposit: Zoning and distribution of copper oxide minerals. Society of Economic Geologists Newsletter, No. 41.

Chong, G. (1973) Reconocimiento geología del área Catalina-Sierra de Varas y Estratigrafía del Jurásico del Profeta. Memoria de Título (Unpublished), Universidad de

Chile, p. 1-294.

Coira, B., Davidson, J., Mpodozis, C., and Ramos, V. (1982) Tectonic and magmatic evolution of the Andes of northern Argentina and Chile. Earth-Science Reviews, Special Issue Magmatic Evolution of the Andes, v. 18, p. 303-332.

Coira, B., Mahlburg-Kay, S., Peréz, B., Woll, B., Hanning, M., and Flores, P. (1999) Magmatic sources and tectonic setting of Gondwana margin Ordovician magmas, northern Puna of Argentina and Chile. *In* Ramos, V., and Keppie, J. (eds) Laurentia-Gondwana connection before Pangea, Geological Society of America, Special Paper, No. 336, p.145–170.

Coldwell, B., Petford, N., Murphy, P., Smith, M. (2005) 'Adakite' rocks of the Yungay Formation, Peru: Problems with tectonic setting and origin. Geophysical Research Abstracts, v.7, 02656.

Collinson, J. (1996) Alluvial sediments. *In* Reading, H.G. (ed) Sedimentary Environments, Processes, Facies and Stratigraphy. Blackwell, New York, 688 p.

Coney, P., Edwards, A., Hine, R., Morrison, F., and Windrim, D. (1990) The regional tectonics of the Tasman orogenic system, eastern Australia. Journal of Structural Geology, v. 12, p. 519-543.

Corbett, G., Leach, T. (1996) Southwest pacific rim gold-copper systems: Structure, alteration and mineralization. Workshop manual, p. 1-185.

Cornejo, P., Mpodozis, C., Ramírez, C., Tomlinson, A. (1993) Estudio Geológico de la Región de El Salvador y Potrerillos. Servicio Nacional de Geología y Minería, Informe Registrado (IR-93-1), p. 1 –258.

Cornejo, P., Mpodozis, C. (1996) Geología de la región de Sierra Exploradora 25°-26°S. Servicio Nacional de Geología y Minería, Informe Registrado (IR-96-09), 2 v., p. 1–330.

Cornejo, P., Tosdal, R., Mpodozis, C., Tomlinson, A., Rivera, O., and Fanning, C. (1997) El Salvador, Chile porphyry copper deposit revisited: Geologic and geochronologic

framework. International Geology Review, v. 39, p. 22-54.

Cornejo, P., Matthews, S. (2000) Relación entre magmatismo-tectónica y su implicancia en la formación de sistemas de pórfidos cupríferos: Yacimiento El Salvador, III Región, Chile. *In* Noveno Congreso Geológico Chileno, Puerto Varas, 2000, v.1, p. 184-188.

Cornejo, P., Matthews, S. (2001) Evolution of magmatism from the uppermost Cretaceous to Oligocene, and it relationship to changing tectonic regime, in the Inca de Oro-El Salvador area (Northern Chile). *In* Tercer Simposio Sudamericano de Geología Isotópica, Pucón, 2001, Sesión Temática 6, CD.

Cornejo, P., Matthews, S., Pérez de Arce, C. (2003) The "K-T" compressive deformation event in northern Chile (24-27° S). *In* Décimo Congreso Geológico Chileno, Concepción, 2003, Sesión Temática 1, CD.

Cornejo, P., Matthews, S., Marinovic, N., Pérez de Arce, C., Basso, M., Alfaro, J., and Navarro, M. (2006) Alteración hidrotermal y mineralización recurrente de Cu y Cu-Mo durante el Pérmico y el Triásico en la Cordillera de Domeyko (Zona de Zaldívar-Salar de Los Morros): Antecedents geocronológicos U-Pb, $^{40}Ar/^{39}Ar$ y Re-Os. *In* Undécimo Congreso Geológico Chileno, Antofagasta, 2006, v. 2, p. 219-222.

Coward, M., Gilcrist, R., and Trudgill, B. (1991) Extensional structures and their tectonic inversion in the W. Alps. *In* Roberts, A., Yielding, G, and Freeman, B. (eds) The Geometry of Normal Faults. Geological Society of London Special Publication 56, p. 93-112.

Davidson, J., Ramirez, C., Gardeweg, M., Hervé, M., Brook, M., Pankhurst, R. (1985) Calderas del Paleozoico Superior-Triásico Inferior y mineralización asociada en la Cordillera de Domeyko, Norte de Chile. Universidad de Chile, Comunicaciones, No. 35, p.53-57.

Dingman, R. (1963) Cuadrángulo Tulor: Provincia de Antofagasta, Escala 1:50.000. Instituto de Investigaciones Geológicas, Carta Geológica de Chile, No. 11, p. 1-35.

Drummond, M., Defant M. (1990) A model for trondhjemite-tonalite-dacite genesis and

crustal growth via slab melting: Archean to modern comparisons. Journal of Geophysical Research, v. 95, p 503-521.

Farley, K. (2000) Helium difusion from apatite: general behaviour as illustred by Durango fluorapatie. Journal of Geophysical Research, v. 105, p. 2903-914.

Ferraris, F., and Di Biase, F. (1978) Hoja Antofagasta: Región de Antofagasta, escala 1:250.000. Instituto de Investigaciones Geológica, Carta Geológica de Chile, No 30, p. 1-48.

Fleck, R., Sutter, J., and Elliot, D. (1977) Interpretation of discordant $^{40}Ar/^{39}Ar$ age spectra of Mesozoic tholeiites from Antartica. Geochimica et Cosmochimica Acta, v. 41, p. 15-32.

Flowers, R., Bowring, S., and Reiners, P. (2006a) Low long-term erosion rates and extreme continental stability documented by ancient (U-Th)/He dates. Geology, v. 34, p. 925-928.

Fuenzalida, G. (1986) Estratigrafía y estructura del Paleozoic y Mesozoic en el area Cerro Bayo-Cerro Chinchilla. Taller de Título II (Unpublished), Universidad de Chile, p. 1-84.

Gani, M. (2004) From turbid to lucid: A straightforward approach to sediment gravity flows and their deposits. The Sedimentary Records, v.2, p. 4-8.

García, F. (1967) Geología del Norte Grande de Chile. Sociedad Geológica de Chile, Empresa Nacional del Petróleo, Symposium sobre el geosinclinal Andino, Santiago, p. 1-138.

Gardeweg, M., Pino, H., Ramírez, C., Davidson, J. (1994) Mapa geológico del area de Imilac y Sierra Almeida, Escala 1:100.000, Región de Antofagasta. Servicio Nacional de Geología y Minería, Documentos de Trabajo No. 7, 1 mapa.

Garver, J., Reiners, P., Walker, L., Ramage, J., and Perry, S. (2005) Implications for timing of Andean uplift from thermal resetting of radiation-damaged zircon in the Cordillera Huayhuash, northern Peru. Journal of Geology, v. 113, p.117-138.

Gill, J. (1981) Orogenic Andesites and Plate Tectonics. Springer-Verlag, p. 1-390.

Gillespie, M., and Styles, M. (1999) Classification of igneous rocks. Volume 1 of the BGS rock classification scheme. British Geological Survey Research, Report Number RR 99-06, p. 1-52.

Gilmour, P. (1995) A field guide to leached capping interpretation. *In* Pierce and Bolm (eds) Porphyry Copper Deposits of the American Cordillera, Arizona Geological Society Digest 20, p. 169-179.

González, J., Niemeyer, H., Benedetto, J., Brussa, E. (2006) La Formación Quebrada Grande, Arenigiano superior-Llanvirniano inferior del Cordón de Lila, Región de Antofagasta, Norte de Chile. I*n* Undécimo Congreso Geológico Chileno, Antofagasta, 2006, v. 1, p. 49-52.

González, J., Niemeyer, H., Benedetto, J., Brussa, E. (2007) The Ordovician Quebrada Grande Formation, Cordón de Lila Antofagasta Región, northern Chile: Stratigraphic and paleogeographic significance. Revista Geológica de Chile, v. 34, p. 277-290.

Grocott, J., and Taylor, G. (2002) Magmatic arc fault systems, deformation partitioning and emplacement of granitic complexes in the Coastal Cordillera, north Chilean Andes (25°30'S to 27°30'S). Journal of the Geological Society of London, v. 159, p. 425-442.

Gröschke, M., Wilke, H. (1986) Lithology and stratigraphy of Jurassic sediments in the North Chilean Pre-Cordillera between 21°30' and 22°S. Zbl. Geol. Palaönt. Teil. 1, 1317–1324.

Gustafson, L., and Hunt, J. (1975) Porphyry copper deposit at El-Salvador, Chile. Economic Geology, v. 70, p. 857–912.

Harris, A., Allen, Ch., Bryan, S., Campbell, I., Holcombe, R., and Palin, J. (2004) ELA-ICP-MS U-Pb zircon geochronology of regional volcanism hosting the Bajo de la Alumbrera Cu-Au deposit: implications for porphyry-related mineralisation. Mineralium Deposita, v. 39, p. 46-67.

Hartley, A., and Chong, G. (2002) A late Pliocene age for the Atacama desert: implications for the desertification of western South America. Geology, v. 30, p. 43–46.
Hartley, A. (2003) Andean uplift and climate change. Journal of the Geological Society, v. 160, p. 7-10.

Hartley A., Rice C. (2005) Controls on supergene enrichment of porphyry copper deposits in the Central Andes: A review and discussion. Mineralium Deposita, v. 40, p. 515-525.

Haschke, M., Siebel, W., Günther, A., and Scheuber, E. (2002a) Repeated crustal thickening and recycling during the Andean orogeny in North Chile (21°–26°S). Journal of Geophysical Research, v. 107 (B1), doi: 10.1029/2001JB000328.

Haschke, M., Deeken, A., Insel, N., Sobel, E., Grove, M., and Schmitt, A. (2005) Growth pattern of the Andean Puna plateau constrained by apatite fission tracks, apatite (U-Th)/He, K-felspard $^{40}Ar/^{39}Ar$, and zircon U-Pb geochronology. *In* 6th International Symposium of Andean Geodynamics (ISAG), Barcelona, 2005, Extended Abstract, p. 360-363.

Haschke, M., Günther, A., Melnick, D., Echtler, H., Reutter, K.-J., Scheuber, E., and Oncken, O. (2006) Central and Southern Andean Tectonic Evolution Inferred from Arc Magmatism. *In* Oncken, O., Chong, G., Franz, G., Giese P., Götze, H.-J., Ramos V., Strecker, M., and Wigger P. (eds) The Andes: Active Subduction Orogeny, Springer Berlin-Heidelberg, Frontiers in Earth Science Series, p. 337-354.

Hawkesworth, H., Gallagher, K., Hergt, J., and McDermott, F. (1993) Mantle and slab contributions in arc magmas. Annual Review of Earth and Planetary Sciences, v. 21, p. 175-204.

Hedenquist, J. (1987) Mineralisation associated with volcanic-related hydrothermal systems in the Circum-Pacific Basin. *In* Horn, N. (ed), Transactions of 4th Circum Pacific Energy and Mineral Resources Conference, Singapore, American Association of Petroleum Geologists, p. 513–524

Isaacson, P., and Díaz-Martinez, E. (1995) Evidence for a Middle and Late Paleozoic Foreland Basin and Significant Paleolatitudinal Shift, Central Andes. *In* Tankard, A.,

Suarez, R., and Welsink, H. (eds) Petroleum Basins of South America, American Association of Petroleum Geologists, Memoir 62, p. 231-249.

Jaunousek, V., Farrow, C., and Erban, V. (2007) Geochemical Data Toolkit (GCDkit) for Windows. http://www.gla.ac.uk/gcdkit

Jordan, T., Isacks, B., Allmendinger, R., Brewer, J., Ramos, V., Ando, C. (1983) Andean tectonics related to geometry of subducted Nazca Plate. Geological Society of America Bulletin, v. 94, p. 341-361.

Jordan, T., Reynolds, J., and Erikson, J. (1997) Variability in age of initial shortening and uplift in the Central Andes, 16-33°30'S. *In* Ruddiman, W. (ed) Tectonic uplift and climate changes, Penum Press, p. 41-66.

Kay, R., Kay S. (1993) Delamination and delamination magmatism. Tectonophysics, v. 219, p. 177-189.

Kay, S., Mpodozis, C., and Coira, B. (1999) Neogene magmatism, tectonism and mineral deposits of the Central Andes (22° - 33°S Latitude). *In* Skinner, B. (ed) Geology and ore deposits of the Central Andes, Society of Economic Geology Special Publication No. 7, p. 27-59.

Kim, S. (2001) Petrographic description of samples from Chimborazo area. Brownfields Exploration Program. Minera Escondida Ltds., Internal report.

Kojima, S., Salazar, P., and Fukimaki, H. (2005) Petrological and geochemical characteristics of the Cerro Colorado plutonic complex in the Precordillera of northern Chile. Resource Geology, v. 55, p. 45-54.

Kosler J. (2001) Laser-ablation ICPMS study of metamorphic minerals and processes. *In* Sylvester, P. (eds) Laser-ablation-ICPMS in the earth sciences; principles and applications. Mineralogical Association of Canada, v. 29, p. 185-202.

Kramer, W., Siebel, W., Romer, R., Haase, G., Zimmer, M., Ehrlichmann, R. (2005) Geochemical and isotopic characteristics and evolution of the Jurassic volcanic arc

between Arica (18°30'S) and Tocopilla (22°S), North Chilean Coastal Cordillera. Chemie der Erde. v. 65, p. 47-68.

Ladino, M., Tomlinson, A., Blanco, N. (1999) New constrains for the age of Cretaceous compressional deformation in the Andes of northern Chile [Sierra de Moreno, 21°-22°10']. *In* Symposium International on Andean Geodynamics, 4th, Göttingen, 1999, p. 407-410.

Lindsay, D., Zentilli, M., and Rojas de la Rivera, J. (1995) Evolution of an active ductile brittle shear system controlling mineralisation at the Chuquicamata porphyry copper deposit, northern Chile. International Geological Review, v. 37, p. 945-958.

Lira, G. (1991) Geología y paleografía mesozoica de la Precordillera de Calama, región de Antofagasta, Chile. Sexto Congreso Geológico Chileno, Viña del Mar, 1991, p. 645-648.

Lucassen, F., Franz, G., Thirlwall, M., Mezger K. (1999a) Crustal recycling of metamorphic basement: Late Paleozoic granites of the Chilean Coast Range and Precordillera at ~22°S. Journal of Petrology, v. 40, p. 1527-1551.

Lucassen, F., Becchio, R, Wilke, H., Thirlwall, M.F., Viramonte, J. ,Franz, G., Wemmer, K. (2000) Proterozoic-Paleozoic development of the basement of the Central Andes (18°–26°) - 2 mobile belt of the South American craton. Journal of South American Earth Sciences, v. 13, p. 697–715.

Lucassen, F., Trumbull, R., Franz, G., Creixell, C., Vásquez, P., Romer, R., and Figueroa, O. (2004) Distinguishing crustal recycling and juvenile additions at active continental margins: The Palaeozoic to recent compositional evolution of the Chilean Pacific margin (36-41°S). Journal of South American Earth Sciences, v. 17, 103-119.

Lucassen, F., Kramer, W., Bartsch, V., Wilke, H., Franz, G., Romer, R, Dulski, P. (2006) Nd, Pb and Sr isotope composition of juvenile magmatism in the Mesozoic large magmatic province of northern Chile (18-27°): indications for a uniform subarc mantle. Contributions to Mineralogy and Petrology, v. 152, p. 571-589.

Macdonald, R., Smith, R., and Thomas, J. (1992) Chemistry of the subalkaline silicic

obsidian. U.S. Geological Survey, Professional Paper 1523, p. 1-214.

Maksaev, V. (1990) Metallogeny, geological evolution and thermochronology of the Chilean Andes between latitudes 21 ° and 26° south, and the origin of the major porphyry copper deposits. Ph.D. Thesis (Unpublished), Dalhousie University, Dalhousie, p. 1-554.

Maksaev, V., Marinovic, N., Smoje, I., Mpodozis, C. (1991) Mapa geológico de la hoja Augusta Victoria, Escala 1:100.000 Región de Antofagasta. Servicio Nacional de Geología y Minería, Documentos de Trabajo No 1, 1 mapa.

Maksaev, V., and Zentilli, C. (1999) Fission track thermochronology of the Domeyko Cordillera, northern Chile; implications for Andean tectonics and porphyry copper metallogenesis. Exploration and Mining Geology, v. 8; p. 65-89.

Marinovic, N., Smoje, I., Maksaev, V., Hervé, M., Mpodozis, C. (1995) Hoja Aguas Blancas: Región de Antofagasta, escala 1:250.000. Servicio Nacional de Geología y Minería, Carta Geológica de Chile, No. 70, p. 1-150.

Marinovic, N., Cortés, J., García, M. (1996) Estudio geológico regional de la zona comprendida entre Sierra del Buitre y Pampa San Román. Servicio Nacional de Geología y Minería, Informe Registrado (IR-96-8), 2 v., p. 1-150.

Marquardt, J., Rojas, O., Puig, A., Valdés, R. (1994) El distrito Anillo, un sistema hidrotermal alto tipo pórfido de oro del Eoceno, en la Depresión Central de la II Región de Chile. *In* Séptimo Congreso Geológico Chileno, Viña del Mar, 1994, v. 2, p. 855-859.

Marsh, T., Einaudi, M., McWilliams, M. (1997) $^{40}Ar/^{39}Ar$ geochronology of Cu-Au and Au-mineralization in the Potrerillos district, Chile. Economic Geology, v. 92, p. 784-806.

Masterman, G., Cooke, D., Berry, R., Walshe, J., Lee, A., and Clark, A. (2005) Fluid chemistry, structural setting, and emplacement history of the Rosario Cu-Mo porphyry and Cu-Ag-Au epithermal veins, Collahuasi district, northern Chile. Economic Geology, v. 100, p. 819-834.

Matthews, F., Caric, Y., Díaz, J., Carrasco, N. (2004) Programa de Exploraciones

Brownfields Escondida, Blancos de Sierra de San Carlos. Minera Escondida Ltda., Internal report, p. 1-72.

Maturana, M., and Saric, N. (1991) Geología y mineralización del yacimiento tipo pórfido cuprífero Zaldivar en Los Andes del norte de Chile. Revista Geológica de Chile, v. 18, p. 109-120.

May, G., Hartley, A., Stuart, F. (1996) Oligocene-recent sedimentary and tectonic evolution of the Calama basin, N Chilean forearc. *In* 3e Symposium International sur la Géodynamique Andine, Saint-Malo, 1996, p. 435-437.

May, G., Hartley, A., Chong, G., Stuart, F., Turner, P., and Kape, S. (2005) Eocene to Pleistocene lithostratigraphy, chronostratigraphy and tectonosedimentary evolution of the Calama Basin, northern Chile. Revista Geológica de Chile, v. 32, p. 33–60.

McClay, K., Skarmeta, J., and Bertens, A. (2002) Structural controls on porphyry copper deposits in northern Chile: New models and implications for Cu-Mo mineralization in subduction orogens: Applied structural geology for mineral exploration and mining, Kalgoorlie, Western Australia, 2002, p. 127.

McDougall, I., and Harrison, T. (1999) Geochronology and Thermochronology by the $^{40}Ar/^{39}Ar$ Method, Oxford University Press, New York, NY, 269 p.

McInnes, I., Farley, K., Sillitoe, R., and Kohn, B. (1999) Application of Apatite (U/Th)/He thermochronometry to the determination of the sense and amount of vertical displacement at the Chuquicamata porphyry copper deposit, Chile. Economic Geology, v. 94, p. 937-948.

McPhie, J., Doyle, M., Allen, R. (1993) Volcanic textures. A guide to the interpretation of textures in volcanic rocks. Centre for ore deposits and exploration studies, University of Tasmania, p. 1-189.

Meffre, S., Scott, E., Glen, R., and Squire, R. (2007) Re-evaluation of contact relationships between Ordovician volcanic belts and the quartz-rich turbidites of the Lachlan Orogen. Australian Journal of Earth Science, v. 54, p. 363-383.

Mégard, F. (1987) Cordilleran and marginal Andes: a review of Andean geology north of the Arica elbow (18°S). *In* Monger, J., and Francheteau, J. (eds) Circum-Pacific belts and evolution of the Pacific ocean basin. American Geophysical Union, Geodynamic series, v. 18, p. 71–95.

Mitra, S. (2002) Structural models of faulted detachment folds. Bulletin of the Geological Society of America, v. 86, p. 1673-16974.

Miyashiro, A. (1974) Volcanic rock series in island arc and active continental margins. American Journal of Science, v. 274, p. 321-355.

Mon, R., and Salfity, J. (1995) Tectonic evolution of the Andes of northern Argentina. *In* Tankard, A.J., Suarez-Soruco, R., and Welsink, H.J (eds) Petroleum Basins of South America, American Association of Petroleum Geologists, Memoir 62, p. 269–283.

Monroy, C. (2000) Nuevos antecedentes geológicos del pórfido cuprífero Zaldivar II región, Chile. In Noveno Congreso Geológico Chileno, Puerto Varas, 2000, p. 293-297.

Montaño, J. (1976) Estudio geológico de la zona de Caracoles y areas vecinas, con énfasis en el Sistema Jurásico, provincia de Antofagasta, II Región, Chile. Tesis de Doctorado, Departamento de Geología, Universidad de Chile, p. 1-169.

Mortimer, C. (1973) The Cenozoic history of the southern Atacama desert, Chile. Journal of the Geological Society, v. 129, p. 505-526.

Mote, T., Becker, T., Renne, P., and Brimhall, G. (2001) Chronology of exotic mineralization at El Salvador, Chile, by $^{40}Ar/^{39}Ar$ dating of copper wad and supergene alunite. Economic Geology, v. 96, p. 351-366.

Mouslopoulou, V., Nicol, A., Little, T., Walsh, J. (2006) Displacement transfer between intersecting regional strike-slip and extensional fault system. Journal of Structural Geology, v. 20, p. 1-17.

Mpodozis, C., and Ramos, V. (1989) The Andes of Chile and Argentina. *In* Ericksen, G., Cañas, M., and Reinemund, J. (eds) Geology of the Andes and its relation to hydrocarbon

and mineral resources. Earth Science Series, Circum-Pacific Council of Energy and Mineral Resources, Houston, p. 59-89.

Mpodozis, C., and Kay, S. (1992) Late Paleozoic to Triassic evolution of the Gondwana margin: Evidence from Chilean Cordilleran batholiths (28°–31°S). Geological Society of America Bulletin, v. 104, p. 999–1014.

Mpodozis, C., Marinovic, N., Smoje, I., Cuitiño, L. (1993a) Estudio geológico-estructural de la Cordillera de Domeyko entre Sierra Limón Verde y Sierra Mariposas región de Antofagasta, Escala 1:100.000. Servicio Nacional de Geología y Minería, CODELCO, Informe Registrado (IR-93-04), p. 1-282.

Mpodozis, C., Marinovic, C., Smoje, I. (1993b) Eocene left lateral strike-slip faulting and clockwise block rotations in the Cordillera de Domeyko, west of Salar de Atacama, Northern Chile. *In* Proceedings of the Second International Symposium on Andean Geodynamics (ISAG), Oxford, 1993, p. 195-198.

Mpodozis, C., and Thiele, K. (2002) Geological evolution of northern Chile chart. BHP Chile Inc., Internal report, 1 figure.

Mpodozis, C., Arriagada, C., Basso, M., Roperch, P., Cobbold, P., and Reich, M. (2005) Late Mesozoic to Paleogene stratigraphy of the Salar de Atacama basin, Antofagasta, Northern Chile: Implications for the tectonic evolution of the Central Andes. Tectonophysics, v. 399, 125–154.

Muir, R., Ireland, T., Weaver, S., Bradshaw, J., Evans, J., Eby, G., and Shelley, D. (1998) Geochronology and geochemistry of a Mesozoic magmatic arc system, Fiordland. New Zealand. Journal of the Geological Society of London, v. 155, p. 1027-1053.

Muñoz, J., Amilibia, A., Carrera, N., Mon, R., Chong, G., Roca, E., and Sàbat, F. (2005) A geological cross-section of the Andean orogen at 25.5° L.S. *In* 6th International Symposium of Andean Geodynamics (ISAG), Barcelona, 2005, Extended Abstract, p. 536-539.

Navarro, A., Niemeyer, H., Boucot, A., Aceñolaza, F. (2006) El Silúrico del Cordón de

Lila, Región de Antofagasta, Chile. *In* Undécimo Congreso Geológico Chileno, Antofagasta, 2006, v. 1, p. 85-92.

Nicolae, I., and Saccani, E. (2003) Petrology and geochemistry of the Late Jurassic calc-alkaline series associated to Middle Jurassic ophiolites in the South Apuseni Mountains (Romania). Schweiserische Mineralogische und Petrographische Mitteilungen, v. 83, p. 81-96.

Niemeyer, H., Urzúa, F., Aceñolaza, F., and González, R. (1985) Progresos recientes en el conocimiento del Paleozoico de la región de Antofagasta. *In* Cuarto Congreso Geológico Chileno, Antofagasta, 1985, v. 1, p. 410-438.

Niemeyer, H. (1989) El complejo ígneo-sedimentario del Cordón de Lila, región de Antofagasta: significado tectónico. Revista Geológica de Chile, v.16, p.163-181.

Niemeyer, H. (1996) Informe sobre geología structural del área de Chimborazo. Minera Cyprus Ltda., Antofagasta, p. 1-18.

Niemeyer, H., Urzúa, F., and Rubinstein, C. (1997) Nuevos antecedentes estratigráficos y sedimentológicos de la Formación Zorritas, Devónico-Carbonífero de Sierra Almeida, Región de Antofagasta, Chile. Revista Geológica de Chile, v. 24, p. 25-43.

Niemeyer, H. (1999) Nuevos datos cinemáticos para la Falla Sierra Castillo en Quebrada del Carrizo, Precordillera de la Región de Atacama, Chile. Revista Geológica de Chile, v. 26, p.159-174.

Niemeyer, H., and Leiva, G. (2000) Esbozo para un modelo estructural del pórfido Chuqui en mina Radomiro Tomic. *In* Noveno Congreso Geológico Chileno, Puerto Varas, 2000, v.1, p. 306-310.

Niemeyer, H., Berríos, H., Urrutia, C. (2000a) La falla Sierra de Varas al suroeste del salar de Punta Negra. *In* Noveno Congreso Geológico Chileno, Puerto Varas, 2000, v. 2, p. 617-620.

Niemeyer, H., Crignola, F. (2003) Análisis estructural de fallas mediante el método de los

diedros, aplicación al estudio de fallas de rumbo en Sierra de Almeida, Segunda Región de Antofagasta. Universidad Católica del Norte, Facultad de Ingeniería y Ciencias Geológicas, Revista Vertiente, No. 18, p. 11-16. Antofagasta.

Niemeyer, H., Berrios, H., Ruíz Cruz, D. (2004) Temperaturas de formación en cataclasitas triásicas de la Cordillera Domeyko, Antofagasta, Chile. Revista Geológica de Chile, v. 31, p. 3-18.

Niemeyer, H., Munizaga, R. (2008) Structural control of the emplacement of the Potrerillos porphyry copper, central Andes of Chile. Journal of South American Earth Sciences, doi: 10.1016/j.jsames.2008.08.006

Ojeda, J. (1986) Escondida porphyry copper deposit, II region, Chile: Exploration drilling and current geological interpretation. *In* Mining Latin America, Minería Latinoamericana Conference, Santiago, 1986, The Institution of Mining and Metallurgy, p. 299-331.

Ojeda, J. (1990) Geology of the Escondida porphyry copper deposit, II región, Chile. *In* Pacific RIM Congress, Queensland, Australia, 1990, v. 2, p. 473-483.

Oliveros, V., Morata, D., Aguirre, L. (2007) Magmatismo asociado a subducción del Jurásico a Cretácico Inferior en la Cordillera de la Costa del norte de Chile (18°30'-24°S): Geoquímica y petrogenesis. Revista Geológica de Chile, v. 34, p. 209-232.

Orrego, M. (1992) Estratigrafía y sedimentación de una secuencia Triásico Jurásica expuesta en el cuadrángulo Cerro Yocas, Sierra de Moreno, región de Antofagasta, Chile. Memoria de título Universidad Católica del Norte, Depto. Ciencias Geológicas, Antofagasta, p. 1-155.

Padilla, R., Niemeyer, H., and Delgado, J. (1997) Informe geológico estructural del sector northe del distrito Escondida: Predicción del comportamiento estructural para el proyecto Escondida Norte, Región de Antofagasta., Proyecto Escondida Norte, Minera Escondida Ltda., p. 1-11.

Padilla, R., Titley, S., and Pimental, F. (2002) Geology of the Escondida porphyry copper deposit, Antofagasta region, Chile. Economic Geology, v. 96, p. 307-324.

Padilla-Garza, R. (2003) Description and evolution of the Escondida porphyry copper deposit, Antofagasta region, northern Chile, Ph.D. Thesis (Unpublished), University of Arizona, Tucson, p. 1-216.

Palma, L. (1993) Geología del distrito Chimborazo. Minera Cyprus Chile, Internal report, p. 1-20.

Pearce, J. (1982) Trace elements characteristics of lava from destructive plate boundaries. *In* Thorpe, R. (ed) Andesites: Orogenic andesites and related rocks. Chichester, Wiley, p. 525-548.

Pearce, J., Parkinson, I. (1993) Trace element models for mantle melting: Application to volcanic arc petrogesis. Geological Society of London Special Publication 76, p. 373-403.

Pérez, A., Niemeyer, H., Zimmermann, U. (2006) Estratigrafía, petrografía y geoquímica de la parte superior del Complejo ígneo-sedimentario Cordón de Lila. *In* Undécimo Congreso Geológico Chileno, Antofagasta, 2006, v. 2, p. 527-530.

Pérez, A., Niemeyer, H., Benedetto, J., Brussa, E. (2007) The Ordovician Quebrada Grande Formation, Cordón de Lila (Antofagasta Region, northern Chile): Stratigraphic and paleogeographic significance, Revista Geológica de Chile, v. 34, p. 277-290.

Peri, A., and Palma, L. (1997) Evidencias de mineralización de cobre tipo manto en proyecto San Carlos, Cordillera de Domeyko, II región de Antofagasta. *In* Octavo Congreso Geológico Chileno, Antofagasta, 1997, p. 1093-1098.

Petersen, C., Rivera, S., and Peri, M. (1996) Chimborazo Copper Deposit, Region II, Chile; Exploration and Geology. *In* Camus, F., Sillitoe, R.H., and Petersen, R. (eds) Andean copper deposits: New discoveries, mineralization, styles and metallogeny. Society of Economic Geologists, Special Publication Number 5, p. 71-80.

Pollard, P., and Taylor, R. (2001) 40Ar/39Ar ages from porphyry and high-sulphidation Cu mineralization at Escondida Norte, Chile. Minera Escondida Ltda., Internal report, p. 1-6.

Pollard, P., and Taylor, R. (2002) SHRIMP U/Pb and 40Ar/39Ar geochronology of intrusive rocks and mineralization at the Escondida Norte Cu deposit, northern Chile. Minera Escondida Ltd., Internal report, p. 1-16.

Prinz, P., Wilke, H., and Hillebrandt, A. (1994) Sediment accumulation and subsidence history in the Mesozoic marginal basin of northern Chile. *In* Reutter, K.-J., Scheuber, E., and Wigger, P. (eds) Tectonics of the southern Central Andes. Springer-Verlag, p. 219–232.

Pritting, J. (2001) Summary Report of Chimborazo-Cerro Rincones Exploration. Escondida Brownfields Exploration Program, Minera Escondida Ltda., Internal report, p. 1-11.

Pritting, J. (2002) Reconnaissance geological map of Chimborazo-Cerro Rincones area, Region II, Chile Escondida Brownfields Exploration Program, Minera Escondida Ltda, Internal report, 1 map.

Quiroz-Luna, F. (2003) Geology and Hypogene Alteration and Mineralization at Escondida, Northern Chile: Porphyry and High-Sulfidation Events. M.S. thesis (Unpublished), University of Arizona, Tucson, p. 1-82.

Quiroz, F. (2003) Evolution of hypogene alteration and mineralization at Escondida, northern Chile: Porphyry copper and high-sulfidation events. *In* Décimo Congreso Geológico Chileno, Concepción, 2003, Simposium 2: Metalogénesis Andina, CD.

Ramos, V., and Alemán, A. (2000) Tectonic Evolution of the Andes. *In* Cordani, U., Milani, E., Thomaz Filho, A., and Campos Neto, M. (eds) Tectonic Evolution of South America, Rio de Janeiro, 2000, p. 635-685.

Rapp, R., Watson, E. (1995) Dehydration melting of metabasalt at 8-32 kbar: Implications for continental growth and crust-mantle recycling. Journal of Petrology, v. 36, p. 891-932.
Reading, H., and Collinson, J. (1996) Clastic coast. *In* Reading, H. (ed) Sedimentary Environments, Processes, Facies and Stratigraphy. Blackwell, New York, 688 p.

Reagan, M., Sims, K., Erich, J., Thomas, R., Cheng, H., Edwards, R., Layne, G., and Ball,

L. (2003) Time-scale of Differentiation from Mafic Parents to Rhyolite in Northern America Continental Arc. Journal of Petrology, v. 44, p. 1703-1726.

Reagan, M., and Gill, J. (1989) Coexisting calcalkaline and high-niobium basalts from Turrialba volcano, Costa Rica: Implications for residual titanates in arc magma sources. Journal of Gephysical Research, v. 94, p. 4619-4633.

Reiners, P., Spell, T., Nicolescu, S., and Zanetti, K. (2004) Zircon (U-Th)/He thermochronometry: He diffusion and comparisons with $^{40}Ar/^{39}Ar$ dating. Geochemica et Cosmochimica Acta 67:4411-27.

Reiners, P. (2005) Zircon (U/Th)/He thermochronology. *In* Reiners, P., and Ehlers, T. (eds) Low-Temperature Thermochronology: Techniques, interpretations, applications. Review in Mineralogy and Geochemistry, v. 58, p. 151-179.

Reiners, P., and Brandon, M. (2006) Using thermochronology to understand orogenic erosion. Annual Review of Earth and Planetary and Sciences, p. 419-465.

Renne, P., Deino, A.., Walter, R., Turrin, B., Swisher, C., Becker, T., Curtis, G., Sharp, W., and Jaouni, A. (1994) Intercalibration of astronomical and radioisotopic time. Geology, v. 22, p. 783-786.

Reutter K-J, Scheuber E., and Helmcke D. (1991) Structural evidence of orogen-parallel strike slip displacements in the Precordillera of northern Chile. Geologische Rundschau, v. 80, p. 135-153.

Reutter, K.-J., Scheuber, E., and Chong, G. (1996) The Precordilleran fault system of Chuquicamata, northern Chile, evidence for reversals along arc-parallel strike-slip faults. Tectonophysics, v. 259, p. 213-228.

Richards, J., Noble, S., and Pringle, M., (1999) A revised Late Eocene age for porphyry Cu magmatism in the Escondida area, northern Chile, Economic Geology, v. 94, p. 1231-1248.

Richards, J., Boyce, A., Pringle, M. (2001) Geologic evolution of the Escondida Area,

Northern Chile: A model for spatial and temporal localization of porphyry Cu mineralization. Economic Geology, v. 96, p. 271-305.

Richards, J. (2000) Lineaments revisited. Society of Economic Geologists Newsletter, No. 42.

Richards, J., and Kerrich, R. (2007) Adakite-like rocks: Their diverse origins and questionable role in metallogenesis. Economic Geology, v.102, p. 537–576.

Riley, T., Leat, P., Pankhurst, R., and Harris, C. (2001) Origins of large volume rhyolitic volcanism in the Antarctic peninsula and Patagonia by crustal melting. Journal of Petrology, v. 42, p. 1043-1065.

Rogers, G., and Hawkesworth, C. (1989) A geochemical transverse across the North Chilean Andes: Evidence of crust generation from the mantle wedge. Earth and Planetary Science Letters, v. 91, p. 271-285.

Rowland, M., and Clark, A. (2001) Temporal overlap of supergene alteration and high-sulfidation mineralization in the Spence porphyry copper deposit, II Región, Chile [abs.]: Geological Society of America, Abstracts with Programs, v. 33, p. A-358.

Rowland, J., and Sibson, H. (2004) Structural controls on hydrothermal flow in a segmented rift system, Taupo Volcanic Zone, New Zealand. Geofluids, v. 4, p. 259-283.

Orton, G. (1996) Volcanic environments. *In* Reading, H.G. (ed) Sedimentary Environments, Processes, Facies and Stratigraphy. Blackwell, New York, 688 p.

Salfity, J., and Marquillas, R. (1994) Tectonic and sedimentary evolution of the Cretaceous-Eocene Salta Group Basin, Argentina. *In* Salfity, J. (ed.) Cretaceous Tectonics of the Andes, Earth Evolution Sciences, Friedr. Vieweg & Sohn, Braunschweig/ Wiesbaden. p. 266-315.

Salfity, J. (1985) Lineamientos transversales al rumbo andino en el Noroeste Argentino. *In* Cuarto Congreso Geológico Chileno, Antofagasta, 1985, v. 2, p. 119-138.

Sandoval, A. (2001a) Altair Target. Escondida Brownfields Exploration Program. Minera Escondida Ltda., Internal report, p. 1-5.

Sandoval, A. (2001b) Pinta Verde Report. Escondida Brownfields Exploration Program. Minera Escondida Ltda., Internal report, p. 1-31.

Saunders, A., Tarney J., and Weaver, D. (1980) Transverse geochemical variations across the Antarctic peninsula: Implications for the genesis of calc-alkaline magmas. Earth and Planetary Science Letters, v. 46, p. 344– 360.

Scheuber, E., and Andriessen, P. (1990) The kinematic and geodynamic significance of the Atacama fault zone, northern Chile. Journal of Structural Geology, v. 12, p. 243-257.

Scheuber, E., and Reutter, K.-J. (1992) Magmatic arc tectonics in the Central Andes between 21° and 25°S. Tectonophysics, v. 205, p. 127-140.

Schueber, E., and Andriessen, P. (1990) The kinematic and geodynamic significance of the Atacama fault zone. Journal of Structural Geology, v. 12, p. 243-257.

Scheuber, E., Bogdanic, T., Jensen, A., Reutter, K.-J. (1994) Tectonic developement of the North Chilean Andes in relation to plate convergence and magmatism since the Jurassic. *In* Reutter, K.-J., Scheuber, E, Wigger, P. (eds) Tectonics of the Southern Central Andes. Springer-Verlag, p. 121-139.

Scheuber, E., Charrier, R., Gonzalez G., Klotz J., Reuther, C-D., Reutter, K.-J. (2000): Crustal evolution of the southern Central Andes (20-26°S) since the Jurassic. *In* Zeitschrift Für Angewandte Geologie, SH 1 Geoscientific Cooperation with Latin America, 31st International Geological Congress, Rio de Janeiro, 2000, p. 323-329.

Schildgen, T., Hodges, K., Whipple, K., Reiners, P., and Pringle, M. (2007) Uplift of the western margin of the Andes plateau revealed from canyon incision history, southern Peru. Geology, v. 35, p. 523-526.

Sempere, T., Butler, R.,Richards, D., Marshall, L., Sharp, W., Swisher III, C. (1997) Stratigraphy and chronology of Upper Cretaceous - lower Palaeogene strata in Bolivia and

northwest Argentina. Bulletin of the Geological Society of America, v. 109, p. 709 - 727.

Sempere, T. (1995) Phanerozoic Evolution of Bolivia and Adjacent Regions. *In* Tankard, A., Suarez-Soruco, R., and Welsink, H.J (eds) Petroleum basins of South America. American Association of Petroleum Geologists, Memoir 62, p. 207-230.

Sepúlveda, P., López, C., Caric, L., Crignola, F., Ipinza, M., Sánchez, M. (2006) Proyecto Chimalén. Gerencia de Exploraciones, Proyecto Brownfields. Minera Escondida Ltda., Internal report, p. 1-30.

Shuster, D. Flowers, R., Farley, K. (2006) Actinide radiation damage and helium diffusion kinetics in apatite. Geochemica et Cosmochimica Acta, Goldschmidt abstract, Melbourne, Australia, August-September.

Sillitoe, R. (1985) Ore-related breccias in vulcanoplutonic arcs. Economic Geology, v. 80, p. 1467-1515.

Sillitoe, R., and Grappe, I. Jr. (1984) Philippine porphyry deposits: Geologic settings and characteristics. United Nations Economic and Social Commission for Asia and the Pacific, Bangkok, CCOP Technical Publication, v. 14, p. 1-89.

Sillitoe, R. (1995) Exploration of porphyry copper lithocaps. *In* Pacific RIM Congress, p. 527-532.

Sillitoe, R., and McKee, E. (1996) Age of Supergene Oxidation and Enrichment in the Chilean Porphyry Copper Province. Economic Geology, v. 91, p. 164-179.

Skarmeta, J., McClay, K., and Bertens, A. (2003) Structural controls on porphyry copper deposits in northern Chile: New models and implications for Cu-Mo mineralization in subduction orogens [abs.]. *In* Décimo Congreso Geologico Chileno, Concepción, 2003, conference proceedings. Departamento Ciencias dela Tierra, Universidad de Concepción, p. 109-110.

Somoza, R. (1998) Updated Nazca (Farallon) - South America relative motions during the last 40 M.y.: Implications for the mountain building in the central Andean region. Journal

of South American Earth Sciences, v. 11, p. 211-215.

Somoza, R., and Tomlinson, A. (2002) Paleomagnetism in the Precordillera of northern Chile (22°-30°S): implications for the history of tectonic rotations in the Central Andes. Earth and Planetary Science Letters, v. 194, p. 369– 381.

Steiger, R., and Jäger, E. (1977) Subcommission on geochronology: Convention on the use of decay constants in geo- and cosmochronology. Earth and Planetary Science Letters, 36, p.359-362.

Storti, F., Balsamo, F., Rosseti, F., and Salvini, F. (2008) Horsetail fault arrays at strike-slip fault tips in Victoria Land (Antarctica) from the outcrop to the plate scale: fault hierarchy evolution and implications for petroleum exploration. Geophysical Research Abstracts, v. 10, 04523.

Stow, D. (1985) Deep-sea clastic: Where are we and where are we going? *In* Brenchley, P, and Williams, B. (eds) Sedimentology, Recent developments and applied aspects. The Geological Society-Blackwell, p. 67-94.

Suarez, M., and Bell, M. (1992) Triassic rift-related sedimentary basins in northern Chile (24°–29°S). Journal of South American Earth Sciences, v. 6, p. 109–121.

Suthren, R. (1985) Facies analysis of volcaniclasticsediments: A review. *In* Brenchley, P, and Williams, B. (eds) Sedimentology, Recent developments and applied aspects. The Geological Society-Blackwell, p. 123-146.

Swanson, M. (1989) Sidewall ripouts in strike-slip faults. Journal of Structural Geology, v. 11, p. 933-948.

Talbot, M, and Allen, P. (1996) Lakes. *In* Reading, H.G. (ed) Sedimentary Environments, Processes, Facies and Stratigraphy. Blackwell, New York, 688 p.

Tchalenko, J. (1970) Similarities between shears of different magnitudes. Geological Society of America Bulletin, v. 81, p. 1625-1640.

Tera, F., and Wasserburg, G. (1972) U-Th-Pb systematics in three Apollo 14 basalts and the problem of initial Pb in lunar rocks. Earth and Planetary Science Letters, v. 14, p. 281-304.

Tomlinson, A., Mpodozis, C., Cornejo, P., Ramírez, C. (1993) Structural Geology of the Sierra Castillo- Agua Amarga Fault System, Precordillera of Chile, El Salvador- Potrerillos. *In* Second International Symposium on Andean Geology. Oxford, 1993, p. 259-262.

Tomlinson, A., and Blanco, N. (1997a) Structural evolution and displacement history of the West Fault System, Precordillera, Chile: Part 1, Synmineral history. *In* Octavo Congreso Geológico Chileno, Antofagasta, 1997, v. 3, p. 1873–1877.

Tomlinson, A., and Blanco, N. (1997b) Structural evolution and displacement history of the West Fault System, Precordillera, Chile: Part 2, Postmineral history. *In* Octavo Congreso Geológico Chileno, Antofagasta, 1997, v. 3, p. 1878-1882.

Tomlinson, A., Blanco, N., Maksaev, V., Dilles, J., Grunder, A., and Ladino, M. (2001a) Geología de la Precordillera Andina de Quebrada Blanca - Chuquicamata, Regiónes I y II [20°30'-22°30'S]. Servicio Nacional de Geología y Minería, CODELCO, Informe Registrado (IR-01-20), 2 v, p. 1– 444.

Tucker, M. (1985) Shallow-marine carbonate facies and facies models. Sedimentology, Recent developments and applied aspects. The Geological Society-Blackwell, p. 147-169.

Uliana, M., Biddle, K., Phelps, D., Gust, D. (1985) Significado del vulcanismo y extension mesojurasicas en el extreme meridional de Sudamerica. Revista Asociación Geológica Argentina, v. 40, p. 231-253.

Urzúa, F. (1989) Estratigrafía y sedimentología de la Formación Zorritas, Sierra Guanaqueros, extremo sur de la Sierra de Almeida, II Región de Antofagasta, Chile. Memoria de Título (Unpublished). Universidad Católica del Norte, Depto. Ciencias Geológicas, Antofagasta, p. 1-189.

Urzúa, F. (2001b) Geology and evaluation of Poblete Basin. BHP Chile Inc., Internal report, p. 1-3.

Urzúa, F., Valdez, M., and Navarro, R. (2001) Southern extension Escondida Mine project: Progress geological report – F.Y. Escondida Brownfields Exploration Program. Minera Escondida Ltda., p. 1-14.

Urzúa, F. (2005b) Geological map of the Isabel del Carmen project. Brownfields Exploration Program. Minera Escondida Ltda., 1 map.

Urzúa, F. (2005a) Geological map of the San Pablo project. Brownfields Exploration Program. Minera Escondida Ltda., 1 map.

Urzúa, F. (2006) Geological map of the Mirador project. Brownfields Exploration Program. Minera Escondida Ltds., 1 map.

Valente, D., Campbell, I., Allen, C. (2006) The geology, geochemistry and geochronology of the El Abra Mine, Chile, and adjacent Pajonales-El Abra suite of intrusions. The Australian National University, Research School of Earth Sciences, Annual Report. htt://www.rses.anu.edu.au /research/annrep.

Véliz, H., and Padilla R. (1997) Geología estructural del yacimiento Escondida, Antofagasta, Chile. Minera Escondida Ltda., Internal report, p. 1-50.

Véliz, W., and Camacho, J. (2003) Antecedentes Geológicos del yacimiento Escondida. *In* Décimo Congreso Geológico Chileno, Concepción, 2003, Sesión Temática 3, CD.

Vergara, G. (2002) Geología Estructural de Escondida, Segunda Región de Antofagasta, Chile, Implicancias de la deformación frágil en el desarrollo de un sistema de pórfido cuprífero. Tesis de Título, (Unpublished). Universidad Católica del Norte, Depto. Ciencias Geológicas, Antofagasta, p. 1-82.

Vicente, J.-C. (2006) Dynamic paleogeography of the Jurassic Andean Basin: Pattern of regression and general considerations on main features. Revista de la Asociación Geológica Argentina, v. 61, p. 408-437.

Victor, P., Oncken, O., and Glodny, J. (2004) Uplift of the western Altiplano plateau: Evidence from the Precordillera between 20° and 21°S (northern Chile). Tectonics, v. 23,

TC4004, doi:10.1029/2003TC001519.

Viramonte, J., Kay, S., Becchio, R., Escayola, M., and Novitski, I. (1999) Cretaceous rift related magmatism in central-western South America. Journal of South American Earth Sciences, v. 12, p. 109-121.

Warren, I., Kasaneva, S., Robbins, C., Simmons, S. (2003) Alteration and mineralization at El Peñón mine, northern Chile. *In* Décimo Congreso Geológico Chileno, Concepción, 2003, Simposium 2: Metalogénesis Andina, CD.

Wescott, W., Ethridge, F. (1980) Fan-delta sedimentology and tectonic setting - Yallahs fan delta, southeast Jamaica. American Association of Petroleum Geologists bulletin, v. 64, p. 374-399.

White, N. (1991) High sulphidation epithermal gold deposits: Characteristics and a model for their origin. *In* Matsuhisa, Y., Aoki, M., and Hedenquist, J.W. (eds) High temperature acid fluids and associated alteration and mineralization. Geological Survey of Japan Report, v. 277, p. 9-20.

White, N., and Hedenquist J. (1990) Epithermal environments and styles of mineralization: Variations and their causes, and guidelines for exploration. *In* Hedenquist J., White N., and Siddeley G. (eds) Epithermal gold mineralization of the Circum Pacific: Geology, geochemistry, origin and exploration. Journal of Geochemical Exploration, v. 36, p. 445-474.

Wiedenbeck, M., Allé, P., Corfu, F., Griffin, W. L., Meier, M., Oberli, F., Von Quadt, A., Roddick, J., and Spiegel, W. (1995) Three nature zircon standards for U-Th-Pb, Lu-Hf, trace element and REE analyses. Geostandards Newsletter, 19: 1-23.

Williams, S. (1993) Petrographic descriptions of samples from Chimborazo Project. Minera Orion Chile Ltda., Internal report.

Williams, M., Olivares, O., and Turner, R. (2002) Geología proyecto Escondida Norte. Proyecto Escondida Norte, Minera Escondida Ltda., Internal report, p. 1-120.

Williams, M. (2003) Geology and mineral resources of the Escondida Norte deposit, Region II, Chile, Simposium 2: Metalogénesis Andina, CD.

Wilson, J. (1989) Igneous Petrogenesis. Unwin Hyman Ltd, London, p. 1-466.

Winchester, J., and Floyd, P. (1977) Geochemical discrimination of different magma series and their differentiation products using immobile elements. Chemical Geology, v. 20, p. 325-343.

Wigger, P., Schmitz, M., Araneda, M., Asch, G., Baldzuhn, S., Giese, P., Heinsohn, W., Martinez, E., Ricaldi, E., Röwer, P., and Viramonte, J. (1994) Variation of the crustal structure of the southern Central Andes deduced from seismic refraction experiments. *In* Reutter, K.-J., Scheuber, E, Wigger, P. (eds) Tectonics of the Southern Central Andes. Springer-Verlag, p. 23-48.

Wood, D. (1980) The application of a Th-Hf-Ta diagram to problems of tectonomagmatic classification and to establishing the nature of crustal contamination of basalt lava of the British Tertiary volcanic province. Earth and Planetary Science Letters, v. 50, p. 11– 30.

Yang, Y., and Liu, M. (2003) A 3-D geodynamic model of lateral crustal flow during Andean mountain building. Geophysical Research Letters, v. 30, doi: 10.1029/ 2003GL038308.

Zentilli, M., Krogh, T., Maksaev, V., Alpers, C. (1994) Uranium-lead dating of zircons from the Chuquicamata and La Escondida porphyry copper deposits, Chile: Inherited zircon cores of Paleozoic age with Tertiary overgrowths. Universidad de Chile, Comunicaciones, v. 45, p. 101-110.

Zhang H., Niu, H., Sato, H., Yu, X., Shan, Q., Zhang, B., Ito., J., and Naga, T. (2005) Late Paleozoic adakites and Nb-enriched basalts from northern Xinjiang, northwest China: Evidence for the southward subduction of the Paleo-Asian oceanic plate. The Island Arc, v. 14, p. 55–68.